



**Svenska Geotekniska Föreningen**  
Swedish Geotechnical Society



**Rapport 1:2025**

# **Nordic Geotechnical Meeting 2024**

Next Generation Meeting

**Volume 1**



**Svenska Geotekniska Föreningen**  
Swedish Geotechnical Society

SGF Rapport 1:2025

# Nordic Geotechnical Meeting 2024

Linköping 2025

<b>SGF Rapport</b>	<b>Svenska Geotekniska Föreningen</b> <b>E-post: <a href="mailto:info@sgf.net">info@sgf.net</a></b>
<b>Beställning</b>	<b>Svenska Geotekniska Föreningen</b> <b>c/o Ernax Design AB</b> <b>Sveaborgsvägen 16</b> <b>439 73 FJÄRÅS</b> <b>Tel: +46 708 137773</b> <b>E-post: <a href="mailto:info@sgf.net">info@sgf.net</a></b>
<b>ISSN</b>	<b>1103-7237</b>
<b>ISRN</b>	<b>SGF-R-25/1-SE</b>
<b>Upplaga</b>	<b>Digital upplaga</b>
<b>Tryckeri</b>	<b>Digital / Arkitektkopia</b>

## FOREWORD

In 2024 it was the Swedish Geotechnical Society's time to organize NGM. Organizing an event gathering geotechnical people from not only all the Nordic countries, but from countries all over the world requires some planning. We decided for the beautiful city of Gothenburg, on the west coast of Sweden, famous for its rainy weather. However, Gothenburg really exceeded all expectations with summer weather in September.

I think NGM 2024 really managed to show what the Nordic Geotechnical Meeting is all about – getting to interact with fellow geotechnical engineers. During the days we got to see great presentations, a wonderful study visit/bus tour in sunny Gothenburg, a dinner with a magic touch and finally we got to meet a whole bunch of new people all sharing the passion for geotechnical engineering.

Without the management of the NGM 2024-general Victoria Svahn and the working group (Andreas Flyckt, Jonas Axelsson, Helen Kennedy and myself) none of this would have been possible – a huge thanks to all of you! I would also like to thank the secretariat Ragna Hellberg and Hillevi Hellberg, without your support the event would probably have been a disaster. In this book you will find the papers from all the great presentations. Enjoy!



Fanny Deckner  
Chairman of the Swedish Geotechnical Society





## TABLE OF CONTENT

### KEYNOTE PAPERS

IS THERE FUTURE FOR SOFT CLAY MODELLING? .....	10
Minna Karstunen	
RECENT DEVELOPMENTS in DEEP MIXING IN FINLAND .....	26
L. Korkiala-Tanttu and J. Forsman	
ENERGY GEOSTRUCTURES: A REVIEW ON THEIR ENERGY AND GEOTECHNICAL PERFORMANCE .....	42
Lyesse Laloui and Melis Sutman	
VERIFICATION OF ADEQUATE ROTATION CAPACITY FOR STEEL SHEET PILE PROFILES BY LEM WALL CALCULATIONS WITH YIELD HINGES .....	64
O. Møller	
DIGITALIZATION IN GEOTECHNICS .....	82
Magnus Rømøen	
MITIGATION VOLCANIC HAZARDS ON THE REYKJANES PENINSULA - LAVA FLOWS AND PROTECTION OF INFRASTRUCTURE, THE GRINDAVÍK SAGA .....	100
Jón Haukur Steingrímsson	

### ALL PAPERS IN ALPHABETIC ORDER

A NOVEL TECHNOLOGY FOR DETERMINING STRENGTH AND REDUCE CLIMATE-GAS EMISSIONS IN DEEP SOIL MIXED PILES .....	121
Helle T.E., Gerhardsen A., Rekdal T., Eriksson S., Juvik E.S. , Giese S., Wiersholm P., Hegseth I., O’Rawe S., Dahl M., Brendbekken G., Nouri E.H., Wåle M.	
A REVIEW OF STATE OF THE ART ON EROSION-DRIVEN QUICK CLAY LANDSLIDES .....	134
Ankit Tyagi and Ivan Depina	
A SIMPLE METHOD FOR PREDICTING COHESIVE PILE - DEFORMATIONS FROM DISPLACEMENT PILE INSTALLATION INDUCED GROUND MOVEMENT .....	142
Jonatan Isaksson, Yanling Li and Lars Hall	

A SURVEY STUDY of THE ENGINEERING PRACTICE OF PIEZOCONE DEVICES WITH REGARDS TO SATURATION CONDITIONS .....	152
Irene Rocchi, Alena D. Zhelezova	
ALTERNATIVE WAYS OF MODELLING STABILISED EXCAVATIONS .....	160
Sinem Bozkurt, Ayman Abed, and Minna Karstunen	
ANALYSES OF PERFORMED CPT TESTS ON SITE WITH RESPECT TO THE NEW STANDARD .....	174
Caesar Kardan, and Håkan Garin	
AROS – THE NEXT LEVEL, 3D MODELLING OF SWELLING ANCHORS .....	184
Britta S. Heilmann, Martin N. Luxhøj, and Bjørn S. Roesen	
ASSESSING UNDRAINED SHEAR STRENGTH IN DANISH MARINE GYTJIA: INSIGHTS FROM FIELD VANE TESTS AND PLATE LOAD TESTS .....	198
E. S. Brandt, H. Trankjær, N. Mortensen and K. K. Sørensen	
BORED PILES IN COPENHAGEN LIMESTONE .....	216
Kirsten M. Iversen, Bjørn S. Roesen, and Jørgen S. Steenfelt	
BRIDGING GEOPHYSICAL AND GEOTECHNICAL RESULTS: AN AUTOMATED CAD VISUALIZATION METHOD FOR 2D DATA .....	226
Sebastian Buntin, Omid Ahmadi, and Mats Svensson	
BRINGING TECH INTO GEOTECHNICS .....	232
Kristin Paulsen, Truls Martens, and Mats Kahlström	
BYGGEGROPVEILEDNINGEN – A TOOL FOR PLANNING BUILDING PITS .....	236
Gunnvor Baardvik and Astri Eggen	
CC-TEST, CLAY CUTTING TEST .....	250
P. Hedborg	
CEMENTSTABILIZATION OF PEATMATERIAL IN ROAD CONSTRUCTION.....	264
Kristoffer Lauridsen, Andreas Elkjær Riis	
CHALLENGES IN DETERMINE GROUND CONDITIONS FOR THE DESIGN OF WATER RESERVOIR DAMS IN THE AITIK MINE .....	274
Thomas Larsson	
COEFFICIENT OF VARIATION FOR STRENGTH AND DEFORMATION PROPERTIES OF CLAY .....	282
Göran Sällfors, Per-Evert Bengtsson	

COMPLEXITY OF LARGE INFRASTRUCTURE PROJECTS - DISCUSSION OF GEOTECHNICAL CHALLENGES AND RISK TRAJECTORY TO EXTREM COST OVERRUNS.....	292
P. Kylmänen, K. Viking, S. Hintze	
CONCEPT ON SOIL PLUGGING IN CLAY DEVELOPED FROM NUMERICAL CEL- SIMULATIONS CONSIDERING TOTAL STRESSES .....	304
P. Wiesenthal, S. Henke	
CORRELATING $q_{net}$ TO $E_{OED}$ OF PELEOGENE CLAYS OF VERY HITHE PLASTICITY .....	312
N. Okkels, L. Bødker, E. Skouboe and T. Thorsen	
DATA ASSIMILATION IN A HYDROLOGICAL LANDSLIDE MODEL WITH ENSEMBLE KALMAN FILTER .....	325
Amirahmad Vakilinezhad, Signe Othelie Petrohai Pedersen, Ivan Depina	
DESIGN METHODS FOR SHORT SLENDER STEEL PILES IN CLAY .....	333
J. Stener, D. Ebenhardt, A.B. Lundberg and S. Larsson	
DESIGN OF 15 METER HIGH RAILWAY EMBANKMENT on loose silt and clay .....	346
Ibrahim Rashid, Fredrik Clifford	
DIGITAL GEOTECHNICAL INFORMATION MANAGEMENT FOR LIFECYCLE RESOURCE SAVINGS .....	359
M. Svensson, O. Friberg	
DRAINED FAILURES, STRESS DEPENDENCY AND PLANE STRAIN EFFECTS .....	371
Niels Mortensen	
EARLY-PHASE MODELLING OF LIME-CEMENT COLUMNS TO REDUCE CARBON FOOTPRINT .....	384
Nikolaj Børner Hansen, Mats Kahlström, and Magnus Rømoen	
EFFECT OF LOADING RATE ON THE UNDRAINED LIMITING PRESSURE OF DEEPLY-EMBEDDED PILE.....	392
Yuepeng Dong	
EUROCODE 7: A FRAMEWORK FOR GEOTECHNICAL DESIGN .....	397
G. Franzén, B. Hansson, and J. Spross	
EVALUATION OF NORWEGIAN DESIGN METHODS OF AXIAL CAPACITY OF DRIVEN PILES IN SAND .....	402
F. Kolsgaard, S.A. Degago, A. Emdal and F. Oset	

EVALUATION OF SOLIDIFICATION/STABILIZATION TECHNOLOGY PERFORMANCE BY COMBINING ECONOMIC AND ENVIROMENTAL IMPACTS ASSESSMENT FOR A PORT IN SWEDEN.....	410
E. Tamadonyazdian, M. Gholampoor, K. Farsäter, and M. Bayat Pour	
EXCAVATIONS IN SOFT SOILS: REVIEW OF DESIGN APPROACHES.....	422
G. Portmann, A. Arnold	
FENICS SIMULATION OF ARTESIAN CONDITIONS IN CLAY SLOPE .....	435
K. Muratova, A. A. Abed, and M. Karstunen	
FIELD VANE TEST WITH NEW STANDARD .....	445
Panu Tolla, Juha Selänpää, Monica S. Löfman, Sami Kankaanpää and Fredrik Winqvist	

## KEYNOTE PAPERS IN ALPHABETIC ORDER BY AUTHOR



# IS THERE FUTURE FOR SOFT CLAY MODELLING?

**Minna Karstunen<sup>1</sup>**

## KEYWORDS

Constitutive modelling, Numerical modelling, Soft clay engineering

## ABSTRACT

Constitutive models for natural sensitive clays have significantly evolved since the introduction of critical state models in 1950's. They can now be applied with high accuracy to geotechnical engineering problems as part of numerical analyses, thus assisting in geotechnical design. With the current rate-dependent models that combine initial anisotropy and its evolution, as well as the effects of bonding and destructuration, it is possible to capture the system-level response of a wide range of geotechnical problems in natural clays. Thus, a question arises if there is need for further developments in soft soil modelling. The paper will discuss the current state, followed by a discussion on future challenges that necessitate further developments. Despite the recent progress in model development, a major concern is that the gap between academia and practice is increasingly widening. Consequently, the geotechnical profession may not yet be able to fully exploit the latest modelling advances and the huge opportunities they offer for digitalisation and generation of training data for low probability events in geotechnics.

## INTRODUCTION

The preference for the human population to live close to waterways, due to the good transport links and favourable conditions for farming, is the reason why mankind tends to live in areas underlain by soft soil deposits. In particular, the construction on soft sensitive clays in the Nordic countries comes with excessive costs and risks. Ideally, these risks are identified already in the planning stage, to avoid unnecessary delays, cost overruns and project cancellations. We may have been building on soft soils for thousands of years, but due to the unprecedented pressures from urbanisation and climate change, we are faced with additional challenges, and thus need new approaches.

Until now, the geotechnical design of road and railway embankments has relied on breaking up the problem into two separate analyses. We calculate the stability in undrained conditions of embankment slopes for the Ultimate Limit State (ULS) using Limit Equilibrium Method (LEM). That is followed by

<sup>1</sup> Chalmers University of Technology

simple 1D consolidation analyses for settlements for the Serviceability Limit State (SLS), assuming groundwater levels and flow boundary conditions to be stationary. Similarly for natural slopes, LEM is the standard design method to assess stability, even though the accuracy of the analyses is unknown, as the design approach has no links with quantities we are able to monitor. The current methods of analyses are unlikely to remain adequate, as the future will entail more radical changes in pore pressures, temperature fluctuations and saturation levels. Furthermore, from stormwater drainage point of view, keeping the design alignment of embankments will become increasingly more important. Multi-dimensional displacement predictions under linear infrastructure, such as roads and railways, will become increasingly important.

In geotechnical engineering we cannot control the direction of loading. Yet, we need to design the foundation systems to be able to handle the external loads, as well as the body forces due to the self-weight of the soil and transfer them to layers with sufficient bearing capacity in the sub-soil. This needs to be done with a safety margin against failure that can be quantified. In parallel, we need to ensure the functionality of the geostructure during its design life. The loading directions in the soil in an urban setting are complex, as illustrated in Figure 1, where some typical total stress paths have been plotted in terms of mean stress ( $p$ ) and deviatoric stress ( $q$ ). Due to the low hydraulic conductivity and the viscous nature of natural soft clays, the emerging effective stress paths that control the stress-strain response, and the ultimate strength, are rate-dependent. The strain rates in laboratory tests differ from those in a geostructure in the field. The soil response for arbitrary loading paths thus needs to be generalised to map the rate- and time-dependent response from laboratory to the field.

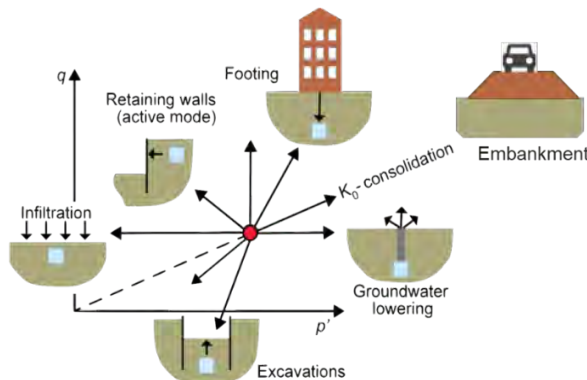


Figure 1 Examples of the complex total stress path associated with urban construction.

A logical method to accomplish the mapping across loading rates and length scales is to use a rate-dependent constitutive model, embedded into a coupled hydro-mechanical numerical framework.



The results of geotechnical numerical analyses largely depend on the constitutive model used to represent the soil response [36]. Furthermore, for accurately modelling natural soft clays, the accuracy of the model parameters relies strongly on the quality of soil sampling and testing [21]. Above all, the results rely on the ability of the geotechnical engineer in choosing a representative numerical model (that includes the selection of the constitutive model, numerical framework and boundary conditions) for the problem at hand, as well as deriving representative values for the model parameters and (initial) state variables.

The commercially available numerical codes utilise different numerical frameworks to solve the system of governing partial differential equations, considering equilibrium, strain compatibility, boundary conditions and stress-strain relationships. The numerical codes offer numerous, increasingly complex, constitutive models. Most of these constitutive models have been developed either via testing reconstituted soil samples, such as kaolin clay, or using generic data not designed to systematically test for the particular model features considered. Thus, element level comparisons between constitutive model simulations and experimental data found in geotechnical literature are often not a representative model validation for natural clays. Without access to raw data, it is also not possible to assess the quality of the data used for model validation. Consequently, only very few constitutive models have been validated against high-quality systematic data on intact samples of natural clays.

Finally, as important as the selection of the constitutive model is, the results of the numerical analyses are meaningless, unless the numerical framework adopted can ensure convergence within a well-defined tolerance. Fundamentally, all numerical models are approximations. The quality of results will thus depend on the general numerical framework utilised, which often includes assumptions that cannot be controlled by the user. These include the solution methods for the non-linear equations and time integration methods, including the iterative procedures, sub-stepping schemes and convergence checks adopted (at local and/or global level). Regardless, the user must be rather knowledgeable to properly discretise the problem, in selecting the correct model geometry, element types and boundary conditions, as well as the tolerances controlling the accuracy of the solution and the speed of the iterative processes.

Given the availability of user-friendly geotechnical numerical codes, people with limited background in numerical modelling per se are using these programs as black boxes for analysing complex problems, with constitutive models they do not truly master. So, no wonder many experienced geotechnical engineers are somewhat sceptical about what geotechnical numerical modelling can offer. The Ballina Embankment Prediction Symposium [42] highlighted how poor the predictions of the deformations of an embankment are,

yet demonstrating significant progress from the settlement calculation competition on Haarajoki test embankment [48]. However, when geotechnical numerical analyses are done properly, they are powerful tools for understanding the complex time-dependent system response of geostructures and can assist the process of geotechnical design of both simple and complex cases.

The paper starts by discussing where we are now in terms of modelling sensitive clays. Following on, future challenges, opportunities and difficulties will be discussed.

## **WHERE ARE WE NOW IN SOFT SOIL MODELLING**

The start of contemporary soft soil modelling can be attributed to the developments at the University of Cambridge in 1950s. Based on systematic testing of reconstituted kaolin clay, the unifying concepts of critical state soil mechanics were developed, ultimately resulting in the Modified Cam Clay (MCC) model [37]. With a single set of four model parameters and two state variables, i.e. specific volume (or void ratio) and preconsolidation pressure, it was possible to describe in a comprehensive manner the complex multi-dimensional stress-strain response of fine-grained soils, both in overconsolidated and normally consolidated state. In early 1990s, the MCC model and some of its derivatives were made available for practitioners via commercial finite element codes, such as SAGE Crisp, Z-Soil and Plaxis, making it possible to use the models in geotechnical boundary value problems. However, as the MCC model was developed for reconstituted clays, some of the key features of the response of natural clay were missing. Furthermore, the model significantly overpredicts the earth pressures in the normally consolidated state, resulting in poor predictions of horizontal displacements and earth pressures.

The pioneering research at Laval University in Canada, by Leroueil and his co-workers, highlighted some of the many complexities in the response of natural sensitive clays. Most importantly, the rate-dependency of the strength and stiffness was highlighted [29]. The anisotropy of yield, and the temperature effects on yielding, were also studied for example in Mexico, Canada, Finland and Sweden (e.g. [13], [26], [44]). Finally, the effects of bonding and degradation of the bonds, as typical for sensitive clays, see e.g. [9] and [30], became better understood.

Observing experimentally the soil response, however, is not sufficient. Even though e.g. [12] and [34] proposed elasto-plastic model frameworks that account for initial anisotropy and its evolution with irrecoverable strains, there was no systematic data for formulating the kinematic hardening laws. Many of the experimental researchers above only studied the shape of the initial yield envelope. This major gap was tackled by the author and her co-workers

by systematically testing four very different Finnish clays, both in their natural and reconstituted state (see e.g. [49], [24], summarised in Koskinen [27]. Using the ideas by Gens & Nova [15], the S-CLAY1 model [49] was extended to account for the bonding and degradation of bonds in sensitive clays [25]. The resulting S-CLAY1S model [25], however did not include the essential rate-effects and creep. Thus, by utilising the ideas of Leoni et al. [28] & Grimstad et al. [18], Creep-SCLAY1S model was developed [40], [17]. With the current version of Creep-SCLAY1S, a rate-dependent model that combines initial anisotropy and its evolution, as well as the effects of bonding and destructuration, it is possible to capture the system-level response for many geotechnical problems, such as embankments and excavations, as discussed in the following.

## MODELLING GEOSTRUCTURES ON NATURAL CLAYS

For accurate predictions using a numerical model, the laboratory testing programme needs to be planned to suit for the constitutive models to be selected. For Creep-SCLAY1S, a systematic test series needs to be performed for each representative soil layer. The test series should consist of CRS (constant rate of strain) & IL (incrementally loaded) oedometer tests to assess the preconsolidation pressure, compressibility and hydraulic conductivity. For strength estimation, CAUC triaxial tests (anisotropically consolidated undrained shearing in compression) are needed. Additionally, for problems where both SLS and ULS are important, or significant rotations of principal stresses are expected, an undrained triaxial test sheared in extension (CAUE) is recommended. For problems where large amplitude loading/unloading loops are encountered, it is also important to plan tests with appropriate loading-unloading loops. The effect of sample disturbance can be quantified by using the sample quality metrics, e.g. by Lunne et al. [32], considering the sample quality relative to the initial state ( $\Delta e/e_0$ , with  $\Delta e$  being the change in void ratio when consolidating to the in situ effective stress state at a corresponding void ratio of  $e_0$ ).

The next step is to derive the values for the model and state parameters. For those parameters that cannot be directly derived, recommendations in [16] can be used, followed by calibration of the parameter set via element level simulations (see <https://soilmodels.com/calibsoftware/> for examples of single element drivers). Once the calibration is completed, i.e. that the test response along different loading paths can be simulated with a single set of parameters, we are ready for numerical analyses. Calibrating parameters for a relatively simple model, such as MCC, is more difficult than for Creep-SCLAY1S that captures the overall response of natural clays more accurately than MCC.

As summarised in [22] [23], Creep-SCLAY1S has been used successfully to simulate test embankments, such as Haarajoki [3] and Ballina tests embankments [4]. More recently, the Onsøy test embankment [6] [7] was simulated

considering both SLS and ULS, including the time for failure (preliminary results by Hernvall shown in [22]. The simulations of the Göta tunnel excavation [46], a permanent sheet pile wall in Uppsala [45], the Marieholm tunnel (yet unpublished) and the lime-cement-column -supported excavation in Gothenburg central station [8] demonstrate the ability of the Creep-SCLAY1S model to capture the time-dependent system response of embedded retaining structures. The latter include the wall movements, the generation and dissipation of pore pressures, strut forces and induced ground movements. However, the larger the distance from the excavation, the poorer is the match between the simulations and measurements. The likely reason for that is the poor performance at small strain magnitudes. A small-strain feature was recently added to the model formulation, to overcome this limitation, following the ideas by Sivasithamparam et al. [41]. Furthermore, the visco-plastic model formulation of Creep-SCLAY1S enables extension of the model for other long-term predictions, such as cyclic degradation [51] in soft natural clays due to railway traffic.

While Creep-SCLAY1S can be used for individual case studies and forecasting, the true power comes from understanding the system performance and thus model simulations can be used for generalisation of the system performance. As an example of the former, Hernvall et al., [19], used the model for studying the increase of the stability of an embankment as a function of time. In the FE analyses of [19] the mobilised strength along the failure plane is automatically predicted by the constitutive model, even accounting for strain softening. This overcomes difficulties in evaluating the evolution and mobilisation of the undrained shear strength along the failure surface. Tornborg et al. [47] in turn used numerical analyses in combination with non-dimensional groups to create design charts for the effective heave pressure that develops over time under the slab at the bottom of a deep excavation.

As shown by Sellin [38], the rate of loading to failure affects both the time of failure of natural slopes, as well as the mode of failure (i.e. the depth and

extent of the failure surface). Furthermore, using a simpler model, such as an isotropic model or a model with fixed anisotropy is not conservative [39]. Moreover, in natural slopes and in sloping ground, the initialisation (of the initial state variables) is a challenge that requires careful consideration [38] [46]. This definitely needs further investigation, as the initialisation affects the mobilised undrained shear strength in natural slopes.

In the West Coast of Sweden the natural slopes have been formed by erosion processes. Sellin [38] simulated the formation of a typical slope by numerically modelling the erosion process. The in Figure 2d, suggest that due to these processes, the slope has become overconsolidated.

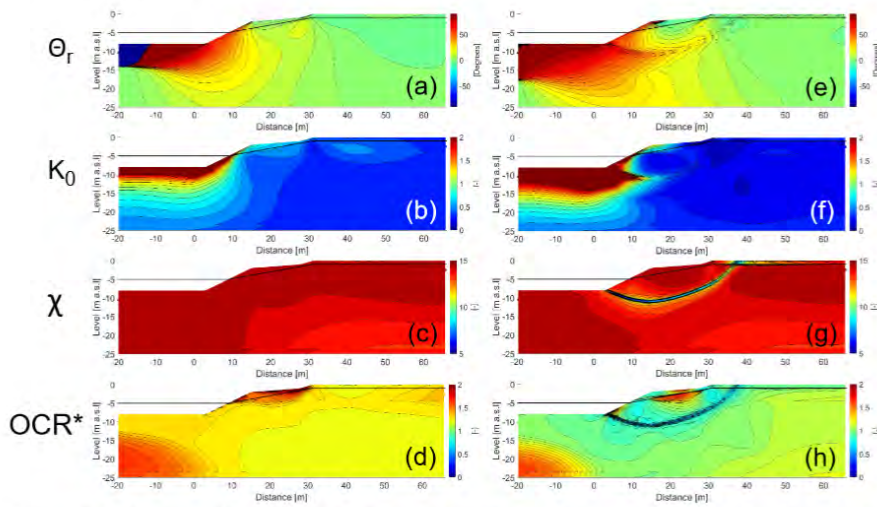


Figure 2 Contour plots of principal stress direction  $\Theta_r$  (upper row),  $K_0$  (second row),  $\chi$  (third row) and modified over consolidation ratio  $OCR^*$  (lower row) after unloading (left) and after additional gravity is applied to drive the slope to failure (right) [38].

The erosion process was found to cause significant rotation of principal stress axes, changes in  $K_0$  (coefficient of earth pressure at rest) and the amount of bonding  $\chi$ . These changes in the state of the soil will affect the stability and mode of failure, when the slope is subsequently driven to failure by increasing the gravity (see Figure 2 on right). Our knowledge of the rate-dependent response of natural clays in the overconsolidated region is very limited, and systematic experimental investigation and combined with model development is required. For understanding the movements and vulnerability of existing slopes in sensitive clays, it is instrumental to study the strength upon unloading and rotation of principal stress axes, which is far from trivial.

## CHALLENGES IN NEAR FUTURE

In the Nordic countries, like in most of the developed world, most of our transport infrastructure is ageing. Thus, characterisation of the state of existing transport infrastructure is of utmost importance, to enable predictive maintenance and smartly designed timely upgrades. The latter include e.g. increasing embankment heights in preparedness for new flood levels, replacing culverts in the view of extreme rainfall incidents, as well as widening of existing embankments to increase the capacity. Increasing traffic and axle loads also imply that our roads and railways are facing increased static, cyclic and dynamic loading. This paired with increasing number of environmental loading cycles due to climate change (droughts vs. downpours, number of freeze-thaw cycles), creates additional challenges and demands for our ageing infrastructure. Thus, we need model developments that enable us to predict future extreme events (with low probability) starting from the current state that often is unknown.

Due to climate change, we will experience more extreme drying-wetting cycles, and there will be a notable increase in the periods of intense precipitation and drought. The more extreme temperature fluctuations will affect in particular the surface layers in the ground, such as the pavement structures and the dry crust, potentially accelerating deterioration and cracking. In the Nordic countries, the increases in the annual number of freezing-thawing cycles [43] and fluctuations of pore pressures, have already increased the demand for maintenance, as well as caused embankment and slope failures in unexpected locations [33].

Both the mobilised shear strength and the stiffness are functions of effective stress, which is controlled by suction (the negative pore pressures), affecting the most critical shallow modes of failure in natural and man-made slopes. As demonstrated in [31], even small increases in temperature will accelerate creep in sensitive clays, resulting in increases in the rate of ground movements when the effective state is close to the preconsolidation pressure. The effects of these climate-change driven changes need to be quantified, to understand which issues are most important in a given environmental setting and geotechnical engineering problem. This requires multi-physics models, currently being developed at Chalmers [1]. Understanding the role of vegetation in the current safety levels is also a multi-physics problem [43]. Consequently, development of advanced physics-based numerical models for natural clays should be a high priority.

Historically, geotechnical design of underground construction and the potential impacts on the surroundings, both in the short and long term has been made with 2D simulations. In Geotechnical Engineering context the simulations are fully coupled transient analyses in either axisymmetric or plane strain conditions. Hydrogeologists may also consider 3D groundwater flow

simulations that are weakly coupled with 1D settlement simulations. Most simulations consider so-called green-field conditions when estimating possible building damage from underground construction, thus largely ignoring the effect of foundations. New constructions inevitably affect the existing structures and buildings, some with high cultural and/or historic value. Thus, there are more demands on combining predictions and monitoring. Monitoring alone is insufficient, as the rigorous use of Observational Method [35], relies on predictions of the quantities that are being monitored, to set up the trigger levels. In case of tunnels and deep excavations, this means (vertical and horizontal) displacements, stresses and pore pressure changes, the latter often affecting large areas. The problems we need to analyse are 4D, with time as the 4<sup>th</sup> dimension. Thus, from a project-scale we need increasingly to move to regional scale, as demonstrated in [50].

In an urban environment, the site characterisation needs to consider, in addition to the geological history, the effects of anthropological loading history. The installation effects of retaining structures, piles and ground improvement in soft soils often result in ground movements that are of the same order of magnitude as the effects of the excavation and tunnelling themselves. Numerical modelling can be used to simulate these processes (see e.g. [10] [14] [20]). The deepening of waterways and canals and the deposition of fills in and next to the waterways for new developments, as well as historic land and water use may cause significant background subsidence. An example is Gothenburg, with background creep settlements varying between 3 mm/year to over 30 mm/year. The cumulative effects of these in tens of years (the planned lifetime of building and infrastructure) and hundreds of years (flood protection), means that the background creep settlement cannot be ignored. They need to be considered in all planning and design of new developments, as they affect the connections of infrastructure to buildings and most importantly, future flooding scenarios. Namely, the background creep settlements are rarely uniform, and thus areas that were not deemed flood-prone based on their current elevation may in the long-term perspective become vulnerable for floods (due to the settlements from fills). Fortunately, new sources of monitoring data that cover large areas, e.g. InSAR data from the European Ground Motion Service [11], can assist in identifying areas with elevated long-term risks. The measurements on the surface will of course not suffice, and need to be complemented with depth-integrated measurements of pore pressures and displacements to understand the source and nature of the time-dependent deformations at the surface.

All in all, as discussed above, future geotechnical design cannot be based on simplified semi-empirical methods, as we no longer have the conditions for which those methods have been calibrated for, and most importantly we do not have experience on those conditions. As a result of urbanisation and climate change, we have to be able to understand ever more complex systems of



systems, and thus, we will increasingly need to rely on physics based numerical modelling to understand, and predict, the performance of these complex systems in a changing environment.

## **OPPORTUNITIES & DIFFICULTIES**

In society at large, as well as in the construction industry, there are huge expectations on using artificial intelligence (AI) and big data to make processes more efficient and predictions more reliable. Furthermore, there is the impression that the conservatism (as expressed in safety factors) can be reduced. Yet, there are several obstacles that preclude the use of AI and big data in geotechnical engineering:

- 1) The low probability of most extreme events (storms, floods, slope failures, bearing capacity problems) implies that, even in case we can monitor all these events, there is an insufficient amount of data for developing AI-based techniques. There is a significant opportunity to use the physics-based numerical models discussed herein to for example train meta-models (a simplified surrogate model) that are computationally more efficient for analysing large scale problems [50].
- 2) For serviceability limit state, there is opportunity to use data driven approaches. Yet, the often-poor reliability of the data and the incompleteness of the datasets prevents the widespread use of purely data-driven approaches. A method to overcome some of the limitations of the data reliability and sparsity is to combine site investigation and monitoring data with numerical forecasting (prediction) models using Data Assimilation [2], as demonstrated in Figure 3.
- 3) There is a general lack of access to high quality public data that is in digital format and properly annotated. Furthermore, the geotechnical quality and reliability (quality of the soil samples tested in the laboratory, reliability of the porewater transducers in the ground after some time, control of temperature) is not always sufficient. Major players in Swedish geotechnical engineering, such as Swedish Geotechnical Institute, Swedish Geological Union, Trafikverket and municipalities have already been developing great tools. What is needed is to integrate those resources in a fully open database linked to other resources such as Land Survey (Landmäteriet) and Swedish Meteorological and Hydrological Institute (SHMI).

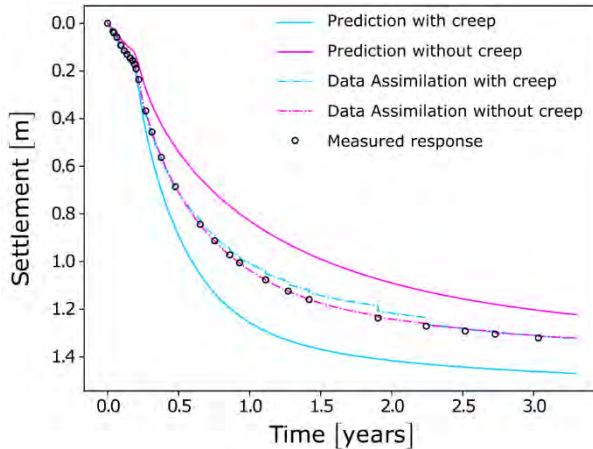


Figure 3 Prediction of settlement of Ballina test embankment with and without creep, combined with data assimilation (modified from [2]).

Finally, the developments discussed above require a strong commitment to further develop physics-based models that are tailored to the Nordic conditions. In addition, we need to reinforce our efforts to not only teach geotechnics, but also the opportunities and limitation of numerical modelling and computational methods associated to AI and big data. The education does not stop at university, there is an imminent need for the discipline to develop a framework for life-long learning in geotechnical engineering.

## ACKNOWLEDGEMENTS

I would like to thank all former and current colleagues, students, and collaborators for the interactions we have had over the years. The financial support by FORMAS, Vetenskapsrådet (Swedish research councils) and Swedish Transport Administration (as part of BIG -Branchsamverkan i Grunden project) in recent years is greatly appreciated. The work is done as part of Digital Twin Cities Centre that is supported by Sweden's Innovation Agency VINNOVA.

## REFERENCES

- [1] Abed, A., Gerolymatou, E. & Karstunen, M. FEniCS simulation of a partially saturated slope under varying environmental loads. Proceedings of NUMGE 2023 London, UK, 26 - 28 June 2023
- [2] Amavasai, A. Beyond the deterministic approach-on the feasibility of data assimilation methods in geotechnics. Doctoral thesis, Chalmers University of Technology. 2023.

- [3] Amavasai, A., Gras, J. P., Sivasithamparam, N., Karstunen, M., Dijkstra, J. Towards consistent numerical analyses of embankments on soft soils. *European Journal of Environmental and Civil Engineering*, 26(7), 2616-2634. 2022
- [4] Amavasai, A., Sivasithamparam, N., Dijkstra, J., Karstunen, M. Consistent Class A & C predictions of the Ballina test embankment. *Computers and Geotechnics*, 93, 75-86. 2018
- [5] Amavasai, A., Tahershamsi, H., Wood, T., & Dijkstra, J. Data assimilation for Bayesian updating of predicted embankment response using monitoring data. *Computers and Geotechnics*, 165, 105936. 2024
- [6] Berre, T. Test fill on soft plastic marine clay at Onsøy, Norway. *Canadian Geotechnical Journal* 51 (1), 30–50. 2014
- [7] Berre, T. Test fill brought to failure on soft plastic marine clay at Onsøy, Norway. *Canadian Geotechnical Journal* 55 (4), 563–576. 2018
- [8] Bozkurt, S., Abed, A., & Karstunen, M. Finite element analysis for a deep excavation in soft clay supported by lime-cement columns. *Computers and Geotechnics*, 162, 105687. 2023
- [9] Burland, J. B. On the compressibility and shear strength of natural clays. *Géotechnique*, 40(3), 329-378. 1990
- [10] Castro, J., Karstunen, M., Sivasithamparam, N. Influence of stone column installation on settlement reduction. *Computers and Geotechnics* 59, 87-97. 2014.
- [11] Crosetto, M. et al. The evolution of wide-area DInSAR: From regional and national services to the European Ground Motion Service. *Remote Sensing* 12(12): 2043. 2020
- [12] Dafalias, Y. F. An anisotropic critical state soil plasticity model. *Mechanics Research Communications*, 13(6), 341-347. 1986
- [13] Diaz-Rodriguez, J. A., Leroueil, S., & Aleman, J. D. Yielding of Mexico City clay and other natural clays. *Journal of Geotechnical Engineering*, 118(7), 981-995. 1992
- [14] Dijkstra, J., Broere, W., Heeres, O. M. Numerical simulation of pile installation. *Computers and Geotechnics* 38(5), 612-622. 2011
- [15] Gens, A., Nova, R. Conceptual bases for a constitutive model for bonded soils and weak rocks. In: *Geomechanical Engineering of Hard Soils and Soft Rocks*, Vol. 1, pp. 485-494. 1993

- [16] Gras, J.-P., Sivasithamparam, N., Karstunen, M., Dijkstra, J. Permissible range of model parameters for natural fine-grained materials. *Acta Geotechnica* 13(2), 387-398. 2018
- [17] Gras, J. P., Sivasithamparam, N., Karstunen, M., Dijkstra, J. Strategy for consistent model parameter calibration for soft soils using multi-objective optimisation. *Computers and Geotechnics* 90, 164-17. 2017.
- [18] Grimstad, G., Degado, S. A., Nordal, S., Karstunen, M. Modeling creep and rate effects in structured anisotropic soft clays. *Acta Geotechnica* 5(1), 69-8. 2010.
- [19] Hernvall, H., Karlsson M., Karstunen, M. A numerical study of the time effects on the stability of a test embankment on sensitive clay. *Proceedings of NUMGE 2023, London, UK, 26 - 28 June 2023.* 2023.
- [20] Isaksson, I., Karlsson, M., Dijkstra, J. Modelling pile installation in soft natural clays. *Proceedings of NUMGE 2023, London, UK, 26 - 28 June 2023*
- [21] Karlsson, M., Emdal, A., Dijkstra, J. Consequences of sample disturbance when predicting long-term settlements in soft clay. *Canadian Geotechnical Journal* 53(12), 1965-1977. 2016.
- [22] Karstunen, M. Advanced numerical models for geotechnical problems on soft clays. 10th Raúl J. Marsal Córdoba Lecture, XXXI Reunión Nacional de Ingeniería Geotécnica, Guadalajara, Mexico, November 16 - 19, 2022
- [23] Karstunen, M. From theory to practice - numerical modelling of geostructures on soft natural clays. Invited keynote lecture. *Proceedings of NUMGE, London, UK, 26 - 28 June 2023.*
- [24] Karstunen, M., & Koskinen, M. Plastic anisotropy of soft reconstituted clays. *Canadian Geotechnical Journal*, 45(3), 314-328. 2008
- [25] Karstunen, M., Krenn, H., Wheeler, S. J. Koskinen, M., Zentar, R. Effect of anisotropy and destructuration on the behaviour of Murro test embankment. *International Journal of Geomechanics* 5 (2), 87-97. 2005
- [26] Korhonen, K. H., & Lojander, M. Yielding of Perno clay. In *Proc., 2nd Int. Conf. on Constitutive Laws for Engineering Materials*, Vol. 2, 1249-1255. 1987.
- [27] Koskinen, M. Plastic anisotropy and destructuration of soft Finnish clays. PhD thesis. Aalto University, Espoo, Finland. 2014.
- [28] Leoni, M., Karstunen, M., Vermeer, P. A. Anisotropic creep model for soft soils. *Géotechnique* 58(3), 215-226. 2008.

- [29] Leroueil, S., Kabbaj, M., Tavenas, F. & Bouchard, R. Stress-strain-strain rate relation for the compressibility of sensitive natural clays. *Géotechnique* 35(2), 159-180. 1985.
- [30] Leroueil, S. & Vaughan, P.R. The general and congruent effects of structure in natural soils and weak rocks. *Géotechnique*, 40(3), 467-488. 1990
- [31] Li, Y., Dijkstra, J., & Karstunen, M. Thermomechanical creep in sensitive clays. *Journal of Geotechnical and Geoenvironmental Engineering*, 144(11), 04018085. 2018
- [32] Lunne, T., Berre, T., Andersen, K. H., Strandvik, S. & Sjursen, M. Effects of sample disturbance and consolidation procedures on measured shear strength of soft marine Norwegian clays. *Canadian Geotechnical Journal*, 43(7), 726-750. 2006
- [33] Löfroth H., Fritzson H., Holmén M., Lundström K., Rudebeck D., Abed A., Karstunen M., Jia Q., Laue J. Långsamma skred i skiktad siltig jord. Förstudie – BIG A2022-01. Statens geotekniska institut, SGI, Linköping. 2024.
- [34] Nova, R. Mathematical modelling of anisotropy of clays. *Proc.*, 11th ICSMFE, San Francisco, Vol. 1, 607–66. 1988
- [35] Peck, R. B. Advantages and limitations of the observational method in applied soil mechanics. *Géotechnique*, 19(2), 171-187. 1969
- [36] Potts, D. M. Numerical analysis: a virtual dream or practical reality? *Géotechnique*, 53(6), 535-573. 2003
- [37] Roscoe, K.H. & Burland, J.B. On the generalized stress-strain behaviour of 'wet' clay, in: J. Heyman and F.A. Leckie, eds., *Engineering Plasticity* (Cambridge Univ. Press, Cambridge), 535-609. 1968
- [38] Sellin, C. On modelling of slope stability in sensitive clay. Doctoral thesis. Chalmers University of Technology. 2023
- [39] Sellin C., Karstunen, M. Slope stability assessment in sensitive clay with an advanced constitutive model. *Proceedings of NUMGE 2023*, London, UK, 26 - 28 June 2023
- [40] Sivasithamparam, N., Karstunen, M., Bonnier, P. Modelling creep behaviour of anisotropic soft soils. *Computers and Geotechnics* 69, 46-57. 2015
- [41] Sivasithamparam, N., D'Ignazio, M., Tsegaye, A. B., Castro, J., & Madhus, C. Small strain stiffness within logarithmic contractancy model for structured anisotropic clay. *IOP Conference Series: Earth and Environmental Science*, 710(1), 012042. 2021.

- [42] Sloan, S. Ballina Embankment Prediction Symposium (Editor). Computers and Geotechnics, 93, 1-280. 2018.
- [43] Tang, A. M., Hughes, P. N., Dijkstra, T. A., Askarinejad, A., Brenčič, M., Cui, Y. J., ... Van Beek, V. Atmosphere–vegetation–soil interactions in a climate change context; impact of changing conditions on engineered transport infrastructure slopes in Europe. Quarterly Journal of Engineering Geology and Hydrogeology, 51(2), 156-168. 2018.
- [44] Tidfors, M., & Sällfors, G. Temperature effect on preconsolidation pressure. Geotechnical Testing Journal, 12(1), 93-97. 1989
- [45] Tornborg, J., Karlsson, M., Karstunen, M. Permanent sheet pile wall in soft sensitive clay. Case study. Journal of Geotechnical and Geoenvironmental Engineering, 149(6), 05023003. 2023
- [46] Tornborg, J., Karlsson, M., Kullingsjö, A., Karstunen, M. Modelling the construction and long-term response of Göta Tunnel. Computers and Geotechnics, 134, 104027. 2021
- [47] Tornborg, J. , Karlsson, M. , Kullingsjö, A. , Abed, A. and Karstunen, M. Generalisation of effective heave pressure considering the effect of small strain stiffness. Proc. NGM 2024, 18-20 September, 2024
- [48] Vepsäläinen, P., Lojander, M. , Koskinen, M. Competition to calculate settlements at Haarajoki test embankment competition programme, competition materials, FinnRA, Finland. 1997
- [49] Wheeler, S. J., Näätänen, A., Karstunen, M., Lojander, M. An anisotropic elastoplastic model for soft clays. Canadian Geotechnical Journal, 40(2), 403-418. 2003
- [50] Wikby, P., Haaf, E., Abed, A., Rosén, L., Sundell, J., & Karstunen, M. A grid-based methodology for the assessment of time-dependent building damage at large scale. Tunnelling and Underground Space Technology, 149, 105788. 2024
- [51] Zuada Coelho, B., Dijkstra, J., Karstunen, M. Viscoplastic cyclic degradation model for soft natural soils. Computers and Geotechnics, 135, 104176. 202





# RECENT DEVELOPMENTS IN DEEP MIXING IN FINLAND

**L. Korkiala-Tanttu<sup>1</sup> and J. Forsman<sup>2</sup>**

## KEYWORDS

Deep mixing, deep stabilization, low-carbon binders, carbon emissions, environmental impacts, leaching, mechanical properties

## ABSTRACT

Deep mixing has established its role as one of the most commonly used ground improvement methods in Finland over the last few decades. Research on deep mixing has been active, covering topics such as execution, quality control, design, design guidelines, and binder development. Although alternative low-carbon materials have been used as binders since the 1990's, their use has been modest. However, the pressure to apply low-carbon binders is now higher than ever. All research indicates that it is possible to decrease the carbon emissions of stabilised soils by using alternative binders without compromising structural performance or environmental impacts. This is important to demonstrate to the industry and stakeholders. This presentation highlights the results of recent studies and developments of low-carbon binders in Finland, concentrating on research conducted at Aalto University with partners.

## INTRODUCTION

Deep mixing, or deep stabilisation, is one of the most widely used ground improvement methods in Finland [1]. The mean annual deep mixing volumes have stabilised at approximately 850,000 m<sup>3</sup> [2], of which about 83% involve mixing with columns and 17% involve mass stabilisation. In the Nordic stabilisation method, dry mixing is employed. Finnish design guidelines have been based for decades on the principle of equal settlement presented by Broms and Boman [3] and on the concept of elastic columns. The use of lime–cement mixtures as binders has predominated. However, the situation is changing rapidly, as it has been noted that lime–cement mixtures have significantly higher carbon emissions compared to other binder types [4,5]. According to

<sup>1</sup> Aalto University, School of Engineering, Department of Civil Engineering, Espoo Finland

<sup>2</sup> Ramboll Finland Oy, Espoo, Finland

Lehtovaara [5], on average, 2.6% of the total CO<sub>2</sub> emissions from Finnish infrastructure construction (57 kt CO<sub>2</sub>eq annually) originate from the manufacturing of binder materials for deep mixing. Therefore, the city of Helsinki is now planning to relinquish the use of lime–cement in 2024.

The next Eurocode will also include ground improvement methods. Additional drivers for developing deep mixing methods and guidelines include the need to standardise the preparation of stabilisation test samples and their testing to improve quality control methods, to prove that low-carbon binders are environmentally acceptable, and to adapt and update Finnish design guidelines [10].

Researchers at Aalto University, formerly Helsinki University of Technology, have studied the behaviour of natural Finnish clays for decades. Since the late 1990s, the deep mixing of clays has also been a focus [6]. Early studies concentrated on the development of deep mixing techniques (e.g. mixing tools) and stabilisation test methodology [6]. Recent research topics have focused on the long-term performance of stabilised soil and peat, the performance of alternative binders in laboratory and field conditions, environmental impacts, and CO<sub>2</sub> emissions. The objective of this keynote lecture is to introduce the key findings of recently published Finnish research results.

## **PERFORMANCE OF ALTERNATIVE BINDERS COMPARED TO LIME–CEMENT MIXTURES**

### **2.1 Laboratory tests**

#### **Material properties and tests**

The performance of low-carbon binders has been reported in several laboratory studies. López Ramirez et al. collected and analysed the results of several researchers [7,8]. The stabilised soil presented is mainly soft, sensitive, non-organic Malmi clay from the northern part of Helsinki. The studied clays had a water content between 80% and 120% and undrained shear strength varying between 8 kPa and 20 kPa. The binder materials included lime–cement (LC or KC) as a reference and several commercial binders produced by Nordkalk, Finnsementti, and Ecolan. A binder mixture tailored by Oulu University was also tested (CSAB calcium sulfoaluminate belite). The binders consist of blast furnace slag, quick lime, Portland cement and cement mixtures, lime kiln dust, slaked lime, gypsum, fly ash, slags from the steel industry, and phosphogypsum [7]. The fly ashes are biobased from paper industry UPM and energy production (PVO). Table 1 includes the typical index properties of Malmi clay, and Table 2 lists the binder materials<sup>3</sup> and the associated raw ma-

<sup>3</sup> Due to the existence of several sources, the naming of binders was not always possible to harmonise.

terials. The extensive laboratory studies comprised index tests, uniaxial compression, fall cone, oedometer, and triaxial tests, and even autoradiography. The curing times varied from 7 to 91 days.

Table 1. Malmi clay index properties according to [8].

Property	Value	Standard
Depth (m)	3–4.5	-
Density (g/cm <sup>3</sup> )	1.50	ISO 17892-2:2014
Specific gravity	2.70	ISO 17892-3:2015
Water content (%)	95	ISO 17892-1:2014
Clay content (%)	73	ISO 17892-4:2016
Plastic limit (%)	32.1	ISO 17892-12:2018
Liquid limit (%)	82	ISO 17892-12:2018
Undrained shear strength (kPa)	17.8	ISO 17892-6:2017
Sensitivity	35.4	ISO 17892-6:2017
Organic content	1.3	SFS-EN 15935:2021
pH	7.5	ISO 10390:2021

### Failure modes

One study concentrated on radial deformations and failure modes using a photogrammetric method. Failure modes were divided into three categories: axial splitting, inclined shearing, and hybrid splitting–shearing. The results implied that most of the stabilised specimens remained ductile. Another conclusion was that the unconfined shear strength was predominantly determined by the composition and dosage of the binder rather than by the failure mode [9].

### Porosity studies

The porosity of stabilised samples was compared at the age of 28 days for four binders provided by Nordkalk. The porosity stabilized clay samples mixed with LC50, Terra Green, and Terra Poz varied between 74% and 78%. However, Terra GTC had less porosity (around 64%). This difference might be explained by the presence of gypsum, a component that has been shown to have a significant closing effect on the porosity of stabilised clay samples with high water content [8].

Table 2. Raw materials and pH values of the tested binder materials [7].

Binder Name	Raw Components	Reference	Percentage	pH Value
CEMIII/A	Portland cement clinker	Finnsementti (2022a)	35–64 %	12.6
	Blast furnace slag		36–65 %	
OIVA lime-cement	Portland cement clinker	Finnsementti (2022b)	65–79 %	13.0
	Limestone and blast furnace slag		21–35 %	
Nordkalk Terra KC50	CEM II	Nordkalk (2021)	50 %	13.0
	Quicklime		50 %	
Nordkalk Terra KC30	CEM II	Nordkalk (2021)	70 %	13.1
	Quicklime		30 %	
Nordkalk Terra Green	Lime kiln dust	Nordkalk (2021)	50 %	13.0
	CEM II		50 %	
Nordkalk Terra Poz	Lime kiln dust	Nordkalk (2021)	33 %	13.0
	CEM II		33 %	
	Quicklime		33 %	
Nordkalk Terra GTC	Slaked lime	Nordkalk (2021)	33 %	12.9
	Gypsum (calcium sulphate $\text{CaSO}_4$ )		33 %	
	CEM III		33 %	
	Fly ash		80 %	
Ecolan InfraStabi80	Rapid cement CEM I 52.5 N	Ramboll (2021)	20 %	12.9
CSAB cement	Ladle slag	Isteri et al. (2022)	68.1 %	11.5
	Fe-slag		3.8 %	
	Phosphogypsum		11.5 %	
	Limestone		8.6 %	
	Clay		3.8 %	

### Preparation of samples and round-robin tests

The Finnish guidelines for preparing and storing laboratory samples were harmonised in 2018 [10]. Koivulahti et al. [11] presented these guidelines in English. To test the usability of these guidelines, three round-robin (interlaboratory) test series were conducted in Tankovainio (2018) and Topinpuisto (2020 and 2021). Eight anonymous (L1–L8) laboratories took part in this effort. The uniaxial compression test results were examined to determine the internal (within one laboratory) coefficient of variation (COV) of individual test series and the external variation between test series performed in parallel in different laboratories [12]. The internal variation ranged from 1% to 34%, depending on the laboratory. After the preliminary results from 2018, the laboratories with the highest variation re-evaluated their sample preparation techniques. In the next rounds (2020 and 2021), the internal variation percentages decreased to between 1% and 24%. Despite the new guidelines, a large external variation was found between laboratories, ranging from 13% to 36% [12]. Figure 1 shows the variations for the two binders and two dosages. The binder type did not have a clear effect on the variations, nor did the binder dosage [13]. Forsman et al. [12] stated that it is possible to achieve COVs of less than 10%. This can be accomplished if ‘(i) the instructions [are] followed, (ii) laboratory personnel [are] qualified to conduct stabilization, and iii) laboratory [are] equipped with proper test apparatus (mixing, compaction, curing, testing, etc.)’. In the concrete industry, the quality of accredited laboratories

is monitored using annual round-robin tests. For comparison, the internal COVs in 2024 varied between 0.5% and 4.2%, with an average of 2.6% [14].

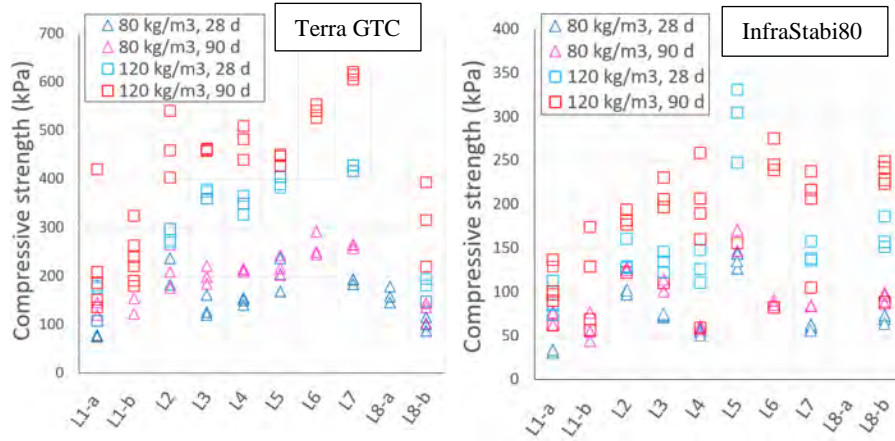


Figure 1. Topinpuisto (2021): the results of the unconfined compression tests of eight laboratories with Terra GTC and InfraStabi80 binders and two curing times and dosages [12].

#### Performance of low-carbon binders in triaxial tests

Different binder materials were tested in isotropically consolidated drained triaxial tests (CID) for Malmi clay with a binder content of 120 kg/m<sup>3</sup> [8]. The effective strength parameters were calculated for the maximum and residual strength values (see Figure 2). For the 28-day tests, the maximum effective friction angle ( $\phi'$ ) varied between 35° and 37.2° and the residual effective friction angle ( $\phi'_{\text{res}}$ ) varied between 35.3° and 38°. The maximum effective cohesion ( $c'$ ) was estimated to be lowest for InfraStabi80 at 18.7 kPa and highest for Terra Green at 75.2 kPa. The residual effective cohesion ( $c'_{\text{res}}$ ) varied from 6.5 kPa to 30.2 kPa. For a curing time of 60 days,  $\phi'$  and  $\phi'_{\text{res}}$  varied about 35–38.5°, but the maximum cohesion values  $c'$  clearly increased to 66.6–127.9 kPa, and  $\phi'_{\text{res}}$  ranged from 8.3 kPa to 35.9 kPa. The Terra Green, Terra GTC, and Terra LC30 binders exhibited the best performance in the 28-day tests compared to the reference LC50 binder. In particular, the  $c'$  values were higher than for the reference. The Terra Green and Terra GTC binders were also tested for 60-day triaxial strength, showing further strength development that surpassed that of the reference binder. The LC50, Terra Green, and Terra Poz binders exhibited about 40% higher effective cohesion values than after 28 days, while the hardening of Terra GTC was much more significant, with 90% of the cohesion values being higher than after 28 days. The breakage of cementation bonds at maximum deviatoric stress and the consequent strength reduction were reflected in significantly smaller cohesion values for the fully softened state, especially for the GTC binder. It seems that the relationship between  $c'$  and  $c'_{\text{res}}$  depends entirely on the type of binder [8].

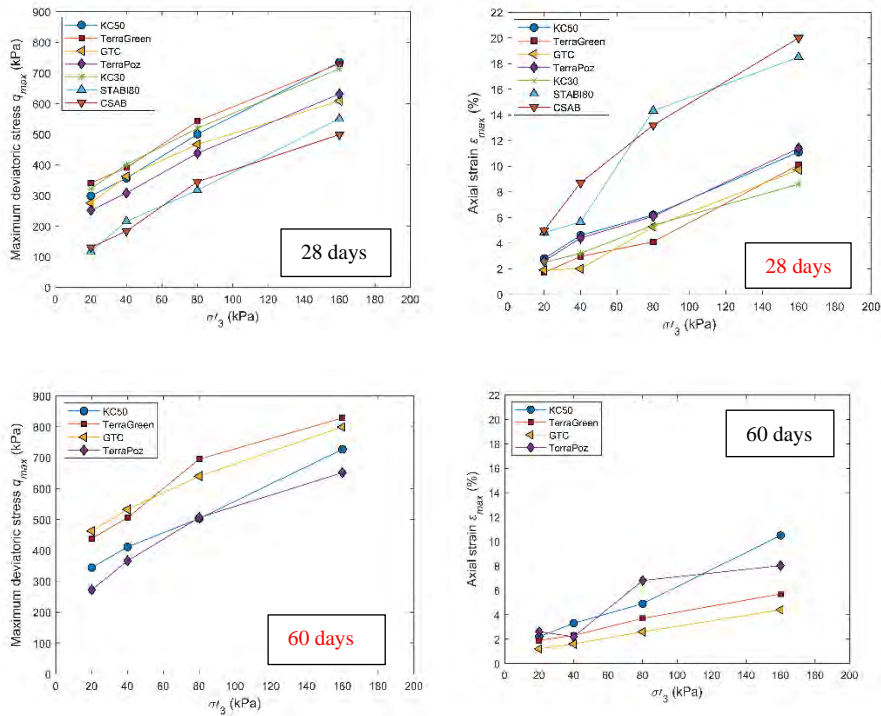


Figure 2. Malmi clay: triaxial test results for seven binders with a dosage of  $120 \text{ kg/m}^3$  and curing times of 28 and 60 days [8].

Although the cohesion and strength of the GTC binder surpassed those of the reference binder LC50, this formula can result in a highly brittle admixture compared to the rest of the binders. The binder reactions used the water inside the samples, rendering them partially saturated. Therefore, it was decided to conduct drained triaxial tests with a back pressure of 20 kPa. Åhnberg [15] stated that the difference between drained and undrained test results with high water content can be small. Nonetheless, the samples in the study were assumed to be sufficiently saturated. The base soil had a high initial water content, and upon stabilisation, the samples had saturation degrees within the 94–96% range [8].

#### Fall cone tests compared to uniaxial compression test results

In the laboratory, the fall cone test can be used to evaluate, for example, the curing process. Lopez Ramirez et al. [7] studied the correlation between fall cone measurements and the undrained shear strength obtained from uniaxial compression tests. The results showed a relatively good correlation between these test types up to the shear strength level of 650 kPa in the fall cone test (Figure 3). Above 650 kPa, the fall cone is no longer sensitive enough. The fall cone overestimates the shear strength, giving values about three times

larger than UCS. Therefore, there is a clear need to redefine the empirical fall cone correlations for stabilised in future. In this study, binder type and curing time did not affect the results.

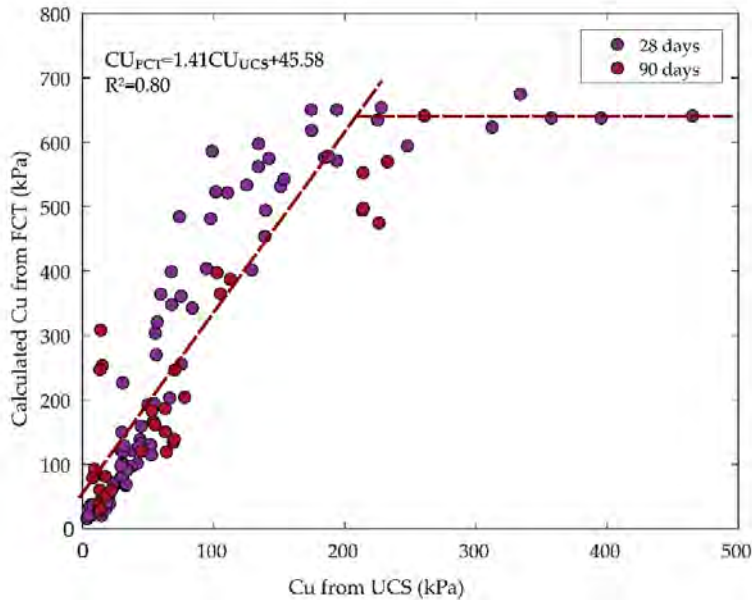


Figure 3. Correlation between the undrained shear strength  $C_u$  obtained from the fall cone test and that obtained from the uniaxial compression test [7].

#### Water content and binder dosage

Low-carbon binders are mixtures of several constituents that cause both pozzolanic and hydration reactions. Sometimes, binder mixtures are less active, or the development of strength might be slower. Typically, this is connected to the underlying chemical reactions: hydration reactions occur quicker than pozzolanic reactions [10]. In some cases, a slightly higher binder dosage for low-carbon binders is needed compared to traditional lime–cement mixtures. This trend appears to become more pronounced as the water content of the soil increases. Figure 4 illustrates the test results of several low-carbon binders for a curing time of 90 days, grouped based on the water content of the Malmi clay. The target compressive strength was 150 kPa. For lower water contents, it was possible to achieve this target value with a low dosage of binder (50–70 kg/m<sup>3</sup>). When the water content exceeds 100%, it is challenging to achieve the target strength with a lower binder content. Only two InfraStabi80 samples out of three surpassed the target value with a binder dosage of 80 kg/m<sup>3</sup> and even 60 kg/m<sup>3</sup>. For the other low-carbon binders, the dosage had to be at least 100 kg/m<sup>3</sup>. In this case, even the reference binder LC50 did not reach the target strength [7].



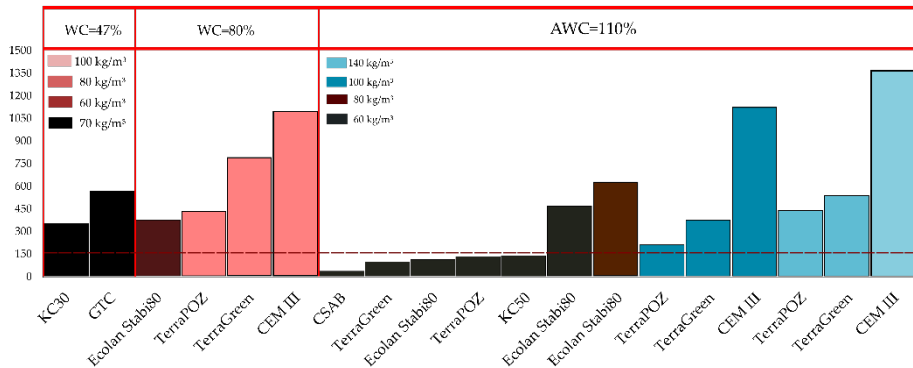


Figure 4. Uniaxial compression strength [kPa] for low-carbon binders grouped based on the water content of the Malmi clay 90 days [7].

#### Effect of curing time

All the stabilisation tests were stored according to the Finnish guidelines: the first two days at room temperature and then in a cold room at 6 to 10°C [10]. This temperature corresponds to the soil temperature, which is around 6°C in the Helsinki region. The effect of curing time has been investigated to some extent in nearly all studies. One way to estimate the time effect is by using time-strengthening coefficients normalised to the 28-day strength, as outlined in the design guidelines [10]. Nguyen [4] discovered that the time-strengthening coefficients for low-carbon binders differed from the guidelines. To better understand this behaviour, Aalto University has been collecting test results into a database, which will be analysed in future studies.

## 2.2 Field tests

### Variations in field samples

The variation in undrained shear strength (COV) for some natural Finnish clays is between 22% and 32% [16]. Deep mixing makes the soil more heterogeneous than natural clay. In Savila's master's thesis [17], the field properties of stabilised soil of varying ages were tested using field samples extracted from columns. The coefficient of variation of the uniaxial compressive strengths of stabilised clays measured from field samples was typically around 70% [17]. Figure 5 addresses these variations in the shear strength of the Malmi field samples for five low-carbon binders, two dosages, and three clay depths. The results are challenging to interpret. However, it can be observed that as the strength increases, the variance also increases.

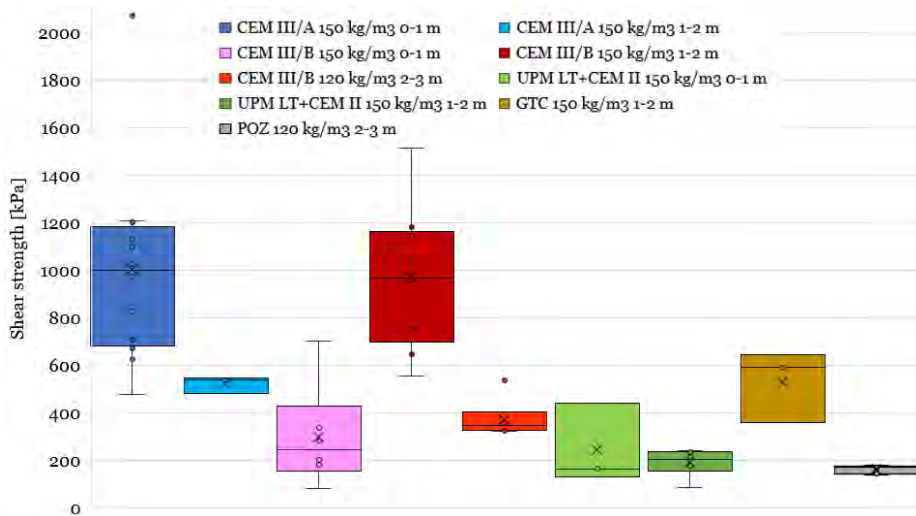


Figure 5. Malmi clay: variations in the shear strength of field samples for different binders, dosages, and depths [17].

### Long-term performance of low-carbon binders

Piispanen et al. [18, 19] collected data to analyse the long-term performance of mass-stabilised soils, including peats, clays, and dredged sediments. The analysis was mainly based on strength comparisons from quality control / quality assurance (QC/QA) soundings. QC/QA sounding methods for mass-stabilised soil were studied by Melander in 2017 [20,21]. The studied sites are presented in Table 3. The quality control methods included the column penetrometer test, static-dynamic penetration test, and cone penetrometer test with tip areas of 100 cm<sup>2</sup>, 50 cm<sup>2</sup>, and 10 cm<sup>2</sup>. Heterogeneity is common and typical for mass-stabilised soil due to variability in the mixing process and in the soil. Therefore, it is necessary to carry out sufficient QA tests. To determine shear strength, a minimum of approximately 10 representative soundings (e.g.

column penetrometer) should be performed, and at least 3 vane shear tests should be carried out in a given subarea.

Piispanen [17] concluded that the strength of mass stabilised soil increased regardless of binder or soil type. Short-term strength development was faster in hydraulic binders than in pozzolanic or gypsum binders. Over a period of 6.5–23 years, the strength increased by an average of 1.6 times for hydraulic binders and by 2.0 times for pozzolanic or gypsum binders compared to their 30-day strength. This result – although obtained for mass-stabilised peat – is in line with the long-term results of Savila in 2024 [17].

*Table 3. Sites of peat mass stabilisation. Binder type and amount, hardening time of the peat, sounding types and the number of sounding points, sample size, strength increase ratio, and COV variations [21].*

Site and number of areas	Binder type and amount [kg/m <sup>3</sup> ]	Age [year]	Sounding type and number	Sample size N *	Strength increase ratio [-] **	COV ***
Kivikonlaita 1, Finland (3)	Ce + F [70-113 + 70-113]	18.5	CPT 60 VP 9	1011 27	1.7 1.7	0.60-1.17 0.14-0.30
Kivikonlaita 2, Finland (3)	Ce + sand [100 + 150]	9.5- 16.5	CP 10 CPT 12 SDPT 20	401 729 762	1.2 3.4 1.5	0.24-0.30 0.79-1.07 0.43-0.79
Veittostensuo 1, Finland (1)	RCe + F [125 + 125]	23	CP 6 VP 6	109 24	3.8 2.6	0.17-0.23 0.44-0.84
Veittostensuo 2, Finland (1)	RCe + BFS [150 + 150]	23	CP 6 VP 6	288 24	1.9 2.3	0.39-0.62 0.40-0.62
Kose-Mäo 1, Estonia (4)	Ce + OSA [70-100 + 100-200]	6.5	CP 24	418	1.4	0.19-0.52
Kose-Mäo 2, Estonia (4)	Ce [150-250]	6.5	CP 24 VP 3	581 11	1.1 1.7	0.02-0.45 0.18-0.55

Ce = Cement (Portland)  
F = Finnstabi (lime, gypsum)  
RCe = Rapid cement (Portland)  
BFS= Blast Furnace Slag  
OSA = Oil shale ash  
sand =extra aggregate

CPT = Cone penetration test, tip 10 cm<sup>2</sup>  
PK = Column penetrometer, tip 100 cm<sup>2</sup>  
SDPT = Static-dynamic penetration test, tip 50 cm<sup>2</sup>  
\* Number of collected readings of soundings  
\*\* Strength increase compared to 30-day-strength  
\*\*\* Variation of COV values calculated to 0.5 m depth ranges of mass stabilized layer

### Correlation between laboratory and field tests

Ikävalko [13] investigated field test results from three test areas in Malmi and from five other test stabilisation sites. His objective was to define the ratio between the strengths determined in the field and in the laboratory. There are several reasons for the discrepancies between these two strengths. According to Piispanen and Åhnberg [18, 22], the following issues affect this ratio:

- the mixing is better in the laboratory;
- differences in temperatures in situ and in the laboratory;

- the temperature released during the binding reaction has a different effect in the laboratory compared to in situ;
- in dry mixing, the water content of the soil decreases after mixture and stays partly saturated in the laboratory, whereas in situ, the water content slowly increases.

Ikävalko [13] grouped the test results of low-carbon binders into three categories based on their strength properties: 1) Terra Poz, Terra Green, and LC; 2) Infrastabi80, Terra GTC, and Fly ash + CEMII; and 3) CEMIIIs. His results corresponded to 90 days of strength. As the target strengths of Finnish column stabilisation normally lie between 50 kPa and 150 kPa, the strengths gained in situ were clearly higher than in the laboratory, including for low-carbon binders, and than the guidelines [10] suggest.

## ENVIRONMENTAL IMPACTS

### 3.1 Carbon emissions

Concerning climate change, the most important environmental impact of deep mixing is the reduction in carbon emissions. The issue of rising carbon emissions has gained increased attention over the last decade. The development of low-carbon binders has concentrated on low-carbon materials, which are typically recycled materials or by-products. This means that besides low CO<sub>2</sub> emissions, the use of these materials supports the circular economy. Several calculations of the carbon emissions of deep mixing have been conducted [4,7,23].

Binder producers have recently developed low-emission products and have succeeded in significantly reducing the carbon footprint of binders. The use of primary materials, such as Portland cement and lime, has decreased. This means that older carbon footprint calculations may be outdated. Nguyen [4] stated that transportation plays only a small role in the carbon emission comparisons of binder manufacturing. She estimated that the carbon emissions of the stabilisation work in the field were the same for all binder types (about 72 kgCO<sub>2</sub>-eq/ton). Therefore, Figure 6 shows only a comparison of the carbon emissions from the production of different binders using the latest information obtained from binder producers and Nguyen [4].

### 3.2 Local impacts of deep mixing on groundwater and surface water

Deep mixing using the dry method has been used in Finland for about 50 years. No remarkable harmful local environmental effects were reported during this period. In the few studies conducted, the impact data originated mainly from leaching test results and field observations. No significant problems were observed in these studies, and the leaching tests also indicated low concentrations of harmful ingredients. Therefore, the need to monitor local

impacts has been low. As the sector now uses more low-carbon binders, this need has been re-evaluated. In general, the stabilisation or solidification of soils has been used to treat contaminated soils or waste [24]. Therefore, the risk of large local environmental impacts can be estimated to be comparatively low.

In the southern part of Finland, local impacts on groundwater have been monitored in five deep-mixing areas. Additionally, the cities of Helsinki and Vantaa are constantly monitoring the quality of water in at least six other deep-mixing areas [25]. Valjakka's thesis also presented the current understanding of the effects of stabilisation through expert interviews [25]. In his study, Valjakka used data from 20 standpipes for groundwater sampling at the inspected sites. The standpipes were installed upstream and downstream of the column stabilisation. Groundwater samples were extensively studied using field and laboratory measurements for different concentrations and basic properties of water. The results showed no statistically significant differences between the upstream and downstream samples.

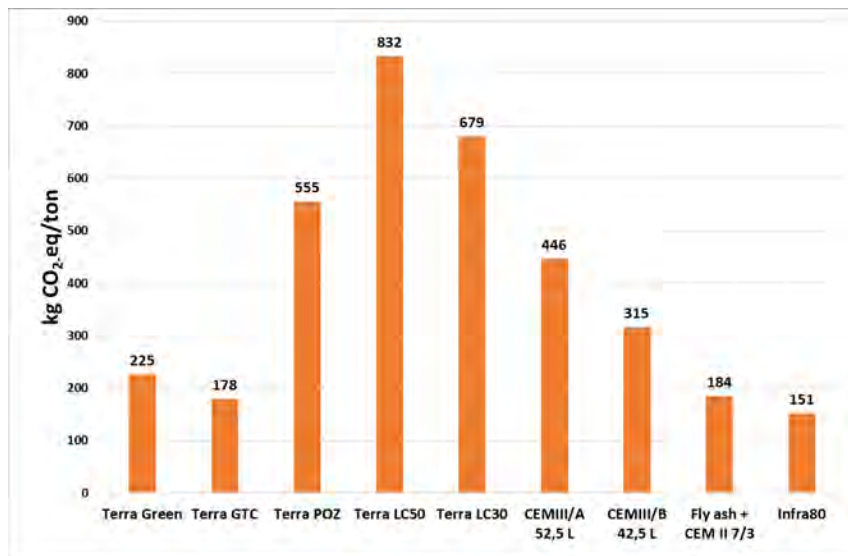


Figure 6. The unit carbon emissions associated with the manufacturing of the most used low-carbon binders and lime–cement binders (LC50 and LC30) in Finland.

Valjakka [25] found that soluble calcium dissolved from the column stabilisation in low volumes. In addition, there were indications that the concentrations of soluble cobalt, manganese, and nickel may also increase due to stabilisation. The conclusion was that the effects of column stabilisation on the groundwater were minor. The monitoring of water quality continues, and the results are reported annually. The situation has remained stable.

These conclusions are in line with earlier Finnish studies [26]. In Kuninkaan-tammi, Helsinki, several low-carbon binders were used. In addition to the water quality tests, samples of the clay surrounding the columns were also collected. The pH values of clay just around the column (<40 mm) have increased. In this case, the pH values of groundwater remained the same; calcium content increased slightly in some pipes but decreased in others.

## **MAIN CONCLUSIONS AND FUTURE RESEARCH**

The mechanical and environmental performance of low-carbon binders has proven to be the same as that of traditional binders. Ductile behaviour was the dominant failure mode for all tested binders. The effective friction angles of different binders resemble each other. However, some differences exist in the effective cohesion values. The variation in strength values increases as the strength increases. Round-robin tests revealed that the variation between different testing laboratories was significant. However, the authors believe that it is possible to reduce this variation to less than 10%. In particular, field results can exhibit significant variances in strength. Long-term studies prove that stabilised structures have mainly kept on increasing strength.

The impacts of deep mixing with low-carbon binders on the quality of groundwater have been shown to be small or even non-existent in some cases. As the emissions of low-carbon binders are manifold lower compared to lime–cement mixtures, their environmental benefits are clearly higher and support the transition towards their use.

Research on the stabilisation of soil is ongoing. For example, Bruk et al. [27] studied the carbon sequestration capacity of stabilised soft clays with low-carbon binders, with promising results. Additional efforts include, for instance, the development of databases of stabilisation outcomes and the properties of stabilised soils.

## **ACKNOWLEDGEMENTS**

The authors would like to thank Kari Kuusipuro from Nordkalk for the carbon emission data. We are also grateful to Alejandra López Ramirez and Ida-Maria Savila, who helped with the figures.

## REFERENCES

- [1] E. Kivi: Pohjanvahvistusmenetelmät Suomessa – käyttömäärät ja hiilijalanjälki. In Finnish, Master's thesis, Aalto University. 2022. <https://aaltodoc.aalto.fi/items/0a309556-72a4-468b-b089-cd6da2ec962a>
- [2] K. Kuusipuro: Syvästabilointikatsaus. Presentation in Pohjanvahvistuspäivä 24.8.2023. In Finnish. 2023. <https://sgy.fi/content/uploads/2023/05/syvastabilointikatsaus-kari-kuusipuro.pdf>
- [3] B. Broms, and P. Boman: Stabilization of soil with lime columns. Design Handbook, 2<sup>nd</sup> edition, Jord- och bergmekanik, KTH. 1977.
- [4] T. Nguyen: Uusiosideaineet pilaristabiloinnissa: kuninkaantammen koestabilointi. In Finnish, Master's thesis, Aalto University. 2021. <https://aaltodoc.aalto.fi/items/89c084b5-69bf-4974-aecb-e44c4b77b5c5>
- [5] T. Lehtovirta: Infrarakentamisen hiilidioksidiekvivalenttipäästöt Suomessa. In Finnish, Master's thesis, Aalto University. 2023. <https://aaltodoc.aalto.fi/server/api/core/bitstreams/3cb869c5-ceb3-4973-bd3d-bdd6339ed222/content>
- [6] A. Aalto: Syvästabilointitutkimus – yhteenveto projektin III vaiheesta. TKK. In Finnish. 2002.
- [7] A. López Ramírez, Y. Zhang, J. Forsman, and L. Korkiala-Tanttu: Stabilization of soft clay with sustainable binders for dry deep mixing design. Geotechnical Testing Journal. 2023. <https://doi.org/10.1520/GTJ20220255>
- [8] A. López Ramírez, and L. Korkiala-Tanttu: Stabilisation of Malmi soft clay with traditional and low-CO<sub>2</sub> binders. Transportation Geotechnics, 38. 2023. <https://doi.org/10.1016/j.trgeo.2022.100920>
- [9] Z. Li, Y. Zhang, M. Janiszewski, and L. Korkiala-Tanttu: Radial deformation and failure of stabilized clay under uniaxial compression. Soils and Foundations, 62. 2022. <https://www.sciencedirect.com/science/article/pii/S0038080622001214?via%3Dihub>
- [10] Liikennevirasto 2018: Syvästabiloinnin suunnittelu, Liikenneviraston ohjeita 17/2018. 2018. [https://ava.vaylapilvi.fi/ava/Julkaisut/Liikennevirasto/lo\\_2018-17\\_syvastabiloinnin\\_suunnittelu\\_web.pdfhttps://ava.vaylapilvi.fi/ava/Julkaisut/Liikennevirasto/lo\\_2018-17\\_syvastabiloinnin\\_suunnittelu\\_web.pdf](https://ava.vaylapilvi.fi/ava/Julkaisut/Liikennevirasto/lo_2018-17_syvastabiloinnin_suunnittelu_web.pdfhttps://ava.vaylapilvi.fi/ava/Julkaisut/Liikennevirasto/lo_2018-17_syvastabiloinnin_suunnittelu_web.pdf)
- [11] M. Koivulahti, H. Jyrävä, T. Niemelin, J. Forsman, V.-M. Uotinen, and L. Korkiala-Tanttu: Deep soil mixing – Finnish guideline for stabilisation tests. Proceedings of the 17th ECSMGE, Reykjavik. 2019. [https://www.ecsmge-2019.com/uploads/2/1/7/9/21790806/0738-ecsmge-2019\\_koivulahti.pdf](https://www.ecsmge-2019.com/uploads/2/1/7/9/21790806/0738-ecsmge-2019_koivulahti.pdf)

- [12] J. Forsman, J. Ikävalko, M. Löfman, L. Korkiala-Tanttu, and T. Teittinen: Stabilization tests for deep mixing – Round-robin tests in eight Finnish laboratories. *Geotechnical Testing Journal*. 2024.  
<http://doi.org/10.1520/GTJ20230377>
- [13] J. Ikävalko: Pilaristabiloinnin kenttä- ja laboratoriolujuuksien suhde koestabilointikohteissa. In Finnish, Master's thesis, Aalto University. 2023.  
<https://aaltodoc.aalto.fi/items/3f6f0026-a308-4a87-ad39-7d0184db5bbd>
- [14] J. Punkki: Testauslaboratorioiden tasokokeet 2023. *Betoni* 2/2024. 2024. [https://betoni.com/lehti/wp-content/uploads/sites/4/2024/06/BET\\_2402\\_62-71.pdf](https://betoni.com/lehti/wp-content/uploads/sites/4/2024/06/BET_2402_62-71.pdf)
- [15] H. Åhnberg: Effects of back pressure and strain rate used in triaxial testing of stabilized organic soils and clays. *Geotechnical Testing Journal*, 2004;27, 250–259. 2004. <https://asmedigitalcollection.asme.org/geotechnical-testing/article-abstract/27/3/250/1176106/Effects-of-Back-Pressure-and-Strain-Rate-Used-in?redirectedFrom=fulltext>
- [16] M. Löfman: Perniön saven luotettavuuden ja saven eri ominaisuuksien välisten korrelaatioiden arviointi. In Finnish, Master's thesis, Aalto University. 2016. <https://aaltodoc.aalto.fi/items/a09c7be3-e2fb-48af-bc34-12d6b981b3d5>
- [17] I.-M., Savila: Syvästabiloinnin maastonäytteiden lujuusvertailu ja laadunvalvonnan kokemukset. In Finnish, Master's thesis, Aalto University. 2024. <https://aaltodoc.aalto.fi/handle/123456789/128093>
- [18] P. Piispanen: Massastabiloinnin pitkäaikaistoimivuus. In Finnish, Master's thesis, Aalto University. 2017. <https://aaltodoc.aalto.fi/items/330d2bb6-3cb0-4734-926b-a7739ce616a2>
- [19] J. Forsman, L. Korkiala-Tanttu, and P. Piispanen: Mass stabilization as a ground improvement method for soft peaty soil. Chapter 7 in the open access book “Peat,” Intech, pp. 107–139. 2018.  
<https://www.intechopen.com/chapters/59545>
- [20] M. Melander: Massastabiloinnin laadunvalvontakairaukset (Mass stabilization quality assurance soundings, abstract in English). In Finnish, Master's thesis, Aalto University. 2017.
- [21] J. Forsman, M. Melander, F. Winqvist, H. Halkola, and L. Korkiala-Tanttu: Mass stabilization quality control methods. *Proceedings of the 19th International Conference on Soil Mechanics and Geotechnical Engineering*, Seoul, pp. 2511–2514. 2017.
- [22] H. Åhnberg: Strength of stabilized soils – A laboratory study on clays and organic soils stabilized with different types of binder. Doctoral thesis.



Svensk Djupstabilisering Report, 16. 2006 <https://www.sgi.se/globalassets/publikationer/svensk-djupstabilisering/sd-r16.pdf>

[23] O. Kaukoranta: Vähähiilinen pilaristabilointi ja hankintamenettelyt. In Finnish, Master's thesis, Aalto University. 2024. Not published.

[24] A. Al-Tabbaa: State of practice report – Stabilisation/solidification of contaminated materials with wet deep soil mixing. Proceedings of the International Conference on Deep Mixing, Stockholm. 2005.

[25] T. Valjakka: Pilaristabiloinnin ympäristövaikutukset pinta- ja pohjavesissä. In Finnish, Master's thesis, Aalto University. 2022.  
<https://aaltodoc.aalto.fi/items/39c7f92b-373a-49f5-a3e4-a32c6c26196b>

[26] I. Reijonen: Kuninkaantammi, Yhteenveto koestabiloinnin ympäristötutkimuksista. In Finnish, Ramboll Finland Oy. 2021.

[27] D. Bruk, A.S.S. Raghuram, L. Korkiala-Tantt, J. Forsman, and H. Gustavsson: Carbon sequestration capacity of stabilized soft clays with recycled binders. Geotechnical Testing Journal. Open Access. January 2024.

# **ENERGY GEOSTRUCTURES: A REVIEW ON THEIR ENERGY AND GEOTECHNICAL PERFORMANCE**

**Lyesse Laloui<sup>1</sup> and Melis Sutman<sup>2</sup>**

## **KEYWORDS**

Energy geostructures, Renewable energy, Thermo-mechanical, Design, Application.

## **ABSTRACT**

Energy geotechnology provides low carbon, cost-effective and local energy solutions to structures and infrastructures, which opens a new era for the geotechnical engineering practice, by extending the conventional role of structural design to the one of addressing acute energy challenges of our century. The paper initially goes over the idea behind energy geotechnology by highlighting its scope and applications to various geostructures for structural support and energy supply of built environments. Aspects of primary importance for maximizing the energy, geotechnical and structural performance of energy geostructures and solutions to address this challenge are presented. Moreover, analytical solutions and design tools, as well as performance-based design of energy geostructures are introduced. The goal of this paper is to uncover the great potential of energy geotechnology on the path of less dependency on fossil fuels and to emphasize the new critical role of geotechnical engineers to take full advantage of this technology.

## **INTRODUCTION**

The residential sector was responsible for 25.8% of final energy consumption in Europe in 2022, of which space heating and hot water production represented 78.4% in total (Eurostat, 2022), leading to around 2 400 Mt of direct CO<sub>2</sub> emissions and 1 700 Mt of indirect CO<sub>2</sub> emissions (IEA, 2022). Fossil fuel based and conventional electric equipment still dominates the global building market, accounting for more than 60% of space heating (IEA, 2022).

<sup>1</sup> Laboratory of Soil Mechanics, Swiss Federal Institute of Technology Lausanne (EPFL), Lausanne, Switzerland

<sup>2</sup> Institute for Infrastructure & Environment, University of Edinburgh, Edinburgh, UK

Moreover, due to global warming, economic growth and urbanization, cooling is the fastest growing use of energy in buildings (IEA, 2018), which is mainly covered by electricity. Without action to address energy efficiency, energy demand for space cooling will more than triple by 2050 (IEA, 2018).

Several initiatives and policies at national and international levels are being established in the construction sector (ASHRAE, 2008 and European Directive 2010/31/EU, 2010) for the implementation of zero- or nearly zero-energy buildings. For instance, ASHRAE Vision (2008) presents requirements to enable buildings to produce as much energy as they use by 2030. On the other hand, European Directive 2010/31/EU (2010) requires all new public buildings to be nearly zero-energy by 2018 and all new buildings by the end of 2020. Therefore, the development and the diffusion of reliable, economically viable and environmental-friendly technologies to satisfy a noteworthy part of the energy needs of the building sector is an important challenge.

Conceptually, energy geostructures is a technology enabling the use of renewable energy sources for efficient space heating and cooling. In this technology, any geo-structure in contact with the soil and already required for structural support are equipped with geothermal loops, for heat exchange operations to exploit the near surface geothermal energy. The idea behind energy geostructures comes from the fact that the temperature of the ground remains the same throughout the year below a depth of 6-8 meters. Therefore, with the integration of the geothermal loops and the water-antifreeze mixture circulating within them, the heat is extracted from the ground to heat the buildings during winter. Similarly, during summer, the extra heat coming from the building side is injected into the ground to cool them. In this system, ground source heat pumps (GSHP) are often required which works intermittently in order to adapt the temperature of the circulating fluid to meet the energy demands from the building side.

The heat energy that can be provided by the energy geostructures depends on various factors, including, but not limited to, the thermal and hydraulic properties, and mean temperature of the ground, geothermal and geotechnical design of the geo-structures, and the energy demand from the building side. However, 40-150 W/m, 20-40 W/m<sup>2</sup> and 20-60 W/m<sup>2</sup> are achievable energy extraction or withdrawal amounts from energy piles, energy walls and energy tunnels, respectively. As a practical example, a recent numerical investigation was performed at the Laboratory of Soil Mechanics (LMS), considering a five-storey office building, with net heated/cooled area of 2400 m<sup>2</sup>, bearing on 32 piles with 0.5 m diameter and 20 m length which were used as energy piles. The results of the analysis show that the energy piles can supply 100% of the heating demands and most of the cooling demands of the office building in Sevilla, Spain. An auxiliary air conditioning system was required only during July and August, to provide the remaining 11% and 6% of the cooling demand (Sutman et al., 2019).

## ENERGY ASPECT

### Typical energy problem

Operation of energy geostructures to meet the heating and cooling demands from the building side involves heat exchange within the three components of the ground source heat pump system, being the primary circuit, the GSHP and the secondary circuit (Figure 1).

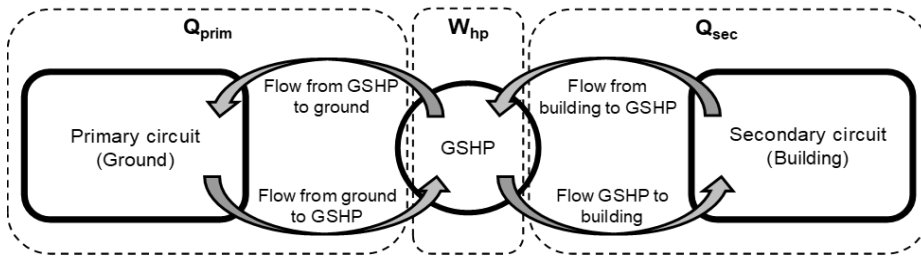


Figure 1 Heat exchange within three components of ground source heat pump system.

In the primary circuit, the heat exchange occurs between the ground and the GSHP, where the heat is extracted from or withdrawn into the ground for heating or cooling the building side, respectively. The heat exchange mechanism that occurs between the ground and the energy geostructure is shown in Figure 2, through the example of an energy pile, for both building heating and cooling purposes.

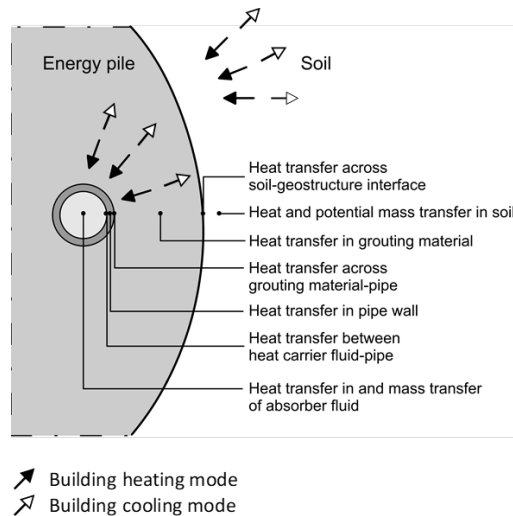


Figure 2 Heat exchange between the energy pile and the ground.

Regarding the building cooling mode, shown by the white arrows, the temperature of the circulating fluid returning from the building side is warmer than the ground temperature, which results in a thermal gradient. The circulating fluid exchanges heat with the ground loop wall through convection, which is

followed by a heat conduction through the wall of the ground loop and the pile until reaching the pile-soil interface. Finally, the heat is transferred within the ground mainly by conduction and partially with convection if a moisture migration takes place. Similarly, during the building heating mode, the returning fluid temperature is colder than the ground temperature and the heat exchange occurs in the reverse direction, as shown by the black arrows.

Assuming pure thermal conductivity within the energy pile and the ground, the energy conservation equation reads:

$$\rho c \frac{\partial T}{\partial t} - \text{div}(\lambda \mathbf{grad} T) = 0 \quad (1)$$

where  $\rho$  is the density,  $c$  and  $\lambda$  are the specific heat capacity and thermal conductivity, respectively, including both fluid and solid components,  $T$  is the temperature,  $t$  is the time and  $\text{div}$  and  $\mathbf{grad}$  are the divergence and gradient operators, respectively. The energy conservation equation for the incompressible circulating fluid within the loops can be written as:

$$\rho_f A_p c_f \frac{\partial T_f}{\partial t} + \rho_f A_p c_f \mathbf{u}_{f,i} \cdot \mathbf{grad} T_f = \text{div}(A_p \lambda_f \mathbf{grad} T_f) + \frac{1}{2} f_D \frac{\rho_f A_p}{d_h} |\mathbf{u}|^3 + q'_w \quad (2)$$

where  $\rho_f$ ,  $c_f$ , and  $\lambda_f$  are the density, specific heat capacity, and thermal conductivity of the fluid, respectively;  $A_p$  and  $d_h$  are the cross-sectional area and hydraulic diameter of the pipe, respectively;  $T_f$  is the temperature of the fluid;  $\mathbf{u}_{f,i}$  is the velocity vector;  $f_D$  is the Darcy friction factor; and  $q'_w$  represents the heat flux per unit length that is exchanged through the pipe wall.

In the secondary circuit, the heat is transferred to or from the building side for heating or cooling purposes, respectively. In between the two circuits, there exists the GSHP to transfer the heat between the two circuits. The efficiency of the GSHP is quantified by the coefficient of performance ( $COP$ ) through examining the amount of energy input to operate the GSHP ( $W_{hp}$ ) and the energy that can be supplied to the building side ( $Q_{sec}$ ), as shown below:

$$COP = \frac{Q_{sec}}{W_{hp}} \quad (3)$$

### State of the Art on the Application of Energy Geostructures

To reveal the actual energy performance of energy geostructures, a comprehensive investigation was performed by incorporating information from (i) a survey targeting international construction companies involved in energy geostructures, (ii) available literature on operational energy geostructures and (iii)

complementary results by Di Donna et al. (2017). Figure 3 presents the state of the art on energy piles, based on the integration of the information from 157 energy pile projects, in terms of extracted thermal power with respect to the diameter and length of the piles. On the other hand, Figure 4.a and Figure 4.b represent extracted and injected heat for heating and cooling purposes for energy walls (17 projects) and energy tunnels (11 projects), respectively.

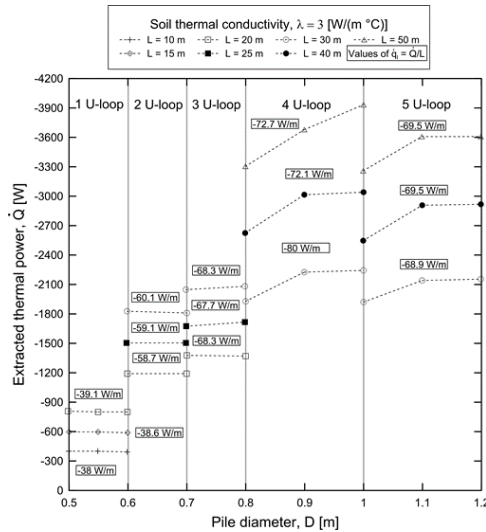


Figure 3 State of the art on application of operational energy piles (Laloui and Rotta Loria, 2019).

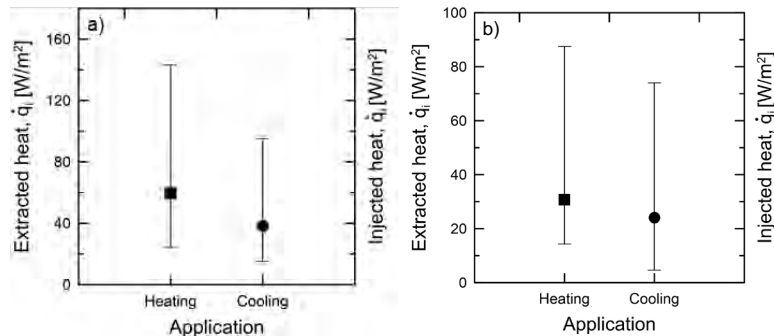


Figure 4 State of the art on application of energy walls and tunnels (Laloui and Rotta Loria, 2019).

## GEOTECHNICAL ASPECT

As shown in the previous section, energy geostructures concept, a technology capable of exploiting geothermal sources for both space heating and cooling, is undoubtedly an outstanding candidate to cut down the governance of unus-

tainable resources. Yet, the use of conventional geostructures for heat exchange purposes is associated with temperature changes, hence thermal loads and displacements, along the geo-structures and within the surrounding soil, which needs to be taken into consideration in addition to the typical geotechnical design (Laloui and Sutman, 2021, Laloui et al., 2014).

In order to understand the extent of temperature change effects on energy geo-structures, several in-situ tests were performed on single (Laloui et al., 2006; Bourne-Webb et al., 2009; You et al., 2016; Loveridge et al., 2016; McCartney and Murphy, 2017; Sutman, 2016; Sutman et al., 2017; Sutman et al., 2019) and a group of energy piles (Mimouni et al., 2015; Rotta Loria et al., 2016), energy walls (Xia et al., 2012) and energy tunnels (Adam and Markiewicz, 2009; Frodl et al., 2010; Nicholson et al., 2014; Barla et al., 2019). Moreover, several models or tools with varying complexity were developed for the analysis and design of energy piles (Knellwolf et al., 2011; Bourne-Webb et al., 2014; Salciarini et al., 2013; Rotta Loria and Laloui, 2016; Makasis et al., 2018, Sutman et al., 2018), energy walls (Kürten et al., 2015; Sterpi et al., 2017; Sailer et al., 2019) and energy tunnels (Barla and Di Donna, 2018; Bidarmaghz and Narsilio, 2018). The previous research answered the most fundamental questions on the mechanisms governing the thermal and structural behavior of energy geostructures. These efforts opened a new era for the geotechnical engineering practice, by extending the conventional role of geotechnical design to the one of addressing acute energy challenges of our century.

### **Full-Scale Experimental Analysis on Energy Piles**

The two pioneering full-scale in-situ tests on energy piles performed at Swiss Federal Institute of Technology in Lausanne (EPFL), investigating (i) the response of a single energy pile to combinations of thermal and mechanical loads and (ii) the response of a group of closely spaced energy piles to thermo-mechanical loads are presented in this section. Compressive stresses and upward shaft resistance mobilization are considered positive, according to the adopted sign convention.

- (i) Response of a Single Energy Pile to Combinations of Thermal and Mechanical Loads (Laloui et al., 2003):

A pioneering field test was performed at EPFL campus, on a single energy pile, with a diameter of 0.88 m and length of 25.8 m, under a newly constructed 5-storey building (Bâtiment Polyvalent). The single energy pile was one of the 97 bored piles constructed under the building. Along the test pile, polyethylene (PE) tubes were installed vertically on the reinforcing structure with a U-shaped configuration to permit the passage of the heat-carrying fluid. The test pile was instrumented by a considerable number of sensors to

enable the measurement of temperature, strain and toe load variations during the thermal load applications.

The soil profile at the field test site consists of alluvial soil at the first 12 m (Layers A1 and A2) which is followed by a sandy gravelly moraine (Layer B) and bottom moraine (Layer C) until around 25 m. Finally, a molasse layer (Layer D) is found under the moraine. The ground water table at the test site is located at ground surface. Further information on soil and soil-pile interaction, as well as the test pile and instrumentation can be found in Laloui et al. (2003).

A heating and passive cooling cycle was applied to the test pile following the completion of each storey of the building with the purpose of evaluating the influence of structural load on the development of thermally induced axial stresses and displacements. Figure 5.a shows the results of the last test which was performed after the construction had been finalized. The distribution of the mechanical load profile shows the absence of toe resistance which implies that the structural load was entirely carried by the mobilized resistance along the shaft of the test pile. The following temperature increase, with a magnitude of 13.4°C, resulted in generation of thermally induced compressive axial loads with a significant mobilization of the toe (2000 kN) and thermally induced axial loads at the pile head (1000 kN).

Shaft resistance mobilization due to mechanical and thermal loads along the same test pile is shown in Figure 5.b and Figure 5.c. The mechanical load application resulted in downward displacement of the pile which is associated with positive shaft resistance mobilization. The subsequent temperature increase caused the portion of the pile, above the null point, the depth at which no thermally induced displacement is observed, to possess an upward displacement, resulting in a decrease in corresponding shaft resistance mobilization due to mechanical and thermal loads along the same test pile is shown in Figure 5.b and Figure 5.c. The mechanical load application resulted in downward displacement of the pile which is associated with positive shaft resistance mobilization. The subsequent temperature increase caused the portion of the pile, above the null point, the depth at which no thermally induced displacement is observed, to possess an upward displacement, resulting in a decrease in corresponding shaft resistance (Figure 5.b). On the other hand, the portion below the null point displaced downward, further mobilizing the positive shaft resistance (Figure 5.c).



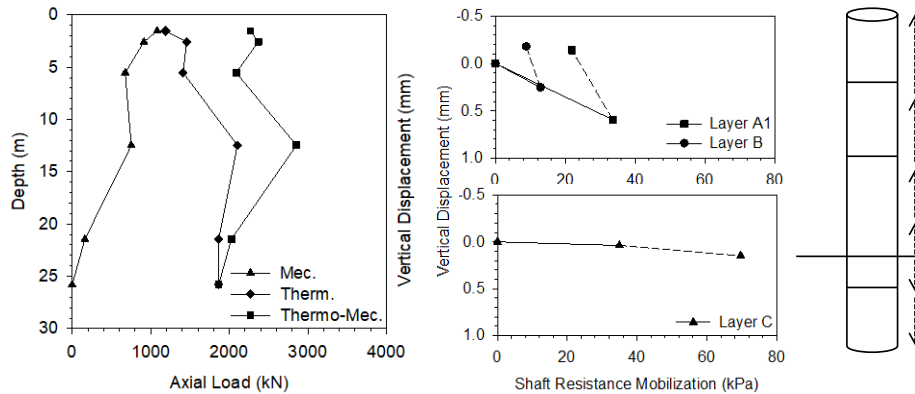


Figure 5 a) Mechanical, thermal and combined thermo-mechanical loads. b, c) Shaft resistance mobilization along the test pile.

(ii) Response of a Group of Closely-Spaced En-Ergy Piles to Thermo-Mechanical Loads (Mimouni and Laloui, 2015; Rotta Loria and Laloui, 2017)

A second field test was implemented at EPFL campus by equipping four out of 20 piles under a water retention tank within the Swiss Tech Convention Center to evaluate the thermally induced group effects among closely-spaced energy piles. The piles were 0.9 m in diameter and 28 meters in length. Each test pile was equipped with four 24 m long U-loops connected in series which were installed 4 m below the pile heads in order to prevent the thermal interaction with the water retention tank. The test piles were instrumented with vibrating wire strain gages at every 2 meters along the length, a pressure cell at the toe and radial optical fibers. Moreover, thermistors and piezometers were installed within boreholes at close proximity to the test piles to monitor the temperature and pore water pressure changes during the field test. The field test site is 200 m away from the single energy pile test location, resulting in similar stratigraphic characteristics (Mimouni and Laloui, 2015).

Heating with maximum temperature increase of 20°C and passive cooling cycles were applied to single (EP1) and the group of four energy piles (EPall) (Rotta Loria and Laloui, 2017). Figure 6 shows (i) thermally induced axial strains and stresses along EP1 when serving as the only operating pile among the group of four piles (20EP1) and (ii) average thermally induced axial strains and stresses along the length of all four piles during full geothermal activation of the group (EPall). The comparison of tests 20EP1 and 20EPall shows that the presence of thermally induced group effects govern the higher development of axial strain when more energy piles operate as geothermal heat exchangers in a closely spaced pile group than when only one energy pile serves this purpose (Figure 6.a).

Figure 6.b shows the comparison in terms of thermally induced axial stresses where an opposite behavior was attained corresponding to a decrease in thermally induced axial stresses as the number of thermally active energy piles increases. This phenomenon is associated with the increased deformation of energy piles operating in a group (Figure 6.a) which results in lower thermally induced blocked strains, since the temperature change and hence the free thermal strains are the same for Test 20EP1 and 20EPall, and therefore lower observed axial stresses. Moreover, tensile stresses were observed at the bottom portion of the energy piles during test 20EPall, which is associated with the thermally induced deformation of the molasse layer resulting in a pull-down effect. This effect was less pronounced during the test 20EP1 since the compressive stresses induced by the restrained expansion of EP1 overcame the tensile stresses exerted by the surrounding molasse layer.

Comparison of thermally induced strains and axial stresses per unit temperature change corresponding to geothermal operation of a single energy pile (Test 20EP1) and a group of energy piles (Test 20EPall) is presented in Figure 7.a and Figure 7.b, respectively, which are average values along the active length of the piles. The figures clearly show greater average vertical strains and lower average axial stresses with increasing number of active energy piles. In terms of design aspects, analysis of a single pile in a closely-spaced group will lead to a conservative estimate of vertical stresses that can be employed during the preliminary design stages, but is not the case for the vertical strains.

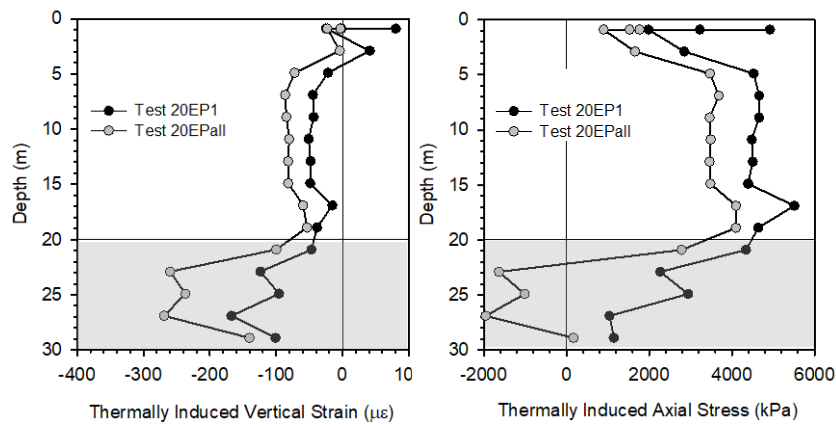


Figure 6 a) Thermally induced axial strains b) Thermally induced axial stresses during tests EP1 and EPall.

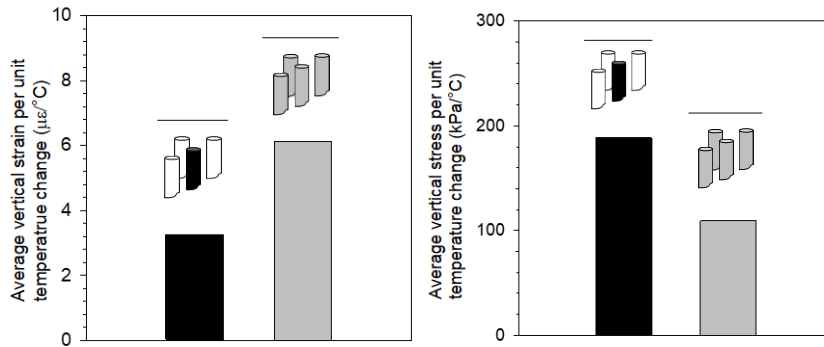


Figure 7 a) Thermally induced group effects in terms of a) Axial strains and b) Axial stresses (redrawn after Rotta Loria, 2019).

### Analytical Methods for the Analysis of Energy Piles

Full-scale in-situ tests provided the most fundamental information regarding the response of a single and a group of energy piles to thermo-mechanical actions. Moreover, finite-element methods, the majority of which have been validated by the results of the in-situ tests, were developed, and are considered to be the most rigorous approach for the analysis of energy piles. However, these comprehensive methods require a considerable number of geotechnical parameters, as well as high computational efforts, which renders them more suitable for research purposes rather than for practical piling problems. For the design and wider application of energy piles, a reasonable balance between excessive complexity and unsatisfactory simplicity should be established for the development of practical analytical models. Therefore, several simplified analytical methods have been developed by the Laboratory of Soil Mechanics to serve as preliminary design guidance of single and groups of energy piles.

- (i) Load-Transfer Approach for Single and Group of Energy Piles (Knellwolf et al., 2011; Ravera et al., 2020)

The load-transfer approach, where the soil-pile interaction is represented by springs distributed along the pile shaft and toe by neglecting the continuity of the soil domain, is one of the most common analytical methods employed for the analysis of conventional piles (Seed and Reese, 1957; Coyle and Reese, 1966). In this approach, numerous analytical and empirical methods have been proposed to define the load-transfer curves (Randolph and Wroth, 1978; Frank and Zhao, 1982; Kraft et al, 1981). Later on, considering that most piles are implemented in groups in practice, the load-transfer curves have been modified to consider group effects (Randolph and Clancy, 1993; Comodromos et al., 2016). Given the great potential of the load-transfer approach in providing a practical tool for the analysis of axial loaded conventional piles, the approach has been implemented for the analysis of single and groups of energy piles.

The load-transfer approach has first been modified for single energy piles by Knellwolf et al. (2011), where the pile is divided into rigid elements that are connected to each other and to the surrounding soil by the springs (Figure 8.a). In order to define the relationships between the mobilized shaft friction/toe resistance and displacement, the method from Frank and Zhao (1982) was utilized, relating the shaft and toe stiffness to Menard pressuremeter modulus and dividing the load-transfer curve into three main sections: (i) initial linear part characterizing the elastic response, (ii) second linear part associated with the elastoplastic response and (iii) final plateau referring to perfectly plastic response as represented in Figure 8.b by full lines for single isolated piles. The presence of a slab above energy piles was considered in a simplified way by introducing an additional spring linked to the pile head. The analytical model is validated by the results of both EPFL single pile in-situ test (Laloui et al., 2006) and Lambeth College in-situ test (Bourne-Webb et al., 2009) and has also been implemented in the Thermo-Pile Software developed by Laboratory of Soil Mechanics for the analysis and design of energy piles.

Following the same logical sequence as the one of conventional piles, the load-transfer approach for single energy piles has subsequently been extended to characterize the response of groups of energy piles to thermo-mechanical loads in a simplified, yet rational manner (Ravera et al., 2020). To represent the interaction between a group of energy piles, a displacement ratio ( $R_d$ ) was introduced adapting the displacement response of a single isolated energy pile to the one of an energy pile in a group:

$$R_d = \frac{w_{gr}}{w_{is}} \quad (4)$$

Where  $w_{gr}$  is the average displacement of group and  $w_{is}$  is the displacement of a single pile subjected to same average load. As in the case of the approach proposed for conventional piles (Comodromos et al., 2016), the displacement ratio depends on the geometric configuration as well as the variations in the displacement field introduced by thermal and mechanical loads. In this approach, the ultimate shaft resistance of an energy pile in a group is considered to be the same as the one of a single isolated energy pile, while the displacement ratio is applied to adapt the displacement necessary to mobilize it. The load-transfer curve attained for a single energy pile in a group is represented by dashed lines in Figure 8.b and is determined as follows:

$$w_{gr} = R_d w_{is} \quad (5)$$

$$t_{s,gr} = t_{s,is} \quad (6)$$

where  $w_{gr}$  and  $t_{s,gr}$  are the displacement and shaft resistance of an energy pile in a group, and  $w_{is}$  and  $t_{s,is}$  are the displacement and shaft resistance of a single isolated energy pile, respectively. The load-transfer curve in Figure 8.b is determined using the method proposed by Frank and Zhao (1982), yet, any method developed for single conventional piles can be employed provided that a displacement factor is applied. Finally, since the behavior of a pile in the group highly depends on its location, the displacement ratio may also be corrected by introducing a location weighting factor (Comodromos et al., 2016).

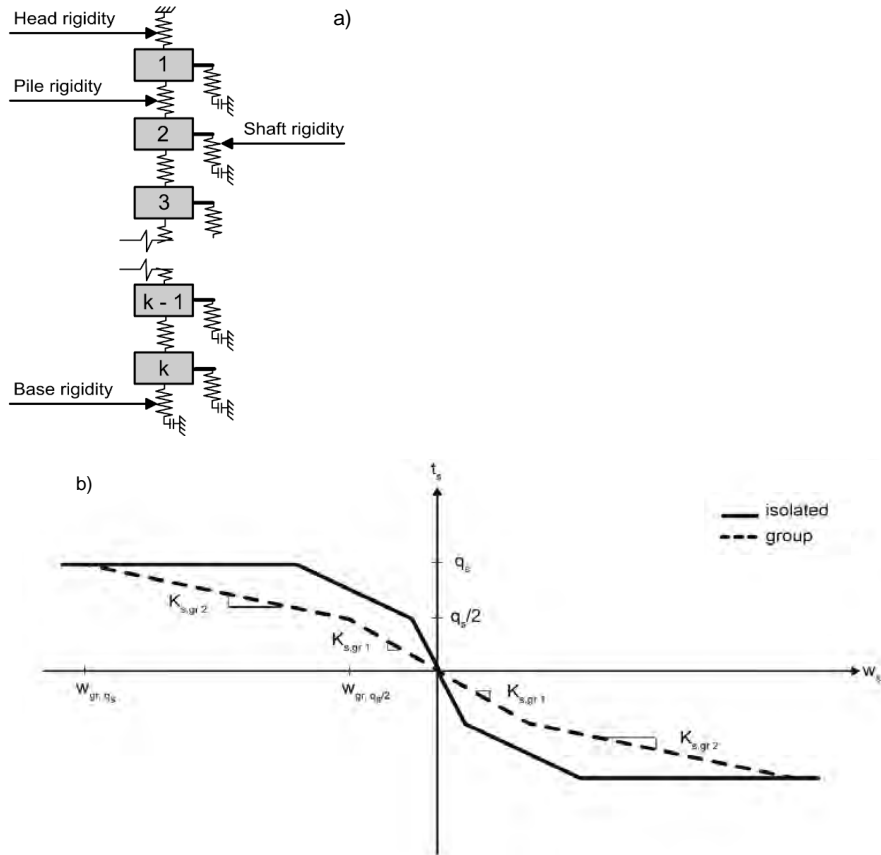


Figure 8 a) Modelling approach b) Load-transfer relationship for single isolated energy pile and energy pile in a group.

The proposed method has been implemented in Comsol Multiphysics Software and its competence in analyzing the behavior of a group of energy piles has been investigated through the results of the full-scale in-situ test performed at EPFL campus, on a group of four energy piles. The material properties considered in the analysis as well as the development of the load-transfer curves are explained in detail by Ravera et al. (2020). Comparison of experimental data from the full-scale in-situ test (Rotta Loria and Laloui, 2018)

and the numerical results obtained through the implemented method is presented in Figure 9.a and Figure 9.b, in terms of thermally induced axial stress and mobilized shaft resistance, respectively at 20°C temperature increase. The numerical results were attained employing two sets of parameters for the molasses layer in compliance with the ones presented in Knellwolf et al. (2011).

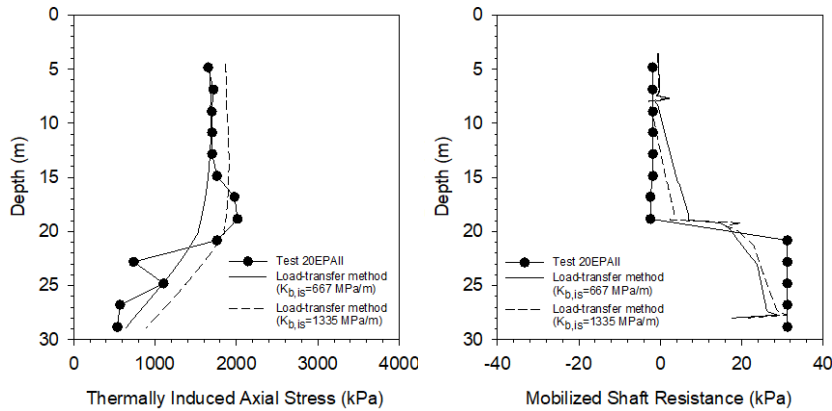


Figure 9 a) Comparison between experimental data and numerical results for a) Thermally induced axial stresses and b) Mobilized shaft resistance (redrawn after Ravera et al., 2020).

The comparison presented in Figure 9 corresponds only to the geothermal activation of the group of energy piles, excluding the stresses generated by the body load and structural loads. The stress variation corresponds to the average value of the mean temperature variations along the uninsulated portions of all four energy piles in the group and the mobilized shaft resistance is determined by employing the stress variations. A good agreement between the experimental and numerical results is observed in the figure, despite the simplifications inherent in the theory.

It was previously shown in Figure 7 that thermally induced vertical stresses decrease for the same temperature change as the number of geothermally active energy piles increases due to increased vertical strains caused by group interactions. The agreement between experimental and numerical results corroborates the additional value of this method, which allows determination of the thermally induced vertical stress along the depth of an energy pile in a group in a simplified and rational manner.

(ii) Interaction Factor Method for Group of Energy Piles (Rotta Loria and Laloui, 2016; Ravera et al., 2019)

A second analytical method was extended from the interaction factor method in the framework of conventional pile groups (Poulos, 1968) to the one of energy pile groups in order to provide a simplified yet rational analysis tool for estimating the vertical displacement of energy pile groups subjected to thermal loads (Rotta Loria and Laloui, 2016). The method allows the estimation

of the head displacement of any energy pile in a group by employing the interactions between two energy piles and the superimposition of the individual effects of adjacent piles in the group as follows:

$$w_k = w_i \sum_{i=1}^{i=n_{EP}} \Delta T_i \Omega_{ik} \quad (7)$$

where  $w_i$  is the vertical head displacement of a single isolated pile per unit temperature change,  $\Delta T_i$  is the applied temperature change to pile  $i$ , and  $\Omega_{ik}$  is the interaction factor for two piles corresponding to the center-to-center distance between pile  $i$  and  $k$ . Interaction factor charts, characterizing a group of two energy piles and taking into consideration pile slenderness ratio and spacing, pile-soil stiffness ratio, Poisson's ratio and non-uniform moduli of the soil have been developed to determine  $\Omega_{ik}$  (Rotta Loria and Laloui, 2016).

The formulation above provides solutions regarding the displacement interaction for free standing energy pile groups or energy pile groups with a perfectly flexible slab. However, in practice piles are often rigidly attached to a pile cap which stands on the soil (Poulos, 1968). Therefore, it is essential to consider thermally induced mechanical interactions which are governed by the changes in deformation field, due to the interplay between the energy pile-slab-soil responses. With this purpose, the interaction factor method was further extended to take into account the presence of the pile cap (Ravera et al., 2019). 3D steady state finite element simulations were carried out employing Comsol Multiphysics Software to propose a formulation of the interaction factor for energy pile groups under a slab and to propose design charts for the analysis compatible with the former study. The influence of the rigid pile cap is expressed in terms of pile-cap displacement ratio as follows:

$$R_c = \frac{\text{displacement of pile with cap}}{\text{displacement of free standing pile}} \quad (8)$$

Employing the pile-cap displacement ratio, displacement determined in free standing conditions can be adjusted to consider the contacting slab as follows:

$$w_k = R_c w_i \sum_{i=1}^{i=n_{EP}} \Delta T_i \Omega_{ik} \quad (9)$$

The combination of the two methodologies (1) interaction factor method for free standing energy piles and (2) extension of the method to consider the

presence of the slab yields the following ultimate methodology illustrated in Figure 10. The first three steps belonging to the original methodology (Rotta Loria and Laloui, 2016) and the following two steps corresponding to the extension of the method (Ravera et al., 2019), are as follows:

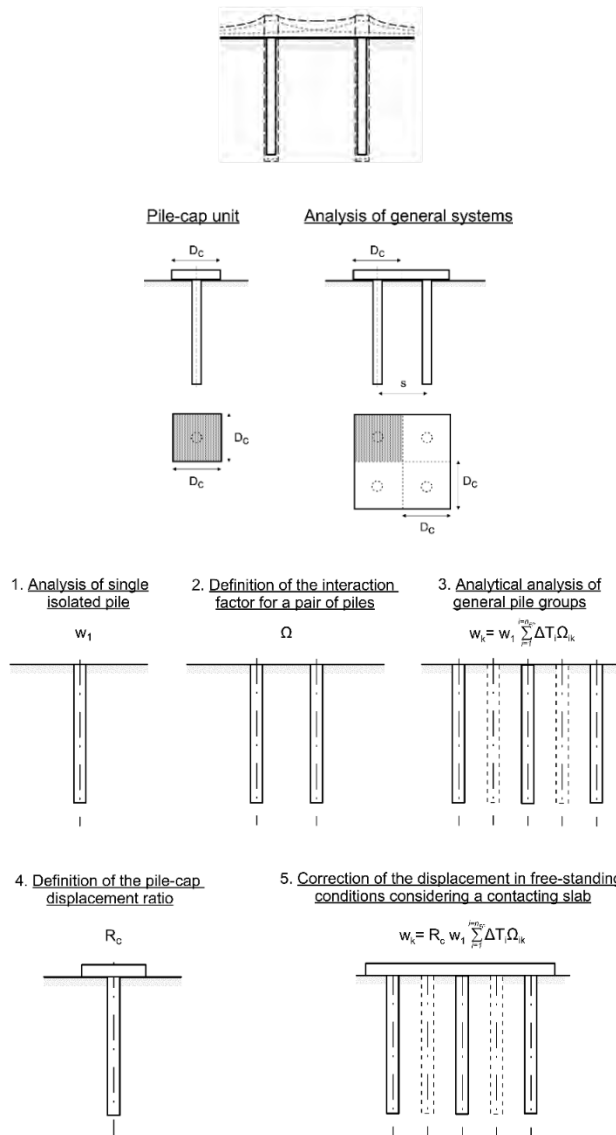


Figure 10 Steps of interaction factor method for the analysis of energy piles with contacting slab.

Step 1: Displacement of an isolated energy pile is computed by employing any suitable practical or sophisticated method as long as it returns representative displacement values for the considered case.



Step 2: Interaction factor is determined for a pair of two energy piles employing the design charts provided by Rotta Loria and Laloui (2016). A sample design chart regarding an energy pile with a slenderness ratio of twenty-five bearing in a soil with a Poisson's ratio of 0.3 is presented in Figure 11.a, for various soil-pile stiffness and normalized displacement.

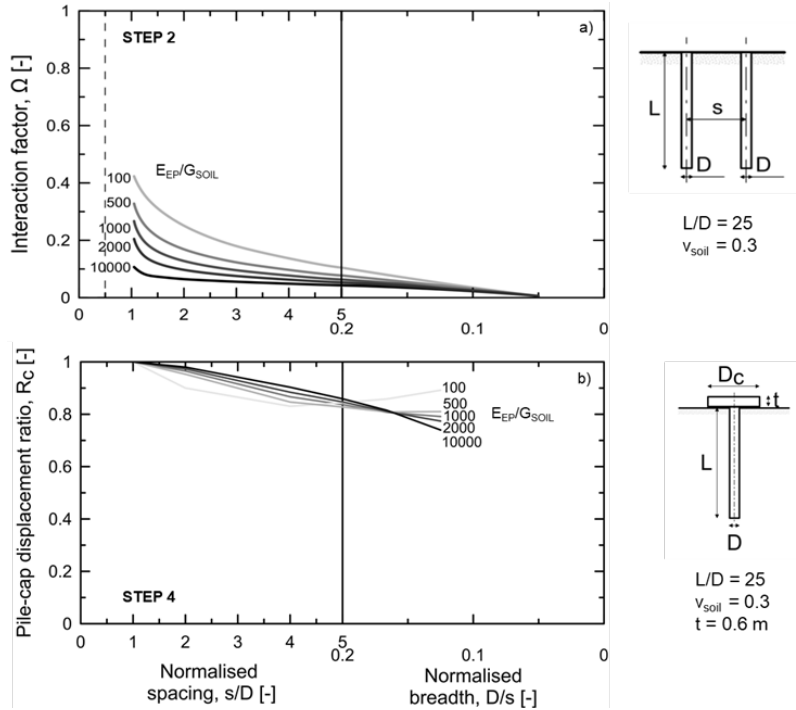


Figure 11 a) Interaction factors, b) Pile-cap displacement ratio for  $L/D = 25$ .

Step 3: Vertical head displacement of any pile in the group in free standing conditions is calculated employing Equation (7).

Step 4: Pile-cap displacement ratio is determined referring to the design charts presented by Ravera et al. (2019). A sample design chart, compatible with the one presented for Step 2, is shown in Figure 11.b for pile cap thickness of 0.6 m.

Step 5: Displacement determined in Step 3 for free standing conditions is corrected by employing Equation (9).

The rather approximate yet rational methodology presented above enables the estimation of the head displacement of any energy pile group configuration with a slab supported on soil through the displacement of a single isolated energy pile and superimposition of the individual effects of adjacent piles and the slab in the group, providing a practical tool to perform displacement analysis of energy pile groups in the early stages of the design process.

## DESIGN OF ENERGY PILES

Full-scale in-situ tests that have been performed on energy piles, as well as the numerical and analytical tools that have been developed over more than two decades, revealed the most fundamental information leading to the recommendations regarding the design of energy piles. According to these findings the design of energy piles at ultimate limit states can be considered as a conventional process by considering that the reactions provided by the soil above and below the null point compensate for each other ensuring equilibrium and, provided that the structural elements are characterized by adequate ductility and rotation capacity (Rotta Loria et al., 2020). However, regarding the serviceability limit states, the effects of both mechanical and thermal loads should be examined by taking into consideration the vertical displacement of single and group of energy piles, as well as the deflection or angular distortion.

Regarding the combinations of actions, Rotta Loria et al. (2020) recommended  $\psi_0 = 0.60$ ,  $\psi_1 = 0.50$  and  $\psi_2 = 0.50$  for the combination, frequent and quasi-permanent values of variable actions, respectively. Regarding the consideration of thermal loads during cooling of the building side (i.e. temperature increase along the energy piles), two design combinations must be considered, assuming the effects of the thermal loads make them the dominant load ( $\Delta T_k = Q_{k,1}$ , where  $Q_{k,1}$  is the dominant variable load) or if not ( $\Delta T_k = Q_{k,i}$ , where  $Q_{k,i}$  is the  $i^{\text{th}}$  general variable load), since it is not known if the thermal loads are dominant with respect to the mechanical ones. Regarding the heating of the building side (i.e., temperature decrease along the energy piles) a single design combination must be considered ( $\Delta T_k = Q_{k,1}$ ).

Finally, when the influence of thermal loads is analyzed during the design of energy piles, (i) piles free at the head and (ii) piles that are fully restrained should be considered to attain conservative estimations of vertical displacement and stress, respectively.

## CONCLUSIONS

The fundamental research in the field of energy geostructures, compiled and expanded by the Laboratory of Soil Mechanics over more than two decades, revealed that this emerging technology provides low carbon, cost-effective and local energy solutions to structures and infrastructures, which opens a new era for the geotechnical engineering practice.

The research activities performed by LMS in this field has exclusively covered various elements related to energy geostructures, including but not limited to energy, geotechnical, structural and design aspects. Related to the energy aspect, it has been revealed that typically, 40-150 W/m heat energy can be extracted from and withdrawn into the ground with the use of energy piles,

while 20-40 W/m<sup>2</sup> and 20-60 W/m<sup>2</sup> are achievable with energy wall and energy tunnels, respectively. Furthermore, two state-of-the-art in-situ tests have been performed on single and a group of energy piles, which not only revealed the most fundamental knowledge regarding their thermo-mechanical behavior, but also provided invaluable information for the validation of numerical models and analytical tools developed in the area.

To provide satisfactory tools for design and wider application of energy piles, several practical analytical tools have been developed for energy piles including the load-transfer method for the assessment of axial stress, displacement and mobilized shaft resistance along single and groups of energy piles, as well as the interaction factor method for the estimation of vertical displacement of energy pile groups with and without a rigid slab. Incremental research efforts performed in the area, from both experimental and analytical points of view, have eventually led to development of recommendations for the design of energy piles for both ultimate and serviceability limit states. Overall, research outcomes achieved over more than two decades revealed that the energy geostructures concept is a mature and ready-to-be-employed technology.

The questions that remained to be answered now are no longer about how an energy geostructure responds to thermal actions, but rather on how the energy performance, as well as the geotechnical and structural adaptations should be assessed to maximize its cost efficiency.

## ACKNOWLEDGEMENT

The financial supports from the Swiss National Science Foundation N. 160117 (Division III), Swiss National Science Foundation N. 200021\_175500 (Division II), Swiss Federal Office of Energy (contract Nb. 154'426) are greatly appreciated.

## REFERENCES

- [1] A. Bidarmaghz and G. A. Narsilio: Heat exchange mechanisms in energy tunnel systems. *Geomechanics for Energy and the Environment*, 16, 83-95, 2018.
- [2] A. Di Donna et al: Energy performance of diaphragm walls used as heat exchangers. *Proceedings of the Institution of Civil Engineers-Geotechnical Engineering*, 170(3), 232-245, 2017
- [3] A. F. Rotta Loria: Performance-based design of energy pile foundations. *DFI Journal* 12 (2), 94-107, 2019.
- [4] A. F. Rotta Loria et al: The role of thermal loads in the performance-based design of energy piles. *Geomechanics for Energy and the Environment*, 21, 100153, 2020.

- [5] A. F. Rotta Loria and L. Laloui: The interaction factor method for energy pile groups. *Computers and Geotechnics*, 80, 121-137, 2016.
- [6] A. F. Rotta Loria and L. Laloui: Thermally induced group effects among energy piles. *Géotechnique*, 67(5), 374-393, 2017.
- [7] A. F. Rotta Loria and L. Laloui: Group action effects caused by various operating energy piles. *Géotechnique*, 68(9), 834-841, 2018.
- [8] ASHRAE 2008: ASHRAE Vision 2020.  
<https://www.isiaq.org/docs/sponsor%20material/ASHRAE%20Strategic%20Plan%20Jun08.pdf>. Last accessed June 2024.
- [9] C. Knellwolf et al : Geotechnical analysis of heat exchanger piles. *Journal of Geotechnical and Geoenvironmental Engineering*, 137(10), 890-902, 2011.
- [10] C. Xia et al: Experimental study on geothermal heat exchangers buried in diaphragm walls. *Energy and Buildings*. 52, 50-5, 2012.
- [11] D. Adam and R. Markiewicz: Energy from earth-coupled structures, foundations, tunnels and sewers. *Géotechnique*, 59(3), 229-236, 2009.
- [12] D. P. Nicholson et al: The design of thermal tunnel energy segments for Crossrail, UK. *Proceedings of the Institution of Civil Engineers Engineering Sustainability*, 167 (3), 118-134, 2014.
- [13] D. Salciarini et al: Thermomechanical effects induced by energy piles operation in a small piled raft. *International journal of Geomechanics*, 15(2), 04014042, 2013.
- [14] D. Sterpi et al: Investigation on the behaviour of a thermo-active diaphragm wall by thermo-mechanical analyses. *Geomechanics for Energy and the Environment*, 9, 1-20, 2017.
- [15] E. M. Comodromos et al : Contribution to the design methodologies of piled raft foundations under combined loadings. *Canadian Geotechnical Journal*, Vol. 53 (4), 559–577, 2016.
- [16] E. P. B. D. Recast: Directive 2010/31/EU of the European Parliament and of the Council of 19 May 2010 on the energy performance of buildings (recast). *Official Journal of the European Union* 18, no. 06, 2010.
- [17] E. Ravera et al : Analysis of the interaction factor method for energy pile groups with slab. *Computers and Geotechnics*, Vol 119, 2019.
- [18] E. Ravera et al: Load-transfer method for energy piles in a group with pile-soil-slab-pile interaction. *Journal of Geotechnical and Geoenvironmental Engineering*, Vol 146 (6), 2020.

- [19] E. Sailer et al: Fundamentals of the coupled thermo-hydro-mechanical behaviour of thermo-active retaining walls. *Computers and Geotechnics*, 109, 189-203, 2019.
- [20] Eurostat, (2022): [https://ec.europa.eu/eurostat/statistics-explained/index.php?title=Energy\\_consumption\\_in\\_households](https://ec.europa.eu/eurostat/statistics-explained/index.php?title=Energy_consumption_in_households) (last accessed June 2024)
- [21] F. A. Loveridge et al: Long-term monitoring of CFA energy pile schemes in the UK. *Energy Geotechnics*, 585-592, 2016.
- [22] H. B. Seed and L. C. Reese: The action of soft clay along friction piles. *American Society of Civil Engineers Society*, 122 (1), 731–754, 1957.
- [23] H. G. Poulos: Analysis of the settlement of pile groups. *Géotechnique*, 18 (4), 449-471, 1968.
- [24] H. G. Poulos: The influence of a rigid pile cap on the settlement behaviour of an axially-loaded pile. *Civ. Eng. Trans., Inst. Engrs*, CE10 (2), 206-208, 1968.
- [25] H. M. Coyle and L. C. Reese: Load transfer for axially loaded piles in clay. *J. Soil Mech. Found. Div. ASCE*. 92 (2), 1–26, 1966.
- [26] International Energy Agency, I. E. A. 2022: Heating, <https://www.iea.org/energy-system/buildings/heating#tracking> (Last accessed June 2024).
- [27] International Energy Agency, I. E. A. 2018: <https://www.iea.org/reports/the-future-of-cooling> (last accessed June 2024)
- [28] J. S. McCartney and K. D. Murphy. Investigation of potential dragdown/uplift effects on energy piles. *Geomechanics for Energy and the Environment*, 10, 21-28, 2017.
- [29] L. Laloui et al: Comportement d'un pieu bi-fonction, fondation et échangeur de chaleur. *Canadian Geotechnical Journal*, 40(2), 388-402, 2003.
- [30] L. Laloui et al: Experimental and numerical investigations of the behaviour of a heat exchanger pile. *International Journal for Numerical and Analytical Methods in Geomechanics*, 30(8), 763-781, 2006.
- [31] L. Laloui and A. F. Rotta Loria. *Analysis and Design of Energy Geostructures: Theoretical Essentials and Practical Applications*. Academic Press, 2019.
- [32] L. Laloui and M. Sutman: Experimental investigation of energy piles: From laboratory to field testing. *Geomechanics for Energy and the Environment*, 27, p.100214, 2021.

- [33] L. Laloui et al: Issues involved with thermoactive geotechnical systems: characterization of thermomechanical soil behavior and soil-structure interface behavior. *DFI Journal-The Journal of the Deep Foundations Institute*, 8(2), pp.108-120, 2014.
- [34] L. M. Kraft et al: Theoretical T-Z curves. *Journal of Geotechnical Engineering*, American Society of Civil Engineers, 107 (11), 1543–1561, 1981.
- [35] M. Barla and A. Di Donna: Energy tunnels: concept and design aspects. *Underground Space*, 3(4), 268-276, 2018.
- [36] M. Barla et al: A novel real-scale experimental prototype of energy tunnel. *Tunnelling and Underground Space Technology*, 87, 1-14, 2019.
- [37] M. F. Randolph and P. Clancy: Efficient design of piled rafts. *Proceedings of 5th International Conference on Deep Foundations on Bored and Auger Piles*, 1-4 June, Ghent, Belgium, 119-130, 1993.
- [38] M. F. Randolph and C. P. Wroth: Analysis of deformation of vertically loaded piles. *Journal of Geotechnical Engineering*, American Society of Civil Engineers, 104 (2), 1465–1488, 1978.
- [39] M. Sutman et al: Full-scale in-situ tests on energy piles: Head and base-restraining effects on the structural behaviour of three energy piles. *Geomechanics for Energy and the Environment*, 18, 56-68, 2019.
- [40] M. Sutman et al: Effect of end-restraint conditions on energy pile behavior. *Geotechnical Frontiers*, 165–174, 2017.
- [41] M. Sutman et al: Cyclic Load–Transfer Approach for the Analysis of Energy Piles. *Journal of Geotechnical and Geoenvironmental Engineering*, 145(1), 04018101, 2018.
- [42] M. Sutman et al: Long-term performance and life cycle assessment of energy piles in three different climatic conditions. *Renewable Energy*, 146, 1177-1191, 2020.
- [43] M. Sutman: Thermo-mechanical behavior of energy piles: Full-scale field testing and numerical modeling (Doctoral dissertation, Virginia Tech), 2016.
- [44] N. Makasis et al: A machine learning approach to energy pile design. *Computers and Geotechnics*, 97, 189-203, 2018.
- [45] P. J. Bourne-Webb et al : Energy pile test at Lambeth College, London: geotechnical and thermodynamic aspects of pile response to heat cycles. *Géotechnique*, 59(3), 237-248, 2009.
- [46] P. J. Bourne-Webb et al: Thermal and mechanical aspects of the response of embedded retaining walls used as shallow geothermal heat exchangers. *Energy and Buildings*, 125, 130-141, 2016.

- [47] P. J. Bourne-Webb et al: Design tools for thermoactive geotechnical systems. *The Journal of the Deep Foundations Institute*, 8(2), 121-129, 2014
- [48] R. Frank and S. R. Zhao: Estimation par les paramètres pressiométriques de l'enfoncement sous charge axiale de pieux forés dans des sols fins. *Bulletin de Liaison Laboratoires des Ponts et Chaussées*, No. 119, 17–24, 1982.
- [49] S. Frodl et al: Design and construction of the tunnel geothermal system in Jenbach. *Geomechanics and Tunnelling*, 3(5), 658-668, 2010.
- [50] S. Kürten, S et al: Design of plane energy geostructures based on laboratory tests and numerical modelling. *Energy and Buildings*, 107, 434-444, 2015.
- [51] S. You et al: Experimental study on structural response of CFG energy piles. *Applied Thermal Engineering*, 96, 640-651, 2016.
- [52] T. Mimouni, L. Laloui: Behaviour of a group of energy piles. *Canadian Geotechnical Journal*, 52(12), 1913-1929, 2015.

# VERIFICATION OF ADEQUATE ROTATION CAPACITY FOR STEEL SHEET PILE PROFILES BY LEM WALL CALCULATIONS WITH YIELD HINGES

**O. Møller**

## KEYWORDS

Limit Equilibrium Method (LEM), ductility, failure modes, mobilisation of plastic earth pressures, yield hinges, steel sheet piles, rotation capacity  $\phi_{Cd}$ , necessary rotation  $\phi_{Ed}$ , cross section classes, link between steel (EC3-5) and geotechnical design (EC7-3).

## ABSTRACT

Where LEM wall calculations involve yield hinges (by plastic global analysis), adequate rotation capacity of the sheet pile cross section shall be verified. The paper highlights the interface between EC3-5 and EC7-3 regarding way and background for verification of adequate rotation capacity of sheet pile profiles even for cross section Class 3 by guidance to determination of the rotation capacity  $\phi_{Cd}$  and the necessary rotation  $\phi_{Ed}$  beyond the elastic rotation of the cross section. A calculation example is provided.

## INTRODUCTION

Since the early fifties designing of retaining walls in Denmark has been based on plastic earth pressures calculated according to the earth pressure theory developed by J. Brinch-Hansen. The earth pressure is redistributed according to the failure mechanism including none, one or more yield hinges and/or involving relieving (yielding) supports like anchors. Plastic design is more cost effective (requires less material) than elastic design. At that time most sheet pile profiles were quite compact and of a moderate steel strength, i.e. ductile, so nobody cared about rotation capacity of the sheet pile profiles. Since then, the sheet pile manufacturers have developed wider and thinner sections with higher steel strength to utilise the weight of the steel optimally. However, this has created the need for verification of the adequate rotation capacity of sheet pile profiles used for retaining walls based on calculation models with yield hinges. This paper provides guidance of such verification with reference to the new EN 1993-5 Design of steel structures – Part 5: Piling (EC3-5) and EN 1997-3 Geotechnical design – Part 3: Geotechnical structures (EC7-3).



## LIMIT EQUILIBRIUM METHOD (LEM)

By limit equilibrium methods for retaining structures (constant) plastic earth pressures are assumed on both the retained and excavated side. The length (embedment) of the wall is increased until moment and force equilibrium are achieved. The method does not give any information of the displacement of the retaining structure. It is just presupposed that the displacement is adequate to mobilise the plastic earth pressures.

### Failure mechanisms

To mobilise plastic earth pressures a failure mechanism must be anticipated. Safety factors applied either directly on the calculated earth pressures or indirectly on the soil strength parameters provide the necessary safety against the anticipated failure mechanism.

Some but not all failure mechanisms cause an earth pressure redistribution compared to a triangular pressure distribution, and some but not all failure mechanisms require yielding of the wall or the anchorage. All mechanisms can be composed by a rotation and/or a translation of the wall. Some typical examples of failure mechanisms are shown in the Figure 1 below.

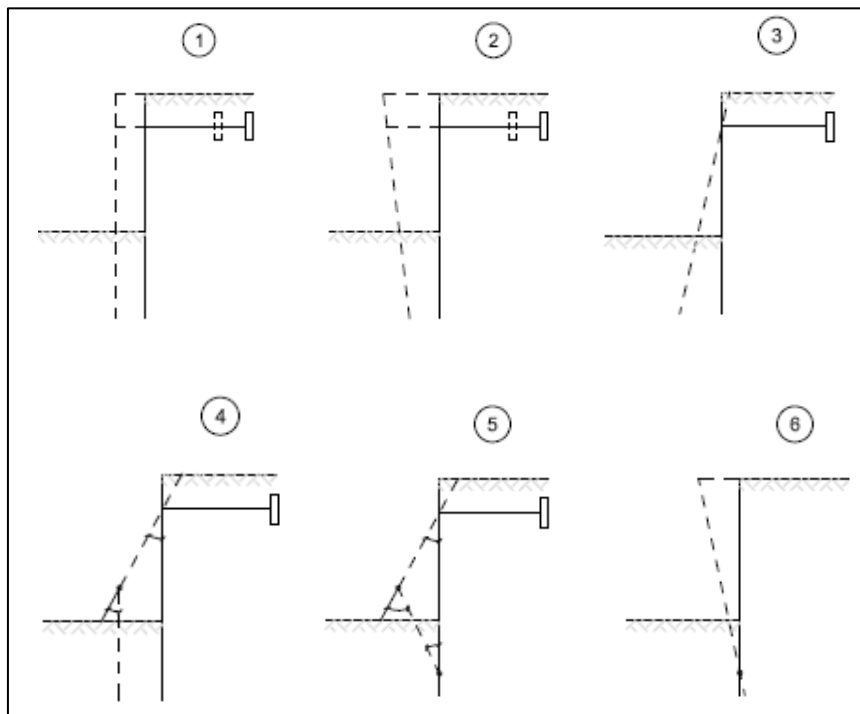


Figure 1 Failure mechanisms

In mechanism 1 and 2 the anchor is yielding, by yielding of the steel tendon or by translation of the anchor plate, the dead man (anchor) mobilising passive earth pressure on the front side of the dead man.

In mechanism 3 and 6 the wall is rotating like a rigid body around a fixed point, in mechanism 3 around the fixed anchor point, in mechanism 6 around the fixation point in the ground.

In mechanism 4 and 5 the upper part of the wall is rotating about a fixed anchorage point, and the lower part of the wall is translating in 4 and rotating about a fixation point in the ground in 5.

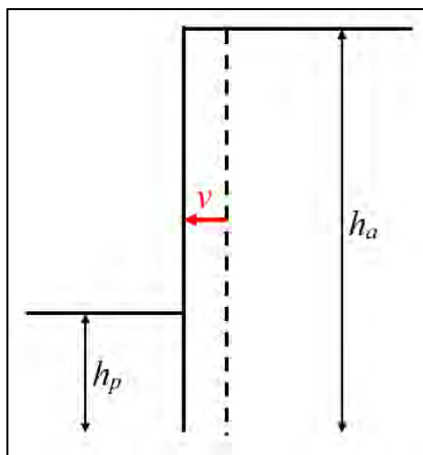
Only mechanism 4 and 5 involves a yield hinge in the wall.

### Mobilisation of plastic earth pressures

The limiting criteria for mobilisation of plastic earth pressures appear from EC7-3, Annex D.8 Limit equilibrium models, paragraph (2) and corresponding note:

(2) When limit equilibrium models are used to justify plastic hinges in metallic structures accordingly with EN 1993-5, limit displacements associated with limit earth pressures may be estimated based on conventional order of magnitude, traditionally expressed as a proportion  $\lambda_a$  of the wall height on the retained side, and  $\lambda_p$  of the embedded depth on the excavated side.

NOTE The values of  $\lambda_a$  and  $\lambda_p$  are 0,1 to 0,3 % and 1 to 5 % respectively, unless different values are given in the National Annex.



$$\lambda_a = v / h_a$$

$$\lambda_p = v / h_p$$

$v = \max (v_a ; v_p)$  to mobilise active as well as passive plastic earth pressure

Assume  $\lambda_p \sim 10 \lambda_a$ .

Then  $v_p$  is most critical, if  $h_p > 0,1 h_a$  which is very typical.

Index a for active and p for passive pressure/side.

Figure 2 Mobilisation of plastic earth pressures

## ELASTIC OR PLASTIC GLOBAL ANALYSIS

Methods of analysis considering material non-linearities (of steel) appear from Cl. 7.4 in EC3-5 as well as EC3-1-1 (same clause number).

Quote from EC3-5, 7.4:

(1) The internal forces and moments may be determined in accordance with EN 1993-1-1, using either

a) elastic global analysis or

b) plastic global analysis.

(2) For elasto-plastic cross-section verification of Class 3 sections, in combination with elastic global analysis, use Annex E (normative), according to Table 7.1

(3) To replace EN 1993-1-1:2022, 7.4.1(3) for U and Z sheet piles, a plastic global analysis may be used in accordance with Annex C for structures made of steel grades up to S460. For other cross-sections EN 1993-1-1:2022, 7.4.1(3) applies.

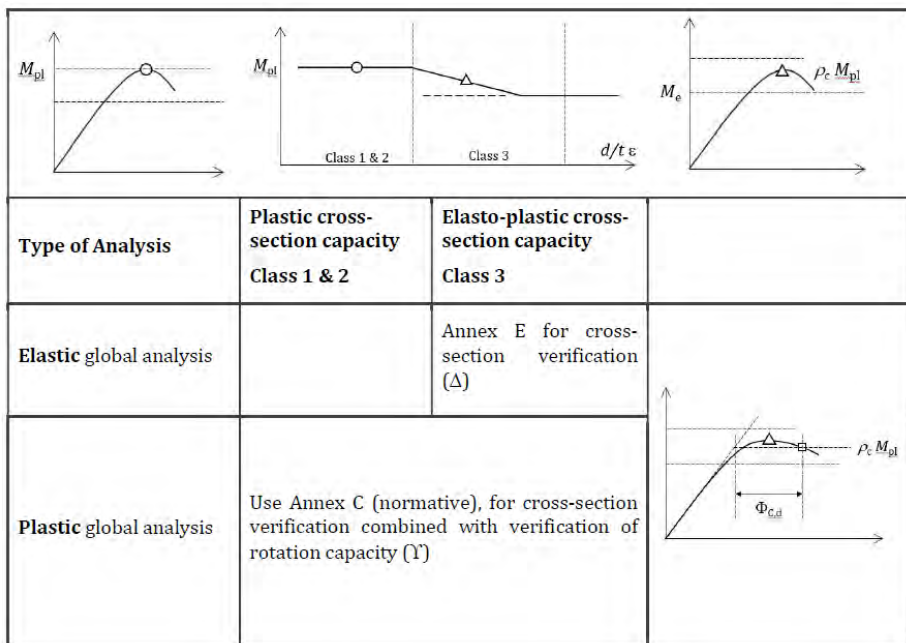


Figure 3 Resistance in bending according to the type of analysis  
(draft Table 7.1 from FprEN 1993-5)

Normally you would consider and calculate a cross section as plastic being Class 2 OR as elastic being Class 3. However, EC3-5 Cl. 7.4 allows for utilization of the semi-plastic capacity of Class 3 cross sections.

In EC3-5 Table 7.1 it is misleading that “Class 1” is mentioned at all. You can turn a Class 2 section into a Class 1 section, provided you can document that the cross section has the adequate rotation capacity, but you do not know that until you have determined the necessary rotation capacity from the wall calculation, i.e. the necessary  $\lambda_a$  and  $\lambda_p$ , and by this  $v_a$  and  $v_p$ . On the other hand, even if you manage to document adequate rotation capacity for a Class 3 cross section you would not term that a Class 1 cross section ... by “jumping” over the Class 2 term. Hopefully / probably the term “Class 1” will disappear from Table 7.1 in the final version of EC3-5 for Formal Vote.

This paper deals with documentation of the adequate rotation capacity using plastic global analysis in accordance with EC3-5 Annex C for Class 2 and Class 3 sheet pile cross sections.

## CROSS-SECTION CLASSES

The cross-section classes are described in EC3-1-1, 7.5.2 (1). Table 1 below illustrates the stress distribution and degree of plasticity depending on the cross-section class.

Table 1 Stress distribution depending on cross section class

Stress distribution					
Edge stress	$\sigma < f_y$	$\sigma = f_y$	$\sigma = f_y$	$\sigma = f_y$	$\sigma = f_y$
Class	4	3			2
Type	elastic	elastic	elasto-plastic		plastic

Class 3 sections cover all stress distributions from pure elastic up to pure plastic. Class 2 covers only one stress distribution: the full plastic.

To quantify the limits between Class 2, 3 and 4, a kind of relative slenderness ratio  $\lambda = b_t / t_f / \varepsilon$  is defined, where  $b_t$  and  $t_f$  is the width and the thickness of

the flanges, and  $\varepsilon$  is a weighting factor taking the yield strength  $f_y$  into consideration. The higher yield strength the higher relative slenderness ratio. The limits appear from EC3-5, Table 7.2 which is inserted as Figure below.

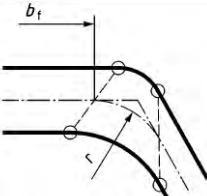
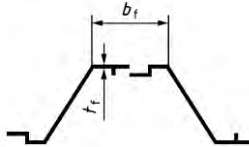
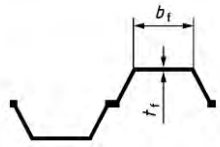
Classification		Z-profile				U-profile			
									
Class 1		— the same boundaries as for Class 2 apply — a rotation check shall be carried out according to Annex C							
Class 2		$\frac{b_f/t_f}{\varepsilon} \leq 35$				$\frac{b_f/t_f}{\varepsilon} \leq 35$			
Class 3		$\frac{b_f/t_f}{\varepsilon} \leq 60$				$\frac{b_f/t_f}{\varepsilon} \leq 49$			
$\varepsilon = \sqrt{\frac{235}{f_y}}$	$f_y$ [N/mm <sup>2</sup> ]	240	270	320	355	390	430	460	
	$\varepsilon$	0,99	0,93	0,86	0,81	0,78	0,74	0,71	

Figure 4 Classification of cross-sections for U- and Z-profiles  
(Table 7.2 from EC3-5)

It is not clear why  $b_f$  is determined in such a sophisticated way. Using the inner straight part of the flange width, which is listed in every (or most) sheet pile catalogues seem precise enough. The free software Durability from Arce-lorMittal renders the value of  $b_f$ . The error of using the inner straight part of the flange width is insignificant, e.g. for AZ20-800  $b_f$  is 436 mm whereas the inner straight part is 428 mm. Assuming  $f_y = 240$  MPa,  $b_f = 436$  mm means  $b_f/t_f/\varepsilon = 46,4 \sim 46$ . With  $b = 428$  mm  $b_f/t_f/\varepsilon = 45,5 \sim 46$ .

## ROTATION CAPACITY

The design rotation capacity  $\phi_{cd}$  is defined as the rotation capacity of the cross section beyond the elastic limit as appear from Figure C.2 in EC3-5, pasted below.

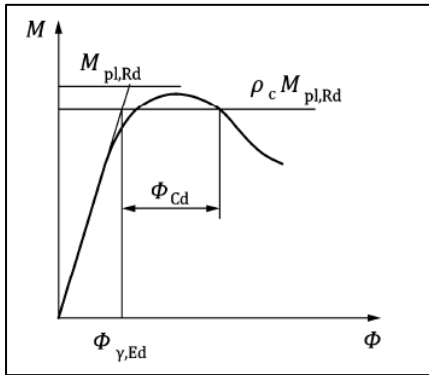


Figure 5 Definition of the rotation capacity angle  $\phi_{Cd}$   
(Figure C.2 from EC3-5)

$\phi_{Cd}$  depends on the utilisation or reduction of the plastic bending resistance  $M_{pl,Rd}$  defined by the reduction factor  $\rho_c$ , which ranges from 1,00 (full plastic) to 0,85 (pure elastic). Comparison between the elastic modulus  $W_{el}$  and the plastic modulus  $W_{pl}$  will for most sheet pile profiles be close to 0,85.

The elastic rotation  $\phi_{elastic}$  is assumed linear up to the elastic limit  $\phi_{y,Ed}$  corresponding to the reduced plastic moment resistance  $\rho_c M_{pl,Rd}$ , which is an approximation.

The residual bending moment resistance of a cross-section may be determined by using relative slenderness ratios  $b_f / t_f / \varepsilon$  according to table C.1 in EC3-5, pasted below.

Table 2 Reduction of bending moment resistance  $M_{pl,Rd}$  (Table C.1 from EC3-5)

Reduction factor $\rho_c$ on $M_{pl,Rd}$	1,00	0,95	0,90	0,85
Class	2	3		
U-piles	$\frac{b_f/t_f}{\varepsilon} \leq 35$	$\frac{b_f/t_f}{\varepsilon} \leq 40$	$\frac{b_f/t_f}{\varepsilon} \leq 44$	$\frac{b_f/t_f}{\varepsilon} \leq 49$
Z-piles	$\frac{b_f/t_f}{\varepsilon} \leq 35$	$\frac{b_f/t_f}{\varepsilon} \leq 43$	$\frac{b_f/t_f}{\varepsilon} \leq 52$	$\frac{b_f/t_f}{\varepsilon} \leq 60$

$\phi_{Cd}$  can be found from graphs in Figure C.1 in EC3-5, pasted below based on results from bending tests with steel sheet piles as well as finite element simulations.  $\rho_c$ -curves are plotted in a  $(b/t_f/\varepsilon)$ - $\phi_{Cd}$  diagram.

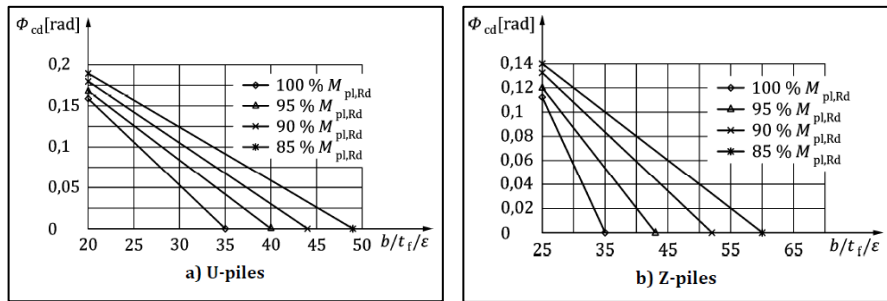


Figure 6 Rotation capacity angle at different levels of reduction of  $M_{pl,Rd}$   
(Figure C.1 in EC3-5:2024-06-24, Ref. [2])

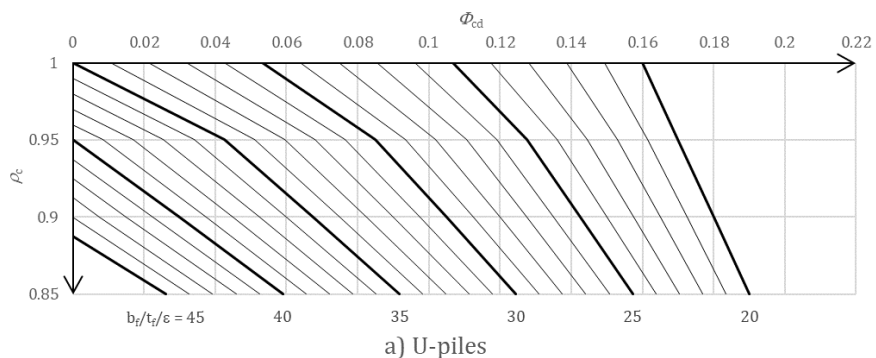
The limiting values on the horizontal axis appear from Table C.1 in EC3-5, cf. Ref. [2].

The limiting values on the vertical axis in EC3-5 Figure C.1 appear from Table below.

Table 3  $\phi_{cd}$  - values [rad] on vertical axis in Figure C.1 in EC3-5

$\rho_c$	1,00	0,95	0,90	0,85
U-piles ( $b_f / t_f / \varepsilon = 20$ )	0,16	0,17	0,18	0,19
Z-piles ( $b_f / t_f / \varepsilon = 25$ )	0,11	0,12	0,13	0,14

However, in the latest draft of EC3-5 prepared for FV (SC7 Doc N4032, Ref. [3]) the format of Figure C.1 is changed to figures as appear below



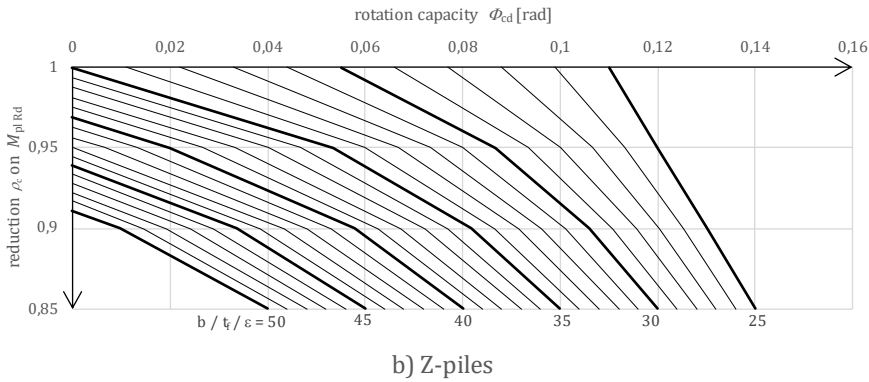


Figure 7 Rotation capacity depending on slenderness and utilisation  $\rho_c$  of plastic bending resistance (Figure C.1 in EC3-5:2024-07-23, Ref. [3])

The figures represent the same data. The idea is to make ease of use. Each line in the figure corresponds to one slenderness ratio (rounded up to a whole number, i.e. an integer, considered to be precise enough for all practical applications). With this slenderness for a particular sheet pile profile you can determine the rotation capacity  $\phi_{Cd}$  for any degree of utilisation of the profile  $\rho_c$  between 85 % and 100 % of the plastic bending moment capacity  $M_{pl,Rd}$ .

However, this form does not facilitate a quantitative determination of the rotation capacity, only a graphically determination, for which reason the SC3-WG responsible for the revision of EC3-5 has provided formulas for  $\phi_{Cd} = f(b/t_f/\epsilon)$  for  $\rho_c = 0,85; 0,90; 0,95$  and  $1,00$  to allow for determination of “knee points” in the new form of Figure C.1, cf. table below.

Table 4 formulas for  $\phi_{Cd}$ , where  $\lambda = b/t_f/\epsilon$

$\rho_c$	0,85	0,90	0,95	1,00
U-piles	$0,19 \left[ 1 - \frac{\lambda-20}{29} \right]$	$0,18 \left[ 1 - \frac{\lambda-20}{24} \right]$	$0,17 \left[ 1 - \frac{\lambda-20}{20} \right]$	$0,16 \left[ 1 - \frac{\lambda-20}{15} \right]$
Z-piles	$0,14 \left[ 1 - \frac{\lambda-25}{35} \right]$	$0,13 \left[ 1 - \frac{\lambda-25}{27} \right]$	$0,12 \left[ 1 - \frac{\lambda-25}{18} \right]$	$0,11 \left[ 1 - \frac{\lambda-25}{10} \right]$

### Consistency between Annex C and D in EC3-5

The limiting values of the relative slenderness  $\lambda = b/t_f/\epsilon$  in Table 2 represent the maximum utilization of the plastic modulus  $W_{pl}$  for a given relative slenderness ratio leaving no (extra) plastic rotation capacity ( $\phi_{Cd} = 0$ ). They are consistent with the elasto-plastic section modulus  $W_{ep}$  values you can determine from EC3-5, Annex E *Properties of semi-compact sections*.



For Z-piles

$$W_{ep} = W_{pl} + (W_{el} - W_{pl}) \frac{b_f/t_f - 35\varepsilon}{25\varepsilon} \quad (\text{EC3-5, E.1})$$

Introducing  $\lambda = \frac{b_f/t_f}{\varepsilon}$  and dividing by  $W_{pl}$  in (E.1) gives:

$$\frac{W_{ep}}{W_{pl}} = 1 + \left( \frac{W_{el}}{W_{pl}} - 1 \right) \frac{\lambda - 35}{25}$$

Valid for  $35 < \lambda < 60$

For U-piles

$$W_{ep} = W_{pl} + (W_{el} - W_{pl}) \frac{b_f/t_f - 35\varepsilon}{14\varepsilon} \quad (\text{EC3-5, E.2})$$

Introducing  $\lambda = \frac{b_f/t_f}{\varepsilon}$  and dividing by  $W_{pl}$  in (E.2) gives:

$$\frac{W_{ep}}{W_{pl}} = 1 + \left( \frac{W_{el}}{W_{pl}} - 1 \right) \frac{\lambda - 35}{14}$$

Valid for  $35 < \lambda < 49$

$W_{ep}/W_{pl}$  is comparable to  $\rho_c$

If you assume  $W_{el}/W_{pl} \sim 0,85$  you get a very fine fit of  $W_{ep}/W_{pl}$  with  $\rho_c$  from Table C.1 in EC3-5 as appear from the table below.

Table 5  $\rho_c$  and  $W_{ep}/W_{pl}$  for Z- and U-piles assuming  $W_{el}/W_{pl} = 0,85$

Table C.1	Z-piles	E.1	$\frac{\rho_c}{W_{ep}/W_{pl}}$	U-piles	E.2	$\frac{\rho_c}{W_{ep}/W_{pl}}$
$\rho_c$	$b_f/t_f/e$	$W_{ep}/W_{pl}$	-	$b_f/t_f/e$	$W_{ep}/W_{pl}$	-
1,00	35	1,000	1,000	35	1,000	1,000
0,95	43	0,952	0,998	40	0,946	1,004
0,90	52	0,898	1,002	44	0,904	0,996
0,85	60	0,850	1,000	49	0,850	1,000

This means that even if you are (just) doing an **elastic** global analysis – and thus not chasing a rotation capacity - you can still utilise a Class 3 section to more than just the pure elastic section modulus capacity, depending on the relative slenderness of the profile.

## REQUIRED ROTATION

As the rotation capacity  $\phi_{Cd}$  is defined and determined as the plastic rotation beyond the elastic rotation the necessary rotation  $\phi_{Ed}$  is likewise defined as the extra rotation (if needed) beyond the elastic rotation, which makes determination of the elastic rotation relevant.

The necessary (extra) rotation capacity beyond the elastic rotation can be determined in three ways according to EC3-5, Annex C:

1. Direct determination from the rotation in a plastic hinge
2. Based on the total rotation in a span between two supports or
3. Based on the beam displacement at certain points along the span

The first option is relevant when analysing / calculating the wall with an elasto plastic finite element program, which allows for direct reading of the plastic rotation of the section with maximum bending moment.

The two last options can be expressed as

$$\phi_{Ed} = \phi_{total} - \phi_{elastic}$$

where both terms are based on either the rotation or the displacement.

Considering a simply supported beam, the elastic mid (and max) deflection  $u_{max}$  and rotation  $\alpha$  at the supports from a uniform load  $q$  can be expressed as appear from the figure below

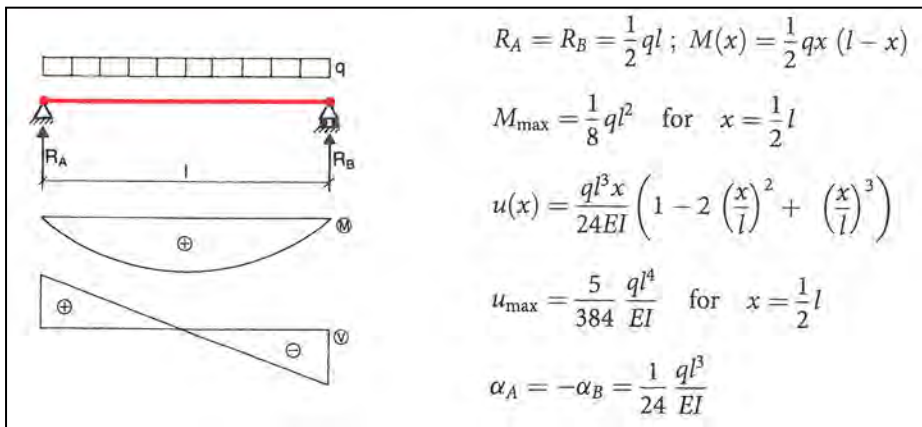


Figure 8 elastic rotation and displacement (from Teknisk Ståbi, 25. Udg.)

Substituting  $1/8 q l^2$  with  $M$  in the expressions for  $u_{max}$  and  $\alpha$  renders

$$u_{max} = \frac{5}{384} \frac{q l^4}{EI} = \frac{5}{48} \frac{M l^2}{EI} \quad \text{and} \quad \alpha_A = -\alpha_B = \frac{1}{24} \frac{q l^3}{EI} = \frac{1}{3} \frac{M l}{EI}$$

where

$M = \rho_c M_{pl,Rd}$  and

$$M_{pl,Rd} = \beta_B W_{pl} \frac{f_y}{\gamma_{M0}}$$

$\beta_B$  (B for bending) is a reduction factor that takes account of the lack of shear force transmission in the interlocks and oblique bending in double U-piles.

Similarly, the stiffness  $EI$  is reduced with a(nother)  $\beta$ -factor:  $\beta_D$ . D for deflection.

$\beta_B$  and  $\beta_D$  depend on the number of anchors/supports and the soil conditions. Recommended values appear from Table 8.1 (NPD) in EC3-5. For a Z-profile both  $\beta$ -factors are 1,0.

Based on the total rotation in a span between two supports the value of  $\phi_{Ed}$  may be found as

$$\phi_{Ed} = \phi_{tot,Ed} - \phi_{y,Ed} \quad (\text{C.2 in EC3-5})$$

where

$\phi_{tot,Ed}$  is illustrated in the figure below and

$$\phi_{y,Ed} = \alpha_A - (-\alpha_B) = \alpha_A + \alpha_B = \frac{2 \rho_c M_{pl,Rd} L}{3 \beta_D EI} \quad (\text{C.3 in EC3-5})$$

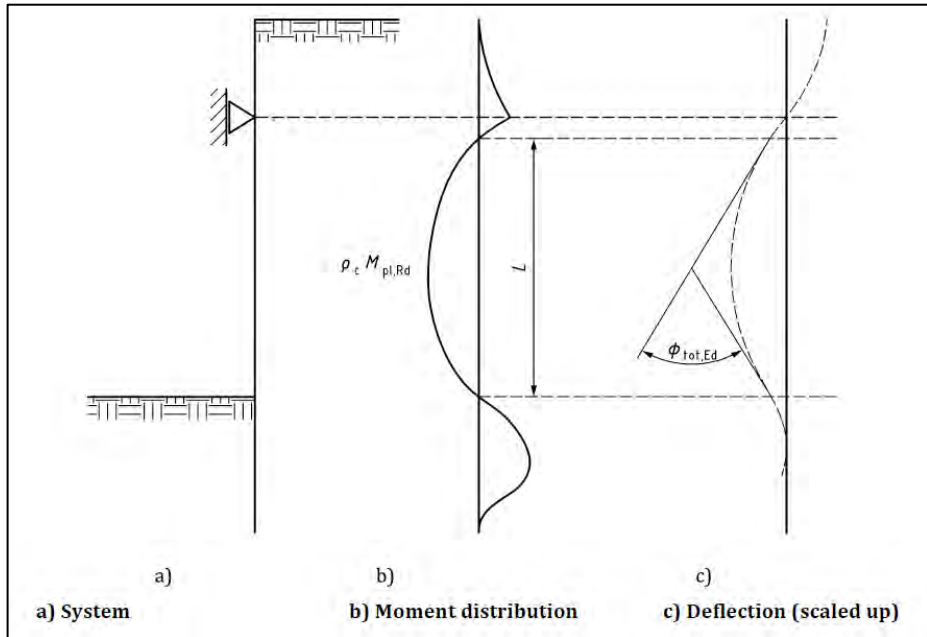


Figure 9 Definition of the total rotation angle  $\phi_{rot,Ed}$  using rotation angles (Figure C.3 in EC3-5)

Based on the calculated displacements of the wall the value of  $\phi_{Ed}$  may be found as

$$\phi_{Ed} = \phi_{w,Ed} - \phi_{wy,Ed} \quad (\text{C.4 in EC3-5})$$

with

$$\phi_{w,Ed} = \frac{w_2 - w_1}{L_1} + \frac{w_2 - w_3}{L_2} \quad (\text{C.5 in EC3-5}) \text{ illustrated in figure below and}$$

$$\phi_{wy,Ed} = \frac{u_{max}}{L/2} + \frac{u_{max}}{L/2} = \frac{4}{L} u_{max} = \frac{4}{L} \frac{5}{48} \frac{\rho_c M_{pl,Rd} L^2}{\beta_D EI} = \frac{5}{12} \frac{\rho_c M_{pl,Rd} L}{\beta_D EI} \quad (\text{C.6})$$

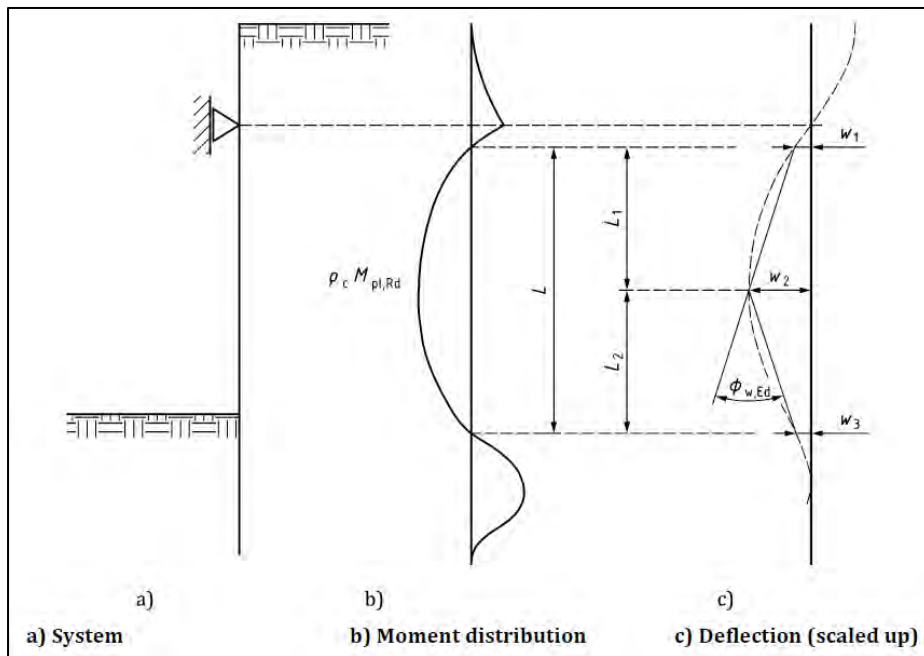
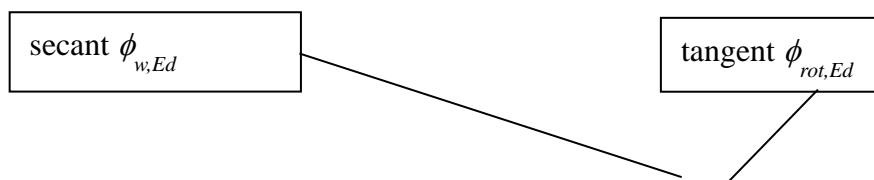


Figure 10 Definition of the total rotation  $\phi_{w,Ed}$  based on displacements (Figure C.4 in EC3-5). In the figure an example of a wall with fixed earth support is shown.

The two methods render completely same and exact result ( $\phi_{Ed}$ ) for a simply supported beam with a uniform load. The reason for this is, that the two terms in the expression for ( $\phi_{Ed}$ ) in (C.2) and (C.4) are both either based on the tangent angle (in C.2) or on the secant angle (in C.4) as illustrated in figure below.



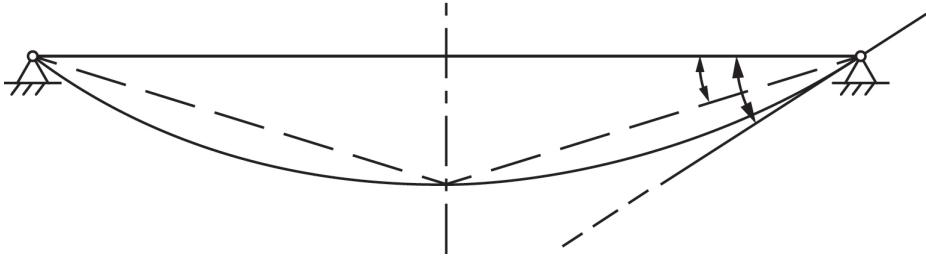


Figure 11 Secant and tangent rotation angles

However, when determining the necessary rotation by a LEM calculation it is practical to use the last/third method based on the displacements of the wall.

Considering three typical failure mechanisms in the figure below and comparing it with figure C.4 in EC3-5 it is a reasonable approximation to calculate the rotation for a wall with one yield hinge (free earth support) as

$$\phi_{w,Ed} = \frac{w_2 - w_1}{L_1} + \frac{w_2 - w_3}{L_2} \approx \frac{v - 0}{d} + \frac{v - v}{\infty} = \frac{v}{d}$$

For a wall with two yield hinges (fixed earth support), the rotation is calculated as

$$\phi_{w,Ed} = \phi_1 + \phi_2 = \frac{w_2 - w_1}{L_1} + \frac{w_2 - w_3}{L_2} \approx \frac{v}{d_1} + \frac{v}{d_2}$$

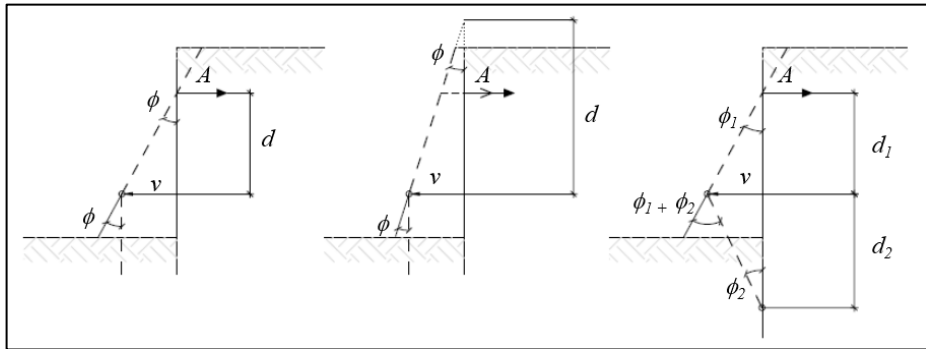


Figure 12 Rotation around rotation points by LEM failure mechanisms

## EXAMPLE

LEM calculation of anchored wall with one yield hinge.

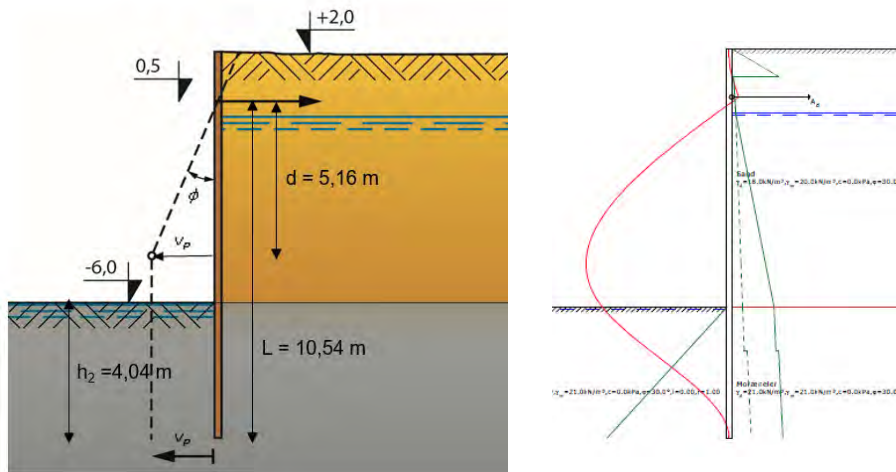


Figure 13 Wall with one yield hinge, bending moment and earth pressure distribution

Results of wall calculation

$$A_d = 212 \text{ kN/m (at level +0,5)}$$

$$M_{Ed} = 543 \text{ kNm/m}$$

Yield hinge at -4,66

Toe level = -10,04

$h_1 = h_a$  = wall height on back (active) side = 12,04 m ~ 12,0 m

$h_2 = h_p$  = wall height on front (passive) side = 4,04 m ~ 4,0 m

$d$  = distance between anchor and plastic hinge = 5,16 m

$L$  = distance from anchor level to toe level = 10,54 m

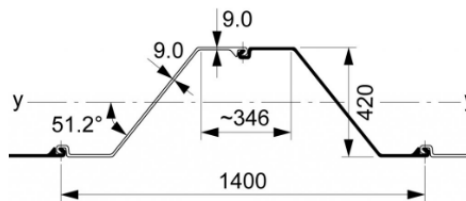
## Profile

AZ 18-700

S320 GP  $\Rightarrow f_y = 320 \text{ MPa}$

$E = 200.000 \text{ MPa}$

$I = 37.800 \text{ cm}^4/\text{m}$



### Cross section Class

$$\varepsilon = \sqrt{235/f_y} = 0,857$$

$$\lambda = b_f / t_f / \varepsilon = 346 / 9,0 / 0,857 = 44,9 \Rightarrow \text{Class 3, cf. Table C.1 in EC3-5}$$

Bending resistance

$$Z\text{-pile} \Rightarrow \beta_B = \beta_D = 1,0$$

$$W_{el} = 1800 \text{ cm}^3/\text{m} \Rightarrow M_{c,Rd} = M_{el,Rd} = \beta_B W_{el} f_y / \gamma_{M0} = 524 \text{ kNm/m} < M_{Ed} !$$

$$W_{pl} = 2116 \text{ cm}^3/\text{m} \Rightarrow M_{c,Rd} = M_{pl,Rd} = \beta_B W_{pl} f_y / \gamma_{M0} = 616 \text{ kNm/m}$$

$$\text{Possible reduction factor } \rho_c = M_{Ed} / M_{pl,Rd} = 543 / 616 = 0,88$$

( $W_{el} / W_{pl} = 0,85 \dots$  as usual and claimed)

### Rotation capacity $\phi_{cd}$

Draw the 88%  $M_{pl,Rd}$  line in the Figure C.1 by interpolation as shown in figure below.

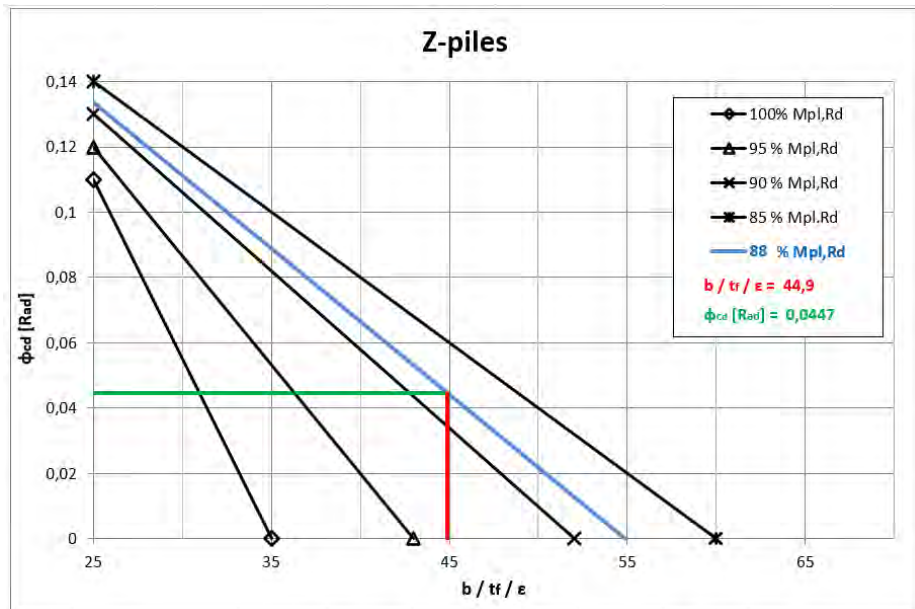


Figure 14 Determination of the rotation capacity  $\phi_{cd}$  for a given  $\rho_c$  and  $b/t/\varepsilon$

The intersection between  $\lambda = 44,9$  and the 88%  $M_{pl,Rd}$  line renders a design rotation capacity  $\phi_{cd} = 0,0447 \text{ rad} = 2,56 \text{ deg}$ .

Alternatively, using the new format of Fig. C.1 in EC3-5 from figure below:

$\lambda = 45$  and  $\rho_c = 0,88 \Rightarrow \phi_{Cd} \sim 0,045 \text{ rad} = 2,57 \text{ deg}$ .

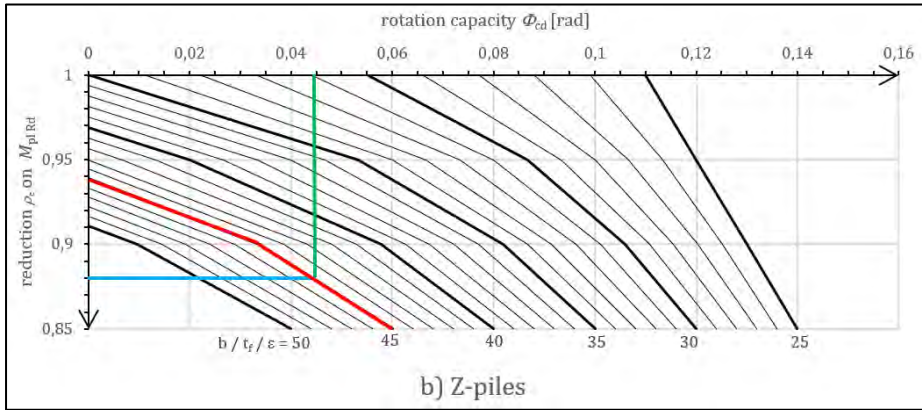


Figure 15 Determination of the rotation capacity  $\phi_{Cd}$  for a given  $\rho_c$  and  $b/t/\varepsilon$

### Mobilisation of plastic earth pressures

Back side (active side):

Assume  $v_a = 0,3\%$  of  $h_a = 0,3/100 \times 12,0 \text{ m} = 36 \text{ mm}$

Front side (passive side):

Assume  $v_p = 5\%$  of  $h_p = 5/100 \times 4,0 \text{ m} = 200 \text{ mm}$

$v = v_p = 200 \text{ mm}$

Required rotation  $\phi_{Ed}$  vs. rotation capacity  $\phi_{Cd}$

$$\phi_{w,Ed} = \frac{v}{d} = \frac{200}{5160} \text{ rad} = 0,0388 \text{ rad} = 2,22 \text{ deg}$$

$$\phi_{wy,Ed} = \frac{5}{12} \frac{\rho_c M_{pL,Rd} L}{\beta_D EI} = \frac{5}{12} \frac{543 \cdot 10^6 \cdot 10,54 \cdot 10^3}{2,0 \cdot 10^5 \cdot 37800 \cdot 10^4} = 0,0315 \text{ rad} = 1,80 \text{ deg}$$

$$\phi_{Ed} = \phi_{w,Ed} - \phi_{wy,Ed} = 2,22 \text{ deg} - 1,80 \text{ deg} = 0,42 \text{ deg} < \phi_{Cd} = 2,56 \text{ deg}$$

It is very close that the elastic rotation is enough. If the required displacement to mobilise the passive earth pressure is moderated to say 3% (i.e. 10 x the 0,3% for mobilising the active pressure), a thinner profile like AZ 17-700 being 5% less heavy could have been chosen.

### CONCLUSIONS

The reliability of the verification of adequate rotation capacity depends on the precision of the determination of the rotation capacity  $\phi_{Cd}$  as well as the necessary rotation  $\phi_{Ed}$ . EC3-5 provides an operational, approximate but experimentally well documented method of determining the rotation capacity,



whereas EC7-3 does not provide a similarly precise method for determining the necessary rotation. EC7-3 does give a recommended range of displacement rates to mobilise plastic earth pressures, but the values are a national choice. It is the hope and request from the author that the geotechnical engineers in Europe will work for a more comprehensive, consistent and operational (realistic) set of limiting criteria for mobilising plastic earth pressures in any kind of ground.

## **ACKNOWLEDGEMENT**

Thanks to the MG of SC7: Andrew Bond, Adriaan van Seters, Gunilla Franzén and Geert Kraijema for appointing me as liaison officer for SC7 in SC3/WG18 revising EC3-5. Also, thanks to the PT13 of SC3: Cecile Prüm, Colin Jacobs and Dirk Jan Peters for fruitful dialogue on content of EC3-5 and interface to EC7-3.

## **REFERENCES**

- [1] FprEN 1993-5:2024-05-24 Design of steel structures – Part 5: Piling (SC3 Doc N4006).
- [2] FprEN 1993-5:2024-06-24 Design of steel structures – Part 5: Piling, (No SC3 doc number, corrected version of N4006).
- [3] FprEN 1993-5:2024-07-23 Design of steel structures – Part 5: Piling (SC3 Doc N4032).
- [4] FprEN 1997-3:2024 Geotechnical design – Part 3: Geotechnical structures (SC7 Doc N1753), termed EC7-3 in the paper.

# DIGITALIZATION IN GEOTECHNICS

**Magnus Rømoen<sup>1</sup>**

## KEYWORDS

Digitalization, geotechnics, BIM, AI, data management, Gartner's hype cycle, keynote, NGM

## ABSTRACT

This paper explores emerging technologies in geo-engineering within the framework of Gartner's Hype Cycle, focusing on the adoption and practical application of digital tools in the Nordic region. It examines the progress of Building Information Modelling (BIM), highlighting its benefits and challenges in geo-engineering, particularly in data modeling and standardization. The paper also delves into Artificial Intelligence (AI), including machine learning and digital twins, evaluating their potential and current limitations. Furthermore, it underscores the critical role of data management in advancing these technologies and discusses NGI's development of tailored digital solutions for improved data handling and project efficiency. The study concludes that while significant advancements are being made, further development of digital skills, particularly coding, is essential for continued progress.

## INTRODUCTION

The purpose of this paper is to present a few emerging technologies within geo-engineering in relation to the Gartner's hype cycle. The paper also looks into some fundamental requirements for any novel and data-driven technology to succeed in the world of geo-engineering.

The paper does not address the most advanced ongoing research and development but focuses on the development within the daily use of digital tools for geotechnical engineers in the Nordics.

<sup>1</sup> NGI – Norwegian Geotechnical Institute, Sandakerveien 140 0488 Oslo, [magnus.romoen@ngi.no](mailto:magnus.romoen@ngi.no)

## EXPECTATIONS AND REALITY THOROUGH THE DEVELOPMENT OF NEW TECHNOLOGIES

### Gartner's Hype Cycle

Gartner's Hype Cycle [1] is a graphical representation that illustrates a common pattern that arises with new technologies. The graph combines the hype level curve, arising from a novel technology, and the typical curve of engineering or business maturity. The hype level curve, the maturity curve and the combined hype cycle is shown in figure 1. On all graphs the X-axis shows time.

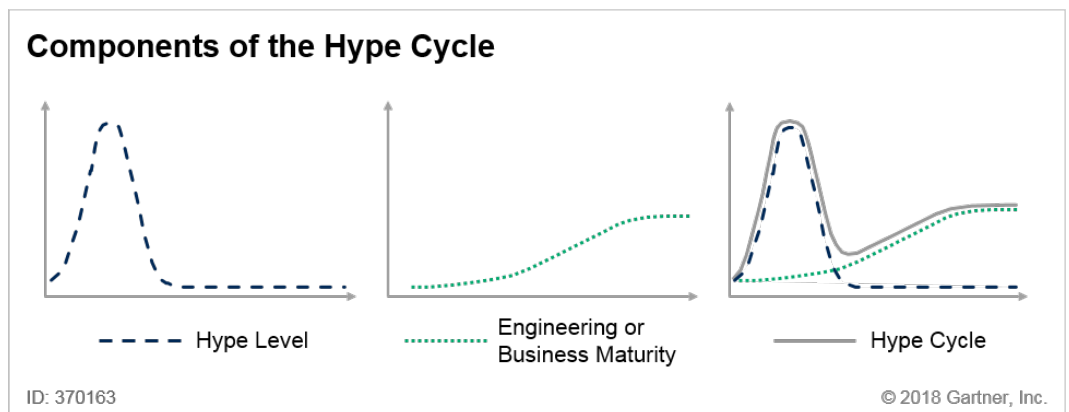
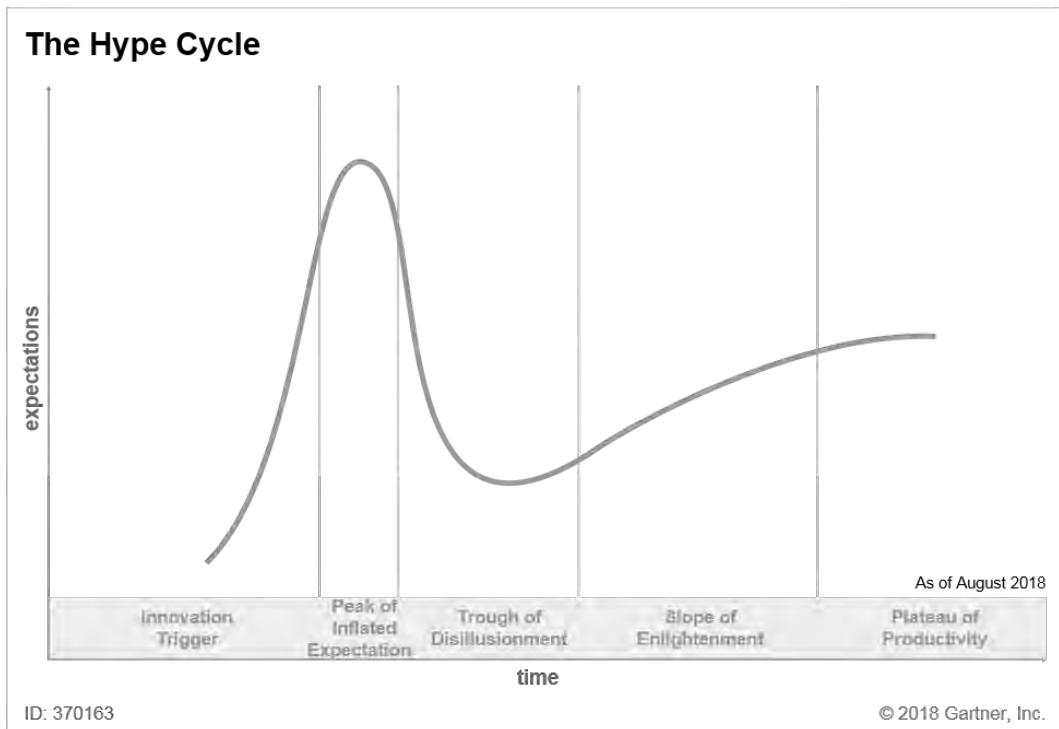


Figure 1 Principle of the hype cycle [1].

Gartner's Hype Cycle is a valuable tool for organizations navigating the complexities of digitalization. It provides a framework for understanding the lifecycle of emerging technologies, enabling better strategic decisions and more effective digital transformation initiatives. It is also a good reminder of the struggle many technologies experience in the phase between very high expectations in an early phase and the final phase where the full potential of the technology is obtained.

The hype cycle can be divided into different stages, which shows the road to productivity, as shown in figure 2.



*Figure 2 Different stages of the hype cycle [1]*

### **Adoption for geoengineering technologies**

In his keynote for the 5<sup>th</sup> International Conference on Information Technology in Geo-engineering, Erharter [2] assessed several geo-engineering technologies and their position in the hype cycle during spring 2024. The assessment is given in figure 3.

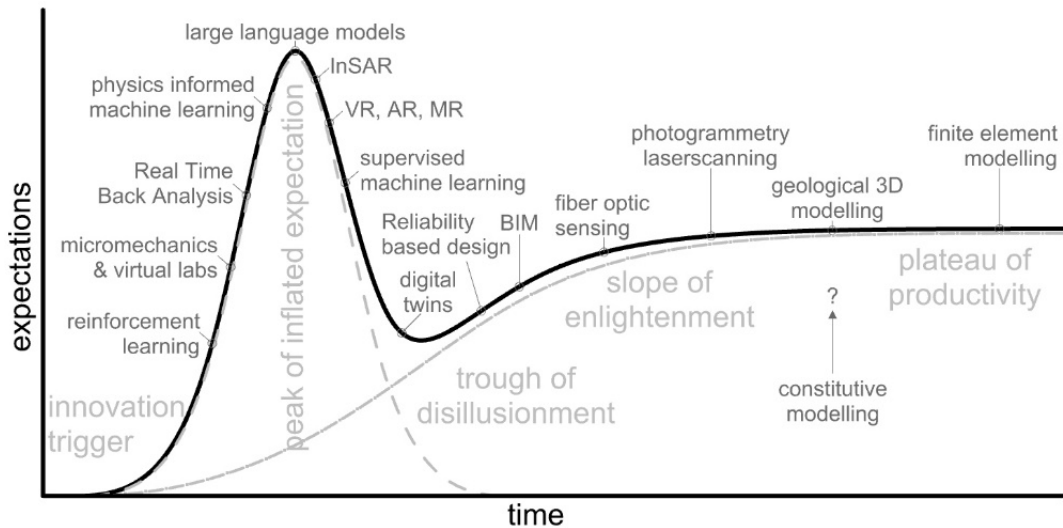


Figure 3 Assessment of geo-engineering technologies in the hype cycle

It is important to emphasize that this is a subjective assessment of the different technologies made by the author. The actual position for each technology is also influenced by factors such as geography, time of assessment, and for what field within engineering that is considered.

Even though, this is still a state-of-the-art assessment for how far we have come in digitalization within geo-engineering.

## BIM – BUILDING INFORMATION MODELLING

### Introduction to BIM

Building Information Modelling (BIM) is a process involving the creation and maintenance of a digital 3D-model which includes a set of information properties embedded in the model. The information describes the physical and functional characteristics of the asset, such as materials, demands, execution of construction, maintenance, etc when it comes to both construction and operation phase. A full BIM model can therefore be seen as a replacement of a combination of 3D-models, drawings and to some extent also the written report.

BIM has been used in the Nordics for several years already, and as in the rest of the world, the development seems to have been pushed by projects working with the construction of buildings rather than linear infrastructure.

There are several advantages with BIM, highlighted by Borrmann et. al. [3]:

- Better visualizations
- Improved collaboration
- Increased productivity
- More accurate documentation
- Enhanced coordination
- Cost and time savings
- Better lifecycle management
- Improved quality

All these benefits are probably more applicable in a situation where the full potential of BIM is utilized. As shown earlier in figure 3, Erharter assessment predicts that BIM has passed the hype peak but is yet to reach the full plateau of productivity.

From personal experience gained over the past years, both the general focus as well as utilizing BIM in the construction phase has increased. Especially early in the projects, the client or contractor wants to use BIM for the construction. What often happen though, as the start of the construction work is getting closer, is that the wish or need for supplementary drawings arises and sometimes even removes the wish for BIM. This is sometimes also due to different wishes and expectations in the client or contractor organisation. The people making the early decision has another wish than those responsible for the construction. As a result, BIM models tend to be more used in the design phase than in the construction phase.

### **BIM for geo-engineering**

For the modelling part, BIM-models for geo-engineering can roughly be divided into three different types of models:

- Factual data models
- Interpretation models of the stratigraphy/layering
- Geo-structures, for examples sheet piles, deep-soil-mixing etc.

The factual data models are 1D or 2D models with results from soundings, lab-tests, observations, geophysical surveys etc, while the interpreted models give a 3D-model of the geological, geotechnical or hydrogeological conditions.

### **The M in BIM - modelling**

In recent years, Leapfrog Works has gained traction in the industry for creating a combined factual and interpreted model of the soil and/or bedrock. However, a limitation with the current version of the software is that it cannot natively produce a project-specific property set during IFC export and hence is a simple 3D-model instead of a full BIM-model.

There is several other software that also can be used alone or together, making these factual and/or stratigraphy models. Erharter et. al. [5] for example, shows how one can combine different software to make such models for a large linear project. In his work a combination of MOVE, Rhino/Grasshopper and BricsCAD BIM is used.

One challenge when going from factual data models to interpretation models is communication of uncertainty. With borehole data gathered in 1D or 2D, and models illustrated in 3D, one must perform e.g. linear interpolation or use geostatistical methods such as kriging to model the full 3D geometry. This yields a 3D model where the modelled geometry in between the data points is, at best, inaccurate. This fact is often obvious to the geotechnical engineer but may not be so for the client, contractor or other designers using the geotechnical model as baseline for further design, such as mass balance calculations. NGI have used colour-coding, as shown in figure 4 to communicate uncertainty in 3D geometry. Here, the colour in the 3D-model gets lighter with the increasing distance from the borehole.

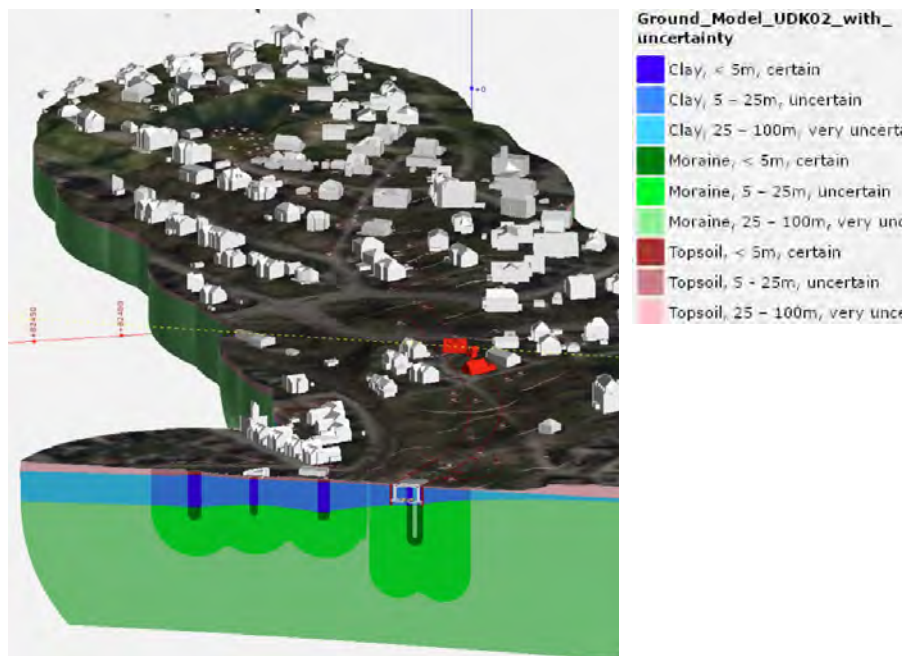


Figure 4 Communication of uncertainty [4]

When it comes to the geo-structures, there has been a shift over the last couple of years. Traditionally, the 3D modelling was a highly manual and time-consuming process. However, with the use of parametric modelling techniques in software like Rhino/Grasshopper and Revit/Dynamo, things have changed a lot. Parametric programming involves creating complex geometric

models using variables and mathematical rules, allowing the model to be easily adjusted and modified by changing parameter values.

Development of the parametric programming scripts will (likely) take some time for the first model. This will normally give a larger time use for the first model. But as there is need for the first revision of the model, the code can be re-used and the designer will save time for each new revision. The scripts are also re-usable for other projects and will therefore definitely be time- and cost-cutting over time.

This has also drastically changed the timing of delivery for the geo-structure models. While most of the models earlier were created and delivered at the end of the design phase, to avoid re-making every time there was a change, the models are now created as early as possible in the project. This enables communication of the approximate presence, location and size of geo-structures to the other disciplines in the interdisciplinary model. This will also give an early assessment of the quantities from the geo-structures, and hence also the cost.

### **The I in BIM - information**

The property set in the BIM model always contains a value for MMI (model maturity index) or LOD (level of development), which gives a pre-defined value on how developed the model is. And as the model evolves with the project, the MMI or LOD changes with it, from for example “early phase” to “ready for construction” and at the end “as built”. A typical example on the different levels given for the MMI is established in the Norwegian “MMI guide” [20], which is a collaboration between several large governmental organizations and organizations for engineers, architects and contractors to establish a unique system for MMI in Norwegian construction projects.

When it comes to the information given in the BIM models, there is one large challenge: standardization. Very often the property sets are customized and unique for each project, which is challenging when it comes to data sharing and project lifecycle management.

One reason for this, is a limitation in the data schema for the IFC-format. The current version, IFC 4.3 given in ISO 16739-1:2024 [6], does not contain data sets for geo-elements. Hopefully this will be included in future IFC 4.4-version, which will be an important step forward when it comes to BIM-models within geotechnics.

At the same time, do we have to have everything the same at each project? As geotechnical engineers, when making drawings or models for the contractor, we have a lot of requirements and demands when it comes to the execution of the work. This is very often linked to standards but can also be project specific demands that are annotated on the various drawings. This is for example



typical rules when it comes to sequence of work, execution of work, temporary solutions etc. This information is essential during execution, but not so after the construction is completed. We often also want to limit the amount of information in the models the contractor is using as basis for the construction, to prevent an information overload and that the important information disappears.

On the other hand, what is important to have after completion is a good documentation of what was actually installed in the ground and the location and properties of this. The as-built must be in a “language” that everybody can understand, meaning that we must make understandable and precise as-built models that can be understood and used by everybody in the future.

This difference in the needs when it comes to the information in the models, makes it highly relevant to think of different data sets should be used in different stages of the project. This challenge may be one of the reasons why BIM models in many projects are not used in the actual construction phase.

## **AI – ARTIFICIAL INTELLIGENCE**

Artificial intelligence (AI) is a current buzzword within both daily life and digitalization. For many, the term AI is linked to either ChatGPT or similar large language model (LLM), or to the stories about deep fakes in the news. But AI is a lot more than that. The Norwegian Consulting Engineers Association (RIF) divides AI into four different categories [7] which are “recognisable for engineers”:

- Data analysis
- Generative AI
- Generative design
- Digital twin and sensor data

### **Data analysis**

Data analysis is classic recognition of the content of an object, where you have an input and the AI helps understanding this input. This can also be called machine learning (ML) or supervised machine learning. Relating this to geotechnical engineers, this can for example be interpretation of site investigation, correlations based on different types of site investigation etc.

Data analysis through machine learning is probably what we have seen most examples of when it comes to AI within geo-engineering. As shown in figure 3, ML is evaluated to be over the highest hype, but the full potential is so far not reached.

The maybe most used application for ML in geotechnics has been using it for interpretation of soundings. Kydland et. al. [12] showed how they used ML

for automizing the interpretation of stratification in soil based on the results from Norwegian total soundings. The work is done based on approximately 170.000 soundings executed all over Norway, where the algorithm has been trained on data from CPTUs, soil samples and drilling logs. Through APIs (application programming interface), the interpretation is used in software for either calculations or modelling of the ground conditions.

EMerald Geomodelling is a company using ML to get the best out of a combination of airborne resistivity measurements and site investigations. In one of their projects [13] they have combined the results from helicopter based electromagnetic survey, with existing geotechnical site investigations. Combining these two, they get a 3D-model with a given probability of quick clay, shown in bottom left in figure 5. Based on this they can also extract the volumes having the largest probability for quick clay, bottom right in the same figure.

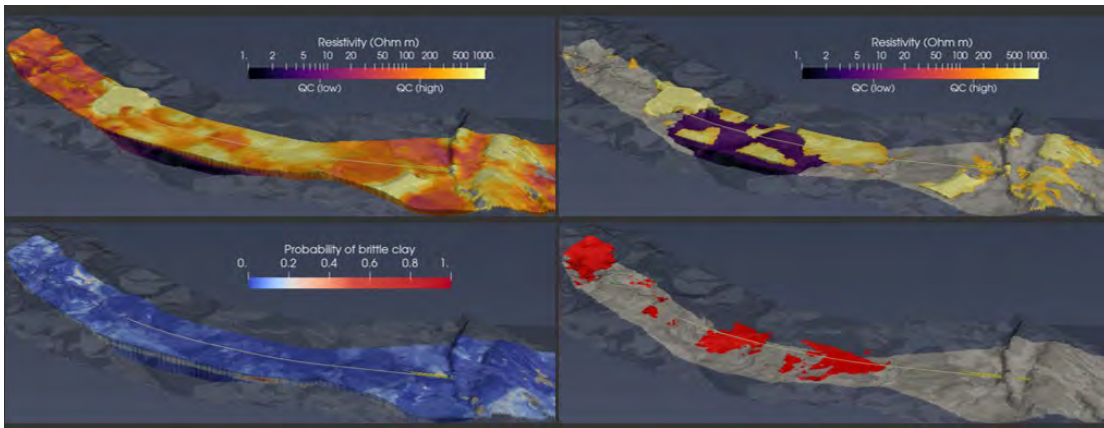


Figure 5 Bedrock and probability for quick clay, from [13].

Ten noorden van de Waddeneilanden Wind farm Zone is a project covering roughly 120 km<sup>2</sup> in the sea north of the Netherlands [14]. Site investigations included CPTs and sampling in 106 locations and almost 200 seismic lines. Combining these data, NGI together with Sand Geophysics used ML to predicted synthetic CPT data across the full 3D of the area. This provides the designer a possibility to obtain the parameters needed for the wind turbine foundation design at any location, making it possible for optimized design for the entire area.

## Generative AI

This category includes e.g. LLMs and the automatic generation of pictures and videos. A perhaps underrated feature, which is highly relevant for geotechnical engineers, is that the generative AI also can help generating code, which again can be used in for example ML or handling of large data sets.

Going back to figure 3, Erharter has placed the LLMs at the peak of the inflated expectations. Which means the hype is at the top, but we are still far from taking out the full potential of the technology.

An example on the use of these LLMs is the worked recently shown on LinkedIn by Henning Frodahl Firman [18]. Here, he developed a web application that incorporated a standalone GPT that is used in the process of searching for certain types of reports (in this case Factual geotechnical report) in a folder system. The application finds the reports, while ChatGPT helps the user in structuring the information found by the application.

### Generative design

Generative design is a design optimization, for most maybe know through software like Autodesk Forma (earlier Spacemaker) [8] or Infraspaces [9]. The key here is also that the machine learns from the design, which differs it from a parametric design. This is so far not much used within geotechnics, but there is a clear potential here when it comes to design optimization and material optimization.

### Digital twin and sensor data

The last one is digital twins and sensor data. Or as some call it, the modern and digital observational method. The exact definition of a digital twin is somewhat up for discussion, depending on if there is a two-way real-time data integration or not. Fuller et. al. [10], see figure 6, differs between a digital mode, a digital shadow and a digital twin based on how the data flows between the physical and digital object. Another definition is made by DNV GL, given in figure 7 [11], where one operates with different levels. With reference to figure 6 one can say that level 0 is BIM, level 1 and 2 are a digital shadow, and level 3, 4 and 5 are a digital twin.

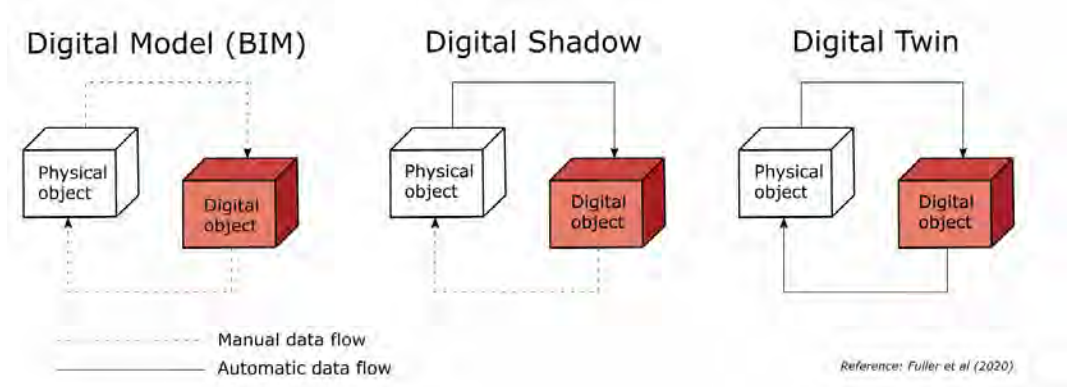


Figure 6 From BIM to Digital twin, after [10]

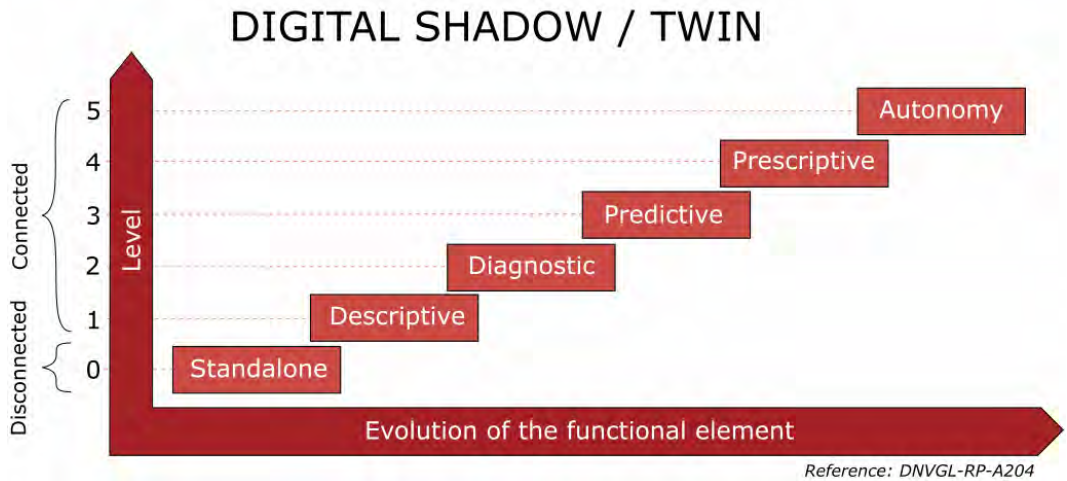


Figure 7 Levels of digital twin, after [11]

Piciullo et al. [19] shows how one can combine real-time hydrological monitoring, public metrological data and automated numerical modelling for a live prediction of the safety factor for a natural slope. In the foot of the slope there is a double track railroad, and the real time safety factor of the slope is there important during heavy rain. This case is a good example of a descriptive digital twin, according to the different levels given in figure 7.

Digital twins and sensor data has an unleashed potential when it comes to the use in geo-engineering. This is the technologic observational method and will have a large impact on geotechnical design an execution in the future. Even though there has been a lot of talk about it, it is still somewhat surprising that this have not had a larger impact on the geotechnical projects already. That might also be the reason why Erharter in figure 3 have placed digital twins in the “trough of disillusionment”. We are well over the over hyped phase where everybody talked about digital twins, but we have not managed to take out the potential in the technology.

## DATA MANAGEMENT

### Historic data management

As geotechnical engineers, we have been used to combine data and result from several different sources in our projects. As an example from NGI, 10 years back, the result from site investigation were stored in one proprietary software and the interpretation of the soundings in another one (or in an Excel spreadsheet). The data from the lab was in several PDF and/or Excel files, while monitoring data was in both a software and in excel spreadsheets. If one had some field observations, this was stored in an Excel or Word file, hopefully in the same folder as the pictures taken in field.

Using data from these different sources kind of worked while working with the project. But going back and find details in these bad data structures years or decades after can be a nightmare. This limits in many cases the potential to reuse this data, which is not only economically poor, but a lot of this data could also had been used for development within geotechnics. As an example, for decades different correlations within geotechnical engineering are developed, correlations that could have been improved and further developed if one had access to all data located on the servers in the industry.

Going back to figure 3, data management is not rated as a technology itself. But data management is basis for many of these technologies, and the quality of the data is essential for many of them. For some of these technologies it is also reasonable to say that the time between the “peak of inflated expectation” and the “plateau of productivity” is longer than it could be, since the data quality and the structure of data is limiting the development. Going back to the two previous examples in this article: what limits the development on BIM is the data set in the BIM models, and what AI is 100% dependent on is the data set that AI either should be trained on or should help the user understand.

### **Improved data management**

To have better management of all the data NGI produces through our own field department, 3 soil and rock labs and 2 instrumentation sections, an internal work started 5-6 years ago to investigate alternative solutions. This work concluded that relaying purely on external software would not solve the demands NGI had set for its data management. This was both because we did not get a good enough structure and system on the data, but also that we did not get the interface to the data that we wanted. We also did not want to rely only on large international companies where we would be bound to both their strategic choices and their licenses. A strategic decision was therefore made that we would start developing our own software for many of the core data producers at NGI, in addition to keep using some off-the-shelf software. This has resulted in numerous cloud-based applications in what is called NGI's GeoHub, see figure 8.

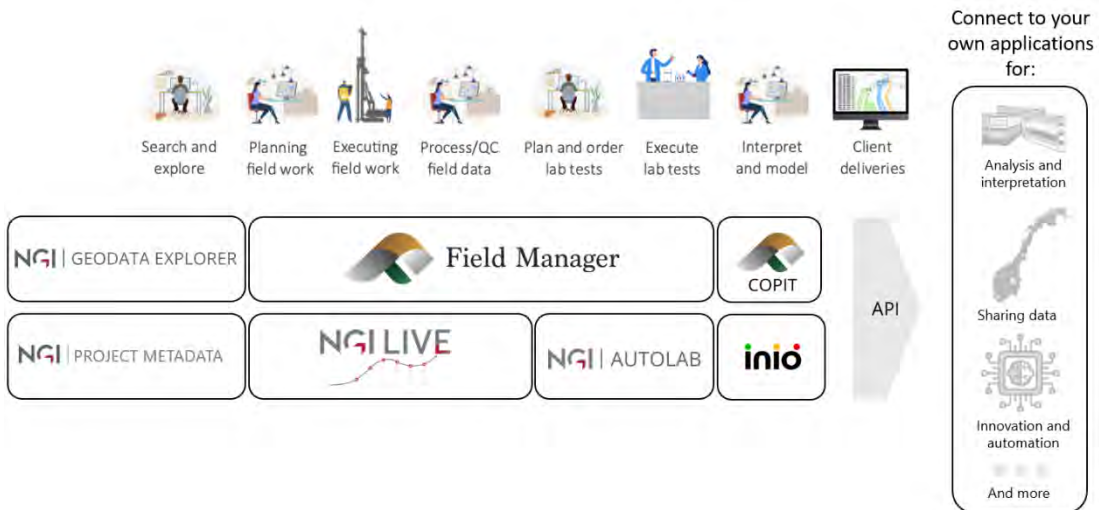


*Figure 8 Overview of the NGI Geo Hub*

In the following, some of the main part of the Geo Hub will be shortly explained.

Field Manager [15] is a web-based tool with API connectivity for the entire value chain for geotechnical site investigations. The tools improve the collaboration between field operators, engineers, clients and other stakeholders, where everybody can access the progress of the campaign and the status and results of each borehole. The data is assessed and approved by the engineers, ensuring a high data quality. Field Manager is the first ever software developed by NGI which is also open for sale as a SaaS (Software as a Service), and so far, more than 1000 unique users are registered.

AutoLab is developed to process data from advanced tests performed in the rock and soil lab. The software improves processing of lab data from start to end, enhancing the overall delivery and storing the data in a structured way. This has been a large step forward, digitalizing the workflow for all advanced lab tests.

NGI Live is an online monitoring service for field sensor measurements. It has a project specific dashboard from Grafana, further enhanced at NGI with a map plugin and alerting system. The system is so far used on 35 different NGI projects, containing app. 13600 sensors and 78 different sensor types. NGI Live has not only improved to storage of sensor data, but it has also improved how we present our monitoring data to the client and given us a whole new flexibility in the user-interface.

COPIT is NGI's internally developed CPTU interpretation software. The software seamlessly connected to both Field Manager and AutoLab through APIs,

which makes it easy to import the data one need for the interpretation. The software makes it possible for the user to do manual interpretation of the CPTUs or use correlations such as e.g. Karlsrud et. al [16] or Paniagua et al [17].

The possibilities through APIs and the use of these are essential for all the software in the GeoHub family. We geotechnical engineers have always dealt with and worked with correlations, and having easy access entry point into these databases will give us unique opportunities to further develop and create new such correlations. Additionally, as we increasingly build in densely populated areas, being able to easily share data about ground conditions and existing underground structures between these projects is crucial for reducing costs related to ground investigations and creating predictability regarding what is already underground for new projects. Perhaps underground structures, whose location and properties are well documented, can also be reused in new projects on adjacent plots.

## CONCLUSION

This paper has, with the basis of Gartner's hype cycle, presented two different technologies which the geotechnical engineers have adopted in recent years, and which they will meet more and more in the future. The paper also presents the importance of good data management, which is a key for further technology development.

Even though the focus in this paper has been mainly on Norway and partly on the Nordics, it has also come clear that there are endless number of initiatives and development going on worldwide. A key for these initiatives and developments seems to be two aspects: geo-engineers with large digital curiosity and support from management/upper management.

To increase the digital curiosity amongst geo-engineers, it is important to help them develop especially one important tool: coding. This is a key for developing skills that is needed for much of the digital development which is presented earlier. It is also a key in optimizing other part of a geo-engineer's daily work. There is a lot of possibilities on optimizing and improve simple and potentially repetitive working processes with coding and programming.

Support from management and upper management is, as mentioned, the other key. Almost every company these days has digitalization as part of their strategy, but not all companies manage to put word into action. The funding for digital development might sometimes be reduced because of securing enough revenue for the company, but in these cases the digital development will probably also stop, or the initiator will in worst case find something else to do. To make sure that these initiatives manage to grow, management/upper management must be both supportive and have funding for the initiatives.

At the same time, one should not throw away money on every digitalization initiative within the company. And assessment of the initiatives and the value of these is needed. Which takes us back to Gartner's hype cycle. The hype cycle can as mentioned be a good tool to assess the engineering or business maturity of the initiative, and help decided if this is the right time to invest in development or not.

## ACKNOWLEDGEMENT

First of all, a thank you to NGM 2024 for asking me to present a keynote and write this paper. It has given me a perfect opportunity to dive into some more details within digitalization, that have been on my mind for a while.

Also, a big thank you to several of my good colleagues for useful input and discussions around the paper, especially Georg Erharter and Mats Kahlström. You have been of great help.

Finally, I want to thank Andi Pfaffhuber and Craig Christensen in Emerald Geomodelling, Niklas Engebretsen in Cowi AS and Henning Frodahl Firmann in Norconsult AS for sharing some experiences and content that I can use in both the paper and presentation.

## REFERENCES

- [1] Understanding Gartner's Hype Cycles:  
<https://www.gartner.com/en/documents/3887767>
- [2] G. H. Erharter: Digitally Empowered Geoengineering Toolbox: From AI-Driven Lab Data Interpretation, BIM Ground Modelling to Parametric Design. Keynote at the 5<sup>th</sup> International Conference on Information Technology in Geo-engineering
- [3] A. Bormann, M. König, C. Koch and J. Beetz: Building information modelling: Why? What? How?: Technology Foundations and Industry Practice
- [4] Faglig Onsdag #18 - "Geologi og beredskap – kommunikasjon av usikkerhet":[https://www.youtube.com/watch?v=6cNBc8XIJ30&list=PLN9yYGLszezTpuxfxBxvZ0zr82W6si\\_L7&index=13](https://www.youtube.com/watch?v=6cNBc8XIJ30&list=PLN9yYGLszezTpuxfxBxvZ0zr82W6si_L7&index=13)
- [5] Erharter, Georg H.; Weil, Jonas; Bacher, Lisa; Heil, Frédéric; Kompolschek, Peter (2023): Building information modelling based ground modelling for tunnel projects – Tunnel Angath/Austria. In Tunnelling and Underground Space Technology 135, p. 105039.  
<https://www.sciencedirect.com/science/article/pii/S0886779823000597?via%3Dihub>



- [6] ISO 16736-1:2024: Industry Foundation Classes (IFC) for data sharing in the construction and facility management industries.  
<https://www.iso.org/standard/84123.html>
- [7] Faglig Onsdag #30 - "åpenBIM og kunstig intelligens":  
[https://www.youtube.com/watch?v=a3EnDDG7kE4&list=PLN9yY-GLszezTpxufxBxvZ0zr82W6si\\_L7&index=3](https://www.youtube.com/watch?v=a3EnDDG7kE4&list=PLN9yY-GLszezTpxufxBxvZ0zr82W6si_L7&index=3)
- [8] Autodesk Forma: <https://www.autodesk.com/products/forma/overview?term=1-YEAR&tab=subscription>
- [9] Infraspaces: <https://www.infraspaces.tech/>
- [10] A. Fuller, Z. Fan and C. Day: Digital Twin: Enabling Technologies, Challenges and Open research. 2020
- [11] DNV GL: Assurance of digital twins. Report DNV-RP-A204, October 2023
- [12] T.Kydland, H. Firman and K. Aunaas: GEOTOLK-Tolkning av totalsonderinger med maskinl ring. Geoteknikkdagen, 2021
- [13] Emerald Geomodelling: Customer story: Gaining information regarding geological conditions and probabilities for quick clay and other brittle clay materials through airborne geoscanning. <https://www.emerald-geomodelling.com/news/customer-story-norwegian-water-resources-and-energy-directorate>
- [14] Ten noorden van de Waddeneilanden Wind Farm Zone animation: <https://www.youtube.com/watch?v=JEenpiAU8Mk>
- [15] Field Manager homepage: <https://www.fieldmanager.io/>
- [16] Karlsrud K, Lunne T, Kort DA, et al. (2005) CPTU correlations for clays. Proceedings of the international conference on soil mechanics and geotechnical engineering, Rotterdam: Balkema, 693–702.
- [17] Priscilla Paniagua, Marco D'Ignazio, Jean-S bastien L'Heureux, Tom Lunne and Kjell Karlsrud: CPTU correlations for Norwegian clays: an update. AIMS Geosciences 2019, Volume 5, Issue 2: 82-103.
- [18] Firman, Henning Frodahl: [https://www.linkedin.com/posts/henning-frodahl-firman-7447a862\\_jeg-har-laget-noe-g%C3%B8y-og-nyttig-](https://www.linkedin.com/posts/henning-frodahl-firman-7447a862_jeg-har-laget-noe-g%C3%B8y-og-nyttig-)

applikasjon-activity-7225222803350855680-7C-  
f?utm\_source=share&utm\_medium=member\_desktop

- [19] Luca Piciullo, Mine Treesa Abraham, Ida Norderhaug Drøsdal and Erling Singstad Paulsen: A fully operational IoT-based slope stability analysis. Manuscript for Environmental Modelling and Software
- [20] MMI guide: <https://mmi-veilederen.no/>



# **MITIGATING VOLCANIC HAZARDS ON THE REYKJANES PENINSULA - LAVA FLOWS AND PROTECTION OF INFRASTRUCTURE, THE GRINDAVÍK SAGA**

**Jón Haukur Steingrímsson**<sup>1</sup>

## **KEYWORDS**

Volcano, lava, infrastructure, eruption

## **ABSTRACT**

Geological evidence shows that volcanic activity on the Reykjanes peninsula follows a periodical pattern with several decades of dormant periods intercepted by shorter volcanic episodes. In 2021 the first eruption in approximately 780 years happened, marking the onset of a new active period. The greatest activity has been near the town of Grindavík and the geothermal area in Svartsengi. To protect the town and power production installations a vast network of lava deflection barriers has been constructed to protect these locations. The barriers extend over 12 km with a fill volume in the range of 2,4 million m<sup>3</sup>. Since November 2023 lava flow from a series of five eruptions have successfully been deflected. Over 10 km of roads have been laid out on fresh lava fields only few days old and a network of central heating hot-water pipes, cold-water pipes and power lines have been successfully restored under very demanding conditions. This paper aims to tell the story of the eruptions and measures undertaken to either protect or reinstate the vital infrastructure, rather than to provide a full scientific account of the situation at hand. As of August 2024, the event is still ongoing, the next eruption is to be expected and the future remains uncertain for the population.

## **INTRODUCTION**

Iceland is situated on the Mid-Atlantic ridge that forms the divide between the North American and Eurasian continental plates. The ridge is a divergent plate boundary where the two continents spread apart by roughly 2 cm per year. As the continents drift apart magma flows to the surface feeding a belt of volcanic systems stretching diagonally across the island. Iceland also hosts an additional uplift by a mantle plume that coincides with the divergent plate boundary and forces it into a slight bend. The oldest rock formations are

<sup>1</sup> Efla Consulting Engineers

about 15 million years old on the west and the east coasts. The youngest rocks follow the active volcanic belt coming ashore on the Reykjanes peninsula, crossing the central highland to the northeast coast where it connects the Jan Mayen ridge via system of transform faults.

Iceland is in a way an infant with very active geology and associated earthquakes and volcanic eruptions, as well as other natural hazards such as landslides, avalanches, floods, storms, and recently, a variety of climate-change induced hazards. Since 2021 a total of 8 volcanic eruptions have occurred on the Reykjanes peninsula affecting greatly the population, especially in the town of Grindavík.

## **REYKJANES PENINSULA**

The Reykjanes peninsula is a direct continuation of the Mid-Atlantic ridge. Series of volcanic systems lie along the peninsula in an echelon pattern under a 40-45° angle to the main rift axis. That angle is partly caused by the curvature of the Mid-Atlantic plate divide through the island and is a combination of a rift zone and a transform fault, essentially a leaking transform zone. It is a matter of an opinion how many volcanic systems are to be defined as individual systems along the peninsula and how well they are connected. For the current paper the systems are regarded to be six in total. The volcanic systems appear to follow a periodical behaviour showing active periods of roughly 400–500 years and intersected with substantially longer dormant periods of 600–800 years (Sæmundsson et al., 2013 & 2020). For the past three volcanic cycles at least four of these systems have been active, while the remaining two behave more sporadically. The latest active period on Reykjanes peninsula was from AD ~800–1240, and for the system closest to Grindavík from 1210 - 1240. Large portion of the peninsula are covered by lava formations that have been produced over the last 14,500 years, or since after the glacial retreat.

Inhabitants of the Reykjanes peninsula are ~30,000, with the majority living in several towns on the northwestern part of the peninsula. Grindavík is the only major settlement in the southwestern part with ~3,600 inhabitants prior to the evacuation of 2023 and is the second most valuable fishing harbour in Iceland. The area also hosts the Keflavík international airport and the well-known Blue lagoon geothermal spa. Two major power plants are located on the peninsula utilizing geothermal power and producing electricity and supplying hot water for central heating for the region, one of them in Svartsengi close to Grindavík.

## REYKJANES AWAKENING

After 780 years of volcanic quiescence on the Reykjanes peninsula, an episode of seismic and later volcanic unrest started in December 2019 that is currently ongoing. Most of the activity has been concentrated around the mountain Fagradalsfjall and Svartsengi geothermal field. Historically there has been a debate on whether those are to be regarded as two separate volcanic systems or not. The seismic unrest started near Svartsengi 4 km north of Grindavík and later moved towards Fagradalsfjall where the first eruption occurred in 2021 (Sigmundsson et al., 2022). This first eruption went on for over six months with rather moderate or small magma flow of 7–15 m<sup>3</sup>/s and became a major tourist attraction. Petrographical analysis showed that the magma originated from a substantial depth of 10–15 km (Halldórsson et al., 2022), while the seismicity around Svartsengi was related to an accumulation in a potential magma reservoir at shallower depths, or some 5 km.

After 14 months of earthquake swarms associated with magma intrusions, possibly at shallow depth and with the general knowledge of the periodical volcanic behaviour of the Reykjanes peninsula, the Department of Civil Protection and Emergency Management of the National Commissioner of the Icelandic Police (NCIP) (hereafter referred to as the Icelandic Civil Defence) put together a team of engineers and scientists to map out vital infrastructure that might be threatened or affected by potential eruption and to portray the possible mitigation methods. The work started in February 2021 with immediate analysis of previous eruption sites, extends of older lava flows, potential lava volume, flow rate and general behaviour of the lavas. Narrowing down the most likely eruption sites, series of lava-flow simulations were carried out by several different methods and a ground plan laid out for barrier system that could compensate a selection of scenarios. The constructability, availability of material and suitable machinery had to be analysed to assess realistic mitigation actions with regards to large uncertainty and most likely a very restricted time frame.

The eruptions at Fagradalsfjall were located well away from any infrastructure and the non-violent behaviour of the first eruption provided a unique opportunity for Icelanders and tourists to witness a relatively small and confined eruption. Although not causing immediate threat to infrastructure, the vast number of visitors caused serious strain on the Icelandic emergency response system as thousands flocked towards the volcano in all weathers. The eruption also provided an opportunity to study the lava flows and to calibrate lava-flow modelling by real-time event. Furthermore, a series of trial barriers were constructed that gave immensely valuable experience for the upcoming events in 2023.

The first eruption at Fagradalsfjall lasted for 6 months. In 2022 and 2023 similar but smaller and shorter eruptions followed. Those required a significant

response due to massive tourist interest and widespread moss fires that followed the 2023 eruption.

## **INCREASED ACTIVITY NEAR SVARTSENGI AND GRINDAVÍK**

On October 24th, 2023, yet another major earthquake swarm started north of Grindavík, with the centre slightly NW of the power plant area in Svartsengi and the Blue Lagoon resort. This area was quite active prior to the volcanic eruption in Fagradalsfjall in 2021, but as events unfolded near Fagradalsfjall in 2021-2023 the Svartsengi area showed much lesser activity. Simultaneously fixed GPS stations showed increased horizontal and vertical displacements indicating ground inflation that were confirmed by InSar satellite data. These events were soon interpreted by the Icelandic Meteorological Office (IMO) and other scientific parties as a magma intrusion that progressed with continuous surface inflation and varying seismicity. On November 10th the seismicity increased significantly along with extensive surface fracturing, subsidence and horizontal displacement in the town of Grindavík. An evacuation was implemented that afternoon although many of the inhabitants of Grindavík had by this time already left town due to the constant unrest. The town has been formally evacuated ever since (in August 2024). In few households the inhabitants have chosen to stay in Grindavík and some workplaces, mainly around the harbour, are still in function.

It has been suggested that these events on November 10th were caused by a major dyke intrusion, extending over 15 km in length and at depth between 1 and 5 km (Sigmundsson et al., 2024). The dyke intrusion caused widespread tectonic displacement in Grindavík, at least ~6-7 fault zones intersect the town, some with a vertical displacement of 1,0 m and horizontal displacement of 1,2 m. A network of open fractures cut through the town, destroying tens of houses, streets and affecting all vital utilities.

During the following weeks following November 10th a continuous surface inflation associated with varying seismic activity was monitored through a vast network of fixed GPS stations that have been in operation on the Reykjanes peninsula. On December 18th, the first of many subsequent eruptions along the Sundhnjúkar crater row began.

Drawing from the earlier preparation work in 2021 and the intensity of the uplift rate and a series of three very recent eruptions in Fagradalsfjall, construction work on lava deflection barriers was commenced on November 10th, the very same day as the major rupturing event in Grindavík. The first and foremost priority was to secure, if possible, the power plant location at Svartsengi which is essentially the only source of geothermal extraction for central heating for the towns spread out on the Reykjanes peninsula. The power plant is set up with geothermal turbines as well with 75 MW electrical generation along with 150 MW of geothermal water. The spill water from the power plant is furthermore the main geothermal water source for the Blue

Lagoon geothermal resort situated few hundred meters away. Both installations are sitting in a topographical depression or shallow basin surrounded by lavas formed during the last two volcanic episodes on the peninsula. The magnitude and hastiness of this construction exceeded all conventional constructional and planning laws, requiring a special bill to be passed through the Parliament with great urgency in the days before.

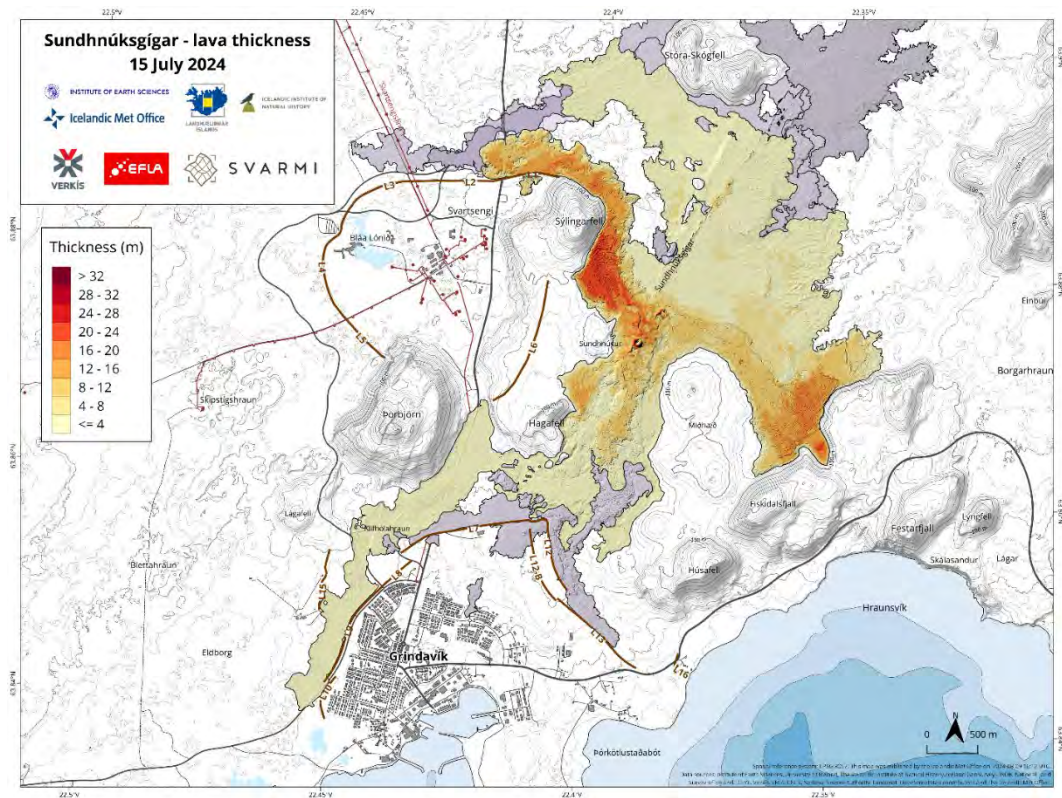


Figure 1. Overview of Svartsengi and Grindavík, status of lava flows in July 2024.

## THE SVARTSENGI BARRIER SYSTEM

As the focal point of uplift and earthquakes coincided with the power plant location it was not known if the mitigation plans had to consider both previous eruption sites located at Eldvörp and Sundhnjúkar crater rows west and east of the Svartsengi basin, respectively, or each one of them individually. The Eldvörp site was active with at least three eruptions in the Middle Ages from 1210-1240 and the Sundhnjúkar crater row that produced vast lava fields surrounding the town of Grindavík and the power plant site was active some 2,400 years ago.



It became quite evident that the Svartsengi basin had to be defended by series of deflecting barriers covering an almost circular envelope around the basin. As both literature study, lava flow modelling and work on the trial barriers in 2021 had shown, the plan had to be to convey or deflect the lava flow to a lower topographical level where it could spread out and accumulate without affecting the heart of the power plant. By doing so it had to be accepted that other important utilities as roads, power lines, hot-water and cold-water pipes would potentially be overrun by new lava. The barriers around the Svartsengi basin, named L1-L6 extended over 5.5 km with varying height from 8-13 m above the surrounding ground level, see figure 1. Estimated volumes for initial design involved some 600,000 m<sup>3</sup> of earth to be piled up. The “lava” side of the barriers were formed with a slope of 1:1.5 (vertical:horizontal), with a top width of 4 m and an “air” side (leeward) of 1:2. Later this basic form was modified as many barriers were elevated or adjusted to suit the ever changing topography.

The first phase of the construction involved immediate barriers that are crudely piled up to provide a first line of defence along the entire barrier system. The fill material was sourced by large bulldozers from the older lava formation immediately along the “outside” of the barrier line and hauled in from a gravel mine some 15 km away by regular lorries. The initial bulldozed fill extended generally some 3–5 m above the intact ground elevation providing a base for the top fill to be hauled in by dump trucks and placed by large excavators shaping the barriers. The first line of defences was largely completed on December 18th, apart from several gaps or passes in the system where the barriers crossed major roads and utility paths.

## **DECEMBER 18<sup>TH</sup> ERUPTION – 2023**

This first major eruption on the evening of December 18th proved to be quite dramatic in the opening phase compared to the previous eruptions at Fagradalsfjall. In a matter of minutes, a 4-km-long eruptive fissure opened. The crater line extended from Stóra-Skógfell in the north and towards Hagafell in the south, crossing the tectonic plate boundary but following the same orientation as the Sundhnjúkar crater row which was active 2,400 years ago. In the first few hours the outermost ends receded quite fast and after the first day the lava flow was confined only to centre part of the crater row slightly north of the old Sundhnjúkar main crater. The immediate response was to close the road passes on the barriers closest to the eruption, which was achieved within few hours. But as the first night went off with receding magma outflow it became evident that a direct contact with the barriers or some vital infrastructure was not imminent. On December 21st the eruption ceased with new lava covering an area of 3,5 km<sup>2</sup>. Estimated lava volume was 20 million m<sup>3</sup>, which is rather small in relation to older lava formations in the vicinity. After an evident ground deflation at Svartsengi during the

eruption a distinct uplift was noted immediately, concurring with continued inflation in the magma domain resting underneath Svartsengi, indicating that these events were potentially only the beginning of a larger and more persisting event.

## **TOWARDS GRINDAVÍK – JANUARY 2024**

Work on the Svartsengi barriers continued towards the Christmas holidays. By that time no decision had been made about the protection of the town of Grindavík. Preparation work with lava-flow simulation and layout design for Grindavík continued along with the barrier construction at Svartsengi. The first plans involved a U-shaped envelope around the town, close to 6.5 km long with a fill -volume of close to 1 million m<sup>3</sup>.

With ongoing inflation in the magma domain and the December eruption situated close to the town an order was given to commence construction of the first Grindavík barrier named L7 on January 2nd, 2024, at the northern border of the town. By that time the uplift at Svartsengi had reached similar levels as for December 18th eruption. The barrier started at the watershed northeast of the town and extended 1.7 km diagonally towards southwest crossing the main road to Grindavík. All major utilities as central heating, cold water, power cables and communications followed the same road, resulting in an 150 m open gap in the barrier where it crossed the road. The barrier layout aimed to lead the potential lava flow under moderate gradient towards west, where the road would later be moved to allow for the road to swing by the tip of the barrier through an overlap with next barrier, L8 and a topographical threshold heading towards the town.

An old gravel pit resting under the south slopes of Hagafell had been put in use by this time allowing for much shorter hauling distance and greater fill capacity. With the continued pressure increase in the magma domain a great urgency was put on the work and by the first week of January an immediate first crude barrier line was in place. The northeastern part was substantially higher than the immediate plan called for as the bulldozers could pile up that part easily, whereas fill material to the middle and westernmost part of the barrier had to be hauled in.

The road and pipe crossing called for some special measures as the hot water main to Grindavík was a surface pipe. Since the preceding summer a new hot-water main and cold-water main had been under construction. Both pipes were planned as underground pipes in the same trench, to replace the older surface pipe and a fragile cold-water pipe. As the situation unfolded in October–November 2023, work on the pipes was abandoned due to safety concerns by the privately owned utility company. Work on the pipes was again well underway, the cold-water main had been put in use, while the new hot-water main lay still in the open ditch with only the final touches remaining

before the trench could be closed. That was the situation north of Grindavík in the second week of the new year.

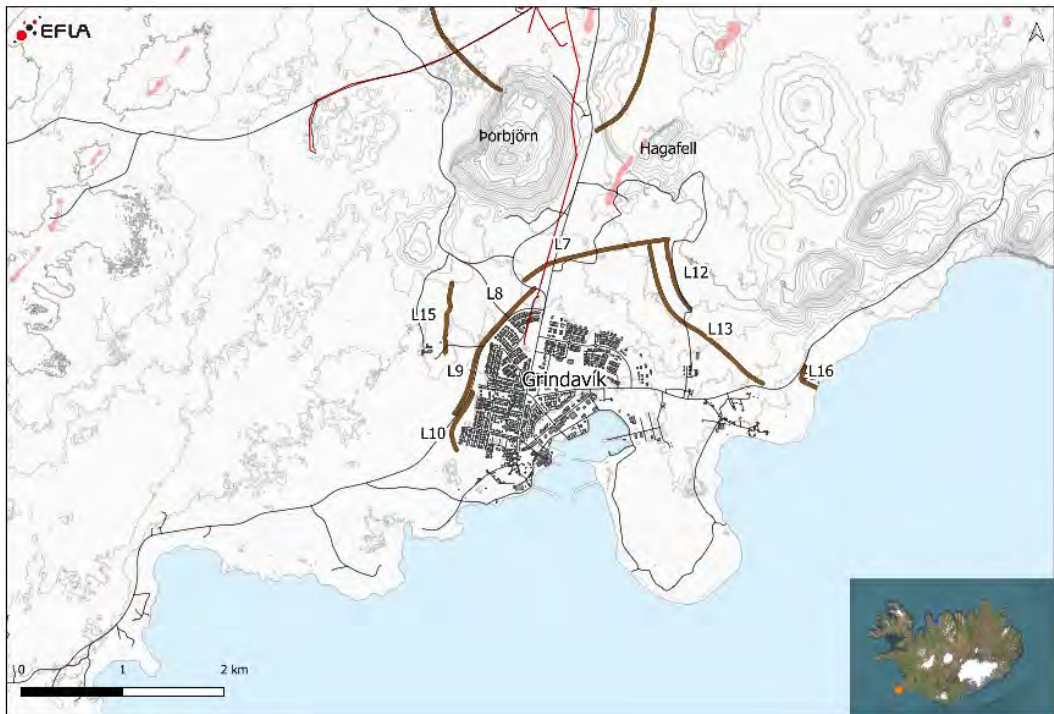


*Figure 2. The Grindavík barrier system, old volcanic craters shown with red polygons.*

## **JANUARY 14TH ERUPTION**

On Sunday morning January 14th the second eruption started, preceded by early warning signs by increased seismicity, tectonic displacement and increased surface fracturing in Grindavík. This time the eruptive vents were located south of Hagafell on a fissure system slightly east to the fissure system associated with the crater row active in December. The new crater row extended through the L7 barrier southward, with one of the main vents located directly in the barrier. As the barrier defined a flow path with sufficient gradient, most of the lava followed the barrier to the west instead of taking the otherwise more direct path towards the town.

As the eruption started on a Sunday morning the construction team had a rare day off. The construction machinery stood parked on top of the barrier few hundred meters away from the craters, including all the heaviest bulldozers and excavators, which are the most vital components of the machine park. The lava flow was rather moderate compared to what would later be seen in

this series of events and the main lava front moved only with a speed of brisk hiking pace. The contractors were obviously eager to get in and save their machines, but the Regional Command Centre situated outside the area and with a limited view of the situation denied that request. After a prolonged communication between the construction site supervision and the Regional Command Centre, and helicopter fly-over to assess the situation the Regional Command Centre granted a permission to save the equipment and start to fill in the gap over the main road, that would otherwise provide an open path for the lava into the town. Work on closing the road gap started immediately with all available machines operating in a confined area with great haste. The final buckets were being shovelled as the lava front reached the road. Again, drawing from the work on the trial barriers in 2021 when work on actively steering the lava front along the main deflecting barrier near Stórhóll gave important lessons in working around the hot moving lava. Soon afterwards the surface hot water pipe broke, but as the pumps had been turned off, there were no steam explosions. To save the cold-water pipes, fire hydrants in the town were opened to allow the water flowing along the pipe to cool off the skin and hopefully save the pipe. Work in the road pass was abandoned when the lava front passed by on the request of the Regional Command Centre, leaving the hastily piled up fill, substantially lower than the remainder of the barrier. As combined result of the lava front interaction with the hot-water pipe and significantly lower fill over the road a minor overflow occurred that could otherwise be most likely be avoided.

During the eruption a small eruptive vent opened inside the town border producing a small lava field that engulfed one house and set two other houses on fire. It has been suggested that the lava travelling laterally along open surface fissures at shallow depth and emerging to the surface only hundred meters from the northernmost houses in Grindavík.

As the day and next night went on, emphasis was put on to pile up an immediate barrier along the northwestern and western border of the town along a road following the outskirts of the town. After some 12 hours the flow rate declined and on the following morning the lava front had come to a rest. The eruption continued, gradually decreasing and on January 16th the eruption was over.

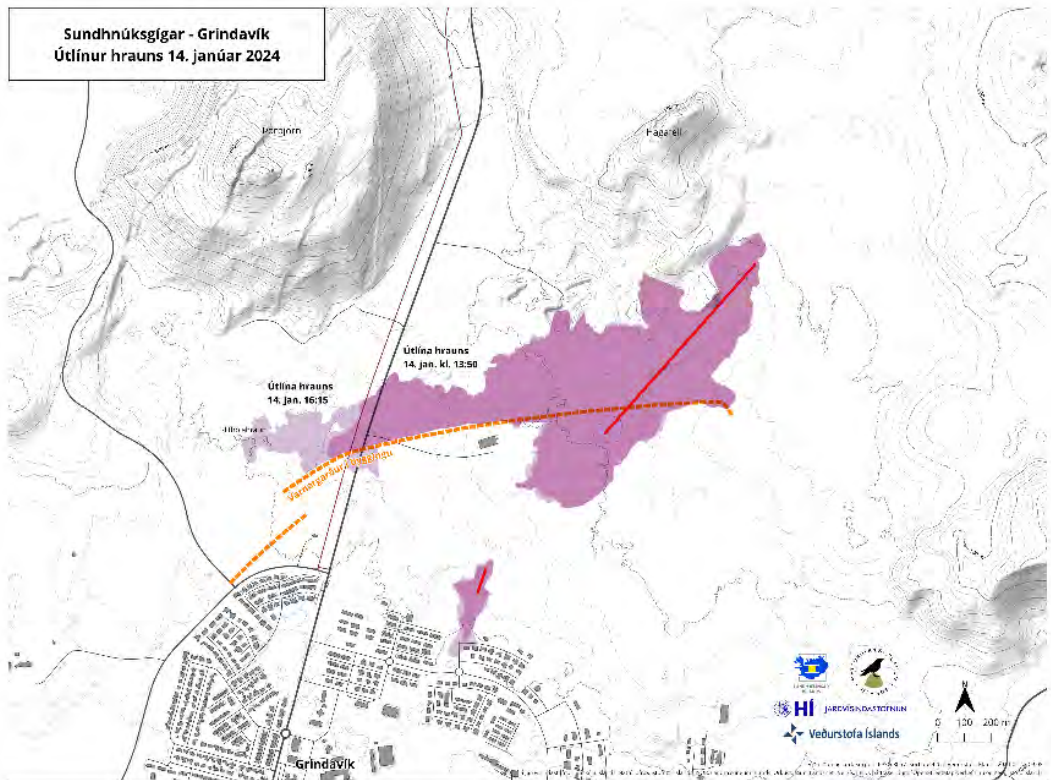


Figure 3. The January lava.

## JANUARY ERUPTION AFTERMATH

This short-lived eruption caused a significant havoc although being rather small in all comparison, covering only 0.7 km<sup>2</sup> and with volume of 2.8 million m<sup>3</sup>. The main road to Grindavík was covered by new lava, the town was without central heating and in three days after the eruption the power cables submerged by lava gave away. The cold-water pipe was conveying water, but the minor lava overflow overran the control station for the water distribution destroying it completely. One week later an overhead transmission line had been erected. The new hot-water pipe was connected, and conveying water, but without pressure buildup caused by leaking heat expanders. Few days after the eruption, work on extracting the cold-water supply from underneath the lava started. There were some successes as the pipe conveyed water, but some damages had occurred. In the end an old asbestos pipe lying on the ground underneath the lava was used as a conduit after being cooled down and new pipe fitted through. Work on trying to repair the leaking hot-water pipe was abandoned and a section of older steel pipe was brought in and placed over the surface of the new lava.

The latter half of January entered with rather strange mood for the people on site. The town had now been completely evacuated by the State Police Commissioner under a special clause in the Civil Protection laws, following a fatal accident in the town and a great uncertainty on the status of fault systems and possible hidden fractures og bedrock weaknesses that could potentially collapse and open without warning. There was also uncertainty regarding the continuation of the barrier construction work, if further action to prevent lava from flowing into Grindavík were to be justified and approved by the government. In the meantime, work on completing the Svartsengi system continued along with repair work. Preparations for barriers along the eastern part of the town were made along with plans for elevating the L7 barrier that took on the January lava flow. That involved installing construction roads and loosening materials from the gravel pit by Hagafell.

On February 4th an order was given for continued barrier work with elevation of L7 north of Grindavík and adjusted barrier along the eastern part of the town, named L12 and L13. The eastern barriers followed slightly diagonally and partly through the watershed formed by an 8,500 years old Hópsnes lava formation. The easternmost tip of L7 was cut off to allow the northern tip of L12 to connect into the eastern boundary of the January lava and facilitate a natural pathway for future lava flows that would likely follow the outskirts of the January lava.

## **GEOTECHNICAL ISSUES CROSSING TECTONIC FRACTURES**

Associated with the January 14th eruption a significant tectonic displacement affected Grindavík. That involved especially the main fissure line which the eruptive vents followed into the town, forming a small graben in the eastern part of the town. The previous displacement associated with the November 10th dyke intrusion formed a 4.5 km wide graben in the western part of the town. Between those grabens is a 200–300 m wide horst formation (De Pascale et al., 2024). Prior to the January eruption measures had been taken to repair some of the most important streets within the town. The most significant faulting system following a known fracture by the name Stamphólsgjá was activated severely during the November event with vertical displacement of 1.2 m, horizontal displacement of up to 1 m and several tens of meter deep. The conventional way in Grindavík and mostly elsewhere in Iceland has been to fill in the fractures after seismic events. As a long-term measure with expected further ground movements that was seen as rather short-lived method. Instead, the most critical crossings were repaired with the aid of geotextiles and reinforced with geonet. After rounding off the bedrock and filling in the bedrock fracture as practicable a layering of

reinforcement was placed over the fractures providing a ductile pass way. The main function of the geotextile is to keep the fill material in place and thus



providing an arching effect over the fractures. Several of these had been constructed prior to the January displacement and all performed very well providing a safe passage through the town.



Figure 4. Grindavík and the fracture system, yellow and orange

## FEBRUARY 8TH ERUPTION

At 5:30 on Thursday morning February 8th an intense seismicity started northeast of Sýlingafell along the Sundhnjúkar crater row. About 30 minutes later an eruption started on approximately 3-km-long fissure following similar location as in the December eruption. The lava flow quickly formed a distinctive front towards west and monitoring through web cams and drone surveillance showed the lava front moving quite fast along towards Stóra-Skógfell where it accumulated for a bit before taking a sharp turn towards Svartsengi. The new lava followed a defined channel in a depression formed by the boundaries of two older lava formations. The lava front progressed at a pace of 600–700 m/hr and by 10:17 it had reached the main road to Grindavík, north of Svartsengi. By 12:00 it reached the utility corridor from Svartsengi connecting all towns on the northern part of the peninsula. By 13:30 the lava front reached the maximum extension towards west, then it had

travelled some 4.5 km in 6 hours. Simultaneously the eruption receded with lava fountaining confined to three active vents, and the following day, February 9th, the eruption ceased. The February lava covered 4,2 km<sup>2</sup> and with a lava volume of approximately 15 million m<sup>3</sup>.

Work on protection measures for the very important hot-water pipe from Svartsengi, which provides geothermal water for central heating for the entire Reykjanes peninsula, started in January. The main pipe was as for Grindavík a surface installation and as such very susceptible to lava flows. As the project stood in February, some 500 m of new Ø700 mm pipe had been laid down in a trench crossing the most obvious depression and potential flow path. Work on the pipe had not been completed and the trench was still open when the eruption began. The construction teams started immediately to cover the pipe with sand and protective gravel fill. As the lava front progressed work on closing the road passages in the barriers also went on. The surface pipe ruptured almost instantly as the lava hit and carried the remainder of the pipe downstream with a great plume of steam rising from the lava. Condition on the new Ø700 mm pipe remained uncertain. Consequently 30,000 inhabitants on the Reykjanes peninsula were without central heating in subzero winter conditions.

The main cold-water supply for Svartsengi power plant is located 3.5 km north of Svartsengi and the pipes follow the same corridor as the hot-water pipes north of Svartsengi. This water supply is essential to operations in Svartsengi as it is the only source of cooling water and after running through heat exchanger it is returned as hot water for central heating, while the remaining brine is discarded. To protect the cold-water pipes under the new lava a continuous flow was maintained to allow proper cooling of the pipes.

A major high voltage overhead transmission line also follows the same corridor, connecting Svartsengi power plant to the main grid. Two of the most exposed transmission towers had been protected by piling up fill material against the towers. To avoid uncontrolled electrical outage the transmission line was shut off temporarily to reduce sagging as the heat flux from the running lava affects the conductors significantly. These measures were essential as by 17:00, when the heat flux had receded, the transmission line was connected again to the main grid without interruption although 6–7 m thick new lava surrounded two towers.

## **RESTORING INFRASTRUCTURE**

The largest blow to the infrastructure was the loss of geothermal power supply to the towns on the Reykjanes peninsula, the international airport included. The main road to Grindavík was also cut off resulting in 1-hour-long diversion along the nearest roads. As the lava front slowed, work on a construction road began immediately to connect the work sites on either side of



the new lava. It was anticipated that the new Ø700 mm pipe had survived as the pipe had been mostly covered before being overrun with new lava. When the protruding northern end of that pipe was inspected a significant lengthening of the pipe had already occurred buckling the end through the new lava. Geothermal pipes are constructed with heat expanders to facilitate pipe expansion when heated to 80°C. The first alternative was to connect the part of this new pipe, now covered by lava with remains of the older surface pipe. The connection was completed on Friday afternoon, but when water started to run through the pipe the water temperature rose towards 100°C at the north side of the lava, while being pumped in at the other end at 80°C. The flow maintained for few hours until the pipe broke in the evening, rendering hope for a quick repair.

In the subzero temperatures it was foreseen that it would only be a matter of 2–3 days before a significant and widespread frost damages would set in as electrical installation in the towns were not capable of running all households by electrical heating. With ~30.000 inhabitants without central heating, widespread actions were taken to safeguard public and private installations against frost damages as plans were drafted on how to reconnect the hot-water connection over the new lava. On Saturday morning, only 48 hours after the eruption started, a suitable Ø500 mm steel pipe material had been located. Welding and auxiliary crews were mobilized to facilitate a 24 hrs operation on two welding platforms. The pipe would be welded into length of two 250 m sections to be moved over the new lava if possible. The lava crossing was very uncertain as by this time there were only 48 hours since the lava crossed the pipe corridor. After careful inspection and drone surveying a small 17 tonne bulldozer started to level the scoriated surface crust. The crust was about 50 cm thick; surface temperature of the lava was ranging from 200–250°C and through cracks in the crust temperatures over 650°C could be measured at 50 cm depth. The lava surface was quite level, thickest at 7 m and gradually thinning towards either side, with this thickness solidification of the lava takes many months up to a year. The surface crust has a certain bearing capacity, but a liquid core remained underneath. Despite the general believe, the leveling went quite smoothly and after only 2 hours on the new lava the bulldozer broke through. Dump trucks waited on the other end ready to place fill material over the levelled crust scoria. Upon completing a “road” connection over the new lava it became certain that the new temporary pipe section could be pulled over the new lava. By Sunday afternoon the new pipe section was installed and connected to the still surviving parts of the main pipe and run up of central heating commenced.

On the main road to Grindavík a 300-m- long section was now covered by new lava. Drone surveying showed that this part of the lava was only 2.5–3.0 m thick, and therefore expected to solidify in few days. Work on levelling the top started on Saturday and on Sunday a useable construction road was in

place. Work on the road continued through the next days, by levelling side areas and finalizing surface course for public use. On Wednesday afternoon, only six days after the eruption started, the road was opened for public use.

### **MARCH 16TH ERUPTION**

Along with the infrastructure restoration after the February eruption, work on the Grindavík barriers continued. Inflation of the magma domain showed the same tendency as before; therefore, a new eruption was to be expected within few weeks. The priority was to elevate the L7 barrier north of Grindavík and the barriers at the eastern border. On March 2nd a dyke intrusion occurred without eruption and without affecting magma accumulation significantly. Two weeks later, on a Saturday evening the March 16th, a fissure eruption started at a similar location as in December and February. During the first hours the lava flow was estimated to be 1100–1200 m<sup>3</sup>/s. After 3–8 hours the lava flow had receded to 100 m<sup>3</sup>/s before settling down to 15 m<sup>3</sup>/s on the second day, gradually decreasing thereafter. The lava fronts followed similar paths as before, a western lobe running towards Svartsengi, covering the main road to Grindavík again before coming at rest close to the utility corridor. Another and more significant front flowed south towards Grindavík. That front followed previous formation but were directed by the January crater row and then by the recently constructed L12 and L13 barriers away from the town before halting some 400 m from the coastal road east of Grindavík. The main road to Grindavík was restored 5 days later again over the new lava.

After the initial phase the newest lava covered 6 km<sup>2</sup> and expanded only slightly over the next weeks although its volume increased. The eruption continued until May 8th and was the longest eruption this winter with estimated lava volume of 34 million m<sup>3</sup>. When the first intense phase was over and the eruption settled into a similar pace as seen during Fagradalsfjall 2021–23 events, the fluid lava started to accumulate in the near vicinity of the craters. The lava accumulated in lava ponds and large open channels with a gradual building up on top of earlier flows. Lower magma flow from the crater does not sustain lava flow over long distance as with reduced effusion the temperature of the running lava is lowered and with more exposure it loses gases resulting in a more viscous mass. After few days of lava accumulation south of the main vent, a thick viscous and slowly moving lava front approached the north corner where barriers L7 and L12 met. This slow flowing mass carried large blocks of solidified lava, up to 5 m in diameter. On average the crust appeared to be in the range of 3–4 m thick. As the lava touched the barriers it stood 3 m above the top and rolled like a belt on a bulldozer along the barriers. Blocks touching the barrier came at rest, while there was a continuous movement further out in the main flow, some 15–20 m away from the barrier. The following days the flow continued by filling completely the precious gravel pit under Hagafell. During Easter holidays another change happened as

small lava outlets began to squeeze out higher up in the system along with rising of the surface crust. That development continued downward along the system, indicating that the lava was flowing slowly in connected tube system under the crust. During the second week of April the expansion of the lava had reached the L12 barrier and lifted the few weeks old surface lava even higher than already seen, building up a pile of large blocks some 5 m above the barrier. Still only a one minor overflow resulted by squeezing. At the same time the first geotechnical deformation of the barrier occurred, when a large flat block was lifted by the expansion, scraped the inside slope until standing vertical near the top of the barrier pushing the top outwards. This deformation only affected the topmost 1 m of the 4 m wide barrier top with an expanding lava approximately 5 m higher than the barrier, thrusting the now vertical block outwards like a giant bulldozer blade.

### **MAY 29<sup>TH</sup> ERUPTION**

On Wednesday May 29th the fifth eruption on the Sundhnjúkar crater row started. The initial phase of the eruption was even more intense than the previous ones. Some estimations have been put forward for lava flow up to 1.500-2,000 m<sup>3</sup>/s (Icelandic Met Office, 2023-2024). The lava flow followed similar patterns as before since the main vents were close to the December, February, and March eruption sites. The main flow headed towards Grindavík and was led by the older lava formations and barriers along the northern and western border of the town, while less significant fronts flowed towards Svartsengi and east of Grindavík. The lava flow was extremely liquid and fast flowing and reached the maximum length at 5.6 km west of Grindavík in ~4–5 hours. The immediate effect of this initial phase was that all roads connecting Grindavík from north and west were covered by the new lava, leaving only one major road connection functioning towards east.

As for the March eruption this initial phase receded fast and on the second day of the eruption all fronts were standing still, and the lava started to accumulate close to the craters. Eventually on June 8th the lava accumulation northwest of the main crater succumbed, and a viscous slow-moving front developed towards Svartsengi, taking out the Grindavík main road for the third time on this specific location. As the viscous lava front reached its terminal length, signs of inflation within the lava body higher up in the system appeared. During the next two weeks the lava expanded from within via tube system and rose to an elevation 7 m higher than the barrier it lay against. Eventually the lava boundary gave in, and multiple small overflows squeezed over the barrier. Those were kept at bay with active plugging and steering by fill material and with the aid of water cooling. Luckily the eruption ceased soon after or by June 22nd. Even though the crater went quiet, the lava continued to move gradually over the next days, not coming fully to arrest until June 28th.

In July and August 2024 inflation has continued in the Svartsengi magma domain with expected eruption within the first three weeks of August. Compared to the Krafla eruptions in North Iceland from 1975–1984 it appears that the Grindavík fires can possibly be reaching the final stages. That might be a wishful thinking, but as long as magma is accumulating more eruption must be expected. How many and for how long remains uncertain. The infrastructures in Grindavík and Svartsengi are still functioning and holding out and with each event the mitigating measures need to be adjusted accordingly.

## CONCLUSIONS

The theme of this meeting is “next generation meeting” and the subthemes of sustainable foundation, digitalization, challenges for the future, construction in urban areas and handbooks or guidance. What can we draw from the past months of our operations on the Reykjanes peninsula that may have relevance to some of these subjects.

Digitalization. This project has been realized mostly without traditional drawings when transmitting the design to construction. The lava flow modelling is highly dependent on accurate topographical models. The topographical models have mostly been sourced by drone surveying both photogrammetric and by Lidar scanning. After finding a suitable barrier elevation and form of the barriers, the model is delivered to the contractor’s cloud service where the operators have instant access to new or updated models. This seamless transfer allows for fast adjustments and adaptability that is badly needed in a constantly changing environment. With the ever-changing topography with each eruption the topographical models need to be updated fast and with great accuracy, mainly by drone surveying. During inflation periods of the viscous slow-moving lavas in the March and June eruptions, the drone surveying has also been vital to recognize the slow movements in the lava fields.

Volcano monitoring, eruption prediction and management of response is obviously very reliant on automation, interpretation of vast data quantities, and remote surveillance. However, there is the danger of remoteness associated with this approach as monitoring operators and command centres are at great distance often lacking communication with the ground, that is both ground personnel and the physical ground conditions. As personnel on the ground may be noticing important signs that are not incorporated in the assessments made at distance. Thereby we are at the risk of missing the trust and understanding between parties that is a crucial part of effective teamwork. Increased compartmentalization in the science community and within the response system may also contribute to misunderstanding as different entities are putting their narrow understanding forward that might shadow a more generalized view of the situation at hand.

Challenges for the future and construction in urban areas. In Iceland we already see present and future challenges related to climate change in both rural and some urban areas. with increased frequency and size of eruptions, landslides, and glacier outburst floods, as well as sea-level changes due to retreating glaciers on local and global scales. In addition, we have now a very definitive situation of a new volcanic episode that has started on the Reykjanes peninsula where we have the highest population density. We have large urban areas placed on lava fields that are relatively young. If we were to compare frequency of lavas flows to landslide and avalanches, we would most likely limit or not allow inhabitation on those areas. The great question is how do we move on? Do we need to restrict further urban development within such areas, or are we going to accept the situation as is and rely exclusively on monitoring and mitigation measures as have been carried out for Grindavík and Svartsengi in the past months? It all come down to the value of acceptable risk which is at presently being evaluated. Central heating for the region is obviously too reliant on one source, alternative sources must be incorporated, either by low temperature harnessing or strong connection to the Reykjavík area.

Handbook and guidance. Familiarize yourself with the terrain! Engineering is in many ways based on a trial and error, to be moulded and adapted into practical theories and methods. There are no applicable handbooks on how direct lava flows or to interact with running lava or how to lay roads or other utilities on a fresh lava. In a way we must gain that experience in the field through the sole of our boots and have the courage to pioneer something that would look absolutely ridiculous in the eyes of the general public or safety managers in industrial complexes used to a very controlled work environment. At the same time, we need to study previous historical undertakings and experiences achieved, constantly learning and adapting. In the end, fresh lava is just a material that we need to learn to work with and around.

We also must maintain a strong focus on the task ahead and not loose sights in all the digital and physical noise surrounding us. There is a good chance that Grindavík and Svartsengi can be protected. If we were to compensate for all possible outcomes that have been suggested, the situation would be near unrealistic. We can only cover the most likely scenarios, but those must be done at full steam, any half-hearted attempts are not likely to secure a positive outcome.

## REFERENCES

De Pascale, Gregory P., Fischer, Tomás J., Moreland, William Michel, Geirsson, Halldór, Hrubcová, Pavla , Drouin, Vincent, Forester, Danielle, Payet Clerc, Méline, Brum da Silveira, Diana, Vlcek, Josef, Ófeigsson, Benedikt, G., Höskuldsson, Ármann, Torfadóttir, Helga Kristín, Valdimarsdóttir,

Iðunn Klara, Jónsdóttir Blöndal, Birta Dís, Jónsdóttir, Ingibjörg, Jónsson, Sigurjón, Thordarson, Thor. 2024; On the Move: 2023 Observations on real time graben formation, Grindavík, Iceland. *Geophysical Research Letters*, 51, e2024GL110150. <https://doi.org/10.1029/2024GL110150>.

Halldórsson, S. A., Marshall, E. W., Caracciolo, A., Matthews, S., Bali, E., Rasmussen, M. B., et al. (2022). Rapid shifting of a deep magmatic source at Fagradalsfjall Volcano, Iceland. *Nature*, 609(7927), 529 – 534. <https://doi.org/10.1038/s41586-022-04981-x>

Icelandic Met Office (2023-2024). Volcanic unrest Grindavik (news collection). <https://en.vedur.is/about-imo/news/volcanic-unrest-grindavik>.

Institute of Earth Sciences (2024). Sundhnúksgíggar (news collection). [https://jardvis.hi.is/is/Sundhnuksgigar\\_frettasafn](https://jardvis.hi.is/is/Sundhnuksgigar_frettasafn).

Kristján Sæmundsson & Magnús Á. Sigurgeirsson. In Náttúrvá á Íslandi (Natural Hazards in Iceland, Volcanic Eruptions and Earthquakes). Ed. Júlíus Sólmes, p 379– 402.

Sigmundsson F., Parks M., Geirsson H., Hooper A., Drouin V., Vogfjörð K. S., Ófeigsson B. G., Greiner S. H. M., Yang Y., Lanzi C., De Pascale G. P., Jónsdóttir K., Hreinsdóttir S., Tolpekin V., Friðriksdóttir H. M., Einarsson P. & Barsotti S. 2024: Fracturing and tectonic stress drive ultrarapid magma flow into dykes. *Science*, 383, p. 1228–1235.

Sigmundsson F., Parks M., Hooper A., Geirsson H., Vogfjörð K. S., Drouin V., Ófeigsson B. G., Hreinsdóttir S., Hjaltadóttir S., Jónsdóttir K., Einarsson P., Horálek J. & Ágústsdóttir Þ. 2022: Deformation and Seismicity decline before the 2021 Fagradalsfjall eruption. *Nature*, 609, p. 523–527.

Sæmundsson K., Sigurgeirsson M. Á. & Friðleifsson G. Ó. 2020: Geology and structure of the Reykjanes volcanic system, Iceland. *Journal of Volcanology and Geothermal Research*, 391, (106501). <https://doi.org/10.1016/j.jvolgeores.2018.11.022>



## ALL PAPERS IN ALPHABETIC ORDER





# A NOVEL TECHNOLOGY FOR DETERMINING STRENGTH AND REDUCE CLIMATE-GAS EMISSIONS IN DEEP SOIL MIXED PILES

**Helle T.E.<sup>1</sup>, Gerhardsen A.<sup>2</sup>, Rekdal T.<sup>3</sup>, Eriksson S.<sup>4</sup>, Juvik E.S.<sup>5</sup>, Giese S.<sup>1</sup>, Wiersholm P.<sup>1</sup>, Hegseth I.<sup>1</sup>, O’Rawe S.<sup>1</sup>, Dahl M.<sup>5</sup>, Brendbekken G.<sup>1</sup>, Nouri E.H.<sup>5</sup>, Wåle M.<sup>6</sup>**

## KEYWORDS

Deep-soil mixing, Laboratory procedure, In-situ testing, Seismic, Temperature, Sustainability

## ABSTRACT

A new non-destructive methodology for documentation and prediction of strength in binder-stabilised piles is developed. The methodology comprises improved laboratory procedures, continuous in-situ temperature monitoring and cross-hole seismics that may be conducted at any time and repeated in the same pile during the curing process. By applying this methodology, climate-gas emissions may be reduced by more than 39% and costs by more than 16%.

## EXAMPLE INTRODUCTION

Today, the strength of deep-dry mixed piles (DDM piles) is documented by in-situ tests such as reversed pile soundings (RPS), (predrilled) lime-pile soundings (FKPS) or cone penetration tests (CPTU). Due to practical limitations of these tests, they are often conducted during the first week after installation of the piles. However, the curing and the strength increase continues over a much longer period. This larger strength is not included in the design

<sup>1</sup> Multiconsult Norge AS, P.O. Box 265 Skøyen, 0213 Oslo, Norway, tonjeeide.helle@multiconsult.no Institution of second author

<sup>2</sup> Cautus Geo, Arnstein Arnebergs vei 28, 1366 Lysaker, Norway

<sup>3</sup> Argeo AS, Nye Vakåsvei 14, 1395 Hvalstad, Norway

<sup>4</sup> Heidelberg Materials Sement Norge AS, P.O. Box 143 Lilleaker, 0283 Oslo, Norway

<sup>5</sup> Norwegian Public Roads Administration, P.O. Box 1010 Nordre Ål, 2605 Lillehammer, Norway

<sup>6</sup> GeoPhysix AS, Merdevegen 8A, 3676 Notodden, Norway

of the piles, thus causing unnecessary excess consumption of binders, and large climate-gas emissions.

The innovation project KlimaGrunn (2018-2023) [1] have developed a new non-destructive procedure for documentation and prediction of strength in DDM piles that may be conducted at any time and repeated in the same pile during the curing process. The procedure is developed combining concrete technology, geotechnical engineering, sensor technology and geophysics.

The KlimaGrunn methodology [1] involves the whole process of deep mixing, from the initial site investigations, preparation and testing of laboratory-mixed specimens, how the results are used in design, and monitoring and testing in the construction phase. A new laboratory procedure for moulding and curing laboratory specimens is developed improving the correlation between the strength determined in the laboratory and in situ. Laboratory results form the basis for correlation models developed for prediction of strength development over time. During the construction phase, the temperature is continuously monitored by sensors installed at various levels in the piles. The temperature is used for estimating the strength of the piles based on the correlation models and is also used for updating the predicted curing time in-situ. Cross-hole seismics are conducted repeatedly in the same pile and documents the as-built strength and homogeneity over the whole depth of the piles.

This paper describes KlimaGrunns methodology, also presenting results from field experiments carried out in the Oslo region [1], and from two sites in Østfold and Nordland, Norway.

## **THE KLIMAGRUNN METHODOLOGY**

### **Site investigations**

The obtained strength of the DDM piles is influenced by the in-situ material properties (i.e. grain-size distribution, water content, density, remoulded shear strength, plasticity index). Therefore, it is necessary to map the variations over the site where DDM is planned, and to collect enough soil from each representative soil layer for moulding laboratory specimens to quantify the effect of binders (preferably various amounts, types and combinations). The extracted soil samples are sealed and stored at 6-8 °C at 100% humidity. Storage time should be kept at a minimum to avoid any chemical alteration or loss of water. Due to loss of material during the mixing and preparation of the specimens, about 600-700 g (about 13-18 cm of a 54-mm piston sample) of soil is needed to prepare one specimen.

### **KlimaGrunns laboratory procedure**

The strength in binder mixed laboratory specimens is affected by the density [2], [3]. In situ, the binders are blown into the soil with an air pressure and mixed with the soil creating a heterogenous matrix with air-filled voids. It is

therefore not possible to predict what density is achieved in the piles in-situ, and there is not much data available documenting the density of DDM soils. Compared to in-situ density of non-stabilised soils, Falle [2] reports less than 4% reduction of the density in samples collected from DDM piles mixed with 30, 50 and 80 kg/m<sup>3</sup> binders and cured for 9 weeks. Multiconsult [4], [5], report less than 6% reduction in piles with 90-100 kg/m<sup>3</sup> binders cured for 25 weeks. To avoid overestimating the strength, it is therefore recommended to mould the specimens to a target density 5% lower than the density of the original, non-stabilised soil.

A new equipment was developed allowing preparation of specimens with the intended target density having a height of 100 mm and diameter of 54 mm maintaining constant volume during curing (Figure 1). The equipment consists of:

- A 180-mm high cylinder with an inner diameter of 54 mm (Figure 1a).
- Two distance pieces with 1-2 mm holes (vents) in the centre is used for compressing the specimens to a final height of 100 mm (H/D ratio of 1,85) (Figure 1a).
- A hand-held rod with structured surface (waffle pattern or similar).
- A 10-20 mm high split ring mounted at the bottom distance piece (Figure 1a and b). When removed this allows for compression of the specimens from both ends (Figure 1c). Moist paper filters placed at the top and bottom of the specimen inhibit material from the specimen to be squeezed out through the vents.
- 180-mm long extruder rod (Figure 1Fel! Hittar inte referens-källa.a).

To ensure comparable results, enough soil from the same representative layer to mould all the specimens (all binder combinations and curing times) should be homogenised simultaneously. Preferably, three (minimum two) specimens with the same soil, binder combination and curing time are moulded. As a minimum three specimens of same type are cured for 28 days, but it is recommended to produce several sets of specimens with different curing times (i.e. 7 and 90 days).

The specimens are moulded by splitting the binder-mixed mass into minimum four parts of equal weight. These parts are filled into the cylinder using the muddler whilst minimising the size of air-filled voids. To avoid defined layers in the specimen, each layer should have an uneven surface prior to filling in the new layer. To make sure that the mass is evenly distributed over the height of the specimen, the first two layers are compressed with the muddler so that they have a height of 5,1-5,5 cm. Thereafter layers no. 3 and 4 are

filled into the cylinder to a total height of 10,1-10,5 cm. The unconfined compression

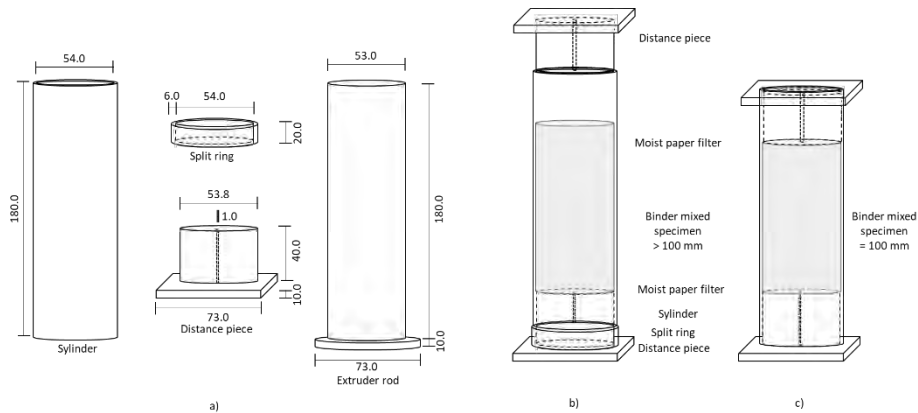


Figure 1 Sketch of a) equipment, b) moulded specimen prior to removal of the split ring and final compression in the unconfined compression apparatus and c) after final compression and ready for curing.

apparatus is used for pressing both the top and bottom pieces into the cylinder until they fluctuate with the cylinder walls. The specimens are stored vertically at  $20 \pm 2$  °C and 100% humidity until extrusion and testing. The temperature in the storage room must be documented.

After curing, the shear wave velocity is measured by bender element (BE) tests prior to unconfined compression (UC) tests ( $\sigma_3 = 0$  kPa) on the same specimens applying a strain rate of 1.5%/min. The undrained shear strength ( $c_{u,UC}$ ) is calculated as half the unconfined compressive strength ( $q_u$ ) [6].

### Correlation models

The quality of the laboratory results may influence the correlation models and must therefore be evaluated, and deviating results must be filtered out from the input data such as:

- Ratios of height to diameter (H/D) deviating from 1.8-2.1.
- Large deviations from target density of the cured specimens (> 5 %)
- Deviating water content of the homogenised soil compared to in-situ water content, and large internal deviations in the water content amongst cured specimens of the same type.
- Poorly prepared specimens (i.e. horizontal layering/cracks, large volumes of air-filled pockets).
- Deviating stress-strain curves, and large internal deviations of the obtained shear strength (> 15 % from median  $c_{u,UC}$ ) and shear wave velocity ( $V_s$ ) amongst three specimens of the same type.

The curing time in the laboratory at  $20 \pm 2$  °C ( $t_{eq}$ ) is not the same as the in-situ curing time in the piles ( $t_c$ ) where the temperature varies over time (Figure 2). Therefore, the laboratory-based correlation model for the development

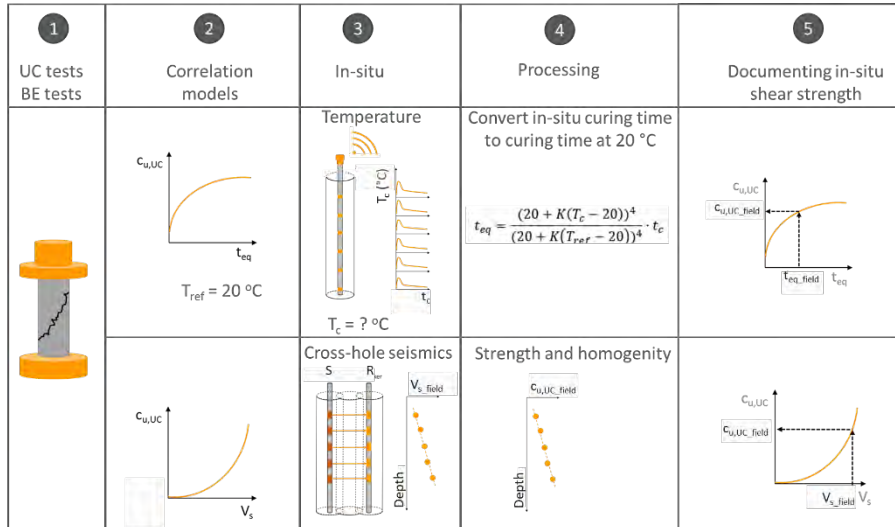


Figure 2 Combining laboratory-based correlation models to in-situ measurements of temperature and cross-hole seismics.  $S$  = source,  $R$  = receiver.

of shear strength over time does not correspond to  $t_c$ . The development of temperature in the piles depends on several factors such as installation grid (degree of coverage), binder type and quantity and the clay's thermal material properties [7], [8], [9], [10], [11], [12].

The temperature in the subsurface in Norway is around 6-8 °C. Exothermal chemical reactions between binders and soils start immediately after mixing. A rapid increase of the temperature is observed in the piles in the days following installation. The temperature is higher than in the surrounding soil and remains elevated for days, weeks or months after installation [7], [11], [12], [13], [14]. Therefore, it is recommended to cure the laboratory specimens at a higher curing temperature than the in-situ soil temperature [15]. Ideally the curing temperature should be as in the piles which, however, is hard to obtain in the laboratory.

In concrete technology specimens are cured at  $20 \pm 2$  °C, which is also recommended by [16]. The maturity number is used in concrete technology to be able to compare the progress of curing for concrete samples with different temperature histories. A principle also adapted for binder-stabilised soils (Equation 1) [7].

$$M(T_c, t_c) = (20 + K(T_c - 20))^2 \cdot \sqrt{t_c} \quad \text{Equation 1}$$

Where  $M$  is the maturity number (degree-days),  $T_c$  is the in-situ curing temperature ( $^{\circ}\text{C}$ ),  $t_c$  is the in-situ curing time after installation (days), and  $K$  is a constant varying with soil and binder types. A  $K$  of 0.5 is applied for Swedish clays and silty clays [7] and is considered applicable also for Norwegian clays and silty clays. By curing the laboratory specimens at a reference temperature of  $20^{\circ}\text{C}$  ( $T_{\text{ref}}$ ), Equation 2 is derived from Equation 1 for estimating how long it will take for piles cured at any temperatures to obtain the same curing time as if they were cured at constant  $20^{\circ}\text{C}$ , referred to as the equivalent curing time ( $t_{\text{eq}}$ ). For instance, at constant  $7^{\circ}\text{C}$  the pile must cure for 135 days to obtain the same  $M$  as a representative specimen cured at  $20^{\circ}\text{C}$  for 28 days.

$$t_{\text{eq}} = \sum \frac{(20 + K(T_c - 20))^4}{(20 + K(T_{\text{ref}} - 20))^4} \cdot \Delta t_c \quad \text{Equation 2}$$

This means that regardless of the temperature history in the pile, temperature measurements in situ can be used for calculating the equivalent curing time at  $20^{\circ}\text{C}$  ( $t_{\text{eq\_field}}$  in Figure 2), and thereby relate the progress of curing in situ to the strength measured on laboratory specimens cured at  $20^{\circ}\text{C}$  ( $c_{u\text{UC\_field}}$  in Figure 2).

In Åhnberg's correlation model [17], the undrained shear strength ( $c_{u,\text{UC}}$ ) is normalised by the average of the shear strength obtained after 28 days of curing ( $c_{u,\text{UC}28}$ ) (Equation 3). This correlation model creates in most cases a conservative, lower boundary for the data produced by applying KlimaGrunns laboratory procedure on soils from Eastern and Northern Norway mixed with various types and amounts of binders. Åhnberg's correlation model is modified by replacing  $t_c$  with  $t_{\text{eq}}$  in Equation 3. In most of the results, a higher shear strength than what appears from the correlation model is developed after a short curing time (Figure 3a). In such cases, a correlation model for the local site conditions may be more appropriate as suggested by the second function in Figure 3a which have a higher rate of strength increase during the first part of curing, but slightly slower than Åhnberg's correlation model after 28 days.

$$\frac{c_{u,\text{UC}}}{c_{u,\text{UC}28}} = 0.3 \cdot \ln(t_{\text{eq}}) \text{ modified after [17]} \quad \text{Equation 3}$$

In general, there is a scatter in the shear wave velocity interpreted from the bender-element tests (Figure 3b). Nevertheless, Dannewitz et al. [18] correlation model in Equation 4 fits well with a rough average of the results in the scatter. Developing locally fitted correlation models may be necessary, such as the upper and lower limits suggested in Figure 3b. In situ, the shear strength estimated based on temperature may be verified by shear-wave velocities interpreted from cross hole seismics (Figure 2).

$$c_{u,\text{UC}} = 0.0424 \cdot V_s^{1.462} \quad [18] \quad \text{Equation 4}$$

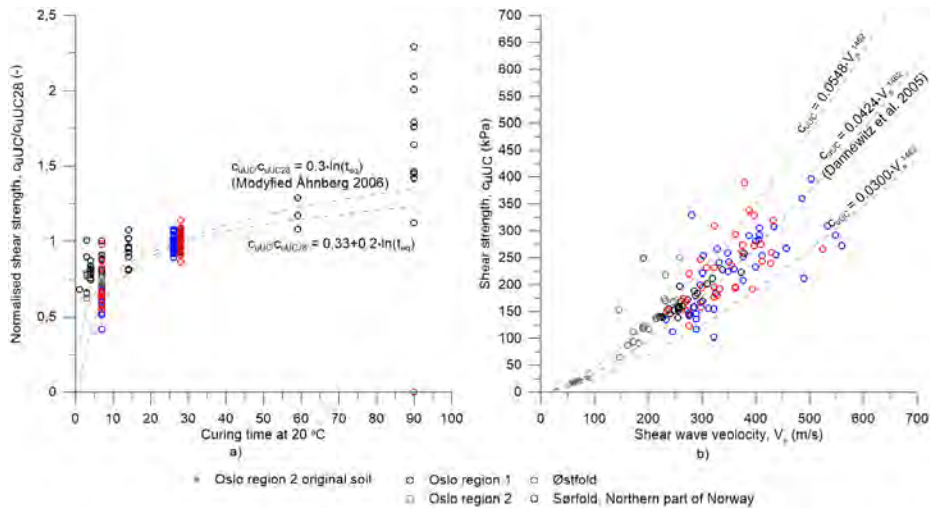


Figure 3 a) Normalised shear strength versus curing time at 20 °C. b) Shear wave velocity versus shear strength.

### In-situ monitoring

The complexity of the site conditions over the area where DDM is planned influences the set-up of the monitoring. To capture temperature variations over the site and differences this may cause in the rate of strength increase, it is recommended to monitor all variations of installation grids, pile diameters, binder combinations and soil types over the site. Furthermore, instruments should be installed in the outskirts as well as in the central parts of the ground-improved areas.

To ensure contact between the DDM soil and instruments, temperature sensors and casings for cross-hole seismics are installed directly after installation of the piles. It is recommended to install temperature sensors at multiple levels in the piles (Figure 2a). Preferably a minimum of four sensors over sections of 10 m length, starting at around 3 m depth down to half-a-meter above the end of the pile. The data are automatically transferred to the cloud and presented live at Cautus Web (Figure 4).

The correlation for shear strength development based on temperature and curing time in Equation 3 is considered conservative. In-situ the piles cure under overburden stress, thus most likely obtaining higher shear strengths than determined from the UC tests. The shear wave velocity increases with increasing shear strength (Figure 5). Thus, the effect of overburden stresses on obtained shear strength may be detected by cross-hole seismics (Figure 6).



Figure 4 Temperature and strength development over time at various depths in the monitored pile as presented at Cautus Web (<https://cautusgeo.com/cautus-web/>).

Cross-hole seismics are conducted between casings installed with a minimum distance of 2 m in panels with overlapping piles. To ensure that the shear wave velocity is calculated correctly, the distance between the two casings at any depths are documented by inclinometer measurements. Waves are transmitted from a source (S) in one casing and received by a receiver (R) positioned at the same level in the other casing (Figure 2b). It is recommended to apply a receiver that registers particle movements in two horizontal directions in the S-R plane allowing the source to be rotated 180 degrees to obtain polarised shear waves in the horizontal direction for easier detection of the first arrival of shear waves. The data are processed by filtering of frequency (keeping 30-300 Hz), subtraction of signals from the opposite directions and analysing of the first arrival.

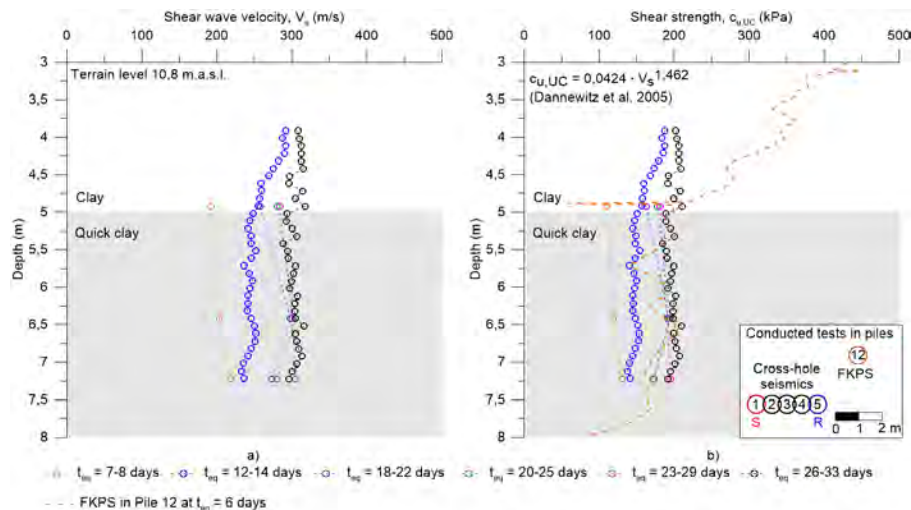


Figure 5 a) Interpreted shear wave velocity measured at several points after installation, and b) corresponding shear strength calculated by Dannewitz et al. (2005), and



also compared to interpreted shear strength from conducted FKPS in nearby single pile no. 12 at equivalent time at 20 °C of 6 days. The cross-hole seismics is conducted with the source in pile no. 1 and the receiver in pile no. 5. The clay is mixed with 80 kg/m<sup>3</sup> 50/50 ByPass Dust (BPD) and CEM II.

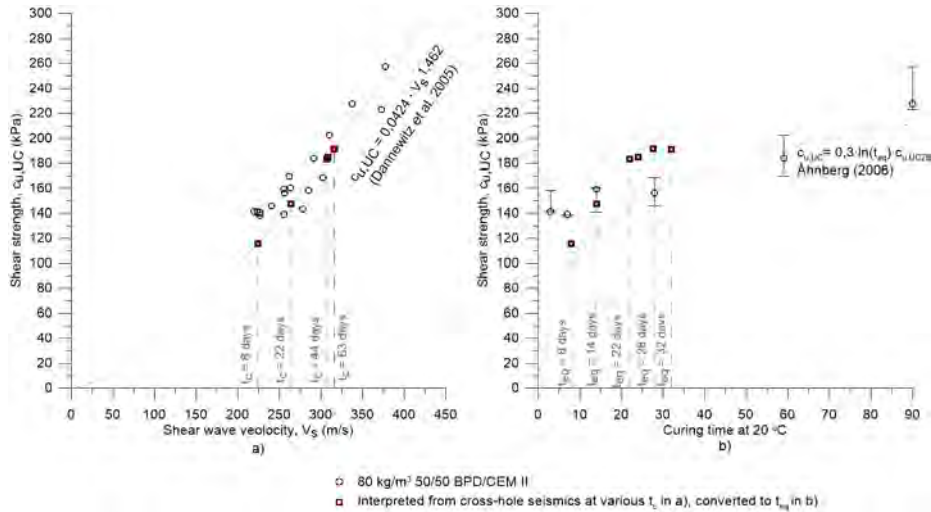


Figure 6 a) Interpreted shear wave velocity measured by cross-hole seismics (red symbols) several times after installation and b) plotted against shear strength over equivalent time at 20 °C. The clay is mixed with 80 kg/m<sup>3</sup> 50/50 BPD/CEM II.

As a minimum cross-hole seismics should be carried out at the same levels as the installed temperature sensors early in the curing process to verify the laboratory-based correlation model, and for example at every 10 cm to document the as-built strength and homogeneity of the piles prior to construction work (Figure 5). Shear strength interpreted from cross-hole seismics is in the case shown in Figure 5b considered to be conservative compared to conventional FKPS carried out in a nearby single pile.

### Data presentation and documentation

All registered users can follow the strength development live during the construction phase via the web application Cautus Web. The temperature measurements are updated continuously, and the equivalent time ( $t_{eq}$ ) is automatically calculated by applying Equation 2. The strength increase is documented by the laboratory-based correlation model (i.e. Equation 3), shown both with the in-situ curing time and equivalent time at 20 °C. It is also possible to add predictions of how the strength will continue to develop over time. In addition, the data from cross-hole seismics are presented together with the inclinometer measurements.

## REDUCED CLIMATE- GAS EMISSIONS AND COSTS

In the following, results from KlimaGrunns site experiment at E18 Vestkorridoren is used in a simplified example to estimate the potential for reducing climate-gas emissions and costs by applying KlimaGrunn's methodology. The calculations are based on 15 m long 800 mm piles installed with a 150 mm overlap in a 20 m long panel of single piles over an area of 100 x 20 m. The piles must obtain a minimum shear strength of 100 kPa, and the average shear strength of the stabilised soil volume must in this case be of 60 kPa minimum.

Until recently it has been common to apply binder quantities of 80-110 kg/m<sup>3</sup>. However, laboratory tests on quick clay from E18 Vestkorridoren showed that it is possible to obtain sufficient shear strength by only adding 45 kg/m<sup>3</sup> (Figure 7a) when allowing the specimens to cure for about 48 days at 20 °C. By applying 80 kg/m<sup>3</sup> sufficient shear strength is obtained during the first week of curing, and a strength of 160 kPa is obtained in specimens by curing for 48 days at 20 °C. There are only minor differences between binders containing CL80/CEM I (lime and cement) and BPD/CEM II (ByPass Dust and cement with fly ash). BPD/CEM II with a smaller climate footprint is therefore considered in the following.

By allowing the 80 kg/m<sup>3</sup> cure for 48 days, the centre distance between the panels may be increased and thereby reduce the total number of piles over the ground-improved area (Alternative A in Figure 7a), and thereby reduce the climate-gas emissions and costs by 39%. By keeping the number of piles and rather decrease the binder quantity from 80 to 45 kg/m<sup>3</sup> in the piles (Alternative B in Figure 7a), the climate-gas emissions are reduced by 44% and the costs by 16%. Be aware that the climate-gas emissions only include the production of binders and not the fuel consumption during installation and transport. How quickly the target shear strength is obtained depends on how the temperature develops in the piles in situ (Figure 7b).

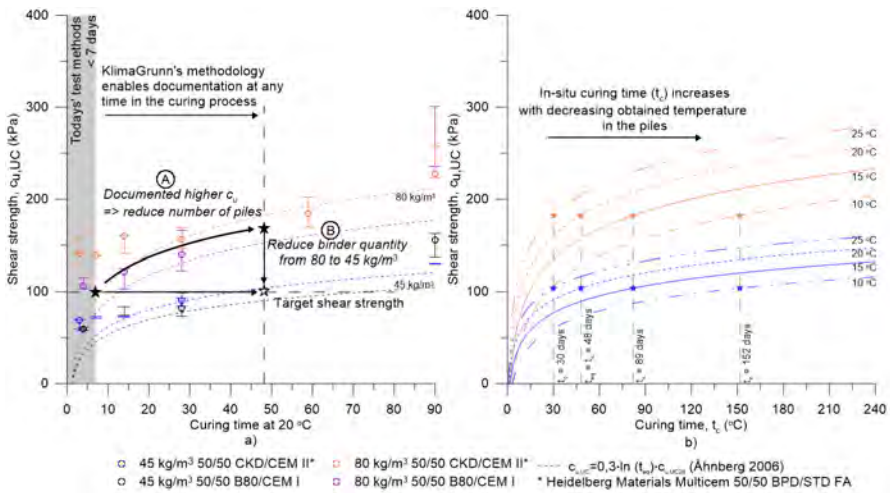


Figure 7 a) Increased curing time allows for reduced climate-gas emissions applying Alternative A or B. b) In-situ curing times ( $t_c$ ) to obtain target shear strength differs from the laboratory curing time at 20 °C, depending on in-situ temperature in the piles.

## CONCLUSIONS AND FURTHER WORK

By applying KlimaGrunn's methodology the binder combination is optimised for local site conditions and design criteria facilitating reduction of both climate-gas emissions and costs. Furthermore, the continuous monitoring and live presentation increases the control of how the strength in the piles develops in the construction phase improving the safety prior to commencing of construction work. The live-updated correlation models may be used actively in the progress planning. Cross-hole seismics may also be used for documentation of the durability of existing piles. Although the method may seem time consuming and expensive, this will pay off as a result of reduced number of piles and/or binder quantities and increased control in the construction phase.

A public database should be established so that correlation models for soils of varying grain-size distributions and properties may be developed to make it easier to optimise the binder combinations for local site conditions without the necessity of large number of laboratory tests.

Laboratory studies show promising results in reducing the binder content and still obtain sufficient strength. However, today's drill rigs may limit how well the binder and soil is mixed when the added quantity of binders decreases below 22.5 kg/m (i.e. 45 kg/m³ for a 800 mm pile and 60 kg/m³ for a 600 mm pile). Therefore, contractors are encouraged to develop rigs with mixing tools that may improve the homogeneity of the piles, and also documenting the installed position.

## ACKNOWLEDGEMENTS

The authors express their sincere gratitude to Innovation Norway and The National Programme for Supplier Development (LUP) for funding and supporting the innovation project KlimaGrunn. The many discussions with many internal and external colleagues are greatly appreciated. Skanska, Marthinsen & Duvholt and Dmix AB are acknowledged for their great contribution during the execution of the field work.

## REFERENCES

- [1] KlimaGrunn: KlimaGrunns arbeidsmetode for grunnforsterkning. Statens vegvesen report no. 915, 2023.  
<https://vegvesen.brage.unit.no/vegvesen-xmlui/handle/11250/3069881>
- [2] F.Å. Falle: Comparing laboratory and field stabilised clay. NTNU Master thesis, 2021.
- [3] P. Baustad: En laboratoriestudie av styrke og stivhet i kalksementstabilisert leire. NTNU Master thesis, 2022.
- [4] Multiconsult: E6 Klett, Jaktøya-Dovrebanen, Grunnundersøkelser datarapport. Report no. 415531-RIG-RAP-001 rev. 01, 1st October 2013.
- [5] Multiconsult: E6 Klett, Datarapport grunnundersøkelser, dagsferske prøver. 415531-RIG-RAP-003, 14<sup>th</sup> May 2014
- [6] ISO: Geotechnical investigation and testing – Laboratory testing of soil – Part 7: Unconfined compression test. ISO 17892-7:2017(E).
- [7] H. Åhnberg and G. Holm: Om innverkan av härdningstemperaturen på skjuvhålfastheten hos kalk- och cementstabiliserad jord. SGI Report 30, 1987.
- [8] H. Åhnberg et al.: Cement och kalk för djupstabilisering av jord. SGI Report 48, 1995.
- [9] S. Christensen et al.: Grunnforsterkning med kalksementpeler. SINTEF Bygg og Miljøteknikk, 1998.
- [10] M. Kitazume and M. Terashi: The deep mixing method. 2013.
- [11] P. Wiersholm: Temperatureffekter ved kalksementstabilisering. NTNU Master thesis, 2018.
- [12] B.K.F. Bache et al.: Erfaringer med ulike kalksementvariasjoner – Laboratieforsøk med ulike typer kalkbaserte bindemidler med hensikt å optimalisere bindemiddeltipe, innblandingmengde og påvirkning på klima og miljø. Geoteknikkdagen, 2021.

- [13] B.K.F. Bache et al.: Effect of Temperature on the Strength of Lime–Cement Stabilized Norwegian Clays. *Journal of Geotechnical and Geoenvironmental Engineering*, vol. 148, 2022.
- [14] T.E. Helle et al.: KlimaGrunns arbeidsmetodikk for dokumentasjon og prediksjon av skjærfasthet og stivhet i bindemiddelstabiliserte peler. *Geoteknikkdagen*, 2022.
- [15] NGF: NGFs beskrivelsestekster for grunnundersøkelser. Melding nr. 10, Rev. nr. 2, 2020.
- [16] R.R.E. Vervoorn and A.A.S. Barros: Deep soil mixing for stabilising deep excavations. NGM, 2021.
- [17] H. Åhnberg: Strength of stabilised soils – A laboratory study on clays and organic soils stabilized with different types of binder. Doctoral thesis, Lund University, 2006.
- [18] N. Dannewitz et al.: Seismisk kontrollmetod för KC-pelare. Svensk Djupstabilisering Arbetsrapport No. 35, 2005.

# A REVIEW OF STATE OF THE ART ON EROSION-DRIVEN QUICK CLAY LANDSLIDES

**Ankit Tyagi<sup>1</sup> and Ivan Depina<sup>2</sup>**

## KEYWORDS

Quick Clay Landslide, Literature Review, Erosion.

## ABSTRACT

About 5000 km<sup>2</sup> of Norway is covered by soft marine clay deposits. Nearly 20% of this area consists of highly sensitive or quick clay. Landslides on this sensitive clay cause loss of life and adversely impact infrastructure, environment and communities. Most of the Quick Clay Landslides (QCLs) are caused due to human activities. However, continuous soil erosion activity along the riverbeds is one of the significant natural factors for QCLs. Recently, many researchers have incorporated soil erosion as the triggering factor for analyzing QCLs. The main goal of the present study is to review the research conducted on erosion driven QCLs in Norway and propose a framework for QCL risk assessment and management. We have reviewed some relevant articles and highlighted their limitations with future scope of work. Mitigating all quick clay deposits can be very cumbersome and hence first preference should be given to the extremely high QCL hazard zones. The accurate use of multi-temporal erosion data and its analysis can improve the prediction accuracy of QCL hotspot zones. The study also highlights the research gaps in monitoring soil erosion for predicting erosion driven QCL.

## INTRODUCTION

On average around one large Quick Clay Landslide (QCL) occurs in Norway per year (L'Heureux et al. 2018), causing damage to infrastructure, or even loss of lives. QCL is one of the most devastating landslide types triggered by changes in the near-surface properties of the clay through human intervention and natural factors (Rørstadbotnen et al. 2023). Natural triggering factors include mainly terrain changes such as from erosion from a nearby drainage network (Gregersen, 1981; Regjeringen, 2021). These sensitive clays are known for their potential for large landslides, which poses a serious risk to human lives, infrastructure, and surrounding ecosystems within their reach. More is discussed below in Section 3 about the characteristics of quick clay in

<sup>1</sup> Norges teknisk-naturvitenskaplige universitet - NTNU

<sup>2</sup> Norges teknisk-naturvitenskaplige universitet - NTNU

Norway. QCL can have large consequences as was recently seen in the quick clay landslide in Gjerdrum where 11 people lost their lives and more than 1600 people had to be evacuated from their homes. This landslide also caused extensive damages that cost almost 2 billion Norwegian kroner in damages and reparations after the event (NOU, 2022). Other such historical catastrophic landslides include, e.g., Sørumsund in 2016, Skjeggstad in 2015, Statland in 2014, Byneset in 2012, Saint-Jude in 2010, Lyngen in 2010 and Kattmarka in 2009.

The work to obtain information about the risk of quick clay landslides has been ongoing since 1980 and was initiated after the quick clay landslide in Rissa (1978). NGI (Norwegian Geotechnical Institute) was then commissioned by the Ministry of Agriculture to carry out overview mapping of "potentially landslide-prone quick clay areas" in Eastern Norway and in Trøndelag based on Quaternary geological maps from NGU. The program described in NVE report 14/2011 "Plan for landslide hazard mapping" (NVE 2011) is an update of NGI report 20001008-2 from 2008 (NGI 2008). As of today, overview mapping has been carried out under the auspices of NVE in large parts of the country (NVE, 2020a). This paper reviews some of the latest remarkable work describing the state of the art on erosion driven QCL and proposing a framework for QCL risk assessment and management.

## **TYPES OF QUICK CLAY SLIDES**

Landslides in Norwegian clays can be classified as rotational, retrogressive, and flake slides (NVE, 2020b). In real situations, a landslide can be a combination of several types. For example, the 1978 Rissa landslide is a combination of initial slide, flake type and flow (Gregersen 1981). In the case where the rotational slide triggers further slides, it is referred to as the initial slide (NVE, 2020b). Flake slides happen when large flakes in gentle slopes release and quickly break up into large chunks or disintegrate (Torrance, 2012). This can occur in thin layers of quick clay that collapse and liquefy because of loading at the top of a slope or cuts or erosion at the bottom of the slope leading to a progressive failure along the quick clay layer releasing the flake.

## **QUICK CLAY IN NORWAY**

The Norwegian landscape is characterized by large u-shaped valleys, fjords, and alpine relief – shaped by glacial variations throughout history. Over the past 2.6 million years, Norway has been subjected to more than 40 glaciations, resulting in many glacial processes influencing the Norwegian geography (Ramberg et al., 2008). The ice sheet exerted immense loads on the underlying crust, causing an isostatic depression amounting to several hundred meters. When the overburden ice disappeared, the underlying crust began to rise by means of isostatic uplift. Scandinavia is still rising at present-day. The

Oslofjord and Trondheim area has risen 36 cm the past century (Ramberg et al., 2008).

Quick clay can be found in places that are lower than the marine limit, which corresponds to the highest sea level during and after the last ice age. The marine limit is used as the upper boundary for delineating land areas that was depressed under sea water during the last ice age in Norway, and because of the postglacial land uplift the marine clay is now on land. The marine limit ranges in Norway vary from 0 to 220 meters above the current sea level (NGU, 2021). Sensitive clays are leached marine clays that may change from a stiff and brittle material into a viscous liquid when remolded (Rosenqvist 1953). The classification of a quick clay is in Norway based on the remolded undrained shear strength and sensitivity of the soil. A geotechnical definition is clays that have a remolded shear strength less than or equal to 0.5 kPa (NGF 2011) or 0.33 kPa in ISO 1789-6:2017. According to Thakur et al. 2014, clays with a remolded shear strength of less than 1 kPa, pose a risk for large, retrogressive flow-slides. The NVE uses a more conservative approach and classifies all brittle materials in surficial deposits, clays or silt with a remolded shear strength less than or equal to 2 kPa (NVE 2020b).

The clay in saltwater forms an open card house like structure, where the edges and planes have a different charge and are attracted to each other. The salt contributes to the binding forces keeping the card house structure stable. As the salt is washed out, the card house structure stays the same, but the binding forces are weakened (Regjeringen, 2021). As quick clays become liquid when remolded, these clays pose a serious risk for catastrophic QCL in inhabited areas, especially in mid-Norway and the southeast part of Norway.

## **EROSION AS THE TRIGGERING FACTORS**

The foremost two triggering factors of quick clay landslides can be divided into anthropic factors (filling, excavation, construction activities, urbanization) or natural causes, mainly erosion destabilizing the slope (L'Heureux et al., 2018). Most erosion-initiated landslides in clay soils occur on the banks of watercourses where the toe is subjected to erosion. Erosion in riverbeds and ravines is progressively developed due to wet seasons and years of high precipitation with high water flow in rivers. An increase in precipitation and runoff because of climate change is also expected (IEA, 2022) which could lead to an increase in erosion and erosion-triggered quick clay landslides (Ryan et al. 2022). River erosion can cause destabilization in the long-term situation and erosion protection design should be built (Pytten et al. 2017). In the QCL in Gjerdrum, one of the causes of increased erosion in the river was additional runoff from the urbanization in the catchment (Regjeringen, 2021), exemplifying how quick clay landslides can result from a mix of anthropic factors and natural factors. The autumn season in 2020 was the wettest season in Gjerdrum since autumn 2000, and part of the conclusion for why the quick



clay landslide released in 2020 and not in 2000 was the effect of the erosion over the years reducing the stability of the slope.

Erosion, unfavorable pore pressure conditions and terrain changes are the most common causes of landslides, and these can be due to both natural conditions and human influence (NGU Report 2022). Terrain changes due to natural erosion can lead to a disturbance of the stability equilibrium of a slope are an important contributor to quick-clay landslides (Solberg et al., 2024). According to Alene et al. (2024), a partially collapsed riverbank with fallen trees and exposed rock can suggest representing erosion directly. River channel morphology changes such as migrating of river course toward the riverbank adjacent to the toe of a given slope could be one indicator of dangerous erosion. In addition, river water level rise could represent erosion indirectly as a river flow increase exacerbates erosion.

In the aftermath of the landslide at Gjerdrum in 2020, the Norwegian Public Roads Administration (NPRA) has initiated to work proactively with assessments and protection of quick clay areas connected to the road network. Grøndalen et al. (2021) prepared a new working methodology with more focus on qualitative assessments of the dangers. They first evaluated the significant parameters for slope stability, which includes change in slope geometry, historical landslide activities, geometrical conditions in nearby slopes, stage in the formation of the valley, slope angle, erosion activity. Among them, the slope geometry (regardless of whether it is changing or not) was used as a basis for classifying the slopes stability. The other parameters were considered for additional information. They classified slopes into three main groups with slopes without change in geometry, slopes in change, and slopes with modified geometry. For each group, different stability conditions such as stable, potentially unstable, and assumed unstable were adopted. Central to their methodology was emphasis on the triggering causes of quick clay landslides and assessment of the extent to which they were present in an area with quick clay. The factors investigated were primarily ongoing erosion, landslide activity, slope gradient and height differences. To get a complete overview of the erosion conditions along a watercourse, site inspections and mapping the condition visually was carried out. They used GIS analyzes to get an overview of these factors in the many thousands of quick clay areas in Norway. This helped them in prioritizing areas that should be mapped and assessed first. They initially took the DTM for the study area and identified the streams. Then they calculate the height difference in the slopes adjacent to the waterways by creating a buffer zone of 50 m width. Then they selected the areas with a height difference greater than 10 metres by selecting steep areas ( $> 20$  degrees) within 75 meters from the streams. This new approach was tested in eastern and central Norway and shown promising results with possibilities for further applications.

Godoy et al. (2023) introduces a new method, which is under development at the NVE, which aims to identify areas that may be vulnerable to naturally triggered quick clay landslides. He used publicly available lidar datasets (hoydedata.no/LaserInnsyn2), and automatically identified the terrain changes along ravines and watercourses using machine learning technique. The terrain changes were calculated as a regular raster algebra based on two digital terrain models (DTM) from lidar scans at different times. The data set consists of over 4,000 terrain change polygons that were validated with field visits. This data was divided into training (70%) and testing (30%) of the machine learning U-Net model. To train the model, they correlated the 70% training terrain change data with four chosen terrain parameters (change in height, change in plane curvature, change in slope and change in tangent curvature). The trained model then identified the same type of changes automatically. Further, the identified terrain changes were used as a basis for calculating maximum release areas for potential landslides incorporating NVE's inhouse tool. NVE has developed a tool to calculate the maximum release area based on a given initiation zone. By using a slope of 1:15, landslide's maximum detachment area can be estimated (NVE, Jernbaneverket and Statens vegvesen, 2016). The slope ratio of 1:15 was taken in the steepest direction (normally on the elevations) (NVE, 2020b). By assuming the entire slope profile consists of brittle fracture material and retrogressive landslide development, they run the tool to calculate potential maximum detachment areas over the continuous deposits of marine clay (MSML) if an initial landslide starts at automatic identified terrain changes. Moreover, they estimated the potential risk from these release areas in a semi-quantitative approach by multiplying consequences and danger. Consequences were derived by correlating loosening area with geodatabases from Statistics Norway such as population data or infrastructure information. The degree of danger was estimated qualitatively by using three parameters: Slope (average), Height difference (maximum) and terrain changes/erosion (average volume). This risk assessment by estimation of both hazard and consequence helps in identifying the vulnerable areas that require prior investigation and mitigation measures. However, they have also mentioned the limitation of their work as it delimits very large loosening areas as it assumes that there is quick clay/fractured material everywhere within the MSML.

## **PROPOSED FRAMEWORK**

Following framework is proposed for erosion-driven QCL risk assessment and management (Figure 1). This framework is based on the GIS-based conceptual integrated system for landslide risk assessment and management (Dai et al. 2002). of the proposed framework on erosion-induced QCL risk assessment starts by establishing a comprehensive physical, monitoring, QCL, and socioeconomic databases. The framework then proceeds to identify critical

features or parameters controlling slope stability, erosion processes, and consequences of QCLs. This will be then used to address both aspects of risk assessment, namely hazard and consequences. Hazard estimates can be obtained by physical or data-driven models in a sequential approach. The likelihood of erosion will be estimated, followed by the estimate of the likelihood of the initial slide. This will be estimated through the use of fragility curves. Estimates of consequences will be based on vulnerability assessment, which represents the likelihood of losses (e.g., economic, fatalities) in a QCL release and runoff zones. Finally, the risk assessment will be used for determining the optimal risk management measures.

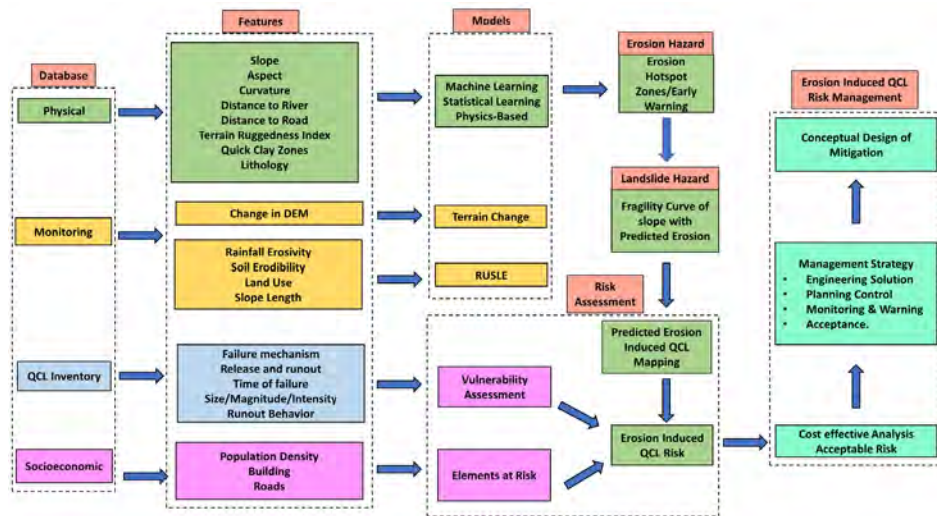


Figure 1 Framework for Erosion Induced QCL Risk Assessment and Management.

## CONCLUSIONS

This review paper is dedicated to the growing community of scholars, practitioners and policy makers concerned with the different scientific aspects of erosion-induced quick clay hazards in Norway. Here, we have discussed work from various government and private organizations and their contributions in mitigating this hazard. Since landslides in sensitive clays possess huge destructive capabilities, there is a need for accurate assessment and prediction of landslide potential in such materials considering significant triggering factors such as erosion. This study proposes a comprehensive and quantitative erosion induced QCL risk management framework that complements and extends existing efforts by providing a more explicit treatment of coupled erosion and landslide hazards through a fragility function and assessment of consequences with a vulnerability function.

## ACKNOWLEDGEMENT

We would like to acknowledge NVE for share their data, insights, and ongoing work on erosion-driven QCL.

## REFERENCES

- Alene, G.H., Depina, I., Thakur, V. et al. QuickAware: a virtual reality tool for quick clay landslide hazard awareness. *Nat Hazards* 120, 1869–1898 (2024).
- Cristian Godoy. (2023). Proactive prevention of quick-clay landslides: use of data and technology for effective identification of vulnerable areas.
- Dai, F.C., Lee, C.F. and Ngai, Y.Y., 2002. Landslide risk assessment and management: an overview. *Engineering geology*, 64(1), pp.65-87.
- Gregersen, O. (1981). The quick Clay Landslide in Rissa, Norway. Norwegian Geotechnical Institute, Oslo, Norway. Publication No. 135, pp. 421–426.
- Grøndalen, G.S., Juvik, E.S., Ottesen, H.B., Degago, S.A., Hellum, Ø. and Kveli, J., 2021. Håndtering av kritiske grunnforhold.
- IEA. (2022). Norway Climate Resilience Policy Indicator – Analysis (Climate Resilience Policy Indicator). IEA.
- Kristiansen, J.B., 2023. Precipitation and Erosion Threshold for Quick Clay Landslides Using Machine Learning Models (Master's thesis).
- L'Heureux, J.-S., Høydal, Ø. A., Paniagua Lopez, A. P., & Lacasse, S. (2018). Impact of climate change and human activity on quick clay landslide occurrence in Norway. Second JTC1 Workshops on Triggering and Propagation of Rapid Flow-like Landslides.
- NGF (Norwegian Geotechnical Society) (2011) Veiledning for symboler og definisjoner i geoteknikk: Identifisering og klassifisering i jord. Norwegian Geotechnical Society, Oslo, Norway, NGF-notification no. 2, 2nd revision.
- NGI 2008, "Method for mapping and classification of danger zones, quick clay," Program for increased safety against mudslides. Report No. 20001008-2, rev.3.
- NGU. (2021, February 10). Marin grense | Norges geologiske undersøkelse. <https://www.ngu.no/emne/marin-grense> Jeg er ikke sikker at man kommer på riktig side med denne lenke- sjekk
- NGU Report (2022), Penna, I; Solberg, IL, Statistical analyzes of morphological parameters for mudslides in Trøndelag and Viken.
- NOU. (2022). On safe ground — Better management of quick clay risk <https://www.regjeringen.no/no/dokumenter/nou-2022-3/id2905694/>

NVE 2011, "Plan for landslide hazard mapping," Report 14/2011.

NVE, Jernbaneverket and the National Road Administration. (2016). Method for assessment of loosened and outlet areas for area landslides. The natural hazard project: Sub-project 6 Quick clay. NIFS report 14/2016

NVE. (2020a). Overview mapping and classification of the degree of danger, consequence and risk for quick clay landslides. Method description, NGI. NVE External report no. 9/2020

NVE. (2020b). Safety against quick clay landslides. Assessment of area stability in land planning and development in areas with quicksand and other soils with brittle fracture properties. Guidelines for planning and development in danger areas along waterways. Guide No. 1/2019.

Pytten, E., Flobak, T., Ottesen, H.B. (2017). Fv. 287 Strandgata: Kjøreplass bru. Road Construction in Quick Clay. Advances in Natural and Technological Hazards Research, vol 46. Springer, Cham.

Ramberg, I. B., Solli, A., Nordgulen, Ø., Binns, R., Grogan, P. & NORSK GEOLOGISK, F. 2008. The Making of a land: geology of Norway, Trondheim, The Norwegian Geological Association

Rørstadbotnen, R.A., Dong, H., Landrø, M., Duffaut, K., Growe, K., Kakhkhorov, U., Wienecke, S. and Jacobsen, J., 2023. Quick clay monitoring using distributed acoustic sensing: A case study from Rissa, Norway. Geophysics, 88(5), pp. B267-B283.

Rosenqvist IT (1953) Consideration on the sensitivity of Norwegian quick-clays. Geotechnique 3:195–200

Regjeringen. (2021). Årsakene til kvikkleireskredet i Gjerdrum 2020.

Ryan, I., Bruvoll, A., Foldal, KM, Hæreid, GO, Muthanna, TM, Nordal, S. Ottesen, HB & Solberg, IL, 2022. On safe ground. Better management of quick clay risk. Norway's public studies, NOU 2022:3. Report to the OED submitted on 28 March 2022.

Solberg, IL. Landslide and ravine distributions related to ground conditions in elevated marine deposit in Mid-Norway. Nat Hazards (2024).

Thakur, V. and Degago, S.A., 2012. Quickness of sensitive clays. Géotechnique Letters, 2(3), pp.87-95.

Torrance, J. K. (2012). Landslides in quick clay. In D. Stead & J. J. Clague (Eds.), Landslides: Types, Mechanisms and Modeling (pp. 83–94).

# **A SIMPLE METHOD FOR PREDICTING COHESIVE PILE DEFORMATIONS FROM DISPLACEMENT PILE INSTALLATION INDUCED GROUND MOVEMENT**

**Jonatan Isaksson<sup>1</sup>, Yanling Li<sup>2</sup> and Lars Hall<sup>3</sup>**

## **KEYWORDS**

Displacement pile installation, SSPM, SSI, Soil movement

## **ABSTRACT**

Prediction of ground deformations resulting from the installation of displacement piles in greenfield conditions can be calculated using theoretical solutions such as the shallow strain path method (SSPM). The induced ground deformation from piling work may cause damage to nearby buildings' deep foundations. To study this potential damage, complex finite-element calculations may be necessary. In this article, a simple approach using the SSPM is presented for estimating the horizontal deformation of existing piles induced by nearby displacement pile installation. The method was based on the results from actual field measurements and finite-element calculations.

## **INTRODUCTION**

With the ongoing urban densification in larger cities, taller buildings are being constructed today on land with poorer ground conditions than before. Foundations on such land require extensive piled foundations. In these urban areas, buildings are constructed in the vicinity of existing structures, imposing increasingly stringent requirements to prevent damage to these existing structures. In recent years, this issue has been particularly emphasized in Gothenburg, where the geotechnical conditions primarily consist of clay to significant depths (>100m), alongside a surge in the construction of tall buildings adjacent to major infrastructure such as tunnels and bridges, as well as near older, fragile buildings.

In Sweden, pile foundations are traditionally prefabricated displacement piles of solid concrete or hollow steel pipes. An effect of installing displacement piles in clay is that the installation causes ground movement, which can lead

<sup>1</sup> NCC Sverige AB, Sweden, Chalmers University of Technology

<sup>2</sup> NCC Sverige AB, Sweden

<sup>3</sup> NCC Sverige AB, Sweden

to damage to nearby buildings and infrastructure. This problem is not new but has lately been a topic of discussion not only in Sweden (e.g., [3], [4]) but also in other countries with similar geotechnical conditions (e.g., [8], [9]). The magnitude of these ground deformations is directly proportional to the installed volume of displacement piles, and the extent of the movement relates to the pile length. In greenfield conditions (GF) - i.e., a flat ground surface, deep clay deposit, and no heavy buildings and structures near the installed piles. The Shallow Strain Path Method (SSPM) ([1]) has been proven to estimate displacements of light buildings and structures, as well as ground deformations, with good agreement with field and laboratory measurements (e.g., [2], [6]). The SSPM method provides a simple and fast tool for calculating ground deformations resulting from installations of displacement piles.

However, in geotechnical design, the primary concern is the deformations and potential damage to existing structures, with the GF movement being of secondary importance. The presence of existing structures supported by deep foundations has been shown to alter the magnitude/distribution of displacements compared to the predicted results from the GF situation ([5], [7]). Simple methods able to quantify this influence are not available, and practicing engineers are left to rely on engineering judgment/experience or need to use numerical methods to analyze this problem. Even simplified numerical analysis of the installation of piles and their effect on nearby structures requires three-dimensional modeling and can become complicated and time-consuming for both personnel hours and computing time.

In this paper, the installation of displacement piles for a new building in central Gothenburg, Sweden, and their effect on two nearby buildings are analyzed by comparing the measured deformations with predictions using SSPM and the Finite Element Method (FEM). Based on the insights gained from the comparison, a practical approach is suggested for estimating the horizontal deformations of existing piles due to displacement pile installation in clay.

## METHODOLOGY

The installation rate of prefabricated displacement piles, in combination with the low permeability of natural clays, results in undrained loading conditions with constant volume behavior of the displaced clay. This constant volume condition has been utilized for two methods of predicting displacements due to pile installation. The first method is the SSPM ([1]). The SSPM is based on theories from fluid mechanics and assumes a frictionless and constant volume material. It provides displacements due to the installation of a pile in an infinite half-space with a stress-free surface. The solution is based on an incompressible material, and the displacements from the installation of multiple piles can thus be calculated by the superposition of the single-pile solution.

The second method relies on FEM where the installation of piles has been simulated by the horizontal expansion of a soil volume where the expanded volume corresponds to the volume of soil displaced by the installed piles. The volume of multiple individual piles will in this work be grouped together to a larger single volume to reduce the number of expanding soil volumes as proposed by [3]. The influence of existing structures in FEM can be modeled using various levels of fidelity. In this study, a simple strategy was used to enable the modeling of the large geometrical system of existing foundations. The soil was modeled using solid elements with a linear elastic material model. The walls and foundation slab of the existing structures were modeled using plate elements connected by interface elements to the soil. Existing piles were modeled using the embedded beam element in Plaxis 3D ([10]), where the stiffness of the pile is applied on top of the existing finite element, avoiding the need to create separate volume elements to represent the pile. The embedded beam formulation has been shown to capture the behavior of the volume pile to a reasonable degree. However, the accuracy of the embedded beam element is not ideal and should be used with caution in the case of lateral loading, especially when approaching failure.

## CASE HISTORY

The analyzed case history involved the development of a new neighborhood in Gothenburg, Sweden, comprising office and residential buildings. This area, situated in the floodplain of the Göta River near its mouth at the sea, was previously a harbor basin. The soil profile consists of a 4-m-thick layer of fill material containing sand, silt, and clay, along with remnants of old dock structures. Beneath this layer lies clay, extending to a significant depth (>100m). This paper focuses on soil displacements resulting from pile installation for the foundation of one of these new office buildings, known as Habitat 7

The construction of Habitat 7 began with the installation of sheet-pile walls (SPW), followed by excavation to a depth of 3 meters, and then the installation of piles from a 1-m-thick gravel bed. In total, 149 piles were driven in a span of 7 weeks. The piles are a combination of concrete and timber where the top 30m part consists of concrete and the bottom 12 of timber. Additionally, a few hollow cylinder steel piles were used in the foundation of a crane. To reduce the displacement during the installation of the piles, soil was extracted up to a depth of 14 m using auger screws in the location of some of the combined displacements piles to reduce the displaced soil volume. A plan of the foundation is presented in Figure 1. An extensive monitoring program was implemented focused on tracking displacements and preventing damage to the two existing office buildings with deep foundations, namely Stuveriet and Brick Studio (see Figure 2). In this analysis, three monitoring points were studied in more detail, with S1 and S2 mounted on the building of Stuveriet



and B1 mounted on the building of Brick Studios. To be able to monitor the displacement of the existing piles, inclinometers were installed at the location of S1 and B1. The inclinometers were fixed at their top to the building foundation slabs of the respective buildings.

The details of the foundations for the nearby buildings Stuveriet and Brick-Studios can be found in Table 1; some simplifications regarding foundation geometry and pile layout have been made. A large number of 28m long timber piles below the left slender part of Stuveriet was excluded from the numerical analysis to reduce the model complexity. All buildings in this study, were founded on so-called cohesive piles. There were a few end-bearing piles installed under Stuveriet, but they were only used to decrease downdrag forces for the cohesive piles.

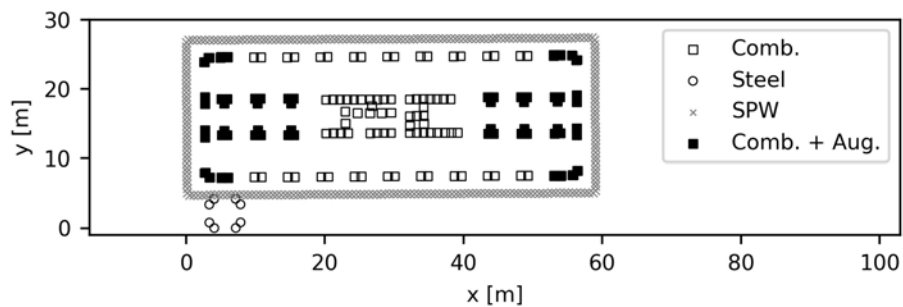


Figure 16 Deep foundation plan for Habitat 7 includes combination (concrete and timber) piles (Comb.), open-ended cylindrical steel piles (Steel), and sheet pile walls (SPW). The locations where auger screws were used before installation of the combination piles are also shown (Comb. + Aug.).

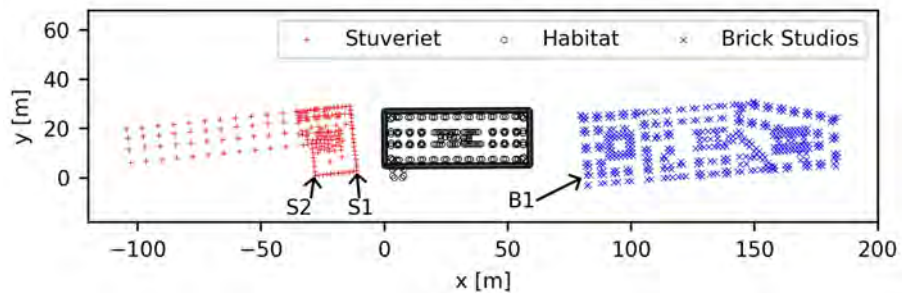


Figure 2. Overview of the existing pile foundations of Stuveriet and Brick studios and the deep foundation works of Habitat.

Table 6 Foundation of Stuveriet and Brick Studios

	Stuveriet	Brick Studios
Basement depth	5.75 m	5 m
Foundation slab	1 m	1 m
Basement wall	0.3m	0.3m
Pile types	Concrete/wood: 43m Concrete: 56 m Steel: End bearing, top at 5 m below basement	Concrete: 48-52 m Various steel piles: 72 – 80 m

## NUMERICAL ANALYSIS

The ground deformations resulting from the deep foundation work for the Habitat building were predicted using SSPM and finite-element (FE) calculations. The predictions entailed calculating and summarizing the deformations from all individual piles and SPW to the points of S1, S2 and B1. Plaxis 3D, 2023 ([10]) was used for the FEM simulations. The FE model is illustrated in Figure 3 and features a horizontal domain size of 600 m by 600 m and a uniform depth of 100 m. The soil was modeled with linear elastic response and a Poisson's ratio of 0.499 to ensure a constant volume condition. The pile installation was simulated using 36 expanding volumes. Each expanding volume comprised individual piles that were grouped together, determined by dividing the building's footprint area into 36 zones, with 4 rows in the width direction and 9 in the length direction. The placement of the expanding volumes within each zone was determined based on a weighted mean of the individual pile locations, considering their respective contribution volumes. The FE model consisted of approximately 300,000 volume elements, 579 embedded beams, and 17 plates. Furthermore, to make a direct comparison of the results obtained from the SSPM calculations, FE calculations were also performed without accounting for the foundations of nearby buildings (i.e., the GF conditions). The location of S1, S2 and B1 corresponds to the location of piles in the FE-model

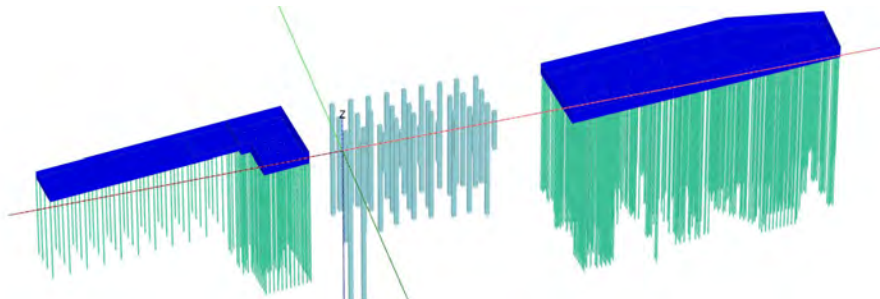


Figure 3 Finite element model for calculating the displacements of Stuveriet (left) and Brick Studios (right) due to the installation of Habitat piles (middle).

## RESULTS

The calculated and measured horizontal and vertical deformations of the two buildings, Stuveriet and Brick Studios are shown in Figure 4. The results indicate that the predicted GF displacements from Finite Element Method (FEM) and SSPM exhibit similar magnitudes and depth-dependent shapes. However, the deformations calculated in FEM show higher horizontal displacement (10-30%) and lower vertical displacement (10-30%). The FE simulation and the inclinometer measurements show that the movement of the top of the pile in point S1 and B1 were reduced in relation to both the GF movement and the predicted and measured movement deeper in the soil. The difference in vertical displacement between S1 and S2 is reduced from 6,5mm to 4,5mm when the existing foundation is included in the FE analysis while the field measurement shows a difference of 3mm.

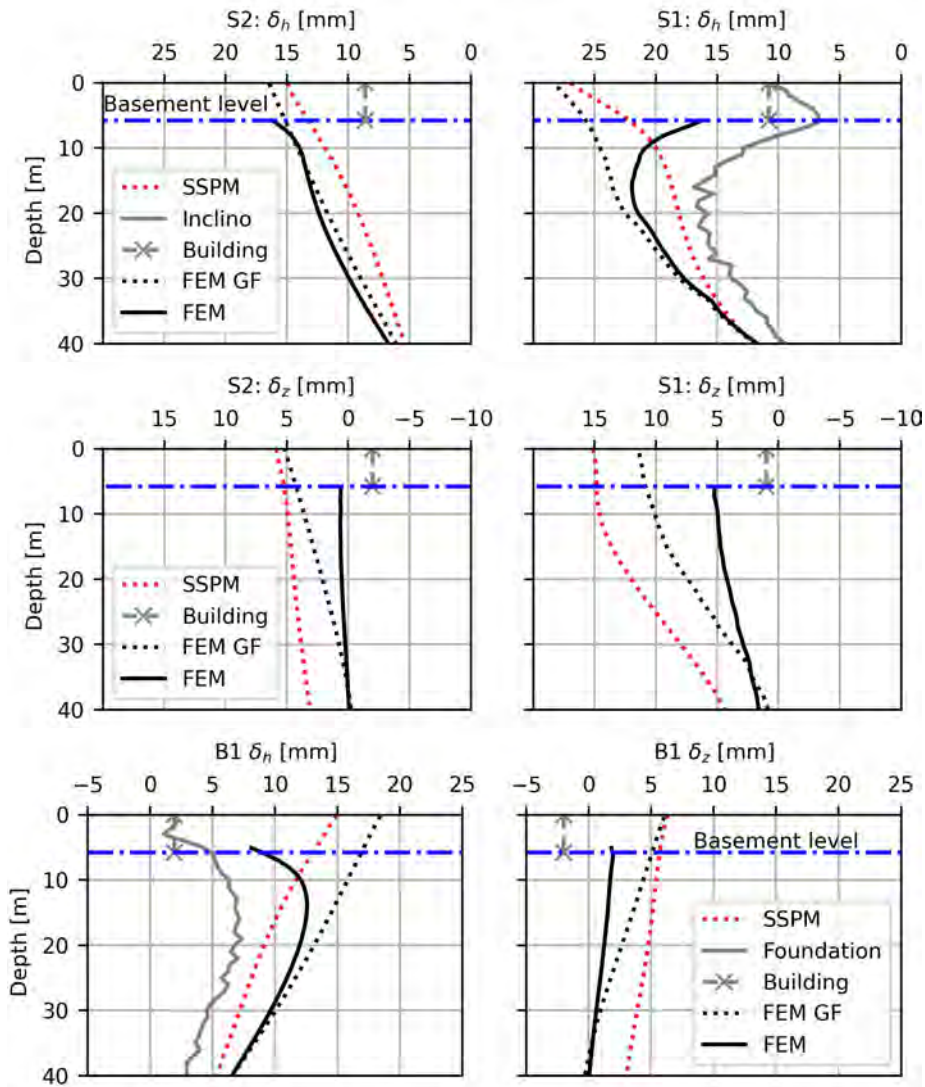


Figure 4 Measured and predicted horizontal and vertical movement for measurements point S1 and S2 on Stuveriet and B1 on Brick Studios.

## A SIMPLE METHOD FOR EVALUATING PILE DEFORMATIONS

Horizontal ground deformation due to displacement pile installation was shown to induce bending of existing piles of nearby buildings. The bend shape of the pile leads to a reduction of the axial load-bearing capacity of the piles due to second-order moments. If the piles are already highly utilized, their capacity may be exceeded. The deformed shape of the piles determined through FE calculations and the measured deformations, from inclinometers fixed at the top of the foundation slab is similar. Large curvatures of the pile

are isolated to the upper part of the pile corresponding to a buckling length equal to about 5m ([11]). Consequently, the pile's shape can be assumed to be equal to the predicted greenfield displacement shape below a depth corresponding to the buckling length. Over the buckling length, the pile has a curvature that connects to the deformations of the building at its top. Figure 5 illustrates the result of this simple adjusted SSPM method for estimating the deformed shape of the piles located at S1, S2, and B1. The proposed methodology results in both larger curvatures and deflection ratios in the piles compared to the FEM and measurements and seems to be conservative for the case studied herein.

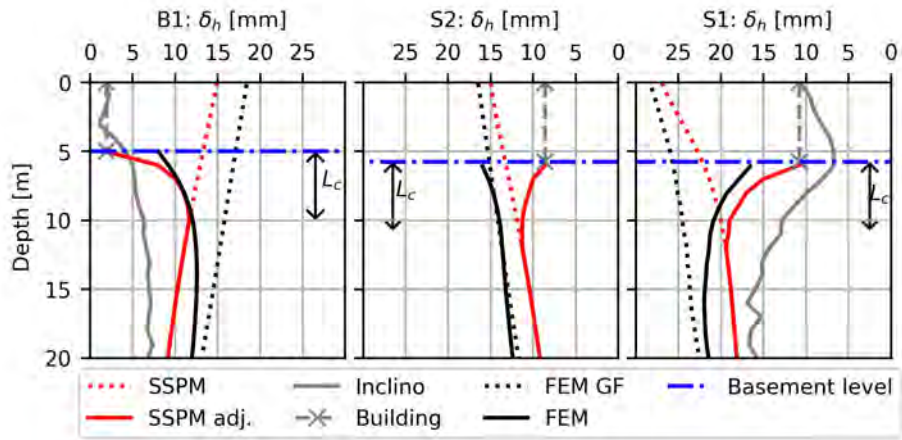


Figure 5 Measured and predicted horizontal and vertical movement for measurements point S1 and S2 on Stuveriet and B1 on Brick Studios.

## CONCLUSIONS

The results of the study revealed that ground deformations resulting from the installation of displacement piles were strongly influenced by nearby building foundation. The study utilized the Finite Element Method (FEM), which successfully accounted for the restraining effect of the existing foundation on both horizontal and vertical movement. Additionally, the study demonstrated that a simple methodology, based on greenfield predictions of ground displacements and measured building movement, could provide an initial conservative estimate of existing pile deformations. The simple methodology gave estimates of the pile deformations with reasonably good agreement with both field measurements and FE calculations.

## ACKNOWLEDGEMENTS

The first author acknowledges the financial support provided by SBUF (Development fund of the Swedish construction industry, grants 13614 and 14186) and

BIG (Better Interaction in Geotechnics, grant A2019-19 and B2019-19, from the Swedish Transport Administration).

## REFERENCES

- [1] C. Sagaseta et al.: Deformation analysis of shallow penetration in clay. *International Journal for Numerical and Analytical Methods in Geomechanics* 21(10), 1997.
- [2] Q. Ni et al.: Physical modelling of pile penetration in clay using transparent soil and particle image velocimetry. *Géotechnique* 60(2), 2010.
- [3] T. Edstam & A. Kullingsjö: Ground displacements due to pile driving in Gothenburg clay. *NUMGE 2010*, 2010
- [4] L. Hall et al.: “Piling made less boring” - Minskad omgivningspåverkan genom samverkan. *Grundäggningsdagen*, 2020.
- [5] J. P. J. Dugan & D. L. Freed: Ground Heave Due to Pile Driving. *International Conference on Case Histories in Geotechnical Engineering* 28, 1984.
- [6] C. Sagaseta & A. Whittle: Prediction of ground movements due to pile driving in clay. *Journal of Geotechnical and Geoenvironmental Engineering* 127(1), 2001.
- [7] D. J. Hagerty & R. B. Peck: Heave and lateral movements due to pile driving. *J. Soil Mech. and Found. Div.* 11, 1971.
- [8] L. T. Chen & H. G. Poulos: Piles subjected to lateral soil movements. *Journal of geotechnical and geoenvironmental engineering*, 1997.
- [9] P. Zhou et al.: Analysis of the existing pile response induced by adjacent pile driving in undrained clay. *Computers and Geotechnics* 138, 2021.
- [10] R.B.J Brinkgreve et al... *Plaxis 3D 2010 Manual*. Bentley, 2024.
- [11] A. Fredriksson, Å. Bengtsson & P.E. Bengtsson. *Pålkommisionen rapport 84*, 1991.



# A SURVEY STUDY OF THE ENGINEERING PRACTICE OF PIEZOCONES WITH REGARDS TO SATURATION CONDITIONS

Irene Rocchi<sup>1</sup>, Alena D. Zhelezova<sup>2</sup>

## KEYWORDS

piezocone, CPTU, saturation

## ABSTRACT

For many projects, Cone Penetration Testing with pore-pressure measurements (CPTU) is the main source of information regarding stratigraphy, mechanical and hydraulic properties of soils. Uncertainty in measurements may arise from malfunctioning of the piezocone equipment, poor calibration and/or maintenance, but also a lack of complete saturation. While a correct measurement of the pore-pressure is key to reliable results, and lack of saturation in the piezocone has long been acknowledged as a large source of error, the issue remains unresolved in common engineering practice. The great variety of saturation methods and media encountered in engineering practice is a symptom of the uncertainties persisting on the topic. To mitigate the issue, the saturation process is often explicitly detailed in contractual terms. However, since the quality of saturation can only be assessed *a posteriori*, after the test is completed, unwanted outcomes cannot be entirely avoided. This paper collects information on current engineering practices related to the saturation of piezocone from the perspective of operators and geotechnical engineers. The results highlight the need to implement tools to measure the saturation degree of the pore-water pressure system of piezocones in engineering practice.

## INTRODUCTION

Cone Penetration Test (CPT) is possibly the most employed field technique deployed to obtain information about soil stratigraphy and geotechnical properties. Piezocone testing (CPTu), which includes a sensor to measure the pore-water pressure, was proposed in 1974 and dates back half a century. Defects in the piezocone saturation have since been cited as a major source of

<sup>1</sup> Department of Resource and Environmental Engineering, Technical University of Denmark

<sup>2</sup> Department of Resource and Environmental Engineering, Technical University of Denmark



uncertainty and the comparison of pore-water pressure profiles presented by Lunne et al. [1], which was obtained with instruments having different saturation degrees, has become the epitome of the problem. Yet in engineering practice there is still uncertainty on the best methods and materials to be used for saturation, as indicated by a relatively recent survey [2]. The most acute problem is that saturation is assessed based on data quality, and this cannot be done unequivocally and for obvious reasons cannot be performed beforehand. Because it is more typically done after the test is completed, rather than while it is running, unwanted outcomes cannot be entirely avoided. As a result, operators and clients (or their consultants) may enter into conflict when results are unsatisfactory both because of the economic implications and because the sources and reasons for pore or loss of saturation cannot be objectively established. At the same time, manufacturers tend to minimize the occurrence of poor saturation, which is not conducive to a solution to the problem.

This research presents the results of a survey aimed to estimate the use of piezocone compared to other techniques, the occurrence of poor saturation, its relative importance compared to other issues, and solutions currently adopted in practice. It continues to summarize some preliminary results that have been gathered following the development of a tool that is able to measure the saturation degree of the piezocone pore-water pressure measuring system, based on the same concept applied before performing triaxial test to verify saturation of the hydraulic system.

## **METHOD**

The survey consists of 11 questions both provided as multiple-choice questionnaire and open questions (see Appendix for the questions and the participants for each). Answers were collected in the period from 01.10.2023 to 31.03.2024 using several channels: 1) Google Forms questionnaire posted on LinkedIn and follow-up after meetings (10 responses), 2) during online meetings (8-10 responses), 3) sending emails (3 responses out of 15 contacts), 4) private messaging to contacts on LinkedIn (2 responses out of 15 contacts). The survey was sent to 50 potential participants and resulted in 21 geotechnical firms/engineers answering (42% response rate), which in two cases they also own and operate a CPT truck. Google form responses were anonymous, while the answers obtained through other means were personal. The participants country of operation was varied and included: Norway, Sweden, Belgium, Netherlands, Italy, France, Switzerland, UK, and Australia. While all designers/consultancies performed work both nationally and internationally, no information about extended geography was collected. The results of multiple-choice questions are expressed as % based on the number of answers obtained for each question, since this latter value changes from question to question.

## SURVEY RESULTS

Based on answers to questions 1 and 2 there is no difference in the type of tests used for ground investigation based on whether a project is or not abroad. Laboratory tests, CPT/CPTu tests and other field tests are all always employed (where the relative weighting was not required to be specified), except for one response where only CPT/CPTu tests were considered.

The soil types that participants mentioned being relevant to their projects were varied and included sands, normally and overconsolidated clays, boulder clays, alluvial soils, marine sediments, mine tailings, and also chalk and rocks.

A limitation of the results collected is that most participants interpreted less than 10 tests in the previous 2 months, based on the assumption that far away memories are more likely to be less reliable.

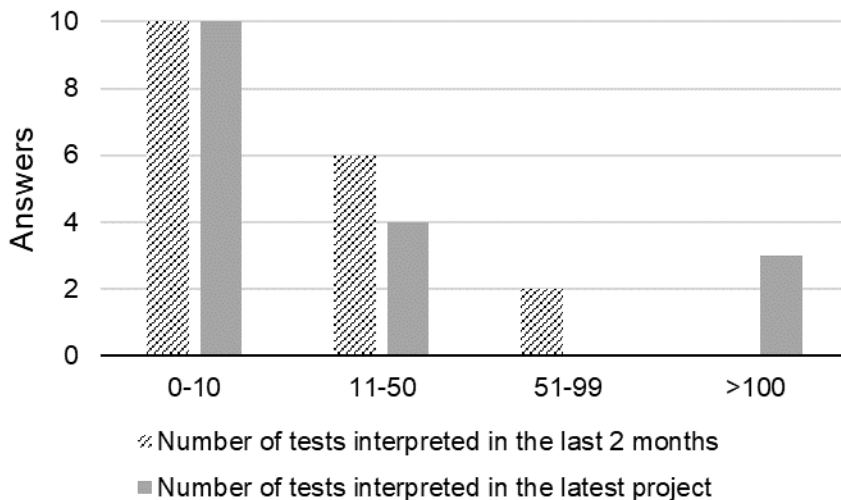


*Figure 1 Representativeness of the survey response based on time proximity of the task and its volume, where the task is interpretation of CPT/CPTu profiles.*

Based on question 6, CPT/CPTu results are the primary source for defining stratigraphy and measuring undrained shear strength (100%), followed by calculation of other mechanical parameters such as stiffness (64%) and angle of shearing resistance (55%), while they are used to a lesser extent to estimate hydraulic parameters (permeability and consolidation both scoring at 36%). The most employed quality check to assess reliability of results are comparison with stratigraphic description of boreholes (mentioned by 6 participants), checking pore-water pressure response with respect to hydrostatic values and

its speed of response (mentioned by 10 participants). With regards to questions 8 and 9, Figure 2 shows from top to bottom the most reported issues and how many of the participants considered this to be a frequent issue, not so frequent or not an issue. Almost unanimously (20 responses out of 21) the most mentioned issue was reported to be pore-water pressure measurements, and associated issues such as occurrence of cavitation and unreliable dissipations, out of which 15 participants reported this to be encountered often. Sleeve friction and depth/inclination were also reported as frequent (4 responses) or not (1 response), alone (1) or combined with pore-water pressure measurements (4).

Finally, when it comes to ways to account for or mitigate the uncertainty linked to pore-water pressure measurements, the following strategies were adopted: test repetition, alternative sources (such as laboratory testing) and adopting conservative values, either together or in combination, the most common being to use laboratory testing as an alternative source (66% of participants adopting this strategy). In equal numbers, participants either repeated the test or adopted a conservative value (about 30% of responses).

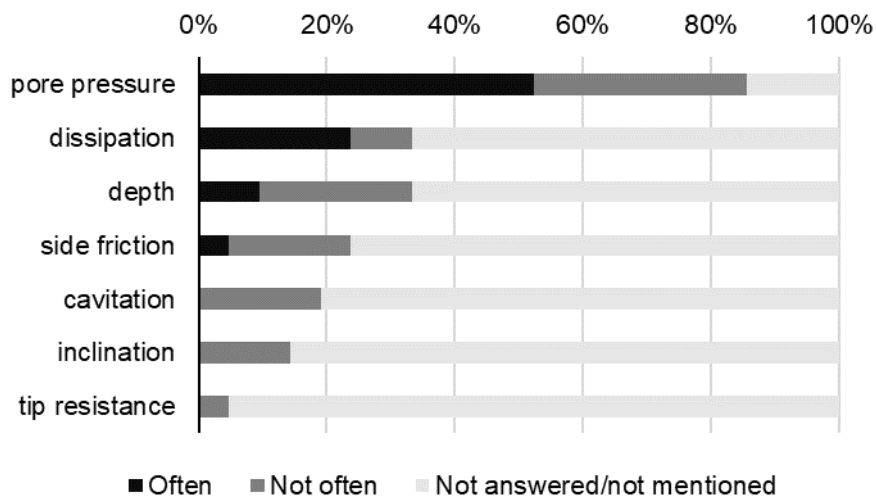


Figure 2 Main issues encountered and their frequency when performing and interpreting CPT/CPTu.

## MEASUREMENT OF SATURATION CONDITIONS AND IMPACT

Figure 3(a) shows a summary of the results obtained when measuring the  $B^*$  value of the pore-water pressure measuring system of a piezocone in laboratory conditions, under different saturation conditions of the filter and the hydraulic system behind it [3,4], which are more extensively described in [5]. A clear link between the saturation degree of the filter and measured  $B^*$  is observed. Furthermore, it is observed that both procedures recommended by the

standards are effective in saturating the instrument. Figure 3(b) compares the pore-water pressure profiles obtained from 2 CPTu soundings performed at the test site of Boretto (Italy), for which  $B^*$  was measured to be 1.0 and 0.84, respectively. Despite the relatively small difference in  $B^*$ , which can only be attributed to poor saturation of the instrument, since the corrected tip resistance ( $q_t$ ) and the sleeve friction ( $f_s$ ) are virtually identical, the pore-water pressure response ( $u$ ) is stunningly different. More detailed information about these field tests can be found in [7].

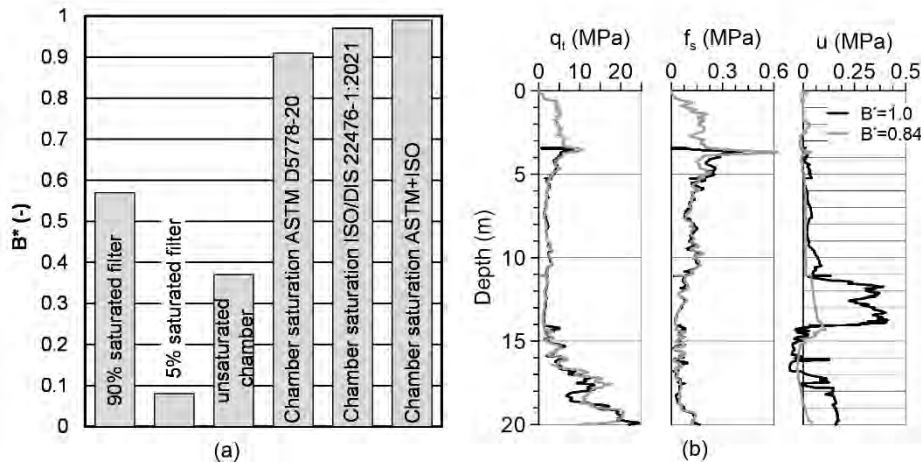


Figure 3 (a) Measurement of piezocone saturation by  $B^*$  and (b) Comparison of pore-water pressure measurement performance based on initial measured  $B^*$ .

## CONCLUSIONS

Pore-water pressure measurements are commonly used as an a posteriori quality check for CPTu results, despite or perhaps because they are the main source of error in CPTu results. Survey results show that there is a need for proper quality control for piezocone saturation, such as provided by the tool developed by Rocchi et al. [8]. This tool, which has been proved to be effective at a laboratory scale, and preliminary validated in the field, allows to quantify the degree of saturation in piezocone tips prior to testing. The ultimate objective of the research is to introduce such tool as a benchmark for quality assessment of piezocone testing with regards to its saturation.

## ACKNOWLEDGEMENT

This work has been funded by the Proof of Concept fund granted by the Sky-lab, Technical University of Denmark and grant Spin-outs Denmark.

## APPENDIX

The survey contains 11 questions (6 multiple choices, with answers reported under the question) followed by the number of responses in brackets.

1. What ground investigations do you recommend to your clients in national projects? (16)
  - a. Laboratory testing
  - b. Cone penetration test (CPT/CPTu)
  - c. Other field tests
  - d. Other
2. What ground investigations do you recommend to your clients in international projects? (19)
  - a. Laboratory testing
  - b. Cone penetration test (CPT/CPTu)
  - c. Other field tests
  - d. Other
3. What types of soils do you mostly work with? (10)
4. How many CPT/CPTu did you interpret in the last 2 months? (18)
5. How many CPT/CPTu did your last project have? (18)
6. For which parameters do you rely most on CPT results? (19)
  - a. Undrained shear strength
  - b. Friction angle
  - c. Stiffness modulus
  - d. Permeability
  - e. Consolidation parameters
  - f. Stratigraphy
  - g. Other...
7. How do you check if the results obtained are of good quality? (20)
8. How often do you encounter issues with CPTu? (21)
9. What are the main issues you encounter with CPTu? (21)
  - a. tip resistance

- b. side friction
  - c. pore pressure
  - d. depth
  - e. inclination
  - f. dissipation
  - g. cavitation
10. What do you usually do to fix/mitigate these issues? (20)
- a. ask for the CPTu to be repeated
  - b. rely on input from a different test
  - c. assume a conservative value
  - d. Other...
11. With regards to filter saturation in CPTu (19)
- a. Good saturation is critical in my typical design tasks
  - b. I do not have knowledge/preference about slot or porous filters being used
  - c. When possible I prescribe guidelines about filter saturation
  - d. Other...

## REFERENCES

- [1] T. Lunne T. et al.: Cone Penetration Testing in Geotechnical Practice. Blackie Academic & Professional, London, 312 pp. 1997
- [2] J. T. DeJong et al.: Design of a Miniature Piezoprobe for High Resolution Stratigraphic Profiling. *Geotechnical Testing Journal*, 30(4), 292–302, 2007.
- [3] ASTM International, 2020. ASTM D5778-20 Standard Test Method for Electronic Friction Cone and Piezocone Penetration Testing of Soils. West Conshohocken: ASTM International.
- [4] International Organization for Standardization, 2021b. ISO/DIS 22476-1:2021 Geotechnical Investigation and Testing – Field Testing – Part 1: Electrical Cone and Piezocone Penetration Test. Geneva, Switzerland.
- [5] I. Rocchi et al.: Novel procedure for measuring the saturation of the pore-pressure system in piezocone tips. *Geotechnique Letters*, 13(4), pp. 191–195, 2023.

- [6] I. Rocchi et al.: Quantitative assessment of tip saturation for high quality piezocone testing. Proceedings 7<sup>th</sup> International Conference on Geotechnical and Geophysical Site Characterization, ISC7 Barcelona, Spain, 2024.
- [7] Rocchi, I., Tonni, L., Gottardi, G.; University of Bologna 2017. Device for checking the degree of saturation of a pressure sensor unit of a piezocone and method for performing the check. Italian patent PCT/IB2017/053104, filed 26/05/2017.

# ALTERNATIVE WAYS OF MODELLING STABILISED EXCAVATIONS

**Sinem Bozkurt<sup>1</sup>, Ayman Abed<sup>1</sup>, and Minna Karstunen<sup>1</sup>**

## KEYWORDS

deep mixing, deep excavations, volume averaging, soft clay, lime-cement columns

## ABSTRACT

The realistic estimation of the soft clay response in deep excavations stabilised with lime-cement columns highly relies on the consideration of nonlinear elastoplastic soil behaviour and three-dimensional (3D) effects. In this paper, deep-mix columns were simulated using both linear elastic and nonlinear elastoplastic constitutive models to illustrate their influence on the deformations of the sheet-pile wall. Model parameters were calibrated using high-quality laboratory tests conducted on both field-mix and laboratory-mix samples. Subsequently, the inherent 3D nature of stabilised soft clay was incorporated into a plane strain analysis using a volume averaging technique. The technique, implemented for 2D analysis, accommodates the use of different advanced soil models to represent the stabilised clay, consisting of the soft clay and columns. The results indicate that relying solely on one-dimensional compression tests when modelling stabilised clay leads to an underestimation of the deformations and structural forces of the sheet-pile wall. The proposed technique maps the actual 3D problem into an equivalent 2D, thus holding the potential to efficiently capture real soil behaviour.

## INTRODUCTION

Deep mixing using lime and/or cement as a cementitious binder has been used over 50 years simultaneously in Japan and Scandinavian countries to improve the strength and compressibility of soft soils. In Nordic countries the dry soil mixing method (DSM) is widely accepted solution in stabilising soft clay (e.g. [1-3]). Additionally, there are applications for sandy soils with insufficient natural water content for proper hydration of the binder using the wet or modified dry mixing methods (i.e. [4, 5]).

<sup>1</sup> Chalmers University of Technology, Department of Architecture and Civil Engineering, Gothenburg, Sweden



The hydromechanical response of the stabilised clay when mixed with stabilising agents differs from the natural or reconstituted states. To simulate the response of artificially cemented clays, traditionally, simple elastic perfectly plastic soil models like Mohr-Coulomb are widely adopted, despite its limitations in realistically representing soil behaviour, such as the absence of hardening/softening plasticity and stress-dependent stiffness. Current guidelines (e.g. [6-9]) for deep mixing design typically propose rigid-plastic solutions and the weighted strength/stiffness based on [10, 11], primarily tailored for embankment applications. These guidelines establish empirical links between the undrained shear strength (determined via vane, unconfined compressive strength (UCS), fall-cone, static penetration tests (FKPS/ FOPS), etc.) and the stiffness. In stabilised excavations with deep mixing, especially in urban settings where serviceability governs the design, stress-dependant stiffness and the influence of the soft clay on the overall response becomes equally critical.

In this paper, a braced excavation stabilised with lime-cement (LC) columns using DSM was investigated by adopting both linear elastic and nonlinear elastoplastic soil models for plane strain (2D) fully coupled consolidation analyses. In the analyses, the stabilised material in the passive side of the excavation was first simulated based on current practice by using averaged strength and stiffness. Later, a three-dimensional (3D) analysis was performed to account for the hydromechanical response of both the soft clay and LC columns separately. Finally, to take into account 3D effects and the different response of individual materials, a volume averaging technique was implemented into a 2D finite element code. The response of the homogenised material involving the soft clay and columns was described based on the 3D simulation. The lateral deformation profile and maximum moment of the sheet-pile wall (SPW) were compared among the alternative methods.

## NUMERICAL MODELLING

The numerical analyses were performed based on a five-meter-deep braced excavation for an arbitrary consolidation period taking into account transient flow. LC column construction in the excavated region was assumed to be wished-in-place, and therefore no installation effects during and after the deep mixing were considered. These effects can be incorporated into simulation through an external strain/load application if field instrumentation data exist (i.e. [12]). The excavation was supported by a fifteen-meter-long SPW and single row of struts with a five-meter spacing in the out-of-plane axis. LC columns, each with a diameter of 0.7 m and a length of 10 m, were arranged in a square grid pattern with a spacing of 2.5 m and a 20 cm overlap, as illustrated in Figure 1(a).

The 2D analyses consisted of utilising simple averaging of stiffness/strength with a linear or nonlinear soil model. In contrast, in the 3D simulation, the columns and soft clay were simulated separately using different nonlinear

elastoplastic soil models to include the varied soil responses (i.e. stress/strain) in a homogenised material (i.e. stabilised clay) (refer to Figure 1(b)). In the 3D case, the overlapping column grid was simplified into a rectangular form for the sake of simplicity, as the primary focus is not on optimising 3D analysis but rather on assessing the influence of the individual constituents on the deformation profile and the structural forces of the SPW. Additionally, to describe the hydromechanical response of the homogenised material, a volume averaging technique (VAT), elaborated in Section 3, was adopted for 2D analysis.

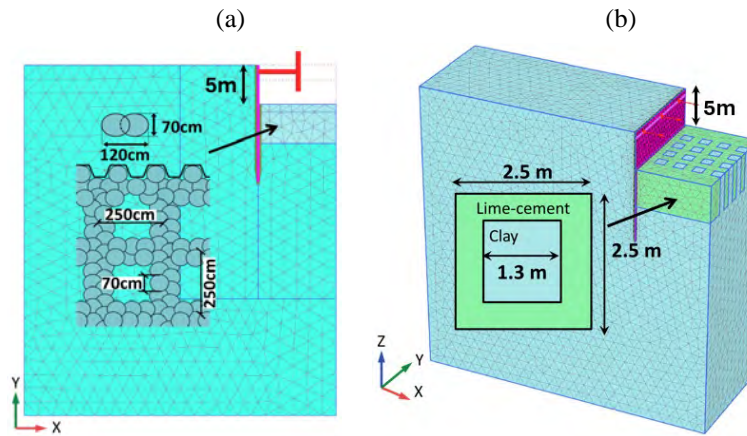


Figure 1. The used FE model in (a) 2D and (b) 3D analyses.

To reduce the effect of discretisation, comparable meshes were utilised in the 2D analyses with 1,125 15-node triangular elements totalling 9276 nodes, whilst in the 3D simulation, 42,294 10-node tetrahedral elements totalling 67,835 nodes were employed. The discretised geometry in the 2D and 3D simulations (PLAXIS 2D & 3D, version 23) at the final excavation phase are presented in Figure 1.

## 2.1. Modelling soft clay

The hydromechanical response of the soft clay was represented by the S-CLAY1S model [13]. The model accounts for the initial anisotropy, the evolution in fabric and in interparticle bonding of natural soft clays owing to plastic straining. The plastic straining governs the progressive loss of bonding ( $\chi$ ) and the volumetric component changes in the size of the intrinsic yield surface. The isotropic preconsolidation pressure ( $p'_m$ ) defines the size of the natural yield surface.  $p'_m$  is linked with the size of the imaginary intrinsic surface where all bonding is destroyed ( $p'_m = (1 + \chi)p'_{mi}$ ). Both the yield and the intrinsic surfaces have the same orientation.

To ensure a more realistic simulation, model parameters for soft clay were taken from a West Link railway tunnel construction project, underneath the centre of Gothenburg, based on a previous study [12]. The hydraulic conductivity of the stabilised clay and natural clay were assumed to be of the same order ( $0.75 \times 10^{-4}$  m/day). The model parameters, computed from several CAUE/CADE (anisotropically consolidated undrained/drained triaxial tests in extension) and IL (incrementally loaded oedometer) tests performed on the field samples, are shown in Table 1.

Table 1. S-CLAY1S parameters for the soft clay.

	Definition	Value [-]
$\lambda_i$	intrinsic compression index	0.2
$\kappa$	swelling index	0.02
$\nu'$	Poisson's ratio	0.2
$M$	critical state stress ratio	1.10
$\mu$	absolute effectiveness of rotational hardening	50
$\beta$	relative effectiveness of rotational hardening	0.64
$a$	absolute rate of destructuration due to volumetric strain	12
$b$	relative rate of destructuration due to shear strain	0.4
$\chi_0$	initial amount of bonding	6
$\alpha_0$	initial anisotropy	0.42
$OCR$	overconsolidation ratio	1.20
$K_0$	coefficient of earth pressure at rest	0.54
$e_0$	initial void ratio	1.90

## 2.2. Modelling deep-mix columns

The deep-mix columns were modelled using the Matsuoka-Nakai hardening (MNhard) [14] and Mohr Coulomb (MC) soil models. The MNhard model employs hyperbolic stress-strain relationship for shear hardening and the ultimate failure is computed based on the Matsuoka-Nakai failure criterion [15].

During the stages of primary loading (secant modulus,  $E'_{50}$ ) and unloading-reloading (un-/reloading modulus,  $E'_{ur}$ ), stress-dependent moduli can be computed with a power law using Equation (1).

$$E'_{50,ur} = E'_{50,ur}{}^{\text{ref}} \left( \frac{\sigma'_3 + c' \cot \phi'}{\sigma'^{\text{ref}} + c' \cot \phi'} \right)^m \quad (1)$$

where  $m$  defines the amount of stress dependency and controls the shape of the yield surface. Shear modulus can be estimated using elasticity theory ( $G = E'/(1 + \nu')$ ) and can be simulated using triaxial test data.

The Matsuoka-Nakai failure criterion is determined by the average of the mobilised planes (SPM) in 3D effective stress space using Equation (2), while the MC failure is defined by shear ( $\tau$ ) and normal ( $\sigma$ ) effective stresses considering major and minor principal stresses on the failure plane with Equation (3). As demonstrated in Section 4, for serviceability limit states neither failure criterion nor strength ( $c'$  and  $\phi'$ ) are influential.

$$\frac{\tau_{\text{SMP}}}{\sigma_{\text{SMP}}} = \frac{2}{3} \sqrt{\frac{(\sigma_1 - \sigma_2)^2}{4\sigma_1\sigma_2} + \frac{(\sigma_2 - \sigma_3)^2}{4\sigma_2\sigma_3} + \frac{(\sigma_3 - \sigma_1)^2}{4\sigma_3\sigma_1}} \quad (2)$$

$$\tau_f = c' + \sigma'_f \tan \phi' \quad (3)$$

The parameters for the MC model parameters were computed using the unconfined compression strength (UCS) from data provided by [16]. The tests performed on field-mixed samples, taken from various depths for the West Link project, are presented in Figure 2. The proportion of binder was 50% lime and 50% cement with 80 kg/m<sup>3</sup> by dry weight.

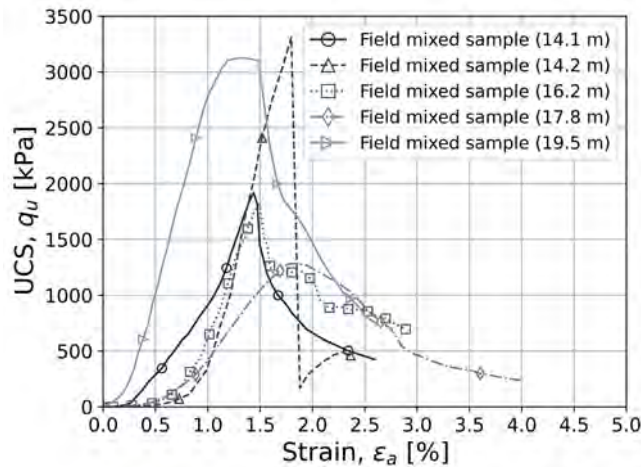


Figure 2. UCS tests performed on field mixed samples (adopted from [16]).

According to Figure 2, although the available samples were selected to be able to conduct the unconfined compression tests (UCT), possible low-strength regions along the stabilised zone are likely to affect overall response, as the available samples may not fully represent the LC columns. The significant variation of the unconfined strength,  $q_u$ , is noteworthy, with a coefficient of variation of 46%. The minimum, maximum and average values of  $q_u$  are 1.3-3.3 and 2.3 MPa, respectively. The average  $E'_{50}$  was computed as 216 MPa from the laboratory data, which corresponded to 230 MPa using the lower bound estimation of  $E'_{50}/q_u$  defined as 100 in [9]. Considering the large variation in measured  $q_u$ , the upper and lower boundaries were investigated for the 2D simulations using the simple stiffness averaging method.

To explore the influence of the strength, the lower boundary was determined by averaging the effective strength parameters of the column and *in situ* clay, while the upper boundary values belong to the LC columns calculated from triaxial tests. Effective strength parameters are derived from triaxial tests. The averaged stabilised clay properties using the MC model are presented in Table 2.

Table 2. The averaged MC soil model parameters for stabilised region (2D FEA).

	$\gamma_n$ (kN/m <sup>3</sup> )	$E_{50}$ (kPa)	$\Phi'$ (°)	$c'$ (kPa)	$v'$ (-)
<b>Lower, <math>q_{u(min)}</math></b>	16.5	97500	35	15	0.25
<b>Upper, <math>q_{u(avg)}</math></b>	16.5	171220	37	20	

The parameters for the MNhard model for the stabilised clay were determined and calibrated using a series of CAUE and IL tests performed on both *in situ*

mixed and laboratory mixed samples [11]. In this study, for the 2D finite element analysis (FEA), a simple stiffness/strength averaging technique was initially applied, using a simplified area replacement ratio of 0.73 ( $a_r = (2.5^2 - 1.3^2) / 2.5^2$ ), based on the overlapping column square-grid (see Figure 1(a) and Table 3). The average stiffness of the stabilised clay was computed using the arithmetic mean of the soft clay ( $E'_{50}=15\text{MPa}$ ,  $E'_{ur}=39\text{MPa}$ ) and LC column ( $E'_{50}=85\text{MPa}$ ,  $E'_{ur}=180\text{MPa}$ ) stiffness. In contrast, in the 3D analysis and in the subsequent 2D analysis with VAT, LC columns were represented without the averaging by using the values presented in Table 4.

*Table 3.* The averaged MNhard soil model parameters for stabilised region (2D FEA).

$\gamma_n$ (kN/m <sup>3</sup> )	$G_{50}^{\text{ref}}$ (kPa)	$G_{ur}^{\text{ref}}$ (kPa)	$p^{\text{ref}}$ (kPa)	$m$ (-)	$\phi'$ (°)	$c'$ (kPa)	$u'$ (-)
16.5	25000	56000	100	0.65	37	20	0.25

*Table 4.* MNhard soil model parameters for the columns (2D VAT and 3D FEA).

$\gamma_n$ (kN/m <sup>3</sup> )	$G_{50}^{\text{ref}}$ (kPa)	$G_{ur}^{\text{ref}}$ (kPa)	$p^{\text{ref}}$ (kPa)	$m$ (-)	$\phi'$ (°)	$c'$ (kPa)	$u'$ (-)
16.5	28000	75000	100	0.65	37	20	0.25

## VOLUME AVERAGING TECHNIQUE

The volume averaging technique (VAT) has been used to describe the response of the composite materials consisting of two or more materials [17]. The method has been employed to simulate settlements in soft clay underneath the road embankments stabilised with deep mixed/stone columns [18, 19]. The stress-strain increments within the composite material can be calculated by averaging the increments of the individual constituents, under the assumption of an equivalent homogenised material. The averaging rules that form the basis for describing the response of the equivalent material are given in Equations (4) and (5).

$$\Delta\sigma^{eq} = \Omega_s\Delta\sigma^s + \Omega_c\Delta\sigma^c \quad (4)$$

$$\Delta\epsilon^{eq} = \Omega_s\Delta\epsilon^s + \Omega_c\Delta\epsilon^c \quad (5)$$

where  $\Omega$  represents the fraction of individual materials, while  $\Delta\sigma$  and  $\Delta\epsilon$  stand for the increments of stress and strain tensors, respectively. The subscripts  $c$ ,  $s$  and superscript  $eq$  denote the columns, soft clay and equivalent material.  $\Omega$  can be computed considering the representative plan area of the

constituents for evenly distributed columns. Alternatively, the geometry can be divided into subsections to increase the accuracy of the calculations.

VAT has not been applied to stabilised excavation problems owing to difficulties in assessing interaction mechanism between the soft clay and deep-mix columns. In this study, the stress-strain distribution of the equivalent material, comprising the natural clay and deep-mix columns, was generalised based on the 3D analysis by investigating the relevant equilibrium and kinematics conditions. The fundamental considerations to preserve local equilibrium are presented in Equations (6)-(8). In the equations, global coordinate system for plain strain analysis was utilised where  $x$  and  $z$  designate the horizontal axes, and  $y$  is the vertical axis.

$$\Delta\sigma'_{zz}{}^{\text{eq}} = \Delta\sigma'_{zz}{}^{\text{c}} = \Delta\sigma'_{zz}{}^{\text{s}} \quad (6)$$

$$\Delta\tau_{yz}^{\text{eq}} = \Delta\tau_{yz}^{\text{c}} = \Delta\tau_{yz}^{\text{s}} \quad (7)$$

$$\Delta\tau_{zx}^{\text{eq}} = \Delta\tau_{zx}^{\text{c}} = \Delta\tau_{zx}^{\text{s}} \quad (8)$$

Similarly, compatibility in kinematics of the strain field is maintained using Equations (9)-(11).

$$\Delta\varepsilon_{xx}^{\text{eq}} = \Delta\varepsilon_{xx}^{\text{c}} = \Delta\varepsilon_{xx}^{\text{s}} \quad (9)$$

$$\Delta\varepsilon_{yy}^{\text{eq}} = \Delta\varepsilon_{yy}^{\text{c}} = \Delta\varepsilon_{yy}^{\text{s}} \quad (10)$$

$$\Delta\gamma_{xy}^{\text{eq}} = \Delta\gamma_{xy}^{\text{c}} = \Delta\gamma_{xy}^{\text{s}} \quad (11)$$

The elastic stiffness matrix of the equivalent material ( $\mathbf{D}^{\text{eq}}$ ) is constituted using the stress equality conditions that results in an independent strain distribution within the soft clay and columns. The independent strain distribution can be formed analytically through the strain redistribution matrices,  $\mathbf{S}_1^{\text{s,c}}$  using continuity constrains (Equations (9)-(11)). Thereby, the stress increments in the equivalent material can be expressed in terms of effective stresses of the individual materials using Equations (4) and (12), and  $\mathbf{D}^{\text{eq}}$  can be established, provided that the elastic stiffness matrix of the individual materials,  $\mathbf{D}^{\text{s,c}}$ , are known (Equation (13)).

$$\Delta\mathbf{D}^{\text{eq}}\boldsymbol{\varepsilon}^{\text{eq}} = \Omega_s\mathbf{D}^{\text{s}}\mathbf{S}_1^{\text{s}}\boldsymbol{\varepsilon}^{\text{eq}} + \Omega_c\mathbf{D}^{\text{c}}\mathbf{S}_1^{\text{c}}\boldsymbol{\varepsilon}^{\text{eq}} \quad (12)$$

$$\mathbf{D}^{\text{eq}} = \Omega_s\mathbf{D}^{\text{s}}\mathbf{S}_1^{\text{s}} + \Omega_c\mathbf{D}^{\text{c}}\mathbf{S}_1^{\text{c}} \quad (13)$$

VAT was implemented into the commercial finite element code Plaxis2D (version 23) as a user-defined soil model (UDSM). Local integration was achieved using an implicit scheme to solve nonlinear equations iteratively. During the iterative calculations, if the equilibrium constraint is not achieved, stress states revert to previous values and strain increments are redistributed between the constituents, initiated by the return mapping scheme. The technique therefore always satisfies both the local balance and maintains the continuity of kinematics.

## RESULTS

The stress-strain response of the braced excavation stabilised with LC columns was initially investigated following the current design guidelines. The investigation involved using the average stiffness/strength of the clay and column materials. In the simulations, both linear and nonlinear elastoplastic constitutive models were utilised to model the stabilised clay in the passive side of the excavation. Either the MC or MNhard model was employed, incorporating the averaged stiffness and strength parameters as indicated in Table 2 and 3. The natural soil, the soft clay, was represented by the anisotropic S-CLAY1S model. However, the adopted simple stiffness/strength averaging approach unfortunately does not account for the hydromechanical response of the soft clay.

The results of the simulations were compared to evaluate the effects of choosing between linear and nonlinear model options, as depicted in Figure 3. When calculating the average stiffness using the MC model, the stiffness of the columns was determined, taking into consideration the variability of  $q_u$ . Consequently, both the minimum and average values were investigated. The stiffness calculated from the average strength ( $q_{uav}$ ) led to a significantly lower maximum lateral deformation of approximately 3 mm, along the first 5 meters of the excavation. In contrast, using the minimum strength ( $q_{umin}$ ) resulted in approximately 5 mm (see Figure 3(b)). Employing the MNhard model yielded a maximum lateral deformation of 9 mm. Evidently, regardless of the model choice, averaging the strength appears to have no effect on the lateral deformation profile of the SPW, as it is governed by the serviceability limit state. This is particularly relevant for braced excavations in urban areas, where the excavations are designed for restricted lateral deformations. In Figure 3(a), the lateral deformation profile was affected by the averaged strength only marginally. The difference arises from the formulation of the MNhard model in which the stress dependent stiffness is a function of the strength parameters ( $c'$  and  $\phi'$ ) outlined in Equation (1).



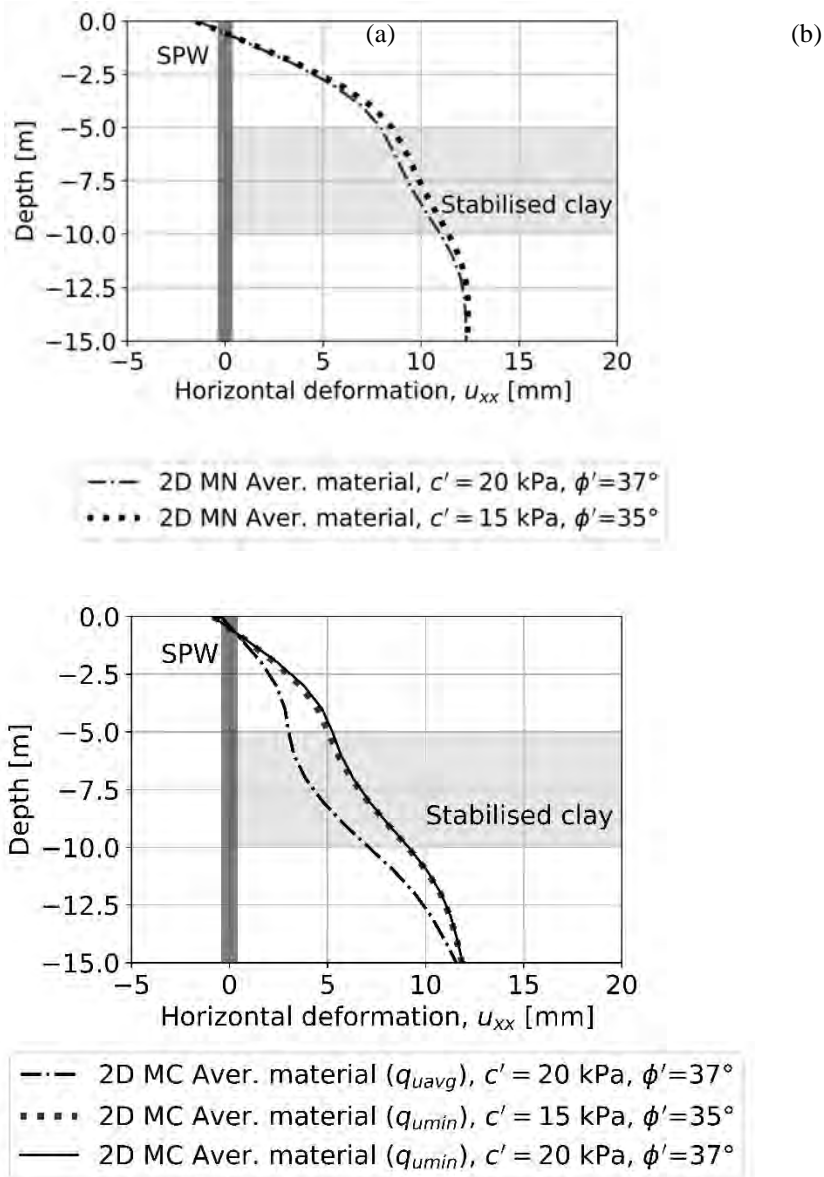


Figure 3. Lateral pile deformation profile at the final excavation stage with/without averaging strength. (a) MNhard model and (b) MC model.

To take into account the hydromechanical response of the soft clay, the braced excavation was investigated using a 3D analysis. The distinct mechanical properties of the natural clay and columns were simulated using different advanced constitutive models (S-CLAY1S and MNhard models, respectively) with conventional separate soil clusters (Figure 1(b)). Subsequently, the stress-strain response of the individual materials identified in the 3D simulation was incorporated into 2D analysis using VAT elaborated in Section 3.

The results of the numerical simulations on the lateral deformation profile and moment distribution of the SPW, using the alternative methods with different constitutive model choices, were compared in Figure 4 and 5.

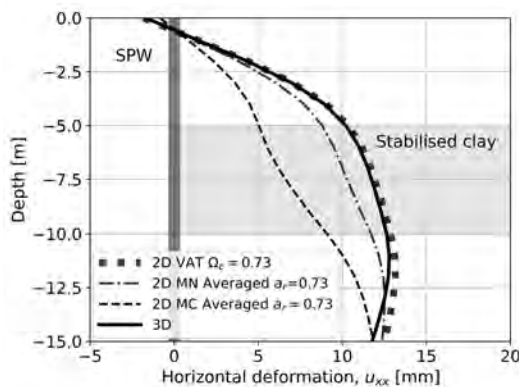


Figure 4. SPW lateral deformation profile at the final excavation stage for alternative methods.

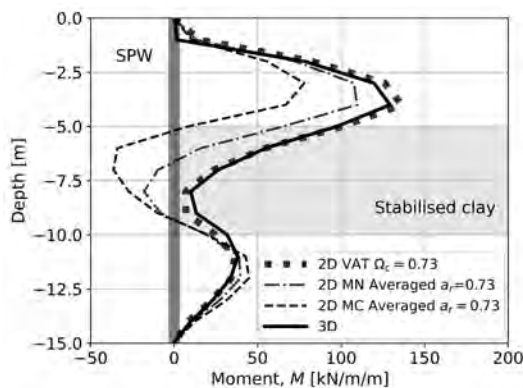


Figure 5. SPW moment profile at the final excavation stage for alternative methods.

The choice of the linear elastic perfectly plastic MC model led to an underestimation of the lateral deformations as well as the maximum moment of the SPW (see Figures 4 and 5). Employing a hardening/softening plasticity model (i.e. MNhard) resulted in a deformation and moment profile more closely aligned with the 3D simulation. Nevertheless, the closest representation of the deformation profile in the 3D simulation was achieved by incorporating the soft clay response using VAT in a plane strain simulation. The results of the 2D simulation with VAT demonstrate robust agreement with those obtained from the 3D simulation.

## CONCLUSIONS

2D and 3D fully coupled numerical analyses of a braced excavation stabilised with LC were performed. Initially, the stabilised clay in the passive side of the excavation was simulated using the averaged strength and stiffness based on current practice by adopting both linear elastic perfectly plastic and nonlinear elastoplastic soil models for the 2D analyses. The results highlight the inadequacy of one-dimensional compression tests (UCT) for modelling stabilised soft clay, which leads to underestimation of deformations and structural forces.

Subsequently, a separate 3D analysis was performed to address the hydromechanical response of the soft clay and LC columns individually. To account for the 3D nature of deep excavations stabilised with deep-mix columns and the distinct response of the clay and columns, a volume averaging technique (VAT) was integrated into a 2D finite element code. The proposed VAT is a computationally efficient tool, with the potential to capture real soil behaviour with high fidelity. Using soil models that employ hardening/softening plasticity and/or stress-dependent stiffness led to a more accurate representation of the stabilised clay, accounting for the response of both the deep-mix columns and soft clay.

## ACKNOWLEDGEMENT

The work is funded by Formas (Research Council for sustainable Development) and Swedish Transport Administration via BIG (Better Interaction in Geotechnics). The work is done as part of Digital Twin Cities Centre that is supported by Sweden's Innovation Agency VINNOVA.

## REFERENCES

- [1] H. Löfroth: Properties of 10-year-old lime-cement columns. Deep mixing 5, 2005.
- [2] R. Ignat, S. Baker, M. Karstunen, S. Liedberg, & S. Larsson: Numerical analyses of an experimental excavation supported by panels of lime-cement columns. Comput. Geotech. 118, 103296, 2020.
- [3] S. Larsson: The Nordic dry deep mixing method: Best practice and lessons learned. In Deep Mixing-An Online Conference (pp. 30-p). DFI Deep Foundation Institute, 2021.
- [4] J. Gunther, G. Holm, G. Westberg, & H. Eriksson: Modified Dry Mixing (MDM) – A New Possibility in Deep Mixing. In Geotechnical Engineering for Transportation Projects, 2004.
- [5] S. Hov, P. Paniagua, C. Sætre, H. Rueslåtten, I. Størdal, M. Mengede, & C. Mevik: Lime-cement stabilisation of Trondheim clays and its impact on carbon dioxide emissions. Soils and Foundations, 62(3), 101162, 2022.
- [6] EuroSoilStab: Development of design and construction methods to stabilize soft organic soils: Design guide for soft soil stabilization. CT97-0351, European Commission, Industrial and Materials Technologies Programme (Rite-EuRam III) Bryssel, 2002.
- [7] EN14679: European Standard, Execution of Special Geotechnical Works – Deep Mixing, 2005.
- [8] TK GEO: Technical requirements for geotechnical constructions. Publication 2013:0667, Swedish Transportation Administration, Borlänge. In Swedish, 2013.
- [9] SGF: Lime and lime cement columns - Guide for project planning, construction and inspection. SGF Report 2:2000, Swedish Geotechnical Society. In Swedish, 2000.
- [10] B. B. Broms, & P. Boman: Lime Columns—A New Foundation Method. Journal of the Geotechnical Engineering Division, 105(4), 539–556, 1979.
- [11] B. B. Broms: Lime and lime/cement columns. Ground Improvement, 2, 252–330, 2004.
- [12] S. Bozkurt, A. Abed, & M. Karstunen: Finite element analysis for a deep excavation in soft clay supported by lime-cement columns. Computers and Geotechnics, 162, 105687, 2023.
- [13] M. Karstunen, H. Krenn, S. J. Wheeler, M. Koskinen, & R. Zentar, Effect of Anisotropy and Deconstruction on the Behavior of Murro Test Embankment. International Journal of Geomechanics, 5(2), 87–97, 2005.

- [14] T. Benz: Small-Strain Stiffness of Soils and its Numerical Consequences. PhD thesis, University of Stuttgart, Germany, 2007.
- [15] H. Matsuoka, & T. Nakai: Stress-deformation and strength characteristics of Soil Under Three Different Principal Stresses. Proceedings of the Japan Society of Civil Engineers, 1974, Volume 1974, Issue 232, 59-70, 1974.
- [16] Swedish Transport Administration: Fullskaleförsök DDM (Dry Deep Mixing) i passivzon, delprojekt E02 Centralen, Västlänken. Technical report. TRV 2015/74805. Swedish Transport Administration, 2018.
- [17] Z. Hashin: Analysis of Composite Materials—A Survey. Journal of Applied Mechanics 50, 481–505, 1983.
- [18] H. F. Schweiger, & G. N. Pande: Numerical analysis of stone column supported foundations. Computers and Geotechnics, 2(6), 347–372, 1986.
- [19] U. Vogler: Numerical modelling of deep mixing with volume averaging technique. PhD thesis, The University of Strathclyde, 2009.

# ANALYSES OF PERFORMED CPT TESTS ON SITE WITH RESPECT TO THE NEW STANDARD

**Caesar Kardan<sup>1</sup>, and Håkan Garin<sup>2</sup>**

## KEYWORDS

CPT, CPTU, Cone penetrometer, Cone resistance, Sleeve friction, Eurocode, Guidelines, Standards, Operator performance, Calibration

## ABSTRACT

*“Quality of CPTU – Analysis and Comparison of data from Commercial Actors in Stockholm/Mälardalen”* was a study conducted by the Royal Institute of Technology during the autumn of 2014. The scope (aim) of the study was to evaluate the quality of CPTU with respect to SS-EN ISO 22476-1:2012 and mostly based on the choice of equipment since the equipment is different in design and functionality but also the execution and factors related to the performance of the operators.

The main purpose of this study is to evaluate the results from the conducted field test in the previous paper from 2014 with respect to the new guideline SS-EN ISO 22476-1:2023 and study the difference in the results of the classification of performed CPTUs.

## INTRODUCTION

There are some other differences between the old guideline and the new one such as dimensional tolerances of cone penetrometer and minor updates to figures and text. Still, the more important changes are related to requirements for the calibration of cone penetrometers, introduction of temperature influence on measurement monitoring and requirements of internal temperature sensor for cone penetrometer class 0 and differences in classification of CPTUs.

## DIFFERENCES BETWEEN OLD AND NEW GUIDELINES

### **Maintenance, checks and calibration**

Maintenance, checks and calibration of the cone penetrometers have been described in Annex B in the new standard SS-EN ISO 22476-1:2023. The

<sup>1</sup> Skanska Teknik, Stockholm

<sup>2</sup> GeoVerkstan, Kungsbacka

first part is maintenance and checks which is not significantly changed compared to the old standard and includes the aspects below:

- ❖ Linearity of pushrods.
  - Minor updates in the text have been made, updated with regards to Test Category instead of Application Class.
- ❖ Wear of cone penetrometers.
  - Updated with the procedure for determining cross-sectional area and sleeve friction using cone penetrometer class 0.
- ❖ Gaps and seals.
  - No updates in this section.
- ❖ Pore pressure measuring system.
  - No updates in this section.
- ❖ Maintenance procedure.
  - Minor updates in Table B1 (Table A1 in the old standard) regarding the control scheme for maintenance routines.

According to the new standards, the reference readings of the measured parameters should be taken twice. The first reading should be taken after the cleaning of the cone penetrometers and this reading is more useful for compression of cone resistance ( $q_c$ ) and sleeve friction ( $f_t$ ).

The second reference reading should be performed with the cone penetrometer unloaded under similar temperature conditions as close to the ground temperature as possible. The second reading is more useful for the correction of the pore pressure concerning instability in the output and for gathering long-term measurement series.

The section regarding calibration has been revised significantly. This section has been divided into 8 subsections.

The first subsection is about “*Environment and preparation*” which provides the reader with requirements regarding the range of temperature and standard uncertainty, time and cleaning of the cone penetrometer and that the cone penetrometer should be fully assembled during calibration.

The second subsection is about measuring intervals for calibration with general information about measuring intervals and typically selected intervals for calibration of inclination.

The other subsections (from B.2.3 to B.2.8) are listed below:

- ❖ Cone resistance and sleeve friction calibration
- ❖ Calibration of pore pressure sensor
- ❖ Determination of cone and friction sleeve dimensions
- ❖ Calibration of a cone penetrometer for inclination
- ❖ Verification of a cone penetrometer for temperature influence
- ❖ Verification of a cone penetrometer for bending influence

Each subsection has been divided into three parts:

- ❖ General
- ❖ Test method
- ❖ Assessment of calibration uncertainty
- ❖ Test results

In the “*General*” part for each subsection, there are some descriptions regarding how the test will be conducted, the devices needed to perform calibration and the environmental aspects such as air temperatures etc.

The “*Test method*” is the most important part of each subsection. In this part, there are some detailed descriptions regarding how the calibration needs to be done in a certain order. Each step is described with detailed instructions and every step needs to be performed for three different angles ( $\Theta = 0^\circ$ ;  $\Theta = 120^\circ$ ;  $\Theta = 240^\circ$ ) perpendicular to the axis of the cone.

The part regarding “*Assessment of calibration uncertainty*” is the calculation procedure with several mathematical equations to evaluate the uncertainties for each calibration phase.

The part “*Test results*” includes how the results should be documented. Besides the general information such as the serial number for the cone penetrometer, the manufacture of the cone penetrometer and so on, every moment of the calibration procedure should be documented with all the data for each rotational position ( $\Theta = 0^\circ$ ;  $\Theta = 120^\circ$ ;  $\Theta = 240^\circ$ ) and the results from each phase. Some results such as expanded measurement uncertainty for cone resistance or bending influence for all four major parameters ( $q_{c,a}$ ;  $f_{s,a}$ ;  $u_a$ ;  $T_a$ ) should also be illustrated graphically. An example of how a calibration report should be compiled is presented in Annex C in SS-EN ISO 22476-1:2023.

## CLASSIFICATION

The classification in the previous version of Standard SS-EN ISO 22476-1:2012 was based on the Application class in which test type, allowable minimum accuracy for the measured parameters, the maximum length between the measurements, the type of the soil and some instructions regarding interpretation and evaluation. The application classes from SS-EN ISO 22476-1:2012 are presented in Figure 1.





Table 3 — Test categories of CPT/CPTU

Test category	Cone penetrometer class	Reference reading checks		
		Parameter	Maximum allowable difference of reference values before and after test	Maximum variation in output stability
A	0	Cone resistance	15 kPa	1 kPa
		Sleeve friction	5 kPa	0,5 kPa
		Pore pressure	3 kPa	0,5 kPa
B	0, 1	Cone resistance	35 kPa	5 kPa
		Sleeve friction	5 kPa	1,5 kPa
		Pore pressure	10 kPa	3 kPa
C	0, 1, 2	Cone resistance	100 kPa	11 kPa
		Sleeve friction	15 kPa	3 kPa
		Pore pressure <sup>a</sup>	25 kPa	8 kPa
D	0, 1, 2, 3	Cone resistance	200 kPa	33 kPa
		Sleeve friction	25 kPa	5 kPa
		Pore pressure <sup>a</sup>	50 kPa	16 kPa

<sup>a</sup> Pore pressure applies only to CPTU.

Figure 2 Table 3 in SS-EN 22476-1:2023.

In this system, cone penetrometers will be categorized during the calibration of them from class 0 up to class 3 where class 0 has the most accurate requirements and class 3 has the least accurate ones. Based on the results from achieved cone resistance  $q_c$  from performed attempts in the field, each one of these classes will give a confidence level which can be high, medium, low or not applicable.

So basically, depending on the class of cone penetrometer and the achieved cone resistance  $q_c$  the requirements for one category will be fulfilled. For example, to achieve test category A, the chosen cone penetrometer for the attempt has to be a class 0 penetrometer and the measured  $q_c$  should be less than 1 MPa ( $q_{c,max} > 1$  MPa). This means that the new standard is a planning tool as well as it can be used for evaluation. To achieve a certain test category, the choice of cone penetrometers should be right from the beginning. The requirements for the confidence level with respect to cone penetrometer class and the result of cone resistance  $q_c$  are presented in the SS-EN ISO 22476-1:2023 Appendix A and illustrated in Figure 3.

**Table A.1 — Confidence levels of measurements for the characterisation of geotechnical properties depending on the cone type and test category**

Application	Confidence level	Cone penetrometer class			
		0	1	2	3
Characterisations of geotechnical proprieties of soil deposits with $q_{c;max} \leq 1$ MPa	High	A			
	Medium	B			
	Low	C			
Characterisations of geotechnical proprieties of soil deposits with $1 \text{ MPa} < q_{c;max} \leq 3$ MPa	High	B			
	Medium	C			
	Low	D			
Characterisations of geotechnical proprieties of soil deposits with $q_{c;max} > 3$ MPa	High	Not recommended	B and C		
	Medium		D		
NOTE A, B, C and D are the test categories according to <a href="#">Table 3</a> .					

Figure 3, Table A.1 in SS-EN 22476-1:2023.

## TEMPERATURE INFLUENCE

The new Standard SS-EN ISO 22476-1:2023 has been updated with requirements regarding the verification of cone penetrometers for temperature influence. The operation shall be conducted in two thermostat baths the first one being a bath with tap water or a mixture of water and antifreeze with the capability of maintaining a constant temperature of fluid at 30°C with a standard uncertainty of <0,5°C during the entire test. The second bath on the other hand has the capability of maintaining a constant temperature of fluid at 0°C with a standard uncertainty of <0,5°C.

The test method is generally based on recording the apparent cone resistance  $q_{c;a}$ , apparent sleeve friction  $f_{s;a}$  and apparent pore pressure  $u_a$  and also the temperature  $T_a$  throughout the test at  $\geq 1$  Hz to determine and record the temperature-corrected cone resistance  $q_{c;ac}$ , sleeve friction  $f_{s;ac}$  pore pressure  $u_{ac}$  by transferring the cone penetrometer several times between thermostat 1 and 2. The entire procedure of verification of a cone penetrometer for temperature influence and also reporting the results is described in SS-EN ISO 22476-1:2023 Annex B chapter B.2.7.

The results from the verification of CPTU with respect to temperature influence can be used to apply corrections to the measurements of  $q_c$ ,  $f_s$  and  $u_2$ . Temperature sensors can be integrated into any cone class with the main purpose of monitoring the temperature changes that can affect the cell loads and pressure transducer. For the cone penetrometers with application class 0, the requirement is that the integrated sensor in the cone penetrometer has the range of -10°C to +50°C with a maximum allowable uncertainty of 0,5°C.

The temperature influence is an important aspect of achieving reliable results from CPTU. However, the gathered data historically from cone penetrometers in Nordic countries indicate suitable results and that the values fulfil requirements regarding the temperature aspect.

## RESULTS & EVALUATION

The evaluation from the performed CPTU in the field in the previously mentioned study from 2014 has been performed based on the reference values (zero values) of each penetration before and after that penetration is performed (Calibration Drift) and with respect to both the old standard SS-EN ISO 22476-1:2012 and the new standard SS-EN ISO 22476-1:2023. The results from reference values are presented in the study under section 4.4.2 and Table 1.

Penetration ID	Cone resistance (kPa)			Pore pressure (kPa)			Sleeve friction (kPa)		
	Before	After	Diff	Before	After	Diff	Before	After	Diff
14C001	9660	9588	-72	920.7	933.6	12.9	332.4	330.8	-1.6
14C004	9654	9600	-54	934.4	937	2.6	325.4	324.7	-0.7
14A005	7196	7160	-36	285.6	285.7	0.1	184.6	183.5	-1.1
14A006	7306	7234	-72	287.5	285.8	-1.7	184.3	6553.5	6369.2
14A007	7148	7250	102	283.2	287	3.8	184.5	184.2	-0.3
14A008	7262	7262	0	292.8	290	-2.8	183.8	183.4	-0.4
14A009	7236	7204	-32	294.1	298.9	4.8	182.8	183.1	0.3
14A010	7232	7200	-32	290.9	288	-2.9	183.5	183.6	0.1
14A011	7136	7100	-36	286	305.6	19.6	185.7	185.9	0.2
14A012	7244	7210	-34	284.4	309.8	25.4	185.4	184.3	-1.1
14A016	7218	7192	-26	282.3	308.2	25.9	181.4	180.7	-0.7
14D017	6456	6453.1	-2.9	255.5	256.4	0.9	132.5	132.5	0
14D018	6453.7	6465.4	11.7	255.9	255	-0.9	132.1	132.4	0.3
14D019	6452.5	6460.1	7.6	254.8	264.1	9.3	133.1	132.8	-0.3
14SD20b	6461.3	6454.9	-6.4	255.7	255.2	-0.5	132.8	132.4	-0.4
14B021	3170.6	3173.1	2.5	273.4	280.1	6.7	112.2	112.5	0.3
14B022	3204.9	3184.2	-20.7	274.7	273.9	-0.8	112.5	112.8	0.3
14B023	3212.7	3150	-62.7	290.3	273.4	-16.9	112.6	113	0.4
14B024	3174	3166.2	-7.8	274.5	270.4	-4.1	112.7	112.8	0.1
14B025	3204.9	3168.5	-36.4	273.8	272.9	-0.9	112.7	112.9	0.2
14B026	3171.2	3174.5	3.3	274.1	273.7	-0.4	112.6	112.7	0.1
14E027	4612	4622	10	597.7	610.4	12.7	147.2	148.9	1.7
14E028	4598	4474	-124	598.5	598.6	0.1	149	149	0
14E029	4480	4470	-10	594.5	607.3	12.8	150.9	151.3	0.4

Table 1, The registered zero values for each borehole during penetration.

The results from the performed CPTU based on the reference values (zero values) in the previous Figure and with respect to the old standard SS-EN ISO 22476-1:2012 and the new standard SS-EN ISO 22476-1:2023 presented in Tabell 4-1. For the new standard, all the cases had measured cone resistances  $q_c$  less than 1 MPa ( $q_{c,max} > 1$  MPa) along the entire penetration which means that the criteria for the first case in Table A-1 in Appendix A is fulfilled.

The results from the performed CPTU based on the reference values (zero values) in the previous Figure and with respect to the new standard SS-EN ISO 22476-1:2023 are presented in Table 2. For all the cases are the measured cone resistance  $q_c$  less than 1 MPa ( $q_{c:\max} > 1$  MPa) which means that the criteria for the first case in Table A-1 in Appendix A are fulfilled.

Penetration ID	Reference Values			SS-EN ISO 22476-1:2012	SS-EN ISO 22476-1:2023	
	$u_2$ [kPa]	$f_s$ [kPa]	$q_c$ [MPa]	Application Class	Test Category	Cone Penetrometer Class
14C001	12,9	1,6	0,072	2	C	1
14C004	2,6	0,7	0,054	2	C	1
14A005**	0,1	1,1	0,036	-	-	1
14A006**	1,7	6369,2	0,072	-	-	1
14A007**	3,8	0,3	0,102	-	-	1
14A008*	2,8	0,4	0	4(1)	D(B)	1
14A009*	4,8	0,3	0,032	4(1)	D(B)	1
14A010*	2,9	0,1	0,032	4(1)	D(B)	1
14A011*	19,6	0,2	0,036	4(1)	D(C)	1
14A012*	25,4	1,1	0,034	4(3)	D	1
14A016*	25,9	0,7	0,026	4(3)	D	1
14D017	0,9	0	0,0029	1	B	1
14D018	0,9	0,3	0,0117	1	B	1
14D019	9,3	0,3	0,0076	1	B	1
14D020b	0,5	0,4	0,0064	1	B	1
14B021	6,7	0,3	0,0025	1	B	0
14B022	0,8	0,3	0,0207	1	B	0
14B023	16,9	0,4	0,0627	2	C	0
14B024	4,1	0,1	0,0078	1	B	0
14B025	0,9	0,2	0,0364	2	C	0
14B026	0,4	0,1	0,0033	1	A	0
14E027	12,7	1,7	0,01	2	C	1
14E028	0,1	0	0,124	3	D	1
14E029	12,8	0,4	0,01	2	C	1

\*) The cone penetrometer was not equipped with an inclinometer. Since the target penetration was deeper than 5 meters, the performed CPTU cannot reach a higher test category than category D in the new standards or a higher application class than class 4 in the old one. Obtained test category/application class is indicated in parentheses if this requirement was disregarded.

\*\*) The penetration was not valid since the criteria regarding the accuracy of the penetration rate was not fulfilled.

Table 2 The results from CPTU with respect to the old and new standards.

## DISCUSSION & CONCLUSION

A comparison has been made between the old standard and the new one regarding the criteria for the reference values (zero values) for each Application Class/Category. It can be considered that there are similarities between some of the test categories in the new standard with some of the application classes in the old one, see Table 3.

The criteria for the reference values in Application Class 1, 2 and 3 in the old standard is the same as for the Test Category B, C and D in the new one. However, the new standard has been updated with the Test Category A which is higher requirements than Application Class 1 in the old standard. Also, there is no equivalent for Application Class 4 in the new standard.

Based on these two aspects it can be stated that there are higher requirements in the new standard compared to the old one.

SS-EN ISO 22476-1:2012				SS-EN ISO 22476-1:2023			
Application Class	Pore pressure $u_2$ [kPa]	Sleeve friction $f_s$ [kPa]	Cone resistance $q_c$ [MPa]	Test Category	Pore pressure $u_2$ [kPa]	Sleeve friction $f_s$ [kPa]	Cone resistance $q_c$ [MPa]
-	-	-	-	A	3	5	0,015
1	10	5	0,035	B	10	5	0,035
2	25	15	0,100	C	25	15	0,100
3	50	25	0,200	D	50	25	0,200
4	>50	50	0,500	-	-	-	-

Table 3 Comparison between criteria for reference values for old and new standards.

Considering aspects above and other aspects such as compensation for the temperature influence and the new calibration procedure for cone penetrometers, it can also be stated that the level of accuracy in the performance, calibration, and evaluation of CPTU has been increased.

Based on the discussion above a comparison has been accomplished between the evaluation of the results from performed CPTU in the study from 2014 with respect to the old standard and the new one. The comparison is presented in Table 4.

Penetration ID	SS-EN ISO 22476-1:2012	SS-EN ISO 22476-1:2023	
	Application Class	Test Category	Cone Penetrometer Class
14C001	2	C	1
14C004	2	C	1
14A005 <sup>(c)</sup>	-	-	1
14A006 <sup>(c)</sup>	-	-	1
14A007 <sup>(c)</sup>	-	-	1
14A008 <sup>(c)</sup>	4(1)	D(B)	1
14A009 <sup>(c)</sup>	4(1)	D(B)	1
14A010 <sup>(c)</sup>	4(1)	D(B)	1
14A011 <sup>(c)</sup>	4(1)	D(C)	1
14A012 <sup>(c)</sup>	4(3)	D	1
14A016 <sup>(c)</sup>	4(3)	D	1
14D017	1	B	1
14D018	1	B	1
14D019	1	B	1
14D020b	1	B	1
14B021	1	B	0
14B022	1	B	0
14B023	2	C	0
14B024	1	B	0
14B025	2	C	0
14B026	1	A	0
14E027	2	C	1
14E028	3	D	1
14E029	2	C	1

Table 4 Comparison between the evaluation of the results from performed CPTU in the study from 2014.

It can be considered that the similarities that have been discussed earlier in this chapter can be identified in most of the attempts. The attempts that have been labelled as Application Class 1, 2 or 3 in the old system have got the equivalent Test category in the new one (B, C and D). However, one of the attempts differs from that matter, the evaluated result from the penetration in 14B026 has been labelled as Application Class 1 according to the old standard. This penetration should be categorized as a Test Category B in the new system, but it can be considered that this attempt has been categorized as a Test Category A. Based on that it can be stated that with higher accuracy in the performance of the CPTU, better results can be achieved. It should also be mentioned that the achievement of Test Category A in that attempt was not possible if the cone penetrometer was not classed as 0 in the Cone Penetrometer Class according to the new standard.

Although there was not so much of a difference in the other performed attempts in this study, it should be considered that all the attempts had a  $q_c$  less than 1 MPa ( $q_{c;\max} \leq 1$  MPa) along the entire penetration. The case will be completely different if the  $q_c$  was higher than 1 MPa, the Test category will remain the same, but the confidence level of each category will be different. The conclusions from the study in this paper can be compiled as:

- ❖ The level of accuracy in the performance, calibration, and evaluation of CPTU has been increased in the new standard.
- ❖ New requirements regarding the correction of parameters with regard to temperature influence.
- ❖ New requirements regarding calibration of cone penetrometer.
- ❖ The relation between cone penetrometer class and confidence level with respect to  $q_{c;\max}$  in the evaluation of Test Category.
- ❖ Addition of Test Category A and removal of equivalent Test Category to Application Class 4 in the old standard.
- ❖ The new standard is a planning tool as well as a new evaluation method.

## REFERENCES

- [1] C. Kardan: Quality of CPTU, Analyses and Comparison of data from Commercial Actors in Stockholm/Mälardalen. Master thesis, Royal Institute of Technology, 2014.
- [2] SS-EN ISO 22476-1:2023: Geotechnical investigation and testing – Field testing – Part 1: Electrical cone and piezocone penetration test. Swedish Standards Institute, 2023.
- [3] SS-EN ISO 22476-1:2012: Geotechnical investigation and testing – Field testing – Part 1: Electrical cone and piezocone penetration test. Swedish Standards Institute, 2012.

## **AROS – THE NEXT LEVEL, 3D MODELLING OF SWELLING ANCHORS**

**Britta S. Heilmann<sup>1</sup>, Martin N. Luxhøj<sup>1</sup>, and Bjørn S. Roesen<sup>1</sup>**

### **KEYWORDS**

Swelling, Anchors, 3D finite element modelling, High plasticity clay

### **ABSTRACT**

”The Dome” is a semi-subterranean art installation designed by the world-famous American artist James Turrell and is a part of the expansion project ”The Next Level” of ARoS Aarhus Art Museum in Denmark. The Dome is a 40 m wide hollow half-sphere skyspace construction extending approximately 9 m below and 10 m above the ground surface. The Dome will become the largest skyspace in the world within a museum context.

The excavation of the large soil mass and the large swelling potential of the underlying very high plasticity Palaeogene clay has led to significant geotechnical design challenges for the foundation.

The foundation is secured using swelling anchors with a free length in the swelling zone and an anchoring zone under the swelling zone to absorb the swelling force on the foundation corresponding to the unloading of the soil.

This article describes the development of a 3D finite element model in PLAXIS 3D using the incorporated linear interpolation between several geotechnical boreholes. Furthermore, different approaches to model the swelling anchors are compared, including “fixed-end anchors” and “node-to-node anchors” with the anchoring zone modelled by embedded beams. Finally, the swelling of the Palaeogene soils is modelled with two different approaches. The first approach uses a predefined swelling phase, while the second approach applies time-dependent consolidation phases in full depth. The latter examines the difference between applying different oedometric modulus  $E_{\text{oed}}$  and the coefficient of permeability  $k$ . The different modelling methods are compared by their influence on the size of the swelling of the ground surface and the anchor forces.

<sup>1</sup> COWI A/S, Aarhus Denmark



## INTRODUCTION

The light art installation “The Dome” is designed by the world-famous American artist James Turrell. It is a semi-subterranean construction extending approximately 9 m below and 10 m above the ground surface. From the inside, The Dome is a 40 m wide hollow skyspace, and seen from the outside, it is a 10 m high perfectly round grass-covered hill. The Dome is a part of the expansion project “The Next Level” of ARoS Aarhus Art Museum in Denmark and will become the largest skyspace in the world within a museum context.

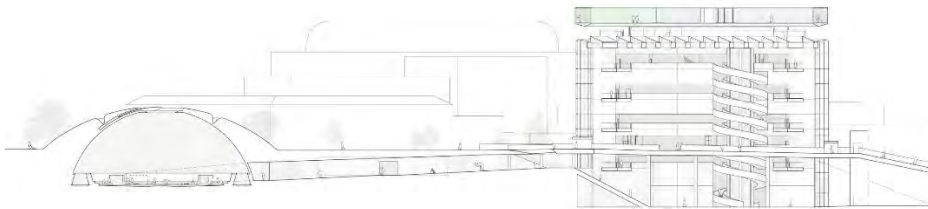


*Figure 1 Cross-section through The Dome and ARoS Aarhus Art Museum, ref. [1].*

To construct The Dome, a large soil mass must be excavated. As The Dome is a relatively light and hollow structure, the very high plasticity Palaeogene clay will consequently experience a large unloading. This can potentially give rise to swelling problems for The Dome under the assumption of sufficient water flow.

To avoid potential damage to the construction due to swelling, the direct foundation along the edge of the Dome is anchored to counteract the swelling force corresponding to the unloading of the soil. The swelling anchors are designed with an anchoring zone below the swelling zone. The swelling zone is defined as the penetration depth for the swelling based on the permeability of the soil and the design life of the structure.

The floor in the centre of The Dome is allowed to rise. For the same reason, the floor in The Dome is made of paving stones, which enables a relatively uncomplicated restoration.

The focus of the article is to describe different modelling methods with regard to the swelling issue and swelling anchors. The methods are compared by their influence on the size of the swelling of the ground surface and the anchor forces.

## Site Geology

The overall geological stratigraphy at the site can be described as 1.5 to 3.4 m of topsoil under which a thin layer of Late Glacial clay was encountered. The Late Glacial clay overlies Glacial deposits of clay till and meltwater sand. The primary Glacial deposit is meltwater sand in one half of the site, whereas clay till dominates the other half of the site. From about 12.2 to 18.4 m below the ground surface, the Palaeogene clays are encountered, consisting of marine Oligocene clay and marine Eocene clay. In general, the Palaeogene clays have a very high plasticity index and are fissured.

## METHODS

A one-dimensional method is applied to address the swelling issue and give a crude estimate of the size of the swelling before advanced models are initiated.

In PLAXIS 3D, different modelling methods regarding the swelling anchors and swelling of the Palaeogene clay have been applied. The methods are compared by the size of the swelling of the ground surface and the anchor forces. The following methods are addressed:

1. Plastic calculation phases with drained materials and swelling anchors modelled as Fixed-end anchors.
2. As method 1 with swelling anchors modelled as Node-to-Node anchors and embedded beams.
3. Consolidation phase in full depth with the swelling anchors modelled as Node-to-node anchors and embedded beams.
4. As method 3 with a different oedometric modulus,  $E_{\text{oed}}$ .

## 1D ESTIMATION OF THE EXPECTED SWELLING

To assess the extent of the swelling issue before advanced models are initiated, an estimation of the expected swelling is made based on the expressions presented in ref. [2]. As the swelling process needs an inflow of water to occur, the calculation is based on one-dimensional consolidation theory and rectilinear drainage compared with measurements of swelling from a site.

The extent of the swelling zone can be estimated by  $n = 2 \cdot \sqrt{c_k \cdot t}$ , where  $c_k$  is the coefficient of consolidation ( $\text{m}^2/\text{s}$ ) and  $t$  is the time corresponding to the lifetime of the building (s). With a service life of 100 years and a coefficient of consolidation of  $c_k = 5 \cdot 10^{-9} \text{ m}^2/\text{s}$ , a thickness of the swelling zone of  $n \approx 8 \text{ m}$  is obtained.

An estimation of the expected swelling is based on  $\delta_{1D} = -H \cdot Q_{\text{swell}} \cdot \log(\sigma'_{\text{after}}/\sigma'_{\text{before}})$ , where  $H$  is the size of the swelling zone,  $Q_{\text{swell}}$  is the swelling ratio, and  $\sigma'_{\text{before}}$  and  $\sigma'_{\text{after}}$  is the vertical effective stress in the middle

of the swelling zone before and after excavation, respectively. The expected swelling of the Dome is calculated to  $\delta_{ID} = 210$  mm, as  $\sigma'_{\text{before}} = 290$  kPa and  $\sigma'_{\text{after}} = 125$  kPa, corresponding to an unloading from excavation of 9.3 meters of soil.

This estimation of the swelling assumes the foundation is constructed directly on top of the Palaeogene clay. This is a conservative assumption and not the case at the site, as the geotechnical boreholes present a varying top level of the Palaeogene clays from about 5.3 to 11.5 m below the foundation level.

## THE PLAXIS 3D MODEL

The following sections describe the general input for the PLAXIS 3D model, which is applied in all four methods unless otherwise stated.

### Stratigraphy

To model the stratigraphy in PLAXIS 3D, the geotechnical boreholes made in or near the modelled project area are modelled using the "borehole" function. The location of each individual borehole is modelled directly from the Autodesk Revit file for the foundation plan, on which the location of the boreholes is indicated. The location of the boreholes is shown in Figure 2. PLAXIS 3D has formed the geological model by interpolation between all the geotechnical boreholes. The model is stopped at a depth where the unloading corresponds to less than 20% of the in situ vertical stress.

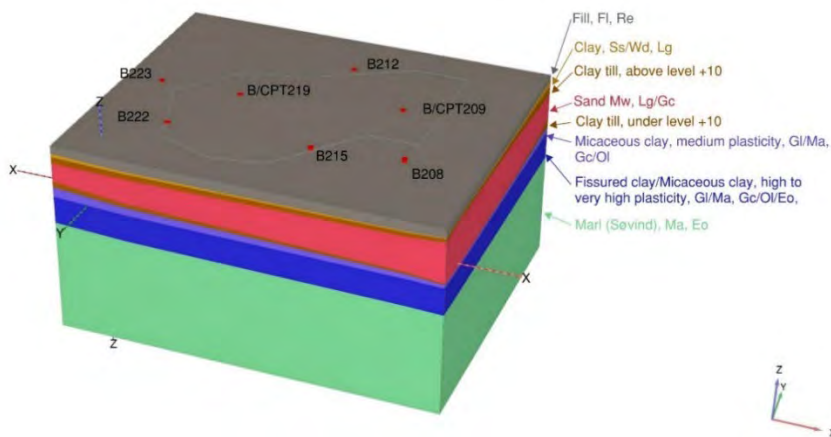


Figure 17: The soil stratigraphy modelled using interpolation between the soil layers.

### Constitutive Models

All soil materials are modelled as drained with the Mohr-Coulomb constitutive model, which was applied instead of more advanced models due to sim-

pler calibration and time constraints in the design phase. Further, it is assumed that all soil materials are normally consolidated with  $K_0 = 1 - \sin(\phi')$ , Poisson's ratio of  $\nu = 0.30$ , and apply "Tension cut-off" with a tensile strength of 0 kPa.

Table 1 lists the deformation parameters for the materials with swelling potential. The oedometric modulus,  $E_{\text{oed}}$ , is calculated based on the expression,  $E_{\text{oed}} = \ln(10) \sigma'_a / Q_{\text{swell}}$  from ref. [3], as the swelling ratio,  $Q_{\text{swell}}$ , must be converted to be applied in a Mohr-Coulomb material model.

The deformation parameters for the micaceous clay and fissured clay are based on swelling tests, whereas no swelling tests were performed for Søvind Marl. The Søvind Marl is located far below the foundation level, therefore, it is uncertain whether a sufficient water inflow for the Marl to swell will occur. Therefore, deformation parameters for both loading and unloading are given. For unloading, the parameter  $Q_{\text{swell}}$  is assumed to be similar to the one for the fissured clay and converted to  $E_{\text{oed}}$  using the expression in ref. [3]. The oedometric modulus for primary consolidation is estimated based on experience from the area using  $E_{\text{oed}} = 10 \text{ MPa} + 150 \cdot \sigma'_a$ , where  $\sigma'_a$  is the lowest vertical effective stress.

Soil type	$Q_{\text{swell}}$ [%]	$c_k$ [m <sup>2</sup> /s]	$E_{\text{oed}}$ [MPa]
Very high plasticity micaceous clay and fissured clay	7	$5 \cdot 10^{-9}$	5.5
High plasticity micaceous clay	1.5	$5 \cdot 10^{-9}$	25
Søvind Marl, primary consolidation	-	$5 \cdot 10^{-8}$	34.8
Søvind Marl, swelling ratio	7	$5 \cdot 10^{-8}$	5.4

Table 7 Deformation parameters for the soil layers with swelling potential.

The oedometer modulus for primary consolidation (loading) is applied in methods 1 to 3, and the parameters for secondary loading (unloading) are applied in method 4.

### Geometry and mesh

An excavation pit is made consisting of anchored sheet pile walls, although the sheet pile wall itself is not modelled in PLAXIS 3D, as it is not of interest in determining the number of swelling anchors and the size of the swelling. However, the excavation sides formed by the sheet pile wall are retained by

limiting the horizontal displacements to  $u_x = u_y = 0$ , where the z-axis is the vertical axis.

It is assessed that the model size is sufficient thus, the boundary effects do not affect the results of the swelling under the foundations or the 3D effects of the ground anchors. It should be noted that due to the retained sides (instead of sheet pile walls), it has been possible to limit the model approximately to the area of the excavation pit.

The models are meshed using 10-noded tetrahedral elements, which are the standard elements in PLAXIS 3D. Initially, a convergence analysis was made, showing that the calculated swelling in the centre of The Dome remains constant if the element mesh is discretized as coarser or finer than the medium mesh setting. Therefore, a slightly finer "medium" element mesh is used.

## **METHOD 1 – PLASTIC PHASES WITH FIXED-END ANCHORS**

The first method in PLAXIS applies plastic calculation phases, a predefined swelling phase together with swelling anchors modelled as Fixed-end anchors.

Plastic calculation phases in PLAXIS are an elastoplastic deformation analysis where time effects are not considered.

A Fixed-end anchor is a point element [4] where the free length and grouted length are not directly modelled. These are represented by an equivalent length.

The swelling anchors are strand anchors with five strands, each with a cross-sectional area of 150 mm<sup>2</sup>. The grouted length of the anchors is 10 m and is located below the swelling zone, yielding a free length of 17.2 m. The equivalent length,  $L_{\text{equivalent}}$ , is the free length and half of the grouted length.

### **Phases modelling**

In the PLAXIS 3D model, swelling is only allowed to occur when construction is finished. This is a simplification where any swelling that may occur during construction is neglected.

The predefined swelling phase is controlled by a surface at the upper level of the Palaeogene clay, where the displacement in the vertical direction is retained ( $u_z = 0$ ) until the foundations, swelling anchors and loads from the building are applied. Hereafter, the retained surface is released, and swelling can occur. Excavation and construction stages are modelled as plastic, allowing swelling to full depth of the model.

### Results from the first method

Figure 3 shows a cross-section through The Dome with the calculated swelling for the first method. The maximum displacement occurs at the centre of the Dome, with a vertical upward displacement of approximately 263 mm. It should be noted that the swelling is considerably lower at the foundations, which is caused by the applied loads and the swelling anchors. The maximum anchor force is calculated to 702 kN in the fixed-end anchors.

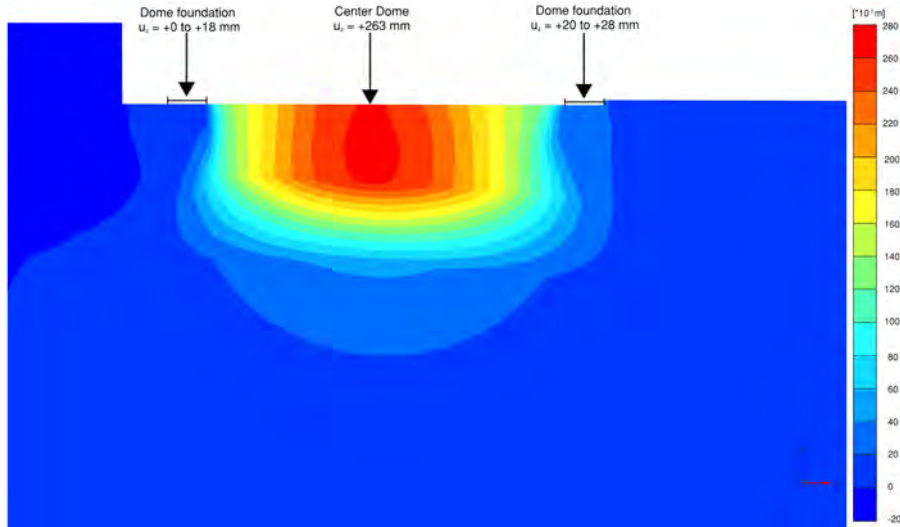


Figure 3: Cross-section through The Dome and calculated swelling for method 1.

### METHOD 2 – PLASTIC PHASES WITH NODE-TO-NODE ANCHORS AND EMBEDDED BEAMS

The second method applied in PLAXIS is similar to the first method, however, the modelling approach for the swelling anchors is different. In the second method, the swelling anchors are modelled using a combination of node-to-node anchors and embedded beams.

The node-to-node anchor represents the free length of the swelling anchor, while the embedded beam represents the grouted length. The connection between the node-to-node anchor and the embedded beam is automatically set to free to avoid unrealistic loss of axial force in the connection point [4]. The node-to-node anchors are modelled as in the first method.

The embedded beams are modelled as linear elastic with a stiffness based on the stiffness of the five strands, as it is assumed that the grout will crack

upon loading of the anchor and, therefore, not contribute to the axial stiffness. An embedded beam is modelled without any width, and the weight is therefore calculated as the difference between the weight of the grout and the weight of the surrounding soil. The grouted length transfers the axial force to the soil through skin friction, which is assumed to be constant for the entire length of the grouted zone. Field tests have yielded a bearing capacity of the swelling anchors of 725 kN.

### Results from the second method

The maximum displacement appears at the centre of the Dome, with a vertical upward displacement of approximately 271 mm. The maximum anchor force is calculated to be 667 kN in the node-to-node anchors.

### METHOD 3 – CONSOLIDATION PHASES WITH PRIMARY CONSOLIDATION

In the first and second methods, a surface at the upper level of the Palaeogene clay was used to control when swelling was allowed to occur, thereby only allowing swelling in the final phase after construction was finished. In the third method, this surface is removed, and all phases are modelled as consolidation phases, where swelling can occur, assuming sufficient water flow to the soil layers with swelling potential.

Each construction phase has a consolidation time of 25 days, except for the last phase, where the consolidation time is 100 years, corresponding to the construction lifetime. The coefficient of permeability,  $k$ , of the soil layers with swelling potential are estimated based on ref. [2],  $k = c_k \cdot \gamma_w / E_{oed}$ , where  $c_k$  is the coefficient of consolidation ( $\text{m}^2/\text{s}$ ),  $\gamma_w$  is the unit weight of water ( $10 \text{ kN}/\text{m}^3$ ), and  $E_{oed}$  is the oedometric modulus.

For the third method, the oedometric modulus of Søvind Marl is based on primary consolidation. The parameters used to estimate the coefficient of permeability for the soil layers with swelling potential and the estimated coefficient of permeability are given in Table 2.

Soil layer	$c_k$ [ $\text{m}^2/\text{s}$ ]	$E_{oed}$ [MPa]	$k$ [m/day]
Micaceous clay	$5 \cdot 10^{-9}$	25.6	$1.688 \cdot 10^{-7}$
Fissured clay	$5 \cdot 10^{-9}$	5.5	$7.855 \cdot 10^{-7}$
Søvind Marl	$5 \cdot 10^{-8}$	34.8	$1.240 \cdot 10^{-6}$

*Table 8: Parameters used for estimation of the coefficient of permeability for the soil layers with swelling potential.*

### Results from the third method

The maximum displacement appears at the centre of The Dome with a vertical upward displacement of approximately 69 mm. The maximum anchor force is calculated to 546 kN in the node-to-node anchors.

### METHOD 4 – CONSOLIDATION PHASES WITH UNLOADING STIFFNESS

The fourth method is similar to the third method, but instead of estimating the coefficient of permeability based on primary consolidation, the swelling ratio,  $Q_{\text{swell}}$  of 7 %, is applied.

The coefficient of permeability for the Micaceous clay and Fissured clay is the same as for the third method. The estimated coefficient of permeability is given in Table 3.

Soil layer	$c_k$ [m <sup>2</sup> /s]	$E_{\text{oed}}$ [MPa]	$k$ [m/day]
Søvind Marl	$5 \cdot 10^{-8}$	5.4	$7.935 \cdot 10^{-6}$

*Table 9 Parameters used for estimation of the coefficient of permeability for the soil layers with swelling potential.*

### Results from the fourth method

The maximum displacement appears at the centre of the Dome, with a vertical upward displacement of approximately 65 mm. The maximum anchor force is calculated to 532 kN in the node-to-node anchors.

### COMPARISON OF 3D METHODS

The four methods are compared by their influence on the size of the swelling of the ground surface at the centre of The Dome and the force in the swelling anchors, which is summarised in Table 4.

	Method 1	Method 2	Method 3	Method 4
$u_z$ - Center of The Dome [mm]	263	271	69	65
Anchor force [kN]	702	667	546	532



*Table 10: Swelling at the centre of The Dome and anchor force for each method.*

The modelling approach of the swelling anchors is compared in method 1 and 2.

From Table 4, it appears that method 1, applying fixed-end anchors, yields a lower swelling at the centre of The Dome and a larger anchoring force than method 2, which uses a combination of node-to-node anchors and embedded beams.

The difference can be caused by the displacement required to activate the full shaft resistance of the grouted zone. In method 1 (fixed-end anchors), the resistance is active without any displacement, as the grouted zone is not modelled, whereas displacements are required to activate the shaft resistance of the grouted zone in method 2, which is modelled using embedded beams. The difference in swelling corresponds approximately to the displacement required to activate the full shaft resistance, according to [5] and [6].

In methods 1 and 2, all materials are modelled as drained and the construction stages as plastic phases, where swelling of the Palaeogene clays is allowed to the full depth of the model and not an 8 m swelling zone as estimated in the 1D approximation in section 79. When the construction stage is modelled as plastic phases, the coefficient of permeability of the soil layers and the time aspect is therefore neglected in the calculations, yielding an overestimation of the swelling and associated anchor forces.

The construction stages for methods 3 and 4 were changed from plastic phases to consolidation phases to account for the coefficient of permeability of the soil layers and include the time aspect. Including these parameters reduces the swelling zone of the Palaeogene Clays. These changes have yielded a large reduction in swelling at the centre of The Dome and lower anchoring force between method 1-2 and method 3-4, as shown in Table 4.

From Table 14, it should be noted there is only a small difference between methods 3 and 4. The difference between methods 3 and 4 is the applied stiffness of Søvind Marl, with the odometer modulus for primary consolidation and the swelling ratio,  $Q_{\text{swell}}$ , respectively. The change in stiffness is also associated with a change in the coefficient of permeability. As expected, the lower stiffness and higher coefficient of permeability reduce the swelling of the Palaeogene Clays.

## **COMPARISON BETWEEN 1D ESTIMATION AND PLAXIS 3D**

A comparison of the PLAXIS 3D models with consolidation phases has been performed, comparing the expected swelling calculated to the 1D calculation, see Table 5. In PLAXIS 3D, a phase without swelling anchors and foundation loads has been performed to compare with the 1D calculation.

	1D	Method 3	Method 4
Swelling in the centre of The Dome [mm]	210	214	419

Table 11: Calculated swelling in the centre of The Dome without swelling anchors and foundation loads.

Method 4 applies the swelling ratio,  $Q_{\text{swell}}$ , for the Søvind Marl, which is associated with a higher coefficient of permeability compared to method 3. This leads to a larger swelling zone compared with method 3, where the stiffness of the Søvind Marl is based on primary consolidation, thus, the swelling contribution of the layer is limited. The 1D calculation does not have any contribution from the Søvind Marl, as it assumes a swelling zone of 8 m, which corresponds well with method 3.

Comparing the calculated swelling in the centre of The Dome listed in Table 15, it is indicated that the swelling zone is overestimated by method 4. Assuming that the 1D calculation is reasonable as it is compared with measurements of swelling from a site. The results from the PLAXIS 3D model with method 3 are shown in Figure 4.

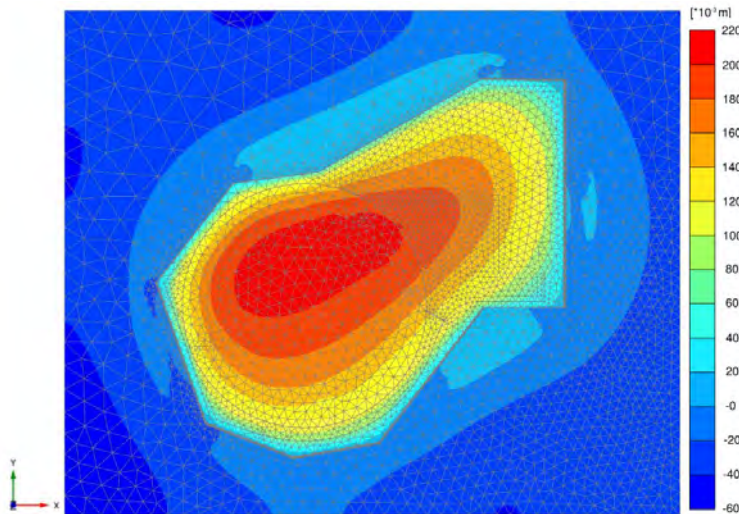


Figure 418 Swelling calculated in PLAXIS 3D for method 3 in the situation of full excavation in The Dome before implementing the foundations, loads, and swelling anchors.

Figure 4 shows that the swelling of the excavation closest to the sheet pile wall is affected by the "boundary effect" as there is no excavation and thus no

heave on the other side of the sheet pile wall. Therefore, the calculated swelling decreases from the centre of the excavation towards the sheet pile wall. As the expected swelling by the 1D calculation did not take the "boundary effect" of the sheet pile wall into account, it must be compared with the calculated swelling in the centre of the excavation, which was calculated to 214 mm in PLAXIS 3D. This indicates a good correlation between the PLAXIS model method 3 and the 1D calculation. The minor difference might be due to the "boundary effect" and a minor difference between the applied water table, which was assumed to be at level +9.0 in the 1D calculation and at level +11.0 before excavation in the PLAXIS 3D model.

## CONCLUSION

This article describes the development of a PLAXIS 3D model using the incorporated linear interpolation between several boreholes.

In PLAXIS 3D, different modelling methods have been applied to the swelling anchors and swelling of the Palaeogene clay. The methods are compared by the size of the swelling of the ground surface in the centre of The Dome and the anchor forces.

The two modelling approaches of the swelling anchors yield close to the same swelling at the centre of The Dome and anchor force. However, method 2 with node-to-node anchors and embedded beams represents the most realistic behaviour since displacement is essential to activate the shaft resistance.

The different approaches to modelling the swelling of the Palaeogene soils distinguish between plastic phases and consolidation phases in full depth. When the construction stage is modelled as plastic phases, the coefficient of permeability of the soil layers and the time aspect is neglected, yielding an overestimation of the swelling and associated anchor forces.

When different stiffnesses of Søvind Marl, primary consolidation or swelling ratio are applied, the lower stiffness and higher coefficient of permeability increase the swelling of the Palaeogene Clays.

The complexity of the PLAXIS 3D model is increased from methods 1 to 4. The PLAXIS 3D model with method 3 exhibits a good correlation with the 1D estimation when results are compared before the installation of the swelling anchors, foundations, and loads. Therefore, it is also expected that method 3 provides the best predictions for swelling when swelling anchors, foundations, and loads are active in the calculations. Method 3 shows that the centre of The Dome will swell approximately 69 mm over the lifetime of the structure, corresponding to 100 years.

## REFERENCES

- [1] Schmidt Hammer Lassen, ARoS – The Next Level, 04-2024, URL: <https://www.shl.dk/work/aros-the-next-level>
- [2] N. Okkels et. al.: Beregning af hævn timer under antagelse af retlinjet dræning, GEO/Aarhus University, 2008.
- [3] J. S. Steenfelt: Formelsamling for kursus 5811 – Geoteknik 1 og 5821 Geoteknik 2. Laboratoriet for fundering. Danmarks Tekniske Højskole, 1980.
- [4] PLAXIS 3D-Reference Manual, Bentley systems, 2021.
- [5] Den Norske Pelekomité: Peleveiledningen. Norsk Geoteknisk Forening, 2012.
- [6] K. Fleming et. al.: Piling Engineering Third Edition, CRC Press, 2020.



# ASSESSING UNDRAINED SHEAR STRENGTH IN DANISH MARINE GYTTJA: INSIGHTS FROM FIELD VANE TESTS AND PLATE LOAD TESTS

**E. S. Brandt<sup>1</sup>, H. Trankjær<sup>1</sup>, N. Mortensen<sup>2</sup> and K. K. Sørensen<sup>3</sup>**

## KEYWORDS

Soft soil deposits, field vane tests, undrained shear strength, plate load tests, marine gyttja

## ABSTRACT

In Denmark, the presence of soft soil deposits in construction projects has gained a lot of attention due to more focus on sustainability, a decreasing access to natural granular fill materials and a laboured process of permits from the authorities to deposit unusable soft soils onshore and offshore.

Field vane tests (FVT) have a long tradition of being the most common field investigation method for assessing the undrained shear strength of cohesive fine-grained soils in Denmark. For soft soils, the conversion from field vane strength ( $c_{fv}$ ) to undrained shear strength ( $c_u$ ) is currently a rather uncertain task and conservative estimates of the  $c_{fv}/c_u$  ratio is often set to cover this uncertainty in geotechnical designs resulting in overconsumption of materials.

To gain basis for a better understanding of the  $c_{fv}/c_u$  ratio and hence narrow the uncertainty, plate load tests (PLT) have been performed on Danish marine gyttja of various plasticity, for direct measurement of  $c_u$ . At the same locations, FVTs have been carried out and intact samples (Shelby tubes) of gyttja have been recovered from geotechnical boreholes for determination of  $c_u$  by undrained triaxial tests.

The results show a decrease in the  $c_{fv}/c_u$  ratio with increasing plasticity index analogous to results found by Bjerrum for (primarily) mineral deposits, however the results furthermore indicate that the empirical correlations suggested in literature tend to result in too conservative estimates of  $c_u$ .

<sup>1</sup> COWI A/S, Aarhus C, Denmark

<sup>2</sup> nmGeo, Allerød, Denmark

<sup>3</sup> Aarhus University, Department of Civil and Architectural Engineering, Denmark

## INTRODUCTION

### Background

The current urban growth and the need for public transport and services are leading to increased demand for new buildings and infrastructures. However, the lack of urban space and the desire to optimize infrastructure locations result in the need to build on soft soil sites with challenging conditions, frequently found in wetland and coastal areas. Recently, disposal of soft organic deposits (gyttja, peat, high plasticity organic clay) has gained a lot of political and public attention due to media coverage of major construction and landfill projects. Soft soils are, due to their problematic material properties with low strength and stiffness, often disposed and replaced by dwindling natural granular fill resources or expensive (economical and CO<sub>2</sub>-wise) lightweight expanded clay. The increased public and media attention labours the process of permits from the authorities to dispose or dump soft soil putting pressure on the clients and hence the consultants to utilise the soft soil deposits within the projects. The present paper focuses on estimations of undrained shear strength of marine postglacial gyttja.

### Danish marine gyttja

The Danish marine postglacial gyttja is typically found in the coastal and wetland areas of Denmark as indicated on Figure 1 (left). Marine gyttja is characterized by its organic origin often mixed with mineral content as a result of activity of bioturbators on the sea floor. The plasticity index, *PI*, of Danish gyttja usually ranges from less than 5% to 200%, but values of 250% or more are occasionally observed.

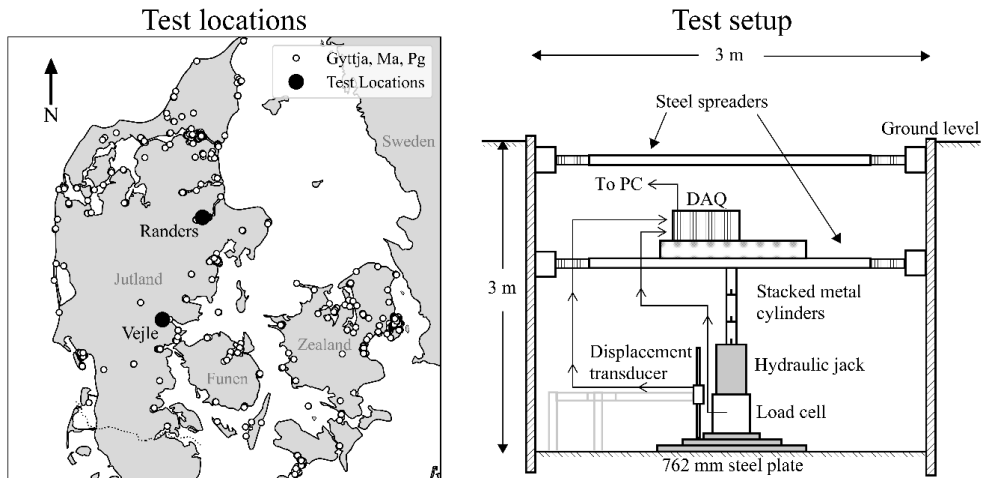


Figure 1: Map of Denmark showing boreholes (>2100) containing marine postglacial gyttja and location of test sites at Randers and Vejle (left) and sketch of plate load test setup (right).

### Field vane tests

Since its invention in 1947 [1] and introduction to Danish engineering practice in the early 1950's the field vane test has been and still is considered as one of the most cost-effective, practical and convenient methods for assessing the undrained shear strength of cohesive fine-grained soil in-situ [2]. It often serves as a reference for Danish literature, experience and in situ soil strength. In Denmark, the concept and equipment itself is similar to standardised procedures in other Nordic countries but the Danish procedure has been developed to cover a wider range of shear strengths ( $10 < c_{fv} < 700$  kPa) and the test rate is set to be significantly faster [2] – standardised by Danish Geotechnical Society to aim for one revolution per minute [3].

### Field vane correction factor

The ultimate undrained shear strength of soils is their ability to resist a load during constant volume and a specific set of conditions (effective stresses, temperature, pore water chemistry, shear rate, constraints, mode of shearing etc.). Hence, the undrained shear strength of a specific soil (sample) is not unique but dependent on the conditions during shearing. Therefore, various methods for assessing the undrained shear strength will provide different results.

It is commonly accepted that the measured field vane strength,  $c_{fv}$ , is generally not equal to the average undrained shear strength typically used for failure analyses. To take into account the effects of progressive failure, anisotropy, shear rate and plasticity L. Bjerrum [4] suggested adjusting the field vane strength,  $c_{fv}$ , by a factor  $\mu$ , dependent on the plasticity index,  $PI$ , to yield



a better estimation of the undrained shear strength,  $c_u = \mu(PI) \cdot c_{fv}$ . A similar, but apparently bilinear, concept was officially adopted in Danish practice in 1977 [5]. The concept was modified in 1984 [6] to mimic that of L. Bjerrum [4] by

$$\frac{c_u}{c_{fv}} = \mu = \frac{1.2}{1+0.01 \cdot PI} \leq 1.0 \quad (1)$$

to be used for organic clay. The basis for the curve suggested by L. Bjerrum eq. (1) was a comprehensive compilation of failures and landslides in low plastic clays from Norway and clays with varying plasticity from mainly Europe and North America. No high plasticity ( $PI > 115\%$ ) or organic soil from Scandinavia was evaluated. Organic soils were considered but mainly organic Bangkok clay.

Even though some literature suggests that back calculations of failures in (Danish) gyttja agree with the equation (1) i.e. [7] there seems to be no documented research confirming this issue. Some published literatures have tried to evaluate the validity of eq. (1) by correlating results from undrained triaxial tests on gyttja and organic clay with representative field vane tests showing a significant scatter [2]. The current authors contend that the observed correlation frequently exhibits unreliability, primarily attributable to the significant influence of errors stemming from the test procedure and sample disturbance. This is particularly relevant in the context of soft soils, and even more so with gyttja, given their inherently low strength and stiffness.

An alternative approach to that of L. Bjerrum, recommended by the Swedish Geotechnical Institute (SGI), relies on the liquid limit,  $w_L$ , rather than the plasticity index [1]:

$$\mu = \left(\frac{0.43}{w_L}\right)^{0.45} \cdot \left(\frac{OCR}{1.3}\right)^{-0.15} \quad (2)$$

where  $1.2 \geq \mu \geq 0.5$ . The idea of reducing field vane strength and fall cone test results by a factor that is influenced by the liquid limit to estimate the undrained shear strength was already initiated in the 1950's yielding different correction factors, culminating in the first SGI correction factor in 1969. The basis for equation (2) was originally developed for organic and high plasticity clays [8] and eq. (2) is currently recommended for organic clay and soft soils [9].

## TEST SITES

In an attempt to yield a reliable estimate of the actual mean (across the failure line) undrained shear strength governing failure and to assess the validity of eq. (1) and eq. (2) two series of plate load tests have been performed on marine gyttja at two different locations in Denmark. To evaluate the validity of

the field vane tests, oedometer tests and one series of triaxial and direct simple shear tests on the marine gyttja have been performed.

### Test locations

Two different test locations were chosen based on the following criteria: 1) marine postglacial gyttja near terrain 2) expected high plasticity index 3) constant  $c_u$  (or  $c_{fv}$ ) with depth 4) accessibility. Trawling various borehole databases against the mentioned criteria was automated to locate the apparently most suitable locations. A test site in Randers, near the fjord, and a test location at Vejle Fjord was chosen for the plate load test series. Figure 29 shows the test locations at Randers and Vejle.

### Geology and classification

Figure 2 shows the stratigraphic profiles from the test sites at Randers and Vejle based on the results from two geotechnical boreholes at each site executed prior to the plate load tests. Both sites are dominated by marine post glacial gyttja immediately or close to the ground level. In Randers the gyttja is covered by a thin layer of top soil and vegetation and in Vejle the gyttja is covered by approximately two metres of fill from reclamation and extension of the city of Vejle into the fjord between 1945 and 1976. The gyttja from Randers and Vejle is generally described as clayey, slightly silty (Randers) and high plasticity (Vejle), suggesting the gyttja found in Vejle to possess a greater plasticity index compared to that of Randers.

At both locations the gyttja is underlain by postglacial marine sand deposits. At Randers the field vane strengths and the water contents are rather constant ( $c_{fv} \approx 20$  kPa,  $w \approx 100\%$ ) with depths greater than approximately 2.5 metres. At the Vejle test site, the water contents are more scattered at depths greater than 3 metres, with water content ranging approximately from 100 to 200% ( $w \approx 100$  to 200%). In contrast, the field vane strengths are almost constant, with values around 20 kPa ( $c_{fv} \approx 20$  kPa). Although not directly related, it is expected for the field vane strength (or shear strength) to display a trend with depth opposite that of the water content (assuming constant  $PI$ ). This can possibly be explained by the test methods (FVT and water content measurement) not being equally sensitive in the low strength gyttja and  $c_u$  and  $w$  not being linearly related.

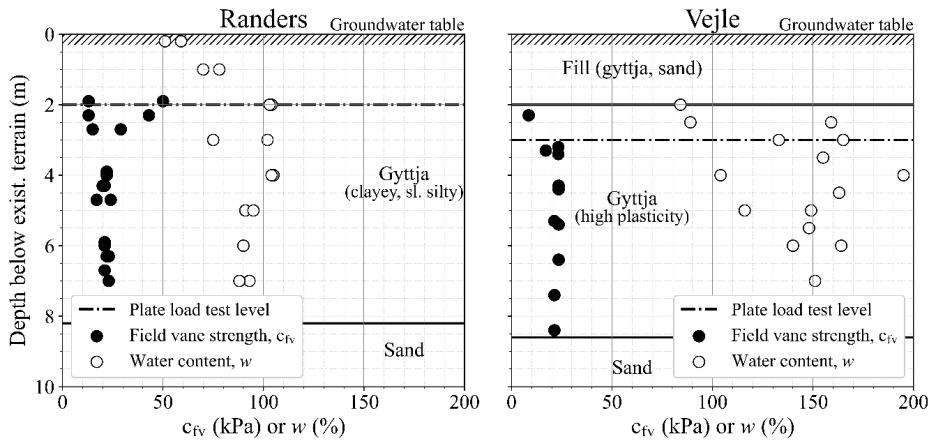


Figure 219: Stratigraphic profiles for test site locations Randers (left) and Vejle (right) including the approximate level for execution of the plate load tests. Based on two geotechnical boreholes at each site.

The plasticity index,  $PI$ , and the liquid limit,  $w_L$ , range from 47 - 57% (mean = 51%) and 96 - 98% (mean = 97%), respectively, in Randers and 74 - 83% (mean = 79%) and 169 - 179% (mean = 174%), respectively, in Vejle. The Atterberg limit tests support the geological descriptions suggesting the gyttja at the Vejle test site to possess a greater plasticity index.

## TEST METHOD

### Plate load tests

Figure 3 (right) shows the plate load test setup. The plate load tests were setup in 3 m wide trench boxes to reduce excavation volumes and costs. In addition to retaining the soil the weight of the trench boxes was used as dead load for the plate load tests. The test area within the trench boxes was prepared in accordance with BS 1377 [10] and allowed levelling of the test level at least three times the plate radius at each test the complying with recommendations from the Danish Geotechnical Society [11].

The transmission of force from the fixed support (trench box) to the loading plates was done by stacking solid metal cylinders of varying sizes each with a pin in one end a socket in the other end. The test plates were 762 mm diameter steel plates in accordance with DIN 18134 [12].

The load increments were applied at a constant penetration rate, increasing the applied stress by 5 kPa within 1 minute, followed by maintaining this stress level for an additional minute. In accordance with BS 1377 [10] it was striven to reach a displacement of at least 15% of the plate diameter, equiva-

lent to 114 mm displacement or until a well-defined failure plateau is observed as suggested in ASTM D1194 [13]. At total of 10 and 5 plate load tests were performed at Randers and Vejle, respectively.

### **Field vane tests**

In Randers the FVTs were conducted at depths ranging from 0.2 to 0.4 m beneath the centre of the plate load test and in Vejle they were performed in the immediate vicinity of the plate load tests. The FVTs were performed immediately before the commencement of the PLTs. The authors have assessed that the FVTs are unlikely to exert a significant or measurable influence on the outcomes of the plate load tests. The FVTs were performed and assessed according to Danish standard [3], using vane type V9.5 at Randers and V7.5 at Vejle. A total of 20 and 10 field vane tests were performed by hand at Randers and Vejle, respectively, after excavation. The field vane test results were calibrated according to Danish practice [3].

### **Laboratory tests**

Triaxial tests (compression and extension), direct simple shear tests (DSS) and oedometer tests (IL) have been performed on gyttja samples from the Randers test site. Only oedometer tests (CRS) have been performed on gyttja from the Vejle test site. Based on results from oedometer tests, the overconsolidation ratios (*OCR*) range between 1 – 2 in Randers and 1 – 1.2 in Vejle.

## **ANALYSIS**

### **Plate load tests**

Figure 3 shows the load-displacement curves from the plate load tests performed at Randers (left) and Vejle (right). The displacements are normalised by the plate diameter (762 mm) to yield the displacement ratio,  $r_\delta = \text{displacement}/\text{plate diameter}$ .

In Vejle the tests were limited by loss of effect of the metal cylinders transmitting the forces between the fixed support and the load cell. This happened due to small gradual rotation of the load plates causing the cylinders to shoot out resulting in loss of load transmission. The same limiting effect was also learned at the Randers test site but several tests were successfully strained beyond the maximum applied stress yielding the post-peak behaviour.

The load-displacement response is observed to behave rather differently in Randers and in Vejle. The load-displacement curves from the tests at the Randers site generally mimic that of a foundation on stiff soil (clear plateau of failure) and the Vejle tests as a foundation on soft soil (increasing stress towards an asymptote, or linear increase, with deformation and no clear failure or elbow).

To yield a consistent evaluation of the maximum applied stress,  $q_{\max}$ , considering the different stress-deformation behaviour of the plate load tests from the two test sites, the inference of  $q_{\max}$  is evaluated as the maximum applied stress within a displacement ratio,  $r_{\delta} = 10\%$ , equivalent to 76 mm deformation. This approach is recommended by BS 1377 if no clear failure plateau is observed, though suggesting a displacement ratio,  $r_{\delta} = 15\%$  [10]. As the majority of the PLTs in Vejle were limited before reaching  $r_{\delta} = 10\%$ , the load-displacements curves are extrapolated to  $r_{\delta} = 10\%$ .

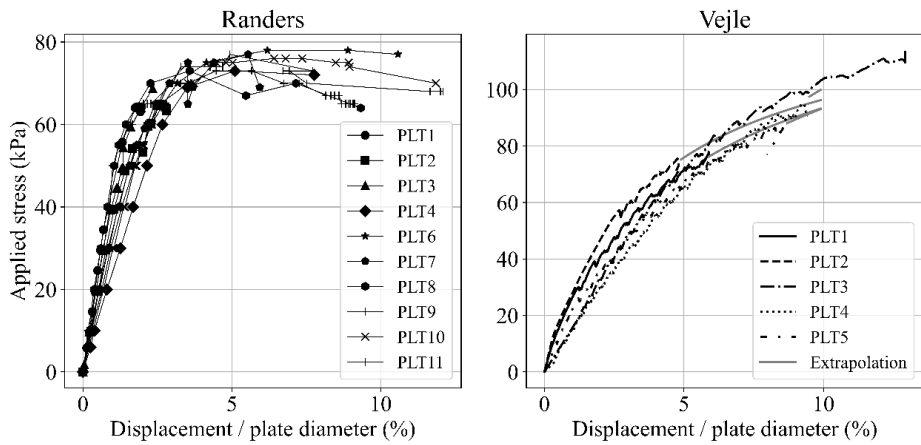


Figure 20: Results of plate load tests on marine gyttja from the plate load test site locations in Randers (left) and Vejle (right).

### Back calculation of undrained shear strength

To estimate the mean undrained shear strength from the plate load test results, the following equation is used:

$$q_{\max} = c_{u, \text{PLT}} \cdot N_c^0 \cdot s_c^0 \quad (3)$$

where  $c_{u, \text{PLT}}$  is the mean mobilised undrained shear strength,  $N_c^0$  is the undrained bearing capacity factor and  $s_c^0$  is the shape factor. In the case of stiff or dense soil (a stress-deformation response with a clear plateau at failure), a bearing capacity factor of  $N_c^0 = 2 + \pi \approx 5.14$  is well established. A shape factor of  $s_c^0 = 1.2$  [14] corresponding to a completely rough interface between a circular plate and the soil surface is used, resulting in

$$q_{\max} = c_{u, \text{PLT}} \cdot 6.17 \quad (4)$$

assuming a fully developed circular failure surface.

### Field vane correction factor

The field vane correction factor is calculated as:

$$\mu = \frac{c_{u,PLT}}{c_{fv}} \quad (5)$$

where  $c_{u,PLT}$  and  $c_{fv}$  are the undrained shear strength inferred from back calculation of results from plate load tests and the field vane strength, respectively.

As the plate load tests and the field vane tests are performed under the approximately same conditions (temperature, effective stresses etc.) at the individual test sites,  $\mu$  is derived based on average values of  $c_{u,PLT}$  and  $c_{fv}$  making the result of  $\mu$  less sensitive to outliers. This assumption seems reasonable for the reasons that 1) the field vane activates only a small volume of soil and only two FVTs were performed at each PLT, making the local mean highly sensitive to outliers. Furthermore, the PLTs at the individual test sites behave rather uniformly, indicating little variation in the soil behaviour. 2) As statistical methods to estimate averages are used more and more, correction factors should be based on averages as well [8]. 3) The correction factor proposed by L. Bjerrum was established on averages of the shear strength values measured by shear vane tests [8]. Table 1 summarises the inferences of  $\mu$  from the two test locations using the above-mentioned approach.

Location	$c_{fv}$ (kPa) <sup>a</sup>				$c_{u,PLT}$ (kPa) <sup>b</sup>				$\mu$ (-) <sup>c</sup>
	No. of tests	Mean	Min.	Max.	No. of tests	Mean	Min.	Max.	
Randers	20	14.2	10.2	17.1	10	12.2	11.8	12.6	0.86
Vejle	10	20.0	18.0	24.6	5	15.8	15.1	16.8	0.79

<sup>a</sup>  $c_{fv}$  with vane types V9.5 at Randers and V7.5 at Vejle

<sup>b</sup>  $c_{u,PLT} = q_{max}/6.17$

<sup>c</sup>  $\mu = c_{u,PLT,mean}/c_{fv,mean}$

*Table 12: Inference of  $\mu$  from plate load tests and field vane tests performed in gytta at the test site locations in Randers and Vejle*

To estimate the relative impact of variations in  $c_{fv}$  and  $c_{u,PLT}$  on  $\mu$ , the change in  $\mu$  with  $c_{u,PLT}$  is computed by  $\Delta\mu_{cuPLT} = (c_{uPLTmax} - c_{uPLTmin})/c_{fvmean}$  and vice versa for the relative impact of variations in  $c_{fv}$ . In Randers  $\Delta\mu_{cuPLT} = 0.06$  and  $\Delta\mu_{cfv} = 0.48$ , indicating the variations in the PLT results to be negligible. A similar, though less pronounced, trend is supported by the results from Vejle where  $\Delta\mu_{cuPLT} = 0.09$  and  $\Delta\mu_{cfv} = 0.23$ . These findings suggest  $\Delta\mu$  to primarily

reflect the variation in  $c_{fv}$  rather than variation in undrained shear strength (bearing capacity).

Figure 4 illustrates the inferred  $\mu$  against the plasticity index,  $PI$  and the liquid limit,  $w_L$ , including existing data and the correlations suggested in literature given by eq. (1) and eq. (2). The results are based on average values of  $c_{uPLT}$  and  $c_{fv}$ . Table 2 summarises the soil types and sources of the existing data plotted on figure 32.

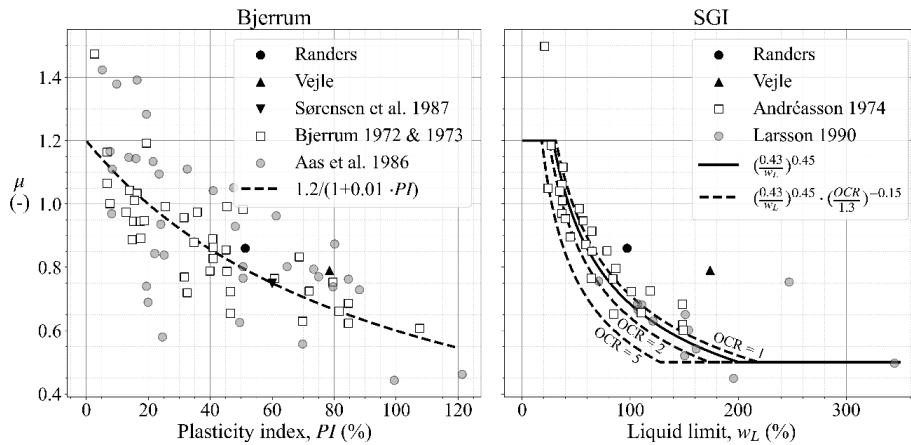


Figure 421: Inferred  $\mu$  against plasticity index,  $PI$  including existing data (left) and liquid limit,  $w_L$  including existing data (right) from plate load test results and field vane tests at test sites in Randers and Vejle.

Table 2: Sources and soil types for existing data plotted on figure 32.

Identification (figure 32)	Soil types	Method *	Source
Bjerrum 1972 & 1973	Low plastic European and North American clays, organic Bangkok clay	BC, PLT	[4] & [15]
Aas. et al. 1986	Clay	Un-	[16]
Sørensen et al. 1987	Gyttja	BC	[17]
Andréasson 1974	Recalculation of Bjerrum 1972	BC	[8]
Larsson 1990	Gyttja and organic clay	L, BC	[9]

\* BC = back-calculation (full scale failures), PLT = plate load tests, L = laboratory tests

The Bjerrum curve in figure 4 (left) is observed to be a conservative estimate in relation to the test results from Randers and Vejle. The test results from both Randers and Vejle are observed to lie above the Bjerrum curve within the scatter of the original data for the curve fit and supplementary data (primarily mineral clay). The original data collected by L. Bjerrum and the supplementary data collected by Aas. et al. show considerable scatter. Considering the present mean plasticity indices  $PI_{\text{Randers}} = 51\%$  and  $PI_{\text{Vejle}} = 79\%$ , the Bjerrum curve underestimates  $\mu$  by 0.06 and 0.12, respectively. As the basis for the Bjerrum curve primarily consist of mineral soils it is considered too weak to conclude the general validity of the Bjerrum curve in relation to gyttja, based on only the two data points from the test sites from Randers and Vejle.

The basis for the present reduction factor  $\mu$  in the SGI approach was originally including Scandinavian organic soils. The right plot on figure 32 shows the test results from Randers and Vejle against the liquidity index,  $w_L$  including the data collected by L. Bjerrum recalculated by L. Andréasson [18] and by R. Larsson [9]. The reduction factor proposed by SGI seems to yield less scatter of the (Bjerrum) data - probably and partly due to the fact, that the estimation domain includes uncertainty only in  $w_L$  as opposed to  $PI$  ( $w_P$  and  $w_L$ ) or that  $w_L$  is closer related to the in situ strength. Even though the oedometer tests from Randers and Vejle indicate  $OCR$  up to 2 the SGI approach seems conservative relative to the present test results, underestimating  $\mu$  by at least 0.14 and 0.24 at Randers and Vejle, respectively. Considering the existing data from mineral soils and organic soils the SGI approach generally seems fair. Most organic postglacial soil in Denmark is normally to slightly preconsolidated ( $OCR < 2$ ) but it does seldomly appears over consolidated ( $OCR > 5$ ) when performing laboratory tests.

### Laboratory tests

Oedometer tests (IL), triaxial tests (compression and extension) and direct simple shear tests (DSS) were performed on samples of gyttja from the Randers test site. While only oedometer tests (CRS) were performed on gyttja from the Vejle test site. Based on the test results the samples are considered disturbed to varying degree and hence do not yield a reliable estimate of the undrained shear strength. This is confirmed when comparing the results of the strength tests to the plate load tests ( $c_{u,\text{laboratory}} < 0.5 c_{u,\text{PLT}}$ ). When samples are recovered from a soft clay deposit they are always disturbed even with perfect sampling and results in a loss of shear strength of up to 10% [19]. These considerations do probably advocate for an inappropriate correlation of field vane strengths against results of laboratory undrained strength tests on gyttja and very soft clay where perfect sampling is considered quite a challenge. The gyttja samples at Randers and Vejle were recovered using a 76 mm steel tube sampler. Several authors have found sampling diameter to significantly impact the laboratory strength and deformation results in soft soils [20] and



D.W. Hight and S. Leroueil recommend using large diameter (200 mm) thin walled open sampler to minimise the disturbance in soft soil [21].

## DISCUSSION

### Field vane correction factors

The present plate load test results indicate that the  $\mu$  curve suggested by Bjerrum underestimates  $\mu$  for gyttja, though the dependency on  $PI$  appears plausible. The data volume (two data points) is not considered sufficient for suggesting a less conservative approach to estimate  $\mu$  for gyttja and organic soils – but the indications suggest further collection of data using the same approach (plate load tests).

As mentioned, one apparent advantage of the SGI approach over the Bjerrum approach is that the basis for the curves includes Scandinavian organic soils and gyttja. Although Bjerrum's original data, when plotted against the liquid limit ( $w_L$ ) as shown on the right side of figure 4, exhibit less scatter around the SGI curve, the dataset from Larsson [9], which includes organic clay and gyttja, appears to result in greater scatter. This dataset is derived from laboratory tests and back-calculations based on full-scale failures. It is unclear which data points originate from laboratory tests and which are from back-calculations. However, it seems reasonable to speculate that the observed scatter may be attributed to variations in sample quality and disturbance associated with the laboratory tests or related to assumptions regarding the failure surface as discussed in the later sections. This indication is supported by the apparently significant underestimation of  $\mu$  based on the results from the present study – though only two data points are available.

Assuming most gyttja to be normally to slightly preconsolidated, the dependence of  $OCR$  on  $\mu$  using the SGI approach appears negligible, compared to the relative underestimation of  $\mu$  given the present test results from Randers and Vejle. Due to the soft response and low strength, often observed for gyttja and high plasticity organic clay, assessing the preconsolidation stress,  $\sigma_{pc}$ , involves significant uncertainty. Generally, models should aim for simplicity as the introduction of each variable add a source of uncertainty and from a practical viewpoint, field vane tests are often not accompanied by consolidation tests. Considering this idea, the correction factor for gyttja might as well be assessed by the relation proposed by [9]

$$\mu = \left( \frac{0.43}{w_L} \right)^{0.45} \quad (6)$$

eliminating the dependence of  $OCR$ . Equation (6) is plotted on figure 32 and falls in the intermediate region of  $OCR = 1$  to 2.

### Plate load tests

Plate load tests were considered ideal for the present purpose of inferring the mean undrained shear strength for the evaluation of field vane correction factors for gyttja and organic clay. Even though plate load tests ideally eliminate the issue of sample disturbance it is challenging to prepare the ground level without disturbing the ground at all – even with great care. The stress conditions are not known but for the present purpose of comparing field vane tests to the average undrained shear strength under the same conditions this is considered irrelevant.

### Field vane tests

The field vane tests used for the present study were performed in accordance with the guidelines provided by the Danish Geotechnical Society [3]. The Danish guidelines for performing field vane tests allow for a more rapid execution ( $\leq 1$  rpm) compared to most international guidelines [2]. As the strain rate affects  $c_{fv}$  (or  $c_u$ ), yielding a higher  $c_{fv}$  with increasing strain rate, the more rapid Danish approach is considered conservative in the current context, yielding a lower  $\mu$  factor. The scatter in the field vane tests performed for the present study account for the majority of the uncertainty in the estimation of  $\mu$ . As the plate load test results were rather uniform, the scatter in the field vane test results are attributed to measurement error rather than natural variability in the undrained shear strength.

Even though the gyttja at the test locations in Randers and Vejle was considered rather clean (absence of coarse-grained soils) intact shell fragments were observed at both test sites. The appearance of shell fragments in marine soil deposits are rather common and can lead to variations in the field vane strength not reflecting the actual variability in the undrained shear strength or measurement error.

### Back-calculation of undrained shear strength

The field vane correction factors established by L. Bjerrum were inferred from the back-calculation of actual full-scale failures and some plate load tests [15]. It is not clear but given the years of publication (1972 and 1973) and the indications in [4] and [15] circular failure surfaces seems to be assumed for the various analyses. Even though the basis for the field vane correction factors established and developed by SGI (right hand side of figure 32) include back-calculation of full scale failures gyttja – these probably also were based on circular failure surfaces, assuming the year of publication (1990). Circular failure surfaces are theoretically valid only for (fairly) homogenous soil conditions. As the (undrained) shear strength is always controlled by effective stresses, it is commonly accepted and observed that the ratio  $c_u/\sigma'_v$  is constant for normally consolidated soils, where  $\sigma'_v$  is the vertical effective stress at the depth considered. A. Skempton [22] found the ratio was

dependent on the plasticity index, typically ranging from 0.1 to 0.4 [23]. If the ratio, defined as the initial undrained shear strength to the strength increase with depth, is sufficiently high, the failure surface tends to be located closer to the surface and exhibits a more elongated shape [7], contrasting with the typically observed circular failure surface when using a constant  $c_u$  – a tendency diminishing with increasing overall soil strength. It is important to recognize that the inference of  $c_u$  by back-calculation is contingent on the length of the failure surface; thus, a reliable estimation of the mean of  $c_u$  critically depends on the assumed shape of the failure surface.

Although the back-calculation of the average  $c_u$  from full-scale failures is deemed reliable and less susceptible to local variations in  $c_u$  along the failure surface and eliminates scaling issues, the average  $c_u$  derived from plate load test theoretically is less sensitive to increasing strength with depth. This is particularly notable in soft soils characterized by a high relative strength increase. Theoretically, the failure surface in plate load tests extends only about one plate radius beneath the plate [24]. Furthermore, the plate load test method eliminates the need for adjusting the results for end effects as pointed out by [25] who adjusted the results originally published by Bjerrum [4] and [15] to account for end effects.

Despite the abovementioned advantages of the plate load test for the assessment of  $c_u$  in soft soils, the inference of maximum applied stress,  $q_{\max}$ , can be discussed when the load-deformation curves from the tests show no clear failure plateau – so can the applicability of the bearing capacity factors and shape factors derived for stiff soils under the assumption of fully developed failure surface. It can also be discussed whether the assessment of  $c_u$  at a displacement ratio,  $r_\delta \approx 10\%$  (76 mm) or more is practically acceptable for conventional geotechnical structures – i.e. foundations – and the superstructures or interacting elements.

## CONCLUSIONS

Based on results from plate load tests on gyttja, the field vane correction factors proposed by L. Bjerrum and the Swedish Geotechnical Institute (SGI) appear to be a conservative estimate for gyttja and organic clay, but further testing using the plate load test method is needed for confirming the present indications.

Due to inevitable sample disturbance laboratory tests are not recommended for assessing the validity of the field vane correction factors.

The field vane correction factor by Bjerrum seems to be conservative for gyttja and less conservative than the approach suggested by SGI. The strength of the SGI is the one parameter domain ( $w_L$ ) – if the OCR is eliminated – resulting in less scatter than that of Bjerrum.

Caution is advised when inferring undrained shear strength from full-scale failures in low-strength soils that exhibit a significant increase in strength with depth, such as normally consolidated gyttja. A relatively high increase of strength with depth will often lead to a more critical failure surface than assuming constant  $c_u$  with depth. Some literature have apparent assessed the undrained shear strength by back-calculating full scale failures in gyttja assuming a circular failure surface – a natural assumption considering the tools available at the time of publication. Further research could involve recalculating the full-scale failures using more contemporary methods that allow for variations in undrained shear strength with depth and do not presuppose a fixed mode of failure.

## ACKNOWLEDGEMENT

The present research has been funded by COWIfonden and Ellen og Ove Arkils fond. The authors would like to thank Rødkilde Gymnasium for making available the test site in Vejle. Furthermore, we would acknowledge students Camilla Hesel, Gustav Krogh and Mads Roholm from Aarhus University involved in the execution of the plate load tests in Randers. Finally, we would like to thank Arkil and Svend Jørgensen for the great collaboration and discussions on execution etc.

## REFERENCES

- [1] H. Löfroth, „Report 71. Undrained shear strength in clay slopes - Influence of stress conditions. A model and field test study,” Swedish Geotechnical Institute (SGI), Linköping, 2008.
- [2] J. D. Andersen en N. Okkels, „Evaluation of fast field vane tests FVT-F,” in *Nordic Geotechnical Meeting, NGM 2020*, Helsinki, 2020.
- [3] Dansk Geoteknisk Forenings Feltkomité, „Referenceblad for vingeforsøg. Revision 3,” Danish Geotechnical Society (DGF), 1999.
- [4] L. Bjerrum, „Embankments on Soft Ground,” in *American Society of Civil Engineers Conference on Performance of Earth and Earth-Supported Structures*, Purdue, Lafayette, Indiana, 1972.
- [5] Dansk Standard, DS 415. Dansk Ingeniørforenings norm for fundering. 2. udgave., København: Teknisk Forlag, 1977.
- [6] Dansk Standard, DS 415. Dansk Ingeniørforenings norm for fundering, København: Teknisk Forlag, 1984.
- [7] J. K. Frederiksen, N. Foged, N. Okkels en J. L. Rasmussen, „Gytje. DGF Bulletin 16: Danske jordarters forekomst og

- tekniske egenskaber,” Dansk Geoteknisk Forening, Not yet published.
- [8] R. Larsson, U. Bergdahl en L. Eriksson, „Evaluation of shear strength in cohesive soils with special reference to Swedish practice and experience,” Swedish Geotechnical Institute (SGI), Linköping, 1984.
  - [9] R. Larsson, „Rapport No 38. Behaviour of Organic Clay and Gyttja,” Swedish Geotechnical Institute (SGI), Linköping, 1990.
  - [10] British Standard, „BS 1377: part 9: 1990,” Bristish Standards Institution, London, 1990.
  - [11] Dansk Geoteknisk Forenings Feltkomité, „Referenceblad for statiske pladebelastningsforsøg,” Danish Geotechnical Society (DGF), Lyngby, 2005.
  - [12] DIN, „18134:2012-04: Soil - Testing procedures and testing equipment - Plate load test,” Deutsches Institut für Normung, Berlin, 2012.
  - [13] American Society for Testing and Materials, „D 1194-94: Standard Test Method for Bearing Capacity of Soil for Static Load and Spread Footings,” ASTM International, West Conshohocken, 1994.
  - [14] K. Terzaghi, R. B. Peck en G. Mesri, Soil Mechanics in Engineering Practice. Third edition, New York: John Wiley and Sons, Inc., 1996.
  - [15] L. Bjerrum, „Problems of soil mechanics and construction on soft clays and structurally unstable soils (collapsible, expansive and others),” in *8th ICSMFE*, Moscow, 1973.
  - [16] H. El-Ramly, N. Morgenstern en D. Cruden, „Probabilistic Stability Analysis of an Embankment on Soft Clay,” in *57th Canadian Geotechnical Conference*, Québec, 2004.
  - [17] C. S. Sørensen en C. Q. Nielsen, „Havnebygning på blød bund,” in *10. Nordiske Geoteknikermøte. NGM-88*, Oslo, 1987.
  - [18] L. Andréasson, „Förslag till ändrade reduktionsfaktorer vid reduktion av vingborr bestämd skjuvhållfasthet med ledning av flytgränsvärdet. Intern rapport. Chalmers Tekniska Högskola, Inst. för geoteknik. Göteborg,” 1974.
  - [19] R. D. Holtz, W. D. Kovacs en T. D. Sheahan, An Introduction to Geotechnical Engineering. 2nd edition, Upper Saddle River: Pearson, 2011.

- [20] S. Lacasse, „Parameters for soft soil,” in *Proceedings of the third international conference on soft soil engineering*, Hong Kong, 2001.
- [21] K. H. Head en R. J. Epps, *Manual of soil laboratory testing, volume III: Effective stress tests*. 3rd edition, Whittles Publishing, 2014.
- [22] A. W. Skempton, „Discussion of "The planning and design on the new Hong Kong Air Port",” *Proc. Inst. Civ. Engrg.. Vol. 7*, 1957.
- [23] P. Harremoës, H. Moust Jacobsen en N. Krebs Ovesen, *Lærebog i geoteknik, bind 1.*, Copenhagen: Polyteknisk Forlag, 1974.
- [24] B. S. Knudsen en N. Mortensen, „Bearing Capacity, Comparison of Results from FEM and DS/EN 1997-1 DK NA 2013,” in *17th Nordic Geotechnical Meeting (NGM-2016)*, Reykjavik, 2016.
- [25] A. S. Azzouz, M. M. Baligh en C. C. Ladd, „Corrected Field Vane Strength for Embankment Design,” *ASCE. Journal of Geotechnical Engineering, Vol. 109, No. 5*, pp. 730 - 734, 1983.



## BORED PILES IN COPENHAGEN LIMESTONE

**Kirsten M. Iversen<sup>1</sup>, Bjørn S. Roesen<sup>2</sup>, and Jørgen S. Steenfelt<sup>3</sup>**

### KEYWORDS

Bored piles, bi-directional testing, shaft & toe resistance, flat-jacks, Copenhagen limestone

### ABSTRACT

On the former Postal Service Centre parcel in central Copenhagen a new urban area of 200,000 m<sup>2</sup> is being constructed, which accommodates service and retail trade as well as apartments for housing. The buildings consist of office buildings in 3-4 stories and 5 high-rise towers up to about 107 m high. Below ground level a parking basement in two levels is established with excavation to 8 m below ground level. Due to exceedingly high concentrated loads the towers and parts of the other buildings with large load concentrations are placed upon bored piles serving as rock sockets in the underlying Copenhagen Limestone. The bored piles are constructed with diameters ranging from 1180 to 1800 mm.

Before installation of the production piles, six test piles were established on the construction site. The purpose of the test piles was primarily to test the shaft resistance of the piles in Copenhagen limestone, as insufficient “Codal comparable experience” was established at the time. However, a second purpose was also to overcome the limitations in the Danish Annex to Eurocode 7 requiring a reduction of the shaft resistance to 30 % of the value for a “comparable driven pile”. Further, the purpose was to test bored piles with a flat-jack device at the bottom. The flat-jack engages toe resistance of the piles by a controlled grouting process enabling pre-stressing of the pile and a stiffer pile/structure interaction.

The results of the tests allowed the design to be optimized beyond the limitations of the Code, and the concept of using flat-jacks on the production piles was proven successful.

<sup>1</sup> COWI A/S, Aarhus C, Denmark

<sup>2</sup> COWI A/S, Aarhus C, Denmark

<sup>3</sup> COWI A/S, Lyngby, Denmark



## INTRODUCTION

### The project

Close to the Central Station in Copenhagen a new urban area of 200,000 m<sup>2</sup> is being constructed on the former Postal Service Centre parcel. The development project consists of a new domicile for a large Danish bank, a building for small and medium-sized companies and five large towers for both business and apartments. Below ground a parking basement in two levels were established with excavation to level -5.5 m, corresponding to approximately 8 m below ground level.

The high-rise buildings are founded on large, bored piles, rock socketed into the Copenhagen Limestone, which forms the sub-base under the entire area.

### Limitations within the Danish annex to Eurocode 7 part 1

In the Danish Annex to Eurocode 7 (DS/EN-1997-1 DK NA:2021), Ref. [1], the resistance of bored piles is restricted by Clause (6) to Annex L (informative). "For bored in situ cast piles, the resistance may be considerably less than for corresponding driven piles. The maximum allowable shaft resistance is limited to 30% of the shaft resistance of the corresponding driven pile, and the toe resistance is limited to 1000 kN/m<sup>2</sup> unless recognized documentation for higher resistance is provided" (COWI translation).

The restriction is not qualified in terms of the soil or rock strata considered. In Denmark, this restriction typically applies to piles in limestone. However, the qualification "30% of the shaft resistance of the corresponding driven pile" implies that the restriction is intended for piles in fine-grained soils where the resistance is mainly derived from shaft resistance.

Unfortunately, this qualification/restriction has been indiscriminately applied to all bored piles, including those in rock. The fact that the qualification/restriction is in an informative Annex seems to be overlooked in its application.

There have been numerous projects in Denmark which proves that the limitations are too strict. Some of the projects are described in the paper "Is it reasonable to reduce the shaft resistance for bored cast-in-situ piles?", Ref. [2]. However, more examples have seen the world after the paper has been published. E.g. a static load test in Miocene sand and clay in Silkeborg, Ref. [3] and "Loading test experience with bored piles in limestone/weak rock", Ref. [4].

To abstain from the codal limitations on the project it was decided to conduct six load tests on piles on the location to gather information about the shaft and base resistance.

## GROUND CONDITIONS

The design of the foundation of the new buildings is based on 36 geotechnical boreholes where 24 were carried out as core drillings 10.5 m to 16.7 m into the limestone.

The ground conditions on the location for the construction pit are relatively uniform. The upper layers at the location consist of fill; mull, sand and clay from level -0,1 to -6,3 m DVR90. Some boreholes showed layers of gyttja fill, postglacial sand and gyttja and late glacial to glacial sand.

Fill, postglacial and late glacial deposits are underlain by glacial deposits of meltwater sand, silt, clay and clay till, gravel till and sand till to level -7.2 á -10.2 m DVR90, followed by a 2.5 to 5.0 m thick layer of Selandian Green sand. Due to the Green sand layer, the underlying Copenhagen limestone was not remoulded and glacially disturbed as frequently seen in the Copenhagen area. The limestone surface varied from level -10.2 to -14.2 m DVR90. The induration of the limestone is typically H2-H4 according to the Danish induration scale (corresponding to R1-R4 on the ISRM rock grade scale). However, some 18 % of the limestone showed hardness H5 (corresponding to R5-R6). The strength of the limestone was tested with 32 UCS (Unconfined Compression Strength) test. The tests were generally made on the weaker layers in the limestone. A plot of the measured strength as a function of depth and hardness is seen in Figure 1.

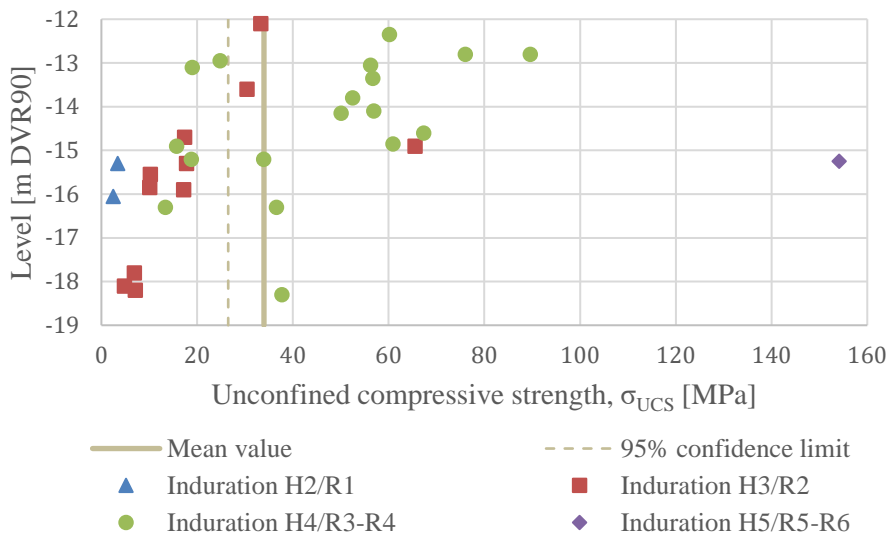


Figure 122. Measured unconfined compression strength as a function of the level of the sample and the induration. The degree of induration was described by the geologist before the conducted UCS tests, which can lead to inconsistency between the judged induration and the resulting strength from the test.

As shown in Figure 1 a lot of scatter is observed in the measured strength of the Copenhagen Limestone. There does not appear to be a relation between the depth of extraction and the measured strength in the limestone. As expected a trend was registered that the strength was a function of the geologically described degree of induration.

## GEOSTATIC CALCULATION

As described in “Loading test experience with bored piles in limestone/weak rock” the design of bored piles follows the international standard adopted for numerous projects with sockets in weak rock carried out by COWI. The characteristic shaft,  $\tau_{char}$ , and the toe resistance,  $q_{toe,char}$ , are based on the measured unconfined compressive strength,  $\sigma_c$ , found by UCS testing. According to Fleming et al., Ref. [5] and Tomlinson, Ref. [6], the characteristic resistance for soft rock may be found as, respectively:

$$\frac{\tau_{char}}{p_a} = 1.3 \sqrt{\frac{\sigma_c}{p_a}}; \quad \frac{q_{toe,char}}{p_a} = 3 \frac{\sigma_c}{p_a}$$

$$\tau_{char} = \alpha \beta \bar{\sigma}_c$$

In the equations  $\sigma_c$  represents the characteristic value and  $\bar{\sigma}_c$  represents the cautious mean value of the strength distribution of individual or total layers of the rock,  $p_a$  is the atmospheric pressure and  $\alpha$  and  $\beta$  are empirical factors. This methodology has been applied on numerous projects and have been found to be conservative for all the pile load tests interpreted by COWI.

The contribution of the layers above the limestone is assessed to be insignificant. In the evaluation of the bearing capacity the bearing capacity of the surface in these layers has been disregarded.

The skin resistance in the limestone has been evaluated to 1300 kPa according to Flemming et. al., Ref. [5] and Tomlinson, Ref. [6].

## CONCEPT OF FLAT-JACK

The quality and resistance of bored piles depend highly on the workmanship, the cleaning of the toe and not least the properties of the surrounding soil/rock. Surprisingly, the strict rules pertaining to ground anchors (investigation, suitability, and acceptance tests) are not implemented for bored piles. To gain the same reliability and robustness of bored piles post grouting, particularly at the toe of the pile, suggests itself.

For the piles at Posten, the post grouting was established by means of flat-jacks where the grouting pressure is ensured over a well-defined area almost corresponding to the cross-sectional area of the pile.

This allowed for (i) enhancement of the toe resistance at a displacement commensurable to the displacement required to mobilize the shaft resistance; (ii) verification of pile capacity to a value of minimum twice the toe capacity; (iii) a cheap and efficient quality assurance; and finally (iv) an increased stiffness of the foundation system where the SLS load may be taken at very limited pile top displacement.

## TEST SETUP

The bored piles were tested by means of an O-cell loading set-up. The O-cell is a bi-directional load cell, that is expanded through hydraulics and can thus apply a load both upwards to test skin resistance and downwards to test the combination of skin resistance below the O-cell and the toe resistance. The piles were not to be considered as production piles and were as far as possible be tested to failure. The load cells (O-cell) were placed 0.7-1.2 m above the pile toe and the piles were instrumented with strain gauges in four levels: half-way between O-cell and top of rock, top of rock and respectively 2 and 4 m above top of rock. The pile was further instrumented with tell-tale extensometers to measure displacement at the toe, the O-cell, top of rock and top of pile. Lastly the expansion of the O-cell is measured with four parallel LVWDTs.

The piles were installed by means of Kelly-boring where the casing is the main drill tool and the soil/limestone inside is brought to the surface with various cutting tools. The piles were drilled with water pressure as to avoid loosening at the pile toe due to inflow of water and the borehole was carefully cleaned both after reaching the final depth and after raising the casing to a level approximately 0.5 m below top of rock. The reinforcement cage with the O-cell, instrumentation and flat-jack, see Figure 2, was lowered into the borehole and the pile was concreted through a submerged tremie pipe to ensure clean high-quality concrete on the entire length of the pile.

Before the loading sequence was commenced the flat-jack injection was carried out to engage the toe resistance. The first injected pile BP3 was not successful, and the procedure was adjusted, after which the remaining flat-jacks were installed successfully.

The load sequence consisted of two load cycles, with the first load cycle being 5 load steps up to 200 % (40 % each) of the expected serviceability limit



*Figure 223: Flat-jack and O-cell mounted on reinforcement cage.*

state (SLS) load applied and a subsequent unloading in 5 steps. The second cycle was subsequently loading in 15 equal load steps to a total load corresponding to 150 % of the guaranteed O-cell capacity or until failure was observed. For each load step in both cycles a 30 min observation time was applied.

## RESULTS

Data from the test piles are summarized in Table 1.

*Table 13. Data from the test piles.*

Test pile	Dimension [mm]	Ground level [m]	Level of pile toe [m]	O-cell break-in-pile [m]	Top level of limestone [m]	SLS load [MN]
BP1	1500	+1.55	-16.70	-15.90	-12.00	7.9
BP2	1500	+1.60	-17.10	-16.37	-11.70	7.9
BP3	1180	+1.70	-16.95	-16.26	-12.10	6.3
BP4	1180	+2.35	-17.40	-16.21	-12.65	6.3
BP5	1180	+2.35	-16.85	-16.20	-12.20	6.3
BP6	880	+2.35	-17.40	-16.21	-12.30	3.3

The load tests on the bored piles were conducted between January 15<sup>th</sup> and January 21<sup>st</sup>, 2019. The load was taken to failure or the maximum capacity of the load cells.

The first load cycle was conducted to the SLS load. The magnitude of the load is shown in Table 1. The test piles were subsequently loaded in 15 equal load steps to a total load corresponding to 150 % of the guaranteed O-cell capacity. Some piles were loaded a bit further to the maximum capacity of the hydraulics.

The load-displacement curves for the pile tests are shown in Figure 3. The horizontal asymptote makes it hard to evaluate failure. Therefore, the rate of creep has been evaluated for each load step for all six test piles as shown in Figure 4. Based on the rate of creep five of the six test piles were loaded until failure. However, test pile BP3 shows a rate of creep of 2 mm/log(t) and has therefore not reached failure.

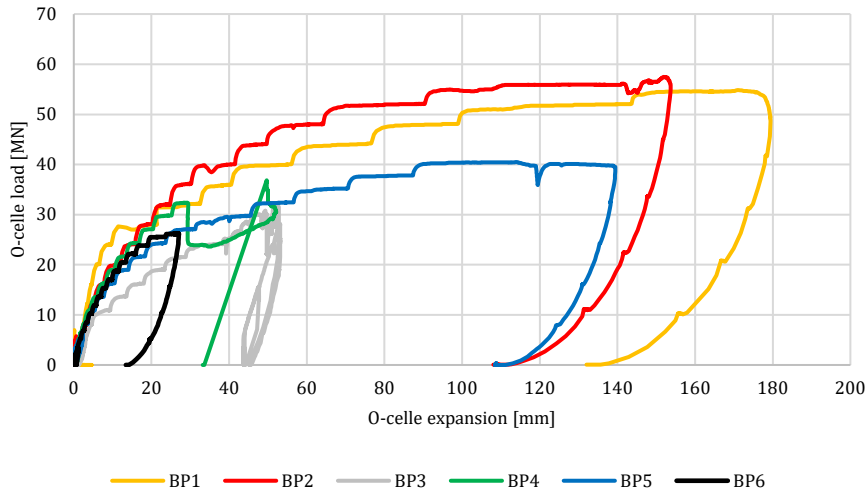


Figure 24. Load-displacement curves for the test piles.

The test piles primarily develop the capacity in the limestone. The test piles were instrumented with strain gauges as described in Section 5. The strain gauges measure the developed strains at the levels of the strain gauges. By using the axial stiffness of the pile (EA) the axial load in the level of the strain gauges can be evaluated. Further this leads to the maximum developed surface resistance between two levels of strain gauges. The result from the evaluation is shown for test pile BP2 in Figure 5.

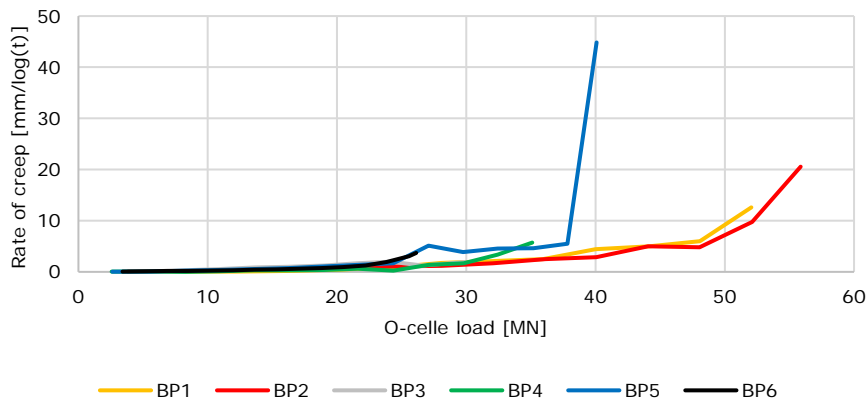


Figure 4. Evaluated rate of creep for all six test piles.

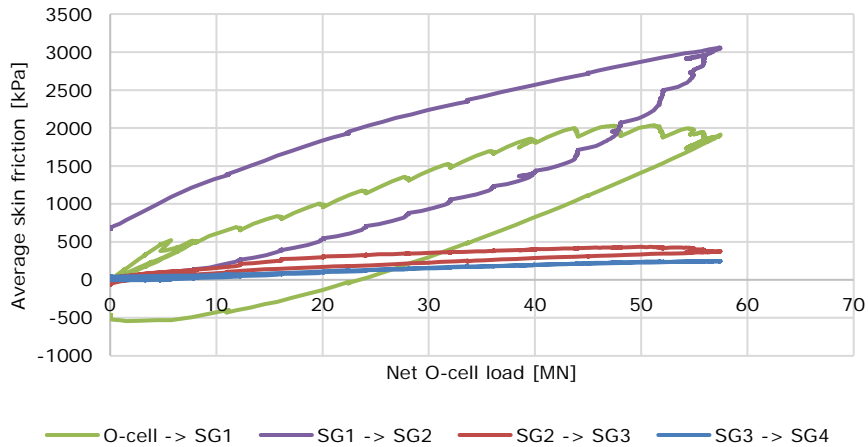


Figure 5. Mobilized shaft resistance for test pile BP2 between O-cell and different levels of strain gauges (SG), respectively.

The maximum and average mobilized skin friction for all the test piles in the limestone were evaluated for all six test piles and summarized in Table 2.

Table 2. Maximum and average shaft resistance mobilized in the limestone.

Test pile	Max. mobilised skin friction [kPa]	Average mob. skin friction [kPa]
BP1	3085	2407
BP2	2952	2402
BP3	1908	1665*
BP4	2444	2139
BP5	2610	2456
BP6	2697	2083

\* Test pile is not loaded till failure.

## CONCLUSIONS

For a construction in the city centre of Copenhagen, six test piles have been established with sockets in the Copenhagen Limestone. The test piles should form the basis of allowing a larger bearing capacity in the production piles compared to the limitation in the Eurocode, which limits the surface resistance to 30 % of the surface resistance of the comparable driven piles.

The piles have been tested with O-cells cast in the pile and with strain gauges to monitor the strains along the pile. The piles are loaded to 150 % of the guaranteed capacity of the O-cell and hydraulics and it is found that five of six piles are loaded to failure. The average mobilized skin friction ranges between 2100 – 2450 kPa for the piles loaded to failure. This corresponds to approximately 160 – 188 % of the estimated skin friction.

## **ACKNOWLEDGEMENT**

The authors would like to thank the owner of the development project, Project Nord, and the contractor Aarsleff for permission to use the site data and to publish the paper.

## **REFERENCES**

- [1] DS/EN 1997-1 DK NA, Nationalt annekst til Eurocode 7: Geoteknik – Del 1: Generelle regler, 2021
- [2] Knudsen J.: Is it reasonable to reduce the shaft resistance for bored cast-in-situ piles. NGM Paper, NGM 2016, Reykjavik.
- [3] Iversen K.M. and Roesen B.S.: Full-scale static compression pile load test in sand with post installation pre-stressing to engage toe resistance. NGM 2020, Helsinki, 2021.
- [4] Steenfelt J.S.: Loading test experience with bored piles in limestone/weak rock. ICSMGE 2017, Seoul, pp 2869-2872.
- [5] Fleming, W.G.K, Weltman, A.J., Randolph, M.F., Elson, W.K. Piling Engineering, 2<sup>nd</sup> ed. Blackie & Son Ltd., London, 1992
- [6] Tomlinson M. and Woodward J. Pile Design and Construction Practice, 5<sup>th</sup> ed., Taylor & Francis, London, 2008





# **BRIDGING GEOPHYSICAL AND GEOTECHNICAL RESULTS: AN AUTOMATED CAD VISUALIZATION METHOD FOR 2D DATA**

**Sebastian Buntin<sup>1</sup>, Omid Ahmadi<sup>1</sup>, and Mats Svensson<sup>2</sup>**

## **KEYWORDS**

geophysical methods, geotechnical engineering, 2D visualization, AutoCAD.

## **ABSTRACT**

Geophysical methods play a crucial role in early subsurface investigations for construction and infrastructure projects, providing valuable complementary data. However, the lack of standardized file formats and visualization protocols across different geophysical techniques hinders seamless interoperability with traditional geotechnical approaches. This paper presents a method designed to address these challenges by enabling the visualization of 2D geophysical results alongside geotechnical soundings within the AutoCAD environment. The methodology is developed in Sweden with consideration of standards set by the Swedish Geotechnical Society (SGF). This approach utilizes automation techniques to simplify the integration process.

By bridging the gap between geophysical and geotechnical data, this method enhances the joint interpretation and utilization of common geophysical techniques, including seismic refraction tomography (SRT), ground penetration radar (GPR), and electrical resistivity tomography (ERT). This approach not only improves the efficiency and effectiveness of subsurface investigations but also encourages the simultaneous use of geophysical methods and traditional geotechnical soundings, fostering a more holistic approach in geotechnical engineering.

## **INTRODUCTION**

In modern engineering projects, the integration of geophysical methods with traditional geotechnical approaches has become increasingly essential for comprehensive subsurface investigations<sup>[1]</sup>. Geophysical techniques, including seismic refraction tomography, ground penetration radar, and electrical resistivity tomography, provide important insights into subsurface conditions,

<sup>1</sup> Bjerking AB, Uppsala Sweden

<sup>2</sup> Tyréns, Helsingborg Sweden

enabling the rapid coverage of larger areas. This, in turn, aids in optimizing the selection of locations for geotechnical soundings and leads to lower uncertainty in the results<sup>[2]</sup>. However, the visualization of geophysical data alongside geotechnical results poses significant challenges due to different file formats and visualization protocols.

## CHALLENGES IN VISUALIZATION PRACTICES

Geophysical methods normally produce 2D profile data, typically visualized using specialized geophysical software. The prevalent software tools for near-surface geophysical processing include Res2DInv for resistivity measurements, ReflexW and Rayfract for seismics, and ReflexW for ground-penetrating radar measurements. However, the incompatibility of these software tools with CAD-systems, coupled with the general absence of standardized file formats across different techniques, complicates interaction with geotechnical soundings.

Geotechnical soundings adhere to well-established standards primarily conveyed through CAD systems, using the standard designation system of the Swedish Geotechnical Society<sup>[3,4]</sup> in Sweden. The current designation system, established in 2001, is not adapted for use with modern geophysical processing software, leading to its infrequent application for presenting geophysical results. Consequently, geophysical, and geotechnical findings are often segregated into separate reports, impeding joint interpretation, and limiting the integration of geophysical methods with traditional geotechnical investigations.

One proposed solution is visualizing both geophysical and geotechnical data through BIM platforms<sup>[5]</sup>. For example, the GeoBIM concept offers a solution by proposing the combined visualization of not only geotechnical and geophysical information, but also all other relevant geotechnical data.<sup>[6]</sup> In this concept all data types are collected in the same database via a complete digital workflow from field planning to interpreted 2D or 3D models, see Figure 1. Developments within GeoBIM have enabled seamless visualization of all data types within BIM tools like Navisworks.

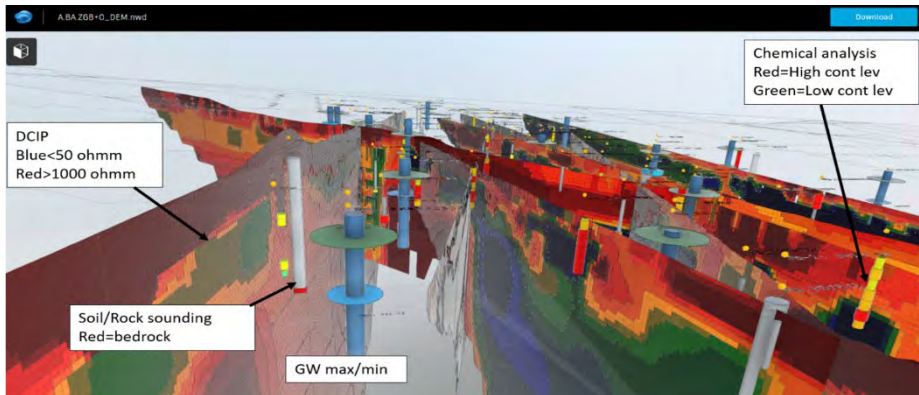


Figure 1. Geophysical DCIP data visualized together with data from hydrogeology, geotechnical sampling and sounding and environmental sampling [6].

But the dominance of CAD software and the relative simplicity of adhering to current standards within those programs presents a challenge for gaining traction for the BIM solutions.

## PROPOSED SOLUTION

To address the complexities inherent in integrating 2D geophysical results with geotechnical data, this paper introduces a novel method designed for seamless visualization within the AutoCAD environment. The method, developed in Sweden, considers standards provided by the Swedish Geotechnical Society and accommodates diverse geophysical techniques.

We have developed GEOSYNK, a specialized software solution that empowers users to effortlessly store geophysical results as images in an AutoCAD-friendly format, preserving the aspect ratio consistent with the 2D sections in AutoCAD. GEOSYNK supports various data file formats, such as SEG-Y for seismic and ground penetration radar data, and r2r, a data format supported by Res2dinv for ERT data. Additionally, compatibility extends to simple ASCII xyz grid files, including those generated using software like Surfer. This makes it suitable for using it with the most common geophysical software in engineering e.g. ReflexW, Rayfract and Res2dinv.

Moreover, GEOSYNK streamlines the creation of profile lines in AutoCAD by leveraging the coordinates from measured geophysical profiles. This generated line, coupled with the associated image, can be seamlessly imported into the AutoCAD environment. Illustrated in Figure 2 are the results of the combined visualization of geophysical and geotechnical data employing different geophysical methods. The visual representation demonstrates how GEOSYNK supports the joint interpretation for identifying specific layers in the subsurface.

This integration facilitates a cohesive visualization of geophysical results alongside geotechnical drilling data, enhancing the overall analytical capabilities of the AutoCAD platform.

## CONCLUSIONS

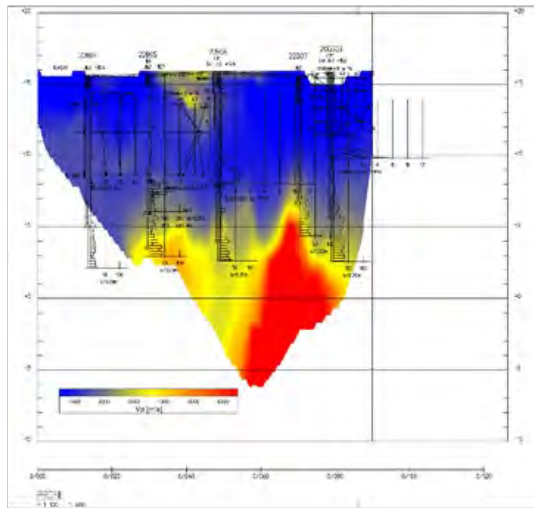
In summary, the integration of geophysical and geotechnical data using the automated 2D visualization method in AutoCAD represents a practical advancement in subsurface investigations. The optimized approach has proven successful in enhancing the efficiency of combined interpretation, providing geotechnical engineers with a detailed representation of subsurface characteristics.

The method's capability to integrate various geophysical techniques ensures versatility and broad applicability, addressing the diverse needs of infrastructure projects. By offering a unified platform for data interpretation, it mitigates challenges associated with disparate visualization practices, and contributes to a more cohesive understanding of subsurface conditions.

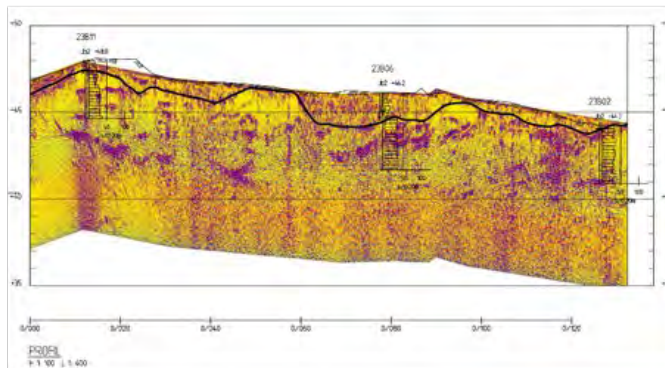
As a notable implication, the adoption of this automated method may lead to an increased utilization of geophysical methods in subsurface investigations. The efficiency and accuracy demonstrated in this approach could potentially encourage a broader application of geophysical techniques, further advancing the field and contributing to the evolution of standard practices in geotechnical engineering.

In conclusion, the proposed automated method serves as a practical tool for geotechnical engineers, streamlining the interpretation process and potentially fostering a wider acceptance and utilization of geophysical methods in subsurface analysis for infrastructure development.

a)



b)



c)

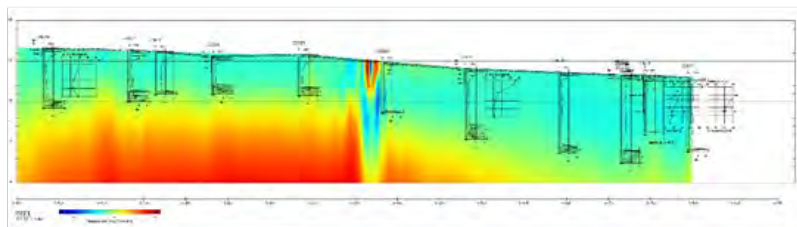


Figure 2. Three examples of the proposed visualization method for geophysical and geotechnical data aligned with the SGF's standards. a) a seismic refraction profile b) a GPR profile c) an ERT profile. All the data have been acquired and processed in Sweden.

## ACKNOWLEDGEMENT

The development of GEOSYNK was funded by the Swedish geotechnical society (SGF, project number: 522304), Bjerking AB, Structorstiftelsen and Tyrens AB, which are gratefully acknowledged.

## REFERENCES

- [1] A. B. Medhus; K. Lone, eds.: Engineering Geophysics. CRC Press, 2022.
- [2] M. Svensson: Slutrapport Osäkerhetsmodeller (in Swedish). Project 13493, SBUF, 2022.
- [3] SGF: SGF/BGS Beteckningssystem 1, Version 2001:2. Swedish Geotechnical Society, Linköping, 2001.
- [4] SGF: SGF:s dataformat, SGF Rapport 3:2012 (in Swedish). Swedish Geotechnical Society, Linköping, 2012.
- [5] M. Svensson; O. Friberg: Communication of geophysics in underground infrastructure projects. SAGEEP 2018, Nashville Tennessee USA, 2018.
- [6] M. Svensson, Friberg O., 2019, BIM – the key for implementation of geophysics in infrastructure planning, EAGE Near Surface Geoscience, Netherlands, September

# BRINGING TECH INTO GEOTECHNICS

**Kristin Paulsen<sup>1</sup>, Truls Martens<sup>1</sup>, and Mats Kahlström<sup>1</sup>**

## KEYWORDS

digitalization, innovation, SaaS, data-driven solutions

## ABSTRACT

The Norwegian Geotechnical Institute (NGI) recognizes the pivotal role of ground engineering in the ongoing digital transformation of the construction industry. We have embraced this challenge by establishing NGI Digital where expertise from the tech industry converges with cutting-edge domain knowledge from geotechnical and geo-environmental engineers. With natural hazards escalating due to climate change, it's imperative for the geo-industry to innovate using data-driven solutions. The goal? Ensuring that we live on safe ground. In addition, to harness the power of emerging technologies and AI, we must first confront and resolve the industry's issues with data quality and availability. Borrowing best practices from the tech world can be transformative. This includes leveraging cloud technologies, deploying DevOps teams, embracing design thinking, and adopting agile methodologies to create high-quality digital products. Over the past 5 years, NGI Digital has grown impressively. Proudly, we introduced Field Manager, our first Software-as-a-Service, to the market in March 2023 and we have developed 4 additional digital products that have redefined how we work. At NGI, we also foster a culture of continuous learning. Our "Code Academy" is a testament to that, propelling innovation across the organization.

## INTRODUCTION

The effective use of digital data represents the future of the digitalisation of the construction sector [1]. In-line with this, NGI has recognized the need for a new strategy to fully leverage emerging technologies, including artificial intelligence (AI). Our journey revealed that capitalizing on these technological advancements posed significant challenges stemming from fundamental

<sup>1</sup> Norwegian Geotechnical Institute, Oslo Norway



issues related to data quality, data availability, and the absence of standardized data formats.

Addressing these fundamental challenges is a formidable task that demands substantial investments. Consequently, NGI's management took decisive ownership to tackle these issues head-on. We recognized the need to embrace cutting-edge technologies and invest in expertise. As a result, NGI established a new department called NGI Digital, specializing in digital product development and technology.

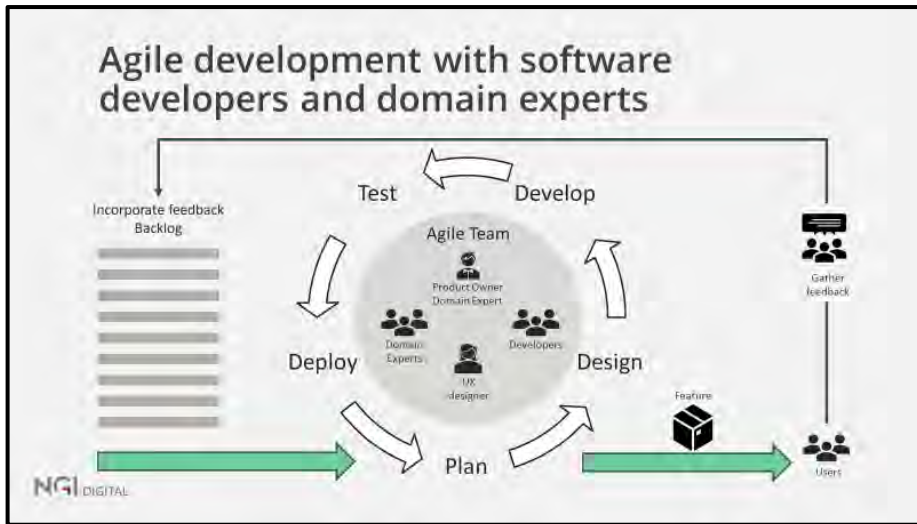


Figure 1: Agile development with software developers and domain experts.

Over the past 5 years, we've built a team of 18 developers, UX designers, and business developers. Given the inherently complex nature of geotechnics, successful outcomes hinge on close collaboration between developers and geoscientific experts within agile teams, as shown in Figure 1.

Furthermore, we have established NGI Code Academy to enhance the proficiency of scientific developers and engineers across the organization. The aim of the course series is to elevate our coding practices by focusing on code quality, improving collaboration, use of API's and creating web applications.

## DIGITAL PRODUCT DEVELOPMENT

The main driver for the initiative Geo Hub, which constitutes our collection of digital products including our flagship product Field Manager, and the establishment of NGI Digital, was to unlock data-driven decisions in the geosciences. Our first mission was to make our core data, from field, lab and instrumentation, easily accessible and useful. A key part of this was to make

the data is available through APIs (Application Program Interfaces). APIs are the backbone of internet communication and digital innovation. They ensure that different digital products can communicate dynamically and seamlessly.

Field Manager is web-based and has quickly become an important tool for both NGI and external customers to improve the processes of collecting data from ground investigations and provides a comprehensive overview of ground conditions in all projects. An example screenshot is shown in Figure 2.

Efficient sharing and transfer of data and information between stakeholders in the value chain is considered a key factor for successful digitalization [2]. In Field Manager, the process of collecting data from field and lab is simplified through intuitive planning tools, collaboration between project stakeholders, immediate visualization, and quick and easy QA. The platform enables safe and secure data sharing and is tailored for improved efficiency and automation of work processes and deliverables.

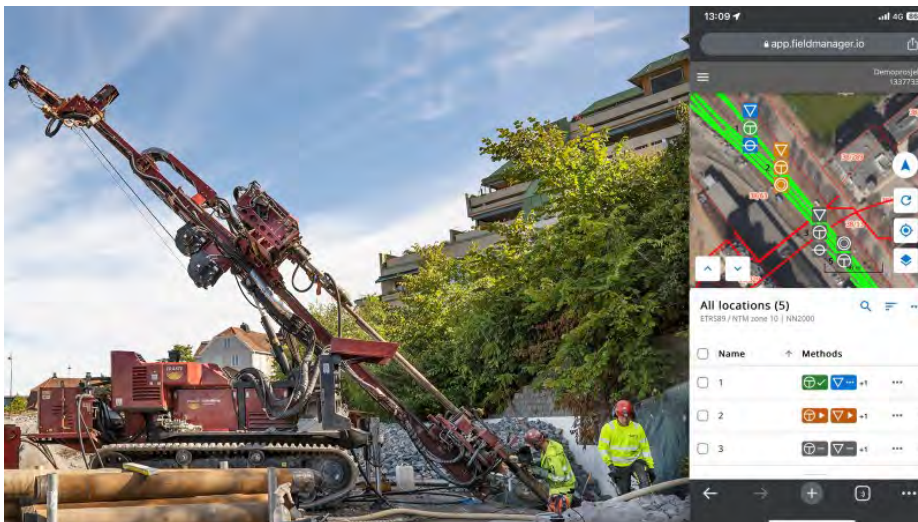


Figure 2: Screenshot of Field Manager mobile view for use during field work.

## HOW WE WORK

At NGI Digital, we adopt a cloud-first approach, focusing on building applications exclusively for the cloud using modern technologies. Our DevOps expertise allows us to create scalable, reliable, secure, and sustainable digital products using open-source technologies. Our DevOps teams are responsible for constantly improving their digital product by owning the whole IT value chain of planning, testing, deployment and operations.

Design thinking is at the core of our product development. We prioritize simplicity and intuitiveness, recognizing that users expect these qualities in the modern age. By closely collaborating with users across the value chain, we empathize with them before designing solutions.

Finally, our agile development process involves software developers and domain experts. We release new features continuously, guided by a domain expert who serves as the product owner. Close dialogue with customers ensures that we address industry needs effectively. This collaborative approach, combining professionalized software developers with domain experts, is our true strength.

## CONCLUSION

Buildings represent approximately 40% of energy consumption in the European Union and account for about 36% of CO<sub>2</sub> emissions. [3] There exists a huge, untapped potential in leveraging technology and data to advance sustainability goals. Improvements must be made in all parts of the life cycle, and ground engineering must carry its fair share. To drive digital innovation effectively, we must adopt a collaborative mindset—one that transcends organizational boundaries. NGI has already embarked on this journey by organizing and structuring high-quality ground investigation data, making it easily accessible and useful. Now, we extend an open invitation to all: join us in transforming the geosciences and contribute to meeting climate goals.

## REFERENCES

- [1] European Construction Sector Observatory. 2021. Digitalisation in the construction sector. Analytical report.
- [2] Labonnote, N., Bryhni, A. and Lech, T.C. 2021. Digital samhandling og datadeling i bygge-, anleggs- og eiendomsnæringen. SINTEF report; 2021:00373
- [3] [The confusion about embodied carbon and scope emissions \(nordesg.de\)](https://nordesg.de)

# **BYGGEGROPVEILEDNINGEN – A TOOL FOR PLANNING BUILDING PITS**

**Gunvor Baardvik<sup>1</sup> and Astri Eggen<sup>2</sup>**

## **KEYWORDS**

Building pits, neighbors, settlement, pore pressure, sheet pile wall, excavation

## **ABSTRACT**

Underground works like building pits have repeatedly led to unexpected and unwanted damage to properties and infrastructure nearby. For that reason, the BegrensSkade I research project was created as a consortium of most Norwegian members in the construction industry together with the Research Council of Norway. One of the main conclusions was that it is necessary to plan better to avoid damage from nearby building pits, and that sufficient mitigating measures must be established for neighbours.

The Norwegian Geotechnical Association took the initiative for a Building Pit Guide - Byggegrupveiledningen. The purpose with this guideline is to increase the level of awareness of the planning adviser in geotechnics. It is agreed that improved execution results in savings through a reduced number of damages and fewer disputes.

The guideline deals with topics such as which regulations must be followed, which preliminary investigations should be carried out and how a building pit can affect the surroundings. It also deals with topics such as simple hydrogeology with a focus on pore pressure and influence zones, leakage and sealing requirements.

Furthermore, it goes into the most common methods for establishing construction pit walls, from open excavation, sheet piling to freezing. Each topic has a reference to the European technical standards for execution of special geotechnical work. There are also recommendations on how each type of wall should be followed up under construction on site, and how they can be dimensioned.

<sup>1</sup> Norconsult

<sup>2</sup> Veidekke Entreprenør AS

## INTRODUCTION

### Old Norwegian Law on Neighbouring Areas:

*Granneloven § 2: Ingen må ha, gjera eller setja i verk noko som urimeleg eller uturvande er til skade eller ulempe på granneeigedom. Inn under ulempe går òg at noko må reknast for farleg. I avgjerda om noko er urimeleg eller uturvande, skal det leggjast vekt på kva som er teknisk og økonomisk mogleg å gjera for å hindra eller avgrensa skaden eller ulempe.*

### Explanatory translation, not legal.

Neighbour law § 2: No one shall have, do, or implement anything that is unreasonable or unnecessary to the detriment or inconvenience of neighbour property. Also included in the disadvantage is that something must be considered too dangerous. When assessing whether something is unreasonable or unnecessary, emphasis shall be placed on what is technically and economically feasible to do to prevent or limit the damages or disadvantage.



Figure 1. Byggegruppveiledningen – The Building Pit Guide

Since the establishment of construction pits and foundations of structures too often lead to building damage to neighbouring areas, a research project on the topic was carried out in the period 2012 – 2015 in Norway. The project was called Begrens Skade (Limit Damage). It is estimated that 3 – 8% of total investment costs for construction projects goes to repairing damage caused by geotechnical circumstances. The research results showed that it is partly the same type of damage that occurs and that it can take time before the damage appear and are discovered. This shows how important it is to carry out the groundworks correctly. Then the damage will be limited to a minimum and

thereby costs for repair. These damages are often a source of conflicts that require a lot of time and resources and can end up in the court system. It is not only the parties who pay a price, but it is the whole society that pays the final bill. By reducing the level of conflict, the focus can be on executing the projects in a good way and not on conflicts.

In the research project Begrens Skade, 23 partners from builders, consultants, suppliers, contractors, research institutes and universities, as well as financial support from the Research Council of Norway contributed. In practice, this meant that the entire building business sector participated, which contributed to a general increase in knowledge.

Ground and foundation work affects the surroundings, and it is necessary that the consequences of the works are assessed to plan and implement any measures. The Eurocodes set requirements for satisfactory design of structures. Furthermore, European standards of execution must ensure that the works are carried out in the best possible way.

In addition, the potential for damage due to installation methods for sheet piles, piles and anchors must be assessed during the design phase. The mapping carried out in the BegrensSkade-project shows that installation effects are usually not sufficiently assessed or probably underestimated. The risk of damage to neighboring property caused by groundwork depends on many factors. Choice of type of construction and foundation method, soil conditions and in particular the margin of the clay's pre-consolidation pressure, soil sensitivity, hydrogeology and pore pressure levels, depth of the construction pit (number of basement levels), choice of execution method, which procedures the contractor uses and construction time are examples of variables that affect adjacent areas to a construction project.

In addition, the understanding of the problem, depending on the expertise and experience of the participants (client, consultant, contractor, and supplier) will play a decisive role for the project. Furthermore, communication and cooperation can be affected by the contracts and the financial framework under which the players work.

## **COMPETENCE OF THE ACTORS**

The Begrens-Skade project has shown that overall competence has a significant potential for improvement among all actors. Those who come out of universities as geotechnical engineers know some theory. They have learned to calculate piles, bracing etc., but it is limited what they have been educated on the totality of a construction project, what laws and regulations apply, can the work lead to damage to third parties, etc.

The Begrens-Skade project was an R&D project in which expertise was shared between the various actors. The geotechnical environment in Norway

is such that one is happy to share experiences if one does not sit on opposite sides in a conflict / court case. This collegial openness came to great news in the R&D project.

Based on Begrens Skade it was concluded that a Building Pit Guide where one collects and compiles the main part of what is important to have knowledge of that can have great significance for the geotechnics part of the industry. There is an understanding of regulations, an overall understanding of what a construction project entails also for the surroundings, the interface between the players (who is responsible for what), HSE/SJA for ground-works, what is important to map before starting work, what opportunities do you have to secure the construction pit and finally something about design.

By gathering the practical part of geotechnics in a book, one will more easily acquire knowledge that would otherwise have taken several years and learn from more experienced colleagues. In other words, the Building Pit Guide is a practical guide for structures in and against the ground.

## **WHAT THE GUIDELINE CONTAINS**

The Building Pit Guide is a practical guide for constructions in and towards the ground. The following provides an overview of the content:

1. Background and regulations
  - The introductory chapter provides definitions of terms such as construction pits, encroachment zones and influence zones. Furthermore, information is provided about and to some extent an overview of the most relevant laws, regulations, standards, guidelines, and manuals.
  - The purpose is to provide an overview and some start-up help.
2. Overall assessments and relationships with neighbours and surroundings
  - The aim of this chapter is to provide an overview of what should be considered to gain a better overall understanding of the impacts a construction project can have on neighbouring areas.
  - At a general level, reference is made to different security options for a construction pit in relation to ground conditions and proximity to neighbouring structures.
  - Experience figures are provided regarding how much impact a construction pit can have on third parties.
  - Technical considerations about accessibility and opportunities are an important topic.
  - Risk assessments, which are currently a useful tool in construction projects, are discussed in a section. Both regulations and Norwegian standards set requirements for this.

### 3. Interface between actors

- There are many actors in a construction project. In this chapter, an attempt is made to shed light on roles and responsibilities:
  - This is seen in relation to how far into the planning and construction process one has come, as well as in relation to different contract forms.
  - Interface between disciplines and actors.
- An assessment is also given of the significance of the type of contract the parties have.

### 4. HSE and SHA during groundworks and planning for groundworks

- It is important that one from the start of planning and engineering in a project, focuses on ensuring that the work is carried out as safely as possible.
- Large machines and an understanding of how the works should be done as safely as possible have been attempted to be shown by examples and with reference to regulations.

### 5. Early investigations and monitoring programs

- For large development projects and infrastructure projects, feasibility studies are required before the project is approved by the competent authorities and politicians. For projects that "only" plan to build a building in a construction pit, the same requirements for feasibility studies are not stipulated, most likely because this is normally carried out in areas that have already been zoned for construction. It is therefore easy to overlook the fact that early investigations and monitoring, outside the actual construction pit, must nevertheless be carried out.
- Ground and neighbouring conditions are of great importance in geotechnical design and construction in the ground.
- Guidance has therefore been provided on what is needed and how to find important information. This applies to both geotechnics and environmental geology.
- References are made to the formal requirements that must be satisfied.
- Control of execution and follow-up of monitoring programs throughout the construction process is shown with examples.

### 6. Support of Excavations

- Support systems for excavations is a large chapter in which 8 types of supporting structures are discussed.



- Furthermore, guidance is given on different types of bracing and anchors for the support structure. Both internal struts and anchors in rock and soil.
- This includes, among other things, securing the sheetpile foot at the rock surface, before excavating (drill&blast) the rock further down.
- Soil nailing, ground reinforcement with lime-cement piles and ground freezing are also covered by this chapter.
- The chapter also provides examples of how to reduce leakage into construction pits, including injection, water infiltration and sealing sheetpile walls.

#### 7. Geotechnical engineering.

- This chapter provides general recommendations for geotechnical design and execution of ground works.
- Many of the solutions and possibilities shown in previous chapters are described in more detail regarding what is important in the design.

This guide will hopefully be of use to all players in the industry who need some more insight into practical issues and solutions.

### **EXAMPLES FROM THE BUILDING PIT GUIDE**

We have selected a few examples to illustrate various topics covered in the guideline. As shown above, there is a wide range of topics that the Building Pit Guide covers. Here are some samples.

#### **Investigations in early planning**

Eurocode 7 sets requirements for geotechnical investigations in early planning phases such as: “Collection and interpretation of geotechnical information must always be carried out. This information must include geology, geomorphology, seismicity, hydrology, and the history of the construction site”. Norwegian environmental legislation sets requirements for investigations of contaminated soil and the Cultural Heritage Act sets requirements to survey for archaeological objects. Nevertheless, issues such as changes in hydrogeological conditions, vibrations and settlements on neighbouring buildings and infrastructure is not covered directly by the regulation and easy to forget.

The Building Pit Guide lists checkpoints that should be reviewed in the design phase for various topics to be surveyed.

#### **Mapping depths to rock surface**

Mapping the depths to rock surface is a useful tool for surveying the potential for subsidence and settlements, and for determining whether neighbours may

experience settlements due to changes in pore pressure or groundwater level. In the Building Pit Guide, it is described how these maps can be used together with pore pressure observations to determine where settlements should be followed up on neighbouring buildings. It is also useful as a tool for predicting vibrations from blasting. An example of a map with soil depths to rock surface is shown in figure 2.

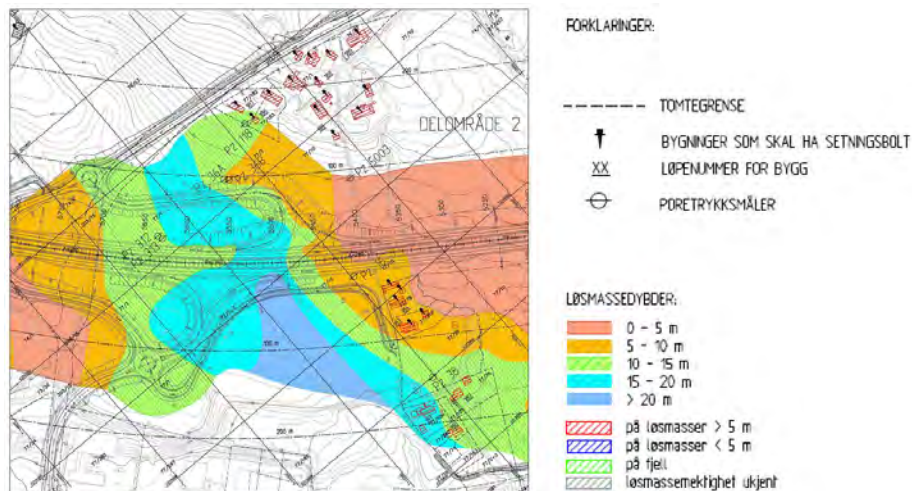


Figure 2 An example of a map with soil depths to rock surface as guide for following up on buildings where settlements may occur due to reduced pore pressure or lowered water table caused by the road construction. [1].

## Survey of neighbouring buildings and infrastructure

Survey of neighbouring buildings and infrastructure that lies within a building pit's influence zone is necessary when blasting is planned in the building pit. It may also be necessary to carry out before sheet piling, or before other earthworks that causes deformations or settlements. The guideline describes how the inspection can be authorised, what must be checked externally and internally in a building and how it must be reported.

## Wells for water infiltration

An example of the practical approach in the guideline is shown in the chapters on Hydrogeology (chapter 5.4) and Infiltration wells (chapter 6.21). In the chapter on hydrogeology, it is illustrated with figures and text that explain hydrogeology in and beneath marine sediments. It is described how a building pit can affect pore pressure and groundwater level, both within the footprint of the pit and also outside the building pit, see figure 3. This is to a small extent captured by Norwegian geotechnical textbooks used in education.

Great emphasis has been placed on explaining the difference between groundwater level and pore pressure. Hydrostatic pore pressure from groundwater level can deviate significantly from measured pore pressure in the case of large thicknesses of marine clay combined with large height differences. With the formation of groundwater in areas lying above the terrain level where a building pit is planned, artesian pore pressure often occurs in the small and almost closed aquifers of moraine under dense and mighty clay layers, see figure 4.

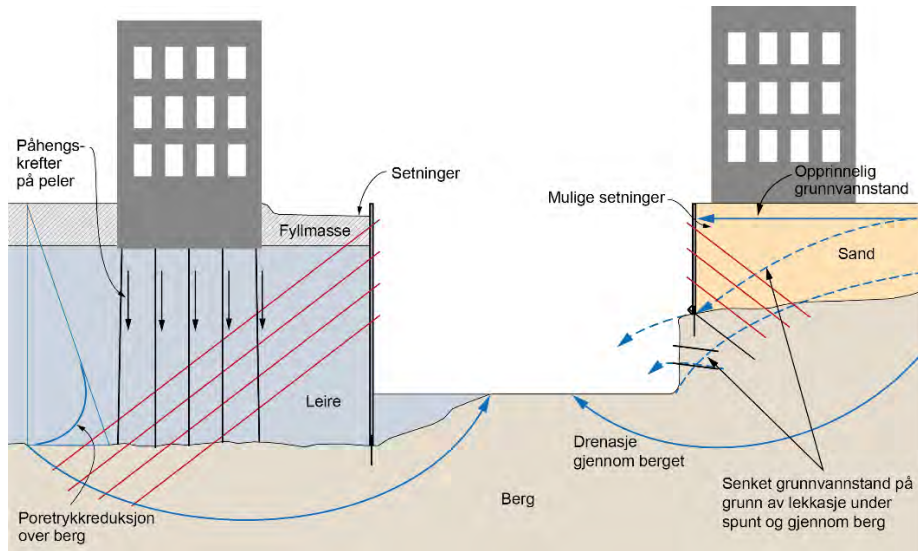


*Figure 3 Two different ways a building pit can affect the groundwater level and pore pressure. On the left, pore pressure reduction at the rock surface is shown. It can be due to direct leakage through rock, or leakage in drilled anchors or drilled piles. On the right is shown the lowering of the groundwater table towards a construction pit. [1]*

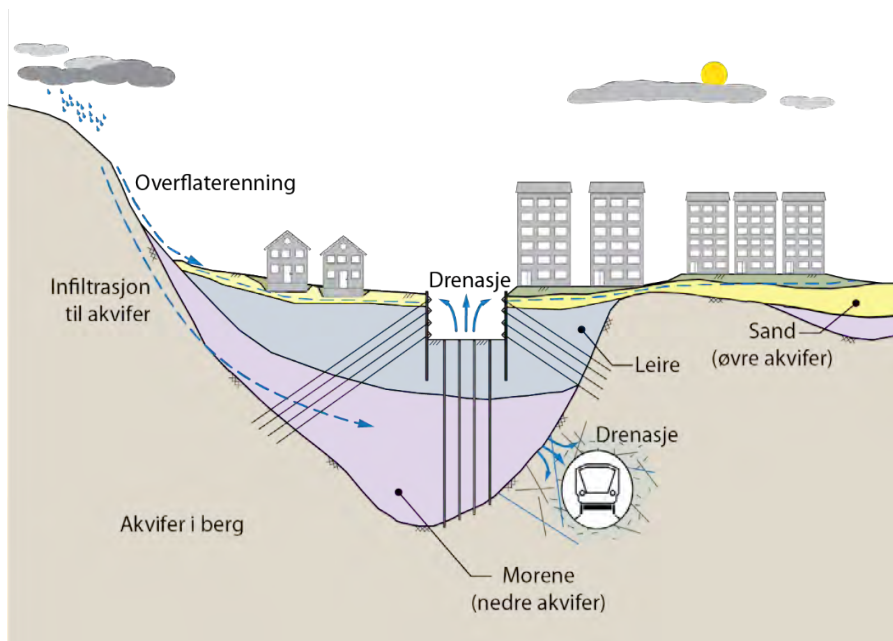


*Figure 4 An artesian pore pressure is often developed in the moraine and rock beneath the clay layer due to the height difference between the area where the groundwater is formed and the aquifers in the rock and the moraine. When the terrain is lowered during the excavation, the gradient increases towards the bottom of the building pit. [1]*

When these pockets with artesian pore pressure are punctured, for example by drilled piles or drilling for anchors without any sealing, the pore pressure drops, and effective stresses increase above the rock surface. It often takes a long time before enough water refills the pockets and restore the pore pressure. In the meantime, settlements arise in the layers above the rock, and buildings and constructions are damaged.

Leakage into the building pit can lower the pore pressure above the rock surface. An important countermeasure in addition to injection is the infiltration of water into the rock using a well, see figure 5. The method has been used for many years with great success. It is included in requests for tenders, but where the well is to be established, how it should interact with the rock surface, geology and fracture directions are not stated in the tender documents. This information is often only handed over orally internally within the different companies. It is important to share this knowledge since the use of infiltration wells can save neighbours from major damages at a low cost.

An entire chapter is devoted to infiltration wells, where the challenges of placement, on terrain and under the rock surface are shown. The location must be adapted to the main geological lines, the local fractural patterns and

directions in the rock masses, and the distance from the rock surface, see figure 6 and figure 7. You can also find in the guideline recommended dimensions and slopes of the wells, information on water consumption and pressure, on the use of packers and sealing, how wells is tested and how they should be followed up, maintained and terminated.

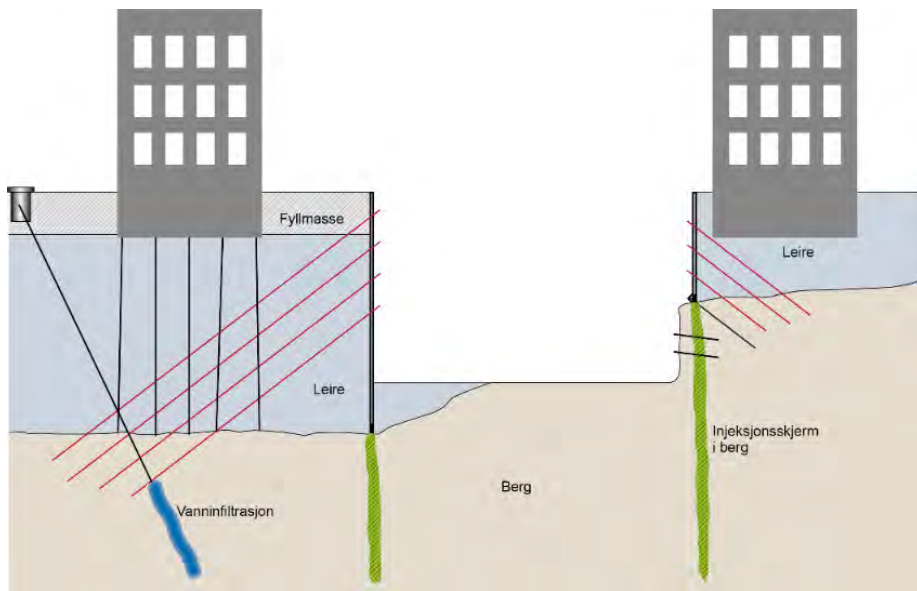


Figure 5 Illustration of an infiltration well close to a building pit [1]



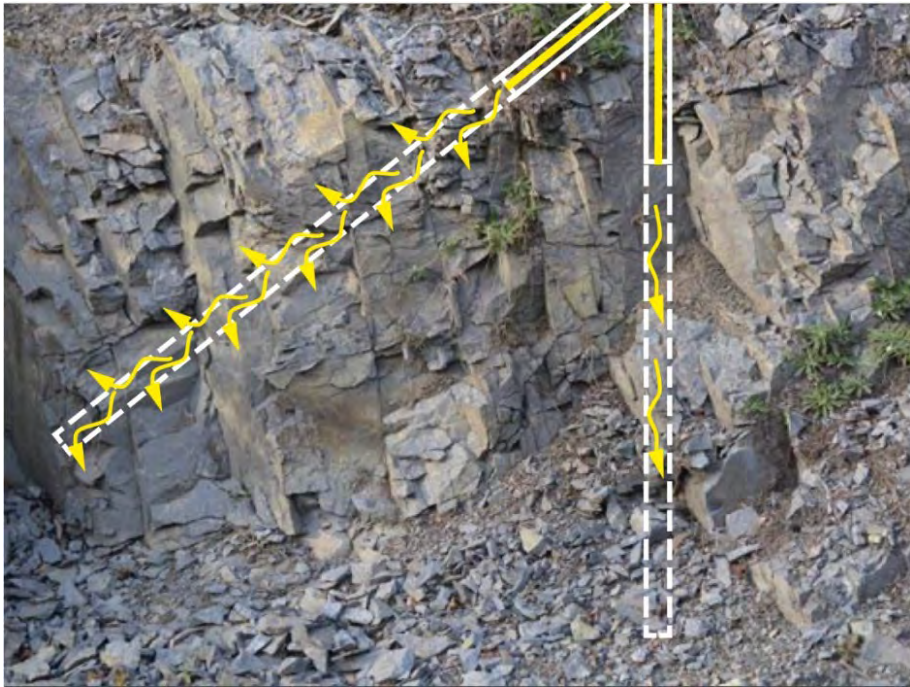


Figure 6 The effect of drilling the water infiltration well through layers and fractures in the rock. The vertical well is mostly in lightly fractured rock, while the inclined well covers many cracks into which it may be possible to infiltrate water [1]

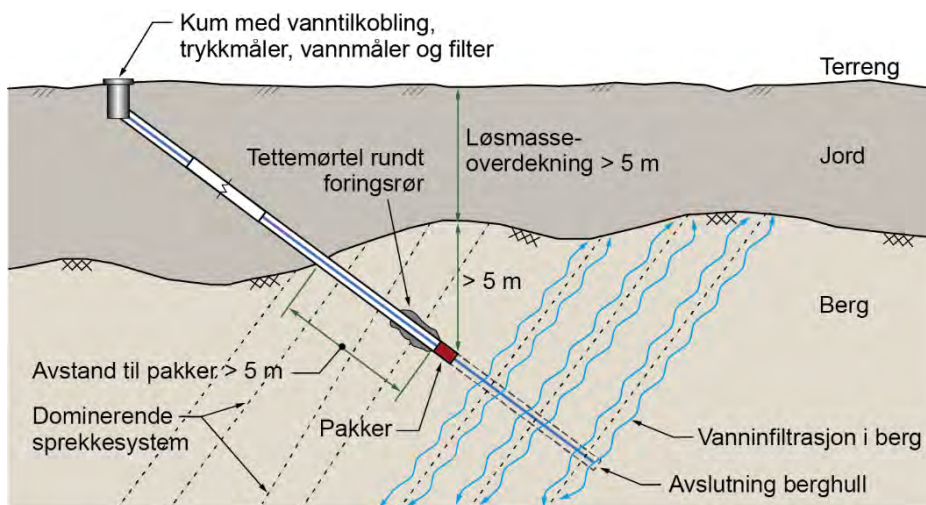
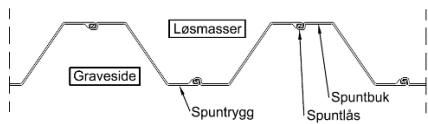
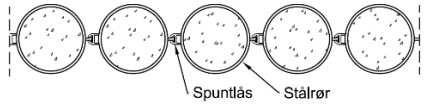
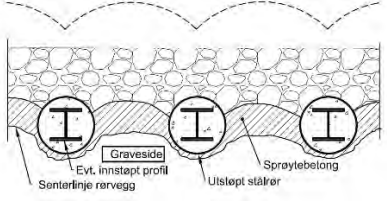
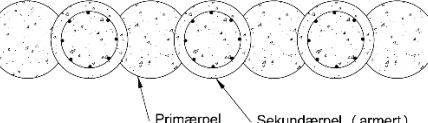
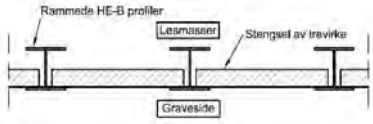


Figure 7 Principles for an infiltration well in bedrock [1]

## Types of excavation support

Another example is the overview of the various types of support constructions shown in chapter 6. The advantages and disadvantages of each method are listed here. In addition, it has been set up what and how the solution is to be controlled during establishment.

	Sheet piling, see chapter 6.3
	Drilled continuous pipe pile wall, see chapter 6.4
	Tubular wall, see chapter 6.5
	Secant pile wall, see chapter 6.6
	Wall of stop logs (Berlinerwand), see chapter 6.9

Figur 8 Excerpt from table showing the most common types of excavation support in Norwegian building pits.

This chapter discusses recommended solutions such as open excavation, sheet piled walls, drilled pipe piling, secant and tangent pile walls, diaphragm walls, jet piles, wall of stop logs and soil freezing.

## SUMMARY

The Building Pit Guide is a tool for spreading knowledge throughout the building and groundworks industry. Either those working with planning and design, contractors who carry out groundwork and foundation on construction sites or owners. The effect on the neighbouring area of the work we do in building pits that was mapped through BegrensSkade is no longer something we can ignore.

The committee for the Building Pit Guide also conducts small webinars, both to elaborate on topics in the book, and to supplement with new knowledge.

The guideline is available on the website for the Norwegian Geotechnical Society.

## ACKNOWLEDGEMENT

We would like to thank the Norwegian Geotechnical Society for funding the secretary work in this project, and all the Norwegian geotechnical consultants, contractors on earthworks and public contracting managements who have contributed through several years with text, photos, quality assurance and hearing statements.

## REFERENCES

- [1] Norwegian Geotechnical Society (NGF): Byggegrøpveiledningen 2019.
- [2] A Eggen et al.: Begrensning av skader som følge av grunnarbeider (BegrensSkade I). Delprosjekt 6: Forbedring av samhandling i BA-prosessen. Lovverk og kontraktens betydning for samspill og produkt. 2014.
- [3] J Langford et al.: Begrensning av skader som følge av grunnarbeider (BegrensSkade I). Sluttrapport. 2026.
- [4] Eurocode 7: Geotechnical design – Part 1: General rules. (NS-EN 1997-1:2004+A1:2013+ NA:2020).
- [5] Norwegian law: Lov om rettshøve mellom grannar (grannelova). § LOV-1961-06-16-15 Justis og Beredskapsdepartementet.





## CC-TEST, CLAY CUTTING TEST

**P. Hedborg<sup>1</sup>**

### KEYWORDS

Clay-Cutting, CC-Test, Shear strength, Test rate/cutting rate

### ABSTRACT

With nearly twenty-five years of experience, I have specialized in geotechnical laboratory testing, using a range of analyses to improve my understanding of soil behavior. These tests include basic methodologies such as the fall cone test, as well as advanced methodologies like triaxial testing. Enhanced understanding of soil behavior is obtained through conducting a larger number of tests on soil samples and compare with different testing methodologies. The result gives a more solid and accurate understanding.

The fall cone test is primarily an index test, measuring cone penetration within a limited part of the soil sample. Usually, the fall cone test is performed on a five centimeter sample per meter, representing a small part of the entire soil profile.

More advanced tests such as direct shear tests can be done, but also here, only a small part of the full sample is tested.

The soil samples often have significant natural variation and the different laboratory test methods do not always give consistent results. In this context the idea of measuring a more extensive sample started to grow.

It was important to see how the shear strength varied with depth within the sample. One way of doing that was to vertically slice the sample and visually observe the changes. Another way was to measure the resistance while cutting the sample.

From the beginning a load frame with constant rate was used and a manual cutter was fixed to a force transducer. The force was measured during the procedure of cutting through the sample. The result gave a good understanding of how the shear strength varied with depth. This simple arrangement was the first prototype of a new laboratory equipment and I call the test, The Clay-Cutting-Test (CC-Test).

<sup>1</sup> AFRY, Gothenburg Sweden

The CC-Test has evolved over time since the first test was performed. The equipment is a simple tool, and the cutter can be recognized as the tool that is used to trim soil samples in other geotechnical laboratory tests. An experienced laboratory engineer can “feel” the shear strength when cutting the clay. The cutter is pressed by hand through the sample and cuts the clay with a metallic thread.

The possibility of gathering a lot of data in a short period of time has been important in develop the CC-Test. The test measures the force over 1000 times per minute. It only takes two minutes to analyze 10 centimeters of a soil sample which made it possible to in several ways validate the method. Thread parameters with focus on material, dimensions, tension, and test rate have been studied to obtain the best results.



*Figure 1 CC-Test Equipment and, handheld Cutter.*

## **SHEAR STRENGTH OF SOIL**

The strength of soil depends mainly on its composition and geological history of deposition and loading. Over time, good empirical knowledge has been created about how the strength in clay varies with plasticity, preconsolidation pressure and degree of overconsolidation, as well as in organic soil with content and type of organic material.[1]

### Using the CC-Test to analyze various empirical relations in soil

Initially, tests were performed to verify the method and to see how the CC-Test can be used. Several types of soil have been evaluated. The resistance of the wire varies as it passes through different soil layers. By combining the results from the CC-Test with a photo of the sliced soil surface it is possible to see how the resistance varies through the sample, which strengthens the method. No major study has been done to analyze this more systematically, but there is a lot of information that potentially can be used to classify the soil.

No empirical correlations have been used to correct the methodology yet, the measurements are completely uncorrected. Focus has been to analyze the shear strength and see how the CC-Test compares with other test types.

### Suggested symbols for the CC-Test

CC-Test = Clay Cutter Test

$F_{CC}$  = Wire Force(kN)

$A_{cc}$  = Wire mantle area in the soil(m<sup>2</sup>)

$L_W$  = Wire length in the soil(mm)

$D_W$  = Wire diameter(mm)

$\tau_{CC}$  = Uncorrected shear strength (kPa)

Equation 1.  $A_{cc} = \pi \times D_W \times L_W$

Equation 2.  $\tau_{CC} = \frac{F_{CC}}{0,5 \times A_{cc}}$

### QUESTIONS

The questions that needed further attention were:

- Test rate/cutting rate
- Repeatability
- Wire parameters (diameter, tension, material)
- Sample height

### Test rate/ cutting rate

To study the effect of the cutting rate homogeneous clay samples from the Gothenburg area with density between 1.55-1.58 t/m<sup>2</sup> and with water content between 75-85% were used.

Two different test rates were initially utilized to see if the rate had some effect on the force on the tread. In the first sequence of tests, the rate of 2 mm/min and 5 mm/min were used and clay from three different depths were studied. These results were compared to see how the force was affected by the cutting rate, see Figure 2. Results from the fall cone test were also used as a reference.

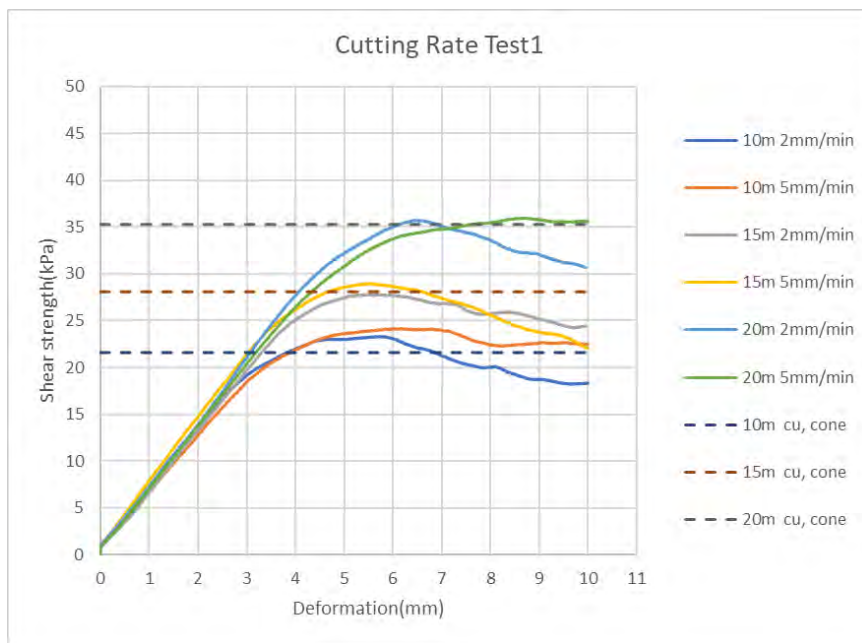


Figure 2 Tests with different cutting rates.

These first series did not indicate that the velocity significantly affected the result. To select a standard velocity more tests were needed to be done, and with a greater span of the soil strength.

Initially the CC-Test was calibrated against the fall cone test. Around twenty parallel tests were performed, and a conversion factor was calculated from the tread resistant load. This made it possible to compare the test from the start and collect data by testing the methodology in different soils.

The conversion factor was then compared with the wire dimensions and what fitted best were the halves mantle area of the wire. This factor was close to the conversion factor from the cone and worked well for other wire diameters. Therefore, the equation 2, was used for from this point.

When tests with considerably lower test rate was performed, the test showed higher shear strength.

The soil sample that was tested had a low shear strength and the cutting area showed significant signs of closing after the tread had passed through, see Figure 4.

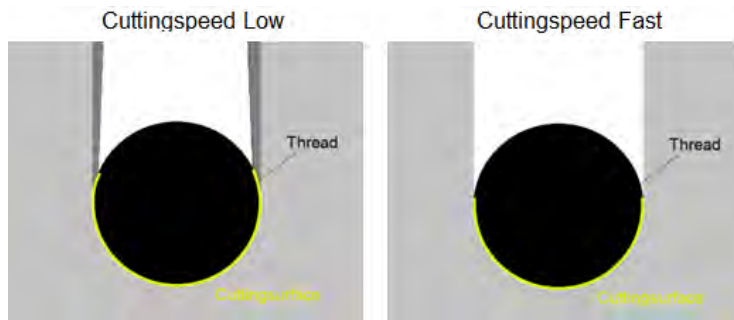


*Figure 3 Contact area between soil and thread depending on the test rate.*

### **Repeatability**

To study and validate the repeatability of the CC-Test, a homogeneous clay used for pottery was tested. Cubic samples were cut out and several tests were done to see how repeatable the test could be. During the whole procedure, the same test rate was used.

The same clay was then used with different cutting rates to see how the test rate affected the shear strength. The conclusion was that it was better to use a higher rate since the soil seemed to reach a certain limit where the contact area between the wire and the soil did not affect the shear strength, see Figure 4.

At this point a test rate of 40mm/min was chosen for further testing and analysis but more tests with different cutting rates in different soils needs to be done to see if it has any effects on the shear strength.

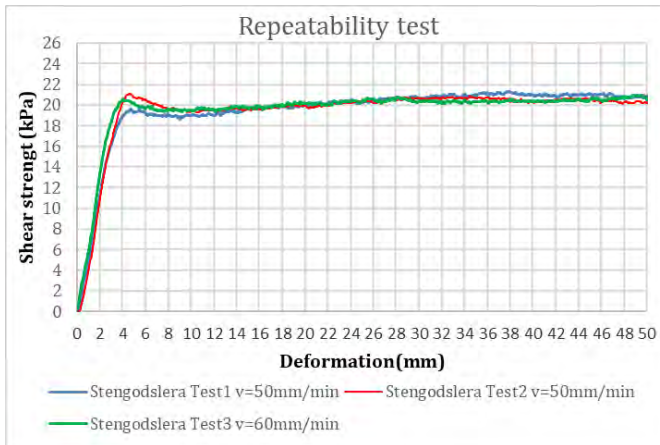


Figure 4 Two tests made on identical samples with different cutting rates.

### Wire parameters

To make a solid and robust equipment the tool had to have a stiff design and a mounting mechanism that enabled changing the thread and get the same tension in the thread every time. The diameter and the tension in the tread have been important parameters to test and see how it affected the output of the test.

The induced force depends on both the cutting length in the soil and the cutting surface on the tread. Therefore, the tread had to be thin and with a high strength, and stiff enough so the length of the thread was constant during the test.

Threads are used in other purposes such as fishing. any of these treads has high strength but one problem with using these treads is the tightening procedure where the roundness easily gets affected. This fact contact area on the wire and soil.

Metallic threads with different diameters have also been studied. The conclusion was that a diameter of 0,20-0,28 mm functioned well for most soil samples. To be able to tighten the tread to the same tension every time a special torque wrench was used.

### Sample Height

In an early period of testing a small sample was used, a height of 20 mm was a good height for many tests. The standard sample tube in Sweden is a 170 mm long tube. For every sample depth there is one upper, one middle and one lower tube.

The CC-Test is a very time efficient test compared to other methodologies, and it generates many measurements during the cutting procedure through the sample. A cutting rate of 2-5 mm/min and the fact that the thread only needs to cut 2-5 mm into the sample before reaching a consistent value, made it possible to do many tests in a short period of time. Different parameters could be tested to see if it affected the result of the evaluated shear strength.

The very first CC-Test that were calculated from the conversion factor from the cone, reminded of a simple direct shear test, see Figure 5. The value obtained also correlated with the result from the direct shear test.

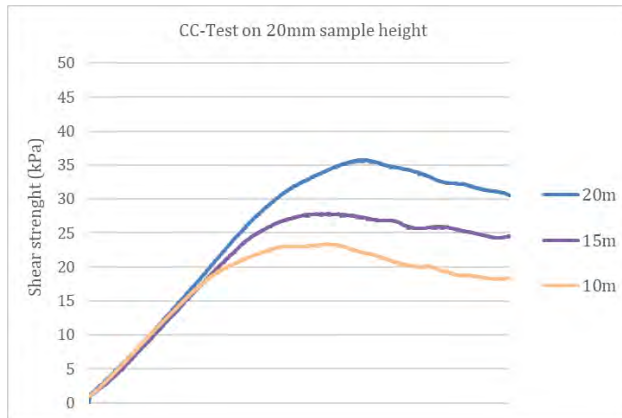


Figure 5 The first result with small sample heights (20mm).

Initially the mantle area of the wire was not included in the preliminary evaluation of the shear strength. It was only the load that was measured from the CC-Test divided with the result from the fall cone test. This factor was then used to the rest of the tests to see how the value compared with the other sample depths, see Figure 6.



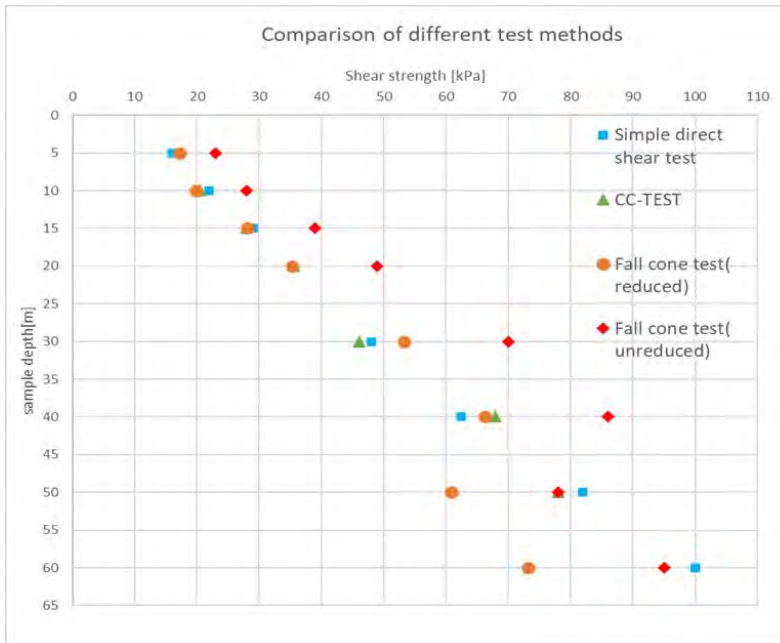


Figure 6 Comparison between different types of tests.

It is well known that the fall cone test is calibrated and representative to a depth of about 15 m in the western part of Sweden. The vane test often shows representative values down to a depth of 20 m. At greater depth, the direct shear test usually is the most reliable methodology. The CC-Test seems to correlate well with the fall cone, the vane, and the direct shear test to a limited depth. As seen in Figure 6, the CC-Test and the direct simple shear test also correlate with depth, and it seems like the unreduced fall cone test fits the trend with depth as well.

After the first test on small sample heights, many more tests were done on different soils. The question was what the thread could measure? Were there any limitations? By performing many comparative tests with both fall cone test, direct shear tests and triaxial tests more trust to this new way of testing the soil was gained. The aim was to adjust the cutting rate, the wire diameter, and the wire material to get closer to the direct shear test, to trim in the CC-Test.

At this stage larger samples were introduced in the CC-Test development. The purpose was to see how the methodology could manage variation in the samples.

When the fall cone is used an analysis is done for every 2 cm layer and the cone penetration length can vary more than one millimeter. That affects the calculation for the shear strength. To study such a small sample will give a

very specific value that in many cases does not represent the variation in the whole soil profile. With the CC-Test and more extensive sample height the variation could be measured in a laboratory.

### Verifying test

To verify the method, the CC-Test have been performed parallel and systematically with the fall cone test in more than 400 cases. By collecting three, 2 cm layers used from the fall cone procedure and run in the CC-Test equipment, data from the same sample can be compared with data from different methods. Shear strength from the CC-Test is illustrated with the reduced and un-reduced shear strength from the fall cone, see Figure 7. The comparison shows that the minimum and maximum shear strength from the CC-Test varies between reduced and unreduced shear strength from the fall cone test. This trend can be seen to a certain depth.

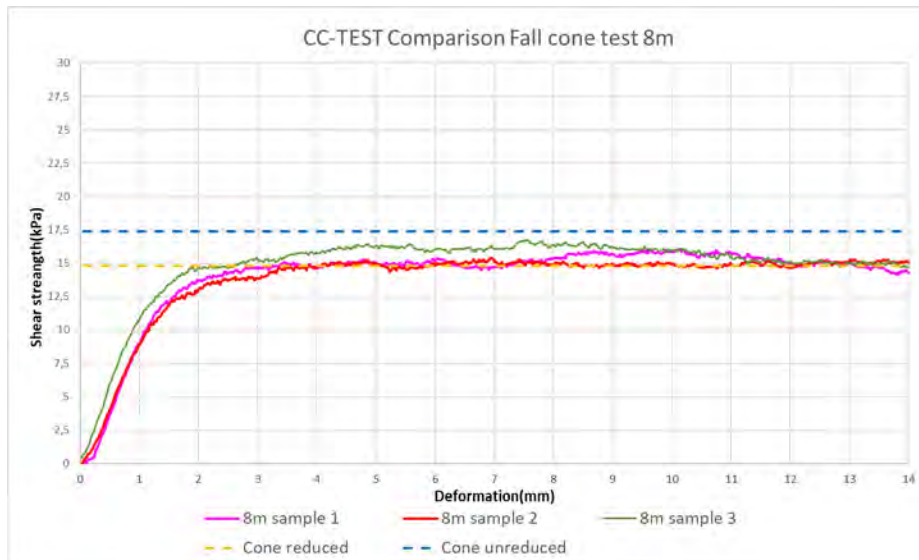


Figure 7 Comparison test with fall cone test.

## CC-TEST WITH DIFFERENT PURPOSES

### CC-Test to measure soil variation

A sample was taken out directly from the sample tube and the test length was chosen to 10 cm. The first step in this test procedure was to cut in the center of the sample through the hole sample length. After that, the sample was divided into pieces of 2 cm horizontal, and each sample was then tested again with a rotation of 90 degrees. The rotation was done to get an undisturbed part of the sample to test again, see Figure 8.

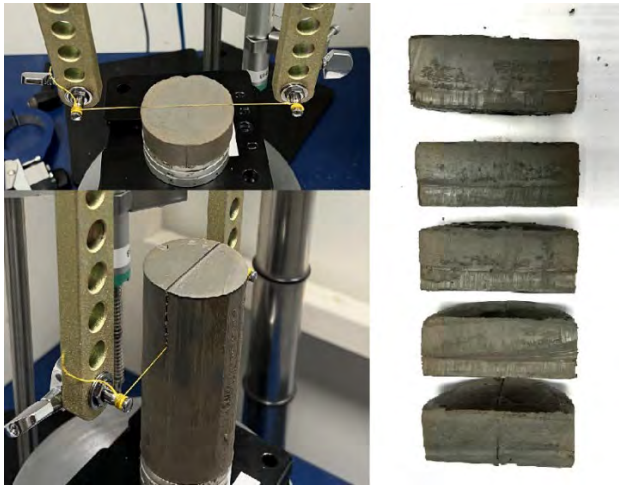


Figure 8 Test in different directions.

The result from the double test showed that the full height test did not affect the test from the five divided parts that was made on the same sample. All measurements from the test were plotted in the same graph, see Figure 9. and the cut in the full height test fitted perfectly with the small sample tests.

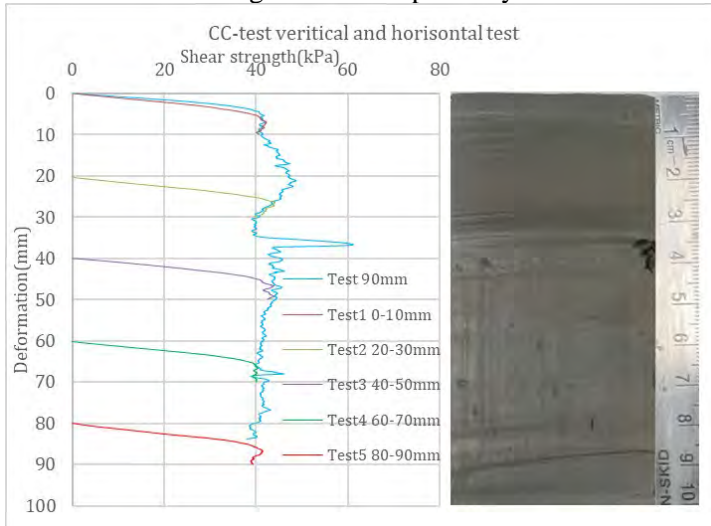


Figure 9 visual fit between a full height sample and five small samples performed with 90 degrees rotation.

### CC-Test to measure variation depending on direction in the soil

Tests has been done on the same sample, but in different directions, see Figure 10. to study the repeatability of the test and to see if there are any differences of the strength in different directions. The result showed that the test could be made in many directions of the sample and almost get the same result and without disturbing the sample.

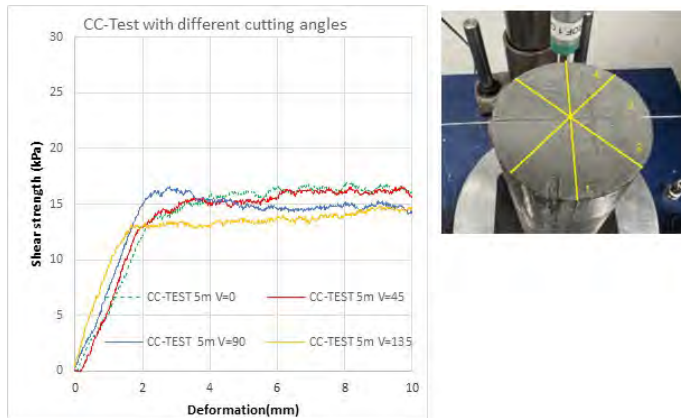


Figure 10 Validation of the results in different directions.

### CC-Test on a sulfide clay

To investigate the possibility to measure variations depending on the sulfide content CC-Tests were done on samples from the north of Sweden. In the soil a substantial variation could be seen and the shear strength from the fall cone test showed different values depending on which sample tube that was used on the same depth (upper, middle, or lower tub). To get a better trend towards the depth some simple direct shear tests were performed. When they were summarized in the graph together with the fall cone test it still showed an extensive variation and it was difficult to explain why there were such a spread between the different methods.

Therefore, some CC-Tests were done to analyze the soil and see if the variation could be measured. The results showed that it was a great variation through the hole section. The darker sulfide layers gave a higher shear strength, see Figure 11.

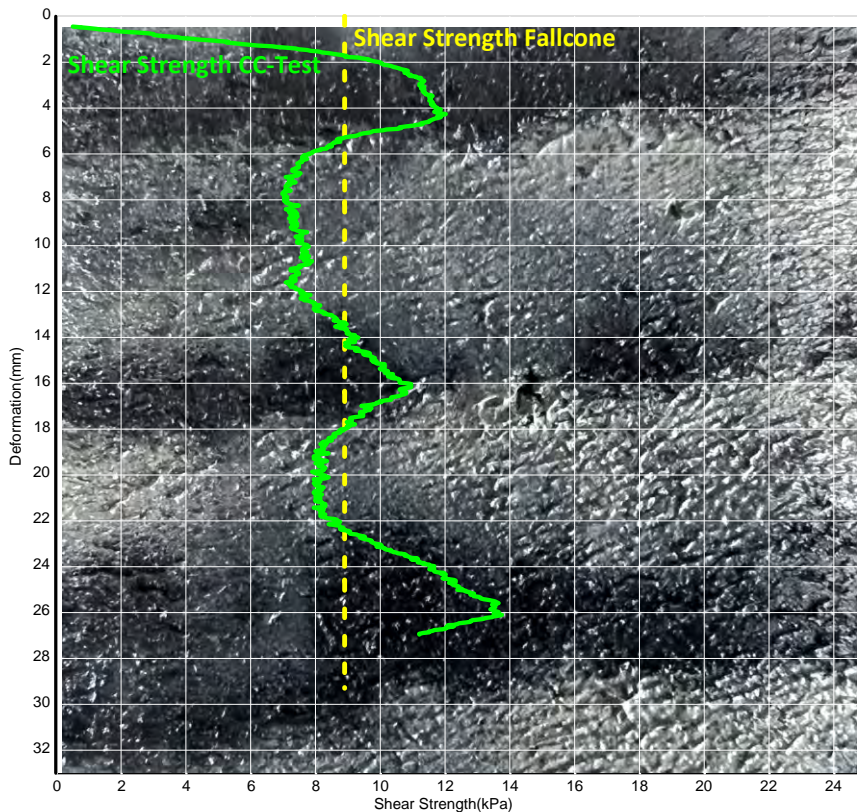


Figure 11 Soil profile with shear strength variation.

## CONCLUSIONS

The combination of measuring the shear strength in the soil and document the cutting surface with a photo gets a better understanding of the soil. Many different analyses have been performed in this study since the methodology is simple, not very time consuming. The fact that the CC-Test is a partly nondestructive test gives the possibility to get measurements in different directions. Hopefully, the CC-Test will be standardized in the future. What need to be done to validate the methodology is something that has to be further discussed.

## ACKNOWLEDGEMENT

I would like to express my sincere gratitude to all those who helped me complete this project successfully.

First and foremost, I would like to thank my Employer AFRY and my colleagues who have been positive and interested about the development of this

project. Especially to my close colleagues in the laboratory, Hanna Karlström and Fanny Molander. They have been very helpful in discussions and their curiosity has encouraged me in the development of the CC-Test.

I also want to thank my colleague Henrik Åslund for all the discussions regarding thread variants and his shown interest in the development.

I would also like to extend my thanks to my mentor Göran Sällfors. Especially with his feedback and expertise regarding the method.

Finally, I would like to thank my family who motivated me and boosted my morale when I was stressed. Without their unconditional love and support this project would not have been possibly.

[1] Shear strength - evaluation in cohesive soil. Information 3.  
SWEDISH GEOTECHNICAL INSTITUTE



# CEMENTSTABILIZATION OF PEATMATERIAL IN ROAD CONSTRUCTION

**Kristoffer Lauridsen<sup>1</sup>, Andreas Elkjær Riis<sup>1</sup>**

## KEYWORDS

Cementstabilization, infrastructure, preloading.

## ABSTRACT

Rv. 4 Roa – Gran grense is a 4.2-kilometer long motorway project that aims to replace the existing two-lane highway with a four-lane motorway between Roa and Gran grense in the southern part of Norway. The project includes the construction of six bridges, one culvert, extensive rock and soil cuts, and significant landfills. The ground conditions in the project area vary greatly, ranging from peat and till to areas with quick clay, moraine, and thin layers of gravel over bedrock.

Given the limited opportunities to adjust the road line, the complexity of the ground conditions and the focus on minimizing the impact on the surrounding area and climate, alternative solutions to conventional concrete bridges and extensive mass replacement have been explored. As a result, an innovative method has been developed to cross an area with peat over quick clay by stabilizing these materials with cement. Calculations conducted by the Norwegian Public Roads Administration have shown that this chosen solution leads to a 30% reduction in CO<sub>2</sub> emissions compared to a traditional low bridge for this specific case.

This method is considered an innovative approach to highway construction, as there were no previous references found for its use on such a scale in Norway.

## INTRODUCTION

As a part of the National transport plan 2014-2023 the road connection between Oslo and Trondheim was to be strengthened. As a part of the strengthening that Norwegian road directorate (Statens vegvesen) tendered the corridor on Rv. 4 between Roa and Gran grense, where the current 2-lane road was to be upgraded to a 2x2-lane highway system, thereby increasing road safety, and accessibility.

<sup>1</sup> COWI A/S



After tough competition, the construction companies Hæhre Entreprenør and Isachsen Anlegg, in a working community, together with the consulting company COWI, were chosen to perform a design and build contract for the road construction.

The alignment of the new road crosses an area with significant variations in the ground conditions, yield several challenges along the way.

One of the challenges was the crossing of an existing peat and soft soil area in the southern part of the project. In this area, the subsoil condition comprised an upper layer of peat with a thickness ranging from a few meters up to 10 m. Beneath the peat, a layer of clay and quick clay was encountered with a thickness of up to 17 m. Reference is given to Figure 1, which contains a longitudinal section of the road.

It was decided to use a combination of mass stabilization and geotextiles to ensure stability, settlement, and progress in the project.

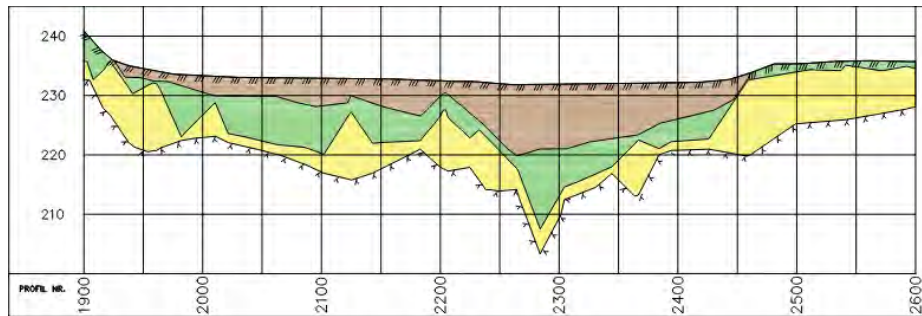


*Figure 1: Sektion view of the encountered soil conditions, peat = brown, clay/silty clay = green, sand/gravel/till = yellow.*

## PROJECT INFORMATION

The Rv. 4 Roa – Gran grense project is located outside the town of Roa in the southern part of Norway, see Figure 2.



*Figure 2: Location of Rv. 4 Roa-Gran grense.*

The soil conditions at the project site have been investigated on several occasions in connection with previous assessments of the feasibility and zoning plan for a new road alignment.

Geotechnical investigations indicate subsoil conditions consisting of an upper layer of organic peat and gyttja, with a depth of up to 10 m, underlain by a layer of clay. In some places, the clay layer is quick, with a thickness ranging from 0 to 10 m.

In addition to the previously performed soil investigations, additional total sounding, CPTu tests, and boreholes were conducted. An example of the encountered soil conditions is shown in Figure 3.

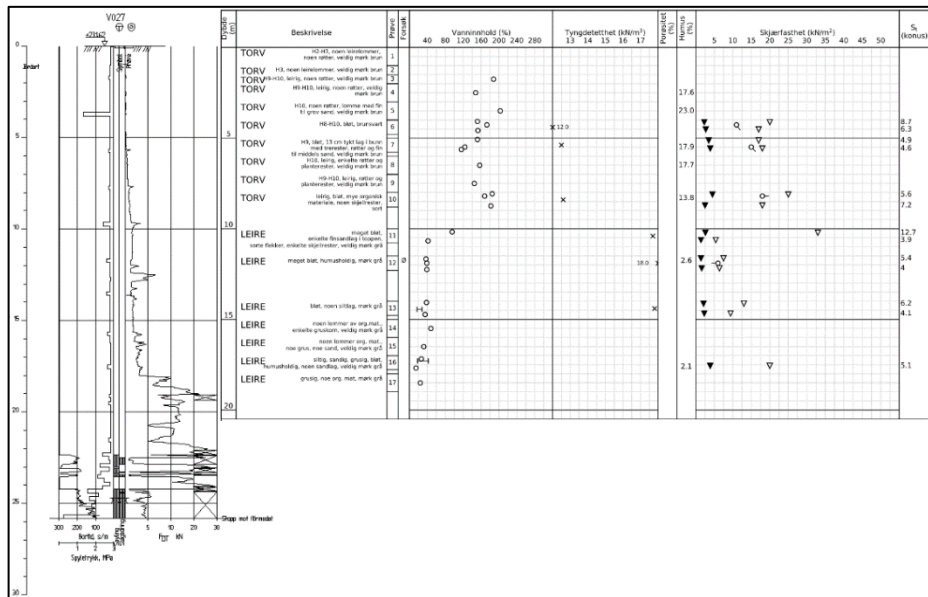


Figure 25 Totalsounding and adjacent borehole.

Considering the limited opportunities to adjust the road alignment due to the previously conducted zoning plan of the Statens vegvesen, the new road needed to cross the marshland. Initially, several methods for crossing the area were considered and discussed in the project team, including a low bridge, full excavation and replacement, and pre-loading. The solution had to take into account for the project's compressed time schedule, the need for the existing road to remain operational, and the requirement for a safe and cost-effective road. Furthermore, there was a general goal of reducing the project's carbon footprint.

It was decided to stabilize the soft soil through a combination of cement piles, pre-loading and a geotextile structure on top. This stabilization method was chosen because it satisfied the forementioned requirements. It enabled the necessary work to be carried out without affecting the existing road. The stabilization provided both settlement reduction (SLS) and stability for the future road (ULS). Moreover, it allowed the surrounding area to be used as a fill area for excess material from the project.

In Figure 4 the layout of the stabilize of the subsoil is presented. A cross section of the proposed stabilization is presented in Figure 5.

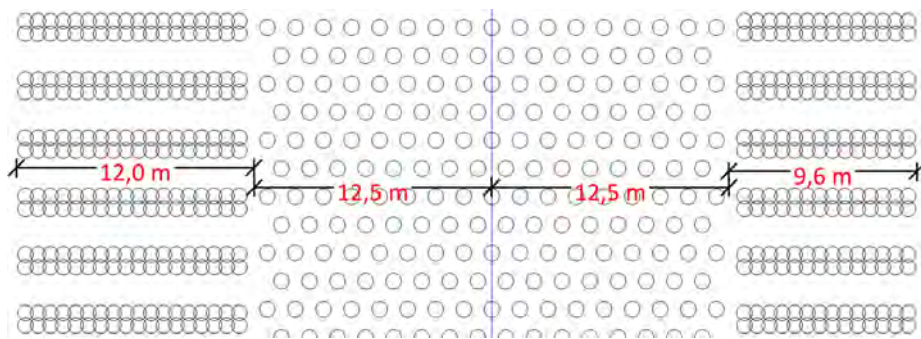


Figure 4 Layout of stabilization.

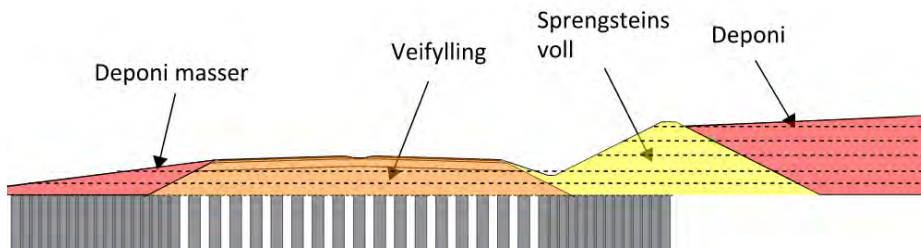


Figure 26 Cross section of the stabilization.

As shown in Figure 6, different stabilization patterns were chosen depending on the purpose of the areas. On the right side of the road, a pattern of interlocked rows of piles was selected to stabilize the noise barrier and land fill. Beneath the road, a pattern of stand-alone piles was chosen to reduce settlement. On the left side, a pattern of interlocked rows was placed to ensure stability. The size of the piles and the distance between rows and individual piles were initially determined using the guidelines provided in references [1] and [2].

Stabilization of clay and quick clay is well-documented in Norway, with established guidelines regarding the required amounts of stabilization material, achievable strength levels, and suitable methods. However, there is significantly less experience with the stabilization of highly organic material. To reduce uncertainty and assess the appropriate method, quantity, and expected strength levels, a test area on site was established before the production piles.

### The test field

The test field consisted of both single piles and interlocked pile rows, utilizing various pile diameters, amounts of material, and installation speeds. A sketch of the test area is presented in Figure 6. A total of 95 piles were installed. To evaluate the impact of the quantity of material used, pile diameter, installation method, and the time elapsed between installation and testing, a test schedule was established. Strength tests were proposed to be conducted using FKPS, and core drilling.

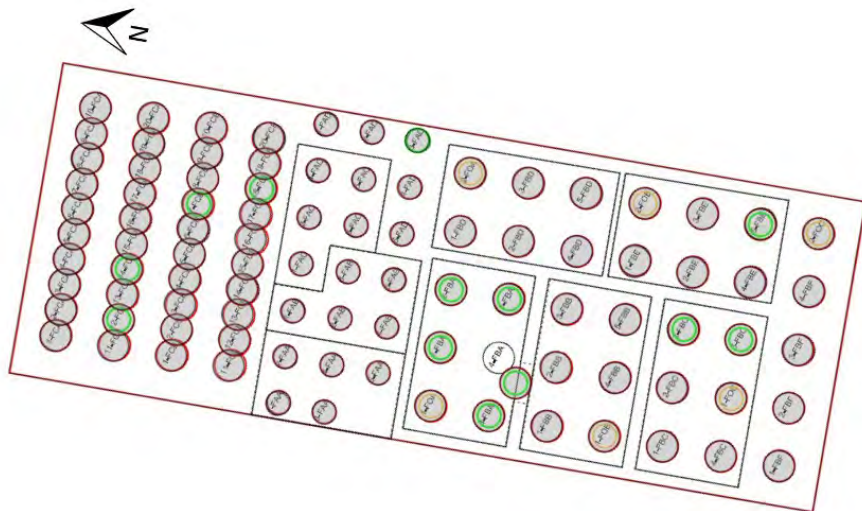


*Figure 6 Test area for stabilization.*

During the testing phase, it was observed that core drilling yielded poor results, and as a result, only FKPS tests were utilized in the final design. Based on the test area outcomes and considering the expected soil conditions, a material ratio was determined, with an allocation of 20-30% more material for organic soils compared to clay and quick clay at the site.

Furthermore, based on the results from the test piles regarding strength development over time, a testing scheme was established for the production piles. Approximately 1% of the installed production piles were tested to evaluate the achieved strength.

Additionally, a monitoring scheme was implemented to track the settlement of the newly stabilized areas.



### Installation and testing

The installations of the cement and the FKPS testing were performed by Soil Mixing Group AB (SMG), as can be seen in Figure 7.



*Figure 7 Soilmixing performed by SMG. Credit T. Bjørhusdal.*

Following the installation, a sandwich construction consisting of geotextiles and crushed rock was placed on top. This was then topped off with a final layer of preloading. The size of the preloading was determined based on the strength results obtained from the test area and calculations of the internal capacity of the piles. Settlement plates were also installed within the preloading area.

### Monitoring and mitigating actions

Results of the FKPS test in the southern part of the area showed consistent results as can be seen in Figure 9. The following monitoring also found that the settlement curves in the course of 3 months were starting to level out, as can be in Figure 8, with settlements ranging from 0 – 12 cm.

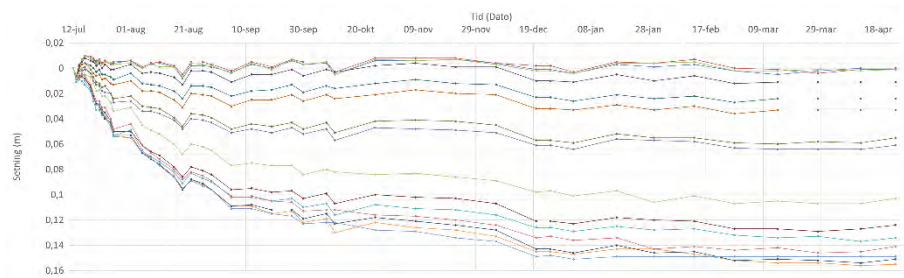


*Figure 8 Settlement of the southern part of the stabilized area.*

In the northern part of the stabilized area, a significantly larger scatter was observed in the achieved strength parameters, as depicted in Figure 9. Furthermore, it was noted that the attained strength parameters did not meet the expected values. To address the lack of strength in certain piles, additional piles were added, and an extended period of preloading was implemented. As shown in Figure 10, a wider range of measured settlement, ranging from 2 cm to 25 cm after 2 months, was observed.

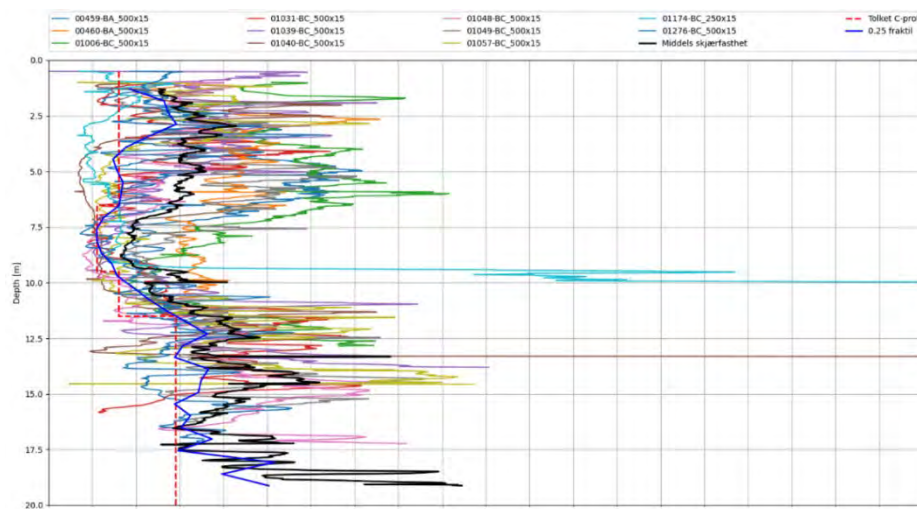


*Figure 9 Measured strength distribution with depth including assed design profile.*

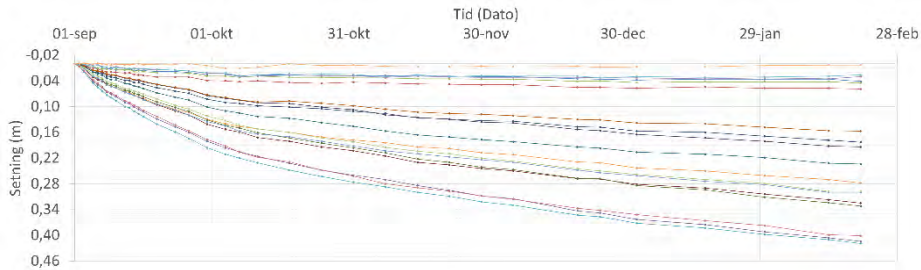


*Figure 10 Settlement curves of the northern part of the stabilized area.*

The settlement development was continuously monitored in the following months, and additional preloading was applied to expedite settlement, thus reducing the remaining settlement when the preloading would eventually be removed.

### **Findings and reflections**

During the monitoring of the stabilized areas, a majority of the area exhibited settlement within 2 to 4 months after the preloading was implemented. However, there was a shorter stretch of approximately 50 meters where the rate of settlement decreased over time but did not come to a complete standstill.

Further examination of this area suggests several possible reasons, with the most likely one being that this area had the thickest layer of organic material, as well as the thickest layer of underlying clay. The increased settlement levels observed in this area could be attributed to the shear thickness of the stabilized material.

To minimize the final settlement of the road after completion, additional measures were taken in the form of a LWA (Lightweight Aggregate) mass replacement in the area where the largest settlements were encountered.

### **EFFECT ON SURROUNDING AREA**

In addition to the geotechnical monitoring and mitigation measures, the local river Vigga is being closely monitored to assess the potential effects of the stabilization on the surrounding area, such as material washout or leaks. The surveillance conducted as of winter 2023 indicates positive results in terms of the impact on the river and local wetlands, according to Statens Vegvesen (the Norwegian Public Roads Administration). Furthermore, a continued test program will be implemented to evaluate the pH levels and presence of heavy metals in the area around the stabilization, in order to assess any long-term effects over time.



## CONCLUSIONS

In the Rv. 4 Roa – Gran grense project, it was concluded that stabilizing organic material with cement is a viable method for crossing areas with a significant amount of soft organic soil.

The method was found to be versatile, particularly when stabilizing larger areas, as it effectively increased stability and reduced settlement. The flexibility of this method allowed for adjustments in the amount of stabilization as needed in specific areas. Traditional monitoring techniques, such as settlement plates and pore pressure measurements, were employed to inform appropriate actions, fostering close collaboration between the contractor and client.

It is worth noting that this project has been carried out parallel to the innovation partnership KlimaGrunn, and the experience and methods gained from that collaboration have not been incorporated. However, the experience and methods from KlimaGrunn can be advantageously utilized in future projects.

## ACKNOWLEDGEMENT

Special thanks are given to Hæhre Entreprenør, Isachsen Anlegg, and Statens vegvesen.

## REFERENCES

- [1] A. B. Andersson: Preparing for the geotechnical challenges. PhD thesis, Chalmers University of Technology, 2020.

# CHALLENGES IN DETERMINING GROUND CONDITIONS FOR THE DESIGN OF WATER RESERVOIR DAMS IN THE AITIK MINE

**Thomas Larsson<sup>1</sup>**

## KEYWORDS

Geotechnical investigation, Hydrogeological investigations, Veiki Moraine, Geotechnical interpretation

## ABSTRACT

Boliden Mineral AB contracted Golder (now WSP) for the investigation for and the design of three new water reservoir dams near the tailings area in the Aitik mine. The dams have crest lengths of approximately 3,7 kilometers and a height ranging from 20 to 25 meters. One of these dams will reach approximately 50 meters in height following tailings deposition. To determine the ground conditions geotechnical investigations were conducted. The investigations included test pit excavations, sondes (Jb-Tot, Jb-2, HfA) including sampling in soil, core drilling in rock, as well as laboratory tests and hydrogeological tests. The investigations were carried out during the years 2017-2020, with a total of over 365 days at the field.

The challenges with this type of investigation are identifying moraine type, its characteristics and establishing a correlation between each investigation method primarily based on sounding. Other challenges included dealing with a type of moraine known as Veiki moraine, local variations in moraine type, layers/lenses of sand and gravel, boulders, and varying strength of the moraine. The works also posed significant challenges with marshy ground, hilly terrain, and harsh weather conditions such as sandstorms, extreme cold, and snow.

The investigations revealed a moraine, sandy-silty moraine to silty-sandy moraine, with a thickness of up to 40 meters. The presence of layers with sand and gravel in the dam's foundation poses a risk of unwanted water transport in the moraine, which could endanger the dams. A significant focus was placed on identifying the layers/lenses, which proved to be a real detective work. Identification of potentially water-bearing layers was mainly based on ram penetration soundings (HfA), supported by correlation analysis with other

<sup>1</sup> WSP

sondes and samplings. This process involved analogously evaluating and interpreting results using crayons on long paper rolls, to the great curiosity and delight of colleagues.

The project's success hinged on close collaboration between Bolidens project organization and contractors, field teams from Ramböll, Sweco, Afry, Drill-con and Golder/WSP, allowing year-round investigations. This synergy, coupled with the experience gained, led to ongoing refinement of the investigation methods and procedures.

## INTRODUCTION

Boliden, in accordance with the current permit [1], has committed to the construction of a new reservoir, the HS reservoir, for the deposition of high-sulfur enrichment sand, a purification plant, and a new Water Reservoir, see Figure 1. The purpose of the reservoir is to manage the water flow from the HS reservoir, increase the water storage capacity in the system, to reduce the amount of water discharged to the recipient, and to better control when water is to be discharged.



Figure 1. Orientation figure with approximate length measurement for dam V1, V2, and VR [11].

carry out the detailed design of the Water Reservoir. The task also involved investigating the appropriate location for the moraine quarries for sourcing material for the construction of the dams.

## OVERALL GEOTECHNICAL CONDITIONS

The terrain is hilly, with low parts in the middle of the investigation area with marshland and lakes/ponds. In the northwestern and southeastern parts of the area, there are higher lying areas. Northeast of the area is the sand magazine and southwest is a transport road. The ground generally slopes from the transportation route down to the sand magazine [4].

Prior to the construction of the Water Reservoir, a feasibility study [2] was carried out and a permit application [3] was prepared. Golder (now WSP) was commissioned by Boliden Mineral AB in 2017 to



Figure 2. Drone photo over the dam area, to the right of the road you can see the construction of the dam V2 [12].

Most of the investigation area has been covered with fir and pine forest, which is now felled, but also marsh areas and smaller ponds exist, see Figure 2. The vegetation and soil layer varies between about 0,6-1,0 m.

The geology in the area according to the Geological Survey of Sweden's (SGU) soil map [5] is Veikimorän, a special type of moraine back landscape (hilly moraine). Veikimorän is characterized by plateaus with ridge edges and intervening depressions that are often filled with water and/or peat. The shapes of the depressions are often round [6]. Veikimorän was formed [7] as dead ice moraines during the melting of the first ice age phase during the Weichselian deglaciation. The material composition for Veikimorän is characterized by varying proportions of sorted sediment and moraine, which is also typical for dead ice moraines.

The investigations showed that the bedrock is overlaid by moraine of varying thickness. The moraine, sandy silty moraine to silty sandy moraine, is mainly quite homogeneous but the investigations show the occurrence of sandy/gravelly layers and vertical lenses and parts with more sandy moraine. Depth to bedrock and rock quality varies along the planned dam lines. The bedrock consists mainly of granitic rocks and gneiss with elements of pegmatitic and mafic rocks. Strongly weathered rock has been observed in some boreholes, mainly near the rock surface.

## CHALLENGES WITH THE INVESTIGATIONS

Generally, the time spent performing the geotechnical investigations has been longer than planned due to boulders, difficulties in sampling loose soil layers at greater depths, and machine breakdowns due to harsh weather.

For the hydrogeological investigations, the irregular soil layer sequence and the proximity to the 450 m deep open pit have created challenging and special hydrogeological conditions. This has meant that conductive soil layers or rock at depth can have unsaturated conditions while water is present in superficial soil layers.

External factors such as peatland, hilly terrain, and harsh weather with sandstorms, severe cold, and snow have also affected where, how, and when certain areas can be investigated.

## INTERPRETATION OF THE INVESTIGATIONS

### Approach, interpretation of the moraine

Direct shear tests have shown that the existing naturally deposited moraine has a friction angle of at least 35 degrees. In the interpretation and evaluation of the moraine, 35 degrees has been used as a reference value for the required strength [4]. When evaluating the friction angle of the moraine, the following equation from the Plattgrundläggningshandboken [8] has been used.

$$\phi' = 29 + 2,3 * HfA_{(netto)}^{0,46}$$

To achieve a friction angle of 35 degrees, at least 12 hammer blows/20 cm subsidence are required after deducting 3 degrees for silt and adding 2 degrees for gravel. The equivalent to achieve a friction angle of 35 degrees for Jb soundings has been correlation-calculated to a sink rate of  $\geq 3$  sec/0,2 m when the hammer is on and the feed force is  $\geq 4$  kN.

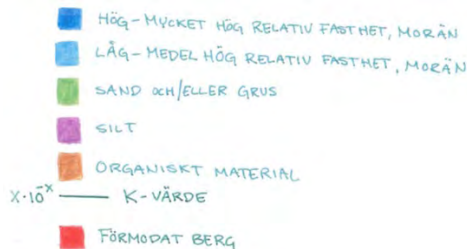


Figure 27. Classification of soil types during interpretation [4].

The interpretation was carried out on printed drawings along each dam with sections every 50 meters and a profile drawing along the centerline of the dams. The soil was classified according to Figure 3. Light blue represents a moraine with a friction angle  $< 35$  degrees and dark blue represents a moraine with a friction angle  $\geq 35$  degrees.

In Figure 4 below, an example of how the interpretation has been reported is shown. The interpretation of these three soundings differs. For the left sounding, there is screw sampling, HfA, and Jb sounding. In the left sounding, mainly screw sampling and HfA results are used and the interpretation is more simple. In the other two soundings, there is only screw sampling and Jb sounding, but the interpretation is more difficult in the right one because the feed force, sinking rate, and hammer drilling vary.

In the left sounding, there are also hydrogeological falling-head tests performed and in the associated groundwater pipes slug tests are also performed. Hydrogeological tests have mainly been performed where screw sampling has shown a high proportion of sand and/or gravel and that low relative strength has been measured in soundings.

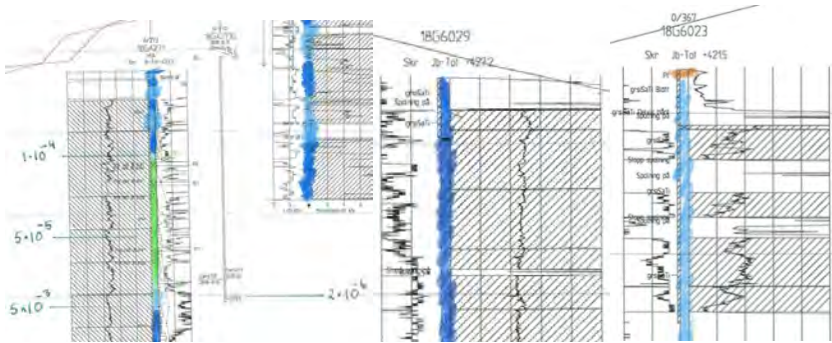


Figure 4. Examples of interpretation of soundings. To the left, interpretation of sounding with sampling, HfA and Jb sounding incl. K-value; middle, interpretation of sampling and Jb sounding; to the right, interpretation of sampling and Jb sounding

### The hunt for water-permeable layers

In the interpretation of the soil's permeability, it is based on the above correlation between HfA/Jb but also with a weighting of results from hydro investigations. Our assessment was that if the hammer sounding shows more than 25 blows/20 cm, hydro investigations often show that the soil is low permeable i.e.,  $k < \text{ca } 10^{-6} \text{ m/s}$ . At fewer than 25 blows/20 cm, the soil can be either high or low permeable. As a complement to the correlation between soundings and permeability, results and ocular assessments from sampling and site visits, field notes on e.g., water losses, and geohydrological assessments have also been weighed in [9].

For dam V2, discontinuous layers and layers of sand and gravel were identified in the beginning of dam V2, called chainage 0, approximately between km 0/200 – 0/550. Hydrogeological investigations in these layers showed a hydraulic conductivity of about  $10^{-5} \text{ m/s}$  [9]. In Figure 5, all investigation points where layers/layers of sand/gravel have been identified are shown.

Generally, the planned chainage 0 is located on top of a ridge and starts at a natural slope in section about 0/150. Along the ridge, high-permeable moraine is found, both on top and along the respective slope. The high-permeable moraine is underlain by moraine with low permeability. The high-permeable moraine decreases in thickness along the chainage and the natural end of the ridge (about section 0/550) [9].

Three different types of sections for the soil profile have been identified, type section A (0/225 – 0/325), B (0/325 – 0/425), and C (0/425 – 0/550), see section marking in Figure 63. Type sections were then used in leakage calculations of the dam's subsoil. In this paper, only type section A (0/225 – 0/325) is described.



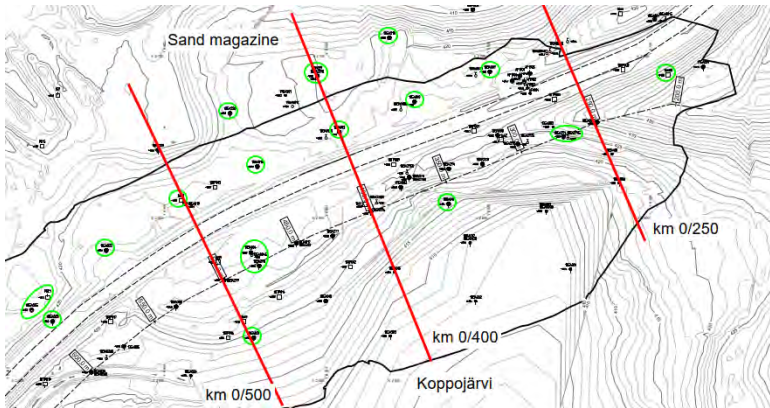


Figure 28. Plan with investigation points over chainage 0, dam V2, and section marks. Green circles around investigation points show where layers of gravel/sand have been identified.

#### 0/225 – 0/325

The soil consists of sandy silty moraine to silty sandy moraine with medium-high relative strength. In places, in two points, inclusions of gravel have been encountered. Towards the depth (>16 m), the investigations show that there are layers in the moraine of coarse sand and gravel. However, the sampling method means that sampling below the groundwater surface at these depths can miss fine material due to washing out. Towards the depth, the relative strength of the moraine increases from medium-high to high to very high.

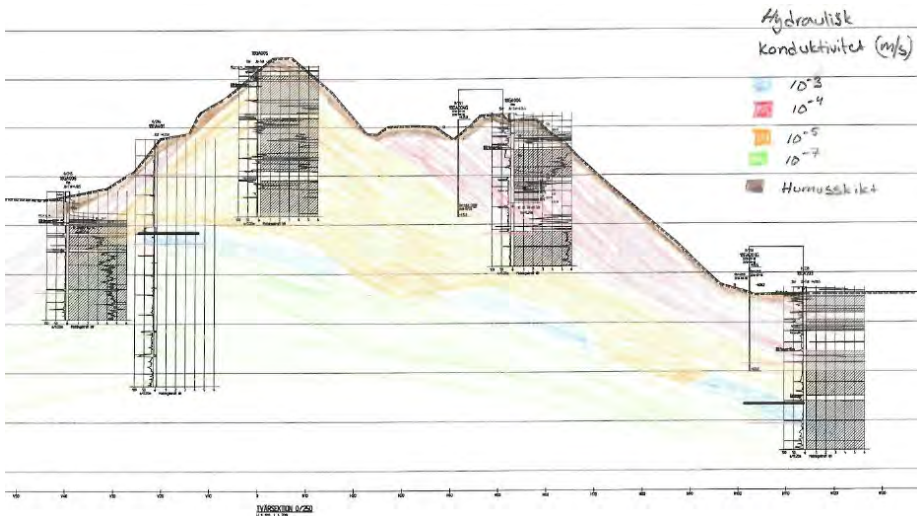


Figure 29. Interpreted soil profile for sections 0/225 – 0/325 (section taken in 0/250).

High-permeable layers occur down to about 10 m depth in the section. In the transition from the high-permeable to the low-permeable materials, there is an approximately 1 m thick non-continuous layer with very high permeability

and with a slope towards the Sand magazine. The non-continuous layer goes from level about +414 at Koppojärvi to about +400 on the Sand magazine side, see Figure 6. The extent of the layer decreases with the length measurement. At section about 0/300, the layer is only found on the side towards Koppojärvi pond.

## INTERPRETATION IN THE CONSTRUCTION PHASE

The results of the investigations and the interpretation, along with other technical results, culminated in, among other things, foundation conditions for the dams. Request documents and work documents were prepared and the contractor began excavation. Dam V2, which was the first of the three dams, served as a pioneer and based on the experiences from investigations and execution, the investigations on the next dam could be optimized.

The dams were to be founded on "dense" moraine, which meant that sand and gravel could not occur in the excavation bottom. During the foundation of the chainage 0 and on other parts of dam V2, the sand and gravel layers identified in the investigation points were encountered. New layers and lenses were also encountered which had not been discovered in the investigations. These layers and lenses could be very local while others were more elongated in both longitudinal and depth directions.

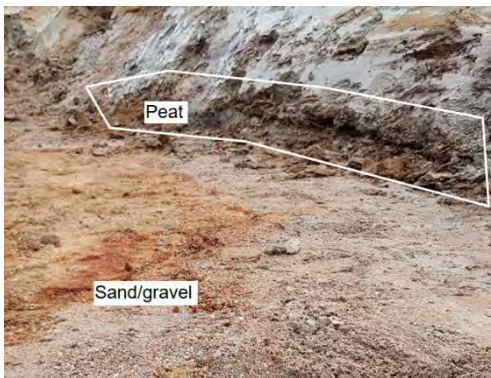


Figure 30. Photo of the occurrence of sand, gravel, and peat in beginning 0 dam V2 [13].

Something that was also encountered in connection with the foundation of dam V2 and in a couple of test pits along the other dams, was 0,1-0,3 m thick peat layers under naturally deposited moraine. The random encounter of sand, gravel, and peat is characteristic of dead ice moraine and Veiki moraine [7].

In connection with the excavation work for the foundation of dam V2, a measure matrix was set up to handle these occurrences more efficiently. The measures depended on the size of the area (larger or smaller diameter than 5 m) and whether it was a single occurrence or not. By single occurrence is meant 1 times/75 m in length and 1 times/20 in width [10]. In Figure 7, the occurrence of sand, gravel, and peat in the dam's subsoil is visible. The different soil materials differ markedly in color, which simplifies the identification of these layers, lenses, and layers during the excavation work for the foundation of the dams.



## ACKNOWLEDGEMENT

I would like to thank everyone who has been involved and contributed to this project. Thank you to all who have stood out and fought with investigations when the weather has been tough. Special thanks to Jonas Nygren, Freja Hoflund, Jakob Eng, Romain Girard, Jörgen Oscarsson and Johanna Lundin.

## REFERENCES

- [1] Umeå Tingsrätt, "Mark- och miljödomstol - Deldom 2014-10-03, Mål nr M 3039-12," Umeå Tingsrätt, Umeå, 2014.
- [2] TCS, "Förstudie, Dammar nytt vattenmagasin och K-L, koncept, daterad 2016-01-22," 2016.
- [3] MalKon konsult, "Bilaga A - Teknisk beskrivning av en utökad verksamhet i Aitik med en årlig produktion av upp till 45 MTon malm, daterad 2012-12-18," 2012.
- [4] Golder Associates, "Vattenmagasin Detaljprojektering - Fältundersökning Tolkningsrapport, daterad 2019-07-05 rev. 2020-10-06," 2020.
- [5] Sveriges geologiska undersökning (SGU), "SGUs kartvisare," 24 1 2024. [Online]. Available: <http://www.sgu.se/sgu/sv/produkter-tjanster/kartvisare/index.html>.
- [6] H. Dittrich, "Jordartskartan 28K Gällivare, skala 1:100 000," Sveriges geologiska undersökning Ak 50, 2005.
- [7] R. Lagerbäck, "The Veiki moraines in northern Sweden - widespread evidence of an Early Weichselian deglaciation," *Boreas* 17, pp. 467-485, 1988.
- [8] U. Bergdahl, E. Ottosson och B. Stigson Malmberg, Plattgrundläggning, Statens geotekniska institut., Solna: AB Svensk Byggtjänst., 1993.
- [9] Golder Associates, Damm v2 – Utredning läckage genom undergrund i anfang 0 sektion 225 – 550, daterad 2018-12-22 rev 2019-07-05, 2019.
- [10] Golder Associates, "11 Teknisk beskrivning, Aitik, Dammexpansion Syd, Vattenmagasin - Dammbyggnation, daterad 2019-04-01 rev 2019-05-10," 2019.
- [11] Lantmäteriet, "Ortofoto," 24 1 2024. [Online]. Available: <https://minkarta.lantmateriet.se/>.
- [12] J. Oscarsson, "Foto id: DJI\_0278," 2018.
- [13] YIT, "Foto id: 20190926\_175707," 2019.

# COEFFICIENT OF VARIATION FOR STRENGTH AND DEFORMATION PROPERTIES OF CLAY

**Göran Sällfors<sup>1</sup>, Per-Evert Bengtsson<sup>2</sup>**

## KEYWORDS

Coefficient of variation, clay, strength and deformation parameters

## SUMMARY

Eurocode opens up for a probabilistic based design in geotechnical engineering. This means that there is a strong need for knowledge about the scatter of geotechnical parameters, such as strength and deformation parameters. In the paper the empirical correlation between the undrained shear strength and the preconsolidation pressure is illustrated through a number of cases from a comprehensive data base.

The coefficient of variation is then calculated for active, direct shear and passive undrained shear strength as well as for the preconsolidation pressure by using a Bayesian statistical method.

The coefficient of variation for these parameters is found to be substantially smaller than usually assumed. This is very important knowledge when the probability of failure shall be estimated for a slope or a foundation.

## BACKGROUND

In the early days of Eurocode the ambition was a design philosophy based on a probabilistic approach. The probability of failure should be less than a given number or the probability that a settlement became larger than a reasonable value should be given.

However, as the knowledge of the scatter of the crucial geotechnical parameters was scarce and also the simulation capabilities were rather limited, the method of partial factors of safety was introduced as a proxy method.

During the last few decades, important progress has been made in the area of simulation, including stochastic parameters. Also, the use of advanced laboratory testing methods, such as triaxial testing and direct shear tests, has increased tremendously in Sweden.

<sup>1</sup> Geo Chalmers University of Technology, Gothenburg Sweden & GeoForce AB

<sup>2</sup> PEB Geoteknik AB

In a separate research project, data were collected from over thirty test sites where high-quality triaxial tests, direct simple shear tests, and CRS (Constant Rate of Strain) oedometer tests were performed on clay samples. These tests constitute the database for the research presented in this paper.

The empirical relation for the ratio of the undrained shear strength and the preconsolidation pressure, as determined by the Swedish standard procedure for CRS tests, is presented in Fig. 1.

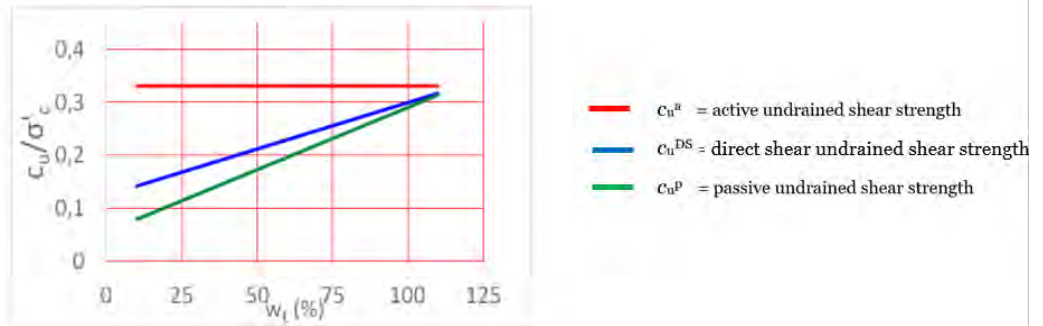


Figure 1. Empirical correlation between the ratio of the undrained shear strength and the preconsolidation pressure as a function of the liquid limit  $w_L$ . [4]

These relations refer to the shear strength for lightly overconsolidated clays. If the OCR is larger than 1.3, the strength should be adjusted for OCR according to eq. 1, to account for the overconsolidation of the sample before  $c_u/\sigma'_c$  is calculated and plotted in Fig.1.

$$\left(\frac{c_u}{\sigma'_c}\right)_{OC} \approx \left(\frac{c_u}{\sigma'_c}\right)_{NC} * OCR^{-0.25} \quad \text{eq 1.}$$

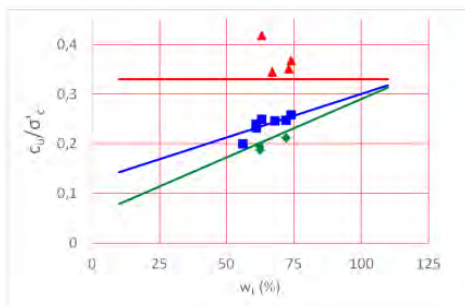
here  $c_u$  = undrained shear strength  
 $\sigma'_c$  = vertical preconsolidation pressure  
 $OCR$  = overconsolidation ratio

A database was established and consists of some thirty different cases, including the four different test methods mentioned above. This is discussed in the next section.

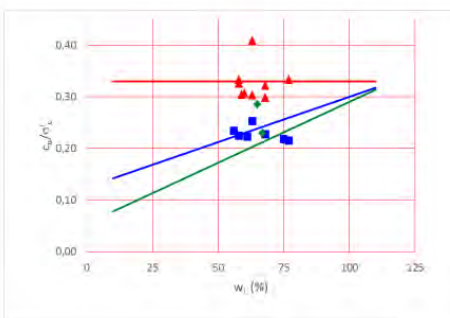
## RESEARCHED MATERIAL

It is well known that there is a close correlation between the undrained shear strength and the preconsolidation pressure. This ratio  $c_u/\sigma'_c$  is usually presented as a function of the liquid limit,  $w_L$ . However, it is evident that the  $w_L$  should be replaced by  $K_o^{nc}$ , where  $K_o^{nc} = \sigma'_{ch}/\sigma'_{cv}$ . It appears logical as  $K_o$  decreases with decreasing  $w_L$ . Also, it is worth noting that the anisotropy,  $c_u^a/c_u^p$  increases with decreasing  $w_L$  and decreasing  $K_o$ . The lines in Fig. 1 clearly illustrate this.

In a rather comprehensive research project, [1], dealing with geotechnical properties of Swedish clays, about 30 test sites were investigated where numerous CRS tests, direct simple shear tests and triaxial tests had been performed, the empirical relation between the undrained shear strength and the preconsolidation pressure was investigated. Here the results from CRS, direct shear tests and triaxial tests were available and the results were plotted together with the empirical correlation. A few examples are given in Fig.2 a – d.



a. Karlatornet



b. Riksvägv45

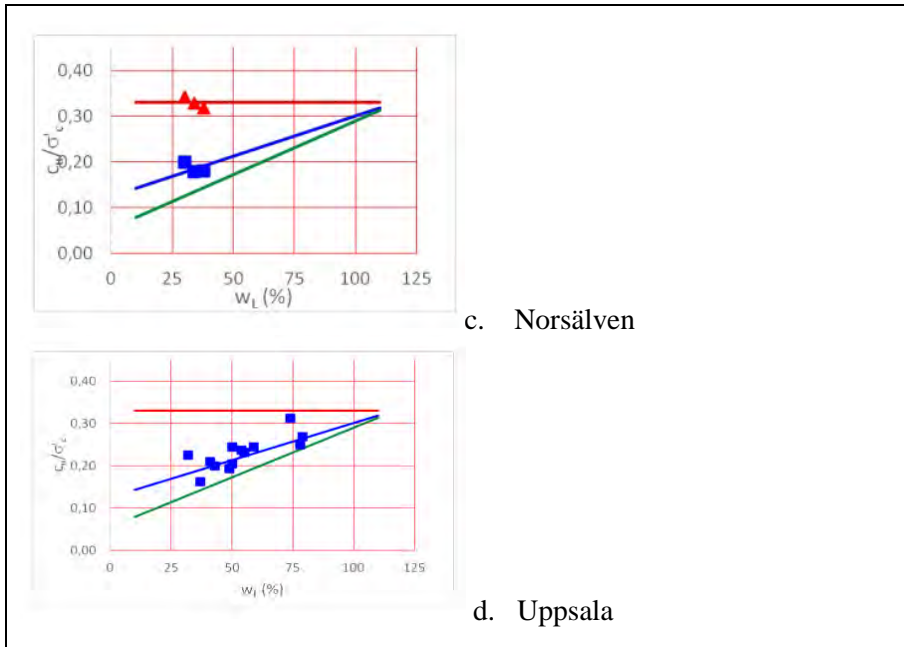
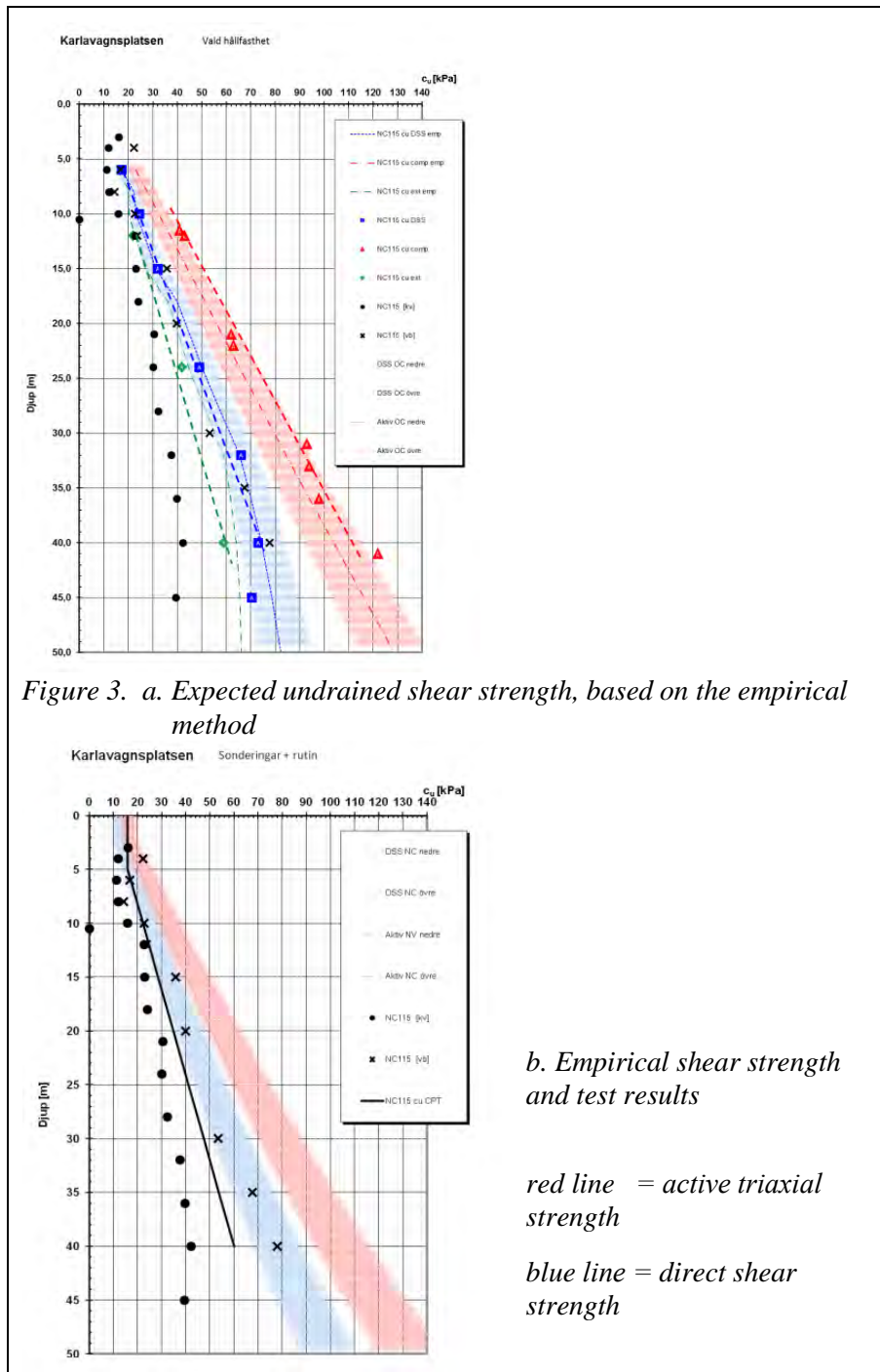


Figure 2. Results from a. Karlatornet, Hisingen, Göteborg. b. Riksväg 45  
 c. Norsälven, Värmland d. Uppsala  
 red line = active triaxial strength  
 blue line = direct shear strength  
 red line = passive triaxial strength

### PROCEDURE FOR ESTIMATING THE UNDRAINED SHEAR STRENGTH, $c_u$ , BASED ON THE VERTICAL RECONSOLIDATION PRESSURE, $\sigma'_c$

In a geotechnical task where the undrained shear strength is of great importance, the recommended procedure includes plotting the preconsolidation pressure determined from CRS tests as a function of depth. A best fit line is chosen for the variation of the preconsolidation pressure with depth and, using the empirical graph described above, then results in an expected variation of  $c_u^a$  and  $c_u^{DS}$ , with depth, see Fig. 3.a. The blue and red areas in the figure indicate a  $\pm 10\%$  range for the estimated shear strengths.



In Fig.3.b the actual results from triaxial tests and direct shear tests are also plotted. Finally the most probable trendlines for the different shear strengths are chosen, indicated by the dashed lines in Fig. 3.b.

It is important to bear in mind that empirical correlations are valid for an aged clay with horizontal ground, and which has not been exposed to leaching or external loading on the surface during the last couple of hundred years.

## THE USE OF BAYESIAN STATISTICAL METHOD

When doing probability-based design, it is imperative to have not only a good knowledge of the trend with depth for the parameters, but also quantitative information about the scatter of the parameters.

The only systematic method for getting a reasonable estimate of the scatter of geotechnical parameters, as the number of test results is limited is through the use of Bayesian statistics.

In Bayesian statistics, prior knowledge of the parameter is used together with the new test data to derive a posterior distribution for the parameter. This type of simulation uses MonteCarlo simulation, combined with Markow Chains (MCMC).

In this case, where the undrained shear strength is of interest, the vertical preconsolidation pressure variation with depth is first estimated based on stratigraphy and results from CRS tests. In this program the preconsolidation pressure is assumed to be constant down to a given depth  $k$ . From then on, the preconsolidation pressure is assumed to increase linearly with depth. By use of the empirical diagram, see Fig. 1, an estimate of the variation of  $c_u$  with depth is obtained. This variation of the undrained shear strength is taken as the prior distribution for the shear strength. Together with the shear strength values evaluated from the laboratory tests, the MCMC simulation is performed. This simulation then results in a posterior distribution of the shear strength variation with depth. The so-called posterior distribution of the undrained shear strength is also constant down to the depth  $k$ , and from then on increases linearly with depth. The coefficient of variation is then assumed to be constant with depth.

A computer program was developed using MCMC simulation and giving the best estimate of the trend line with depth for the undrained shear strength and the coefficient of variation for the shear strength.

The results from such a simulation are given in Fig. 4.

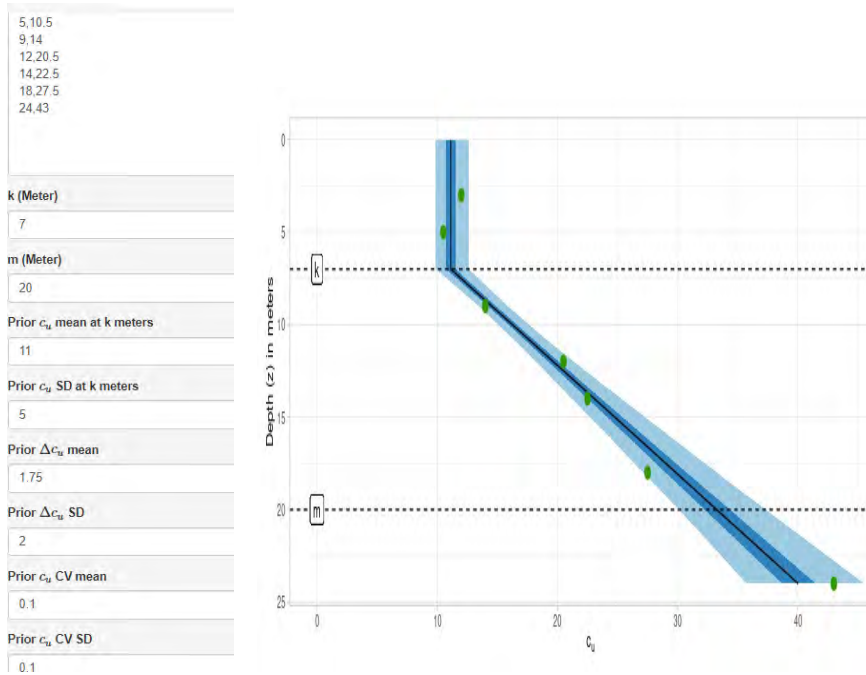


Figure 4. Results from an MCMC simulation of the undrained shear strength variation with depth.

The column to the left indicates the input for the simulation and the graph to the right shows the variation of the shear strength with depth.

dark blue field indicates a 50 % confidence limit and the light blue field indicates a 95 % confidence limit

As can be seen in the figure, the shear strength was assumed to be bi-linear with depth, and the variation of the preconsolidation pressure resulted in a prior distribution of the shear strength being 11 kPa down to 7 m and then increasing with 1,75 kPa/m.

The simulation resulted in a trendline being equal to 11,3 kPa down to 7 m and then increasing with 1,7 kPa/m. The coefficient of variation for the posterior function of the shear strength was estimated to be 6 %.

## APPLICATION OF THE METHODOLOGY TO THE DATABASE OF UNDRAINED SHEAR STRENGTH TESTS

The procedure with the MCMC simulations was applied to the results from all the test sites mentioned above and was presented in [1]. This is a very



comprehensive database and the simulations resulted in rather consistent results.

Apart from the trendlines, which showed some notable consistency, the coefficient of variation for each site and test type was also obtained from the simulation program.

The results were very consistent, and the coefficient of variation was in the order of 5 to 7% for the undrained shear strength and slightly higher for the preconsolidation pressure.

The authors are convinced, that if the geological sorting is made with care, the coefficient of variation for most clays in Sweden is around 6 % for  $c_u^a$  and  $c_u^{DS}$  as well as  $c_u^p$  and 7 % for the  $\sigma'_c$ , probably less.

In order to obtain such low values for the coefficient of variation for these parameters, it is very important that sampling is carefully performed, lab testing made with great care and the results are scrutinized and faulty values, or non representative values are omitted, just in line with what the Eurocode requires. It is especially important to consider whether the samples are undisturbed or not.

## CONCLUSION AND POSSIBLE FUTURE DEVELOPMENT

The empirical correlation between the preconsolidation pressure and the undrained shear strength of clays, active, direct shear as well as passive, is illustrated and found to be very strong. Evaluation of the coefficient of variation is done utilizing Bayesian statistical methods and was found to be around 6 % for a large number of different sites.

## ACKNOWLEDGEMENT

The financial support of The Swedish Road Administration is greatly appreciated.

## REFERENCES

- [1] Sällfors, G., Bengtsson, P-E and Ländström, G.. Val av variationskoefficient för en leras odränerad skjuvhållfasthet och förkonsolideringstryck. In press.
- [2] Richard McElreath. Statistical Rethinking – A Bayesian Course with Examples in R and Stan. CRC Press, Florida, USA 2020.

- [3] Sällfors, G. and Larsson, R. Bestämning av odränerad skjuvhållfasthet med specialiserade metoder i praktiska tillämpningar. Delrapport 3. Sammanställning av "Case Records". Trafikverket, Göteborg 2016.  
[http://fudinfo.trafikverket.se/fudinfoexternwebb/Publikationer/Publikationer\\_003101\\_003200/Publikation\\_003127/2017\\_037\\_%20Best%20av%20odran%20skjuvh-Case%20records.pdf](http://fudinfo.trafikverket.se/fudinfoexternwebb/Publikationer/Publikationer_003101_003200/Publikation_003127/2017_037_%20Best%20av%20odran%20skjuvh-Case%20records.pdf)
- [4] SGI, Information 3. Utvärdering av skjuvhållfasthet i kohesionsjord.



# **COMPLEXITY OF LARGE INFRASTRUCTURE PROJECTS -DISCUSSION OF GEOTECHNICAL CHALLENGES AND RISK TRAJECTORY TO EXTREM COST OVERRUNS**

**P. Kylmänen<sup>1</sup>, K. Viking<sup>1</sup>, S. Hintze<sup>1</sup>**

## **KEYWORDS**

large infrastructure projects, project complexity, geotechnical challenges, cost overruns

## **ABSTRACT**

When considering large infrastructure projects, the phrase "it's a very complex project" is often heard. But what exactly contributes to the complexity of these projects? This paper outlines a conceptualization of complexity and examines the relationship between large Swedish transportation infrastructure projects and cost overruns, focusing on variables such as project type, scale, and geotechnical challenges through the lens of a geotechnical narrative.

## **INTRODUCTION**

Mega-infrastructure projects are characterized as complex, politically-sensitive and often involving a large number of partners [1.]. They are carried out under conditions of high uncertainty, ambiguity and with extremely tight deadlines and budgets and managed in the context of very complex operations, paradoxes, uncertainties, influences and ambiguities which surround these projects [2.].

Comprehending the intricacies of the project holds significance in project management as it correlates with challenges in decision-making and achieving goals [3]. However, extensive infrastructure projects are rarely comprehensively evaluated for the influence of different factors on their results [4].

Frequently, the incapacity of clients - encompassing project managers, team members, and sponsors - to precisely gauge the extent of complexity they confront is recognized as a fundamental underlying problem.

<sup>1</sup> Swedish Transport Administration, Solna Sweden

In most, if not all, one could find as a root cause the inability of the clients [5.]. They often recognize the complexity far too late to effectively address it in order to gain control.

Unanticipated geological conditions and the associated geotechnical problems are known to be a major contributing factor to cost and time overruns in large infrastructure projects [6.] and [7.]. While it is recognized that it is more economically efficient to define geological conditions as early and accurately as possible to reduce surprises during the planning phase rather than during construction [8.]. Despite numerous efforts to address these realities by including various clauses in contract documents, the problem persists.

Therefore, client project managers and planners need to be aware of project complexity from the beginning in order to develop appropriate strategies and assign competent team members.

### **Purpose**

The purpose of this paper is to shed light on the problem of cost overrun within a geotechnical context since there are few theories on how and why it arises. Although there might be several other factors than the variables mentioned in this paper, but another purpose is to hopefully increase the awareness of the problem in order to contribute to launching future studies on geotechnical causes to the problem with extreme cost overruns.

### **Limitation**

The availability of public data is the main limitation of this paper. The data and fact presented in this paper is openly available by sources such as; Swedish National Audit Office (Riksrevisionen), publications found in DIVA (Digitala Vetenskapliga Arkivet), journal articles and news reporting. It should also be mentioned that due to contractor confidentiality, the authors have abstained from providing further details regarding location and properties of mentioned super-structures.

## **THEORETICAL FRAME**

Cost overruns are a common issue affecting large infrastructure projects (LiPs), both domestically in Sweden and internationally. Therefore a good understanding of the *complexity* of the LiPs, see Fig. 1, is vital for project management because it is associated with difficulties in decision making and goal attainment [3.], [8.] [9.].



Figure 1. The Northern Link project, illustrating complexity of LiPs [10.].

The *complexity* of a LIP, along with the level of *uncertainty*, is the characteristic most commonly associated factors. In the literature one can find various types of relationships between *complexity* and *risk* see Fig.2, i.e. *uncertainty*, which can be categorized in the following three groups:

- *Uncertainty* and *complexity* are independent characteristics [1.], [2.],
- *Complexity* is compounded by *uncertainty* [11.],
- Projects *complexity* is the source of *uncertainty* in projects [12.], [3.].

Since above relationships are in contradiction to each other, therefor the following question was raised: – “how are *complexity* and *uncertainty* related in the large infrastructure projects”?

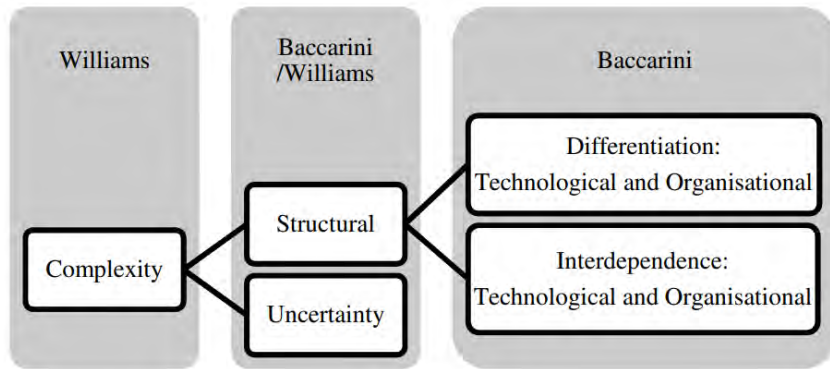


Figure 2. The development of the complexity model, [11.].

### Background

The background to the concept “the project complexity” comes from a systematic approach, which forms the basis of project management [13.] and [14.]. Were it was argued that the complexity of a project reflects "a lot of different interdependent parts".

This was further elaborated to a narrower definition consisting of two types of complexity – organizational and technological [11.].

Mega-large infrastructure projects, and planning for such, in general have the following common characteristics [15.]:

- projects are risky due to long planning and complex interfaces,
- technology is often not standard,
- decision making and planning are often multi-actor processes with conflicting interests,
- project scope or ambition level often change significantly over time,
- such unplanned events are often unaccounted for,
- leaving budget contingencies sorely inadequate.

A common consequence is; misinformation regarding costs, benefits as well as risks is quite normal. The result is cost overruns and/or benefit shortfalls within a majority of mega-large infrastructure projects.

## Understanding

Comprehension of the primary reasons behind cost overruns in mega-large infrastructure projects is crucial. Research indicates that factors including limited experience, project scale, design errors, fluctuations in overall costs, inaccurate estimates and scope adjustments significantly contribute to cost overruns.

## Reasons

Three primary types of explanations are proposed by [15.] to elucidate inaccuracies in forecasts of costs and benefits: technical, psychological, and political-economic rationales.

The technical explanations attribute cost overruns and benefit shortfalls to imperfect forecasting techniques, insufficient data, unintentional errors, inherent challenges in future prediction, and limited experience among forecasters, among other factors. According to this explanation, enhancing forecasting models, improving data quality, and cultivating experienced forecasters may diminish or eradicate technical errors.

The psychological explanations attribute cost overruns and benefit shortfalls to phenomena such as the planning fallacy and optimism bias, as identified by psychologists.

Political-economic explanations suggest that planners and promoters intentionally overestimate benefits and underestimate costs when forecasting project outcomes. This strategic approach aims to enhance the likelihood of securing approval and funding for their projects over competing ones.

## Audit of problems

The STA has pursued a procurement strategy cantered on the concept of a “purely client role”, aiming to increase the volume of turnkey contracts to increase contractors’ freedom regarding project management and execution. However, according to NAO this strategy lacks empirical support, as measurements indicate that the quantity of roads and railways has not increased with turnkey contracts, contrary to the expectations of; the government, the parliament and the STA [18.].

Further analysis conducted by the Swedish National Audit Office indicates the presence of systematic factors influencing LIP:s cost variations. These factors include variances among entrepreneurs, the organizational structure of the STA and the duration of contracts.

## Curatives

It’s evident that there is a need for reform in the planning and execution of large infrastructure projects [15.], [18.] and [20.].



However, it's important to recognize that while costs and benefits are significant factors, they shouldn't be the sole determinants in the decision-making process regarding launching such projects [21.]

When contemplating what can be reformed, it's needed to distinguish between the two following situations: – planners and advocates prioritize accurate forecasts of costs, benefits, and risks and – planners and advocates may prioritize launching projects over precise forecasts, viewing optimistic projections as essential for project initiation.

## LESSONS LEARNED

The long-term lessons learned from LiPs in the STA remain understudied in the literature. As mentioned, there are limited published historical STA analyses available to offer insights into significant events, particularly earlier projects with a geotechnical narrative angle, in the decision-making process of LiPs or other events that influenced the realization of the LiP.

However, by studying and comparing the few analyses found, [18.], [21.], [22.], [23.], [24.] and [25.] the following four general observations can be made.

### Patience

LiP:s requires patience and the remarkable bridge Øresund project is a good example. A LiP with the longest planning history that had the shortest realization time [21.]. For rail projects the average time from planning to construction is ten years and another ten years for the construction period itself. Experience shows that the time for delivery is normally somewhat optimistic. Another extreme example is the Hallandsås railway tunnel project, [25.] with a 23-year construction time, containing complex geotechnical challenges that were unforeseen from the beginning.

To mention a few Swedish ongoing LiP projects requiring patience; E4 the Stockholm bypass project [26], the west link project [27.], the Södertörn crosslink project [28.], the Slussen project (Stockholm) [29.] and [30.], Stockholm Metro expansion project [31.].

### Reasons

Reasons for cost overruns and time delays of LIPs in general, have a tendency of not having a good reputation regarding cost and time control. Cost overruns and the need for more realisation time, have always been topics of disagreements as it is almost impossible to assign them to only one cause. However, from the NETLIPSE research, [21.], it was found that the origin of reasons for cost overrun and time delay more often was found to be related to the planning stage rather than to the construction phase.

The NETLIPS findings consistently indicated that the technical, environmental, and engineering or constructional requirements and scope were inadequately defined during the initial stages of the LiPs.

The geotechnical and geological risks, which always been one of the biggest factors related to uncertainties in LiPs, seems to be a controllable factor, yet, extra costs, caused by geotechnical and geological risks that's been identified, appears almost always to be within the given financial scope.

However, in the study of 258 cases of LiPs by [15.] regarding reliability of initial cost estimate against final cost is set out in table 1.

*Table 1. Example of cost overruns by type of infra project, [15.].*

<b>PROJECT TYPE</b>	<b>NO. OF CASES</b>	<b>COST OVER-RUN %</b>	<b>DEVIATION</b>
<b>RAIL</b>	58	44,7	38,4
<b>BRIDGE &amp; TUNNELS</b>	33	33,8	62,4
<b>ROAD</b>	167	20,4	29,9

### **Context**

Changes of external context factors have a decisive influence on LiPs development. We believe that unexpected or changing conditions, for instance new legislation, change in parliament will always occur and will impact LiPs.

Performance audit has become increasingly common in the public administration and every democracy has today an independent National Audit Office.

In the reports by [16.] and [17.] on the Hallandsås project, it is stated that they conclude that the legal regulations have not effectively served as guiding and controlling instruments. They believe this to be structurally determined rather than simply a consequence of unfortunate circumstances.

### **Feedback**

Public-Private Partnership (PPP) is often hailed as a fusion of the best of both worlds. Consequently, the two parties involved operate under divergent incentives. The public sector's aim is to serve the common good, utilize tax revenue judiciously, and combat corruption, while private entities strive to forge enduring relationships and reap profits from their investments of time and resources. [32.] mentions four major barriers for loops of feedback, trust, and long-lasting relationships to occur in PPP. These disparities can sometimes hinder the establishment of a partnership. Public actors adhere to a collaborative agenda based on the arm's length principle to ensure compliance with

rules, regulations, and laws, thereby mitigating the risk of corruption allegations. However, the use of open tender processes may impede the cultivation of future relationships with contractors [33.], [32.] and [34.].

## DISCUSSION

Large infrastructure projects entail a significant degree of irreversibility, which inevitably influences the decision process. The prevalence of opportunistic compromises in decision making for such projects appears to lead to suboptimal outcomes, [35.].

Numerous and evolving perspectives on policy options are inherent to large infrastructure projects, stemming directly from the distinctive sources of uncertainty and complexity associated with them. The key challenge appears to lie not in overcoming this aspect, but rather in shaping the interaction among stakeholders within a dynamic institutional framework, enabling ongoing learning and facilitating collaborative efforts.

The factors contributing to cost overruns include technical aspects, political considerations, and the perception of complexity influenced by social constructs. These factors often manifest as optimism bias, strategic misrepresentation, or a combination thereof, adding subject risk and the trajectory of cost overrun so complex.

## CONCLUSION

Complexity, along with uncertainty, is a common aspect of large-scale infrastructure projects. As such, the research focused on understanding this characteristic, particularly because these two traits are closely linked and take on different roles relative to each other in various interpretations. Understanding the types of complexity has a significant influence on the selection of a management strategy.

The observation that project complexity, both overall and in specific forms, leads to two possible conclusions: either practitioners need to enhance their perception of complexity by considering additional elements (such as technical and strategic factors), or the perception itself may not be a valid method for analyzing project complexity.

The complexity and simplicity of large infrastructural projects are relative concepts that evolve over time and vary depending on perspective. This leads to the potential conclusion that either the characteristic of the project management approach should also evolve alongside the development of complexity in large infrastructural projects, or that the management approach itself requires further analysis.

We concluded that it still appears to be very challenging in practice to meet the conditions of uncertainty and complexity in large infra project decision making.

## ACKNOWLEDGEMENTS

The authors acknowledge the support by the Swedish Transport Administration organization for the privilege to prepare and writing of the manuscript.

## REFERENCES

- [1.] Clegg S. Pitsis T. Rura-Polley T. and Marooszeky M. (2002) Governmentality Matters: Designing an Alliance Culture of Interorganizational Collaboration for Managing Projects, *Organization Studies*, 23: 3, 317-338.
- [2.] Marrewijk A. (2005) Strategies of Cooperation: Control and Commitment in Mega-Projects, *Dans M@n@gement* 2005/4 (Vol. 8), pages 89 à 104, Éditions AIMS, DOI: 10.3917/mana.084.0089
- [3.] Remington K. Pollack J. (2007) *Tools for Complex Projects*. Hampshire: Gower Publishing Ltd. <https://doi.org/10.4324/9781315550831>.
- [4.] Volden G. H. (2018) Public project success as seen in a broad perspective.: Lessons from a meta-evaluation of 20 infrastructure projects in Norway. *Evaluation and Program Planning*, [Vol. 69, Pages 109-117](#).
- [5.] Ward J. L. Foreman J. H. (2002) Untying the gordian knot of complex projects. [Paper presented at](#) Project Management Inst. Annual Seminars and Symp. San Antonio, TX. Newtown Sq., PA: Project Management Institute.
- [6.] Jansson T. (2021) *Arbetet för hållbart markbyggande i Sverige: Rapport*, [Statens Geotekniska Institut](#).
- [7.] Johnsson A. (2017) Verkliga kostnader för bostadsbyggandet -begrepp och kostnadsfördelning, SBUF Rapport [12666](#).
- [8.] Siljevall A. (2021) Hård kritik mot Trafikverket – Projekten blir 58 miljarder dyrare. [Byggindustrin, 2021-05-12](#).
- [9.] [Nilsson J-E. \(2023\) Experten om röran hos Trafikverket som kan leda till dyrare projekt: "De saknar överblick" Byggindustrin, 2023-09-7.](#)
- [10.] The Swedish Transport Administration -[annual report](#) 2011.
- [11.] Williams T. (2002) *Modelling Complex Projects*, West Sussex: John Wiley and Sons, <https://doi.org/10.4324/9781315550831>
- [12.] Dunovic I. B. Radujkovic M. and Škreb K. A. (2014) Towards a new model of complexity - the case of large infrastructure projects. 27<sup>th</sup> IPMA World Congress, DOI: 10.1016/j.sbspro.2014.03.082.

- [13.] Baccarini D. (1996) The concept of project complexity—a review. *International Journal of Project Management*, 14 (4), 201-204.
- [14.] Mueller R. Geraldi J. and Turner R. (2007) Linking project complexity and leadership competences of project managers. The IRNOP Conf. at Brighton.
- [15.] Flyvbjerg B. (2005) Policy and Planning for Large Infrastructure Projects: Problems, Causes, Cures. World Bank Policy Research Working Paper 3781, DOI: 10.2139/ssrn.2278256.
- [16.] Miljö i grund o botten -erfarenheter från Hallandsåsen (1998) Slutrapport av Tunnelkommissionen [SOU 1998:137](#).
- [17.] Berg A. (2002) Managers found guilty. [Eurofound 2002-02-27](#)
- [18.] Riksrevisionen (2012) Trafikverkets upphandling av vägar och järnvägar -leder den till hög produktivitet? [RiR 2012:14](#).
- [19.] Davey R. A. (2021) Reforming the Execution of Mega Infrastructure Projects: A Response to the Infrastructure Investment and Jobs Act, [LinkedIn article](#).
- [20.] Ferrer S. (2021) The First Infrastructure-Implementation Priority: Invest Efficiently, [LinkedIn article](#).
- [21.] NETLIPSE (2008) European Commission [Report](#) , ISBN/EAN 978-90-810025-2-3.
- [22.] Riksrevisionen (2012) Kostnadskontroll i stora väginvesteringar? [RiR 2010:12](#). ISBN 978-91-7086-234-2.
- [23.] Landslide Småröd, road E6 (2009) Swedish Accident Investigation Authority, Report: [RO 2009:01](#).
- [24.] Nilsson J-E. Nyström J. Salomonsson J. (2019) Kostnadsöverskridande i Trafikverkets entreprenadkontrakt. [VTI rapport 1011](#).
- [25.] Riksrevisionen (2011) Kostnadskontroll i stora väginvesteringar? [RiR 2011:22](#). ISBN 978-91-7086-261-8.
- [25.] Sturk R. (2020) Hallandsås tunnel, Sweden Underground – Rock Engineering and How [It Benefits Society](#), ISBN: 978-91-6377-639-7.
- [26.] Join us in building the Stockholm bypass (2014) Trafikverket, [Diva:1389624](#).
- [27.] The West Link (2015) Trafikverket, [Diva:1389798](#).
- [28.] The Södertörn crosslink project (2024) [Trafikverket](#).
- [29.] The Slussen project (Stockholm), [YouTube](#).
- [30.] Projekt Slussen, [Wikipedia](#).

- [31.] Everything you need to know about Stockholm's new Metro (2022) [Stockholms läns landsting](#).
- [32.] Ling F.Y.Y. Ong S.Y. Ke Y. Wang S. and Zou P. (2014) Drivers and barriers to adopting relational contracting practices in public projects: Comparative study of Beijing and Sydney. [Int. Journal of Project Management 32](#).
- [33.] Ning Y. (2014) Quantitative effects of drivers and barriers on net-working strategies in public construction projects. [Int. Journal of Project Management 32](#).
- [34.] Zou W. Kumaraswamy M. Chung J. and Wong J. (2014) Identifying the critical success factors for relationship management in PPP projects. *Int. Journal of Project Management 32*.
- [35.] Altshuler A. Luberoff D. (2003) Mega-projects: the changing politics of urban public investment. [Brookings Institution Press](#), Washington, DC and Lincoln Institute of Land Policy, Cambridge, MA.



# **CONCEPT ON SOIL PLUGGING IN CLAY DEVELOPED FROM NUMERICAL CEL- SIMULATIONS CONSIDERING TOTAL STRESSES**

**P. Wiesenthal<sup>1</sup> S. Henke<sup>1</sup>**

## **KEYWORDS**

Numerical Modelling, Pile Installation, Soil Plugging, CEL

## **ABSTRACT**

While the topic of soil plugging in open ended piles in sands has been met with great interest by many researchers, in the past very little attention has been paid on the complex interactions during soil plug formation in clayey soils. In recent time breakthroughs in numerical modelling considering large deformations using the coupled Eulerian-Lagrangian (CEL) method have led to new possibilities for investigations on pile installation processes. This paper is dedicated to the numerical modelling of the jacking process of open-ended piles in clay using a total stress approach for deviatoric continuum stresses and for Coulomb contact friction. An analytical approach for determination of plug capacity and plug height is presented and evaluated on the numerical results. It is shown, that from the numerical simulations occurring mechanisms leading to plug formation can be described analytically with good agreement. The derived analytical approach is then applied to a field case from literature, which yields satisfying results. Further development of the approach as well as experimental tests regarding soil plugging in clays are planned in the future.

## **INTRODUCTION**

For the vertical and to some extent the horizontal load transfer of quay walls, offshore-wind turbines or dolphins steel pipe piles are often employed. For piles in general the axial bearing capacity is determined by the outer skin friction as well as the tip bearing resistance, whereas for open-ended pipe piles the tip resistance is controlled by the inner skin friction of soil moving inside the pile. If the bearing capacity of that inner soil column exceeds the bearing capacity of the soil below, soil plugging occurs [1]. The pile base resistance

<sup>1</sup> Helmut-Schmidt-University/ University of the Federal Armed Forces Hamburg, Germany



may drastically increase due to a soil plug, as the pile base area increases from just the annulus to the full circumferential area of the pile tip including the internal soil plug. Furthermore, as the pile behaves as a closed-ended pile during installation, more soil is displaced around the pile, leading to higher lateral stresses and therefore higher skin friction [2].

In the past, investigations on the development of soil plugs were almost exclusively performed on non-cohesive soils, see for example [3], [1], [4] or [5]. Investigations in a geotechnical centrifuge also focus on sands, see [6] or [7]. Soil plugging in clays, in which deep foundations are primarily being employed due to the soil's low bearing capacity, is currently to most extend unexplored and requires further investigations [8].

Plug development in clays is heavily dependent on the applied installation method. While vibrated piles show no tendency [5,9] and driven piles low tendency of plug development [10,11], plugging during jacking is much more likely to occur [2,8]. The type of soil is also pivotal to plugging as higher ratios of over-consolidation go along with a higher tendency to plugging [2].

In this paper, a concept on plug development employing an analytical approach is presented. Verification is done by numerical simulations using the Coupled-Eulerian-Lagrangian (CEL) method, considering undrained soil behavior and total stresses. The concept is validated by comparison with field test data from literature.

## CONCEPT ON PLUG DEVELOPMENT

A new concept on plug development was recently developed in [12] and is briefly presented here. The concept builds on the different stages after [1], which are fully coring, partial plugging and fully plugged behavior, and is extended by also incorporating the stress state of the soil. Four different stages are considered, see Figure 1:

Stage 1: Near the ground surface at shallow depths the pile tip resistance only consists of the soil's weight inside the pile. Note that, as long as the soil body can stand on its own and therefore does not lead to any normal stress on the inner pile wall, no inner skin friction is mobilized. The displaced soil is completely moved into the inside of the pile.

Stage 2: As soon as the stresses inside the soil body exceed the undrained shear strength, effective normal stresses act on the inner pile which determine skin friction [13]. The vertical stress increases exponentially from the soil's weight and the transferred inner skin friction, considering the equation from [14] for drained response. This assumption may only be valid for over-consolidated clays as it implies that from skin friction the resulting increase in vertical stresses generates little to no positive excess pore pressures.

**Stage 3:** The skin friction is limited to the soil's undrained shear strength. It is assumed that shear failure develops in a shear zone close to the pile wall but not at the interface, which is likely to be the case for soft clays [15]. When this critical depth is reached the grade of vertical stress increase slows down.

**Stage 4:** The plug resistance is limited to the pile tip resistance of a closed-ended pile. If this state is reached, no more soil can move into the pile.

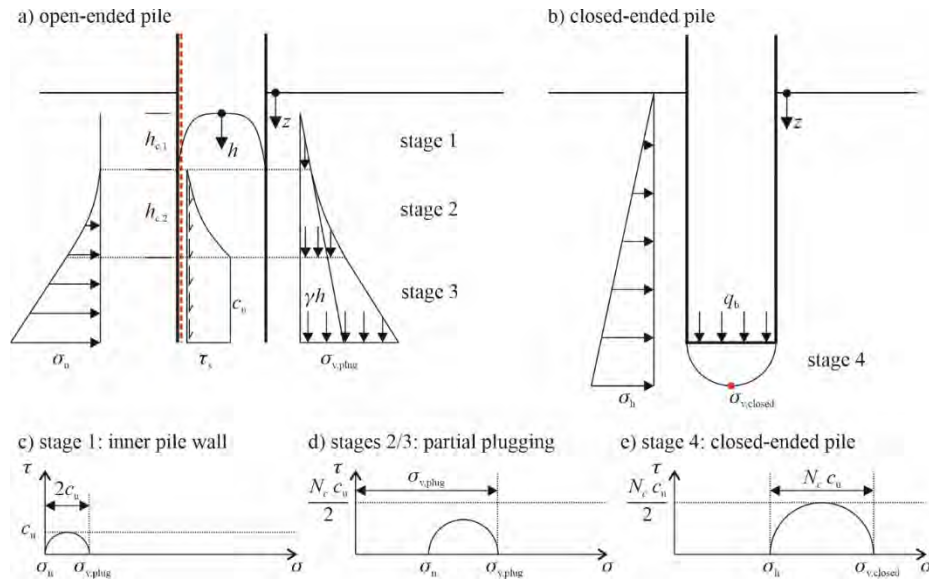


Figure 31 Concept on soil plug development.

The plug resistance can be calculated from equations (1) to (3), depending on the stage, which is determined by the plug height  $h$ .

For  $h \leq h_{c,1}$ :

$$\sigma_{v,plug,1} = (\gamma' + \gamma_w)h \quad (1)$$

for  $h_{c,1} < h \leq h_{c,1} + h_{c,2}$ :

$$\sigma_{v,plug,2} = \gamma' h_{c,1} + \gamma_w h + \gamma' \frac{A}{UK_0 \mu} \left( e^{\frac{(h-h_{c,1})A}{UK_0 \mu}} - 1 \right) \quad (2)$$

for  $h > h_{c,1} + h_{c,2}$ :

$$\sigma_{v,plug,3} = \gamma' h_{c,1} + \gamma_w h + \frac{c_u}{\mu} + (h - h_{c,1} - h_{c,2}) \left( \gamma' + c_u \frac{U}{A} \right) \quad (3)$$

where

$$h_{c,1} = \frac{2c_u}{\gamma' + \gamma_w} \quad (4)$$

$$h_{c,2} = \ln \left( 1 + \frac{c_u}{\gamma'} \cdot \frac{U}{A} \right) \cdot \frac{A}{UK_0\mu} \quad (5)$$

Herein  $c_u$  is the soil's undrained shear strength,  $\gamma'$  the effective unit weight of the soil,  $\gamma_w$  the unit weight of water,  $A$  the inner cross-sectional area of the pile,  $U$  the pile's inner circumference,  $K_0$  the lateral earth pressure coefficient and  $\mu$  the friction coefficient between pile and soil.

For the base resistance of a closed-ended pile a dependency over depth  $z$  is considered. To achieve equilibrium, a connection between plug height  $h$  and penetration depth  $z$  needs to be established. This is done by assuming a bilinear course of the incremental filling ratio  $IFR = \frac{dh}{dz}$ , from which the plug height  $h$  can be integrated, see Figure 2. The depth at which the turning point from constant to linear behavior of  $IFR$  is situated is  $z_{c,1}$  which corresponds to the critical plug height  $h_{c,1}$ . At the depth  $z_{plug}$  the bearing pressure of the plug is equal to that of a closed-ended pile. For further details on the concept see [12].

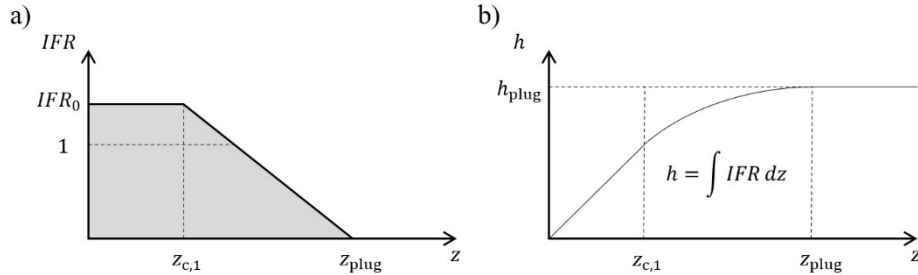


Figure 32 Development of incremental filling ratio  $IFR$  and plug height  $h$  over penetration depth  $z$ .

## NUMERICAL ANALYSIS

To investigate the plugging behavior numerical simulations employing the Coupled-Eulerian-Lagrangian (CEL) method were performed using the commercial software Abaqus. The CEL method has recently been used by other researchers for modelling pile installation processes with great success, e.g. [16,17]. The model used in this study is displayed in Figure 3. For the pile an outer diameter of 0.5 m and a wall thickness of 0.04 m are chosen. The soil is modelled with  $c_u = 25$  kPa,  $E = 5000$  kPa,  $\gamma' = 20$  kN/m<sup>3</sup> and  $\gamma_w = 0$ , as no pore pressure is considered in the total stress analysis. A friction coefficient  $\mu = 0.1$  is selected for the exemplary simulations. Besides the open-

ended pile calculations further simulations are performed considering a closed-ended pile. The results in form of base pressure and incremental filling ratio over penetration depth are given in Figure 4.

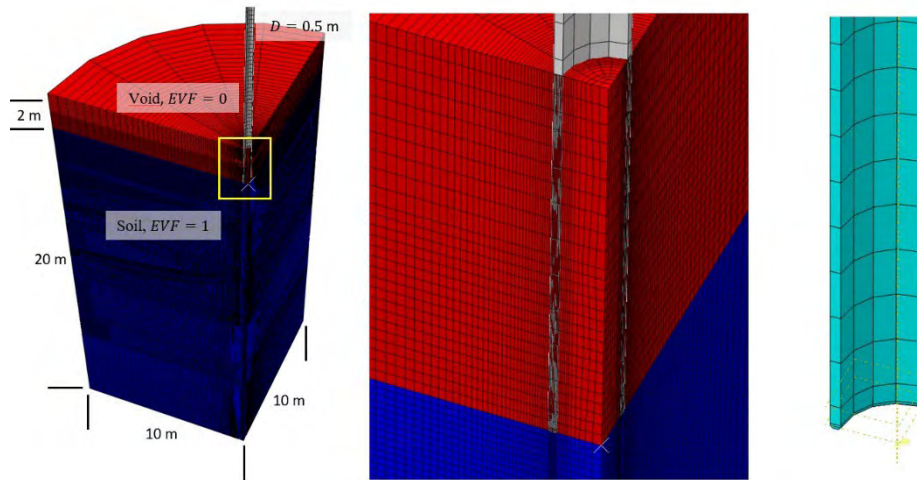


Figure 33 CEL model for pile installation process.

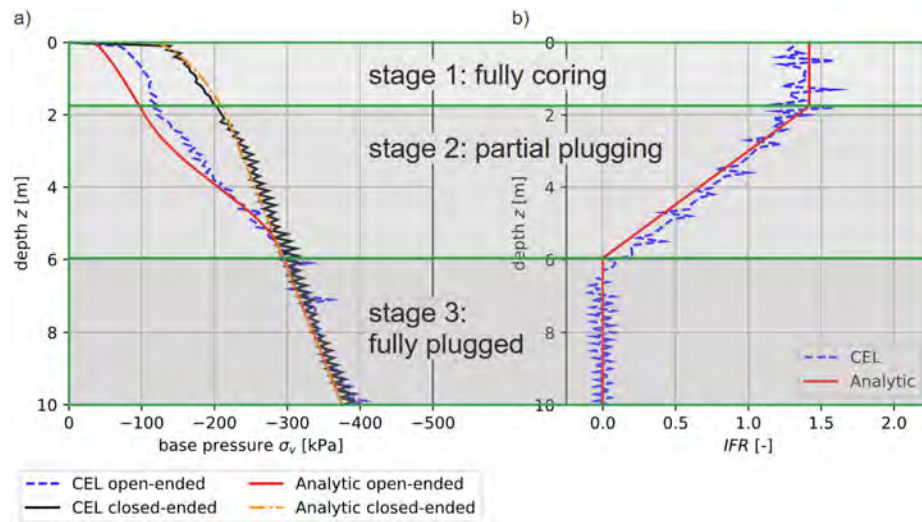


Figure 34 Results of CEL simulations compared to analytical approach.

From the numerical simulations presented in Figure 4, it can be identified that the open-ended pile passes through the stages fully coring, plug development and fully plugged with increasing penetration depth. After reaching the fully plugged state, in which  $IFR = 0$ , base resistance is identical to that of the closed-ended pile. For the analytical approach first the base resistance of the closed-ended pile is taken from the simulation to receive a suitable value for

$N_c$ . Afterwards the analytical calculation is performed. The base resistance and incremental filling ratio behave similarly to the numerical simulation. In total 12 simulations with varying strength and stiffness parameters were performed, which are displayed in [12], showing good agreement for the analytical approach.

## COMPARISON WITH FIELD TEST DATA

For validation of the presented concept, calculations were performed and compared to field test data given by [8]. As with the numerical simulations the base resistance of the closed-ended pile was taken as reference for computing a value for  $N_c$ . Divergences occurred when calculating the critical plug height  $h_{c,1}$  and accordingly the depth at which the incremental filling ratio drops from its initial value and decreases further with depth. By manually choosing a value of  $h_{c,1} = 0.7$  m and  $IFR_0 = 1$  very good agreement with the field test data is achieved, see Figure 5. This shows that the analytical approach, despite its limitations of only considering total stresses, is in good accordance with reality.

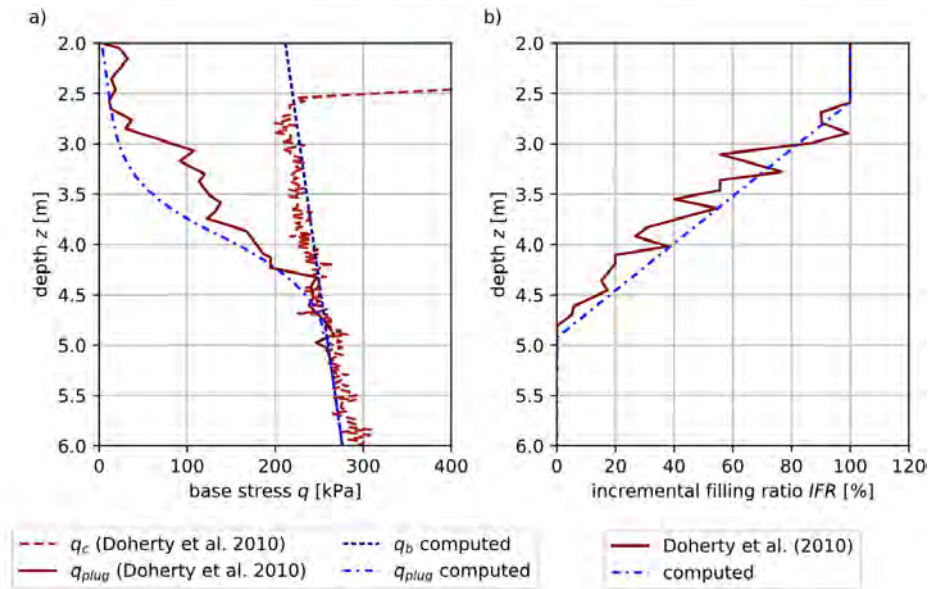


Figure 35 Comparison of field test data from [8] with the analytical approach.

## CONCLUSION

In this paper, soil plugging in clays was investigated and a first concept on evaluating plug development in clayey soils is presented. Performed calculations showed that the new concept for plug development gives results for base resistance and plug height inside the pile during jacking which closely match those from numerical simulations. During jacking of open-ended piles, the

different stages of fully coring, plug development (partial plugging) and fully plugged behavior are considered. When the pile is fully plugged, its base resistance reaches values comparable to those of a closed-ended pile.

The plugging behavior is dependent on employed values like turning point from fully coring to plug development  $h_{c,1}$  and the initial incremental filling ratio  $IFR_0$ . This turned out to be critical for predicting plugging evaluated out of field tests. When employing field test data, the calculations showed good agreement with vertical stresses and plug height. Considering the approach's simplicity and limitations of only employing total stresses, the conformity to observations from field test is very good and further development is planned.

So far, the analytical formulas do not consider excess pore pressures, which will influence the effective stresses and therefore will affect the plugging behavior. For future investigations pore pressure development will be analyzed by means of numerical simulations. For validation purpose of the concept centrifuge tests at the University of Western Australia in Perth are planned.

## ACKNOWLEDGEMENT

The authors would like to thank the German Research Foundation (DFG) for funding the project "Investigations on the vertical bearing capacity of open-ended profiles in cohesive soils under consideration of potential plugging" (project number: 495328022), in which framework this paper was elaborated. The funding is highly appreciated.

## REFERENCES

- [1] S. G. Paikowsky and R. V. Whitman, "The effects of plugging on pile performance and design," *Canadian Geotechnical Journal*, vol. 27, no. 4, pp. 429-440, 1990. DOI: <https://doi.org/10.1139/t90-059>.
- [2] G. A. Miller and A. J. Luttenegger, "Influence of Pile Plugging on Skin Friction in Overconsolidated Clay," *Journal of Geotechnical and Geoenvironmental Engineering*, vol. 123, no. 6, pp. 525-533, 1997. DOI: [https://doi.org/10.1061/\(ASCE\)1090-0241\(1997\)123:6\(525\)](https://doi.org/10.1061/(ASCE)1090-0241(1997)123:6(525)).
- [3] J. Klos and A. Tejchman, "Bearing capacity calculation for pipe piles," *Proceedings of the 10th International Conference on Soil Mechanics and Foundation Engineering*, Stockholm, Sweden, pp. 751-754, 1981.
- [4] J. Lüking, *Tragverhalten von offenen Verdrängungspfählen unter Berücksichtigung der Pfropfenbildung in nichtbindigen Böden*, Zugl.: Kassel, Univ., Diss., 2010, Kassel Univ. Press, 2010.
- [5] S. Henke, *Untersuchungen zur Pfropfenbildung infolge der Installation offener Profile in granularen Böden*, Zugl.: Hamburg, Techn. Univ., Habil.-Schr., 2013, Inst. für Geotechnik und Baubetrieb, 2013.

- [6] A. de Nicola and M. F. Randolph, "The plugging behaviour of driven and jacked piles in sand," *Géotechnique*, vol. 47, no. 4, pp. 841-856, 1997. DOI: <https://doi.org/10.1680/geot.1997.47.4.841>.
- [7] D. Bruno and M. F. Randolph, "Dynamic and Static Load Testing of Model Piles Driven into Dense Sand," *Journal of Geotechnical and Geoenvironmental Engineering*, vol. 125, no. 11, pp. 988-998, 1999. DOI: [https://doi.org/10.1061/\(ASCE\)1090-0241\(1999\)125:11\(988\)](https://doi.org/10.1061/(ASCE)1090-0241(1999)125:11(988)).
- [8] P. Doherty and K. Gavin, "Shaft Capacity of Open-Ended Piles in Clay," *Journal of Geotechnical and Geoenvironmental Engineering*, vol. 137, no. 11, pp. 1090-1102, 2011.
- [9] X. T. Xu, H. L. Liu and B. M. Lehane, "Pipe pile installation effects in soft clay," *Proceedings of the Institution of Civil Engineers-Geotechnical Engineering*, vol. 159, no. 4, pp. 285-296, 2006.
- [10] E. P. Heerema, *Predicting Pile Driveability: Heather As An Illustration Of The "Friction Fatigue" Theory* London, 1978.
- [11] M. Randolph and S. Gourvenec, *Offshore geotechnical engineering* Abingdon: Spon Press, 2011.
- [12] P. Wiesenthal and S. Henke, "Concept on plug development in jacked open-ended piles in clay considering total stresses," Manuscript submitted for publication, 2024.
- [13] A. J. Bond and R. J. Jardine, "Effects of installing displacement piles in a high OCR clay," *Géotechnique*, vol. 41, no. 3, pp. 341-363, 1991. DOI: <https://doi.org/10.1680/geot.1991.41.3.341>.
- [14] M. F. Randolph, E. C. Leong and G. T. Houlsby, "One-dimensional analysis of soil plugs in pipe piles," *Géotechnique*, vol. 41, no. 4, pp. 587-598, 1991. DOI: <https://doi.org/10.1680/geot.1991.41.4.587>.
- [15] H. G. Poulos and E. H. Davis, *Pile foundation analysis and design* New York, Toronto: J. Wiley, 1980.
- [16] G. Qiu, S. Henke and J. Grabe, "Application of a Coupled Eulerian–Lagrangian approach on geomechanical problems involving large deformations," *Computers and Geotechnics*, vol. 38, no. 1, pp. 30-39, 2011. DOI: <https://doi.org/10.1016/j.compgeo.2010.09.002>.
- [17] P. Staubach, L. Tschirschky, J. Macháček and T. Wichtmann, "Monopile installation in clay and subsequent response to millions of lateral load cycles," *Computers and Geotechnics*, vol. 155, no. 105221, pp. 1-16, 2023. DOI: <https://doi.org/10.1016/j.compgeo.2022.105221>.

# CORRELATING $Q_{NET}$ TO $E_{OED}$ OF PALEOGENE CLAYS OF VERY HIGH PLASTICITY

N. Okkels<sup>44</sup>, L. Bødker<sup>1</sup>, E. Skouboe<sup>1</sup> and T. Thorsen<sup>1</sup>

## KEYWORDS

Clay, Oedometer modules, Cone resistance, Correlation, Lateral earth pressure

## ABSTRACT

This paper provides practical formulations for correlating CPTu cone resistance  $q_c$  and net corrected cone resistance  $q_{net}$  to the oedometer reloading stiffness  $E_{OED}$  in highly overconsolidated, fissured, marine Paleogene clays of very high plasticity, from late Eocene and early Oligocene as observed in the Aarhus Denmark.

CPTu measurements provide detailed insights into both soil stratigraphy and geotechnical engineering properties. CPTu's carried out in these Paleogene clay types indicate very variable and fluctuating geotechnical properties spatially.

$E_{OED}$  is determined from oedometer tests and is traditionally used for soil deformation analysis using a Mohr-Coulomb soil model. However, oedometer tests are time-consuming and expensive to perform. In practice, it is rarely possible to carry out a sufficient number of tests per site taking into account the variability and the financial framework. Therefore, it is essential to improve the statistical basis by including a priori knowledge of the stiffness parameters.

By correlation of  $E_{OED}$  from 73 oedometer tests with associated  $q_c$ - and  $q_{net}$ -values from CPTu's carried out near the boreholes from which the oedometer-samples are extracted linear correlations between these properties are found.

The correlations make it possible to derive  $E_{OED}$  directly from CPTu for use in the preliminary analysis of deformations. More importantly, the correlations support the final derivation of  $E_{OED}$  for 3D soil models once the results of all field and laboratory tests for the construction project are incorporated into the correlations.

## INTRODUCTION

Traditionally, odometer tests are used in commercial geotechnical surveys to determine the reload stiffness  $E_{OED}$  for use in a Mohr-Coulomb soil model. In

<sup>44</sup> Geo, Aarhus Denmark



recent years, the test is also used to support the derivation of the coefficient of lateral earth pressure  $K_0$ .

The reload stiffness  $E_{OED}$  should not be confused with the input parameter  $E_{oed}$  for a Plaxis model.  $E_{oed}$  in Plaxis' Hardening Soil model is a stiffness parameter dedicated to primary loading under oedometric conditions - i.e. the soil is in a normally consolidated state and lateral expansion is prevented during testing. Unfortunately, internationally the same nomenclature is used for the stiffness determined by the oedometer test - regardless of whether the soil is in a normal consolidated or overconsolidated state. Following the latter nomenclature,  $E_{OED}$  is defined in this paper as the stiffness of highly consolidated clays under re-loading from the in situ stress level.

At the same time, CPTu has become the preferred investigation method because it is the most effective way to shed light on how stratigraphy, strength and stiffness vary spatially. To exploit this commercially, Geo has correlated  $q_c$  and  $q_{net}$  with the drained triaxial unloading and reloading stiffness  $E_{ur}$  [4] and the maximum small-strain shear modulus  $G_0$  as well [5].

The CPTu's are performed in a single continuous stroke from the ground surface to target depth using Geo's enhanced CPT-system, which reduce the friction on the rod and make it possible to push the cone through more than 80 meters of very firm Paleogene clays.

Geo's CPT-crawler with a maximum push capacity of 15 ton is used together with a 10 or 15 cm<sup>2</sup> piezoelectric cone from the manufacturer A.P. van den Berg. The equipment and the execution agree with ISO 22476-1 with continuous measurement of tip resistance, sleeve friction, pore pressure (measured behind the tip of the probe) and inclination of the probe.

The CPTu's are supplemented with a few geotechnical boreholes for use in interpreting the CPTu's and for extracting soil samples for classification tests and advanced laboratory tests.

## THE PALEOGENE STRATIFICATION

In costal parts of Aarhus, the Paleogene stratification is found near the surface only covered by fill and/or a thin series of glacial and or postglacial layers. The following Paleogene stratification is typically found, cf. figure 1:

Topmost 5-9 meter Viborg Clay, which is an Oligocene clay of very high plasticity with mica.

The Viborg clay is underlain by 0.5-2 m Kysing Marl, which is a highly glauconitic, highly calcareous, and high plasticity clay from the top of the Eocene Søvind Marl formation. It is quite similar to the underlying Søvind Marl, but the geotechnical properties are typically better.

Below the Kysing Marl typically 9 to 13 meters of Moesgaard Clay - which is an Eocene clay of very high plasticity with mica - is found. This clay is somewhat reminiscent of the overlying Viborg Clay - both in terms of appearance and geotechnical properties. In some contexts, it is therefore not possible to distinguish these two clay types from each other by the eye. In such cases, the trivial name "Septarian Clay" is traditionally used for both clay types.

Søvind Marl underlies Moesgaard Clay. Søvind Marl is a clay of very high plasticity that makes up the majority of the Søvind Marl formation. It is predominantly very calcareous. However, calcareous-free or slightly calcareous zones frequently alternate with more calcareous ones.

All these clays are deposited in deep oceans and except for Kysing Marl, they are all fissured with slickensides. Due to the removal of younger layers by erosion and the weight of numerous glaciers during the Quaternary period, they are also highly overconsolidated with a geological preconsolidation stress greater than two MPa.

Large variations in plasticity and calcium carbonate content indicate that also strength and deformation properties vary a lot down through the formations. Variability in CPTu cone resistance confirms this, cf. figure 1. If cone resistance is decomposed into a trend component and a fluctuating component, the CPTu's shows that the fluctuating component is characterized by frequent and violent fluctuations around a trend line. Through the Septarian clays, the trend line is directly proportional to depth, but in the Søvind Marl it varies in large irregular cycles.

The oedometer modules of overconsolidated fine soils are traditionally described by a linear function of the minimum vertical effective stress that the clay has geologically experienced. Accordingly,  $E_{OED}$  increases linearly with depth. The corresponding function is derived based on oedometer tests performed with three unloading path to different minimum stresses. An oedometer stiffness is derived for each unloading for use in a mathematical over-determination of the two coefficients of the function.

In accordance with the traditional model, the trend component in Figure 1 indicates that  $E_{OED}$  increases with depth in the Septarian Clays, while this does not seem to be the case for the Søvind Marl. Furthermore, the fluctuating component in Figure 1 indicates that also the stiffness of both clay types fluctuates violently over short distances, which the traditional model does not predict. The same is likely to apply the coefficients in the above-mentioned function of minimum vertical effective stress. The traditional approach therefore seems unsuitable for overconsolidated Paleogene clay types.

Seismic CPTu, where the maximum small-strain shear modulus  $G_0$  is calculated from the measured shear wave velocity and compared directly with the cone resistance in the same position, documents that  $G_0$  is proportional to the

cone resistance [5]. It is reasonable to assume that this also applies to other stiffness modules including  $E_{OED}$ .

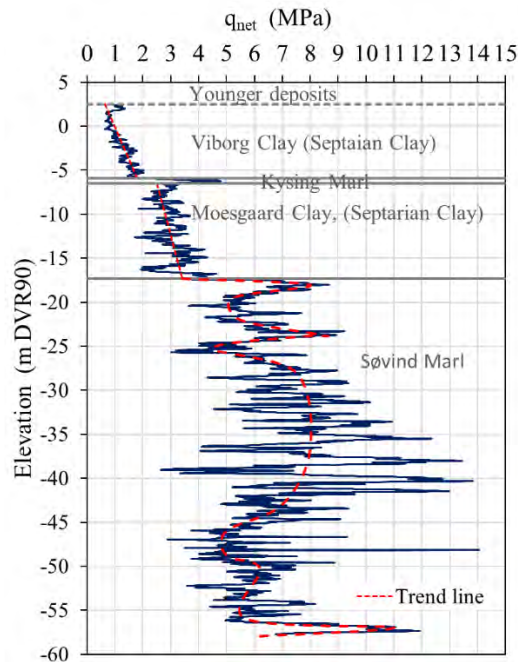


Figure 1. An example of a  $q_{net}$ -profile calculated from one of 36 CPTu's included in this study.

## TEST PROCEDURES

The odometer tests are carried out following the guidelines specified in ISO 17892-5. All samples are extracted from Shelby-tube samples with an inner diameter of 70 mm.

Tests carried out with the very high plasticity Palaeogene clays usually begin with a measurement of the swell pressure, defined as the vertical pressure to be applied to the sample in the oedometer apparatus to prevent the sample from swelling when applied to water. The swell occurs because the in situ mean stress has not been restored in the oedometer apparatus.

After a sample is formed and installed in the oedometer apparatus, it is applied a vertical pressure slightly lower than the estimated effective vertical in situ stress. When the sample is at rest at this load, water is added to the sample, and the swelling pressure is measured by recording the vertical pressure to be applied to the sample to prevent it from deforming (volume constancy) as shown in Figure 2. To prevent the tests from being significantly affected by osmosis forces [6], it is aimed to use apparatus water with the same salinity as the formation water.

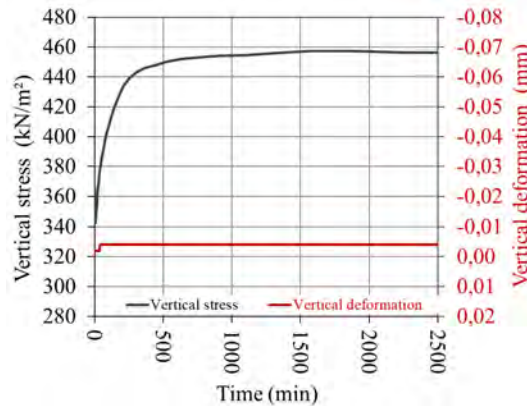


Figure 2. A swell pressure measurement in the oedometer apparatus.

During the preparation and installation of the sample, a negative pore pressure holds it together. Assuming volume constancy the coefficient of lateral earth pressure  $K_0 = 1.0$  while water is added to the sample and the vertical swelling pressure is measured. Therefore, the measured swelling pressure approximately must represent the in situ mean stress  $\sigma'_{mean}$ . This means the in situ  $K_0$  can be calculated from the definition of the mean stress:  $\sigma'_{mean} = \sigma'_{v0} (1+2K_0)/3$ , where  $\sigma'_{v0}$  is the estimated vertical effective in situ stress. However, this method is only applicable when in situ  $K_0 > 1.0$ .

Once the swelling pressure has been measured, the test is continued by loading the sample to a cautiously estimated geological preload stress determined as approximately 2.5 times the field vane strength measured by a fast field vane test (ISO 22476-9). This is done partly to minimize the effect of the inevitable test disturbance and partly to restore the in situ stress state. Next, the sample is unloaded to about the vertical effective in situ stress, after which it is reloaded to the previous maximum load. Finally, the sample is unloaded to the chosen minimum vertical effective stress. Figure 3 shows a typical stress-strain curve.

To facilitate a consistent derivation of the reloading stiffness, it is chosen to determine  $E_{OED}$  from the reloading curve by a polynomial fit to test data for an additional stress of 100 kPa to the minimum vertical effective unloading stress.

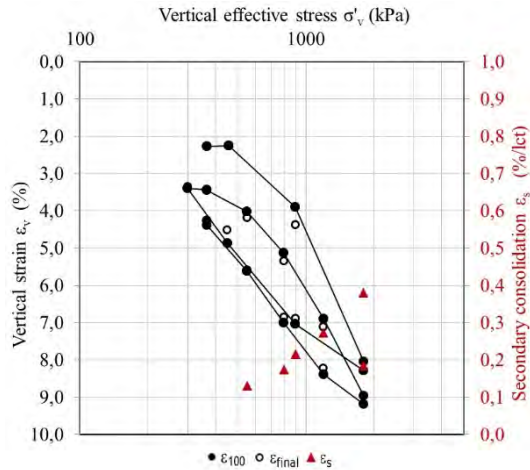


Figure 3. Example of an oedometer test.

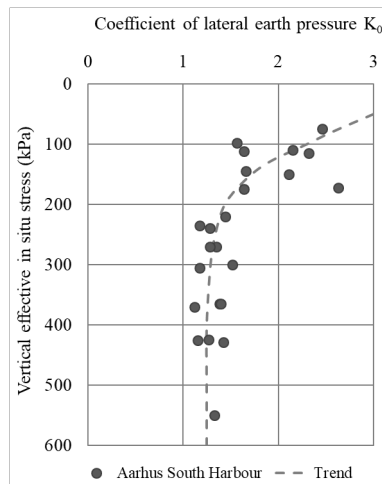


Figure 4. Example of  $K_0$  calculated from swell pressure measurements.

As shown in Figure 5, the polynomial fit completely ignores the last point on the unloading curve. This is because this loading stage is strongly influenced by friction on the sides of the sample, which is working in the opposite direction to the friction during reloading. At the same time, the reloading is initiated before the creep at this stage has reversed direction.

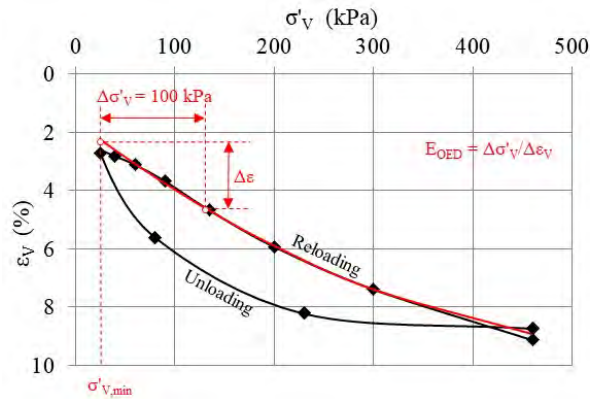


Figure 5. Principle of interpretation of the reloading stiffness  $E_{OED}$ .

The test samples are characterized by the soil index properties in Table 1.

The reload stiffness  $E_{OED}$  from the Septarian Clay tests is presented in Figure 6 and recorded in Figure 7 as a function of the minimum effective unloading stress  $\sigma'_{v,min}$  during testing. The result show as expected a clear rectilinear trend:

$$E_{OED} \approx a \cdot \sigma'_{v,min} + b \quad (1)$$

where  $a$  and  $b$  are constants.

Geo ID	$I_p$	$\sigma'_{v0}$	$\sigma'_{swell}$	$\sigma'_{v,min}$	$E_{OED}$	$a$	$E_{OED, in situ}$	$q_{net}$	$q_c$
	%	kPa	kPa	kPa	MPa		MPa	MPa	MPa
20208219:51	182	247	341	220	13,18	67,4	15,00	2,45	2,90
2020826:71	110	335	445	300	41,79	139,0	46,66	6,72	7,35
20208217:41	125	200	259	180	15,28	124,1	17,76	2,80	3,15
20208217:61	189	290	406	270	16,24	60,4	17,45	3,00	3,52
20208219:31	66	160	218	140	29,61	182,8	33,27	3,30	3,58
2020821:42	85	207	445	180	47,97	163,9	52,39	6,50	6,90
2020821:100	142	470	445	430	61,62	107,2	65,91	6,10	7,00
20208215:32	79	162	445	180	32,77	169,8	29,71	7,20	7,50
20208215:62	108	298	445	270	56,86	141,0	60,81	4,80	5,35
20208215:92	101	430	445	400	56,84	148,0	61,28	7,50	8,25
377231:31	77	140	167	150	20,48	171,8	18,76	3,45	3,75
377231:51	250	240	259	200	7,54	-0,2	7,53	2,35	2,90
3772314:51	222	240	-	40	9,89	27,6	15,41	4,91	5,00
3772317:41	112	200	-	40	13,47	137,0	35,40	2,44	2,80
3772317:61	164	280	-	40	7,72	85,3	28,19	3,20	3,70
37509BH103:13	95	158	-	150	23,90				
37509BH103:21	152	251	-	150	25,07				
37509BH103:27	151	312	-	150	34,50				
37509BH103:33	123	384	-	250	64,60				
37509TR103:64	141	145	-	150	21,58				
37509TR103:81	170	221	-	150	21,20				
2012788:25	121	120	252	40	9,23	128,1	19,47	2,30	2,55
2012788:51	122	250	505	80	25,76	127,1	47,36	4,00	4,50
2012788:230	93	150	-	40	14,19	155,9	31,34	4,70	4,95
383631:41	116	190	275	80	15,82	133,0	30,46	3,20	3,60
2028261:43	136	210	230	120	10,38	113,2	20,57	2,45	2,70
2028261:53	99	250	250	150	20,97	150,0	35,96	6,95	6,65
2028266:31	85	150	145	75	11,34	163,9	23,63	1,20	1,47
2027283:17	128	130	156	100	11,33	121,1	14,96	1,16	1,33
2039497:37	90	175	400	150	27,86	158,8	31,83	5,20	5,25
2039497:46	87	210	550	180	44,81	161,5	49,66	6,50	6,80
2039497:53	123	240	450	220	27,58	126,2	30,10	4,20	4,45
2039497:61	106	270	320	250	60,73	143,3	63,59	6,70	6,80
2042961:101	132	424	503	380	38,45	117,3	43,61	5,80	6,30
2042966:53	112	235	363	150	21,84	137,0	33,49	6,00	6,05
2042966:77	192	333	-	300	28,91	57,5	30,81	4,70	5,20
2042966:85	169	365	457	300	22,70	80,3	27,92	4,70	5,20
2042969:37	79	175	229	150	45,90	169,8	50,14	5,75	5,65
2042969:53	115	240	282	210	30,94	134,0	34,96	4,90	4,85
2042969:69	108	305	340	280	61,60	141,0	65,13	6,00	6,20
2042969:99	119	425	467	380	52,26	130,1	58,11	4,80	5,40
2042969:85	183	370	399	330	34,14	66,4	36,80	5,00	5,50
2042962:44	99	220	285	200	34,65	150,3	37,66	5,10	5,50
2046081:58	131	270	333	250	27,64	118,1	30,01	5,40	5,55
2046081:66	100	300	404	250	47,77	149,3	55,23	6,50	6,50
2046081:82	110	365	461	300	41,68	139,0	50,72	9,70	9,40
2046081:98	162	429	550	350	30,97	87,0	37,85	5,00	5,65
2052311:28	98	135	150	100	18,50	151,0	23,79	3,20	3,40
2052311:44	67	200	250	150	68,35	182,2	77,46	5,75	6,15
2063741:49	112	235	279	160	18,48	137,0	28,76	4,00	4,45
2063741:65	170	305	53	200	35,61	79,3	43,94	3,40	4,00
2063741:73	110	340	452	275	73,53	139,0	82,57	9,30	10,00
2063741:89	192	406	650	350	24,80	57,5	28,01	5,20	6,05

Geo ID	$I_p$	$\sigma'_{v0}$	$\sigma'_{swell}$	$\sigma'_{v,min}$	$E_{OED}$	$a$	$E_{OED, in situ}$	$q_{net}$	$q_c$
	%	kPa	kPa	kPa	MPa		MPa	MPa	MPa
34070 8:51	64	245	-	200	24,29	110,9	29,28	4,00	4,30
34070 11:41	72	200	-	200	27,29	110,9	27,29	2,75	3,15
34070 18:55	81	275	-	200	30,33	110,9	38,65	4,00	4,50
37070 18:39	72	210	-	200	20,04	110,9	21,15	3,70	4,00
38363 1:31	60	150	-	80	11,90	110,9	19,66	2,10	2,35
38363 5:41	67	210	300	80	9,30	110,9	23,71	3,20	3,65
201278 7:8	65	60	152	20	4,63	110,9	9,07	1,40	1,45
201278 8:15	58	70	98	20	7,12	110,9	12,66	1,40	1,55
201278 8:124	67	125	505	40	5,19	110,9	14,61	2,50	2,70
203695 23:24	57	109	-	55	9,30	110,9	15,28	1,40	1,65
203949 7:25	64	115	216	115	13,25	110,9	13,25	1,60	1,80
203949 7:29	56	145	209	135	12,79	110,9	13,89	1,76	2,00
204296 1:37	60	170	-	150	20,80	110,9	23,02	3,93	4,00
204296 8:21	62	110	195	70	9,83	110,9	14,26	2,56	2,70
204296 9:21	70	112	160	90	9,28	110,9	11,71	2,45	2,60
204296 22:11	56	75	148	65	5,74	110,9	6,85	1,05	1,10
204296 22:27	81	150	261	130	11,45	110,9	13,67	2,05	2,25
204607 2:6	78	40	48	25	4,19	110,9	5,85	0,75	0,80
204607 5:7	100	37	66	25	4,44	110,9	5,77	1,20	1,25
204607 8:9	66	57	93	25	4,41	110,9	7,96	1,40	1,47
204608 1:34	76	173	361	150	14,11	110,9	16,66	2,60	2,90
204608 7:16	57	98	135	70	8,21	110,9	11,32	1,73	1,85
205231 1:12	64	70	75	50	7,72	110,9	9,94	1,55	1,65
205231 1:20	62	100	131	70	8,50	110,9	11,83	2,33	2,50
206374 1:17	45	95	150	70	12,95	110,9	15,72	1,75	1,85
206374 1:25	57	130	269	90	10,97	110,9	15,41	1,90	2,20

Figure 6. Test results for Septarian Clays (left) and Søvind Marl (right).

Consequently,  $E_{OED}$  depends on the in situ stress level and must be corrected in case  $\sigma'_{v,min}$  deviates from  $\sigma'_{v0}$  when correlated with the tip cone resistance at the same level. Alternatively, the tip cone resistance should refer to the level where the vertical effective in situ stress is equal to the minimum unloading stress from the test. Due to the wildly fluctuating  $q_{net}$  cf. Figure 1, the first option should be chosen.

Table 14. Natural water content ( $w_{nat}$ ) and plasticity index ( $I_P$ ) of the test samples.

Soil type	Property	Min	Max	Mean
Søvind Marl	$w_{nat}$ (%)	30	52	39
	$I_P$ (%)	66	250	125
Septarian Clays	$w_{nat}$ (%)	24	54	36
	$I_P$ (%)	45	100	64

For the Septarian Clays, the correction is done using Eq. (2) where  $a$  is the slope of the trend line in Figure 7.

$$E_{OED\_insitu} \approx E_{OED} + a (\sigma'_{v\_insitu} - \sigma'_{v\_min}) \quad (2)$$

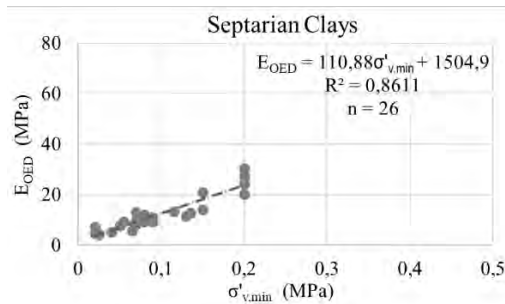


Figure 7. Correlation between minimum vertical effective unloading stress and re-loading stiffness.

According to Figure 7 the slope  $a \approx 110.88$ . Figure 6 list the associated in situ  $E_{OED}$ 's.

The reload stiffness  $E_{OED}$  from the Søvind Marl tests is presented in Figure 6 and recorded in Figure 8 as a function of the minimum unloading stress  $\sigma'_{v,min}$  during testing. According to figure 8, the correction factor depend highly on plasticity.

The trend line for  $I_P$  (%) versus  $a$  in Figure 8 indicate a correction factor  $a \approx 248.42 - 0.9946 \cdot I_P(\%)$  for Søvind Marl. Figure 6 list the associated in situ  $E_{OED}$ 's.



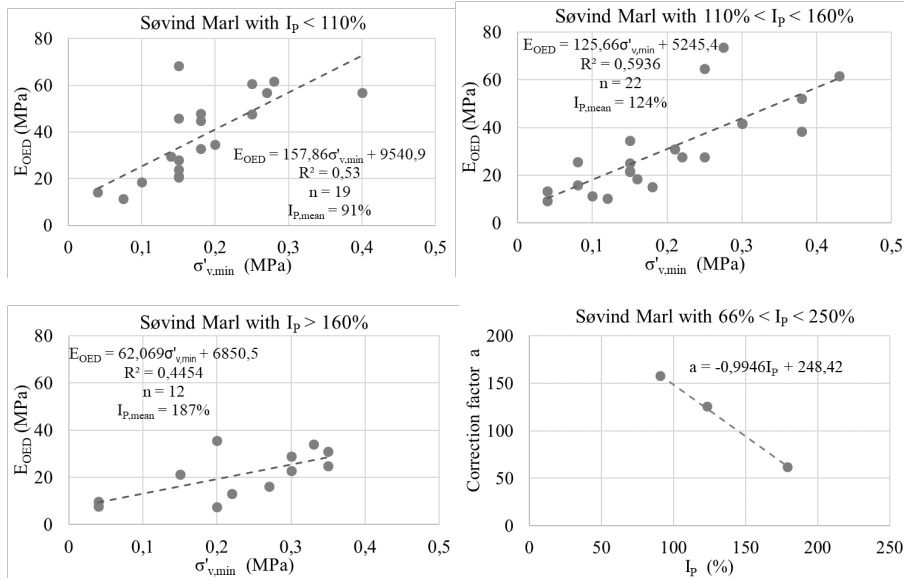


Figure 8. Correlation between minimum vertical effective unloading stress and reloading stiffness and its dependence on plasticity.

## CORRELATING CONE RESISTANCE TO $E_{OED}$

Scatter plots between  $q_c$  and  $E_{OED}$  as well as between  $q_{net}$  and  $E_{OED}$  are presented in Figure 9. The cone resistance is measured in a nearby CPTu at the same level from which the sample for the oedometer test was taken.

The CPT's are typically performed two meters from the borehole. However due to the inevitable deflection, the distance may be many times larger at the base of the CPT stroke. The distance introduces uncertainty and thus scatter when the CPT measurements are correlated with measured soil parameters from in situ testing or laboratory testing on soil samples extracted from the boring. Consequently, a relatively large number of tests is required to achieve a satisfactory strong correlation.

With reference to Lunne et al. (1997) a simple linear correlation is chosen. The trend lines indicate Aarhus correlations between the four data sets as presented in equation (3)-(6).

$$\text{Septarian Clays:} \quad E_{OED} = 6.6 q_c \quad (3)$$

$$\text{Søvind Marl:} \quad E_{OED} = 7.3 q_c \quad (4)$$

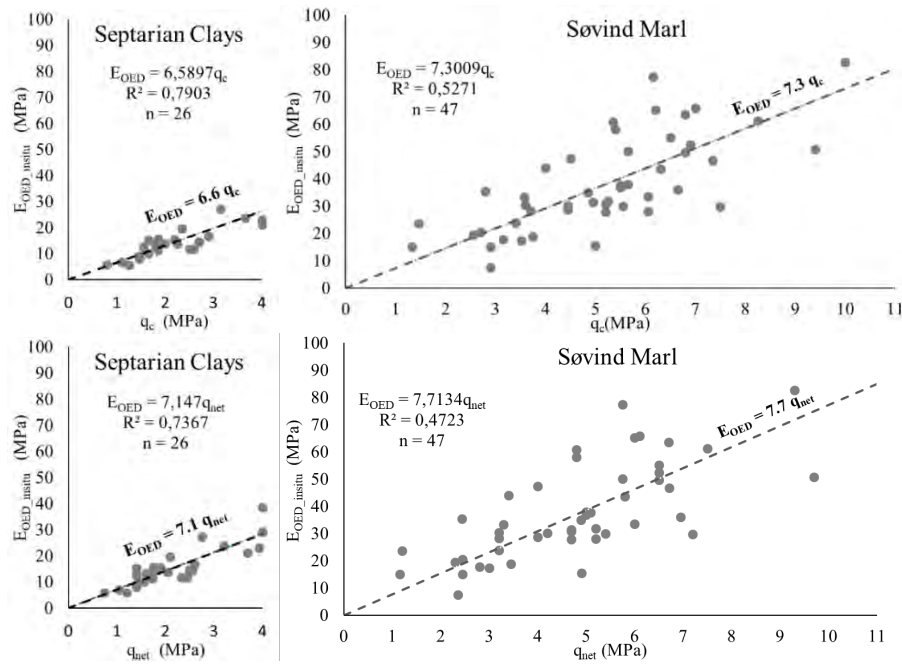


Figure 9. Correlations between  $q_c$  and  $E_{OED}$  (above) and  $q_{net}$  and  $E_{OED}$  (below).

A confidence interval for the  $q_c$ -proportionality factor is computed to be  $CI(95) = 6.6 \pm 0.6$  and  $7.3 \pm 0.8$ , respectively.

$$\text{Septarian Clays:} \quad E_{OED} = 7.1 q_{net} \quad (5)$$

$$\text{Søvind Marl:} \quad E_{OED} = 7.7 q_{net} \quad (6)$$

A confidence interval for the  $q_{net}$ -proportionality factor is computed to be  $CI(95) = 7.1 \pm 0.7$  and  $7.7 \pm 0.9$ , respectively.

As seen from Figure 9, the  $R^2$ -values indicate that correlation is somewhat better for the Septarian Clays than for the Søvind Marl. This is probably because the tip resistance and thus soil stiffness, fluctuates significantly much more in Søvind Marl, cf. Figure 1. It also appears that the correlations with  $q_c$  are stronger than the correlations with  $q_{net}$ .

Figure 10 compares  $E_{OED}$  calculated with correlation algorithms (3) - (6) with the derived  $E_{OED\_insitu}$  values from Figure 6 to evaluate the correlations. As can be seen, the error using the algorithms for the Septarian Clays is symmetric throughout the validity range ( $0.8 < q_c$  or  $q_{net}$  (MPa)  $< 4$ ) for both  $q_c$  and  $q_{net}$ . However for the Søvind Marl, there is a small systematic deviation throughout the validity range ( $1.2 < q_c$  or  $q_{net}$  (MPa)  $< 10$ ), but taking into account the greater scatter, the deviation is considered acceptable - especially for  $q_c$ .

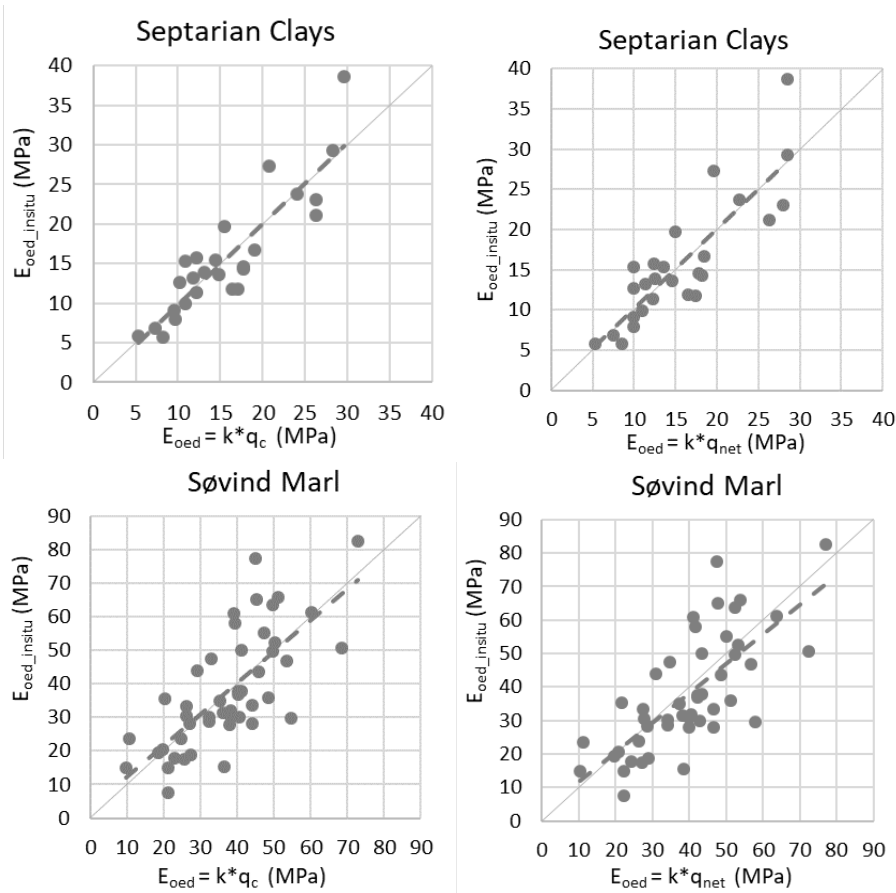


Figure 10. Correlation algorithm check.

## SUMMARY AND CONCLUSION

Geo has determined the reloading oedometer stiffness  $E_{OED}$  from 26 oedometer tests with Septarian Clays and 46 oedometer tests with Søvind Marl in connection with geotechnical surveys for high-rise buildings in Aarhus. This paper demonstrate that simple linear functions of only the cone tip resistance  $q_c$ , or the net-corrected resistance  $q_{net}$ , can predict the reloading oedometer stiffness in highly over-consolidated, fissured, marine Paleogene clays and marls of very high plasticity. The derived Aarhus correlations are presented in equations (3), (4), (5), and (6).

The prediction accuracy is found very satisfactory for practical use given the unpredictability of the soils. The interval of validity of the correlations is documented in Septarian Clay for tip resistances  $0.8 < q_c$  or  $q_{net} < 4$  MPa, meanwhile in Søvind Marl for  $1.2 < q_c$  or  $q_{net} < 10$  MPa.

The performances appear best with  $q_c$ , which may most likely be due to the additional associated uncertainties related to the data acquisition of the excess pore water pressure and the overburden pressure needed for the derivation of  $q_{net}$ .

The proposed correlations make it possible to transform CPTu-profiles in to  $E_{OED}$ -profiles for use in the preliminary analysis of deformations. More importantly, the correlations support the final derivation of  $E_{OED}$  for 3D finite element models once the results of all field and laboratory tests for the construction project are available.

The derived correlations complements corresponding Aarhus correlations between  $q_c$  or  $q_{net}$  and the drained triaxial unloading and reloading stiffness  $E_{ur}$  [4] and the maximum small-strain shear modulus  $G_0$  as well [5].

## REFERENCES

- [1] R. B. J. Brinkgreve and P. A. Vermeer: PLAXIS-Finite element code for soil and rock analysis, Plaxis 3D. Manuals, Delft University of Technology & Plaxis bv, The Netherlands, 2015.
- [2] M. H. Jacobsen: New oedometer and new triaxial apparatus for firm soils, The Danish Geotechnical Institute (Geo), bull. No. 27, Copenhagen, 1970.
- [3] T. Lunne, P. K. Robertson and J. J. M. Powell: Cone Penetration testing in geotechnical practice. Blackie academic & professional, 1997.  
<https://doi.org/10.1201/9781482295047>
- [4] N. Okkels, L. Bødker and T. Thorsen: Correlating  $q_{net}$  to  $E_{ur}$  of Paleogene clays of high plasticity. Proceedings of the XVIII ECSMGE, Lisbon, 2024.
- [5] E. Skouboe, N. Okkels, K. H. Lundvig: Correlating CPTu to  $G_0$  in high plasticity Paleogene clays. Proceedings of the XVIII ECSMGE, Lisbon, 2024.
- [6] L. Thøgersen: Effects of Experimental Techniques and Osmotic Pressure on the Measured Behaviour of Tertiary Expansive Clay. Ph.D. Thesis. Aalborg University, 2001.

# DATA ASSIMILATION IN A HYDROLOGICAL LANDSLIDE MODEL WITH ENSEMBLE KALMAN FILTER

**Amirahmad Vakilinezhad<sup>1</sup>, Signe Othelie Petrohai Pedersen<sup>2</sup>, Ivan Depina<sup>1</sup>**

## KEYWORDS

Data assimilation, Hydraulic parameters estimation, Ensemble Kalman Filter, Uncertainty reduction

## ABSTRACT

Landslides pose significant negative impact on people lives, infrastructures, society, and environment. To reduce the consequences of this natural hazard, spatial and temporal estimations of failure are essential. Yet substantial uncertainties are associated with these assessments. This study is motivated by the need to reduce the uncertainty in soil hydraulic parameters estimations for a better landslide susceptibility and hazard assessment. The research highlights the vital role of diminishing uncertainties in soil hydraulic parameters leading to better estimation of hydraulic conductivity, infiltration, pore pressure distribution and soil strength, therefore improved temporal and spatial slope instability forecasting. The study focuses on a case study in the proximity of Meråker in central Norway because of the complex morphology and geology of the area as well as the available instrumented slopes to measure the soil suction and volumetric water content throughout the year. By utilizing the high-resolution rainfall data from the weather stations in the area together with sensor data, a sequential uncertainty reduction of soil hydraulic properties was implemented with the Ensemble Kalman Filter Method (EnKF) and PLAXIS 2D software. A Python script is employed to implement EnKF and automated Plaxis numerical simulations to assimilate data from sensors and calibrate hydraulic parameters. Preliminary findings reveal considerable reduction in soil hydraulic properties uncertainty leading to improved performance of regional slope stability analysis and ultimately contribute to better geohazard management, effective mitigation strategies and fortifying the community resilience.

<sup>1</sup> Norwegian University of Science and Technology (NTNU)

<sup>2</sup> Geovita AS

## INTRODUCTION

Spatial and temporal prediction of water-induced landslides are crucial to protect people's lives and reduce the socioeconomical consequences through improved spatial planning, engineering protection measures, and early warning systems. In this regard understanding the soil hydraulic properties is the key factor to estimate the water infiltration, ground water condition, soil strength reduction and therefore slope stability. Despite of the importance of soil hydraulic parameters, due to the inherent spatial variability and costly and time consuming soil investigation measures it is common that the hydraulic parameters are associated with great uncertainties. In this paper, Ensemble Kalman Filter (EnKF) data assimilation method is employed together with Van Genuchten unsaturated infiltration theory using PLAXIS 2D to calibrate and update the soil hydraulic parameters continuously, leading to more precise estimation of uncertain hydraulic parameters. The EnKF assimilation of data and dynamic updating features make it exceptional tool for integration of real-time sensor data with conventional models such as Van Genuchten model to evaluate the ground water condition in response to rainfall. Moreover, employing novel data assimilation methods such as EnKF is first step to pave the road for further incorporation of innovative techniques in monitoring and early warning systems for water-induced landslides.

## METHOD

The study utilizes a finite element PLAXIS 2D model combined with EnKF data assimilation algorithm to calibrate the three uncertain soil hydraulic parameters namely Van Genuchten SWCC fitting parameters  $\alpha$ ,  $n$ , and saturated hydraulic conductivity  $K_s$ . The sensors in the study area record volumetric water content, suction and temperature. A slope similar to the instrumented slope is modeled in PLAXIS 2D and using the available geotechnical and hydrological data, infiltration analysis is performed by assuming a probability distribution for unknown hydraulic parameters  $\alpha$ ,  $n$  and  $K_s$ . The results of the PLAXIS 2D model is compared to the actual sensor data in the field and using the EnKF the initial assumptions are calibrated. After updating the parameters with 10 over the period of 9 days, the goals is to reduce uncertainty associated with initial guesses and obtain more accurate parameters probability distribution. Subsequently these hydraulic parameters can be used to perform a slope stability analysis and enhance the accuracy of the deployed early warning systems in the case study area.

### Instrumentation and study area

The instrumented area located along the Stjørdal river in Trøndelag, central Norway. Area covers almost 200 km<sup>2</sup> area and consist of complex geological formation according to Norway National Geological Survey (NGU) shown in

Figure 1. Two locations in the area are chosen to be instrumented with sensors shown in Figure 1.

At each spot, sensors are located at two proximate locations and three depths in Figure 2. This study focuses on sensor data from “Location 2” in Figure 1, where the soil Volumetric Water Content (VWC) has been measured at depths of 0.3, 0.5 and 0.9 m from the

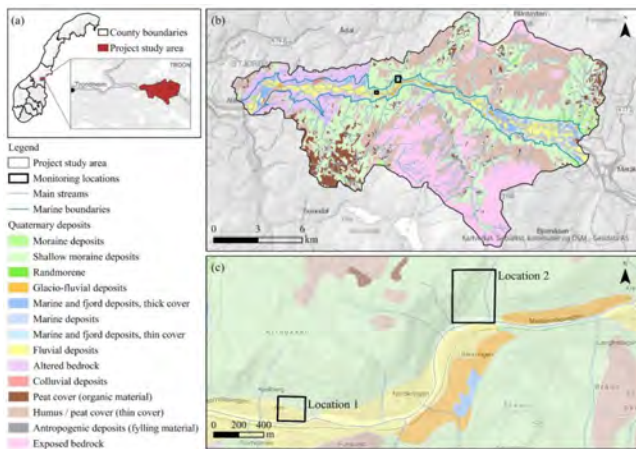


Figure 36. (a) Study area, (b) Geological formation of the area, (c) Two selected monitoring locations. [1]

ground surface, and is accessible in 15-minute resolution. A weather station to measure the daily rainfall also planted at the area.

Annual rainfall of 964 mm to 1205 mm [2] has been registered in the case study area. Soil conditions are characteristic for steep areas with inclination greater than 25 degrees and shallow dept to bedrock with soil thickness varying between 0.5 m to 10 m above the bedrock [1]. Geotechnical soil properties are presented in [1] after literature review and sets of laboratory tests from the soil samples. Soil friction angle and cohesion are measured as  $38^\circ$  and 5.5 kPa respectively and the soil is classified as silty sand. This characteristic for moraine, which is a well-graded soil type consisting of silt, sand, and gravel.

### Ensemble Kalman Filter (EnKF)

The main objective of data assimilation is to successively adjust the state of knowledge about unknown parameter distribution based on the initial assumed distribution, model predictions, and incoming measured state or parameter. Kalman Filter (KF) is one of the well-known data assimilation systems, optimizing the accuracy of the system by processing and adjusting the unknown parameters [3]. Ensemble Kalman Filter (EnKF) is the extension of KF, applicable in processing nonlinear systems by employing the set of samples of unknown parameters known as ensembles to approximate the state or parameter's distribution and therefore optimizing the accuracy of the model [4].

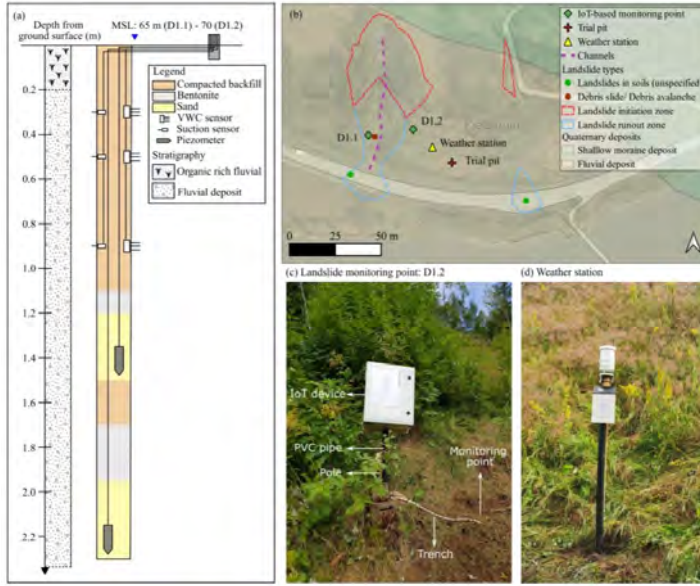


Figure 37. Study area [1] (a) Soil layering and sensor locations, (b) Two sensors, weather station and trial pit locations, (c) Monitoring point and (d) weather station

Comprehensive notation and formulation of the EnKF is provided in [5]. Following the same notation, EnKF is formulated and incorporated in this study.

Let us define the output of a model that aims to capture the considered phenomenon (e.g., rainfall infiltration) as  $g(\mathbf{z})$ . The input to the model,  $\mathbf{z}$ , is a matrix that combines model state (estimation),  $\mathbf{x}$ , and the unknown model parameters (forward calculation input),  $\boldsymbol{\theta}$

$$\mathbf{y} = g(\mathbf{z}) \quad Eq(1)$$

$$\mathbf{z} = [\mathbf{x}, \boldsymbol{\theta}]^T \quad Eq(2)$$

Measurement matrix  $\mathbf{d}$  is defined as observation of the model output  $\mathbf{y}$  with the addition of a measurement error  $\mathbf{e}$ .

$$\mathbf{d} = \mathbf{y} + \mathbf{e} \quad Eq(3)$$

In order to get the close to reality estimations the posterior likelihood of the model parameters given the observations,  $f(\mathbf{z} | \mathbf{d})$ , is maximized, and this can be done by minimizing the cost function [5].

$$J(\mathbf{z}) = (\mathbf{z} - \mathbf{z}^f)^T \mathbf{C}_{zz}^{-1} (\mathbf{z} - \mathbf{z}^f) + (g(\mathbf{z}) - \mathbf{d})^T \mathbf{C}_{dd}^{-1} (g(\mathbf{z}) - \mathbf{d}) \quad Eq(4)$$

$\mathbf{C}_{zz}$ ,  $\mathbf{z}^f$  and  $\mathbf{C}_{dd}$  represent error covariance of  $\mathbf{z}$ , previous estimation of model parameters and error covariance of measurements respectively. The state-parameter vector is updated by maximizing the posterior likelihood [5] as follows:



$$\mathbf{z}^a = \mathbf{z}^f + \mathbf{K}(\mathbf{d} - g(\mathbf{z})) \quad Eq(5)$$

$$\mathbf{C}_{zz}^a = (\mathbf{I} - \mathbf{K}\mathbf{G})\mathbf{C}_{zz} \quad Eq(6)$$

The “a” superscript represents the new estimation. New parameter estimation and error covariance estimation can be obtained through equation 5 and 6 using previous estimation and  $\mathbf{K}$  matrix which is known as “Kalman gain”.

$$\mathbf{K} = \mathbf{C}_{zz}\mathbf{G}(\mathbf{G}\mathbf{C}_{zz}\mathbf{G}^T - \mathbf{C}_{zz})^{-1} \quad Eq(7)$$

For each ensemble the equations can be written:

$$z_i^a = z_i^f + \mathbf{K}^e(\mathbf{d}_i - g(z_i^f)) \quad Eq(8)$$

$$\mathbf{K}^e = \mathbf{C}_{zz}^e\mathbf{G}(\mathbf{G}\mathbf{C}_{zz}^e\mathbf{G}^T - \mathbf{C}_{dd})^{-1} \quad Eq(9)$$

$\mathbf{d}_i = \mathbf{d} + \boldsymbol{\varepsilon}_i$  and  $\mathbf{C}_{zz}^e$  are the measurement matrix with noise and combined covariance matrix respectively.  $\mathbf{C}_{zz}^e$  is calculated using equations 10, 11 and 12 by first finding ensemble members mean and differentiating each ensemble member from the mean value.

$$\overline{\mathbf{z}_t^f} = \mathbf{z}_t^f \mathbf{I}_{Ne} \quad Eq(10)$$

$$\mathbf{z}_f' = \mathbf{z}_f^T - \overline{\mathbf{z}_t^f} \quad Eq(11)$$

$$\mathbf{C}_{zz}^e = \frac{\mathbf{z}_f'(\mathbf{z}_f')^T}{Ne - 1} \quad Eq(12)$$

The measurement matrix is defined as  $\mathbf{D}$  and it is integrated in the main updating function as shown in equation 14.

$$\mathbf{D}_t = (\mathbf{d}_{1,t}, \mathbf{d}_{2,t}, \mathbf{d}_{3,t}, \dots, \mathbf{d}_{Ne,t}) \quad Eq(13)$$

$$\mathbf{z}_t^a = \mathbf{z}_t^f + \mathbf{C}_{zz}^e\mathbf{G}^T(\mathbf{G}\mathbf{C}_{zz}^e\mathbf{G}^T + \mathbf{C}_{dd})^{-1}(\mathbf{D}_t - \mathbf{G}\mathbf{z}_t^f) \quad Eq(14)$$

In this study, 3 soil hydraulic parameters  $\alpha$ ,  $n$  and  $K_s$ , initially characterized by broad probability distribution are selected to be calibrated.  $Ne = 20$  random samples from the distributions are attained and 20 analyses are performed to obtain ensemble of result, which consists of soil VWC predictions at measurement locations. The estimations are updated by incorporating the measurements from sensors data with 0.02 error. This process is repeated for  $N_m = 9$  days and at each day the analysis started with updated parameter probability distribution. Ideally, outputs of analyses should be converging the real sensor data from the field after iterations.

## FINITE ELEMENT PLAXIS 2D MODEL

Python scripting is used to automate the PLAXIS 2D analysis. With 20 random estimations for three parameters the analysis should be performed 20 times for each day. 9 days of data are processed to be used in this study, resulting in total 180 PLAXIS 2D analyses, which would be time consuming to perform manually.

The FEM model begins with defining the geometry and boundary conditions. The geometry of the model is illustrated in Figure 3 where a 35° slope is created with 1.5 m depth to impermeable layer following the available information from trial pits in the field. Soil material is specified following the values presented by [1]. Three unknown parameters  $\alpha$ ,  $n$  and  $K_s$  are defined as a function to be updated at each iteration in the model.

Similar to the sensor locations at 0.3, 0.5 and 0.9 m from the surface, three closest nodes on the mesh at the same depths are chosen to obtain the volumetric water content after each analysis and compared to sensor values. The probability distribution function is updated and subsequently 20 new random samples of unknown parameters are generated to run the model.

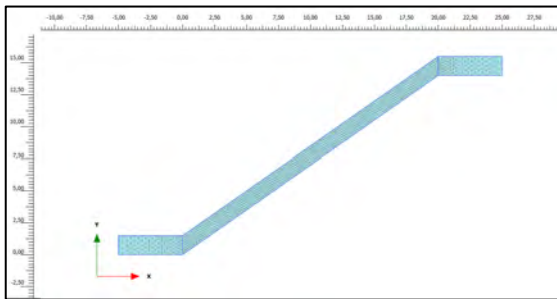


Figure 38. PLAXIS 2D model geometry

## RESULTS AND DISCUSSIONS

Prior and posterior parameters estimations are presented in Table 1. After 9 iterations, the posterior parameters are obtained. It is expected that the output of the FEM analysis resulted from posterior distributions would be getting closer to the sensor data if the model is able to capture the rainfall infiltration process. In Figure 4(a) the VWC recorded from sensors and simulation are shown by the blue line and black crosses respectively. At all depth the initial estimations result in wide range of VWC that converges after a couple of iterations although at the beginning they are far from the real values. At 0.3 m the simulation results are capturing the VWC change after six days. At the 0.5 m depth similarly the simulation results are getting closer to sensor data after six days iteration. However, at 0.9 m depth the predicted VWC is not in good agree-

ment with the measured values. This can be due to the bias in the model, resulting from soil hydrological properties variability at deeper points and inaccurate implementation of initial and boundary conditions in our model.

Figure 4(b) shows the hydraulic parameters estimations. The mean value is shown by blue line and orange dash lines show the one standard deviation from the mean. Saturated hydraulic conductivity shows acceptable convergence and reach to an almost steady number with a small deviation from the mean in 9 days.  $\alpha$  parameter distribution hasn't changes significantly after 9 iterations, however, the model is not dramatically sensitive to  $\alpha$  parameter since at shallower depth, the model shows acceptable performance and captures the actual VWC values although the  $\alpha$  parameter wasn't estimated well.

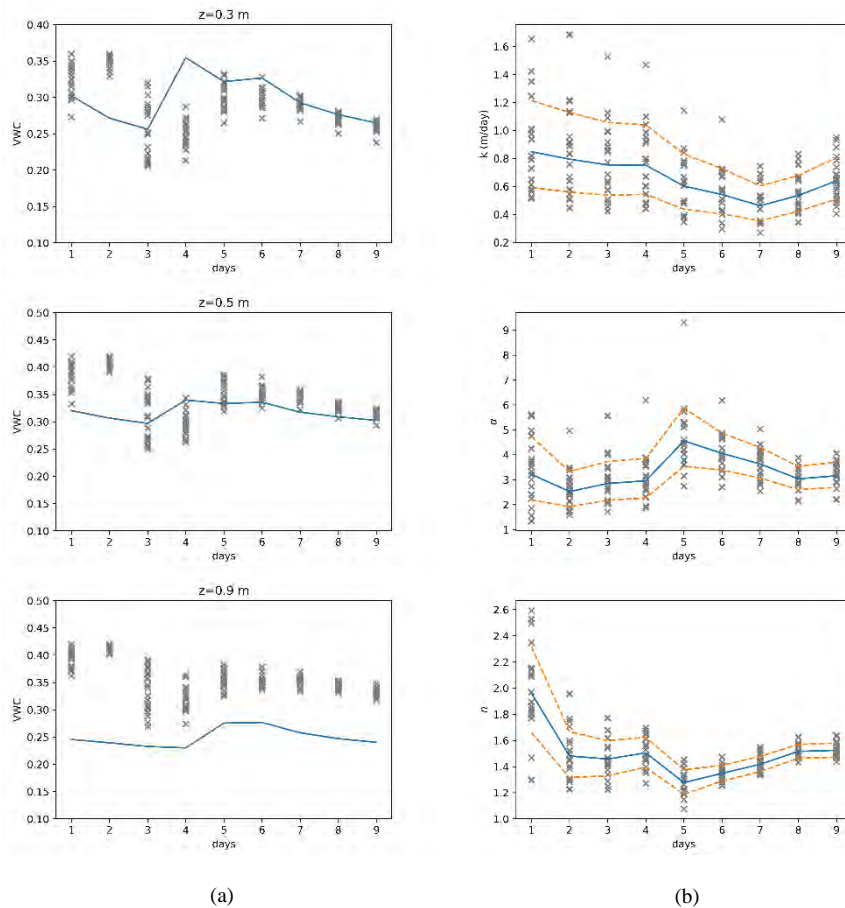


Figure 39. (a) Sensor data and simulation results of VWC at 0.3, 0.5 and 0.9 m. (b) initial  $k_{sat}$ ,  $\alpha$  and  $n$  parameter estimation and distributions in 9 days

Table 15. Mean and standard deviation of the unknown parameters before and after EnKF

Prior Values						Posterior Values					
$\mu_\alpha$	$\sigma_\alpha$	$\mu_n$	$\sigma_n$	$\mu_{Ks}$	$\sigma_{Ks}$	$\mu_\alpha$	$\sigma_\alpha$	$\mu_n$	$\sigma_n$	$\mu_{Ks}$	$\sigma_{Ks}$
4.0	2.0	2.0	0.5	1.0	0.5	3.19	0.49	1.52	0.05	0.65	0.15

On the other hand, the  $n$  parameter deviation from the mean is getting smaller after each iteration and shows acceptable convergence in 9 days.

## CONCLUSIONS

Concluding the study, it is evident that the EnKF can be employed to automate calibration of numerical models with real-time data. In all scenarios the EnKF effectively reduced the uncertainty in initial estimated parameters. Moreover, efficiency of EnKF is showed at 0.3 m and 0.5 m depth where estimations and sensor values converged precisely. Although the results at 0.9 m depth are not as close as our expectations, these issues can be addressed by improving the model capability such as modelling layered soil that can capture the variation in hydraulic parameters, and improve modelling of boundary conditions, accounting for evapotranspiration, and increasing the number or frequency of sensor data.

## REFERENCES

- [1] E. A. Oguz, I. Depina, B. Myhre, G. Devoli, H. Rustad, and V. Thakur, "IoT-based hydrological monitoring of water-induced landslides: a case study in central Norway," *Bull. Eng. Geol. Environ.*, vol. 81, no. 5, 2022, doi: 10.1007/s10064-022-02721-z.
- [2] C. G. Leiva and S. Mechanics, "Report Susceptibility assessment of rainfall," 2019.
- [3] R. E. Kalman, "A New Approach to Linear Filtering and Prediction Problems," *J. Basic Eng.*, vol. 82, no. 1, pp. 35–45, Mar. 1960, doi: 10.1115/1.3662552.
- [4] G. Evensen, "Sequential data assimilation with a nonlinear quasi-geostrophic model using Monte Carlo methods to forecast error statistics," *Journal of Geophysical Research*, vol. 99, no. C5, 1994. doi: 10.1029/94jc00572.
- [5] M. Mohsan, P. J. Vardon, and F. C. Vossepoel, "On the use of different constitutive models in data assimilation for slope stability," *Comput. Geotech.*, vol. 138, no. March, p. 104332, 2021, doi: 10.1016/j.compgeo.2021.104332.

# DESIGN METHODS FOR SHORT SLENDER STEEL PILES IN CLAY

**J. Stener<sup>1</sup>, D. Ebenhardt<sup>2</sup>, A.B. Lundberg<sup>3</sup> and S. Larsson<sup>4</sup>**

## KEYWORDS

Piles, pile buckling, steel pile design, clay, design method.

## ABSTRACT

Slender steel piles in clay, which are driven or drilled to a firm soil stratum, are frequently used in Nordic soil conditions. The design is normally carried out with an analytical calculation model in which the soil response is included as an equivalent spring stiffness for a beam in an elastic medium. However, the natural alterations in the level of the bedrock frequently result in pile group configurations in which some of the piles are shorter than the elastic buckling length. The theoretical base of the pile buckling method is consequently not fulfilled. In this paper, the standard buckling method and the steel column method according to Eurocode are compared to a finite element model of the pile in the soil. The results show that quite different bearing capacities can be calculated, and some recommendations for practical design are given.

## INTRODUCTION

The soil strata in most of the Nordic countries is characterized by the geological processes during the Weichsel ice age, resulting in soft Holocene sediments deposited on the very hard Precambrian bedrock [1]. In Figure 1, a typical soil profile from South-East of Sweden is illustrated, consisting of fill, dry crust, clay, silt and moraine. The clay layer is frequently very soft with an undrained shear strength,  $c_u$ , between 5 - 20 kPa, while the Precambrian rock is very hard with an unconfined compression strength of 150 - 250 MPa. For such a soil profile, piles are drilled or driven into the bedrock and transfer the pile load as a column.

<sup>1</sup> KFS AnläggningsKonstruktörer AB, Solna, Sweden

<sup>2</sup> AFRY AB, Solna, Sweden

<sup>3</sup> ELU Konsult AB, KTH, Stockholm, Sweden

<sup>4</sup> KTH, Stockholm, Sweden

The geotechnical bearing capacity,  $N_{\text{Rd.GEO}}$ , is frequently verified by dynamic pile load tests, allowing a very high utilization of the steel material [2]. The structural design resistance of the pile,  $N_{\text{Rd.STR}}$ , is often calculated by an analytical model in which the soil support is modelled as an equivalent spring stiffness with displacement included softening [3]. The calculation model yields similar results as the full numerical models as studied in [4] and [5]. However, the analytical model developed in [3] considers the buckling of a pile segment equivalent to the elastic buckling length,  $l_{\text{cr.s}}$ . The changes in the depth of the soil frequently results in that many of the piles have a length,  $l$ , which is shorter than  $l_{\text{cr.s}}$  calculated from the  $c_u$  of the clay. This raises the question of how  $N_{\text{Rd.STR}}$  should be calculated. There are essentially three options:

- The pile is assumed to have a length,  $l$ , which exceeds the elastic buckling length,  $l_{\text{cr.s}}$ , and the calculation model in [3] is valid.
- The pile is considered as a column without any support and the calculation model for the specified material is valid, e.g. Eurocode 3 for steel piles [6]
- A full numerical model of the pile and soil is used.

The different options have advantages and disadvantages. The calculation model in [3] is used in practice and the soil parameters can be found from site investigation tests [1]. The calculation model for free columns is found in the literature [6] but is most probably too conservative. The full numerical model of the interaction between the soil and the structure is cumbersome for the practical use.

A comparison of the calculation models has been developed in [7] and is described herein. Initially the methodology is developed, followed by calculation results and conclusions.

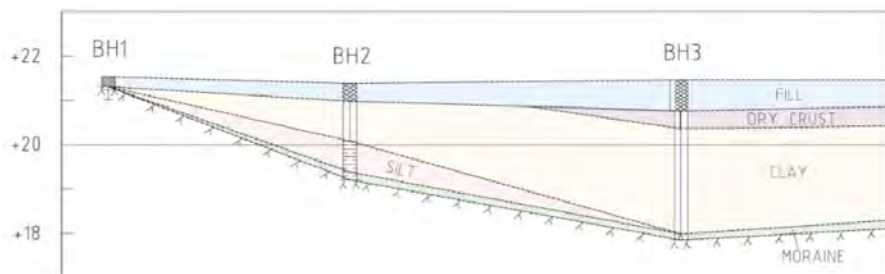


Figure 40. A typical soil profile in the South-East of Sweden, consisting of fill, dry crust, clay, silt and moraine deposited on bedrock.

## METHODOLOGY

A parameter investigation was conducted to compare the assessed  $N_{Rd,STR}$  (minimum value of the critical buckling load,  $N_{cr}$ , and the cross-sectional resistance,  $N_{Rd}$ ) between the two analytical models [3], [6] and the numerical model. The axially loaded pile that was studied was a 4 m long circular steel pipe pile characterized by a diameter,  $d$ , ranging from 110 mm to 220 mm. The pile was presumed to be embedded within a stratum of uniform clay exhibiting a variable  $c_u$  between 4 to 40 kPa. Initial deflection of the pile, denoted as  $\delta_0$ , was assigned according to the guidelines outlined by the Commission of Pile Research in Sweden [9] accounting for initial imperfections, residual stresses and pile driving. In both the model according to reference [3] and the full numerical model,  $\delta_0$  was implemented in accordance with its specifications as outlined in Table 1, alongside the additional material parameters employed in reference [7]. Since  $\delta_0$  is dependent on  $l_{cr,s}$ , it varied when different clays and diameters were considered. To consider the effect of  $\delta_0$  in the model from [6], buckling curves are used which reduces the design resistance of the pile. However, a notable limitation is that the magnitude of  $\delta_0$  cannot be controlled as it is already incorporated in the buckling curves, emanating from experimental studies of steel elements in [8]. In this study, buckling curve d was used for the calculations.

Table 1. Input parameters

Parameter	Range of Values
Thickness, $t$	10 mm
Length, $l$	4 m
Undrained shear strength, $c_u$	4, 6, 8, 10, 12, 15, 20, 30, 40 kPa
Diameter, $d$	110, 140, 170, 220 mm
Initial deflection, $\delta_0$	$2 * \frac{l_{cr,s}}{600} + 0.013 * l_{cr,s}$ [mm]
Modulus of elasticity, $E$	189* GPa
Poisson's ratio, $\nu$	0.3 [-]
Yield stress, $f_y$	460 MPa
Ultimate strength, $f_u$	540 MPa

\* 210GPa x 0.9 = 189 GPa [9]

The finite element software ABAQUS 6.21-1 [10] was used for modelling the pile and Winkler springs were used to represent the clay in the full numerical model. These springs were defined as ideal-elastic-plastic to account for the nonlinear behavior of the soil, which is the same procedure as described in [3].

Eigenvalue buckling analysis combined with Riks method were used in the finite element analysis since this combination of methods considers the plasticity and second order effects in the pile. In order to make sure that the model was representative, a simulation without springs was executed and compared to a classical Euler case, in which the pile is defined as a beam with pinned supports. The difference in terms of  $N_{cr}$  was 1.3%, hence the model gave a good representation of the free beam considering the elastic stability of the structure. A convergence analysis was also performed to decide the distance between the Winkler springs as well as the size and type of mesh.

As the prerequisites in terms of  $\delta_0$  varies between the Eurocode 3 model [6] and the other two studied models, an alternative model was developed in [7]. This model, referred to as the EC3 equivalent model in [7], was a variation of the model in [6] where the reduction from the buckling curves were manipulated in order to replicate initial deflections according to the Commission of Pile Research in Sweden [9]. In this way a more realistic initial deflection of the pile was considered rather than considering an initial deflection used for a steel element.

## RESULTS AND DISCUSSION

Figure 2 and Figure 3 illustrate the variation of the design resistance, denoted as  $N_{Rd,STR}$ , in relation to  $l_{cr,s}$  for the three computational methodologies investigated. The outcomes for the four slender pile diameters are illustrated in the graphical representations, wherein solely  $c_u$  is subjected to variation, thereby influencing  $l_{cr,s}$ . The x-axis is normalized to facilitate the identification of scenarios where the theory, as outlined in reference [3], is considered appropriate for implementation.



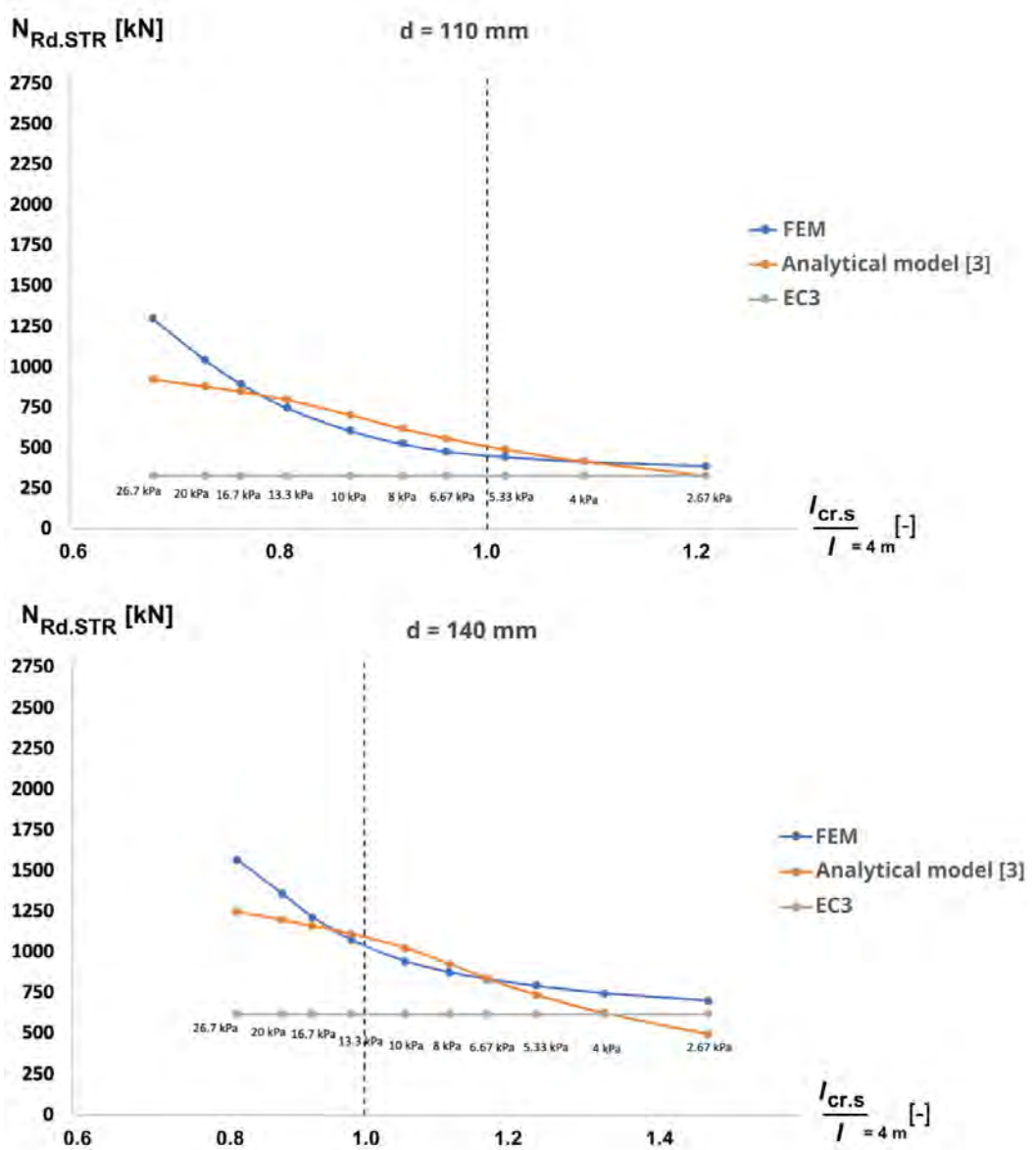


Figure 41. Evaluated design resistance compared to the ratio between the elastic buckling length,  $l_{cr,s}$ , and the physical length of the pile,  $l$ , for test cases where  $d =$

110/140 mm.

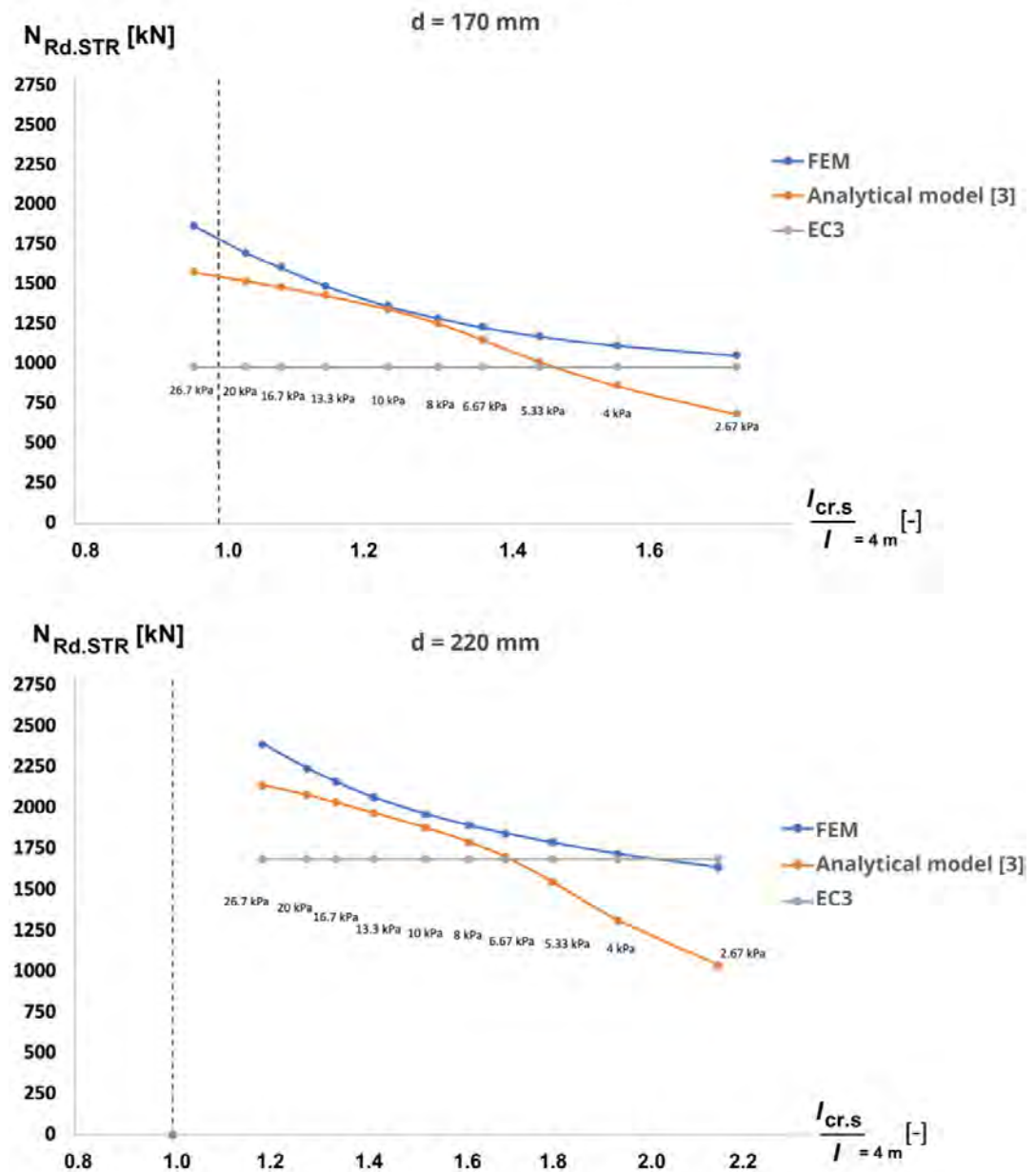


Figure 42. Evaluated design resistance compared to the ratio between the elastic buckling length,  $l_{cr,s}$ , and the physical length of the pile,  $l$ , for test cases where  $d = 170/220$  mm.

Overall, the design resistance,  $N_{Rd,STR}$ , of the different models illustrated in Figure 2 and Figure 3 exhibit expected results. The numerical model, which mirrors the prerequisites of the analytical model in [3], yields  $N_{Rd,STR}$  similar to those of the analytical model. The Eurocode 3 model for steel piles yields lower  $N_{Rd,STR}$  compared to others, as it treats the pile as a freestanding column without the confining pressure exerted by the surrounding soil. Based on the presented diagrams, it is evident that with a pile length of 4 m,  $l_{cr,s}$  frequently exceeds  $l$  given the input parameters. Consequently, the pile design is assumed to be based on an alternative method. The adoption of a comprehensive numerical model in the practical design of a pile is often economically disadvantageous, while analytical alternatives remain as available choices for the designer.

Given an appropriate representation of the pile behavior in the numerical model presented in [7], it becomes evident that  $N_{Rd,STR}$  as per reference [3] yields non-conservative outcomes in certain examined cases. This is observed within intervals where the analytical model [3] is considered both valid and invalid for application. It is notable that this phenomenon seems to be limited to slender piles ( $d < 140$  mm) in clay soils with  $c_u$  below approximately 15 kPa. However, examining the bearing capacity of the numerical model in isolation ( $\frac{l_{cr,s}}{l} > 1$ ) may not yield accurate design resistances. This is because, as discussed in [9], it is stated that: *"If the determination of the actual initial curvature is conducted on a section that deviates from the theoretical buckling length, a conversion to the buckling length must be performed."* A method for conducting this conversion is not provided, and selecting the actual pile length,  $l$ , may not be appropriate as  $l_{cr,s}$  is determined based on both  $c_u$  and the cross-sectional properties. However, the numerical approach can be utilized for comparison with the analytical model outlined in [3] since the preconditions are identical.

By studying Figure 2 and Figure 3 it is evident that the calculation model incorporating a steel pile according to Eurocode 3 in some cases results in design resistances exceeding those obtained from the analytical and numerical models that consider a confining pressure along the pile. This discrepancy prompts further investigation of the models and their preconditions. Given the nonfulfillment of the prerequisite conditions for the analytical method as outlined in reference [3], this may serve as a plausible explanation for the observed discrepancy. In Figure 2 and Figure 3 it is observed from ratios of 1.2 and above. By studying scenarios involving larger pile diameters, the model in accordance with Eurocode 3 also appears to yield design resistances that exceed those generated by the numerical model considering a confining pressure. Through an examination of the foundational assumptions inherent in both methodologies, it becomes apparent that they address imperfections in different ways. Both the analytical model in [3] and the numerical model treat pile imperfections similarly, expressing the initial deflection of the element as a function of the elastic buckling length,  $l_{cr,s}$ . Furthermore, residual stresses are addressed within these models by adding an increase of the initial deflection (which is also dependent

on  $l_{cr,s}$ ) and by reducing the Young's Modulus,  $E$ . However, in the model according to Eurocode 3 these aspects cannot be addressed in the same manner as imperfections are integrated into the buckling curves, which are derived from empirical experiments in [8]. In [8], it is evident that the  $\delta_0$  taken into account during the formulation of the buckling curves outlined in Eurocode 3 is the element length divided by 1000 ( $\frac{l}{1000}$ ), equating to 4 mm in the present context. Conversely, when utilizing the analytical model described in [3] accounting for initial imperfections, residual stresses and pile driving, this value ranges from 13 to 39 mm. Nevertheless, according to the chapter of piles (EN 1993-5), the recommendation is to employ buckling curve d to accommodate the effect of pile-driving, thereby addressing imperfections up to  $\frac{l}{200}$ . This leads to a decrease in  $N_{Rd,STR}$  due to the significant reduction in the chi-factor  $\chi$ . However, it appears that this approach does not adequately consider piles situated in conditions of very soft clay characterized by  $c_u$  falling below 10 kPa.

In reference [7], Stener and Ebenhardt introduce an alternative semi-analytical approach designed to incorporate initial deflection, residual stresses and effects of pile driving into buckling curves. The method uses the numerical model, which has proven to accurately replicate the buckling curves of Eurocode, thereby enabling the formulation of new buckling curves that account for all imperfections specified in reference [9]. Subsequently, in Figure 4 and Figure 5, the design resistances obtained through the semi-analytical method are integrated into the previously presented graphs in Figure 2 and Figure 3.

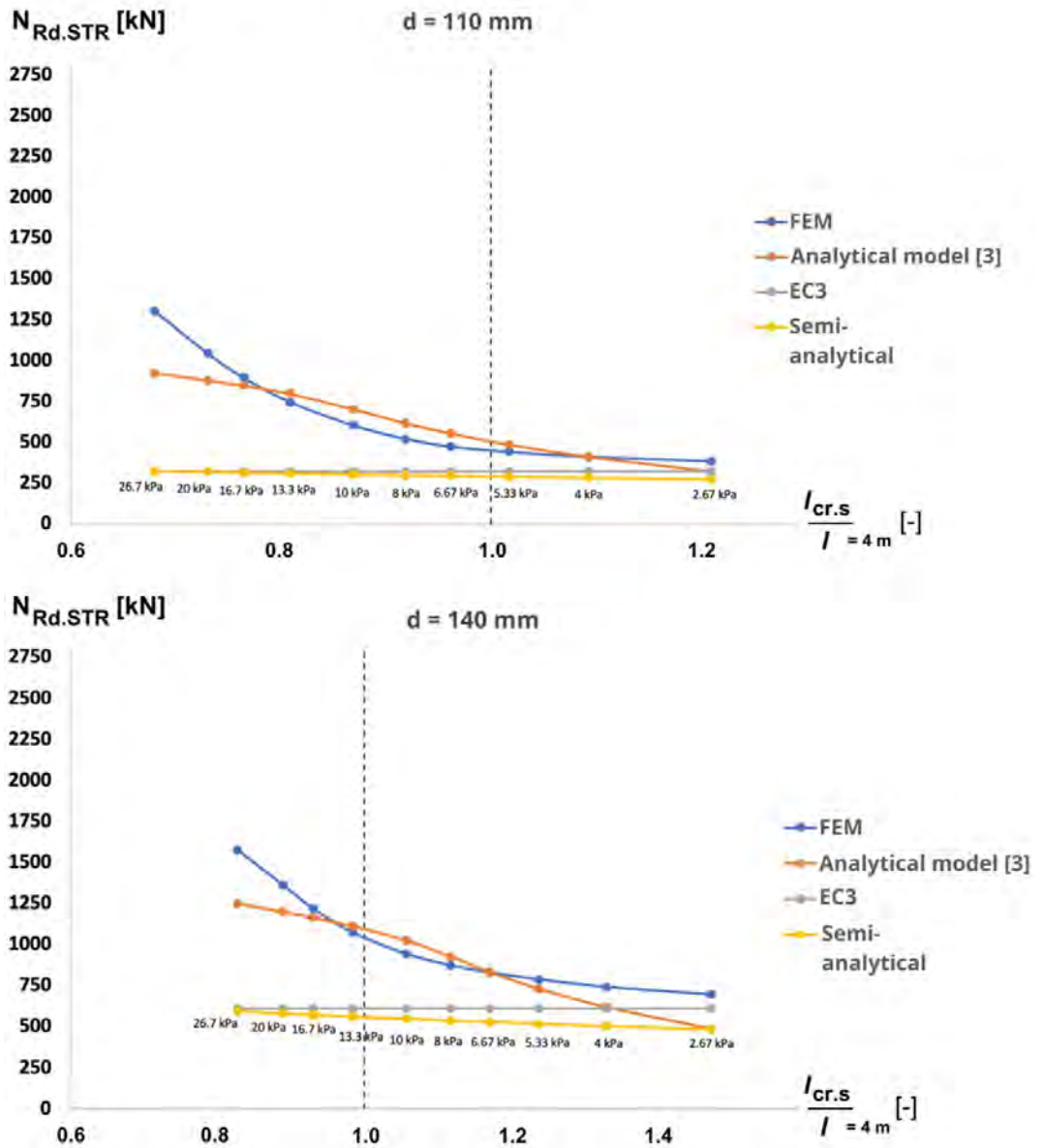


Figure 43. Evaluated design resistance compared to the ratio between the elastic buckling length,  $l_{cr,s}$ , and the physical length of the pile,  $l$ , for test cases where  $d =$

110/140 mm. Semi-analytical represents the model developed in [7].

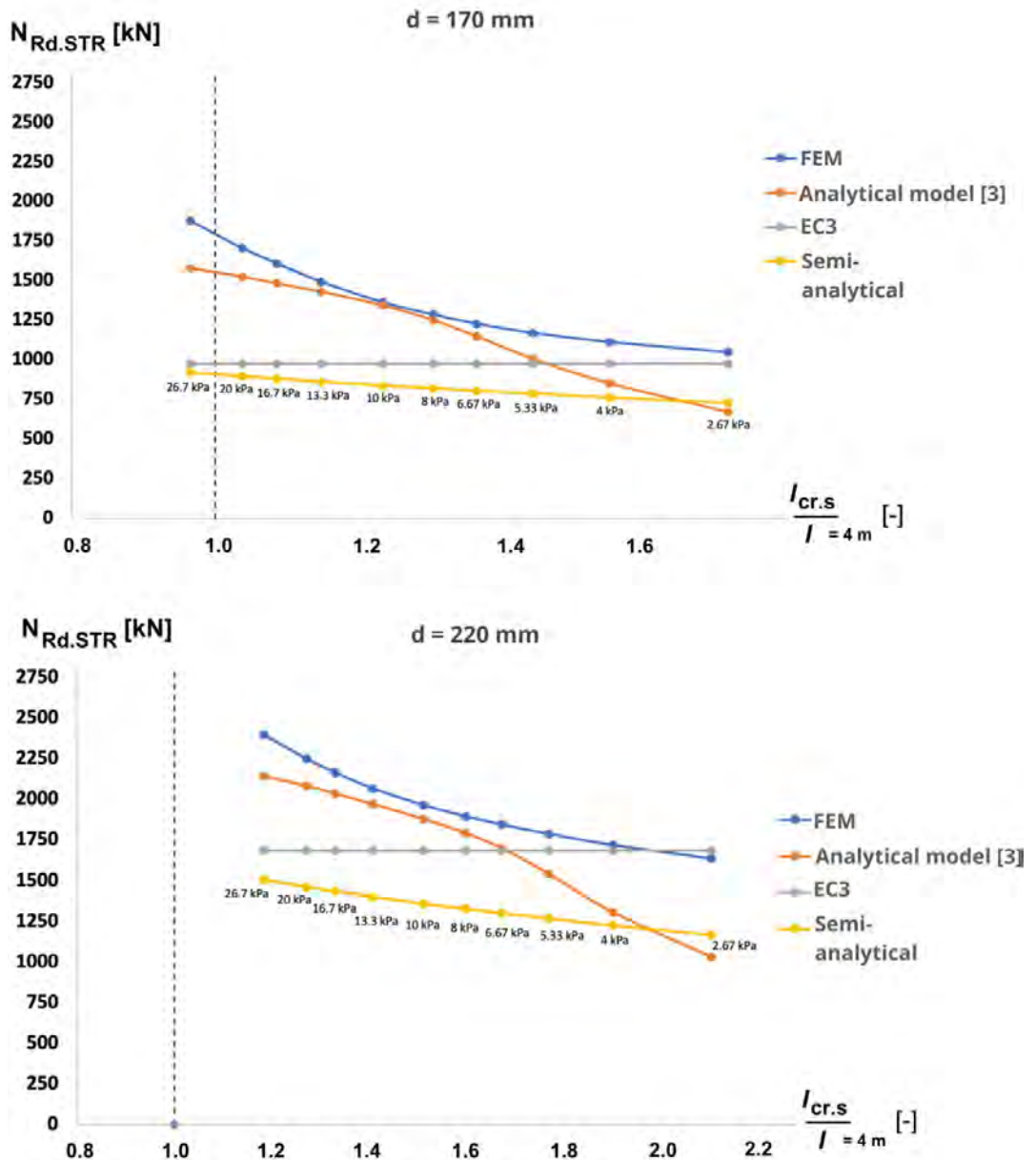


Figure 44. Evaluated design resistance compared to the ratio between the elastic buckling length,  $l_{cr,s}$ , and the physical length of the pile,  $l$ , for test cases where  $d = 170/220$  mm. Semi-analytical represents the model developed in [7].

As expected,  $N_{Rd,STR}$  decline in comparison to those obtained by the Eurocode 3 model when employing the semi-analytical approach, as demonstrated in Figure 4 and Figure 5. The illustrated curves consistently demonstrate a decrease in  $N_{Rd,STR}$  with the increase of pile imperfections,  $\delta_0$ . In other words, based on Figure 4 and Figure 5 one can notice that the use of realistic pile imperfections is essential when determining the design resistance of a pile. Through the examination of cases in which the ratio  $\frac{l_{cr,s}}{l}$  closely approaches 1, a reasonable assessment of the initial deflection of a 4 m pile is undertaken. Notably, the length over which the pile is presumed to buckle coincides with the actual length of the pile. In Figure 6 and Figure 7, two cases where this occurs are presented, with initial deflections of 19 mm in both cases.

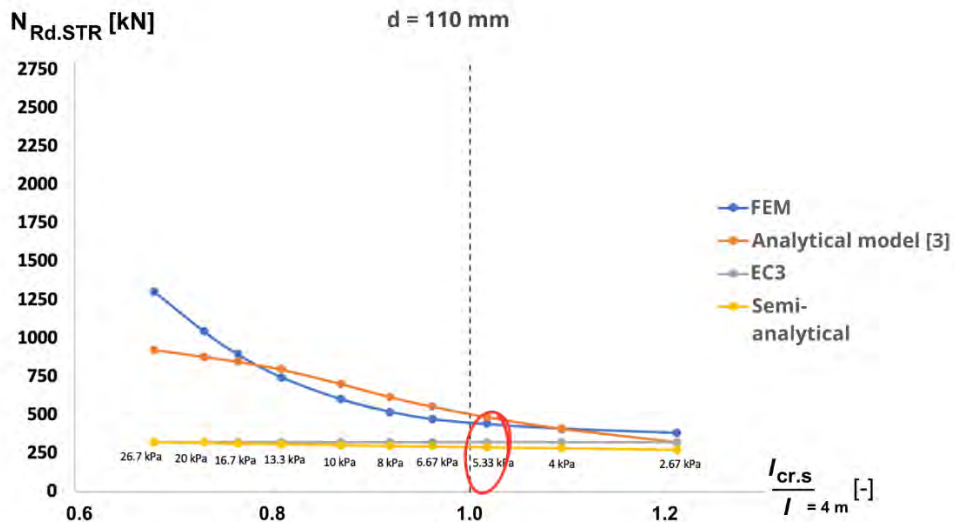


Figure 45. Evaluated design resistance compared to the ratio between the elastic buckling length,  $l_{cr,s}$ , and the physical length of the pile,  $l$ , for the test case considering a diameter of 110 mm. Highlighted case where the initial deflection is equal to 19 mm.

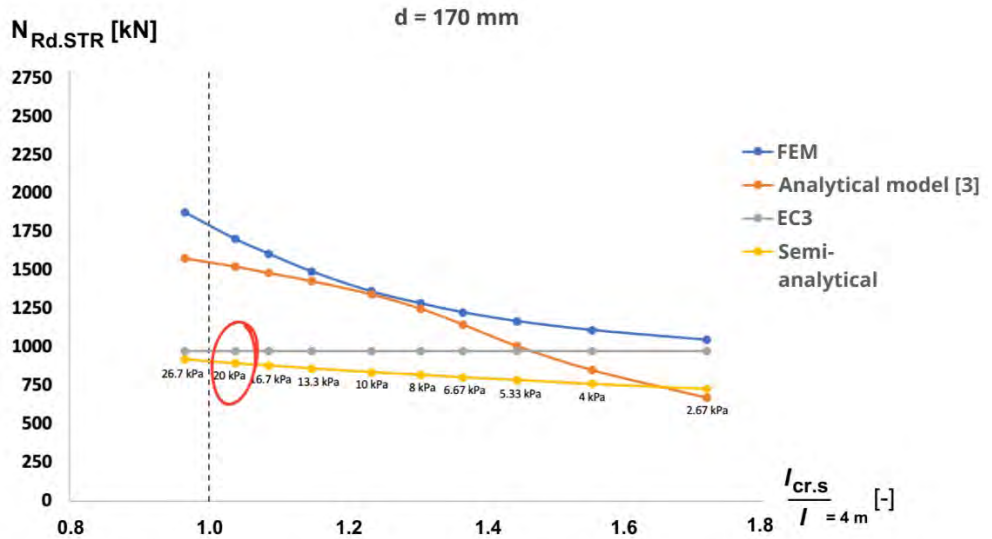


Figure 46. Evaluated design resistance compared to the ratio between the elastic buckling length,  $l_{cr,s}$ , and the physical length of the pile,  $l$ , for the test case considering a diameter of 170 mm. Highlighted case where the initial deflection is equal to 19 mm.

Based on the information presented above, it is evident that the Eurocode 3 model may not accurately account for all pile imperfections with sufficient precision solely by selecting buckling curve d, as stipulated in the code. In such instances, the design resistance,  $N_{Rd,STR}$ , can be overestimated by the designer of the pile.

## CONCLUSIONS

The following conclusions can be stated from this study.

- The analytical model presented in [3] tends to be conservative in the majority of the investigated cases, even when the pile's length,  $l$ , is shorter than the elastic buckling threshold,  $l_{cr,s}$ .
- Modelling a pile as a freestanding column according to Eurocode 3 may underestimate the effect of imperfections, potentially leading to a non-conservative design of the pile.
- Utilizing a numerical model for pile design when the pile's length,  $l$ , is shorter than the elastic buckling length,  $l_{cr,s}$ , is deemed impractical from both a time requirement and economic perspective.



- In practice it is often observed that the same pile diameters are utilized for both shorter and longer piles, resulting in a naturally lower utilization ratio for the former.

## REFERENCES

- [1] Bergdahl, U., Larsson, R., & Viberg, L. *Ground investigations and parameter assessment for different geological deposits in Sweden*. Situ Characterization of Soils. KR Saxena and VM Sharma, ed., AA Balkema Publishers, 119-170. 2003
- [2] Rausche, F. PDA Testing: 2008 State of the art. In *The Application of Stress-wave Theory to Piles: Science, Technology and Practice. Proceedings of the 8th International Conference on the Application of Stress-Wave Theory to Piles*. Lisbon, Portugal 2008.
- [3] Wennerstrand, J & Fredriksson, J. Capacity of slender steel piles. In *International conference on piling and deep foundations*, pp. 371-374. 1989.
- [4] Bhattacharya, S., Carrington, T. M., & Aldridge, T. R. Buckling considerations in pile design. In *Proceedings of the international symposium on frontiers in offshore geotechnics*, pp. 815-821. 2005.
- [5] Reddy, A. S., & Valsangkar, A. J. Buckling of fully and partially embedded piles. *Journal of the Soil Mechanics and Foundations Division*, 96(6), pp. 1951-1965. 1970.
- [6] Lennon, T. *Designers' guide to EN 1991-1-2, 1992-1-2, 1993-1-2 and 1994-1-2: handbook for the fire design of steel, composite and concrete structures to the Eurocodes*. Thomas Telford. 2007.
- [7] Ebenhardt, D & Stener, J. Buckling of Short End-Bearing Piles in Clay. MSc thesis, KTH Royal institute of Technology. 2022.
- [8] Simoes da Silva, L., Simoes, R. & Gervásio, H., Design of steel structures. 1<sup>st</sup> edition ed. Multicomp Lda, Mem Martins, Portugal: ECCS – European Conventino for Constructional Steelwork, 2010.
- [9] Blomdahl, T. et al ., 1995. Beräkning av dimensionerande lastkapacitet för slagna pålar med hänsyn till pålmaterial och omgivande jord. Rapport 84a, Pålkommissionen, Linköping, 1995.
- [10] Dassault Systemes. *ABAQUS 6.14 Documentation-Theory Guide*, Providence, RI. 2015.

# DESIGN OF 15 METER HIGH RAILWAY EMBANKMENT ON LOOSE SILT AND CLAY

**Ibrahim Rashid<sup>1</sup>, Fredrik Clifford<sup>2</sup>**

## KEYWORDS

Ground Improvement methods, FEM modelling, transport infrastructure, railway embankment, observational method, pre-consolidation, preloading, vertical drains

## ABSTRACT

To construct a 15-meter-high railway embankment through pre-consolidation using vertical drain with surcharge on settlement-prone silty clay is rare in Sweden. This poses significant challenges in terms of foundation design, assessment of preloading time, as well as production and environmental considerations.

A combination of analytical and FEM modelling in 2D and 3D has been carried out to assess strength growth in soil and predict settlement development. The FEM model mirrors the production sequence, as the railway embankment will be built incrementally with different laydown times for each stage.

## INTRODUCTION

The Hallsberg-Stenkumla project is part of the Double Track Hallsberg-Degerön and consists of approximately 13 kilometers of rail, with about 12 kilometers in a new alignment. The project also includes construction of ten railway bridges, a road bridge and a 2.4-kilometer-long railway tunnel. Trafikverket (The Swedish transport administration) is developing this area to create grade separated intersections to increase capacity and enable more environmentally friendly transportation.

<sup>1</sup> WSP/COWI Sweden

<sup>2</sup> WSP Sweden



*Figure 47: The project Hallsberg-Stenkumla is situated in the southern part of Sweden, approximately 200 km west from Stockholm.*

This article aims to describe the design process of pre-consolidation using vertical drains with surcharge for the foundation of an approximately 15 meter high railway embankment on a 10 meter loosely layered sediments of silt and clay at Tälleslätten. The embankment is 150 m wide and includes support berms to improve the stability, see Figure 2.

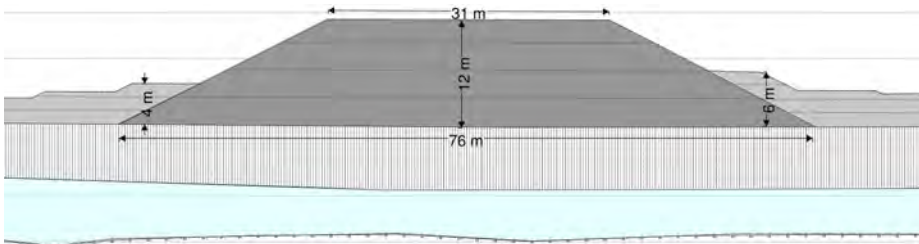


*Figure 48: Typical cross section of the railway embankment over Tälleslätten. Height of the embankment is without surcharge.*

Three foundation methods have been investigated: Soil replacement, pile embankment and pre-consolidation using vertical drains with surcharge. Soil replacement and pile embankment were found to have approximately three times the climate impact as pre-consolidation with vertical drains.

A combination of analytical and Finite Element Modelling (FEM) modelling in 2D and 3D has been carried out to assess strength growth and predict settlement development of the embankment. The FEM model mirrors the production sequence, as the railway embankment will be built in stages with different consolidation time for each stage. These models will be iteratively updated during the construction with field data from monitoring and follow up of the soil behavior to adjust the prognosis in accordance with the observation method.

## GEOTECHNICAL CONDITIONS

The geology of the area consists of an upper layer of sand and silty clay underlain by silt. The sediments overlay a layer of sand.

The clay is silty with layers of silt and sand. The thickness of the clay ranges from approximately 1 - 10 meters and is loose to very loose. The water content varies between approximately 22 - 40 percent, and the liquid limit ranges from approximately 25 - 40 percent. The clay is normally consolidated with an OCR of 1.1 – 1.2. The undrained shear strength is about 15 kPa and increases with depth. Figure 3 shows the layer sequence on the left and the undrained shear strength for the silty clay on the right.

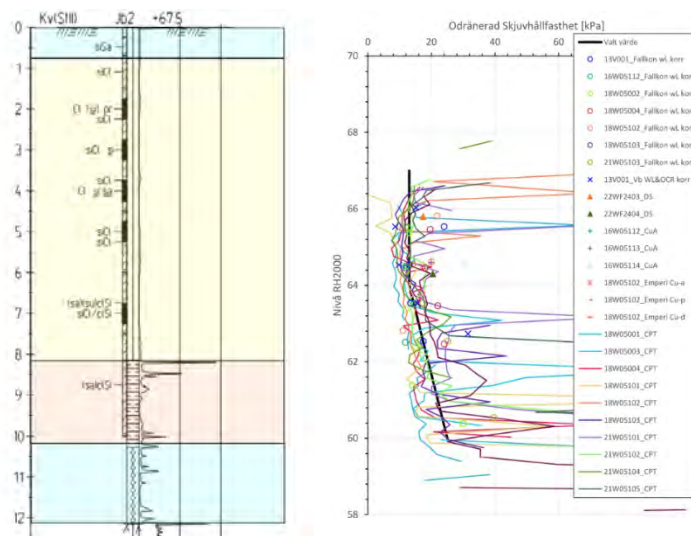


Figure 49: Layer sequence and the undrained shear strength of the area.

The high silt content in the clay made it challenging to obtain undisturbed samples and has led to uncertainty in the interpretation of laboratory results. Only undisturbed samples of high quality have been considered to evaluate the parameters of clay. To capture the deformation behavior of the silty clay, CRS oedometer-test and incremental oedometer tests have been conducted. The value of the undrained shear strength is based on CPT-data, shear vane test, direct shear test and triaxial test.

## DESIGN BASIS

The chosen reinforcement method consists of pre-consolidation with surcharge and vertical drains and support berms. The design has been an iterative process to optimize the consolidation degree and time to ensure that the embankment is stable throughout the process.

The design has been carried out according to the document TRVINFRA-00230 which is the design requirement of the Swedish Transport Administration. The design includes stability checks, short and long-term settlement prediction as well as the design of vertical drains.

The construction time is approximately 48 months, of which the construction of the embankment accounts for 24 months. The remaining 24 months are required to consolidate the clay. The first step is the installation of the vertical drains. The embankment can start to be constructed at the earliest 3 months after their installation. For the construction phase, safety class 2 (SK2) is used, while safety class 3 (SK3) is used for the operational phase.

The spacing between the drains has primarily been determined based on the requirement for strength increase in the clay and the time available for consolidation.

The embankment is constructed through sequential filling in 6 stages. Between each stage, the clay is allowed to consolidate to enable sufficient increase in shear strength to ensure the embankment is stable before the next stage. The additional stress and strength increase in the clay are calculated according to the equation shown below, but also considering that full consolidation is not achieved for each load stage:

$$\Delta c_u = a \cdot [\sigma'_{v0} + \sum_{n=1}^i (\Delta \sigma_{tot.n} \cdot U_n) - \sigma'_{c0}] \quad [1]$$

Where  $\sigma'_{v0}$  is the in-situ effective stress,  $\Delta \sigma_{tot.n}$  is the increase in vertical total stress induce by the embankment fill.  $U_n$  is the degree of consolidation and  $\sigma'_{c0}$  is the in-situ pre-consolidation pressure. The parameter 'a' is a constant that depends on the type of soil and the anisotropic behavior. This constant has been set to 0.1 TRVINFRA-00230 limits it to that if the design is based solely on calculations. This is a conservative assumption. Empirical relationships give an 'a' factor of 0.2 for the specific soil in direct shear, see Figure 85. The design will be optimized during construction with the data collected in the field during construction.

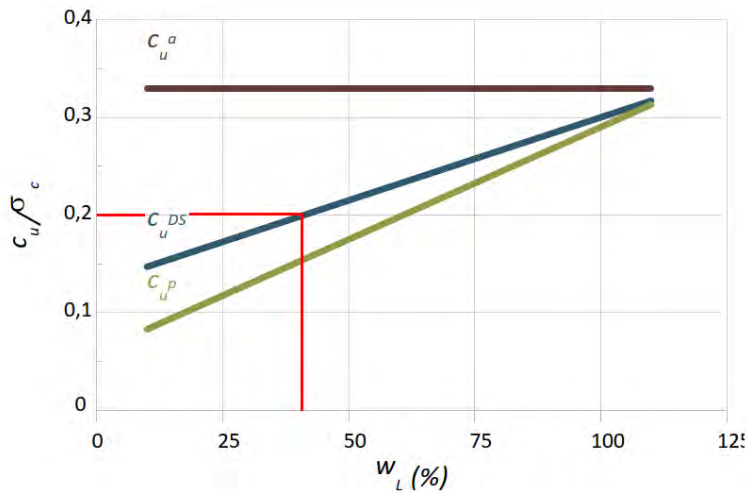


Figure 50. Empirical relationship between undrained shear strength ( $C_u$ ) for different values of liquid limit ( $w_L$ ), (SGI Vägledning 8).

The requirement for stability during the construction stages has driven the size and consequentially the number of load steps. Stability calculations have been performed using Slope/W software with Morgenstern/Price method for both the construction phase and the operational phase. This software was used as the 'a' parameter can be chosen manually while in PLAXIS it is not possible. In the construction phase, a traffic load of 15 kPa is applied, and in the operational phase, a train load equivalent to 32 kPa is applied.

Consolidation and settlements are calculated using FEM in PLAXIS-2D. The soil model "Soft soil creep" has been used for the clay, which is an advanced stress-dependent model that considers creep behavior. The model can be verified against the soil tests performed in the laboratory. It can also be validated and optimized during the staged construction. The Mohr-Coulomb soil model has been used for the remaining soils. The design of the surcharge is performed to ensure compliance with the settlement requirements.

The settlement model has been built with different calculation stages and consolidation time between each stage to reflect reality. Figure 86 below shows several calculation steps from the PLAXIS-2D model.

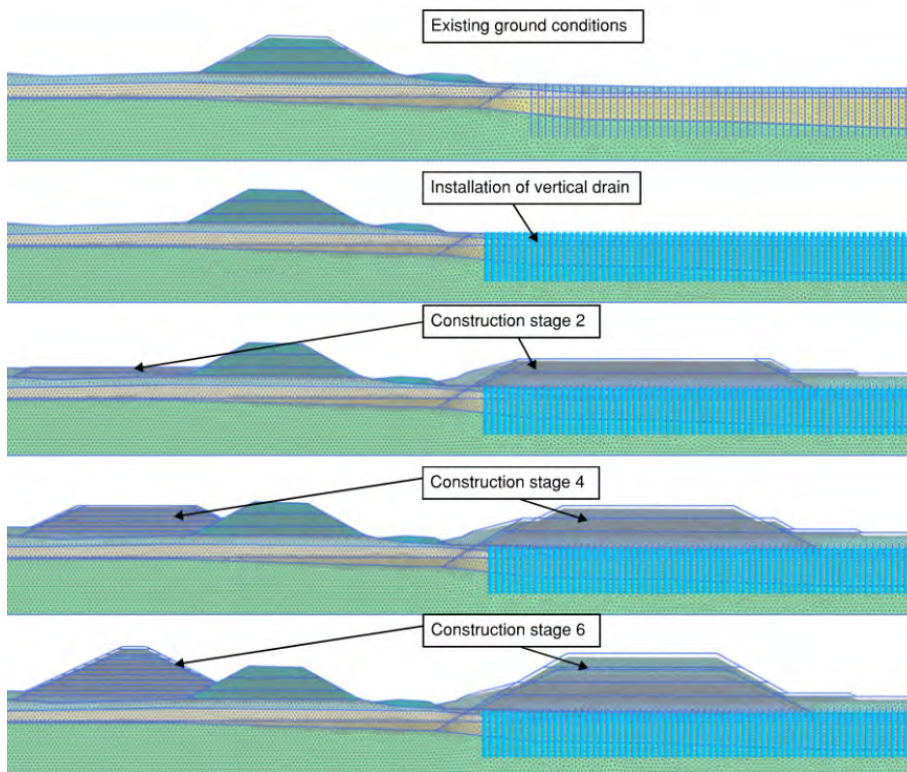


Figure 51: Calculation steps from the PLAXIS-2D model.

## ANALYSIS

The requirements in the serviceability limit state mean that total, differential and transverse settlements, shall be fulfilled during the operational period (40 years). To fulfill the above stated criteria, there should not be any significant primary consolidation remaining in the clay once the surcharge is removed and the risk of secondary creep settlements should be low.

Settlement calculations has been carried out in several sections as shown in the figure below.



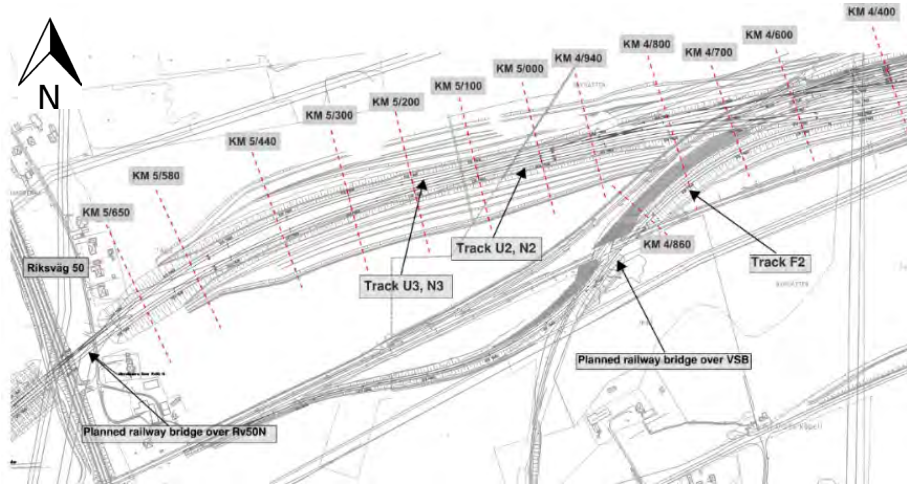


Figure 52: Planview with the calculation sections.

The settlement model has not been able to be verified against a trial bank or settlement data from nearby structures. Therefore, it has been decided to carry out advanced laboratory test to capture the deformation properties of the clay. The soil behavior in PLAXIS has been verified against the performed laboratory tests.

The main parameters in the used soil model for clay are the following:

- $\lambda^*$  (modified compression index)
- $\kappa^*$  (modified swelling index)
- $\mu^*$  (modified creep index).

The parameters  $\lambda^*$  and  $\kappa^*$  describe the stiffness and unloading properties, while  $\mu^*$  describes the creep properties.

The parameters  $\lambda^*$  and  $\kappa^*$  have been evaluated through with simulation of CRS oedometer-test and incremental oedometer tests in PLAXIS. This was done by curve fitting against laboratory results. The creep parameter ( $\mu^*$ ) has only been determined through the simulation of incremental oedometer tests in PLAXIS. Empirical relationships have been chosen as input values for the selection of parameters ( $\lambda^*$ ,  $\kappa^*$ , and  $\mu^*$ ). The chosen empirical relationships are based on the document SGI Info 13 (Swedish geotechnical institution, information 13). The equations are shown below.

$$\kappa^* \approx \frac{2 \cdot \sigma'_V}{M} \quad [2]$$

$$\lambda^* \approx \frac{2 \cdot \sigma'_{CV}}{M_L} \quad [3]$$



$$\mu^* \approx \frac{w_n^{1,5}}{75} \quad [4]$$

The figure below illustrates an example of curve fitting for CRS oedometer-test and incremental oedometer tests.

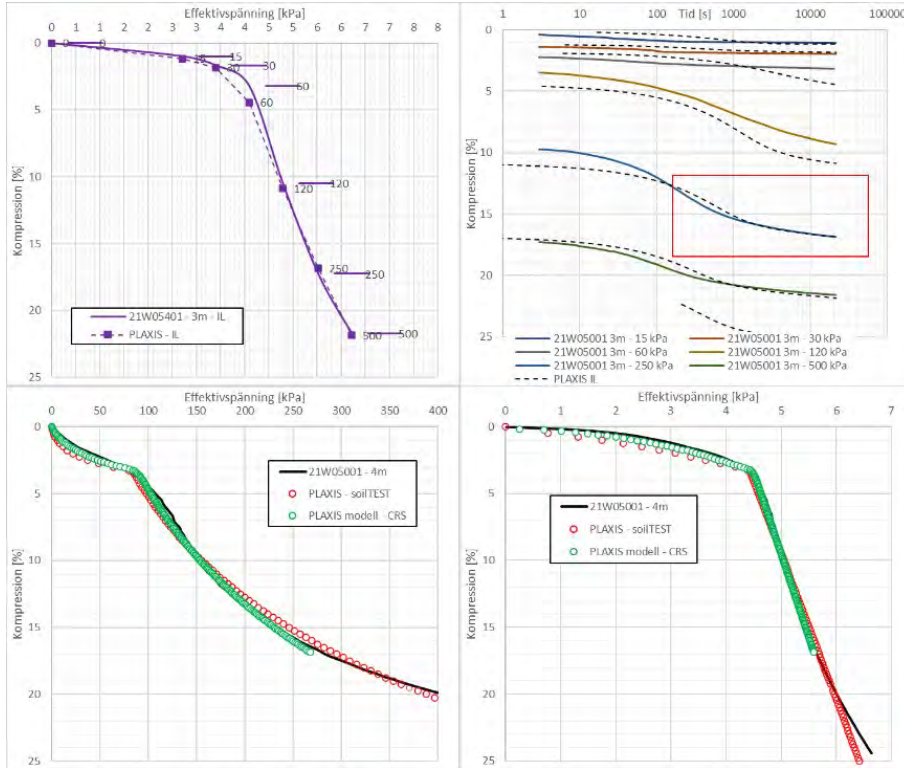


Figure 53: Example of curve fitting against laboratory tests for CRS oedometer-test and incremental oedometer test.

The figure below presents a summary of the parameters obtained through the soil test in PLAXIS.

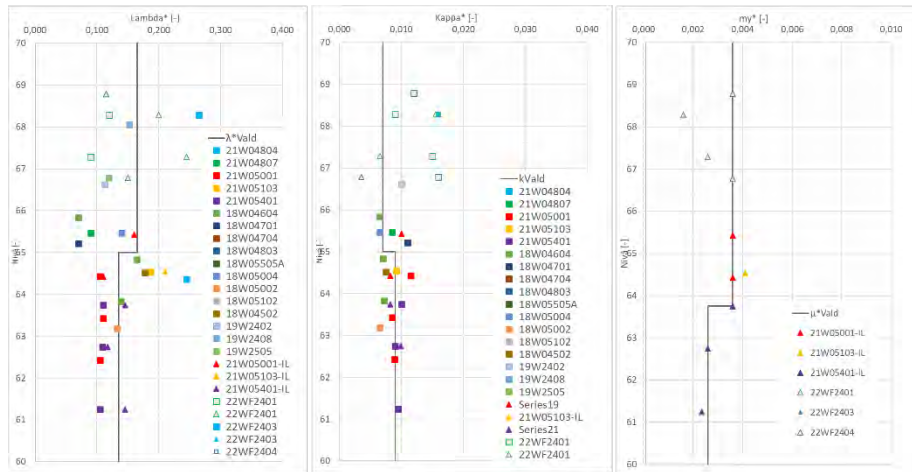


Figure 54: Summary of the parameters obtained through the soil test simulation in PLAXIS (CRS test (squares), Stepwise oedometer test (triangle)).

The permeability of the clay has been assumed from CRS oedometer-test based on the pre-consolidation pressure. Changes in permeability with respect to the loading conditions are adjusted in PLAXIS by using the parameter  $C_k$ .  $C_k$  can be determined using the equation below.

$$C_k = \frac{1}{\beta_k} * e_0 \quad [5]$$

## MONITORING

A monitoring program has been developed to describe the control and follow-up measurements that needs to be performed during the construction period to ensure that the geotechnical requirements in the serviceability limit state and the failure limit state are met.

### Serviceability limit state

The controls in the serviceability limit state require that the allowable total, transverse and longitudinal settlements are not exceeded in the design period. The total settlement must not exceed 20 cm. The maximum tilt on each side of the track is 1%. In the longitudinal direction, the differential settlement must not exceed 5 cm over a distance of 10 m.

To verify that the settlement requirements are met, the following measuring equipment is used:

Measurement of reference markers and settlement tube monitoring are used to track the settlement progress at individual points as well as in sections. The purpose of these measurements is to compare actual settlements with the calculated settlement profiles, thus verifying the calculation model that formed the

basis for the design. The measurements also provide an indication of the development of consolidation settlements and whether there is a need to revise the time between stages.

Pore pressure measurements are carried out to monitor the consolidation in the clay. These measurements provide the basis for calculating the increase in effective stress in the clay, as well as the increase in pre-consolidation pressure and degree of consolidation. However, during the compression of the clay and subsequent settlement, there is a risk that the pore pressure probes may follow the downward movement of the soil. This means that the original measurement levels will change, and the excess pore pressures may not converge to zero but towards a slightly higher value. This is something that needs to be considered when evaluating the measurement results. To get an understanding of the actual settlement towards depth, settlement plate measurements can be used as a complement to the other prescribed measurements.

When the excess pore pressures have dissipated, the consolidation process is considered to be completed. By comparing the increase in pre-consolidation pressure with the effective stress in the clay after the removal of excess load, the degree of overconsolidation (OCR) can be assessed. The design is based on an OCR value  $\geq 1.1$  in the middle of the clay layer, to reduce the risk against potential creep settlements that may occur during the operational period.

Settlement monitoring during the construction period is compared with the predicted settlements, allowing an evaluation of the assumptions that formed the basis for the calculation model. If the measured settlements deviate from the predicted settlement range, the calculation model may need to be adjusted, and a new forecast established. If the excess pore pressures have dissipated completely, consolidation settlements should be completed. The measurements also provide an overall understanding of the settlement process and is an indication of ongoing creep settlements.

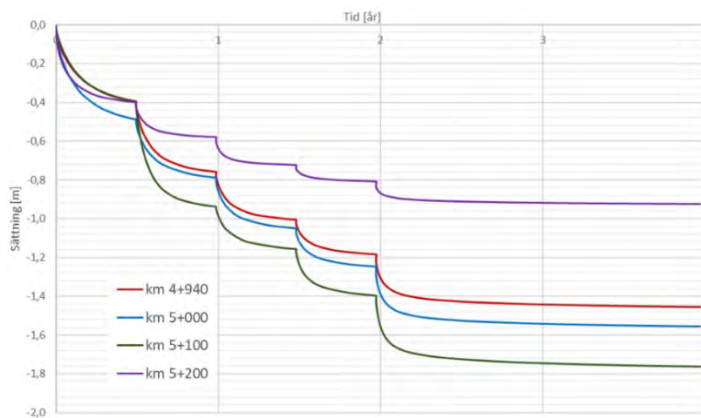


Figure 55: Settlements as a function of time for different sections during a period of four years.

Settlements and consolidation processes have been checked with PLAXIS. Sensitivity calculations have been performed by varying the coefficient of variation by 10% from its base value for parameters  $\lambda^*$ ,  $\mu^*$  and  $k_{\text{init}}$ . This is done to understand how these factors affect consolidation and settlements. Figure 10 shows the results of the sensitivity analysis for parameter  $\lambda^*$  (modified compression index). This parameter is governing the settlement process during the construction phase. In the operational phase, settlements are mainly comprised of creep settlement, which is controlled by the parameter  $\mu^*$ .

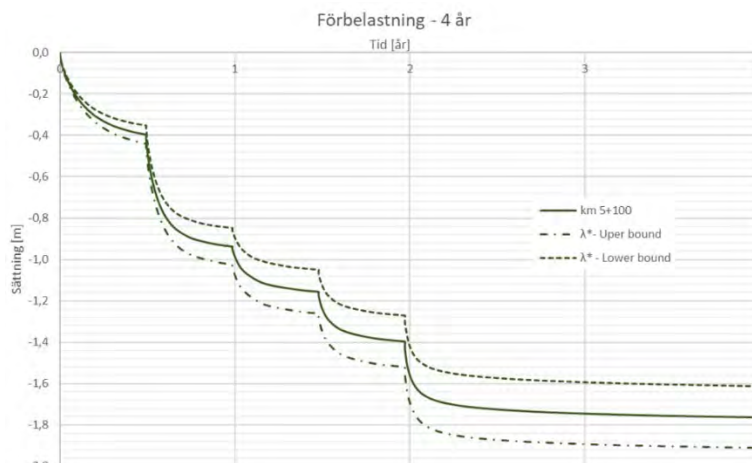


Figure 560: Sensitivity of the parameter  $\lambda^*$  during four years of preloading.

### Ultimate limit state

The requirements in the ultimate limit state are placed on the minimum acceptable safety factor against stability failure. When designing with partial factors (design values of material parameters), the safety factor  $F_{\text{EN}}$  should exceed 1.0 during the construction phase (safety class 2) and 1.1 during the operational period (safety class 3).

To meet the safety requirements during the staged loading of the embankment, it is necessary for the undrained shear strength of the clay,  $c_u$ , to increase along with consolidation. The measured increase in undrained shear strength forms the basis for decisions regarding when the next load step can be applied or if the duration of each stage needs to be adjusted. To evaluate the above, pore pressure measurements and the increase of the undrained shear strength is calculated using the data from CPTu (Cone Penetration Testing) probes.

CPTu probes are used to measure the net cone pressure at different points in time. By comparing this with the net cone pressure from the control probing (baseline measurement) in the undisturbed, naturally deposited clay, the increase in strength of the clay can be calculated with the equation below.

$$c_u = c_{u0} \cdot \frac{(q_t - \sigma_v)}{(q_{t0} - \sigma_{v0})} \quad [6]$$

where  $q_t$  and  $\sigma_v$  are the current total cone resistance and overburden pressure evaluated during the CPTu probing. The parameters  $q_{t0}$  and  $\sigma_{v0}$  and corresponding values from the in situ measurement. The expected strength increase can also be determined from vertical effective stress calculated from pore pressure measurements using the relationship below where  $a$  can be assumed to be in the order of 0,2 according to empirical relationship, see Figure 4.

$$c_u = a \cdot \sigma'_c \quad [7]$$

## CONCLUSIONS

The designed foundation method is cost-effective with low environmental impact. However, one condition is that the construction schedule allow for the consolidation of the clay and that the fill material should be available nearby to minimize transportation distance. This design method requires rigorous geotechnical investigation and laboratory testing. During the construction stage, extensive monitoring is required as well as optimizing the design during the construction phase.

### Some conclusions from the project:

To obtain undisturbed samples, CRS tests and evaluation of permeability and consolidation coefficient have been performed on samples with the highest clay content. In reality, the settlement-prone soil profile consists of silty clay with draining layers of sand. Therefore, the samples and results are not representative of the soil layer sequence. The assumptions made are conservative and result in larger estimated consolidation time.

The consolidation time is highly dependent on the horizontal consolidation coefficient,  $c_{vh}$ . The Swedish Transport Administration [6] advises that  $c_{vh}$  can be set to 2 times the vertical consolidation coefficient  $c_{vv}$ , for clay. To avoid an excessively conservative approach, this parameter could have been determined from in-situ measurements such as pore pressure dissipation time in a piezocone CPTu.

The determination of shear strength increase has been considered with a factor "a" corresponding to 10%, which is a conservative assumption. If direct shear tests (DSS) from various depths and consolidation stresses had been conducted, they would likely have supported the design with a higher rate of strength increase, potentially in the range of 20%, in line with empirical relationships such as those presented in Figure 4.

The design of the embankment is just a preliminary design. The laydown time for each stage and thickness of each fill layer will be updated during construction with respect to the data collected in the field using the observational method.

## ACKNOWLEDGEMENT

We would like to dedicate our special thanks to Per-Evert Bengtsson and Naomi Licudi.

## REFERENCES

- Ericsson, L. (2010). *Vertikaldränering, Varia 609*. Linköping: SGI.
- H.Fellenius, B. (02 2015). *Basics of Foundation Design, Electronic Edition*. Hämtat från [www.fellenius.net](http://www.fellenius.net): <https://www.fellenius.net/>
- Larsson, R. (2007). *Långtidsobservationer av konsolideringsprocesser, Report 70*. Linköping: SGI.
- Müller, R. (2010). *Embankments founded on sulphide clay : - some aspects related to ground improvement by vertical drains*. Stockholm: KTH Royal Institute of Technology.
- Rolf Larsson, P.-E. B. (1993). *Sättningsprognoss för bankar på lös finkorning jord, Infomation 13*. Linköping: SGI.
- Trafikverket. (2023). *TRVINFRA-00230, Version 2.0*. Trafikverket.
- Vägverket. (1989). *Vertikaldränering Publi. 1987:30*. Vägverket.

# **DIGITAL GEOTECHNICAL INFORMATION MANAGEMENT FOR LIFECYCLE RESOURCE SAVINGS**

**M. Svensson<sup>1</sup>, O. Friberg<sup>2</sup>**

## **KEYWORDS**

Uncertainties, geomodelling, digital twins, multivariate analysis, GeoBIM

## **ABSTRACT**

A digital geotechnical data management platform capable of handling all geotechnical information produced through the whole life cycle has been developed. By combining information from desk studies, geophysics and geotechnical sounding and sampling information in the same platform, geomodels of the subsurface conditions can continuously be refined from planning to construction. Finally, an as built 3D model of the subsurface built environment including geology, geotechnical design properties and permanent geotechnical structures can be handed over for asset management to the client for future maintenance use.

Microsoft 365 Teams was chosen as a general platform for implementing the GeoBIM concept for managing all geotechnically related data, including geophysics and geotechnical structures. The tool implements outcomes from recently developments on uncertainty handling in geological layer modelling and soil mechanical design values.

When all data are gathered in the same environment it also enables implementation of advanced interpretation functions. Specifically valuable is the uncertainty module for defining layer models with corresponding uncertainties and objectively determining soil mechanical design values using MVA methodology. Therefore, an updated and much improved geotechnical design process governed by well-defined uncertainties is suggested.

When all geotechnically related subsurface information – data, models, geotechnical structures – are easily available, visualized and communicated in a common platform, and advanced tools for QA and analysis of both data and

<sup>1</sup> Tyréns AB, Helsingborg Sweden

<sup>2</sup> Tyréns AB, Malmö Sweden

models are in place, a geotechnical digital twin of the subsurface can be defined.

Since the database is also prepared for handling sensor data in time series this opens for scenario modelling of future possible geotechnical events. For example, by continuously collecting settlement data or pore pressure data and frequently applying those on stability analyses in sensitive sections defined in the geotechnical digital twin, a proactiveness for preventing for instance landslides will be achieved.

## BACKGROUND

When a road, bridge or railway is to be built it is crucial to know the geotechnical conditions, including hydrogeology and the environmental situation. All information about the subsurface conditions is most often collected using geotechnical drill rigs and is done to a different extent depending on current project type and project phase. At an early stage only archive material is used, whereas at a later stage more detailed investigations are carried out. Every investigation gains valuable information which nowadays most often is digitally collected. Heading towards sustainability and hence a lifetime perspective, today we also need to take the geotechnical asset management phase into account.

Although different initiatives on handling smooth transferring and standardization of geotechnical data formats have been ongoing since many years (AGS, LAS, SGF, buildingSmart, OGC, DIGGS, IFC, CoClass) there is still a long way to go until full compatibility between all data and all software in the geotechnically related subsurface disciplines will come true. Therefore, still planning of geotechnical investigations are often non-optimized and the full potential of the whole geotechnical data set is seldom used. Sometimes data sets are even lost between different phases and different stakeholders.

With the vision of full transparency between all project phases and all stakeholders from idea to demolition of a structure the GeoBIM concept has been developed, see figure 1, enabling:

- Easy access to all data (geotechnical, environmental, geology/rock, groundwater, geophysics) for all stakeholders always
- Design managed by known geotechnical uncertainties
- Flexible workflow and quick adaption to the user needs and specific software

This not only allows a smooth, quality assured and efficient workflow for any geotechnical design applications, it also enables a significantly updated geotechnical process.



Having all data in good order in a professional and well-structured database is fundamental for applying a digital workflow. It is also crucial for making use of the new universe that has opened with IoT and AI methodologies.

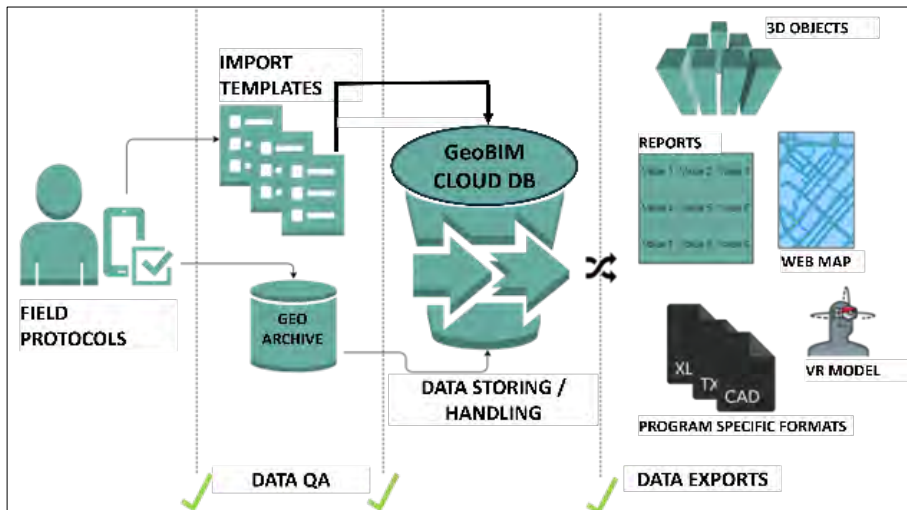


Figure 1 The GeoBIM concept process, enabling a completely closed digital chain from field data collection to 3D geo-model or other deliverables. [1]

## INFORMATION LOSS

Still, and often, unforeseen geological and geotechnical conditions are pointed out for causing delays and more costly infrastructure projects. A limited openness between different stakeholders being reluctant sharing knowledge and data is one of the reasons, often governed by contract issues.

In the procurement phase (design and build contract) the client often only supplies the contractor with the geotechnical factual report, although a lot of job has been spent on interpreting the geotechnical conditions producing geomodels during the design phase. This often results in differing interpretation of the geotechnical conditions, long discussions and possibly a claim situation.

In the end of a project the asset owner, often the client, most often miss systems and routines for storing and manage all information about the subsurface conditions, for example where piles in detail have been installed. Keeping in mind in Sweden infrastructure assets are designed for a lifetime of 120 years, detailed geotechnical as built information, including geotechnical structures, could be very valuable when a bridge is to be widened etc. during it's whole lifetime.

If there was a transparency between different stakeholders and the different project stages data would continuously be shared with the other actors, see figure 2, and many issues would be prevented and less claims would be the case. The GeoBIM concept suggests and facilitates such a process, see chapter 5.

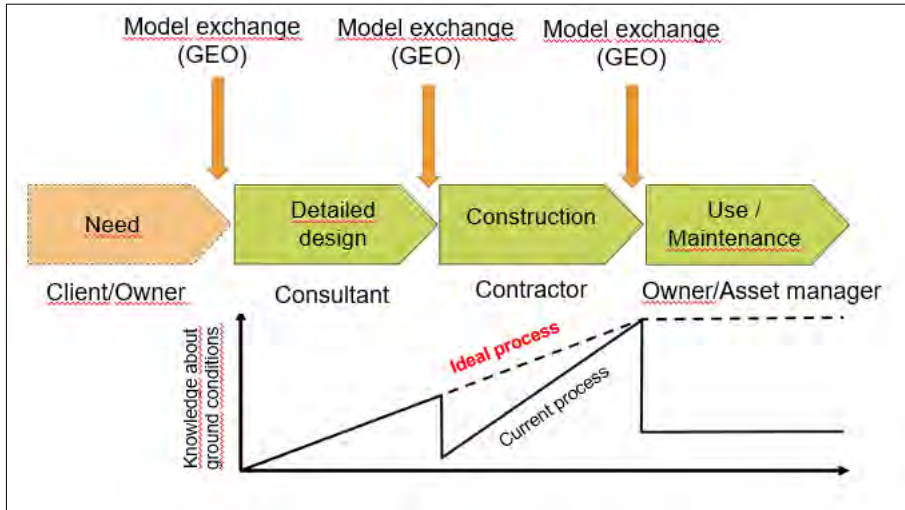


Figure 2 When handling geotechnically related information between each phase and each stakeholder in projects there is an information loss. Often there is also a significant information loss between different disciplines within the same company or project team. The figure also illustrates the preferred process, in red.

## GEOTECHNICAL DATA MANAGEMENT PLATFORM

The GeoBIM data management platform and concept emanate from three principally different uses within the geotechnical process:

- Data handling and storing
- Daily geotechnical craftsmanship
- Advanced data analysis

### Data handling and storing

The database is prepared for importing/exporting all geotechnically related data types used in Sweden (2024). When standards are available, for example the SGF data format [4], this is used. For other methods experts in each field (environmental, geophysics etc.) have defined a preferable data format. After a validation process for quality assurance data is uploaded in the database, which holds approximately 250 000 boreholes (2024). All boreholes are visualized in a map view.

### **Daily geotechnical craftsmanship**

The daily geotechnical design work starts with producing a factual report (GIR) including sounding and sampling data from field investigations. Having all data well organized much of this work could be automated and quality assured. An example is comparing all borehole ground levels with the digital elevation model (DEM). When there is a misfit, the user will be notified to eliminate such fundamental misinterpretations. Transforming all sounding data to shear strength diagrams using all empirical relations is another efficient and quality assured basic tool, enabled by the fully digital workflow.

### **Advanced data analysis**

The efficiency of having access to all data in a project in the same digital environment makes it possible to implement use of advanced interpretation tools that have been developed in previous separate R&D projects, run by experts. In those cases, the specific data sets which are to be used are automatically gathered in the preferred way tailor made for the specific application. Most interesting are tools for handling geotechnical uncertainties and statistical analyses of contaminated volumes, see chapter 4.

### **Microsoft Teams application**

Two key factors while developing the digital concept have, firstly, been to be avoid developing tools and features which are already available in the industry (most often under expensive licenses) and, secondly, give easy access to the digital tools for any stakeholder.

Therefore, all GeoBIM functionality has been implemented in the general Microsoft 365 Teams platform, including for instance tools for determining uncertainties on layer geometries using Monte Carlo simulation technique and design values using MVA methodology, see chapter 4. Each tool is run upon request, see figure 3, and the geometry uncertainty models and the MVA results are stored in the digital platform.

Microsoft Team is used by most of the stakeholders in the industry and hence access to all functionality could easily be given to all parts in projects, including for example environmental authorities, without expensive licensing.



[3]. For determining the uncertainties of the bedrock overburden an algorithm based on individual uncertainties assigned to each sounding have been developed. Also, the distance to the nearest sounding point is used in the algorithm. After a Monte Carlo simulation (1 000 models) the outcome are three bedrock overburden models and an uncertainty map, see figure 5.

The algorithm that has been developed is validated to five uncovered and surveyed bedrocks in infrastructure projects in Sweden. The prediction accuracy was shown to be 0.4-0.9 m [2].

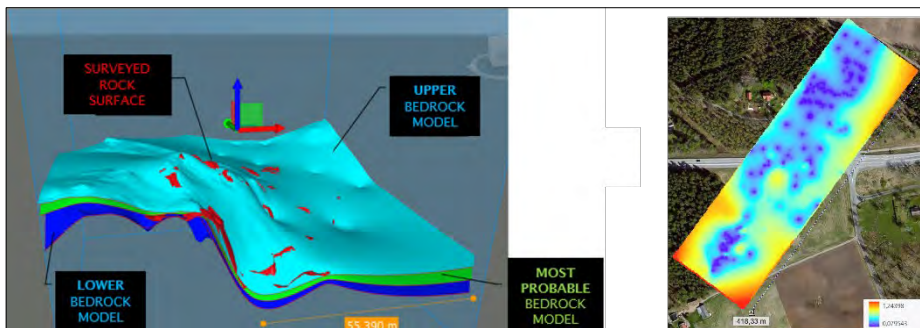


Figure 5 Results from modelling the top of the bedrock. Left: most probable bedrock model, upper and lower bedrock models within 95% probability. Right: Uncertainty map, plan view of most probable bedrock model. [2]

To get an objective prediction of the undrained shear strength a tool using Multivariat analysis (MVA) has been developed. The methodology for geotechnical applications is well validated in [3]. The GeoBIM platform has implemented a module grabbing data of the user's choice in the database and performing an analysis using the MVA methodology. The result is presented with an objectively determined undrained shear strength accompanied by a known uncertainty (COV), see figure 6.

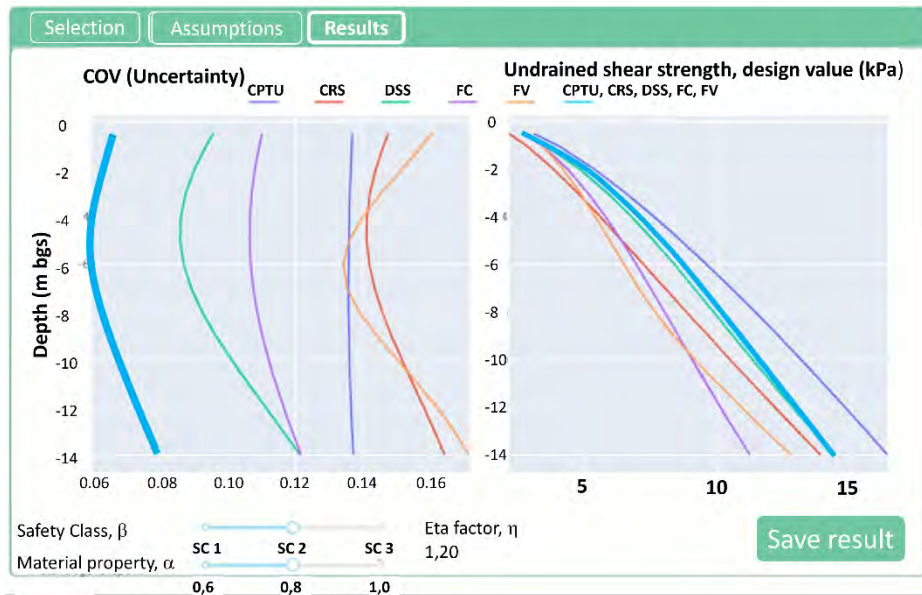


Figure 6 The undrained shear strength determined using MVA methodology. The combined uncertainty is significantly lower than the individual uncertainties from each method. Figure modified from [2].

## UPDATED GEOTECHNICAL PROCESS

Keeping all geotechnical data well-structured and in good order in a professional database shows that the daily geotechnical design work could be fully digitalized, and advanced and novel applications more commonly utilized, such as uncertainty models of geometries and MVA methodology for objective determination of design values.

Irrespective of phase in a project this opens for defining a new geotechnical process and workflow, based on *known uncertainties*, see figure 7. A new geotechnical workflow is suggested, governed by a constant update of the uncertainties both concerning the geologic model and the design values. As soon as any new information is added to the database the uncertainties are recalculated and compared to the allowed uncertainty criteria decided at the beginning of the project or current phase. Following this process activities like investigation programs could be optimized, risk sharing between client and contractor could be clearer and the GBR/GDR could also become more defined.

With the vision of this suggested workflow, not taking legal aspects into account, all stakeholders constantly have access to the same updated information via the same digital platform/database where both data and models can be visualized.



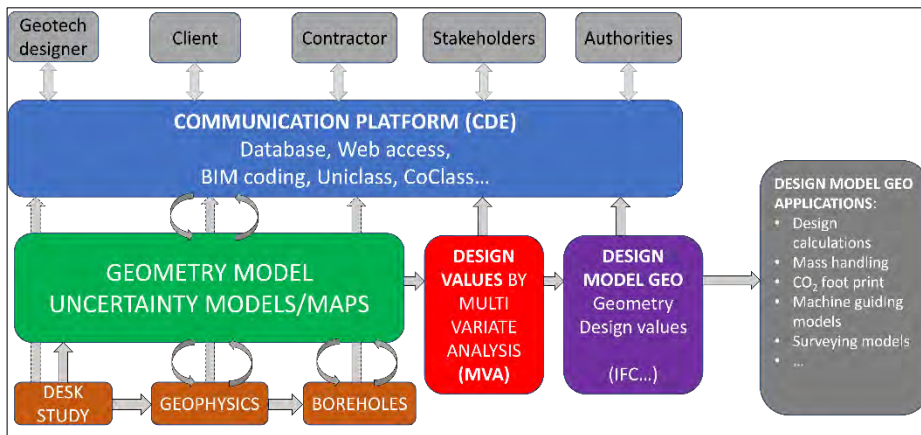


Figure 7 A new geotechnical process is suggested, based on known uncertainties, possible to define within the GeoBIM concept. Figure modified from [2].

## SENSOR DATA AND DIGITAL GEOTECHNICAL TWIN

Having reached the level of fully digitalizing the geotechnical process from field planning to handover of a geotechnical asset management database and model for the client to use in an asset lifetime perspective one could dig deeper into the digital field. Inspired by the IoT sector recently the GeoBIM team therefore has started to implement structured handling and management of streaming sensor data, starting with automatic meters for groundwater levels, see figure 8, and tunnel movements monitored by extensometers, see figure 9. An obvious use of streaming sensor data, certainly during the construction phase, is to continuously compare the movements/levels to set alarm levels.

A more sophisticated and state of the art use is combining the data in the database, the interpreted geomodel from the design phase continuously updated with true values during construction (typically surveyed bedrock surface) and the streaming sensor data, using AI methodology for training an AI algorithm for predicting future geotechnical behavior.

In this process also the design FE models could be calibrated and used for predicting future geotechnical scenarios. The digital geomodel, including not only geometry and physical properties but also a geotechnical behavior, could then be considered a *digital geotechnical twin*.

Even in projects where everything goes according to plan, the continuous follow-up of the geotechnical behavior is highly valuable as it gives the project members a security that everything is under control. By combining information from previous stage investigations and predictions with continuously inflowing sensor data in the same system, reasons for deviations between expected and actual results could also quickly and rationally be identified, enabling the right decisions to be taken in time.

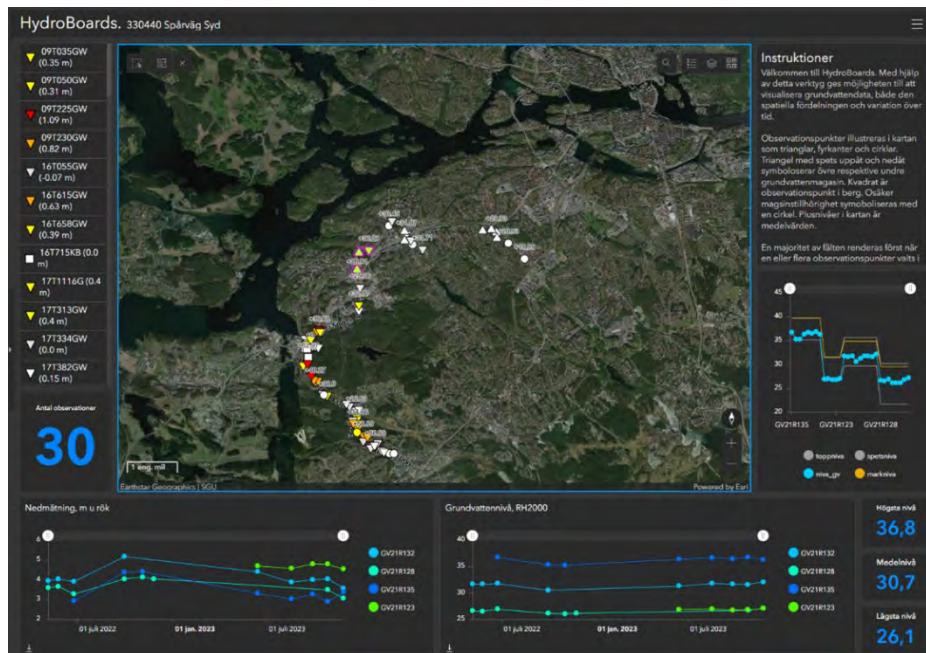


Figure 8 Hydrogeological time dependent sensor data visualized in the Microsoft GeoBIM in Teams platform, currently semiautomatically updated, but soon to be continuously streaming into the database. Project Spårväg Syd, Stockholm.

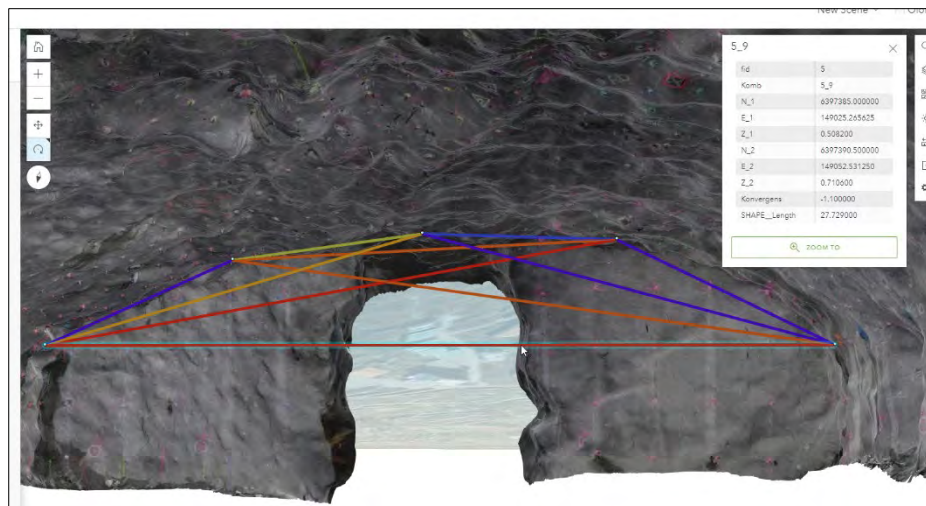


Figure 9 On-line monitoring of extensometers in a tunnelling project in Sweden. All data is monitored and stored in the database and continuously compared to set alarm levels.



## CONCLUSIONS

A digital geotechnical information management platform for a lifetime perspective has been developed, based on the GeoBIM concept, and implemented in the Microsoft 365 Teams shell for increased accessibility in the industry.

The database and the accompanying methodology enable quality assurance, easy access to data, models, and geotechnical structures for all stakeholders through all phases. Using the GeoBIM concept will decrease geotechnically related risks, miscommunication, and the number of claims. It also allows flexible and advanced analyses using the whole data set.

This opens for a new updated geotechnical process governed by uncertainty control of geotechnical parameters. At the end of a project a complete geotechnical model could be handed over to the client for maintenance use.

Implementing a new geotechnical design process as suggested requires overcoming legal issues and since long well-established workflows. Good use cases, education of the geotechnical community, including the environmental, geophysics, rock, and groundwater disciplines, and openminded early adopters among all stakeholders are key elements for succeeding.

In the era of IoT, monitoring of geotechnically related streaming sensor data is implemented in the geotechnical data management GeoBIM concept enabling geotechnical digital twins to be defined. This opens for geotechnical scenario studies in any project and also proactiveness for preventing natural hazards.

However, abovementioned requires commonly agreements on standardized data formats and processes and more transparency and trustfulness between all geotechnical stakeholders. No matter how sophisticated tools and processes that are developed by single players if the geotechnical community as a whole don't collaborate. The technology for giant geotechnical leaps is here. Are we, as a common geotechnical community ready?

## ACKNOWLEDGEMENT

The digital geotechnical information management platform, the GeoBIM concept, has been developed with financial support from Sven Tyréns Foundation, Smart Built Environment, Swedish Rock Engineering Research Foundation (BeFo), The Development Fund of the Swedish Construction Industry (SBUF) and The Swedish Road Administration (TRV).

## REFERENCES

- [1] M. Svensson M. and O. Friberg, Effektiv kommunikation av georelaterad undermarksinformation i ett LCC-perspektiv, Grundläggningdagen 2019, Proceedings, Mars, 2019
- [2] M. Svensson and O. Friberg, GeoBIM for handling geological and geotechnical uncertainties in tunnelling, ITA-AITES World Tunnel Congress, WTC2022, Bella Center, Copenhagen 22-28, 2022
- [3] A. Prästings, Managing uncertainties in geotechnical parameters: From the perspective of Eurocode 7, PhD thesis, KTH Royal Institute of Technology, 2019
- [4] SGF, SGF:s dataformat, SGF Rapport 3:2012 (in Swedish), Swedish Geotechnical Society, Linköping, 2012
- [5] M. Svensson, O. Friberg and D. Hagerberg, GeoBIM for increased efficiency of the remediation process of contaminated sites, Smart Built Environment Report nr U8-2020-06, (in Swedish), 2023

# **DRAINED FAILURES, STRESS DEPENDENCY AND PLANE STRAIN EFFECTS**

**Niels Mortensen<sup>1</sup>**

## **KEYWORDS**

Plane strain effects and representative friction angles (secant peak values).

## **ABSTRACT**

The bearing capacity factor  $N_q$  from Prandtl (1920) was derived for a coarse grained soil, assuming that one friction angle can be used to model the entire range of effective stresses within the rupture figure. A similar rupture figure has been investigated in this paper allowing for stress dependent friction angles throughout the entire failure mechanism using plane and triaxial strain where the friction angle only depends on the density index and on the mean effective stress at failure. To facilitate the continued practical use of the Prandtl solution, the term “representative friction angle” has been introduced and formulas have been established. A representative friction angle will, when used in the work from Prandtl, lead to the same bearing capacity factor or earth pressure coefficient as the stress-dependent model. Differences between plane strain and triaxial strain have been included allowing for establishing factors linking the secant value of a peak friction angle from plane strain to the same parameter in triaxial strain.

## **INTRODUCTION**

The scope of this paper is to investigate the effect of using stress dependent friction angles when analysing the traditional solutions for bearing capacity and earth pressures assuming coarse grained materials. The effective strength properties of a coarse grained material will depend on several factors. Given a reasonable homogeneous sand formation characterised by only small variations in the mineralogy and the angularity of the grains, together with the particle size distribution, the secant value of the effective peak friction angle will mainly depend on the density index,  $I_D$ , and the effective stress state during failure. This was highlighted by Bolton (1986) who also pointed out that plane strain conditions may increase the shear strength of coarse grained material. Plane strain conditions represents a 3D effective stress state where the intermediate principal strain component ( $\varepsilon_2$ ) is zero as the soil cannot dilate or contract

<sup>1</sup> nmGeo, Denmark

in the out of plane direction (y-axis on Figure 1, Part 1). The principal effective stress components acting on the slice of soil in part 1 of Figure 1 represents the stress state in the passive Rankine zone ABCA of part 2 of the same figure. The mean effective stress within a soil element is thus dependent on the three principal stress components but since movements in the soil mass can only develop in the XZ-plane the relevant shear stress component will depend on the minor and major principal effective stresses only,  $\tau = (\sigma'_1 - \sigma'_3)/2$ .

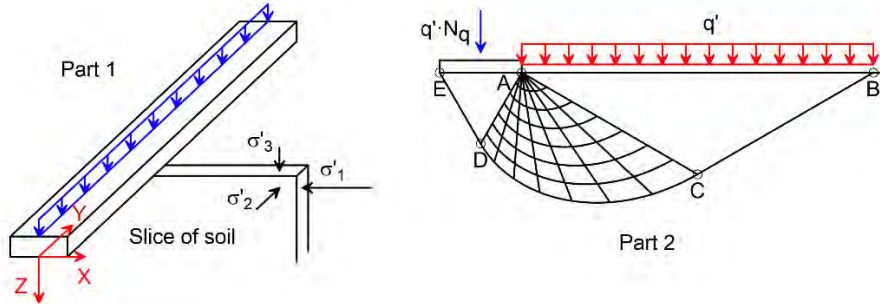


Figure 1 Part 1: 3D view of a strip footing with principal stresses shown on a slice of soil. Part 2: 2D Prandtl rupture figure below a strip footing (surcharge case with zero unit weight and zero effective cohesion).

The symbol  $\phi'$  represents the secant value of the effective peak friction angle in this paper. The effect of unit weight of soil and the effective cohesion has not been included in this work.

## A SINGLE SOIL ELEMENT

### Basic equations

The secant value of the peak friction angle predicted by Bolton (1986) may be computed by Equations (2.1) through (2.3):

$$\phi'_{pl} - \phi'_{cv} = 5 \cdot I_R^\circ \text{ (plane strain)} \quad (2.1)$$

$$\phi'_{tr} - \phi'_{cv} = 3 \cdot I_R^\circ \text{ (triaxial strain)} \quad (2.2)$$

$$I_R = I_D \cdot [Q - \log_e(p'_m / 1 \text{ kPa})] - R < 4.0 \quad (2.3)$$

where  $\phi'_{pl}$  and  $\phi'_{tr}$  are secant values of the plane strain and triaxial peak friction angles, respectively,  $\phi'_{cv}$  is the residual friction angle,  $I_R$  is the dilatancy index,  $p'_m$  is the mean effective stress at failure,  $Q$  is a constant dependent on mineralogy and  $R = 1$ .

The value of  $Q = 10$  was proposed for quartz and feldspar sands. Bolton observed a range of  $32^\circ$ - $37^\circ$  for  $\phi'_{cv}$ , with a mean value of  $34^\circ$  and standard deviation of  $2^\circ$ . The lower end of the interval was dominated by quartz sand, whereas feldspar was found at the upper end. The stress dependency of  $\phi'$  is

introduced through Equation (2.3) where the effective mean stress,  $p'_m$  is estimated using:

$$p'_m = (\sigma'_1 + \sigma'_2 + \sigma'_3)/3$$

$$p'_m = \sigma'_3 \cdot [K_{ps} \cdot (1 + b) + 2 - b] / 3 \text{ (Passive failure state)} \quad (2.4)$$

$$p'_m = \sigma'_1 \cdot [1 + b + K_{as} \cdot (2 - b)] / 3 \text{ (Active failure state)}$$

where the principal effective stress components  $\sigma'_1$ ,  $\sigma'_2$  and  $\sigma'_3$  refer to the state of failure within the sample,  $b = (\sigma'_2 - \sigma'_3) / (\sigma'_1 - \sigma'_3)$  [ $b = 0.35$  for plane strain, cf. Lade et al. (2008), and  $b = 0$  for triaxial strain] and where  $K_{ps}$  and  $K_{as}$  are defined in Equation (2.5).

The mean effective stress during failure is estimated differently depending on the failure state (passive or active). The zone ABCA on Figure 1 (Part 2) represents a passive failure state (Rankine zone) where the minor principal effective stress is vertical ( $\sigma'_3 = \text{surcharge}$ ) for a horizontal soil surface ( $\beta = 0$ ). In an active Rankine zone, the major principal stress is vertical for  $\beta = 0$ .

The failure criterion for coarse grained materials may be defined by:

$$\sigma'_1 / \sigma'_3 = (1 + \sin \phi') / (1 - \sin \phi') = K_{ps} = 1 / K_{as} \quad (2.5)$$

Equations (2.1) through (2.5) form an iterative scheme by which  $\phi'_{pl}$  or  $\phi'_{tr}$  can be estimated when  $\phi'_{cv}$ ,  $I_D$ ,  $Q$  and  $R$  are known together with one of the principal failure stresses  $\sigma'_1$  or  $\sigma'_3$ .

The dilatancy index in Equation (2.3) was given a cut off level of 4.0 by Bolton but the value of four may be a conservative value and data have been observed indicating that  $I_R < 5$  could be used. Results presented in this paper are generally produced using  $Q = 10$ ,  $\phi'_{cv} = 33^\circ$ ,  $R = 1$  and  $b = 0.35$  using a horizontal soil surface combined with a) a vertical wall or b) a horizontal footing.

The parameters  $Q$ ,  $R$  and  $\phi'_{cv}$  in Equations (2.1) through (2.3) can be calibrated to match site-specific conditions using a few CAD tests (triaxial test being anisotropically consolidated and sheared drained).

### Plane strain factor, single soil element

The plane strain factor is defined as the ratio between the secant value of the plane strain peak friction angle and the same parameter in triaxial strain,  $\phi'_{pl} / \phi'_{tr}$ . Figure 2 left illustrates the plane strain factor for single soil elements using Bolton (1986) following the basic equations above.

The curves for the active stress state refer to a major effective principal stress being vertical, while the vertical effective stress is taken as the minor principal effective stress for the passive case. Figure 2 left shows a) The plane strain factor for a single soil element increases with the density index and decreases

for increasing mean effective stress. The active failure state reveals a higher factor than the passive failure state. b) The dilatancy index increases for decreasing mean effective stress. Values of  $I_R$  of 4 and 5 are illustrated on Figure 2 left (curves are not drawn for  $I_R > 5$ ).

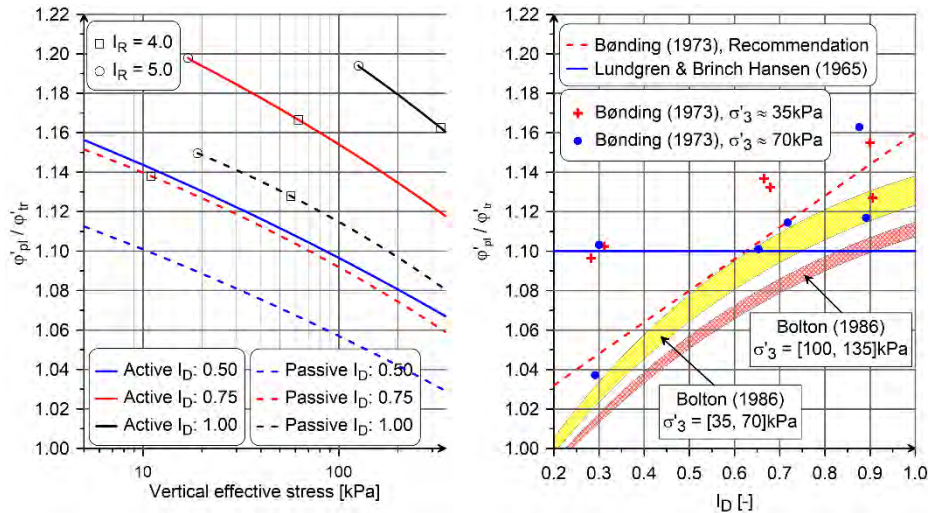


Figure 2 Plane strain factor versus [Left: vertical effective stress for active and passive failure states] and [Right: density index].

The plane strain factor is not strongly linked to the value of  $b = (\sigma'_2 - \sigma'_3) / (\sigma'_1 - \sigma'_3)$ . Using  $b = 0.20$  and  $0.40$  implies a plane strain factor decreasing from 1.192 to 1.182 for an active failure and from 1.125 to 1.117 for a passive failure assuming  $I_D = 0.75$  and a vertical effective stress of 30 kPa.

Bønding (1973) used the results from 12 triaxial and 12 plane strain compression tests to recommend  $\phi'_{pl} = \phi'_{tr} \cdot (1 + 0.16 \cdot I_D)$  as shown as the dashed red line in Figure 2 right, but recommended further testing to support this hypothesis. Lundgren and Brinch Hansen (1965) suggested to use a plane strain friction angle being 10% higher than  $\phi'_{tr}$  with no dependency of the density index and with no data provided to support this conclusion (blue line in Figure 2 right). It is the dilatancy that causes the plane strain factor, so Lundgren & Brinch Hansen (1965) should not be used, cf. also Steenfelt (2004). The yellow filled area on Figure 2 right represents the range of the plane strain factor (passive) using Bolton (1986) with  $\sigma'_3 = 35-70$  kPa (stress range identical to Bønding (1973)). The red filled area represents an identical approach but using  $\sigma'_3$  between 100 and 135 kPa. It is seen that the recommendation from Bønding (1973) [ $\phi'_{pl} = \phi'_{tr} \cdot (1 + 0.16 \cdot I_D)$ ] is an unsafe approximation to the Bolton interval with  $\sigma'_3$  between 35 and 70 kPa and that higher (but still realistic) values of  $\sigma'_3$  may reduce the plane strain factor further. It is indicated by Figure 2 right that a safer approximation accounting for larger mean effective stresses

could be  $\varphi'_{pl} = \varphi'_{tr} \cdot (1 + 0.10 \cdot I_D)$ , which is the expression included in EN 1997-1 DK NA:2021.

## RELATIVE DENSITY INDEX

The x-axis on Figure 2 right refer to the density index  $I_D$ , which is defined by  $I_D = \gamma_{d,max} \cdot (\gamma_{d,i} - \gamma_{d,min}) / [\gamma_{d,i} \cdot (\gamma_{d,max} - \gamma_{d,min})]$  and where  $\gamma_{d,max}$  and  $\gamma_{d,min}$  are the maximum and minimum dry total unit weights, respectively, and  $\gamma_{d,i}$  is the dry in-situ unit weight. Different standards exist for determining the minimum and maximum dry densities and these standards will usually lead to approximately the same value of the minimum dry density, but they will often lead to a significant scatter in the measured maximum dry density and the value of the density index is thus an ambiguous parameter. The subject about density index was investigated in Lunne et al. (2019) reaching the conclusion: *Therefore, it is concluded that there is a need for the development of new standards for a robust determination of  $\gamma_{d,max}$  and  $\gamma_{d,min}$  values. Specifically, a standard for determining  $\gamma_{d,max}$  is required to consistently obtain results at the upper bound of dry unit weight values for the likely range of sands — without crushing the sand grains.*

Knudsen et al. (2020) followed up on the work from Lunne et al. (2019) arriving at a new procedure for identifying the maximum and minimum dry density. It was found that if the suggested approach was followed, different laboratories and different operators within the same laboratory would arrive at almost identical values of the maximum and minimum dry density. The density index has in this paper been used a unique number and with the new method from Knudsen et al. (2020) this approach seems reasonable.

As the challenge with measuring  $\gamma_{d,max}$  unambiguously is solved, one of the main outstanding issues on the laboratory side is to establish a practice for reconstituting sand samples for advanced laboratory testing. The author of this paper was running a laboratory program for a wind farm involving three different geotechnical laboratories with their individual reconstitution procedures. Each laboratory was given an identical sand batch for running two CADc tests using the same  $\gamma_{d,max}$  and  $\gamma_{d,min}$  provided by the Client. One laboratory could reproduce the peak friction angle with an accuracy of  $0.5^\circ$  when comparing the two tests while the reproducibility for the two remaining laboratories was  $2\text{--}3^\circ$ . A difference of more than  $10^\circ$  was observed when comparing the mean value of the friction angle from the different laboratories and these observations highlight the need of an international standard for reconstituting of coarse grained samples in the laboratory.

## STRESS DEPENDENT MODELS

### Introduction

The traditional estimates of either earth pressures or bearing capacities are usually based on closed form expressions defining an earth pressure coefficient or a bearing capacity factor.

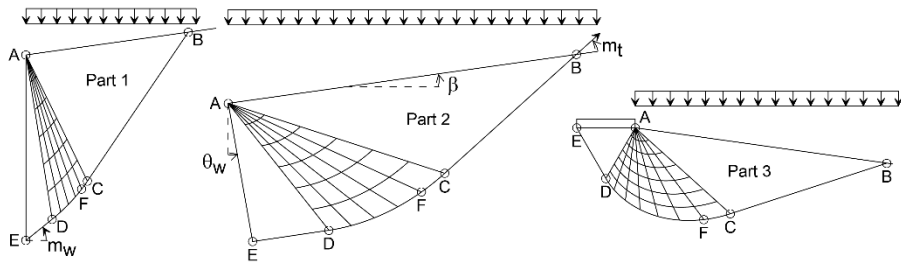


Figure 3 Examples of traditional rupture figures for vertical bearing capacity and lateral earth pressure. Part 1: Active earth pressure, Part 2: Passive earth pressure and Part 3: Bearing capacity.

ABCA on Figure 3 represents a Rankine zone spanned by straight lines and where the mean effective stress within the zone is constant. The zone ACDA is a Prandtl-zone composed of logarithmic spiral arcs and where the mean effective stress increases as the radius in the logarithmic spiral decreases. A stiff soil body ADEA is observed near the wall / footing, and the mean effective stress is constant inside this zone.

The soil surface may be inclined  $\beta$  with horizontal while the wall may be inclined  $\theta_w$  with vertical. At point B the bounding rupture line forms an angle with the soil surface of  $m_t$ , and the angle at point E between the normal to the wall proper and the bounding rupture line is called  $m_w$ .

The rupture figures on Figure 3 are based on one friction angle, used to model the full range of effective stress states. The geotechnical engineer must therefore decide upon a relevant effective stress level reflecting “a representative friction angle” that covers the variation in mean effective stress (and friction angle) throughout the rupture figure in question and this paper will suggest some guidelines as to how this can be performed. The models included in the work are based on zone ruptures only, cf. Figure 3.

### Theoretical basis

A brief description of the theory applied is given below. The reader is referred to either Hansen (2001) or Mortensen & Krogsbøll (2019) for more details. All equations refer to statically admissible rupture mechanisms that are also kinematically admissible when assuming associated flow. The minor principal effective stress within ABCA is estimated by:



$$\sigma'_3 = \frac{q \cdot \cos^2 \beta \cdot (1 - \sin \varphi')}{1 - \sin \varphi' \cdot \sin(2m_t + \varphi')} \quad (4.1)$$

where  $m_t$  can be found by  $\cos(2 \cdot m_t + \varphi' + \beta) = -\sin \beta / \sin \varphi'$  and  $\varphi'$  is computed by Bolton (1986). The effective stress state and the friction angle varies throughout the Prandtl-zone, which is divided into a series of slices each spanning an angle  $\alpha$  of  $\sim 1^\circ$ . Assume that point F is the neighbouring point to C along CD (cf. Figure 3), the minor principal effective stress at point F can then be computed from  $\sigma'_{3,F} = \sigma'_{3,C} \cdot \exp(2 \cdot \alpha \cdot \tan[0.5 \cdot (\varphi'_C + \varphi'_F)])$  representing an iterative procedure. The bounding rupture line at point C is inclined  $m_C = \beta + m_t$  with horizontal while  $m_F = m_C - \alpha$ . The Prandtl-zone can be analysed by this procedure and the result is the minor principal effective stress at point D together with the angle  $m_D$ . The angle at point D needs for statically reasons to be  $m_D = m_w + \theta_w$  (both symbols shown on Figure 3) for earth pressure problems where  $m_w$  is computed by  $\cos(2 \cdot m_w + \varphi'_D + \delta) = \sin \delta / \sin \varphi'_D$  ( $\delta$  is the interface friction angle of the wall). For the bearing capacity problem (Figure 3 Part 3) the value of  $m_D = -(\pi/4 + \varphi'_D/2)$  representing the angle of the rupture line at point D being identical to the angle at point E. The stress dependent bearing capacity factor,  $N_{q,st}$  and the stress dependent earth pressure coefficient,  $K_{q,st}$  can then be computed from the estimated values of  $\varphi'_D$  and  $m_D$ :

$$q \cdot N_{q,st} = (\sigma'_{1,D} + \sigma'_{3,D}) \cdot [1 + \sin \varphi'_D] / 2 \quad (4.2)$$

$$q \cdot K_{q,st} = (\sigma'_{1,D} + \sigma'_{3,D}) \cdot [1 + \sin \varphi'_D \sin(2m_w + \varphi'_D)] / 2 \quad (4.3)$$

The value of  $\sigma'_{1,D}$  can be found from Equation (2.5). Each slice in the Prandtl zone spans  $1^\circ$  and if this value is replaced by  $5^\circ$  the results presented will not change.

### Computed variations of the friction angle

The variation of the friction angle modelled using the theoretical basis is shown in Figure 4 assuming plane strain conditions and a surcharge of 20kPa for the cases bearing capacity, active pressure and passive pressure. The red curve represents  $I_D = 0.60$  for passive and bearing capacity while the blue curve reflects  $I_D = 0.90$  for the same cases. The black curve is an active earth pressure using  $I_D = 0.60$ .

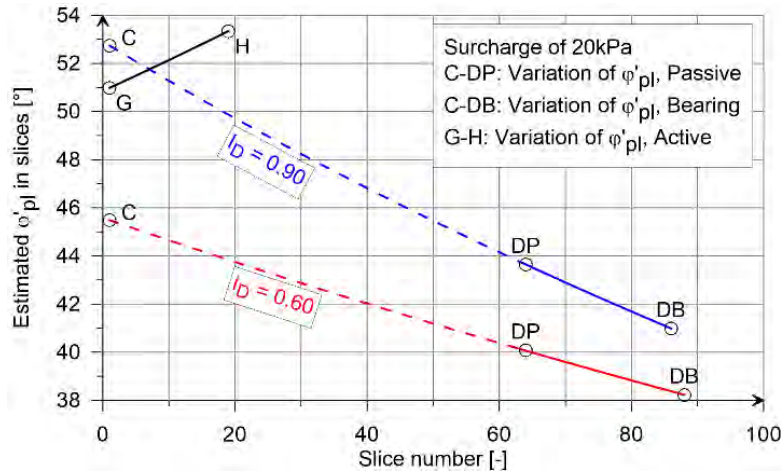


Figure 4 Estimated plane strain friction angle in the slices, where slice number 1 represents point C on Figure 3 and where the highest slice number refer to point D.

The dashed blue curve ( $I_D = 0.90$ ) between C and DP is the estimated friction angles within the Prandtl-zone for the passive earth pressure case, showing  $\sim 9^\circ$  variation in  $\phi'_{pl}$  caused by variation in the mean effective stress. The blue curve between C and DB is the variation within the bearing capacity case showing  $\sim 12^\circ$  variation in  $\phi'_{pl}$ . The red curve ( $I_D = 0.60$ ) in Figure 4 show variations between  $\sim 6^\circ$  and  $\sim 8^\circ$  for the same cases. The black curve between G and H is the active case ( $I_D = 0.60$ ) with only small variations in  $\phi'$ .

### Representative friction angles

The equation for the bearing capacity factor  $N_q$  for an isotropic homogeneous soil is shown in several textbooks, e.g. Hansen (2001):

$$N_q = \frac{1 + \sin \phi'}{1 - \sin \phi'} e^{2\alpha \tan \phi'} \quad (4.4)$$

where  $\alpha = m_t - m_w + \beta - \theta_w$  (leading to  $\alpha = \pi/2$  for  $\beta = 0$ ). The corresponding earth pressure coefficient is:

$$K_q = \cos^2 \beta \frac{1 + \sin \phi' \sin(2m_w + \phi')}{1 - \sin \phi' \sin(2m_t + \phi')} e^{2\alpha \tan \phi'} \quad (4.5)$$

The representative friction angle is defined as the friction angle to use in Equation (4.4) to match the result from Equation (4.2) and similar using (4.5) and (4.3). The intention with this approach is to establish a frame to use when deriving the representative friction angle for a practical design and where the selected friction angle accounts for variations in the effective stresses within the rupture figure in question.

For a bearing capacity case Figure 4 reveals that the maximum friction angle,  $\varphi'_{\max}$  is found at point C in Figure 3 and that the friction angle decreases almost linearly towards point DB where  $\varphi'_{\min}$  is found. Studying the effect of a series of different variations in the surcharge and the density index leads to the following simplification for the bearing capacity case:

$$\varphi'_{\text{rep}} = 0.5 \cdot (\varphi'_{\max} + \varphi'_{\min}) \quad (4.6)$$

The value of  $\varphi'_{\max}$  refer to the zone ABCA in Figure 3, Part 3, and it can be computed directly ( $\sigma'_3 = \text{surcharge}$ ) following Bolton (1986) and  $\varphi'_{\min}$  can be found in a similar way for the zone ADEA provided that a reasonable estimate of the bearing capacity is known ( $\sigma'_1 = \text{bearing capacity}$ ). The value of  $\varphi'_{\text{rep}}$  from Equation (4.6) can be used in Equation (4.4) to absorb the effect of variations in the effective mean stress within the rupture figure. Estimating  $\varphi'_{\text{rep}}$  from  $N_q = N_{q,\text{st}}$  and comparing with the results from Equation (4.6) implies a difference in  $\varphi'_{\text{rep}}$  of less than  $0.1^\circ$  for both plane strain and triaxial strain.

Considering the passive earth pressure case, a similar approach as shown in Equation (4.6) may be given where the maximum friction angle is found in the same zone as found for the bearing capacity case. However, the minimum friction angle in the passive case is found in a zone where the principal effective stress directions vary with the relative roughness of the wall and simple procedures may therefore not be established referring to both  $\varphi'_{\min}$  and  $\varphi'_{\max}$ . Considering a series of different variations in the surcharge and the density index leads to the following simplification for the passive earth pressure case:

$$\varphi'_{\text{rep}} = \varphi'_{\max} - A \cdot I_D \cdot \sqrt{\tan \delta / \tan \varphi'} \quad (4.7)$$

The factor “A” in Equation (4.7) equals 2.1 for triaxial strain and 4.0 for plane strain. The accuracy of the results from Equation (4.7) can be evaluated by comparing with the result obtained using  $K_q = K_{q,\text{st}}$  and Equation (4.7) will imply results within  $\pm 0.2^\circ$  for triaxial strain and  $\pm 0.5^\circ$  for plane strain with the A-factors given. Considering the active earth pressure cases, Figure 4 indicates that the difference between  $\varphi'_{\max}$  and  $\varphi'_{\min}$  is small and that  $\varphi'_{\min}$  is found in the zone ABCA in Figure 3. It is therefore suggested that  $\varphi'_{\text{rep}} = \varphi'_{\min}$  for the active case.

## PLANE STRAIN FACTOR, STRUCTURES

Figure 5 shows the plane strain factor, defined as the representative friction angle for plane strain conditions divided by the representative friction angle for triaxial strain conditions, for the failure types from Figure 3.

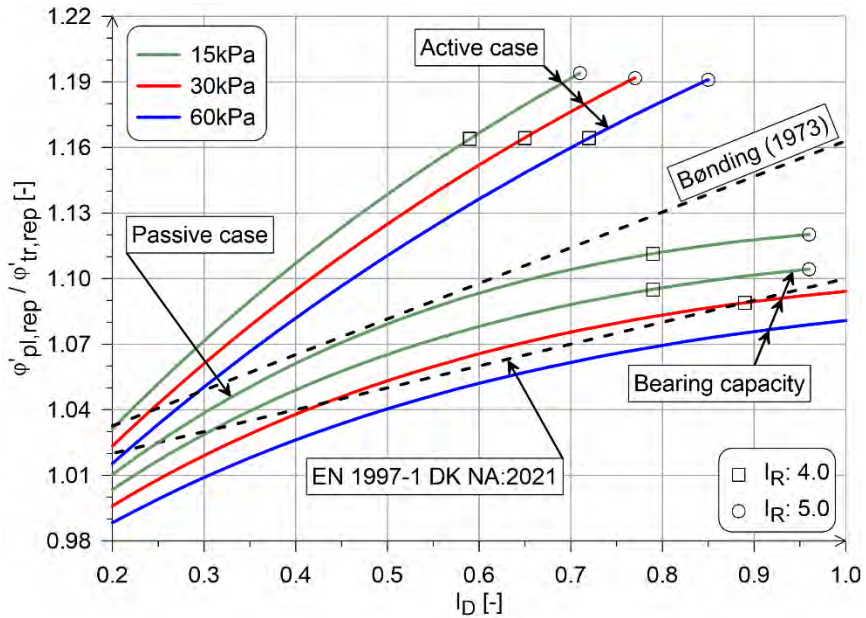


Figure 5 Plane strain factor versus density index for a bearing capacity case, an active case and for a passive case using different values of the surcharge. The earth pressure cases are based on  $\tan \delta / \tan \phi' = 2/3$ .

The individual curves on Figure 5 represent the combined effect of merging a series of stress dependent soil elements into one plane strain factor being dependent on the density index.

Different colour codes on Figure 5 represent different values of the applied surcharge where 15kPa, 30kPa and 60kPa have been used for the active case and the bearing capacity. The passive case is only computed for 15kPa. The earth pressure cases are computed using  $\tan \delta / \tan \phi' = 2/3$ . The recommendation from Bønding (1973) and from EN 1997-1 DK NA:2021 are illustrated through black dashed lines and symbols are included to represent the location of  $I_R$  of 4.0 and 5.0. The 15kPa passive case is seen to deviate only marginally from the 15kPa bearing capacity case so the passive case and the bearing capacity curves are almost identical (at least for a relative roughness of 0.6 or higher). A smooth wall in passive earth pressure implies a plane strain factor of 1.15 for  $I_D = 0.90$  and 15kPa surcharge, which is identical to the recommendation from Bønding (1973) and which exceeds the corresponding factor from bearing capacity by 0.05.

The estimates forming the background for Figures 5 do not include the effect of the unit weight of soil (or the effective cohesion) and this will cause the mean effective stress to be computed too low, implying that the estimated plane strain factor may be on the high side. Most footings gain their main capacity part from the overburden pressure at foundation level so the practical

use of Figure 5 would likely call for the surcharge load in nature to be used as a guideline for selecting the plane strain factor from Figure 5. The conservatism in the approach from EN 1997-1 DK NA:2021 should compensate for the possible effect of using a too low effective mean stress level.

The representative surcharge load for the active and the passive case should likely be the vertical effective in-situ stress halfway down the embedded part of the wall when Figure 5 is used in a design case. This recommendation is based on engineering judgement to compensate for an increasing effective overburden pressure in the nature, which is not included in the estimates behind Figure 5. This recommendation should be on the safe side knowing that EN 1997-1 DK NA: 2021 do not allow utilizing higher plane strain factors than shown as the dashed line in Figure 5. The robustness in a sheet pile wall design is mainly controlled by the relative roughness of the front side of the wall (combined with the applied differential water pressure).

## CONCLUSIONS

When stress-dependent friction angles are accounted for in the traditional rupture mechanisms for vertical bearing capacity and lateral earth pressures, the corresponding coefficients will change. Simple equations are proposed in this paper to ensure that one representative friction angle may be extracted and used in these classical expressions to compensate for variations of approximately  $10^\circ$  in the estimated value of  $\phi'$  within the rupture figures.

Differences between plane strain friction angles and friction angles assuming triaxial strain are studied. The plane strain factor is defined as the factor to multiply on  $\phi'_{tr}$  to estimate  $\phi'_{pl}$ . The factor will depend on the effective mean stress, the density index, and the type of failure in question. EN 1997-1 DK NA:2021 allows for using this effect but results from this paper indicates that the plane strain factor is not fully utilized in EN 1997-1 DK NA:2021.

It is pointed out that the geotechnical community is short of an international standard considering reconstitution of samples of coarse grained material in the geotechnical laboratory.

Bønding (1973), Bolton (1986) and Andersen & Schjetne (2013) seems to align on the subject about triaxial friction angles and the dependency with effective stresses during failure and density index. Furthermore, Bønding (1973) and Bolton (1986) seems to find resembling values for the secant value of the peak friction angle in plane strain. In this way the basis for the present paper seems to be reasonably confirmed when work from other sources than Bolton (1986) is included.

This paper indicates that the shear strength of coarse grained material is significantly higher than what is usually used in Denmark. A high utilization of

the shear strength calls for increased focus on the effect of dilatancy when deriving parameters for models following associated or non-associated flow. This subject has been touched in Mortensen & Steenfelt (2024).

More plane strain testing should be conducted on commercial projects.

## ACKNOWLEDGEMENT

Dr. Anette Krogsbøll has reviewed the paper with corresponding equations, and she has made valuable comments to improve readability. Her efforts are highly appreciated.

## REFERENCES

- Andersen K.H. & Schjetne K. (2013). Database of Friction Angles of Sand and Consolidation Characteristics of Sand, Silt and Clay, *Journal of Geotechnical and Geoenvironmental Engineering*, ASCE, July 2013, pp. 1140-1155.
- Bolton M.D. (1986). The strength and dilatancy of sands, *Geotechnique* 36, No. 1, pp. 65-87.
- Bønding N. (1973). A true triaxial failure criterion in sand (Ph.D.-Thesis in Danish), Technical University of Denmark, Copenhagen, 1973 (Also published in DGI-Bulletin 30).
- Hansen B. (2001). Advanced Theoretical Soil Mechanics, *Dgf-Bulletin* 20, ISBN 87-89833-11-2.
- Knudsen S., Powel, J.J.M., Lunne, T., Thomsen N.V., Krogh, L. and Barwise, A. (2020). Development of New Robust Procedures for the Determination of Maximum and Minimum Dry Densities of Sand, 4th International Symposium on Frontiers in Offshore Geotechnics. Proceedings. (ISFOG).
- Lade P.V., Nam J. & Hong W.P. (2008). Shear banding and cross-anisotropic behaviour observed in laboratory sand tests with stress rotation. *Canadian Geotechnical Journal*, 2008, Volume 45, pp. 74-84.
- Lundgren H. & Brinch Hansen J. (1965). *Geoteknik* (Geotechnics in Danish), Teknisk Forlag, Copenhagen 1965.
- Lunne T., Knudsen S., Blaker Ø., Vestgaarden T., Powell J.J.M., Wallace C.F., Krogh L., Thomsen N.V., Yetginer G. & Ghanekar R.K. (2019). Methods used to determine maximum and minimum dry unit weights of sand: Is there a need for a new standard? *Canadian Geotechnical Journal* 2019. Volume 56, pp. 536-553.
- Mortensen N. & Krogsbøll A. (2019). Effect of tangential surface load components on earth pressure coefficients, *Proceedings of the XVII ECSMGE 2019*.

Mortensen N. & Steenfelt J.S. (2024). L-shaped gravity walls. Recommended practice for ULS. 19<sup>th</sup> Nordic Geotechnical Meeting, Göteborg 2024.

Prandtl L. (1920), Über die Härte plastischer Körper., Nachr. D. Ges. D. Wiss., math-phys. Kl., Göttingen 1920.

Steenfelt J.S. (2004), Guestimate of  $\phi'$ ,  $c'$  and  $\psi$  for coarse grained soil, NGM 2004, XIV Nordic Geotechnical Meeting, May 19<sup>th</sup> – 21<sup>st</sup>, 2004, Proceedings Volume 1.

# EARLY-PHASE MODELLING OF LIME-CEMENT COLUMNS TO REDUCE CARBON FOOTPRINT

**Nikolaj Børner Hansen <sup>1</sup>, Mats Kahlström <sup>2</sup>, and Magnus Rømoen <sup>3</sup>**

## KEYWORDS

Parametric modelling, Early phase planning, Visualization of greenhouse gas emissions, ground improvement

## ABSTRACT

With an ever-increasing focus on greenhouse gas emissions within the construction industry, we must try to change the way we work. Or at least rethink the workflow when we plan and design new linear projects.

In this case, geotechnical engineers at Geovita and NGI, together with the Aas-Jakobsen/ViaNova-network, have prepared a workflow that enables a visual representation of greenhouse gas emissions from a geotechnical point of view in early phase planning.

The result is a unique, early quantification and illustration of the greenhouse gas emission for a planned road or railroad. This gives us a helpful tool for early planning of the alignment of linear infrastructure projects.

## INTRODUCTION

The workflow to perform an early-phase quantification of greenhouse gas emissions from lime-cement columns utilizes a combination of GIS-software and parametric programming in Rhino/Grasshopper, which is explained in more detail in the following sections.

The workflow is demonstrated for a planned road project in Norway showcasing the outcomes of greenhouse gas emissions for three different route options (Alt 1, Alt 2 and Alt 3 shown in Figure 93).

<sup>1</sup> Geovita AS, Oslo Norway

<sup>2</sup> NGI, Oslo Norway

<sup>3</sup> NGI, Oslo Norway



## INITIAL DATA ANALYSIS WITH GIS

### Step 1 - Compilation of existing data in GIS

In the early phase of a project, we often do not have that much data available, so the first thing we must do is try to collect as much relevant data as possible for the project area. However, in our example there are quite a lot of public data available as WMS services, as shown in Figure 1. In addition to looking at terrain data, historical- and sediment maps, much information regarding existing boreholes and ground investigation reports is available through the national database for ground investigations (NADAG) as well as some defined quick clay areas, all published by the Geological Survey of Norway [1].



Figure 57 Project area with current WMS-data shown in QGIS.

### Step 2- Data analysis and soil classification

Reviewing the available data, the authors decided to divide the alignment into three categories of soil classification, presented in Table 1, to inform the need for soil stabilization along the road alignment.

Table 1: Soil classification

Name	Colour in model	Description
Good	Green	Friction soils, stiff clays
Medium	Yellow	Soft clay
Poor	Red	Quick/sensitive clay

The soil classification is defined as 2D surfaces in a GIS-software, as shown in Figure 2. We export the polygons as shape-files (\*.shp) for further use in Grasshopper.

It must be mentioned that the division of these areas obviously will be a very general assessment and such classification should always be performed by someone with geotechnical expertise.

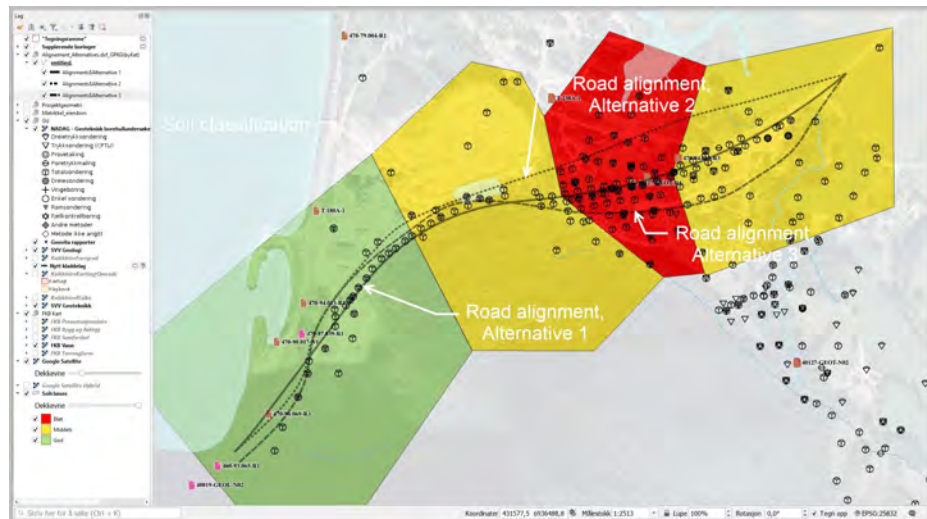


Figure 58 Areas defined by different soil classes together with road alignment alternatives in QGIS.

## PARAMETRIC ANALYSIS IN GRASSHOPPER

### Step 3 - Analysis of road alignment in Grasshopper

With the defined soil class areas in place these areas are imported into a script in Grasshopper, see Figure 3.



Figure 59 Grasshopper script for alignment analysis.

Further on we need to define the existing terrain, an alignment as geometry with the desired width as well as slope for filling and excavation.

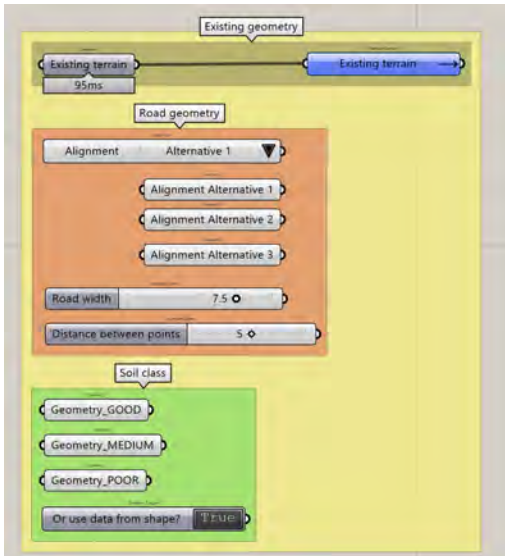


Figure 60 Geometry input in the Grasshopper script.

This script now analyzes the selected alignment and divides this line into points with a user-defined spacing, resulting in “smart points” containing information such as height or depth to terrain, soil class etc. along the alignment. This information is valuable for doing the necessary selection of parameters.



Figure 61 Analyzed points displayed in red in the Rhino 3D viewport.

#### Step 4 – Evaluating the need for ground improvement

For each “smart point” along the road alignment, we have now extracted details that will enable us to determine if ground improvement by use of lime-cement columns is required or not. For this study, a set of criteria are defined in Grasshopper using the Expression-component to categorize parametrically how much, if required, ground improvement should be installed. The chosen criteria need to be established for each individual project and are in this case selected for demonstrative purposes only.

For points within the poor (red) soil class:

- If depth < 2m (cut) or height < 2m (fill), no lime-cement is required.
- If depth > 2m (cut) or height > 2m (fill), install Ø600mm lime cement columns with 40% area coverage and single-column ribs.

For points within the medium (yellow) soil class:

- If depth < 4m (cut) or height < 4m (fill), no lime-cement is required.
- If depth > 4m (cut) or height > 4m (fill), install Ø600mm lime cement columns with 40% area coverage and single-column ribs.

For points within the good (green) soil class:

- No lime-cement columns are required.

The area coverage and spacing between ribs is calculated in accordance with [3]. For this study, a mixing ratio of 50/50 lime-cement with a binder dosage of 60kg/m<sup>3</sup> is used.

The smart points are split categorized in accordance with the criteria. Next, line objects for the lime-cement ribs are created to enable the creation of column volumes.

#### Step 5 - Visual representation of greenhouse gas emissions

By changing the alignment, either sideways and/or in height, it will also change the need for geotechnical mitigations, which again will affect the emissions. The modelling in Rhino/Grasshopper is fully dynamic, helping the engineers to easily compare the emissions caused by the different potential alignment choices.

The visual representation is shown as an example in Figure 6 below. For each defined interval of the road/railroad the amount of greenhouse gases is illustrated as columns. In areas with, for example, a large amount of lime/cement columns, the expected calculated emissions will be high. In areas with only some smaller cuts or fillings, the illustration will indicate much lower future emissions. A figure with the emissions for all 3 routes is shown in Figure 7.



Emission factors are based on data from VegLCA [2] which, in Norway, must be used on large road projects (> NOK 51mio.) to calculate greenhouse gas emissions. A summary of the emissions for each route option is given in Table 2.

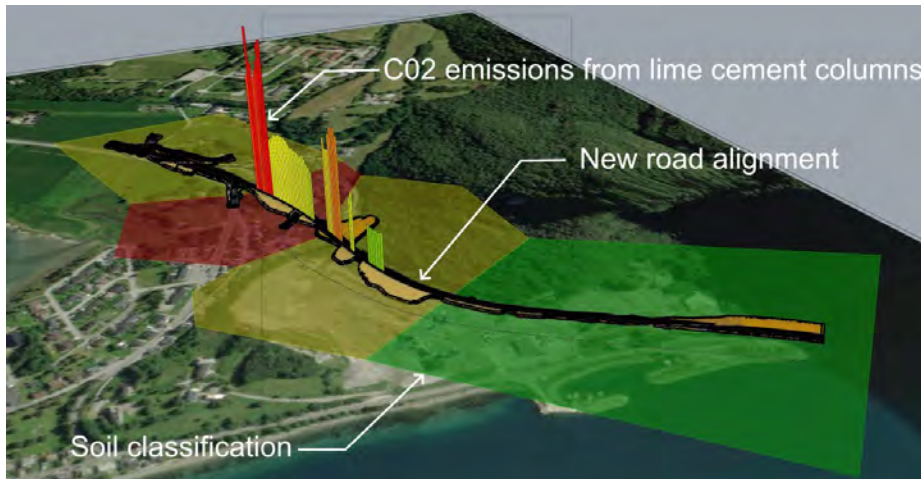


Figure 62 Visual representation of greenhouse gases from ground improvement along route alt 1.

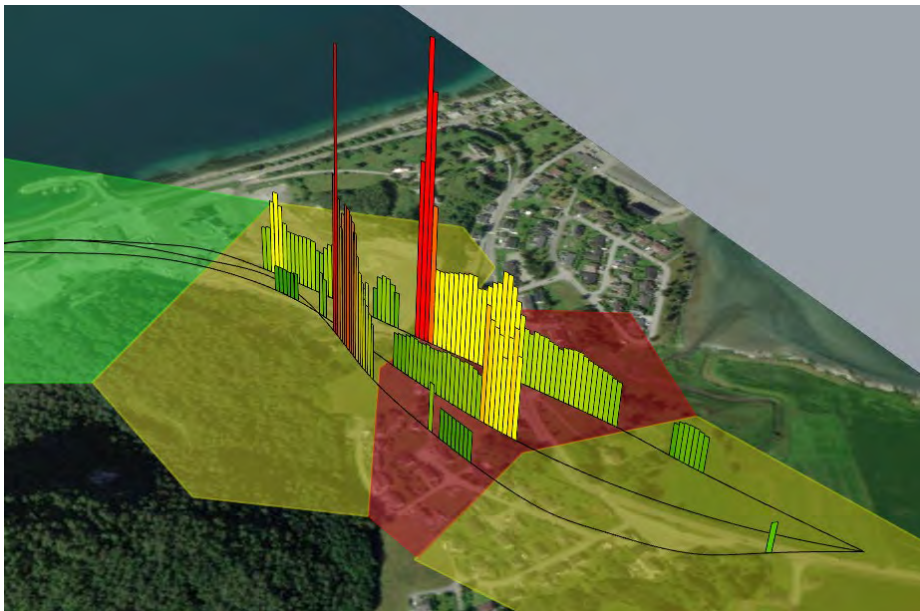


Figure 63 Visual representation of greenhouse gases from ground improvement for all routes.

Table 2: Greenhouse gas emissions from ground improvement for all routes options

Route	Total emissions (kg)
1	953 955
2	2 005 100
3	939 141

## BIM MODELS

The final product is not only a visualization of the emissions, but you will also get detailed generated BIM models of the assumed necessary measures in the early phase of a project. Using developed property set scripts in Grasshopper, all objects are now assigned with discipline- and project-specific properties such as mixing ratio, binder dosage and Model Maturity Index (MMI) among others. Se Figure 8, which is a part of the model from alternative 3, below as an example.

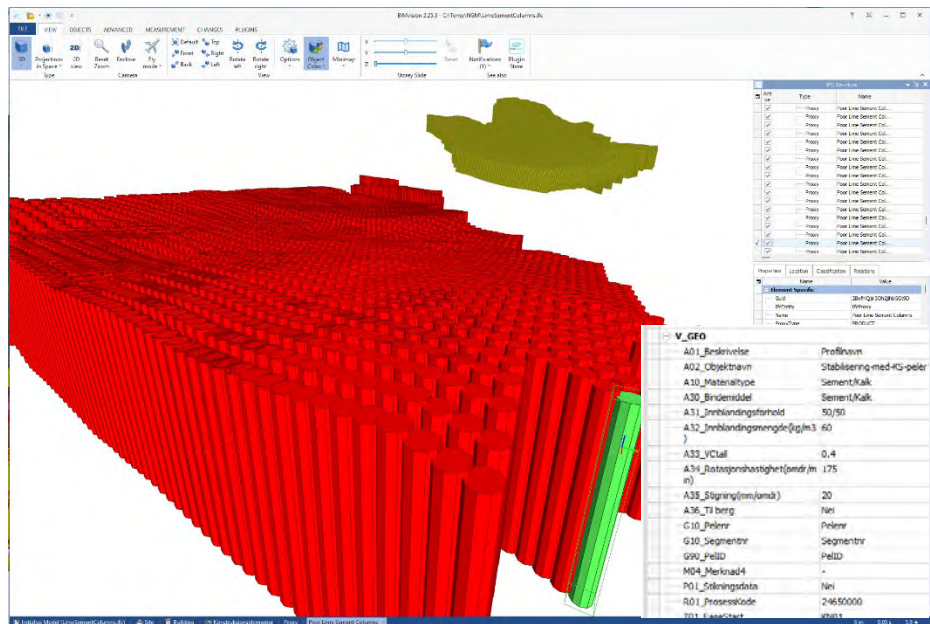


Figure 64 Ifc-model of lime-cement stabilization with specific properties for each Lime Sement Column shown in BIMvision.

## CONCLUSION

This preliminary study shows that the proposed workflow quickly provides a coarse estimate of the need for ground improvement by use of lime-cement columns along the alignment. The fact that we can quickly change various parameters and see the consequences of this in a few seconds will change the way we plan alignments in the future. We also believe that it will increase the focus on the climate effect from groundwork and its importance during early phase planning of a project.

As ground improvement often is a significant part of the emission factor, these figures can, as showcased, be used as a basis for assessment in the early phase of a project. However, this must of course be seen together with emission figures for all other disciplines as well to get a comprehensive overview of the total greenhouse gas emissions for the entire project.

## REFERENCES

- [1] NGU, Geologiske kart: <https://www.ngu.no/en/geologiske-kart> , 2024.
- [2] The Norwegian Public Roads Administration, Bruk av VegLCA: <https://www.vegvesen.no/fag/fokusomrader/klima-miljo-og-omgivelser/utslipp-av-klimagasser/bruk-av-veglca/>, 2024.
- [3] The Norwegian Public Roads Administration, Håndbok V221 Grunnforsterkning, fyllinger og skråninger, 2014.

# **EFFECT OF LOADING RATE ON THE UNDRAINED LIMITING PRESSURE OF DEEPLY-EMBEDDED PILE**

**Yuepeng Dong<sup>1</sup>**

## **KEYWORDS**

Bearing capacity of clay, loading rate, finite element analysis

## **ABSTRACT**

The soil behaviour is rate-dependent as observed in the laboratory and field tests. The foundations can be loaded at various rates in practice, which will cause (i) a wide range of strain rates, and (ii) inhomogeneous strain rate distribution in the surrounding soil. This may cause difficulties to calculate the undrained bearing capacity of clay using the undrained shear strength from standard laboratory and insitu tests at a reference strain rate. This paper investigates the effect of loading rate on the undrained limiting pressure of the deeply-embedded rigid pile section in homogeneous clay using a rate-dependent constitutive model, the MIT-SR. Results suggest that the bearing capacity is strongly affected by the loading rate, which is consistent with observed data.

## **INTRODUCTION**

The soil behaviour is time and rate dependent as observed in the lab tests such as drained creep or secondary compression in 1-D consolidation tests, and the strain-rate effect on the shear resistance in shear tests. In addition, the shear strength interpreted from insitu tests is also affected by the strain rate which can be significantly higher than that in standard lab tests. These rate effects are related to the viscous resistance of soils which is a nonlinear function of strain, strain-rate, stress, and electrochemical reaction. The time and rate dependent soil behaviour has significant impacts on the foundations that are subjected to the long-term dead loads from the structure and to the rapid loading of the environmental factors such as wind and wave. Since the shear strength of soil is rate-dependent, the bearing capacity will also be affected by the loading rate.

This paper investigates the effect of loading rate on the undrained limiting pressure of the deeply-embedded rigid pile section in clay using finite element

<sup>1</sup> Technical University of Denmark



analysis and the MIT-SR model. The computed results clearly demonstrate that the loading rate has significant effect on the undrained bearing capacity on the clay, which is consistent with the observed test data.

## DESCRIPTION OF THE MIT-SR MODEL

### Model description

The MIT-SR model (Yuan and Whittle 2021a) is a generalised elasto-viscoplastic model to describe the time and rate dependent behaviour of saturated clays in shearing, creep and relaxation, and can explain the controversial hypothesis A and B in a unified framework. The model extends the incrementally linearized elastoplastic framework used by the MIT-S1 model, but introduces a generalized hysteretic formulation and a physically-based evolution law that attributes the macroscopic viscoplastic strain to an internal strain rate (occurring within mesoscale soil structure) related to the prior strain rate history.

The MIT-SR model was implemented into Abaqus<sup>TM</sup> through a user-specified subroutine (UMAT), using the explicit substepping algorithm with error control as described in Dong (2023).

### Plane-strain compression tests in the bedding plane

Yuan and Whittle (2021b) evaluated the model performance on the resedimented Boston Blue Clay (BBC) in  $K_0$ -consolidated triaxial compression and extension tests, at four different constant strain rates ( $\dot{\epsilon}_a = 0.05\% / \text{hour}, 0.5\% / \text{hour}, 5.0\% / \text{hour}, 50.0\% / \text{hour}$ ). Fig. 1 shows the computed  $K_0$ -normally consolidated plain strain compression tests on BBC in the horizontal bedding plane (PSK<sub>0</sub>UC-H) at the same four strain rates.

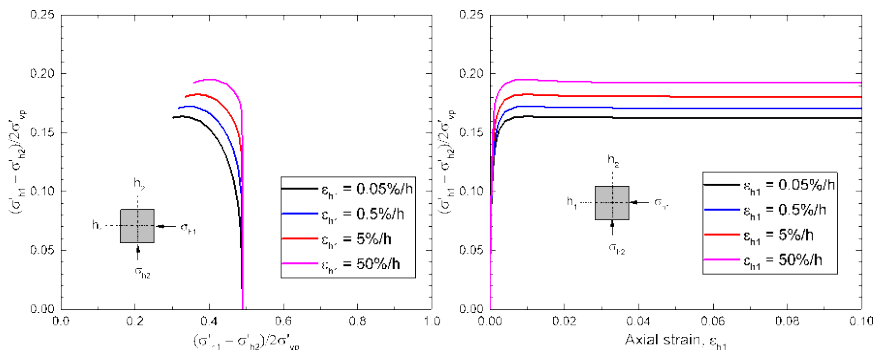


Figure 1 Computed behavior of  $K_0$ -normally consolidated plane-strain compression tests of BBC in the isotropic bedding plane at different constant strain rates

## DEEPLY EMBEDDED PILE SECTION

### Finite element model

The undrained resistance of deeply-embedded pile section in homogeneous clay (Randolph and Houlsby 1984), is conducted to investigate the effect of loading rate on the undrained bearing capacity of clay. The plane strain finite element model is shown in Fig. 2, considering that the pile is long. A normalised displacement ( $s/D = 0.05$ ) is applied on the pile/pipe section in six different durations (0.001hour, 0.01hour, 0.1hour, 1hour, 10hour, 100hour) from seconds to a few days, representing a wide range of loading rate.

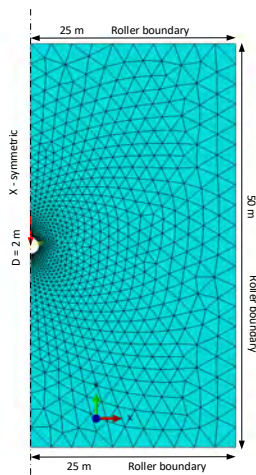


Figure 2 Finite element model of the deeply embedded rigid pile section

### Computed results

Fig. 3 shows the variation of the normalised load ( $N_p = P/Ds_{u,ref}$ ) with the normalised displacement ( $s/D$ ) for the rigid pile section at various loading rates, in the isotropic bedding plane with smooth and rough interface. The undrained shear strength  $s_{u,ref}/\sigma'_{v0} = 0.1722$  is selected as the value derived from the plain strain compression test at a reference strain rate  $\dot{\epsilon}_{h,ref} = 0.5\% / \text{hour}$  in Fig. 1. For the slow loading case ( $0.05\% / \text{hour}$ ) with smooth interface in Fig. 3 (a), the peak resistance factor  $N_p$  is slightly below the lower bound solution (Ukritchon 1998). However, the peak resistance factor  $N_p$  increases with the loading rate and can be significantly larger than the analytical solutions from the limit analysis. Similar rate-dependent observation can be seen in Fig. 3 (b) for the rough interface case.

The computed results in Fig. 3 has strong practical implication in the design of laterally loaded vertical piles (such as monopiles for offshore wind foundations) that can be loaded in a wide range of rates.

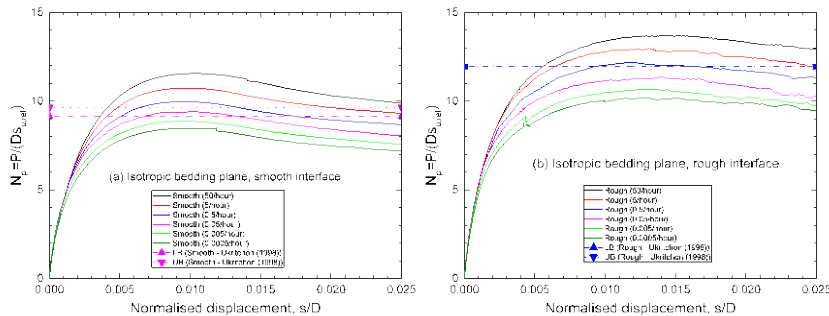


Figure 3 Normalised load-displacement response of rigid pile section in deeply embedded clay at constant loading rates in isotropic bedding plane

## CONCLUSIONS

The undrained bearing capacity is closely related to the undrained shear strength of clay that is rate-dependent. Using the shear strength obtained from the lab at a reference strain rate may cause uncertainties in calculating the bearing capacity of foundations. Finite element analyses with advanced rate-dependent constitutive models are useful to predict the undrained bearing capacity of foundations at various loading rate conditions.

## ACKNOWLEDGEMENT

This work is an extension from previous collaboration with Prof Andrew J. Whittle. Financial support from the Villum Fund is greatly appreciated.

## REFERENCES

- Dong, Y. (2023). "Performance of explicit substepping integration scheme for complex constitutive models in finite element analysis." *Computers and Geotechnics*, 162, 105629.
- Randolph, M. F., and Houlsby, G. T. (1984). "The limiting pressure on a circular pile loaded laterally in cohesive soil." *Géotechnique*, 34(4), 613–623.
- Ukritchon, B. (1998). "Application of numerical limit analyses for undrained stability problems in clay." MIT.
- Yuan, Y., and Whittle, A. J. (2021a). "Formulation of a new elastoviscoplastic model for time-dependent behavior of clay." *International Journal for Numerical and Analytical Methods in Geomechanics*, 45(6), 843–864.

Yuan, Y., and Whittle, A. J. (2021b). “Calibration and validation of a new elastoviscoplastic soil model.” *International Journal for Numerical and Analytical Methods in Geomechanics*, 45(5), 700–716.

# **EUROCODE 7: A FRAMEWORK FOR GEOTECHNICAL DESIGN**

**G. Franzén<sup>1</sup>, B. Hansson<sup>2</sup>, and J. Spross<sup>3</sup>**

## **KEYWORDS**

Eurocode 7, Geotechnical reliability, Sustainability, Robustness

## **ABSTRACT**

During the past 8 years, European engineers have spent many hours discussing, analysing, checking, drafting, and finally approving the next generation of Eurocode 7. The driving force has been to ensure that Eurocode 7 is a useful toolbox for the geotechnical engineers working with soil, rock, fill and groundwater, including all vital aspects for the design, giving guidance but also recognising that the key to a successful geotechnical design is engineering judgement and comparable experience.

This paper gives an overview of part of the content of the second generation of Eurocode and how it can be a useful tool not only as a reference document in procurement but also as a common framework for the development of geotechnical engineering. The paper highlights some new items in the second generation of Eurocode 7; Geotechnical reliability, sustainability, and robustness, and how these items might influence geotechnical engineers' day-to-day work. Finally, the paper elaborates on using the opportunities with a national implementation (EG 2.0).

## **HOW TO MAKE A STANDARD A USEFUL TOOL**

The words "standard" and "tool" are somewhat contradictory. A tool is valuable, and we all happily use it since it facilitates our work. A standard gives a firm recommendation on what to do, and as engineers with creative and free-minded thinking, we hesitate to follow the rules determined by others but try to find our alternative. We do not like somebody else telling us what to do by re-

<sup>1</sup> GeoVerkstan, Kungsbacka Sweden

<sup>2</sup> Keller Grundläggning, Kungsbacka Sweden

<sup>3</sup> Royal Institute of Technology, Stockholm Sweden

ferring to a standard. Hence, is the mandate for the second generation of Eurocode feasible? The aim is to create a user-friendly, up-to-date, harmonised common reference design code that opens for innovation within the civil engineering and building industry on a common market with fair competition. It is a high ambition set out on the European level, and several steps have been taken to make the aim come true. In a few years' time, the second generation will be implemented, and hopefully, it will be the tool that geotechnical engineers need to develop their skills and engineering judgement further.

For Eurocode 7, the key to ensuring that the standard becomes a useful toolbox is to include flexibility and trust that the user fulfils Eurocode's assumption that the user is a competent engineer. The engineer will select the most appropriate tools for the specific project and use them within their limitations and specifications. Let's look at some of the tools in the second-generation toolbox and how they can be used by the competent engineers.

## **PARTIAL FACTORS IS NOT MANDATORY**

If all material codes are considered, The partial factor approach is the most commonly used method to verify structural safety in the Eurocodes. However, Eurocode 7 states that design by calculation using partial factors is only one of at least four options. To verify the ultimate limit state, you can in fact use calculation with any reliability-based method (not only partial factor approach), prescriptive rules, testing or observational method. The basic requirement is that you prove that, with an appropriate level of reliability, the probability of failure is less than the requirement specified by your country. However, using partial factors is a convenient method for most geotechnical structures. Preparing the national annexes includes analyses to ensure that the recommended values will fulfil the probability of failure if used appropriately according to the code. Hence, the engineer does not have to prove it specifically for the considered structure and design. Selecting another verification method is up to the engineer to demonstrate compliance with the requirements in the code.

What is an appropriate level of reliability? The second generation of Eurocode states that different levels of reliability may be adopted, considering the consequences of failure in terms of human lives and injuries as well as social and environmental impacts. The public's reaction and the cost of limiting the risk of failure should also be considered. Once again, Eurocode introduces flexibility that should be used both on the national level to set the requirements on safety linked to consequences and by the engineer for a specific project to use engineering judgement to determine the consequence class, geotechnical complexity class and geotechnical category. The selected geotechnical category will give recommendations on the quality and extent of ground investigation, validation of calculation methods, checking, qualification, documentation, inspection and other measures to ensure that the final product has a quality that fulfils the appropriate level of reliability.

## DESIGN ANNO 2024 IS NOT ONLY RELATED TO SAFETY

In 1975, industry and academia took the initiative to establish a European common design code for civil engineering. Developing the tools that more than 500,000 engineers use daily throughout Europe has been a long process. However, since 1975, a lot has changed in the world: climate change, digitalisation, and urbanisation; the list is long with new items that need consideration in the design of buildings and other civil engineering structures. Therefore, the second-generation Eurocode provides requirements and recommendations not only on structural safety but also on serviceability, durability, robustness, and sustainability.

Opening the Eurocode for design with consideration of sustainability has caused much discussion. Should a design code that traditionally has dealt only with structural safety now also put requirements on sustainable construction, or is that the responsibility of other parties? In the end, the requirement in the Eurocode is vague: Sustainability shall be considered, though how and by whom is up to us as geotechnical engineers. The Eurocode gives flexibility, and it is up to us on a national level to implement a way to consider ecological, social, and economic sustainability. We must take this challenge if we, as geotechnical engineers, want to contribute to a sustainable future.

Robustness is another item where we, as geotechnical engineers, need to tweak our minds. Eurocode is clear: A most probable climate scenario for the design service life of the structure shall be included as an action in the ordinary design of the ultimate and serviceability limit state. So, what is robustness? According to Eurocode, our structures, if designed according to Eurocode, fulfil the requirements of Robustness. But the aim is to review the technical solution and ask – what if? What if there is flooding, storm, or failure in part of the structure or nearby structures, or the loads increase? Are there any adjustments that can be made to minimise the damage and ensure that if the structure fails, it is not catastrophically? Once again, it is up to the engineer to use engineering judgment. Is it worthwhile to adjust the structure, or is it an unnecessary cost?

In 1975, it was still expected to use pen, paper and a slide-rule to verify and design geotechnical structures, see Figure 1.



Figure 1 Eurocode adapting to the designer's environment

The pen is still used; however, the methods are changing with the extensive amount of data and computational resources. Eurocode has adapted to the new working environment by giving more precise guidance on how to use numerical models for the verification of any geotechnical structures, opening the application of statistical approaches in those cases where extensive data is available, and opening the reporting of digital information in BIM (building information model). This is to ensure that the 2<sup>nd</sup> generation of Eurocode will still be applicable in ten years, with respect to the technical developments of computational tools that the engineer uses.

## **IMPLEMENTATION ON NATIONAL LEVEL**

Drafting a standard on a European level is a huge task, and the Nordic group has extensively contributed to it. The result is a standard consisting of three parts: general rules [1], ground properties [2], and geotechnical structures [3]. It is a common framework with flexibility that makes it adjustable for application throughout our Nordic countries [4]. However, we still have a huge amount of work in front of us - the implementation on a national level. Of course, the standard is applicable directly using the default values and choices. Still, if we, at national and project levels, want to ensure that we not only fulfil the requirements but are open to engineers using their knowledge and experience to build the future with economic, innovative, and sustainable structures. We need further discussion and analysis to use the flexibility the Eurocodes provide.

As geotechnical engineers, we love to discuss and argue, but to make sure that the conclusions become useful not only for the debaters, the outcome needs to be formulated into guidelines and national choices. The Implementation Commission for European Standards within Geotechnical Engineering, 2.0 (IEG 2.0) has been reactivated in Sweden to use the revision of Eurocode 7 to facilitate a national joint development of geotechnical engineering practice, where the flexibility of the Eurocodes is used with consideration of all parties views. IEG.2.0 is a non-profit organisation with 56 members from all parts of the Swedish geotechnical industry (authorities, clients, consultants, contractors, academia, societies, and manufacturers). See Figure 2.

The members' funds work together to analyse the changes and flexibility, summarizing the results in recommendations on national choices and preparation of guidelines. Coming together makes it possible to give financing to members who are recognised for their knowledge within the different areas of expertise to do the analyses that will form the base for the national recommendations. This industry-wide collaboration procedure was a great success the first time it was used, and we expect the same outcome this time: it will facilitate an increased competence among Swedish geotechnical engineers and, therefore, increase the competitiveness of the Swedish geotechnical construction industry. More information about the work can be found on IEG's website [5].





Figure 2 Members of IEG 2.0

## CONCLUSION

The second generation of Eurocode is a common step on the European level to update the reference design code to include future challenges. It is open for national adaptation but recognises that we depend more on each other and work across European borders. Hence, there is a need for a common framework to avoid mistakes and unnecessary misunderstandings within our civil engineering and building projects. Eurocode provides the framework where we, on the national level and in the project, can make use of the included flexibility by allowing the competent engineer to use their engineering judgement.

## ACKNOWLEDGEMENT

The authors would like to thank all members of IEG 2.0 for their efforts in contributing to a common understanding of Eurocode and ensuring that engineers will use it in the coming years and consider it an essential tool for everyday work.

## REFERENCES

- [1] EN 1997-1:2024, Eurocode 7 — Geotechnical design – Part 1: General rules, CEN, 2024
- [2] EN 1997-2:2024, Eurocode 7 — Geotechnical design – Part 2: Ground properties, CEN, 2024
- [3] FprEN 1997-3:2024, Eurocode 7 — Geotechnical design – Part 3: Geotechnical structures, CEN, 2024
- [4] G. Franzén, A. Eggen, O. Møller, P. Tolla, D. R. Hauksson. Nordic co-operation gives results. 19<sup>th</sup> Nordic Geotechnical Meeting, 2024.
- [5] [www.ieg.nu](http://www.ieg.nu)

# EVALUATION OF NORWEGIAN DESIGN METHODS FOR AXIAL CAPACITY OF DRIVEN PILES IN SAND

**F. Kolsgaard<sup>1</sup>, S.A. Degago<sup>2,3</sup>, A. Emdal<sup>3</sup> and F. Oset<sup>2</sup>**

## KEYWORDS

Driven piles, Piles in sand, Concrete piles, Steel piles, Axial capacity, Code of design

## ABSTRACT

This study evaluates the Norwegian design methods for axial capacity of driven piles in sand referred to as the PV91 ( $\beta$ -method) and NGI-05 method. The two methods are based on different approach with different input parameters. The semi-empirical PV91-method is recommended to be used for preliminary design with a preference for NGI-05 method as primary design tool. However, since the NGI-05 method demands investigation of sand layers with CPT, the PV91-method serves as an alternative design approach when CPT data is unavailable. Thus, it is important that these two methods are evaluated on the same basis. In this work, a database consisting of 86 international pile tests in sandy soils are analysed and the prediction of shaft friction is evaluated for the PV91-method. PV91-method exhibits variability in axial capacity predictions but is shown to be highly conservative for densely and very densely deposited sand. For loose sand it is shown to overestimate shaft friction capacity for some pile tests. The NGI-05 method is evaluated in several database studies, showing greater accuracy than what the PV91-method performed in this database study. NGI-05 along with other CPT-methods tends also to overestimate capacity in some cases, and especially after friction capacity is corrected for ageing effects. This study offers guidance on the application of the methods and highlights areas for future improvement.

## INTRODUCTION

Various methods are employed for designing the axial capacity of friction piles in sandy soils. In Norway, the prevailing methods are the PV91-method (also

<sup>1</sup> ERA Geo, Molde, Norway

<sup>2</sup> Norwegian Public Road Administration, Trondheim/Oslo, Norway

<sup>3</sup> Norwegian University of Science and Technology, Trondheim, Norway

known as the  $\beta$ -method) and the NGI-05 method [1, 5]. The PV91 is an empirical approach utilizing a fixed side friction factor  $\beta$  and is recommended for preliminary design in the Code of Practice for Piles 2019 [1] and NPRAs handbook V220 [5]. The PV91-method is in general regarded as a conservative approach for estimation of shaft resistance. On the other hand, the NGI-05 method is based on empirical correlations derived from Cone Penetration Test (CPT) data. Since the NGI-05 method demands investigation of sand layers with CPT, the PV91-method serves as an alternative design approach when CPT data is unavailable. CPT is not always available or possible to conduct in sandy soil deposits. This motivated the current study to systematically evaluate both methods based on the same basis. This helps designers to understand the implication of the adopted pile designs.

This article evaluates the semi-empirical method PV91 with a database and compares it to the NGI-05 method and other available full scale pile load test databases. A discussion of the accuracy of the NGI-05 method compared to other frequently used CPT-methods based on former database studies is also presented. This study only focuses on the side friction capacity and does not evaluate the pile tip capacity.

## DESIGN OF FRICTION PILES IN NORWAY

Norwegian design of the axial capacity of driven piles in sand is carried out using two methods referred to as the PV91 ( $\beta$ -method) and NGI-05 method [1, 5]. The empirical PV91-method calculates axial frictional capacity by estimating mobilized friction by use of a side friction factor  $\beta$  along the pile shaft, similar to the semi-empirical method API-RP2A method. The basis for  $\beta$ -values seem to be a redrawing of the comparison of  $\beta$ -values by Kraft & Focht [2] and is based on data from load tests for piles in clay, presented by Eide at a Pile Seminar in Norway in 1987 [3]. Soil density, pile length and mean effective vertical stress  $\sigma'_{v,0}$  is necessary input for estimating shaft friction  $\tau_{s;cal}$ .

$$\tau_{s;cal} = \beta * \sigma'_{v,0}$$

Where  $\beta$  is the coefficient for the normalized side friction. The recommended value for beta is a function of pile length and sand density and is shown as the hatched area in Figure 100.

When CPT-data is available, the Code of Practice for Piles [1] recommends the CPT-based NGI-05 method [4], where side friction is directly correlated to relative density, which is calculated based on CPT-data. Characteristic side friction  $\tau_{s;k}$  is calculated along the pile:

$$\tau_{s;k} = \frac{z}{z_t} * \sigma_a * F_{DR} * F_{last} * F_{spiss} * F_{mat} * F_{\sigma}$$

Where  $z/z_t$  is the relationship between depth and the final pile end depth,  $\sigma_a$  the atmospheric reference pressure,  $F_{last}$ ,  $F_{spiss}$  and  $F_{mat}$  are coefficient for type of

load, pile end geometry and material.  $F_{\text{sigma}}$  is a relationship between effective vertical stress and the reference pressure  $\sigma_a$ .  $F_{\text{DR}}$  is a factor based on the relative density, where the relative density is calculated based on empirical CPT-relations, which is specific for the NGI-method:

$$D_r = 0,4 * \ln \left[ \frac{q_c}{22 * (\sigma'_{v;0} * \sigma_a)^{0,5}} \right]$$

## THEORETICAL EVALUATION OF DESIGN METHODS

A theoretical comparison of normalized side friction for a selection of example piles is presented in Figure 1. Pile length of 20, 40 and 60 m is considered in sand with constant relative density of 0,4 (loose), 0,6 (medium dense) and 0,8 (dense). The comparison is made by back calculating the implied beta from the NGI-method by the formula  $\beta = \frac{\tau_s}{\sigma_{v;0}'}$  based on the mentioned relative densities where  $\sigma_{v;0}'$  is the mean effective stress for the pile length. Comparison between the range of beta factor for PV91-method and NGI-05 implied  $\beta$ -factor is shown in Figure 100.

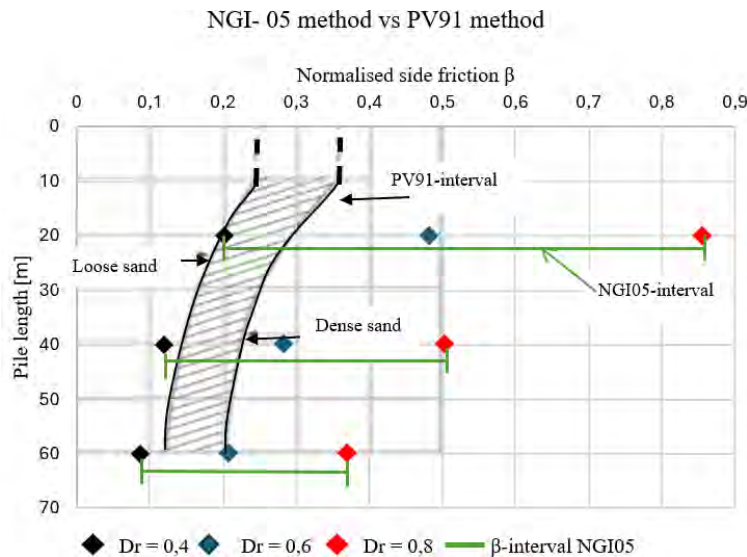


Figure 65 Comparison of normalized side friction factor  $\beta$  for PV91 and corresponding  $\beta$  as implied by NGI-05 back-calculated.

Normalized side friction interval from NGI-05 method is significantly larger than for PV91-method. For loose sand ( $D_r=0,4$ ), both methods tend to give similar estimate of the side friction. For denser sand and shorter pile lengths the NGI-05 method predicts higher normalised side friction than the PV91. For

the six theoretical example piles, the interval is approximately 3,5 – 6,5 times the size compared to the PV91-method. This is shown in table below.

*Table 1. Comparison of  $\beta$ -values for example piles for PV91- and NGI05-method.*

Pile lengths	PV91		NGI05		NGI05 larger interval than PV91
	$\beta$ -values	$\beta$ -interval	$\beta$ -values*	$\beta$ -interval*	
20	0,19 – 0,29	0,10	0,2 – 0,85	0,65	650%
40	0,14 – 0,22	0,08	0,12 – 0,5	0,38	475%
60	0,12 – 0,2	0,08	0,09 – 0,37	0,28	350%

\*Back-calculated side friction factor  $\beta$ .

## EVALUATION BASED ON DATABASES OF FULL-SCALE LOAD TESTS

### a. Evaluation of PV91-method

Load tests results from three former database studies have been used in a database study for evaluation of the PV-91 method: NGI-99 database [7], ZJU-ICL database from 2015 [8] and pile load tests results from Leibniz University Hannover 2018 [9]. Acceptance criteria for the database required that load test results included information about pile type, loading method, measured failure load, CPT-data for estimating relative density ( $D_r$ ), soil layering and soil type. The database incorporates 23 tension tests from the NGI database, 23 tension tests and 20 compression tests from the ZJU-ICL database, and 6 tension tests from Leibniz University. The normalized side friction coefficient  $\beta_{\text{measured}}$  was derived from the failure load and compared to  $\beta_{\text{PV91}}$  from the PV91-method with the relation  $\beta_{\text{PV91}} / \beta_{\text{measured}}$ . Ratio greater than 1 indicates PV91 overestimating the side friction.

The results presented in table indicates that the PV91-method greatly underpredicts shaft resistance, but the statistics indicators show that there are relatively large variations. Among all the samples, the 12 tests on concrete piles have the expectation value closest to 1, and they exhibit the lowest dispersion with a coefficient of variation of 0.44 but with the largest standard error. The expectation value for open-end steel piles is higher than for closed-end steel piles, but with a slightly higher coefficient of variation as well. Results indicate that PV91-method is more conservative for tension piles, than for compression piles.

Table 2. Statistical evaluation of PV91-method for selection of pile tests

Selection	Test piles	$\beta_{cPV91}/\beta_{measured}$			
		Mean $\mu$	Standard deviation $\sigma$	Coefficient of variation CV	Standard error SE
All piles	86	0.57	0.30	0.53	3.2%
Tension load	66	0.54	0.27	0.50	3.3%
Compr. Load	20	0.66	0.35	0.53	7.8%
Open piles	52	0.59	0.31	0.53	4.3%
Closed piles	34	0.53	0.27	0.51	4.6%
Concrete piles	12	0.69	0.31	0.44	8.9%
Steel piles	74	0.55	0.29	0.53	3.3%
Time info.	58	0.54	0.30	0.56	3.9%
Closed end steel	23	0.45	0.20	0.42	4.1%
Open end steel	51	0.59	0.31	0.53	4.3%

Relative density  $D_r$  is the one known geotechnical parameter investigated by CPT for the database tests. Plotted graphically together with  $\beta_{cPV91} / \beta_{measured}$ . Ratio is shown in figure under.

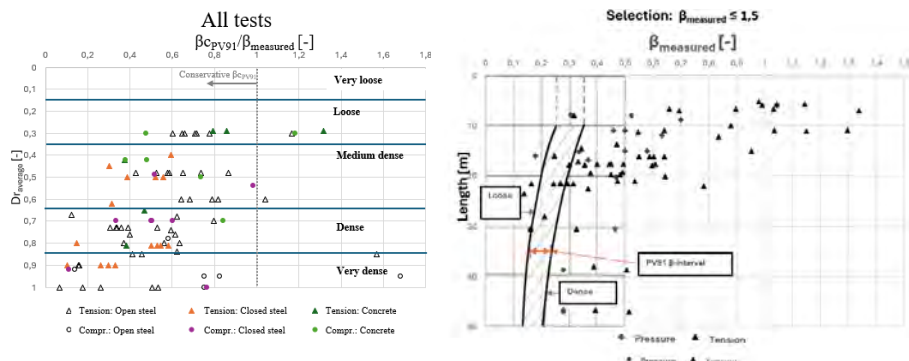


Figure 66 Left: The results are depicted with relative Density  $D_r$ . The blue lines represent the set limits for characterizing density of sand based on the classification from API [11]. Right:  $\beta_{measured}$  vs pile length. Compared to PV91 interval of side friction factor  $\beta$ .

The three tests in loose sands with  $D_r = 0,3$  where the method overestimates the capacity are tests from Norway (Larvik and Drammen). Of the 86 test piles there is only six test results where the PV91-method overestimates shaft capacity, and with mean value of 0,57 it mostly under predicts capacity with a significant margin.

Plotted beta values from the load tests vs the PV91-beta design interval is shown for the selection of tests with  $\beta_{measured} < 1,5$  in

Test results indicate a statistically skewness, suggestion that the PV91-method predicts shaft capacity more accurately in loosely deposited sand ( $Dr$ : 0.15 – 0.35) compared to moderately dense ( $Dr$ : 0.35 – 0.65) and dense/very dense deposited sand ( $Dr$ : 0.65 – 1.0), where the method offers significant conservative shaft capacity design for the pile tests in the database.

### Evaluation of NGI-05 Method

Database studies by Schneider et al. [9], Yang et al. [8], and Lehane et al. [10] demonstrate stronger statistical outcomes ( $\mu$ ,  $CV$ ) for CPT methods than for the API-RP2A method, and for findings of this study concerning the PV91-method. Because the CPT-methods are correlated to pile tests this is somewhat expected.

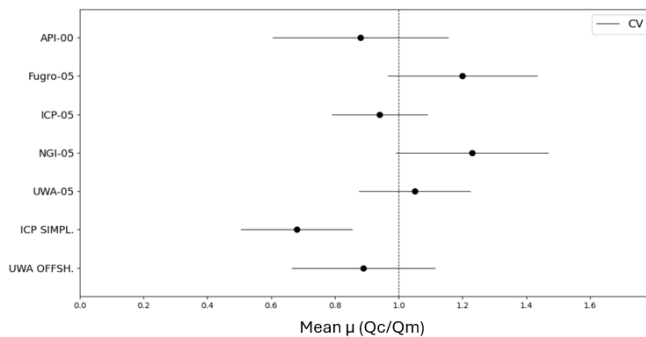


Figure 67 Expectation value  $\mu$  and coefficient of variation  $CV$ : Total capacity of all 80 pile tests with time information in the database study by Yang et al. (2015). The results are not time corrected.

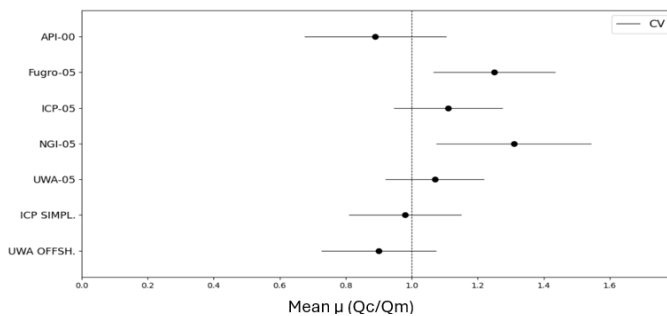


Figure 68 Expectation value  $\mu$  and coefficient of variation  $CV$ : Total capacity for 41 time-corrected and weighted tests in the database study by Lehane et al. (2017).

The NGI-05 method, in several instances, demonstrates an overestimation of both side friction capacity and total capacity compared to pile tests in the database studies, particularly for calculated capacities scaled up using time correction factors. Although there are clear indications that the bearing capacity of friction piles in sand significantly increases with time (Karlsrud et al., 2014a), challenges are associated with increasing friction capacity for time effects in

capacities calculated using CPT-based methods. Results from the study by Le-hane et al. [10] and Yang et al. [8] shown in Figure 3 and Figure 4 indicate that this largely applies to the NGI-05, Fugro-05, and to some extent ICP-05 and UWA-05 methods, in which these methods can overestimate side friction when corrected for time effects.

## FINAL REMARKS

This work evaluates the PV91-method's prediction of shaft capacity against an extensive database of pile tests. Some final remarks are listed below:

- The PV91-method is shown to be highly conservative for densely and very densely deposited sand. Pile tests have shown measured capacities for side friction much higher than those calculated using the PV91-method.
- The PV91-method's calculation of side friction is not necessarily conservative for piles in loosely deposited sand, or for piles in sand material with silt content. This is contrary to the current recommendation from Code of Practice for Piles [1]. For such cases, one should be cautious about scaling up the calculated bearing capacity with time effects in loose sands.
- Several database studies shows that CPT-based design methods for side friction demonstrate better predictions than the semi-empirical PV91-method and the API-RP2A method and should be used when there are available CPT-data.

Based on the results of this study, questions can be raised about whether the PV91-method should be updated and adjusted, given the current availability of numerous pile tests, and the large underestimation of friction capacity for denser sands. It is not always possible to attain CPT-results for pile sites, and there is a need for design methods without CPT data. Consideration about whether a higher relative density can be documented without CPT data in sandy materials should then be considered.

NGI-05 method was not calibrated for time corrections when the method was developed and the method tends to overestimate side friction capacity relative to pile tests in database studies [8,10], particularly when time correction factors are applied. Consequently, caution is advised when increasing the side friction bearing capacity calculated using the NGI-05 method with time effects, as allowed by Norway's Code of Practice for Piles [1].

Fugro-05, ICP-05, and UWA-05 may face similar challenges in accurately predicting capacities when adjusted for time effects.

Additionally, the evaluation of pile tip capacity using various calculation methods should also be addressed, which is not covered in this article.



## REFERENCES

- [1] Norwegian Geotechnical Society: Peleveiledningen 2019: Code of practice for piles, 2019. 380 pages. <https://ngf.no/publikasjoner/peleveiledning-ikke-medlemmer/>
- [2] L.M. Kraft, J.A Focht, S. F, Anerasinghe: Closure to Friction Capacity of Piles Driven into Clay, 1981. Journal of Geotechnical Engineering, Volume 109, Issue 5
- [3] O. Eide: Pelefundamentering: Åpning - dagens situasjon - Utfordring og muligheter, 1987. Unpublished paper presented at Kursdagene, NTH Trondheim
- [4] C. Clausen, P. Aas, and K. Karlsrud: Bearing capacity of driven piles in sand, the NGI approach, 2005. Proceedings of International Symposium. on Frontiers in Offshore Geotechnics, Perth. s. 574-580
- [5] Statens Vegvesen (Norwegian Public Road administration): N-V220 Geoteknikk i vegbygging, 2023 8.th version. <https://viewers.vegvesen.no/product/859978>
- [6] F. Kolsgaard et al: Evaluering av beregningsmetoder for friksjonspeler i sand, 2020. Master thesis, Norwegian University of Science and Technology (NTNU). <https://ntnuopen.ntnu.no/ntnu-xmlui/handle/11250/2779327>
- [7] C. Clausen, P. Aas.: Bearing Capacity of Driven Piles, Piles in Sand, 2001. Internal report NGI
- [8] Z. Yang et al.: A Comprehensive Database of Tests on Axially Loaded Driven Piles in Sands, 2005. Academic Press, eBook ISBN: 9780128047484
- [9] K. A. Schmoor et al.: Reliability of design approaches for axially loaded offshore piles and its consequences with respect to the North Sea, 2018. Journal of Rock Mechanics and Geotechnical Engineering, 10(6), s. 1112-1121
- [10] B. Lehane et al.: Characteristics of unified databases for driven piles, 2017. Proceedings of 8th International Conference on Offshore Site Investigations and Geotechnics, SUT London. s. 162-194
- [11] API: ANSI/API recommended practice 2GEO, 2014. API Washington, DC, USA

# **EVALUATION OF SOLIDIFICATION/ STABILIZATION TECHNOLOGY PERFORMANCE BY COMBINING ECONOMIC AND ENVIRONMENTAL IMPACTS ASSESSMENT FOR A PORT IN SWEDEN**

**E. Tamadonyazdian<sup>1</sup>, M. Gholampoor<sup>2</sup>, K. Farsäter<sup>3</sup>, and  
M. Bayat Pour<sup>4</sup>**

## **KEYWORDS**

Life cycle assessment, Economic analysis, Stabilization, Solidification, Cement mixtures

## **ABSTRACT**

The importance of reducing environmental impacts has gained speed in the contemporary global context. Stabilization/Solidification (S/S) has become a practical method for handling polluted dredged sediments to make them usable as a construction material. This study aims to evaluate the environmental and economic impacts of a 48,586 m<sup>2</sup> port, with stabilized dredged sediment, by focusing on the production and construction stages in Sweden. It encompasses eight distinct scenarios that are proposed based on cement types and binder mixtures. Environmental impact categories, including Global Warming Potential (GWP), Acidification Potential (AP), Eutrophication Potential (EP), and Ozone Depletion Potential (ODP), were assessed. Life Cycle Assessment (LCA) modeling was carried out in the software LCA for Experts (GaBi). The study also incorporates Life Cycle Cost (LCC) calculations to be integrated with LCA results, using the Single-Point Rate (SPR) method to aid decision analysis. The results show that the optimal scenario features cement type I with a 20% cement and 80% slag binder mixture. This choice demonstrated a nearly 29% reduction in environmental impacts and approximately 1.5 MSEK lower initial costs compared to the base case which is cement type I with a 30% cement and 70% slag binder mixture. These results highlight the potential for environmentally responsible and cost-effective decision-making in infrastructure projects through an integrated LCA and LCC approach.

<sup>1</sup> Swegon Operations AB, Sweden

<sup>2</sup> Division of Building Materials, Lund University & Peab Anläggningsteknik, Sweden

<sup>3</sup> Division of Building Services, Lund University, Sweden

<sup>4</sup> Division of Structural Engineering, Lund University, Sweden

## INTRODUCTION

The global emphasis on reducing environmental impacts, as evidenced by the Sustainable Development Goals (SDGs) and the Paris Agreement, underscores the significance of sectors like construction and real estate in advancing sustainable practices [1]. Life Cycle Assessment (LCA) has emerged as a methodology for evaluating the environmental impacts of construction projects [2]. LCA calculation tools like LCA for Experts (GaBi) facilitate analysis of environmental impacts across various life cycle stages of construction materials and processes. Life Cycle Cost (LCC) calculations are performed for evaluating the economic consequences of an item or system, by summing all costs incurred during their life span [2].

Stabilization and Solidification techniques, commonly employed in managing hazardous waste materials, offer practical solutions for transforming contaminants into stable forms suitable for disposal or reuse [3]. In the context of dredging operations, where substantial volumes of sediment require management, stabilization/solidification methods have been proven to effectively manage contaminated dredged sediments [4].

This study aims to evaluate the environmental and economic impacts associated with a port project, located in Gothenburg, Sweden, both for the present situation and also other possible alternatives. Then, eight different scenarios are proposed. By assessing both environmental and economic aspects, the study seeks to provide insights and recommendations for informed decision analysis regarding the project and its alternatives [5].

## METHOD

The Methodology section of this paper encompasses three key steps: LCA, LCC, and Decision Analysis. LCA involves defining the assessment unit, establishing system boundaries, collecting data on raw material inputs, energy consumption, emissions, and assessing environmental impacts such as greenhouse gas emissions [6,7]. LCC analysis identifies cost components, including capital and operational expenses, using historical data and expert opinions [6,7]. Decision Analysis utilizes evaluation criteria aligned with research objectives and applies the Single-Point Rate (SPR) method to rank alternative scenarios based on environmental and economic impacts [6,7].

### Case study and proposed scenarios

The case study focuses on the Köping Port Deepening and Harbor Basin Expansion Project, an integral component of the Mälärprojektet. The project involves deepening and widening the fairway and harbor basin, stabilizing and solidifying dredged sediments, and creating an industrial zone spanning 48,586 m<sup>2</sup> [8]. Key tasks include constructing access roads, establishing temporary quays, implementing drainage systems, and noise barriers to ensure smooth operations [8]. The project aims to efficiently utilize stabilized dredged sediment

and mitigate environmental impact [8]. Figure 1 provides an overview of the project location, emphasizing its proximity to major road connections and neighboring industrial operations.



*Figure 1: Overview of the project location*

This study investigates various alternative scenarios within the Köping Port project to assess their environmental and economic impacts. These scenarios, analyzed through LCA and LCC, aim to understand the project's sustainability implications and identify optimal options. Each scenario, distinguished by different types and proportions of cement and slag in the binder mixture, is outlined in Tables 1 and 2 for easy comparison, providing insights into their environmental and cost considerations.

*Table 1: Proposed scenarios*

Scenario	Type of Cement	Ratio of Cement	Ratio of Slag
Present Situation	type I	30%	70%
Scenario 1	type I	40%	60%
Scenario 2	type I	20%	80%
Scenario 3	type II	30%	70%
Scenario 4	type II	40%	60%
Scenario 5	type II	20%	80%
Scenario 6	type III	30%	70%
Scenario 7	type III	40%	60%
Scenario 8	type III	20%	80%

Table 2: Amount of each material in different portions of binder mixture in [Kg ]

Used material	Slag 70% & Cement 30%	Slag 80% & Cement 20%	Slag 60% & Cement 40%
Cement	4 600 872	2 761 166	5 991 117
Slag	10 734 302	12 573 452	9 343 501
Activated Carbon	774 310	774 310	774 310

### Life Cycle Assessment (LCA)

The LCA methodology applied in this study encompasses defining the assessment unit, establishing system boundaries, and collecting data on environmental impacts, focusing on the Köping Port project's production and construction phases. The LCA evaluation considers various life cycle stages, including raw material extraction, transportation, construction processes, and product delivery to the project site. Employing LCA for Experts (GaBi) software, version 10.6.1, enables analysis, utilizing databases such as Ecoinvent and Sphera to assess environmental impacts across different stages. Additionally, the study utilizes Environmental Product Declarations (EPDs) for slag and activated carbon, covering stages A1-A3, to provide detailed insights into the environmental impact of raw materials. Environmental impact categories such as Global Warming Potential (GWP), Acidification Potential (AP), Eutrophication Potential (EP), and Ozone Layer Depletion Potential (ODP) are investigated. The normalization and weighting methods employed, particularly the CML 2016, excluding biogenic carbon, allow for comparisons and prioritization of environmental impacts [9]. Overall, this approach facilitates a thorough assessment of the Köping Port project's environmental impacts and identifies areas for improvement to promote sustainable development.

### Life Cycle Cost (LCC)

This study examines the initial cost of the Köping Port project, which is related to the production and construction stages [10]. Required data were gathered from Peab (a construction company) and suppliers, including machinery rental fees and material costs as well as reasonable estimations for personnel expenses. Tables 3, 4, and 5 detail machinery types, material costs, and labor force involvement, respectively, providing insights into project finances.

Table 3: Information about machineries

Machinery				
Item	Model	Cost/ (SEK/day)	No. of Machines	Total work days
Excavation Machine	Hitachi Vacker Neuson	5 242.00	1	75
Stabilization Machine	Volvo	7 300.00	1	220

*Table 4: Information about materials*

<b>Material</b>			
<b>Material</b>	<b>Type of Material</b>	<b>Supplier Company</b>	<b>Cost/ (SEK/ tonne)</b>
Cement	BASE (type I)	Cementa	956.34
Cement	type II	Cementa	1 042.36
Cement	type III	Cementa	1 184.04
Slag (GGBS)	Merit	Swecem	176.59
Activated Carbon	AquaSorb CS	Jakobi Group	18.28

*Table 5: Information about Labor Force*

<b>Workmanship</b>			
<b>Item</b>	<b>No. of personnel</b>	<b>Work time/ month</b>	<b>Fee/ SEK</b>
Worker (Excavation)	3	4	30 000.00
Worker (Stabilization )	3	10	30 000.00
Project Manager (Exc.)	1	4	60 000.00
Project Manager (Sta.)	1	10	60 000.00
Site Manager (Exc.)	1	4	55 000.00
Site Manager (Sta.)	1	10	55 000.00
Labor Leader (Exc.)	1	4	40 000.00
Labor Leader (Sta.)	1	10	40 000.00

### Integration of LCA and LCC

The study aims to determine the optimal scenario by integrating LCA and LCC, using the SPR method [6,7]. This method, depicted in Table 6, utilizes weighting factors to gauge the relative importance of LCA and LCC. By considering three options for SPR calculations, the study assesses different scenarios to provide insights into the project's environmental and economic impact viability.

*Table 6: Weighting factors for different options*

<b>Options</b>	<b>Weighting factors</b>	
	<b>LCA</b>	<b>LCC</b>
Option 1	50 %	50 %
Option 2	60 %	40 %
Option 3	40%	60 %

## RESULTS AND DISCUSSION

### Life Cycle Assessment (LCA)

Figure 2 shows the environmental impact of each scenario, focusing on Acidification Potential (AP). Among the scenarios examined, scenario 8 emerges with the lowest impact with  $4.41\text{E}+03$  [kg SO<sub>2</sub> eq.], followed by scenario 6 with  $4.87\text{E}+03$  [kg SO<sub>2</sub> eq.], and scenario 5 with  $5.68\text{E}+03$  [kg SO<sub>2</sub> eq.]. Scenario 1 illustrates the highest AP with  $9.39\text{E}+03$  [kg SO<sub>2</sub> eq.]. The observed differences underscore the importance of considering alternative materials and cement formulations in mitigating the environmental impacts of construction activities. Scenario 8, characterized by cement type III with a higher ratio of slag, demonstrates the potential benefits of utilizing sustainable materials in cement production.

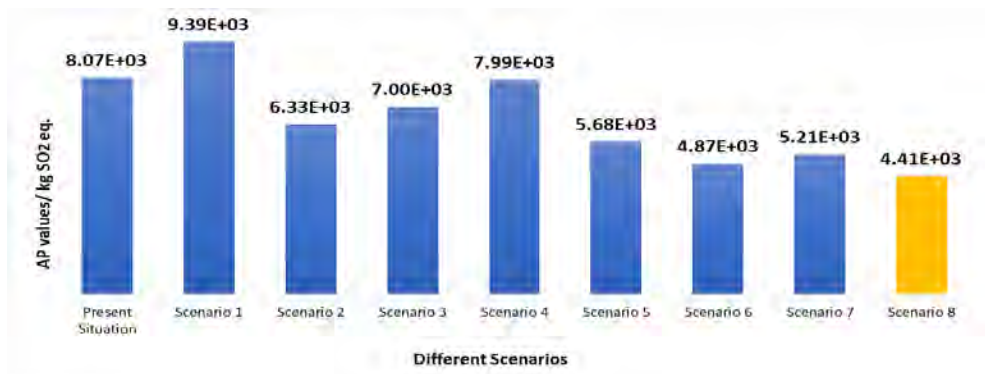


Figure 2: Acidification Potential comparison between different scenarios [kg SO<sub>2</sub> eq.]

Figure 3 presents the Eutrophication Potential (EP) across scenarios. Similar to AP results, scenario 8 has the lowest results with  $3.51\text{E}+02$  [kg Phosphate eq.], with a notable difference from scenario 1 with  $1.18\text{E}+03$ . This highlights the importance of scenario selection in minimizing EP. The analysis highlights the potential of sustainable cement formulations (type and percentage) in mitigating environmental impact and promoting eco-friendly construction practices.

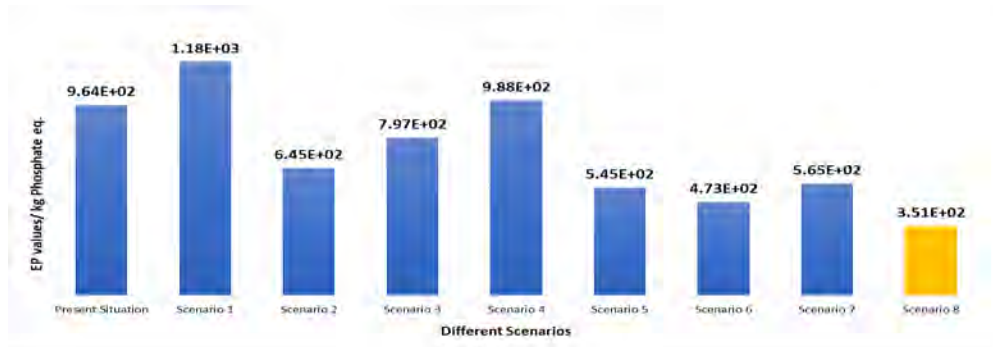


Figure 3: Eutrophication Potential comparison between different scenarios [kg Phosphate eq.]

The subsequent category analyzed in both the present situation and proposed scenarios is the Global Warming Potential (GWP). Once again, scenario 8 shows the best results, this time in the GWP environmental impact category. Scenario 8, defined by specific attributes including cement type III with a binder composition of 80% slag and 20% cement, demonstrates a notable capacity to mitigate GWP, emphasizing its pivotal role in advancing sustainability objectives. Following scenario 8, scenarios 6 and 5 stand out as better performers within the GWP category. Scenario 6, associated with cement type III featuring 70% slag and 30% cement, exhibits the best GWP results after scenario 8. Despite using a higher amount of cement compared to scenario 5, scenario 6's advantageous GWP results can be attributed to its cement type III composition, underscoring the significance of careful material selection in influencing environmental outcomes. This trend is consistent across previously investigated environmental impact categories, where scenario 8 maintains the lowest impact, followed by scenario 6 in second place, and scenario 5 in third place. The pivotal difference lies in the specific cement type utilized in each scenario, highlighting that even when cement weights are comparable, its quality and type exert a more significant influence on environmental impacts.



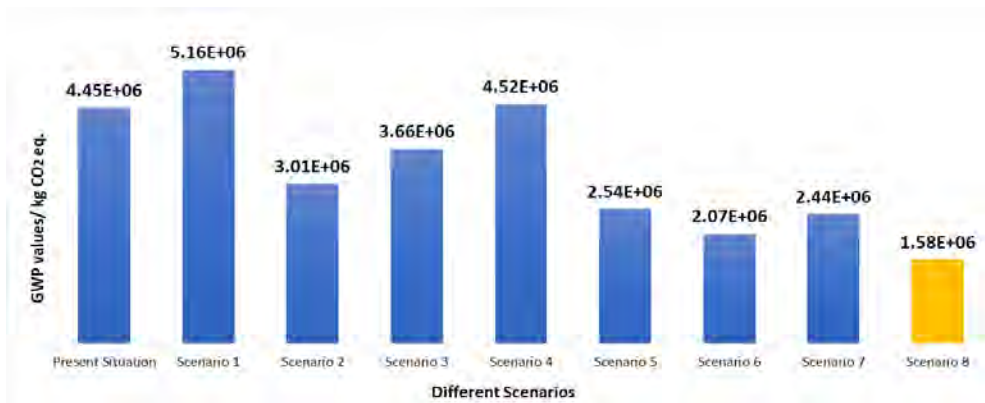


Figure 4: Global Warming Potential comparison between different scenarios [kg CO<sub>2</sub> eq.]

In Figure 5, Ozone Depletion Potential (ODP) was investigated, confirming scenario 8 as the top performer in the life cycle assessment for the fourth time. scenario 8 leads, followed closely by scenario 5 in second place and scenario 2 in third, highlighting their environmental performance in mitigating ozone layer depletion. The analysis of the ODP category in Figure 5 reveals the role of cement in influencing environmental outcomes. scenarios with lower cement content, specifically comprising 20% of the binder weight, consistently outperform others, highlighting the importance of cement management in optimizing ODP. Moreover, the study elucidates a clear correlation between cement quality and ODP, with the transition from type I to type III cement demonstrating a reduction in negative environmental impact, particularly on the Ozone layer depletion potential.

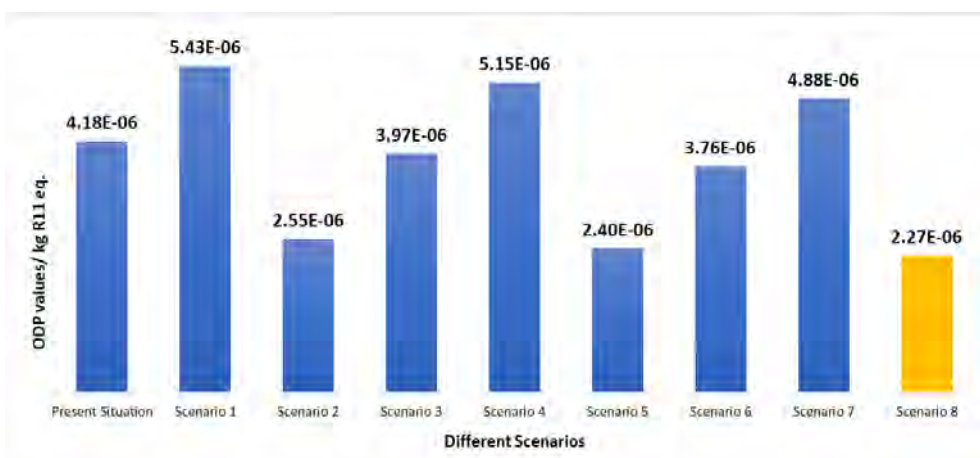


Figure 5: Ozone Depletion Potential comparison between different scenarios [kg R11 eq.]

Figure 6 presents weighted and normalized LCA results, integrating findings from various environmental impact categories. Scenario 8 consistently emerges as the top performer across these categories, demonstrating superior environmental performance compared to others. This reinforces scenario 8's significance in achieving sustainability goals and underscores the critical role of material selection in mitigating environmental impacts.

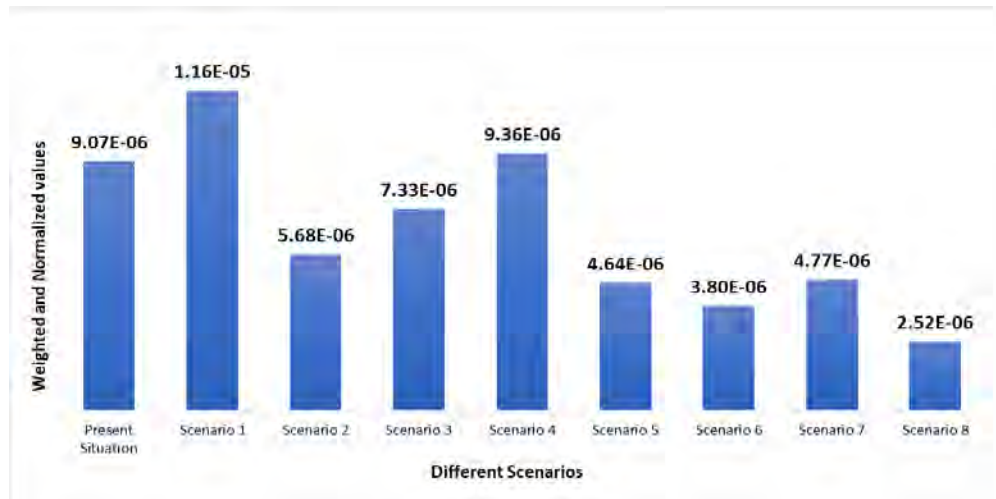


Figure 6: Weighted and Normalized results

### Life Cycle Costing (LCC)

The total initial cost for the project is around 11.73 MSEK. However, it reduced to 10.34 MSEK in scenario 2, indicating a potential cost reduction of approximately 10% in this specific scenario.

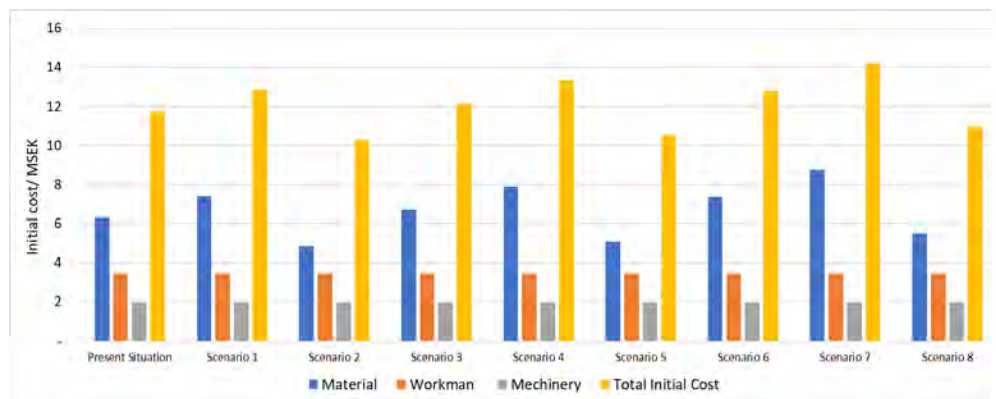


Figure 7: Initial cost in present and proposed scenarios [MSEK]

### Integration of LCA and LCC

SPR calculations integrate LCA and LCC weights to determine the optimal scenario. Table 7 displays weighting factors and minimum SPR values, offering insights into the combined assessment of environmental and economic factors to identify the optimal scenario. The below table shows scenario 2, with the lowest SPR value, features cement type I with an 80% slag and 20% cement binder mixture. Despite expectations favoring scenarios with less cement, scenario 2, with the most cost-effective cement type, strikes the ideal balance between environmental impact and economic feasibility, making it the optimal choice for the Köping port stabilization project.

*Table 7: Lowest SPR values and corresponding scenario*

Options	Weighting factors		Lowest SPR value	Related scenario
	LCA	LCC		
Option 1	50%	50%	5.15E+06	Scenario 2/ cement type I – slag 80% & cement 20%
Option 2	60%	40%	4.12E+06	Scenario 2/ cement type I – slag 80% & cement 20%
Option 3	40%	60%	6.18E+06	Scenario 2/ cement type I – slag 80% & cement 20%

Figure 8 shows the LCA and LCC results for all scenarios. Despite a marginal cost difference of about 1 MSEK, scenario 6 shows approximately 2.38 times lower environmental impact compared to the base case. Similarly, scenario 8, employing cement type III with an 80%-20% slag-cement distribution, yields a cost saving of around 1 MSEK compared to the base case, with a 3.59 times lower environmental impact.

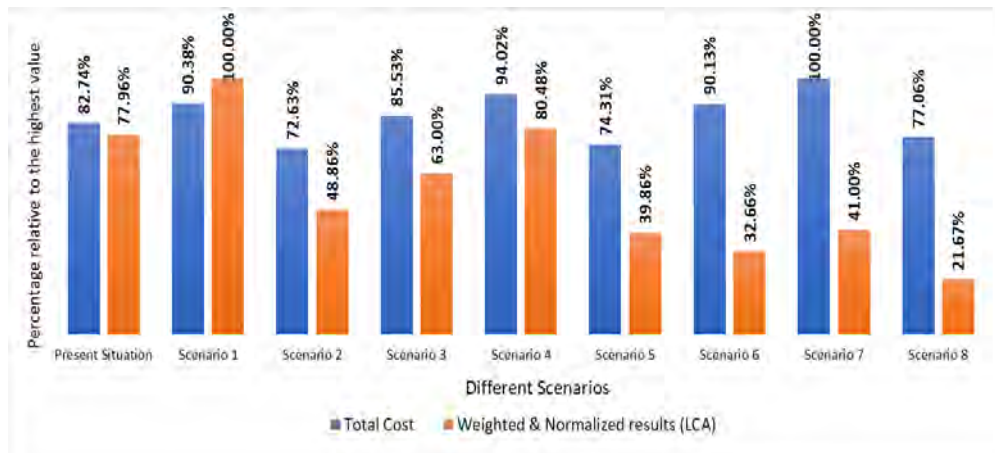


Figure 8: Integration of weighted and normalized LCA results with LCC results

## LIMITATIONS AND FURTHER STUDY

Data validation from the industrial lab and academic sources ensured project-specific insights, although limitations included uncertainties in the A3 stage of the LCA study and emissions due to data constraints. Additional environmental impacts like Freshwater Aquatic Ecotoxicity and Marine Aquatic Ecotoxicity were not fully explored due to data limitations, while contaminants in excavated sediment were not addressed. Further validation and experimentation are recommended to assess the mechanical properties of the proposed stabilization mixture, ensuring its feasibility for this project.

## CONCLUSIONS

This study aimed to investigate the environmental and economic impacts during the stabilization of a port project in Sweden, as well as to identify the most optimal stabilization solution. By considering material, machinery, and workforce costs, it was found that material costs dominated the project's total expenses. Eight scenarios through varying cement types and proportions were analyzed and the results revealed that scenario 8 (cement type III, 80% slag & 20% cement) consistently performed best across selected environmental impact categories.

Based on the LCA analysis, scenario 8, featuring cement type III, resulted in a lower environmental impact, emphasizing the importance of material selection in reducing the project's environmental impact. Moreover, while cement cost significantly influenced total expenses, scenarios with lower cement content, like scenario 2 (cement type I, 80% slag & 20% cement), emerged as the best option from the cost perspective. Integrating LCA and LCC highlighted the decisive role of cost in decision-making, ultimately identifying scenario 2 as the optimal choice, and striking a balance between environmental aspects and cost-

effectiveness. These findings emphasize the importance of thoughtful material selection and strategic decision analysis in construction projects.

## ACKNOWLEDGEMENT

I am grateful to Peab for their collaboration on this project. Additionally, I appreciate their provision of essential data, such as material content, which significantly contributed to its completion.

## REFERENCES

- [1] On the Role of Construction in Achieving the SDGs. *J Sustain Res* 2019;1.
- [2] W. Alaloul, M. Altaf, M. A. Musarat, A. Faisal, A. Mosavi. Life Cycle Assessment and Life Cycle Cost Analysis in Infrastructure Projects: A Systematic Review, 2021/03/08.
- [3] EuDA (European Dredging Association), Dredged Material & Environmental Regulations in EU, 2005.
- [4] T. N. Burt, “Guidelines for the beneficial use of dredged material,” 1996.
- [5] C. M. Wilk, ‘Solidification/Stabilization Treatment and Examples of Use at Port Facilities’, in *Ports 2004*, Houston, Texas, United States: American Society of Civil Engineers, May 2004, pp. 1–10. doi: 10.1061/40727(2004)92.
- [6] M. Bayat Pour and M. L. Elsayed, ‘Assessment of the environmental impacts, energy performance and economic aspects of various construction materials’, Master thesis, Lund University, Faculty of Engineering, 2020.
- [7] E. Tamadonyazdian, ‘Evaluation of in-situ technology performance and decision analysis by combining economic and environmental impact analysis for a case study’, Master thesis, Lund University, Faculty of Engineering, 2023.
- [8] Technical specification from Peab contract with Köping Kommun.
- [9] D. Koch, A. Friedl, and B. Mihalyi, ‘Influence of different LCIA methods on an exemplary scenario analysis from a process development LCA case study’, *Environ Dev Sustain*, vol. 25, no. 7, pp. 6269–6293, Jul. 2023, doi: 10.1007/s10668-022-02302-w.
- [10] B. S. Dhillon, *Life cycle costing for engineers*. Boca Raton, FL: Taylor & Francis, 2010.

# EXCAVATIONS IN SOFT SOILS: REVIEW OF DESIGN APPROACHES

**G. Portmann<sup>1</sup>, A. Arnold<sup>1</sup>**

## KEYWORDS

Excavations, soft soils, earth pressure, bracing loads, mass displacement, failure mechanisms, numerical modelling, combining practice and theory

## ABSTRACT

The design of deep excavations in soft soils is a complex task. Design engineers are typically faced with decisions such as modelling active and passive earth pressures as well as their distribution in terms of bracing loads, the choice of embedment depth of supporting structures with respect to bottom heave and the selected soil-model considered in finite-element codes. The current contribution provides links between these topics in the design of deep excavations in soft soils using the example of an idealised excavation based on selected soil parameters of the “Lilla Bommen” project in soft Gothenburg clay. The modelling of earth pressure distribution is linked to embedment depth and bottom heave as well as to the bracing design. The investigated example of an idealised excavation is analysed with different approaches proposed in literature, allowing for a comparison of earth pressure and bracing load distributions. Subsequently, the excavation is analysed with the finite-element code “Optum G2”. Initial results and comparison to analytical models are provided and discussed.

## INTRODUCTION

Structures in urban areas are increasingly built in and on soft soils. These soils are typically characterised as fine-grained, water-saturated and normally or slightly over-consolidated [1]. Construction in soft soils is challenging as they may respond undrained to changes in load due to a low water permeability. Consequently, excess pore water pressures  $\pm \Delta u$  develop, which reduce over time until drained conditions are finally achieved. In the design of an excavation, it is not known a priori whether drained (long-term analysis) or undrained (short-term analysis) conditions are most relevant for the design. Thus, a clear understanding of the development of relevant earth pressures and their effects

<sup>1</sup> Lucerne University of Applied Sciences and Arts HSLU, School of Engineering and Architecture, Institute of Civil Engineering, Horw Switzerland

on the design of an excavation is essential. Various studies on excavations in soft soils [3][7][9][12][13] indicate a correlation between bottom heave stability and loads and/or deformations of the excavation support.

In this article, different design approaches for deep excavations in soft soils are compared on behalf of a case study. An 8 m deep and 40 m wide excavation in soft Gothenburg clay is analysed, (corresponding approx. to the dimensions of the Lilla Bommen tunnel excavation). The focus of the comparative calculation is therefore not to validate the executed “Lilla Bommen tunnel” project, as has been done by other authors. This contribution summarises relevant findings from the first author’s master’s thesis at HSLU.

## SUBSOIL

The subsoil data was considered as reported in [8][15]. Gothenburg clay is a slightly over-consolidated ( $OCR \leq 2.0$ ), glacial-marine clay. It has a liquid limit of  $w_L = 76\%$ , a plastic limit of  $w_P = 34\%$  and an in-situ water content of approx. 55%. The groundwater table is located just below the surface.

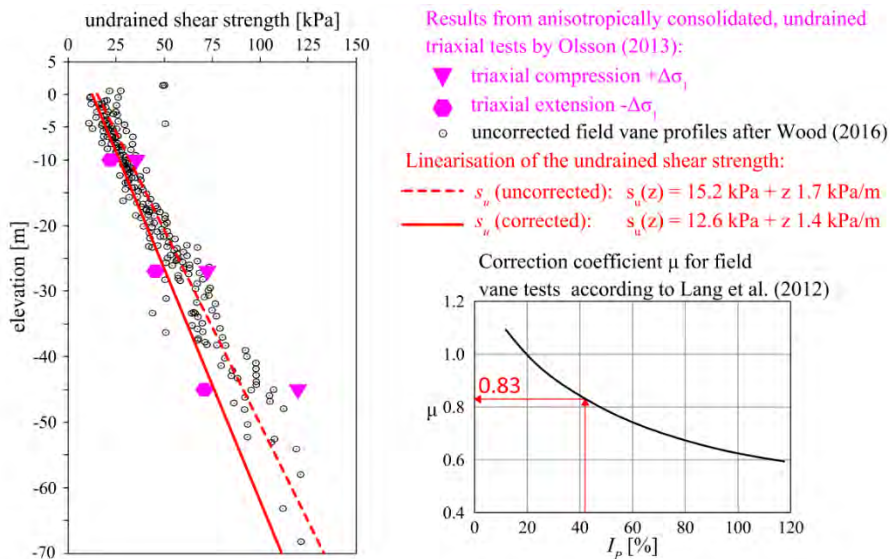


Figure 69 Derivation of an undrained shear strength profile from test data according to Olson [8] and Wood [15].

The subsoil profile was idealised for the calculations as a single layer. Uncorrected soil parameters from field vane shear tests by [15] and the results from undrained triaxial tests on undisturbed soil samples by [8] are summarised in Figure 1. In order to consider the influence of the shear velocity, the  $s_u$ -depth profile obtained in field vane shear tests was modified by the correction factor  $\mu$  as a function of the plasticity index  $I_p$  [6]. The corrected  $s_u$ -depth profile is bounded by the results from triaxial compression and extension, however, it

correlates more closely to the extension tests. This result is to be expected according to [2] and is believed to provide a suitable basis for the design of an excavation as the majority of the soil experiences a stress change similar to that of triaxial extension (unloading by excavation). The relevant parameters are summarised in Table 1.

Table 16 Geotechnical parameters after [8] and [15]

$\gamma$	16.4	kN/m <sup>3</sup>	Unit weight
$\phi'_{cv}$	30.5	°	Critical state friction angle
$s_u(z)$	12.6 kPa + z · 1.4 kPa/m	kPa	Undrained shear strength profile
$k$	$4.97 \cdot 10^{-10}$	m/s	Coefficient of permeability
OCR	1.65 <sup>1)</sup>	-	Over-consolidation ratio
$K_0$	0.68 <sup>1)</sup>	-	Coefficient of earth pressure at rest
$E_{u,50}$	8.5	MPa	Undrained triax. stiff. at 50% of peak strength
$E_{ur}$	34.1	MPa	Unloading-reloading Young's modulus
<sup>1)</sup> In-situ measurement by dilatometer testing [15]			

## RELEVANT DESIGN ASPECTS

### Drained or undrained analysis?

Undrained material behaviour is to be expected in low-permeability, fine-grained soils in the event of rapid changes in the loading level, such as arise during excavations. However, the question remains as to whether the consideration of undrained behaviour is relevant for the design of an excavation? Various authors [1][4] report that negative excess pore water pressures ( $-\Delta u$ ) must be expected due to the unloading conditions in the predominant area around an excavation pit.

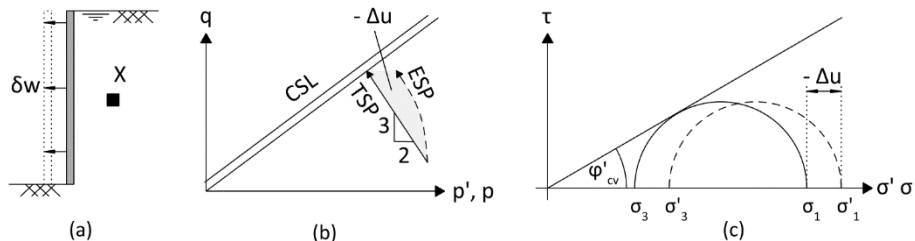


Figure 70 Development of stress paths on the active side of an excavation: (a) Wall displacement leads to unloading on the active side; (b) Effective Stress Path (ESP) and Total Stress Path (TSP) - the ESP reaches the critical state after dissipation of the negative excess pore pressures  $-\Delta u$ ; (c) Mohr's stress representation after the excavation with negative excess pore pressures  $-\Delta u$ .

Generally, negative excess pore water pressures either result in higher short-term failure stresses or that the critical state is only reached during consolidation as illustrated in Figure 2. Thus, a free-standing height in the soil may occur in the short term. However, on the basis of this insight and from the consideration of stress paths, it still cannot be concluded that the undrained case with



the development of negative excess pore water pressures is not relevant for design. Both the magnitude of the shear stress mobilised at the failure state for a specified water content of the soil and the failure mechanism that occurs is decisive for the analysis.

### Bottom heave stability and embedment depth

The bottom heave stability is typically not relevant for soils with  $\varphi' \geq 25^\circ$  in the drained state according to [1][13][14]. In undrained conditions, however, this failure mechanism is to be investigated although it may be assumed that negative excess pore water pressures occur in the soil due to the unloading from excavation [1][12][13][14]. Increasing undrained shear strength with depth, as could be observed in the present example, requires that the width of the considered failure mechanism is to be varied so as not to overestimate the stability [1][14]. The calculation approach according to [14] shown in Figure 106(a) and (b) provides a relevant failure mechanism width of  $x \cdot B = 7.2$  m for the investigated excavation ( $B = 40$  m,  $H = 8.0$  m and soil properties according to Table 23). The stability factor  $F$  can be defined according to Eq. (1) with the partial safety factors  $\gamma_G = 1.20$ ,  $\gamma_Q = 1.30$  and  $\gamma_{GB} = 1.30$  [1].

$$F = \frac{\frac{1}{\gamma_{GB}}(R_{v,k} + R_{GB,k})}{\gamma_G \cdot G_k + \gamma_Q \cdot Q_k} \quad (1)$$

The forces are defined as (see also Figure 106)

$$R_{GB,k} = 5.14 \cdot s_{u2} \cdot x \cdot B; R_{v,k} = s_{u1} \cdot H; G_k = \gamma \cdot H \cdot x \cdot B; Q_k = q_k \cdot x \cdot B \quad (2)$$

and the bottom heave stability is assumed to be sufficient for values  $F \geq 1.0$ . In the excavation under consideration, a value of  $F = 0.79$  results at design level, indicating insufficient bottom heave stability.

Methods for increasing bottom heave stability reported in [13] consist of: (I) Increasing the embedment depth  $t$ ; (II) Increasing the load within the excavation pit (e.g. underwater excavation); (III) Creating a supporting base slab / jetting slab before excavation begins; (IV) Reducing the effective excavation depth by removing soil in a sufficiently large area next to the excavation pit; or (V) Excavating a series of smaller pits. In this way, spatial effects may be mobilised and a greater bearing capacity factor  $N_c$  would result [11].

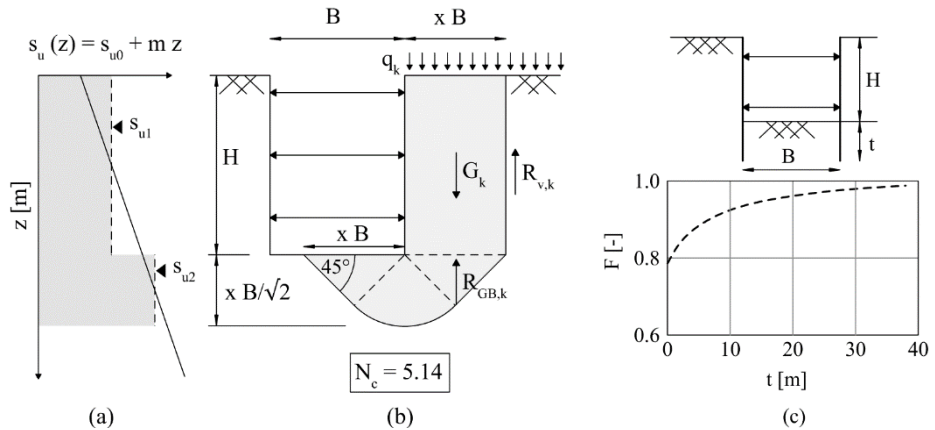


Figure 71 Calculation of the bottom heave stability for  $s_u(z) \neq \text{const.}$  and variable width  $x B$ : (a)  $s_u$ -profile; (b) Approach according to Weissenbach and Hettler [14] with a load-bearing capacity factor  $N_c = 5.14$ ; (c) Influence of the embedment depth  $t$  on the factor of safety  $F$ .

Increasing the embedment depth  $t$  in order to improve the bottom heave stability as a seemingly simple and cost-effective measure is the subject of controversial debate. This can be shown by way of example with the approach according to [14] as formulated in Eq. 1. In the present investigation, even for very large embedment depths of  $t > 20$  m, the calculated level of safety does not fulfil the requirements, see Figure 3(c). It is assumed that the bottom heave failure mechanism develops below the embedment depth as shown in Figure 107(a).

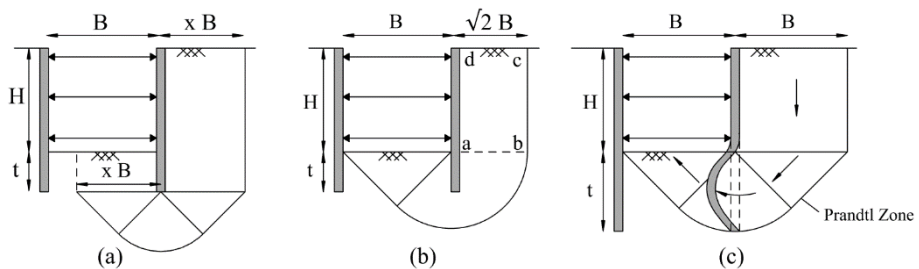


Figure 72 Influence of the embedment depth  $t$  on the bottom heave stability mechanism: (a) The mechanism develops below  $t$  [14]; (b)  $t$  only influences the mechanism if  $t > \sqrt{2} B$  [9]; (c) Dowel effect of the embedment depth [7].

Some other design approaches also imply that large embedment depths are necessary to influence the relevant failure mechanism and thus improve the bottom heave stability [9], see Figure 4(b). In contrast there are approaches that consider dowel action over the embedment depth [3][7], as illustrated in Figure 107(c), whereby in [13] it is suggested that the forces required to retain the soil are transferred upwards in the case of stiff excavation closures, leading to significantly higher bracing forces.

The influence of bottom heave stability is viewed critically as described in [12][13] for another reason. Terzaghi et al. (1996, p.307, [12]) provide the following description: "If the underlying clay experiences a bearing-capacity failure, the bottom of the excavation heaves and the earth pressure against the bracing increases dramatically". This is portrayed in [12] with a larger failure mechanism as seen in Figure 5 for  $F < 1.0$ .

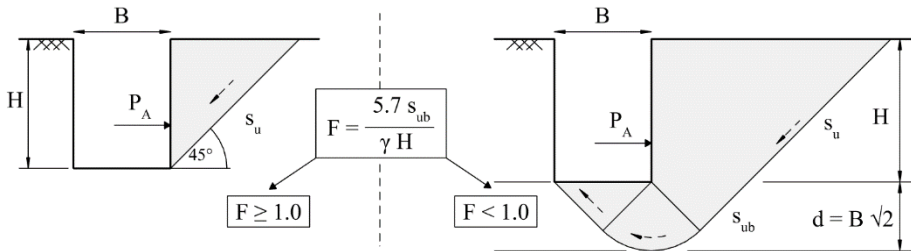


Figure 73 Possible failure mechanism for excavations with bottom heave ( $F < 1$ ) and without ( $F > 1$ ) after [12].

As the requirement for bottom heave stability cannot be satisfied in the current example, a grouted base slab should be constructed before excavation. This construction sequence is generally recommended for excavations in soft soils with depths greater than 5 m [1]. The grouted base slab has the following functions: (I) Creating a base support to ensure the equilibrium of the horizontal forces; (II) Minimising the deformations of the excavation pit support in the foot area in order to limit the settlements outside the excavation pit; and (III) Securing the excavation pit against bottom heave and buoyancy.

The proposed grouted base slab is to be constructed with a thickness of 2 m from -9.0 to -11.0 m, the embedment depth of the diaphragm wall amounts to  $t = 4$  m, see Figure 109(a). The grouted base slab must also be secured with tension piles. Possible design approaches are described in [1][14].

### Earth pressure and bracing forces

The earth pressures and bracing forces are determined analytically and numerically for the excavation illustrated in Figure 109(a). To allow direct comparison with FEM results, characteristic earth pressures are given.

### Earth pressure at rest

Excavation pit supports with prestressed bracings in the upper region and a base support constructed prior to the start of excavation are assumed to be sufficiently rigid so that the earth pressure at rest can be accounted for in the design [1]. Hence, undrained conditions are not considered and earth pressures are calculated as shown in Figure 6. The following aspects should be addressed:

- As a simplification, no passive earth pressure is considered within the excavation – the grouted base slab is activated as a support, see Figure 6(b).

- Earth pressure at rest is considered with a value of  $K_0 = 0.68$ , as determined in the subsoil investigation (Table 23).

$$e'_{0p,k} = K_0 p_k = 6.8 \text{ kPa}; e'_{0,k} = K_0 \gamma' z = 52.2 \text{ kPa}; u_k = \gamma_w z = 120 \text{ kPa} \quad (3)$$

- A degree of earth pressure redistribution is to be considered for prestressed bracings. This can be accounted for in a simplified manner by increasing the resulting support forces by 30% [1]. Hence, the bracing force  $N_k$  is calculated from the upper support force, see Figure 6(c), and increased by 30% for the spacing of  $a = 5 \text{ m}$ :

$$N_k = 1.3 (5 \text{ m}) 252 \frac{\text{kN}}{\text{m}} = 1'640 \text{ kN} \quad (4)$$

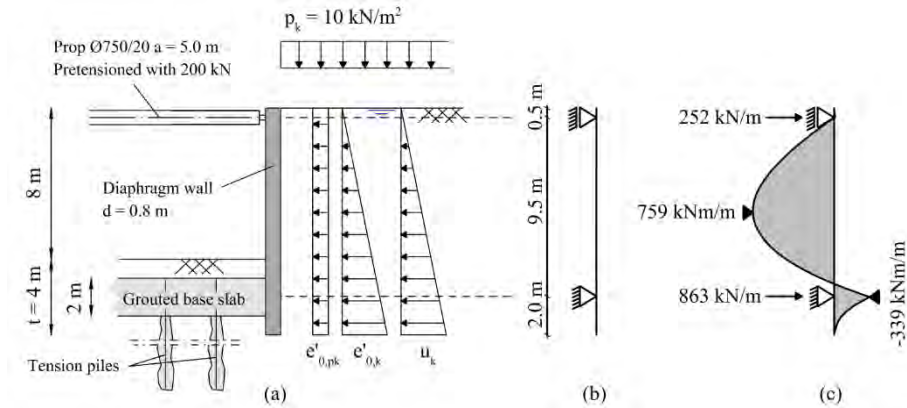


Figure 74 Earth pressure at rest: (a) Actions; (b) Simplified static system; (c) Support reactions and moment distribution.

### Total stress analysis

The active earth pressure may be calculated for the undrained case, neglecting the influence of wall friction:

$$e_{ak} = p_k + \gamma z - 2 s_u(z) = 148 \text{ kPa} \quad \text{for } z = 12 \text{ m} \quad (5)$$

It is assumed that cracks could form due to tensile stresses up to a height of  $h_{cr}$ . When such cracks are filled with water, hydrostatic water pressure takes effect.

$$h_{cr} = \frac{-(2 s_{u0} - p_k)}{2 m - \gamma} = 1.12 \text{ m} \quad \text{with } s_{u0} = 12.6 \text{ kPa} \text{ and } m = 1.4 \text{ kPa/m} \quad (6)$$

In the case of passive earth pressure, it is assumed that the grouted base slab and the soil above act as a surcharge load with a pressure of 56 kPa.

$$e_{pk1} = 56 \text{ kPa} + 2 s_u(11\text{m}) = 112 \text{ kPa} \quad (7)$$

$$e_{pk2} = 56 \text{ kPa} + \gamma 1\text{m} + 2 s_u(12\text{m}) = 131 \text{ kPa} \quad (8)$$

The earth pressure distribution and resulting moment distribution are illustrated in Figure 7. Subsequently, the bracing force can be calculated at a horizontal

spacing of  $a = 5$  m. As before, a degree of earth pressure redistribution is taken into account by increasing the resulting support force by 30%.

$$N_k = 1.3 (5 \text{ m}) 163 \frac{\text{kN}}{\text{m}} = 1'060 \text{ kN} \quad (11)$$

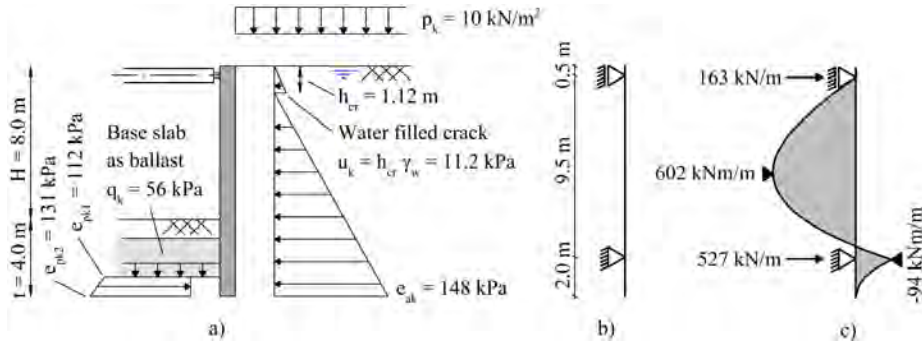


Figure 75 Total stress analysis: (a) Actions; (b) Simplified static system; (c) Support reactions and moment distribution.

### Bracing force diagrams

The critical bracing forces activated across all construction stages may also be estimated using apparent earth pressure diagrams according to Terzaghi et al. [12] or based on Distributed Prop Load (DPL) diagrams according to Twine and Roscoe [13], see Figure 8.

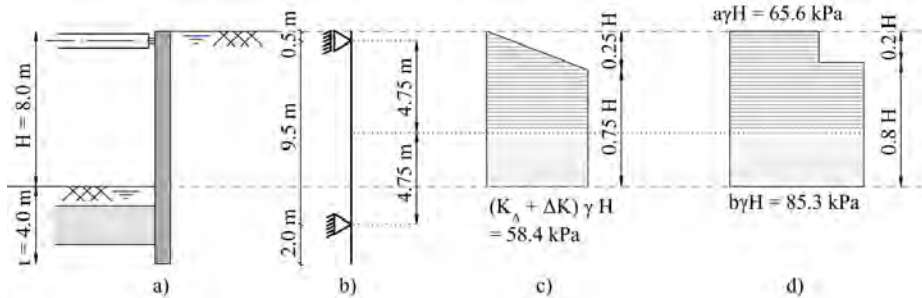


Figure 76 Estimation of maximum bracing force: (a) Excavation pit; (b) Static system; (c) Apparent earth pressure diagram according to Terzaghi et al. [12]; (d) Distributed prop load diagram (DPL) according to Twine and Roscoe [13].

In the investigated case, a jet grouted base slab is constructed as a base support before excavation begins and is secured with tension piles. Thus, it is not assumed that a significant force redistribution results in the bracings from the failure mechanism shown in Figure 108. In the approach according to Terzaghi et al. [12], this results in a value of  $\Delta K = 0$ . Subsequently, the value of  $K_A$  can be calculated for  $s_u(H/2) = 18.2$  kPa, shown in Figure 8, as follows:

$$K_A = 1 - \frac{4 s_u}{\gamma H} = 0.445 \quad (9)$$

According to the approach proposed by Twine and Roscoe [13], the DPL is applied as illustrated in Figure 8(d), which is independent of the undrained shear strength. For the case not at risk of bottom heave, the coefficients result to  $a = 0.5$  and  $b = 0.65$ .

The bracing forces are calculated considering half the distance between the supports as is indicated by the dashed line in Figure 8. Hence, a bracing force of  $N_k = 1'241$  kN results according to Terzaghi et al. [12], whereas  $N_k = 2'080$  kN according to the approach by Twine and Roscoe [13].

## FEM

An undrained, elastoplastic FEM analysis was performed for the current investigation. Structural components such as the diaphragm wall, jetting base and anchors were modelled as wished in place in accordance with [10]. Subsequently, the continued excavation was simulated in 1.5 – 2 m depth increments. The calculations were performed in OPTUM G2 with an axially symmetric model, dimensions of  $b = 120$  m and  $h = 70$  m and an automatically refined FE-mesh consisting of 3'000 elements of type 6-node Gauss. The soil-structure stiffness ratios and the friction mobilised between the soil and the structural component have a significant influence on the development of the deformations and the earth pressures: The diaphragm wall was modelled with a flexural stiffness  $EI^I = 27.23 \cdot 10^4$  kNm<sup>2</sup>/m; the interface-reduction factor was taken as 0.5; the bracing was considered with an axial stiffness  $EA = 96.32 \cdot 10^5$  kN and prestressing force of 200 kN at a spacing of  $a = 5$  m; the grouted base slab was modelled with  $E = 1'800$  MPa,  $\nu = 0.2$  as for concrete and  $c = 2.5$  N/mm<sup>2</sup>,  $\phi' = 0^\circ$  with the Mohr-Coulomb material model. It could be shown that the interface between the base slab and the diaphragm wall has a significant influence on the load-deformation behaviour. The model simulates an incomplete interface between the grouted base slab and the diaphragm wall by considering a reduced wall friction up to a maximum of 50% in relation to the surrounding soil.

Table 17 Input parameters for the soil material models.

Material Model		11 Tresca	12 Tresca	AUS PEAK	AUS ENTF
$E_{u,50}$	[MPa]	8.5	$34.1 \approx E_{ur}$	-	-
$E_u$	[MPa]	-	-	85	85
$\epsilon_{c,50}$	[%]	-	-	0.28	0.28
$\epsilon_{e,50}$	[%]	-	-	0.47	0.47
$s_u(z)$	[kPa]	$12.6+z \cdot 1.4$	$12.6+z \cdot 1.4$	$9.4+z \cdot 2.43$	$11.6+z \cdot 1.54$
$s_{ue}/s_{uc}$	[-]	-	-	0.61	0.61
Tension Cut-Off	[-]	Yes	Yes	Yes	Yes
$\gamma_{sat}$	[kN/m <sup>3</sup> ]	16.4	16.4	16.4	16.4
$K_0$	[-]	0.68	0.68	0.68	0.68

Two undrained material models were implemented to simulate the soil behaviour (total stress analysis), namely, the linear elastic - ideal plastic Tresca and the elasto-plastic AUS (Anisotropic Undrained Shear) soil model [5]. The input parameters were calibrated using a triaxial test according to [8] as summarised in Table 2, resulting in the stress-strain curves shown in Figure 9.

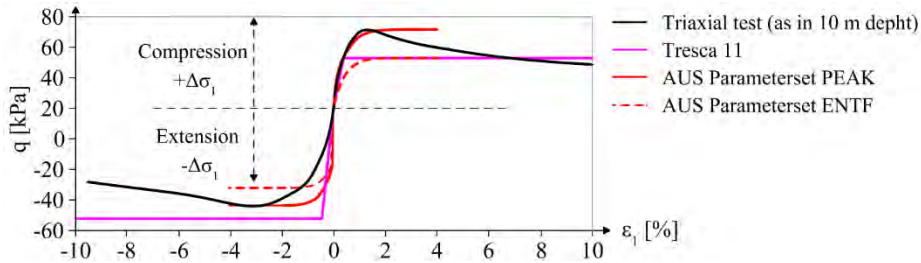


Figure 77 Calibration of the material models using two triaxial tests according to [8] to represent a stress level at a depth of 10 m.

The FE analyses resulted in the earth pressure distributions as illustrated in Figure 10. In addition to the resulting earth pressures, the earth pressure at rest and the total active and passive earth pressures are also shown.

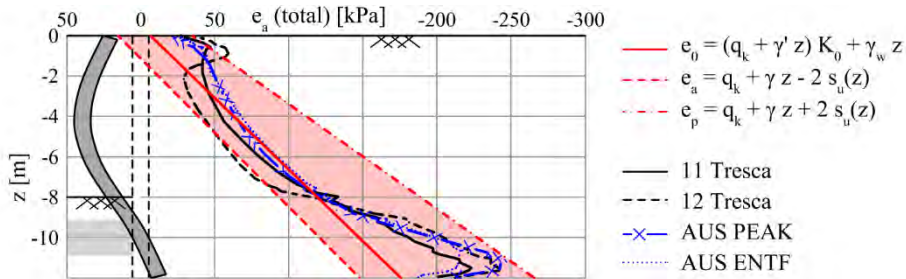


Figure 78 Comparison of mobilised earth pressures resulting from FEM calculations with those from a total stress analysis. Wall deformations are indicated overdrawing.

## COMPARISON OF RESULTS AND CONCLUSIONS

The results from the FE-analysis indicates that the earth pressures react sensitively to the stiffness characteristics in the model as is shown in Figure 10. Consequently, an earth pressure ranging between the earth pressure at rest and the active earth pressure could be mobilised between the bracing and the grouted base slab as a function of the stiffness ratio between the subsoil and diaphragm wall (Tresca 11 & 12). Furthermore, the diaphragm wall appears to rotate around a point approximately at the height of the middle of the base slab. This resulted in the activation of nearly passive earth pressures outside the excavation within the bottom region of the diaphragm wall. Moreover, the analysis indicates a redistribution of forces from the free span length in the direction of the pre-stressed bracings. Figure 11 provides a comparison of the bracing

forces and the maximum span moments obtained from the analytical and numerical calculations. The following three effects could be observed:

- (I) The approach considering earth pressure at rest (drained) appears to result in a safe design for the present investigation, only the approach according to Twine and Roscoe [13] resulted in higher bracing forces, although their diagram is based on multiple-propped excavations in which the greatest bracing forces are known to occur before the next layer of bracings are installed;
- (II) The total earth pressure approach ( $\pm 2 s_u$ ) seemingly results in an underestimation of the bracing force, especially if no increase of 30% due to earth pressure redistribution is taken into account whereas the approach according to Terzaghi et al. [12] compares favourably with the numerical calculations;
- (III) The analytical calculations result in higher bending moments than the numerical analyses.

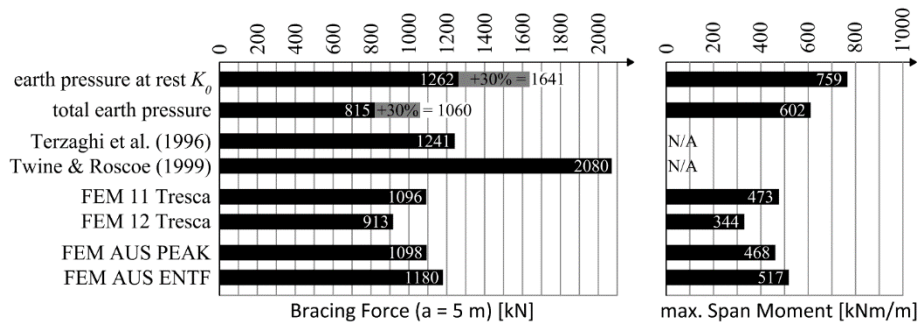


Figure 79 Comparison of the bracing forces and the maximum span moments from the analyses.

The following conclusions could be drawn from the current investigation: For deep excavations in soft soils, there is a risk of bottom heave and large deformations outside the excavation due to ground displacements associated with heave of the excavation base. Thus, the construction practice recommendation that a base support should be provided for excavations in soft soils with  $H > 5$  m before the start of excavation [1] seems appropriate. An overview of literature on the subject and the example calculations indicate that the influence of the embedment depth remains controversial. Insight into the complex soil-structure interaction and activated earth pressure distributions can be obtained through FE-analysis. Interestingly, even the relatively simple, linear elastic - ideally plastic Tresca soil model provides similar results to the elastoplastic AUS soil model with regard to the earth pressure distribution. However, such simple material models are less appropriate in the investigation of deformations around an excavation [10] as they typically do not distinguish between initial and un/reloading in terms of stiffness. A FE-analysis of the undrained conditions with an effective material model (modified cam clay or similar) was not performed. In order to mitigate the risk of unsafe design, the degree of mobilised shear strength must be verified by field measurements for analyses



where the undrained shear strength is a result of the material model and not an input parameter.

## REFERENCES

- [1] Deutsche Gesellschaft für Erd- und Grundbau Arbeitskreis Baugruben: Empfehlungen des Arbeitskrieses Baugruben EAB, 6th ed. Berlin: Wilhelm Ernst & Sohn, 2021.
- [2] A. Hettler, S. Leibnitz, and F. Biehl: Zur Kurzzeitstandsicherheit bei Baugrubenverbaukostruktion. in weichen Böden. Bautechnik, vol. 79, 2002.
- [3] M. Huang, Z. Tang, and J. Yuan: Basal stability analysis of braced excavations with embedded walls in undrained clay using the upper bound theorem. TUST, vol. 79, 2018.
- [4] H.-G. Kempfert and B. Gebreselassie: Excavations and foundations in soft soils. Berlin: Springer-Verlag, 2006.
- [5] K. Krabbenhoft, A. Lymain, and J. Krabbenhoft: OPTUM G2: Materials, 2016
- [6] H.-J. Lang, J. Huder, P. Amann, and A. M. Puzrin: Bodenmechanik und Grundbau: Das Verhalten von Böden und Fels und die wichtigsten grundbaulichen Konzepte, 9th ed. Berlin Heidelberg: Springer, 2011.
- [7] T. D. O'Rourke: Base stability and ground movement prediction for excavations in soft clay. London: Thomas Telford, 1993.
- [8] M. Olsson: On Rate-Dependency of Gothenburg Clay. Doctoral Thesis, Chalmers University of Technology, Göteborg, Sweden, 2013.
- [9] C.-Y. Ou: Deep Excavation - Theory and Practice. London: Taylor & Francis, 2006.
- [10] D. Potts, K. Axelsson, L. Grande, H. Schweiger, and M. Long: Guidelines for the use of advanced numerical analysis. London: Thomas Telford, 2002.
- [11] A. W. Skempton: The bearing capacity of clays, in Proceedings of Building Research Congress Vol.1, 1951.
- [12] K. Terzaghi, R. B. Peck, and G. Mesri: Soil Mechanics in Engineering Practice, 3rd ed. New York: Wiley, 1996.
- [13] D. Twine and H. Roscoe: Temporary propping of deep excavations - guidance on design. CIRIA publication C517. London: Construction Industry Research and Information Association, 1999.
- [14] A. Weissenbach and A. Hettler: Baugruben Berechnungsverfahren. 2nd ed. Berlin: Ernst & Sohn, 2011.

- [15] T. Wood: On the small strain stiffness of some Scandinavian soft clays and its impact on deep excavations. Doctoral Thesis, Chalmers, Göteborg, Sweden, 2016.

# FENICS SIMULATION OF ARTESIAN CONDITIONS IN CLAY SLOPE

**K. Muratova<sup>1</sup>, A. A. Abed<sup>1</sup> and M. Karstunen<sup>1</sup>**

## KEYWORDS

Artesian conditions, Finite element method, FEniCS, safety calculation

## ABSTRACT

This paper presents a numerical simulation of the response of a slope with artesian conditions under the impact of a long heavy rainfall event. Sensitivity analysis of surface and bedrock inclination are presented. The robust FEniCS finite element tool is used to solve the governing coupled Hydro-Mechanical (HM) balance equations. An extended version of the Mohr-Coulomb model is implemented in Fortran and used as soil model. The paper discusses how the stability is influenced by changes in pore water pressure and the occurrence of artesian conditions, exploring slopes with different bedrock inclinations. It also presents potential failure surfaces as part of the discussion. The results provide better understanding of critical geological conditions, which helps to identify regions most at risk and take the required safety measures.

## INTRODUCTION

In recent years, the world has witnessed a notable number of landslides, posing significant challenges to its infrastructure and communities. The understanding of triggering mechanism of landslides is crucial when aiming to predict and mitigate their occurrences.

Instability can happen even in almost horizontal landscapes. Even though most landslides are triggered by human activities, they can also have natural causes. The buildup of artesian pressure could be one of the reasons. Artesian conditions can be found in specific geological conditions: presence of both inclined bedrock beneath a clay deposit and layer of permeable soil between them resulting in a confined aquifer.

One of the most devastating landslides in Sweden, Tuve landslide in 1977, was initiated after a heavy rainfall event, involving artesian conditions [1]. The problem is expected to become even more severe with climate change and the associated extreme weather conditions (i.e., more frequent heavy rainfall with

<sup>1</sup> Chalmers University of Technology, Gothenburg Sweden

long duration) which can lead to sudden pore water changes that can trigger landslides.

This paper aims to explore influence of artesian conditions on the slope stability. Three slope configurations with different inclinations of bedrock were chosen for investigation. For this purpose, Python code based on FEniCS finite element tool created by Abed et al. [2] was used. Additional functionalities have been added to the code to enable the modelling of artesian conditions, including the capability to model multiple soil layers.

## METHOD

The code was utilised to solve the following balance equations:

### 1) Mechanical balance equations

$$\nabla \cdot \boldsymbol{\sigma} + \mathbf{b} = 0 \quad (1)$$

where  $\nabla \cdot \boldsymbol{\sigma}$  is the divergence of the total stress tensor and  $\mathbf{b}$  is a vector containing the body forces.

For considering unsaturated features of the problem, Bishop's effective stress is used:

$$\boldsymbol{\sigma}' = \boldsymbol{\sigma}'' + \chi \mathbf{s} \quad (2)$$

where  $\boldsymbol{\sigma}'' = \boldsymbol{\sigma} - \mathbf{u}_a$  denotes the net stress,  $\mathbf{s} = \mathbf{u}_a - \mathbf{u}_w$  is the matric suction. The pore air pressure and pore water pressure are denoted as  $\mathbf{u}_a$  and  $\mathbf{u}_w$ , respectively. It is generally assumed that the pore air pressure remains at atmospheric levels with  $u_a = 0$ , so  $\mathbf{s} = -\mathbf{u}_w$ . Following the arguments by Gens et al. [3], the code assumes that  $\chi = S_{eff}$  the effective degree of saturation, where:

$$S_{eff} = \frac{(S_r - S_{res})}{(S_{sat} - S_{res})} \quad (3)$$

with  $S_r$ ,  $S_{sat}$  and  $S_{res}$  refer to the soil degree of saturation at normal conditions, the degree of saturation at full saturation and the residual degree of saturation, respectively.

Additionally, information from the Soil Water Characteristic Curve (SWCC) is required to reflect the hydraulic properties of the unsaturated soil. In this study, the SWCC is assumed to have the following simple form (in fact is the code is flexible and any other formula can be easily implemented):

$$S_r = (S_{sat} - S_{res}) \cdot e^{-\alpha \cdot s} + S_{res} \quad (4)$$

where  $\alpha$  is a material parameter. The corresponding hydraulic conductivity function is described by the equation:

$$K(s) = K_{sat} \cdot e^{-\alpha \cdot s} \quad (5)$$

The weak formulation of the mechanical balance equation and the finite element discretization yield:

$$\begin{aligned} \int_{\Omega} \nabla N_b^T \mathbf{M} \nabla N_b \delta \hat{u} d\Omega + \int_{\Omega} \chi \nabla N_b^T \mathbf{m}^T \nabla N_b \delta \hat{u}_w d\Omega - \int_{\Omega} N_b \delta b d\Omega \\ - \int_{\Gamma} N_b \delta \tau d\Gamma = 0 \end{aligned} \quad (6)$$

where  $N_b$  is a shape function,  $\delta \hat{u}$  is the increment of nodal displacements,  $\delta \hat{u}_w$  is the increment of nodal pore water pressure and  $\delta \tau$  is the surface traction increment. The symbol  $\mathbf{m}^T$  denotes the transpose of the unity vector and  $\mathbf{M}$  represents the material stiffness matrix.

### Water mass balance equation

The water mass balance equation for unsaturated soil can be written as (Abed and Sołowski [4]):

$$\nabla^T \left[ \frac{K(s)}{\rho_w g} \cdot (\nabla u_w + \rho_w g) + n \left( \frac{\partial S_r}{\partial s} - \frac{S_r}{K_w} \right) \frac{\partial u_w}{\partial t} + S_r \frac{\partial \varepsilon_v}{\partial t} \right] = 0 \quad (7)$$

where  $n$  is the porosity,  $\rho_w$  is the density of water,  $g$  is the gravity acceleration and  $K_w$  is the water bulk modulus. To solve the equation both the SWCC and the hydraulic conductivity function are required to be defined. The term  $\frac{\partial \varepsilon_v}{\partial t}$  is the rate of volumetric strain representing the coupling term with the mechanical behaviour.

The weak formulation of the water balance equation and the subsequent finite element discretization yield:

$$\begin{aligned} - \int_{\Omega} \nabla N_b^T \frac{K(s)}{\rho_w g} \nabla N_b \delta \hat{u}_w d\Omega + \int_{\Omega} \nabla N_b^T \frac{K(s)}{\rho_w g} \rho_w g d\Omega \\ + \int_{\Omega} \nabla N_b^T n \left( \frac{\partial S_r}{\partial s} - \frac{S_r}{K_w} \right) \frac{\partial \hat{u}_w}{\partial t} d\Omega + \int_{\Omega} N_b S_r \frac{\partial \varepsilon_v}{\partial t} d\Omega = 0 \end{aligned} \quad (8)$$

### Mohr-Coulomb (MC) model for unsaturated soil

Using Bishop 's effective stress instead of Terzaghi's effective stress, the standard form of MC model can be used directly:

$$f_M = \left( \frac{\sigma'_1 - \sigma'_3}{2} \right) - \left( \frac{\sigma'_1 + \sigma'_3}{2} \right) \cdot \sin \varphi' - c' \cdot \cos \varphi' \quad (9)$$

$$g_M = \left( \frac{\sigma'_1 - \sigma'_3}{2} \right) - \left( \frac{\sigma'_1 + \sigma'_3}{2} \right) \cdot \sin \psi \quad (10)$$

$$f_T = g_T = \sigma^t - \sigma'_3 \quad (11)$$

where  $f_M$  and  $g_M$  are the failure and the plastic potential surface, respectively,  $f_T$  is the tension cutoff failure surface,  $\varphi'$  is the effective internal friction angle,  $c'$  is the cohesion intercept and  $\psi$  is the dilatancy angle. Additionally, it is necessary to specify the tensile strength  $\sigma^t$ , which is commonly defaulted to zero. Elasticity is governed by the classical Hooke's linear elasticity law, which relies on two material properties: the effective Young's modulus  $E'$  and the effective Poisson's ratio  $\nu'$ .

## ANALYSIS

During the analysis three models were created with different inclinations of frictional layers (i.e., indicated as 'permeable layer' in Figure 1). The models' geometries are presented in Figure 1. Identical volumes of infiltration of 0.45 m<sup>3</sup>/day are applied to the top of all frictional layer to model environmental loads. The increased infiltration at the top boundary of the frictional layer is used to reflect the runoff due to the accumulation of water at the top of the surrounding, much less permeable, clay. Soil properties of clay, frictional layer and rock are summarised Table 1.

Table 1. Soil properties

Property	Clay	Frictional layer	Rock	unit
MC properties				
$\varphi'$	28	35	40	[ ° ]
$c'$	3	20	20	kN/m <sup>2</sup>
E	3600	240000	1.0e7	kN/m <sup>2</sup>
$K_{sat}$	1.16e-9	1.16e-5	1.16e-9	m/s
Other properties				
$\nu' = 0.2$ , $\psi = 0^\circ$ , $\alpha = 0.01$ 1/kPa, $S_{sat} = 1$ , $S_{res} = 0.23$ , $K_0^{NC} = 0.6$ , $e_0 = 0.667$				

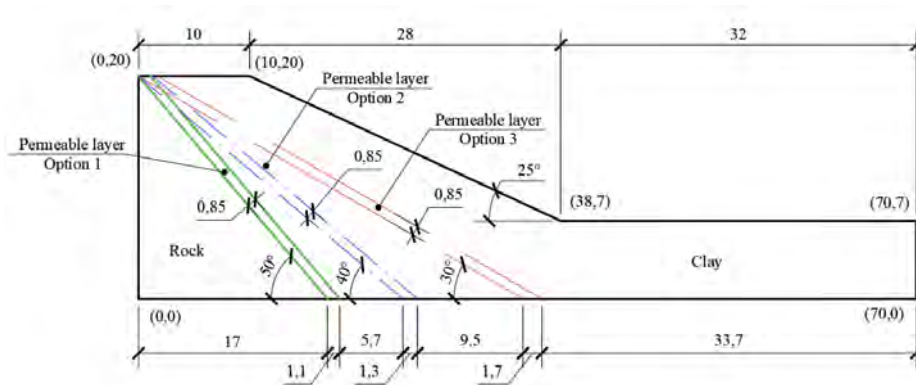


Figure 1 Model geometry

Firstly, the calculations of the stability of the slope in the initial conditions (water level at 0.5 meters above the bottom) using phi-c reduction (strength reduction) method were performed. The ratio between the available shear strength parameters to the critical ones needed to cause failure gives the safety factor SF:

$$SF = \frac{c'}{c'_{critical}} = \frac{\phi'}{\phi'_{critical}} \quad (7)$$

All three slopes in initial conditions have a safety factor higher than 1: 1.26, 1.40 and 1.69 that corresponds to frictional layer inclination of 50°, 40° and 30°, respectively.

Over time under environmental load, due to presence of the frictional layer between two impermeable layers, a confined aquifer is being formed. During this process the pore water pressures are increasing, displacements are developing, and stability is decreasing. The results of the analysis are presented in the following paragraphs.

### Displacements and failure

Failures were observed after 14, 22, and 29 days of infiltration in cases 50, 40, and 30, respectively. Figures 2a-c show slip surfaces at the specified time (displacements are scaled by a factor of 100). White line depicts the contour of zero pore water pressure at failure. On the one hand, since case 50 has the smallest volume of the frictional layer, the rise of the water level happens faster, and it could be the reason of the faster failure. On the other hand, it also has the lowest initial safety factor which indicates that smaller changes in system can lead to failure. Additional investigation needed to understand which factors have the biggest impact.

Figure 3 illustrates horizontal surface displacement at points Q. An increase of the displacement rate is observed before failure. Since failure occurs relatively

fast, the pore water pressure in clay does not have enough time to dissipate and thus the deformation levels before failure are quite low. The largest surface displacements are noted in case 30, it is explained by the lowest thickness of the clay layer above the frictional layer and longest time until failure.

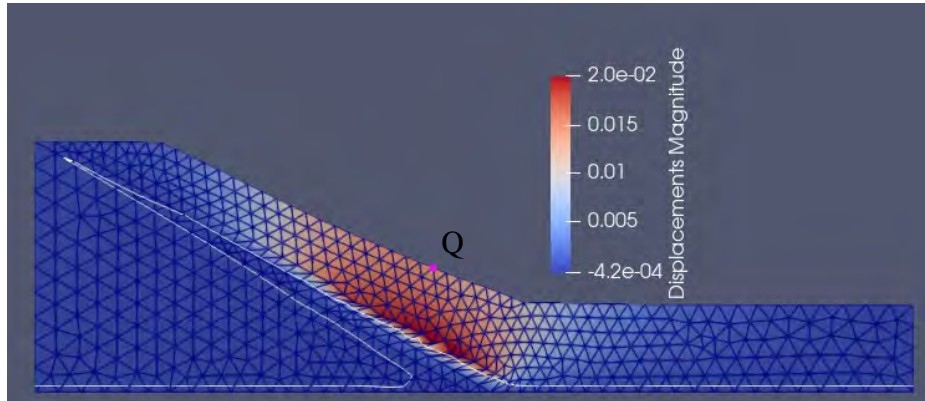


Figure 2a. Displacements (in meters) of the model 30 at day 29

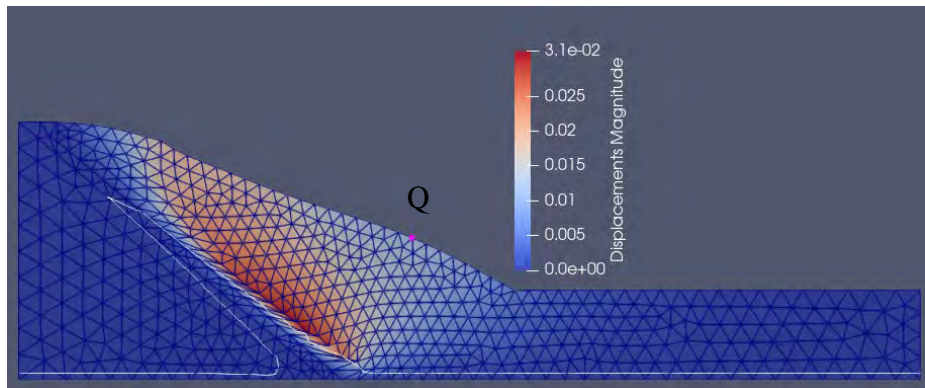


Figure 2b. Displacements (in meters) of the model 40 at day 22

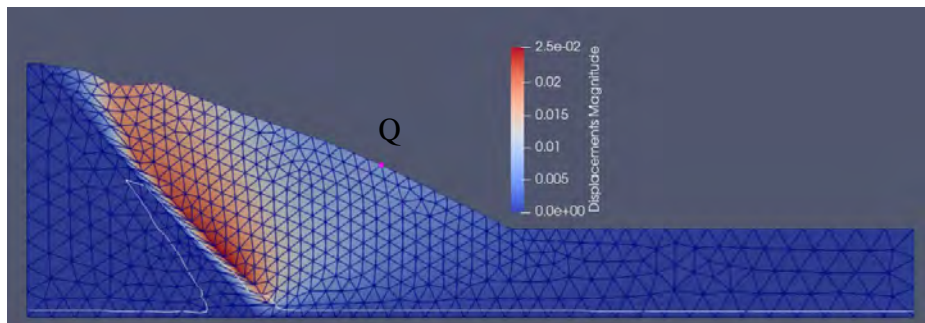


Figure 2c. Displacements (in meters) of the model 50 at day 14



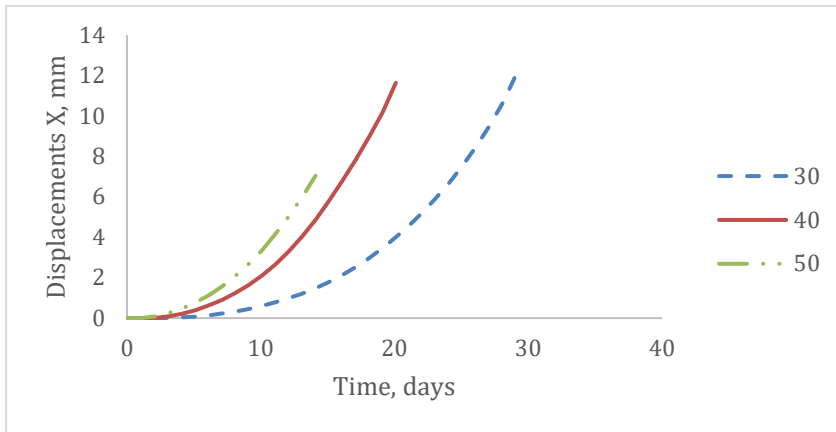


Figure 3. Displacements at points  $Q$  over time until failure.

### Pore water pressure

Different distributions of suction along the layer due to different inclinations of frictional layers lead to different distribution of hydraulic conductivity over layer (see Figure 4), since the hydraulic conductivity is a suction dependant parameter, see Equation 5. The initial hydrostatic distribution of pore water pressure along the frictional layers of the three models is shown on Figure 5a. Due to the different variation of the hydraulic conductivity over depth and the different volume of the frictional layer with equal infiltration rate, the pore water pressure changes differently. The water level in the frictional layer in the case 30 increases slower than in case 50, case 40 showed intermediate result.

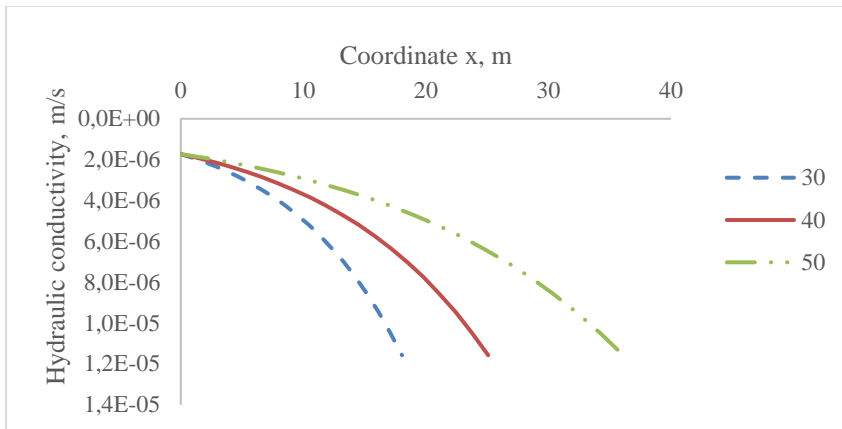


Figure 4. Hydraulic conductivity along the frictional layer

On Figure 5b-f the changes of pore water pressure over time are shown. At day 3, the water level in case A (50) has started to grow and pore water pressure started decreasing in contrast to case C (30) where pore water pressures stay constant. At day 10 in all cases the water level is increasing and the pore

water pressures at the bottom are decreasing. As seen in the figures, the minimum pore water pressures at bottom at failure are similar: -80 (Case 50), -88 (Case 40) and -85 (Case C), the different pressures are observed in the upper part of the slopes. The water levels at failures are at 12, 13 meters above bottom for cases 50 and 40 respectively. For case 30 frictional layer is almost fully filled with water – lowest point of the water level is at 14 meters above bottom, highest – at 18,7 meters.

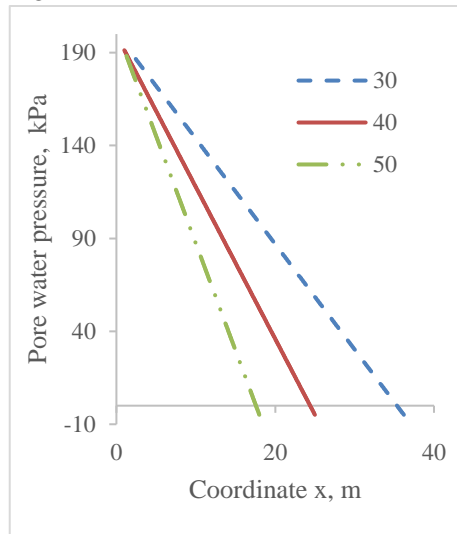


Figure 5a. Initial pore water pressure along frictional layer

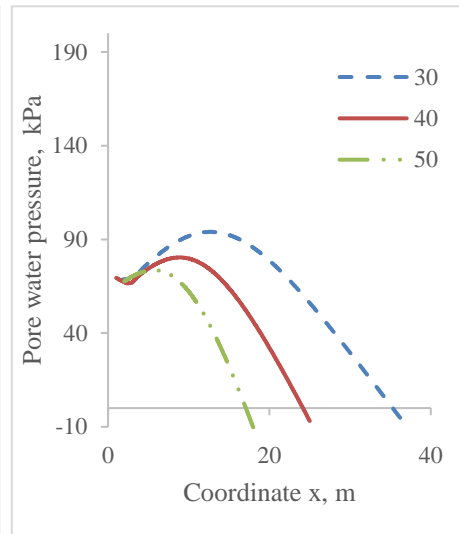


Figure 5b. Pore water pressure along frictional layer at day 3

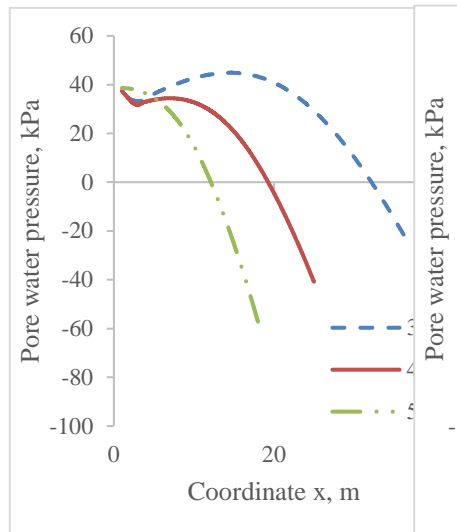


Figure 5c. Pore water pressure along frictional layer at day 10

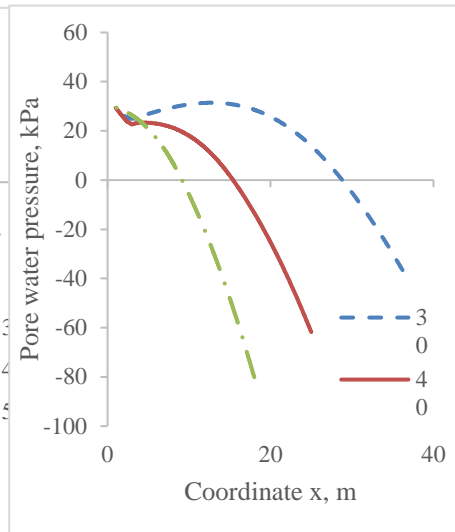


Figure 5d. Pore water pressure along frictional layer at day 14

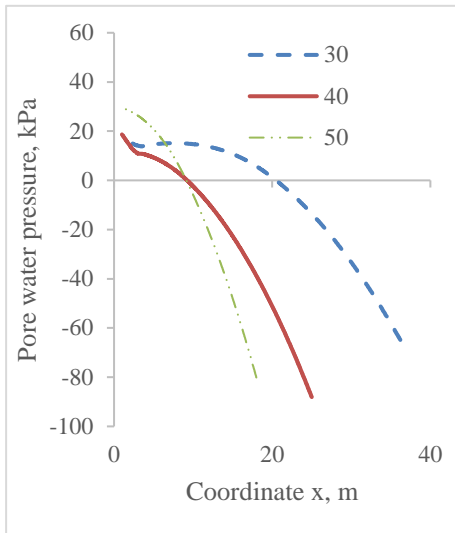


Figure 5e. Pore water pressure along frictional layer at day 24

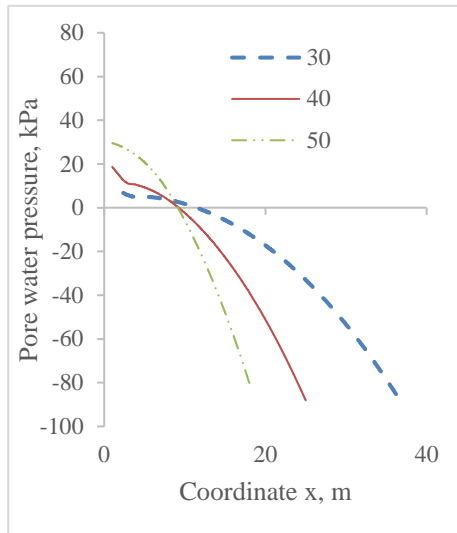


Figure 5f. Pore water pressure along frictional layer at day 29

## CONCLUSIONS

Fully coupled hydro-mechanical analyses considering unsaturated conditions of the soils was performed to model the formation of artesian conditions due to environmental load. The effect of artesian conditions on slope stability was studied. The calculations showed that an infiltration of a specific duration and intensity leads to forming of artesian conditions when having specific geological conditions, which can trigger failure even in the case of relatively flat slopes. The main triggers of decreasing stability are 1) the increase of pore water pressure causing reduction in effective stress; 2) decrease of unsaturated part of the shear strength in the area where decrease of suction happens and 3) the specific stratigraphy of a thin frictional layer sandwiched between two impermeable layers leading to the development of artesian conditions after heavy rain event.

It must be emphasized that the use of this code, which uses many of the capabilities of the FEniCS platform, makes it possible to investigate complex time-dependant hydrogeological phenomena and opens opportunities to solve even more complex tasks. The capability of the code was even extended more by the new functionality of modelling layers with different soil properties which might look simple, but indeed it has far reaching consequences in increasing the flexibility of using FEniCS to model geotechnical problems. One example of these problems is the modelling of the development of artesian conditions as discussed in this paper. Since the problem is of interest and has a big impact on slope stability, further investigations are required to make more comprehensive conclusions.

## FUTURE RESEARCH

There are advancements of the code that needed to be implemented to model artesian conditions more realistically. Among the crucial ones is the implementation of different unsaturated behaviour of different layers. Different soil-water retention curves, such as van Genuchten are going to be implemented as well. In the future, different thermal and hydraulic boundary conditions will be inspected to analyse the slope stability under extreme environmental loads as driven by climate change. While the current work focuses so far on failure, the advanced material model Creep-SClay1S [5] that can consider important aspects of the clay behaviour such as anisotropy, rate-dependency and evolution of the fabric will be used to get more accurate predictions of the evolving pre-failure deformations.

## ACKNOWLEDGEMENT

The work is funded by Formas (Research Council for Sustainable Development, Grant (2021-02400) and the work is done as part of Digital Twin Cities Centre that is supported by Sweden's Innovation Agency VINNOVA (Grant 2019-00041).

## REFERENCES

- [1] R. Larsson, M. Jansson: The Landslide at Tuve. Report No 18, Swedish Geotechnical Institute, 1982
- [2] A. Abed, E. Gerolymatou, M. Karstunen: FEniCS simulation of a partially saturated slope under varying environmental loads. Proceedings 10th NUMGE, 2023.
- [3] A. Gens, M. Sánchez, D. Sheng: On constitutive modelling of unsaturated soils. *Acta Geotechnica* 1, 137–137, 2006.
- [4] A. Abed, W. Sołowski: A study on how to couple thermo-hydro-mechanical behaviour of unsaturated soils: Physical equations, numerical implementation and examples. *Computational Geotechnics* 92, 132–155, 2017.
- [5] J.-P. Gras, N. Sivasithamparam, M. Karstunen, J. Dijkstra: Permissible range of model parameters for natural fine-grained materials. *Acta Geotechnica*, 13(2), 387–398, 2018.

# FIELD VANE TEST WITH NEW STANDARD

**Panu Tolla<sup>1</sup>, Juha Selänpää<sup>2</sup>, Monica S. Löfman<sup>3</sup>, Sami Kankaanpää<sup>3</sup> and Fredrik Winqvist<sup>3</sup>**

## KEYWORDS

Field vane test, standards, Guideline, Undrained shear strength, Remoulded shear strength

## ABSTRACT

New geotechnical investigation and testing standard EN ISO 22476-9:2020 Field vane test (FVT and FVT-F) provides necessary requirements for the test. It introduces various test equipment configurations without classifying their suitability or accuracy for specific ground conditions in details. Observing numerous failed FVTs was led to a research project to improve test specifications by the Finnish Transport Infrastructure Agency. The results show that test reliability can be improved by moderate upgrading device and procedure. The improvements are mirrored in the standard specifications. Despite the standard providing necessary basis for the test, the operator and geotechnical designer need specific knowledge to be able to assess the test results the reliability of shear strength measurements.

## INTRODUCTION

New geotechnical investigation and testing standard EN ISO 22476-9:2020 “Field vane test (FVT and FVT-F)” was published three years ago as the last one of the main field test methods in geotechnics [1]. Active Nordic working group members and the project manager guaranteed that the new standard very well corresponds to the Nordic practices, and it also considers the Danish special heavy duty vane device (FVT-F).

<sup>1</sup> Finnish Transport Infrastructure Agency, Helsinki Finland

<sup>2</sup> Destia Oy, Helsinki Finland

<sup>3</sup> Ramboll Finland Oy, Espoo Finland

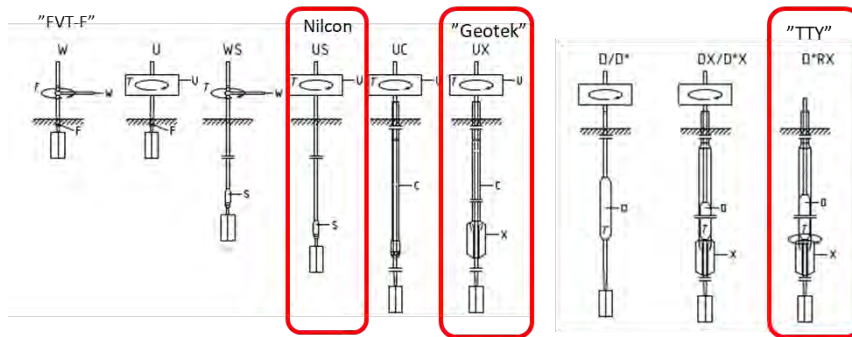


Figure 1. Test equipment configurations in EN ISO 22476-9:2020 [1]. The configurations to be discussed are highlighted and named.

The standard introduces various test equipment configurations without classifying their suitability or accuracy for specific ground conditions in details. In a FTIA (Finnish Transport Infrastructure Agency) project dealing with stability assessment of existing railway embankments called “RATUS”, FVT results that indicate unrealistic low soil strength measured with US configuration test equipment were often observed [7]. Such results were common in silty soil layer units, typically beneath clay units, but also in full depth of soft soil unit composed of lean to fat clay. When the undrained soil strength being the most essential parameter in embankment stability analyses, it was necessary to improve the test method.

## FIELD VANE TESTS IN FINLAND

In Finland, Field vane test (FVT) has been the main test method to measure undrained shear strength of soft clays and silty soils since the beginning of 1960's. It has also been utilized to measure shear strength in peat and in organic soils. At first the devices were equipped with torque wrench and later with torque measuring unit such as the Nilcon type [5]. During the past 20 years, multipurpose tracked sounding machines were equipped with electronic units to carry out vane rotating and torque moment measuring without any significant improvements on the test execution itself.

The test method was investigated in Tampere University in the beginning 2010's. The focus was on US type “Nilcon” device, which was the most common FVT test equipment. Slip coupling device malfunctioning was the major finding in the study. Slip coupling is sensitive to poor maintenance and cheaper quality devices were also discovered to enter the market [7].

In addition to the equipment condition and maintenance, the role of qualified operators was emphasized in discussion. Execution practice on site has a crucial role; That is, pushing into test depth and vane rotating with careful and

precise manner without forcible movements. One relevant quality risk with up-hole test is twisting of extension rods. Increase of testing depth also adds to the twisting. If casing is not used, bending of extension rods is not ensured.

FVT extension rods are small in diameter, only 22 mm. During the down pushing and series of shearing test in previous testing depth, the rods may not maintain straight linear line without the casing. Several meters long extension rods behave as torsion spring during the test and recorded readings may have little to do with actual soil strength.

Following to Geotek Ltd proposal, FTIA tested improved configuration of Nil-con equipment: slip coupling was removed, and the device was equipped with protective shoe for vane and rod casing (Figure 2). The configuration corresponds with new “UX” category [1]:

- Continuous uphole measurement of torque versus rotation
- Transfer of torque by uncased extension rods with a slip coupling
- Torque – apparent rotation
- Electrical rotation unit



*Figure 2. Upgraded “Geotek” field vane equipment of UX category with protective shoe and casing.*

## FIELD TEST RESULTS

FTIA ordered from Tampere University and Geotek Ltd field tests at three sites at Perniö, Kotka and Murro. Perniö site (in south-western Finland) is characterized with slightly over-consolidated fat clay with water content of 80 to 110%. Kotka (in south-eastern Finland) fine soil units compose of lean and fat clays with water content of 50 to 100%. Murro represent typical Österbotten clayey silts with low organic content and lean clay units in deeper depths. Water content is mostly 45 to 70%. The ground conditions are described in further detail in the reference studies [3] [4] [6].

In the field tests Tampere University executed two to three test parallel profiles (labelled as “TTY”). Geotek executed three parallel profiles and an additional one by resting time of 1 hour after the vane blade was pushed down to the test depth (Figure 3)

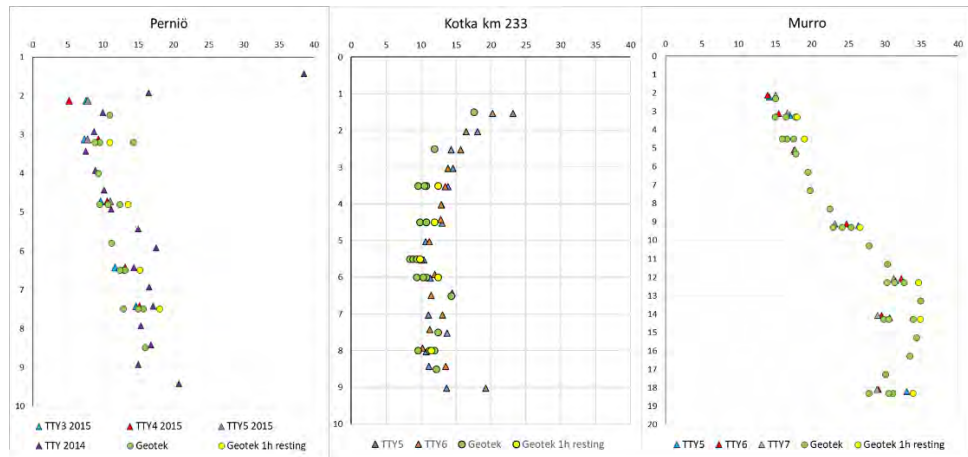


Figure 3. Field vane strength ( $\text{kN/m}^2$ ) versus depth (m) results at Perniö, Kotka and Murro sites carried out by Tampere University (TTY) and Geotek Ltd.

As presented in Figure 3, test results show that the upgraded Nilcon to UX device ("Geotek") can provide similar soil strength as Tampere University's D\*RX downhole device. In Kotka the earlier site investigations indicated that the field vane strength is only 6 to 10 kPa measured with Nilcon device; i.e., some 50% of the latest measurements. On the other hand, in Murro site the old test results varied from similar strength to remarkably low strength in depths of 6 m and deeper in clayey silt soil. And in Perniö results in the old and presented test are in similar range. Another interesting finding was that the measured strengths after 1h resting time were not higher than in the standard procedure test on any test site (Figure 3.). Especially in RATUS project, 1h resting time procedure have been used to compensate for soil disturbance in sensitive silty unit.

Figure 4 presents remoulded field vane strength measured TTY D\*RX and Geotek UX devices. In general, results with D\*RX device present lower remoulded strength compared with UX device result. The measured values of UX type are significantly higher than measured by the D\*RX device although the absolute difference is in similar scale of magnitude as the measured peak strengths differences.



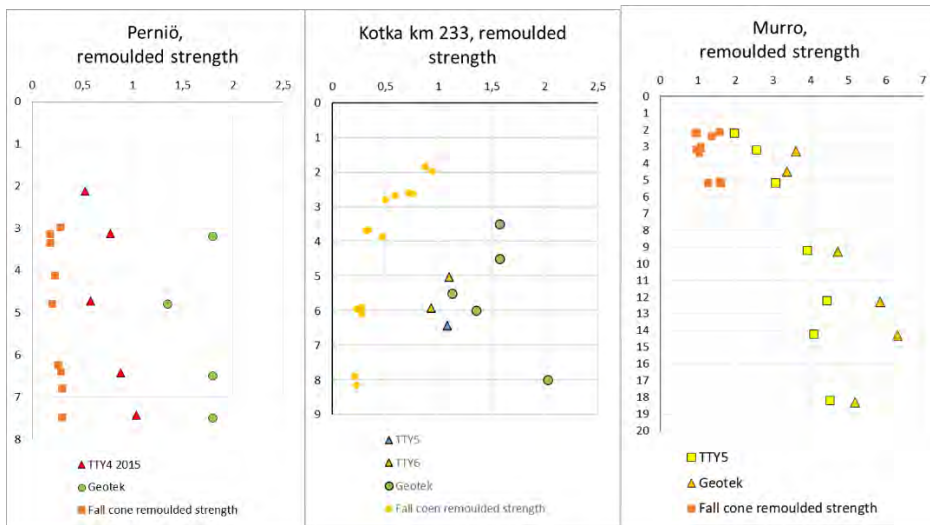


Figure 4. Remoulded field vane strength ( $\text{kN/m}^2$ ) versus depth (m) results at Perniö, Kotka and Murro sites carried out by Tampere University (TTY) and Geotek Ltd and their comparison with fall cone remoulded strength.

When the field vane tests are compared with fall cone test results, the difference can be considered remarkable. Fall cone test results indicate that remoulded strength is approximately 25...35 % of remoulded strength of results measured by the D\*RX device. The difference is even greater when compared to UX measurement. The difference between remoulded vane strength and fall cone remoulded strength is also influenced by different test boundary conditions.

Figure 5 presents another type of problem that was recently identified. Quite high soil strength is measured under embankment slope and old replacement fill. A geotechnical designer may trust in such a result, unless the unusually high remoulded strength is recognized as an indication of quality problem. In this case, the torsion moment-rotation angle graphs provided essential data of the test and proved that the natural strength of soil is not being measured at all. This complete data is not normally available for designers. Possible soil was intruded between the casing and extension rods causing extremely high remoulded strength too. The protection shoe or lower part of casing should be designed so that it prevents soil intrusion inside the casing without increasing external friction.

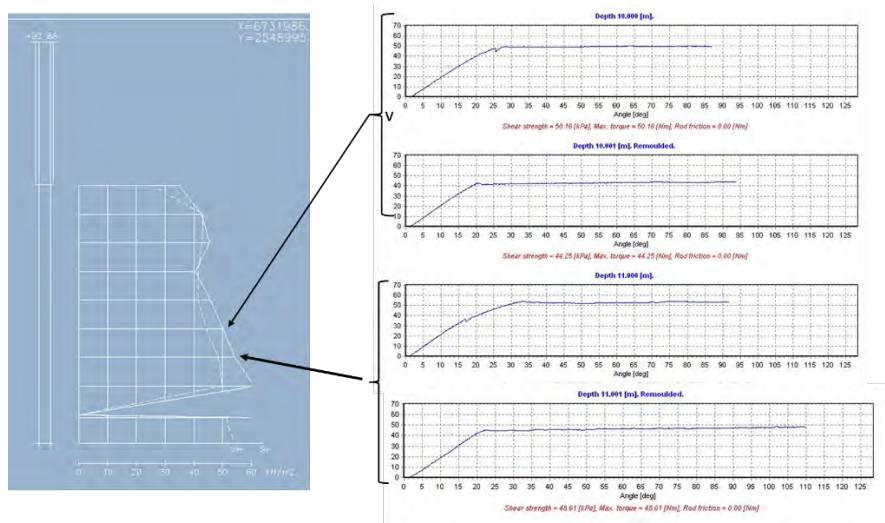


Figure 5. Field vane strength ( $\text{kN/m}^2$ ) versus depth (m) and torsion moment versus rotation angle in two depths as examples.

## DISCUSSION AND CONCLUSIONS

FTIA field test results demonstrate that in typical Finnish soft soil conditions a qualified operator can reach similar investigation test results with the moderately upgraded Nilcon field vane (“Geotek”) compared to the sophisticated and high-quality commercial D\*RX device used by Tampere University.

The tests indicate that with UX or D/D\* type devices a better straightness of the rod system is ensured via casing due to the greater bending stiffness for inner rods. Moreover, the external friction can be remarkably reduced. In addition to mechanical support, the protection shoe can provide cleaner vane blades when penetrating through sticky soil units.

The remoulded strength comparison shows that the strength of fall cone tests is significantly lower than field vane test indicates. Determining the sensitivity based on field vane tests may lead to under estimation of risks related to sub-soil disturbance.

The most important factor for high quality FVT results is the operator. FVT execution requires a person who has knowledge of all the factors that have influence on test results. The operator needs time to carry out this sensitivity test in a careful manner and to conduct the system checks before testing.

Finnish Geotechnical Society (SGY) has published a new national guideline in which the new standard requirements are adopted and the findings of the trial tests, with UX and D\*RX devices, are considered [2]. The new guideline also gives practical guidance for the operators for checking equipment and to maintain good quality in testing. According to the FTIA’s experience, the quality of

FVT results have improved since the request for UX devices was published in 2017, but results with unrealistic low strength do occasionally occur.

New EN1997 states that in Ground investigation report, the geotechnical designer shall verify that ground investigation is executed according to the relevant standard. EN ISO 22476-9:2020 provides excellent bases for FVT, when it defines all the basic test parameters and execution procedure. Unfortunately, it cannot support the operator or geotechnical designer assessing the test results. They still need deep knowledge of test and possibility to assess the results from measured data.

## REFERENCES

- [1] EN ISO 22476-9: Geotechnical investigation and testing - Field testing - Part 9: Field vane test (FVT and FVT-F) (ISO 22476 9:2020), 2020.
- [2] Finnish Geotechnical Society (SGY): Kairausopas II: Siipileikkauskoe. (Ground investigation guide II: Field vane test, <https://sgy.fi/content/uploads/2022/12/kairausopas-2-siipileikkauskoe-2022-12-07.pdf>), 2022
- [3] M. Löfman: Uncertainty quantification for compressibility and settlement response of clays. Doctoral dissertation, Aalto University, 2022
- [4] A. Pelho et al.: Raskaiden junien kuormitusvaikutusten monitorointi. Liikenneviraston julkaisuja 21/2018. (<https://urn.fi/URN:ISBN:978-952-317-542-6>), 2018
- [5] Roctest: Instruction Manual, Field vane shear test, Model M-1000 (NILCON). <https://roctest.com/wp-content/uploads/2017/01/E10046-19032020.pdf>, 2017
- [6] J. Selänpää: Derivation of CPTu Cone Factors for Undrained Shear Strength and OCR in Finnish Clays. Doctoral dissertation, Tampere University, <https://urn.fi/URN:ISBN:978-952-03-2156-7>, 2021
- [7] J. Selänpää et al.: Problems related to field vane testing in soft soil conditions and improved reliability of measurements using an innovative field vane device. Landslides in Sensitive Clays: From Research to Implementation, 109-119, DOI: 10.1007/978-3-319-56487-6\_10, 2017